



**UNIVERSITY OF
BIRMINGHAM**

**Changing Geophysical Contrast between
Archaeological Features and Surrounding Soil**

**By
Daniel Boddice**

**A thesis submitted to
The University of Birmingham
For the degree of
DOCTOR OF PHILOSOPHY**

**School of Civil Engineering
College of Engineering and Physical Sciences
University of Birmingham
June 2014**

UNIVERSITY OF
BIRMINGHAM

University of Birmingham Research Archive

e-theses repository

This unpublished thesis/dissertation is copyright of the author and/or third parties. The intellectual property rights of the author or third parties in respect of this work are as defined by The Copyright Designs and Patents Act 1988 or as modified by any successor legislation.

Any use made of information contained in this thesis/dissertation must be in accordance with that legislation and must be properly acknowledged. Further distribution or reproduction in any format is prohibited without the permission of the copyright holder.

Abstract

Electromagnetic (EM) techniques are widely used to locate and map archaeological features. However, many of these techniques have been found to work poorly on certain soils (especially fine grained soils) and have a poorly understood seasonality to their response. This is due to differences in the soils EM properties, which have been linked by previous research to geotechnical properties of the soil and climatic conditions. Thus this research investigates the changing EM contrasts, which facilitate detection, by using Time Domain Reflectometry (TDR) monitoring stations to collect apparent relative dielectric permittivity (ARDP), bulk electrical conductivity (BEC) and temperature data from archaeological soils and the surrounding soil matrix (SSM) at depths of up to 1.2m. To monitor contrasts in the field, a new bespoke TDR monitoring station capable of operating in remote locations was designed. The use of a datalogger to reduce power consumption and a solar panel system to keep the batteries charged allowed the stations to operate successfully throughout the monitoring period of 16-23 months. Data were collected from four sites located on four different soil types with a wide variety of different soil properties at high temporal resolution to give a dataset of long term and varied soil measurements. Soil samples from site were also taken to study links between their geotechnical and EM properties in the laboratory.

In the laboratory, differences in BEC-VWC (volumetric water content) and ARDP-VWC relationships between the fine and coarse grained soils were found, although differences between archaeological and SSM soils from the same site were smaller, confirming field measured contrasts predominantly result from VWC differences. ARDP-VWC relationships were affected primarily by the EM loss tangent (ratio of energy losses to energy storage) rather than just the amount of bound water as has been previously suggested.

Seasonal variations in the measured properties were found on all of the sites (especially in the near surface soils <0.5m) and were defined by both a dry period with constant low ARDP and BEC values and a wet period after an initial wetting front during which the soil responded to

Abstract

rainfall events. However both the archaeological and SSM soils showed similar trends in recorded values and infiltration responses after rainfall events, and primarily showed differences due to the variable water holding capacities of the soils and variations in drying patterns, which could be explained using the geotechnical properties of the soil. Temperature also followed seasonal trends, affected BEC, especially in fine grained and wet soils but showed minor effects on ARDP due to the influence of conflicting phenomena of the release of bound water, increasing conductive losses and temperature dependence of water permittivity. Whilst the coarse grained soils showed good contrasts throughout the monitoring period, smaller contrasts were found on fine grained soils, with the optimum times for detection found during the dry period when VWC differences were at a maximum and during warm periods where BEC differences were accentuated, allowing for better survey planning.

Dedication

Dedication

This work is dedicated proudly to my friends and family without whom, it would not have been possible

Acknowledgements

The author greatly acknowledges the contribution of several people, without which, this work would not have been possible. Special thanks must go to the author's supervisors, Dr. Nicole Metje and Dr. David Chapman for their continued support and guidance and the UOB Civil Engineering Laboratory staff (Mike Vanderstam, Seb Ballard, Mark Carter, Jim Guest and Dave Cope) for their assistance in making the sensor development and laboratory experiments possible. The author would also like to thank the rest of the DART project consortium, especially the other DART project PhD students (Laura Pring, Dave Stott, Robert Fry), Armin Schmidt, Chris Gaffney, Derek Magee, Bob Evans and Keith Wilkinson for their technical support, data, help and advice. The author is also grateful for the assistance of other University of Birmingham staff and students, most notably Dr. Giulio Curioni, Laura Thring, Dr. KY Foo and Helen Booth. The author gratefully acknowledges the financial support provided by the UK's Arts and Humanities Research Council (AHRC) and Engineering and Physical Sciences Research Council (EPSRC). Special thanks are also due to my family and friends for providing essential support during the research and writing process.

Table of Contents

Table of Contents

| | |
|---|-------|
| Abstract..... | i |
| Dedication..... | iii |
| Acknowledgements..... | iv |
| List of Figures..... | ix |
| List of Tables..... | xvii |
| Abbreviations..... | xviii |
| Notations and Units..... | xx |
| Chapter 1: Introduction..... | 1 |
| 1.1. Background..... | 1 |
| 1.2. Aims and Objectives..... | 6 |
| 1.3. Structure of the Thesis..... | 7 |
| Chapter 2: Literature Review..... | 8 |
| 2.1. Scope..... | 8 |
| 2.2. Heritage Detection Techniques..... | 9 |
| 2.2.1. Aerial Prospection Methods..... | 10 |
| 2.2.2. Geophysical Prospection Methods..... | 11 |
| 2.3. EM Properties..... | 12 |
| 2.3.1. Electrical Permittivity (ϵ)..... | 15 |
| 2.3.2. Magnetic Permeability (μ)..... | 20 |
| 2.3.3. Electrical Conductivity (σ)..... | 24 |
| 2.3.4. Propagation of EM radiation..... | 25 |
| 2.4. Soil Properties..... | 30 |
| 2.4.1. Soil Water..... | 32 |
| 2.4.2. Soil Water Movement..... | 38 |
| 2.5. Effects of Geotechnical Soil Properties and Temperature..... | 44 |
| 2.5.1. Soil Texture..... | 44 |
| 2.5.2. Soil Density..... | 47 |
| 2.5.3. Atterberg Limits and Linear Shrinkage..... | 48 |
| 2.5.4. Effects of Temperature..... | 50 |
| 2.6. Dielectric Mixing Models..... | 53 |
| 2.6.1. Phenomenological Models..... | 59 |

Acknowledgements

| | | |
|---|--|-----|
| 2.6.2. | Volumetric Mixing Models | 60 |
| 2.6.3. | Empirical Mixing Models | 61 |
| 2.6.4. | Semi Empirical Mixing Models | 62 |
| 2.7. | Techniques for Soil Property Determination | 63 |
| 2.7.1. | TDR..... | 66 |
| 2.7.2. | TDR operating principles | 69 |
| 2.7.3. | TDR Limitations | 77 |
| 2.8. | Geophysical Methods and Seasonality | 82 |
| 2.8.1. | Seasonality Tests over Archaeological features | 83 |
| 2.9. | Identified Knowledge Gaps | 86 |
| Chapter 3: Field Monitoring Methodology | | 89 |
| 3.1. | Introduction | 89 |
| 3.2. | Site Locations..... | 89 |
| 3.2.1. | Choice of Sites | 89 |
| 3.2.2. | Identification of Suitable Features | 95 |
| 3.3. | Design of the Monitoring stations | 99 |
| 3.4. | Construction of the stations | 107 |
| 3.5. | Calibration | 111 |
| 3.5.1. | Calibration of Monitoring Stations for Apparent Relative Dielectric Permittivity (ARDP)..... | 111 |
| 3.5.2. | Calibration of Monitoring Stations for Bulk Electrical Conductivity (BEC)..... | 114 |
| 3.6. | Probe Installation Procedure | 119 |
| 3.6.1. | Introduction | 119 |
| 3.6.2. | Excavations..... | 123 |
| 3.6.3. | Recovery of Soil Samples..... | 127 |
| 3.6.4. | Method of Installation..... | 129 |
| 3.6.5. | Post Installation Problems and Remedial action | 141 |
| 3.7. | Automation of Waveform Processing..... | 145 |
| Chapter 4: Laboratory Methodology for Soil Characterisation | | 149 |
| 4.1. | Introduction | 149 |
| 4.2. | Soil Characterisation | 151 |
| 4.2.1. | Geotechnical characterisation..... | 151 |
| 4.2.2. | Magnetic Susceptibility | 151 |

Table of Contents

| | | |
|--|--|-----|
| 4.2.3. | Chemical Characterisation of the Soil | 151 |
| 4.3. | Electromagnetic Characterisation and Water Content Relationships | 155 |
| 4.3.1. | Introduction | 155 |
| 4.3.2. | Sample Preparation..... | 157 |
| 4.3.3. | Measurements | 162 |
| 4.3.4. | Deconstruction of Samples | 163 |
| Chapter 5: Laboratory Soil Testing: Results and Discussion | | 165 |
| 5.1. | Introduction | 165 |
| 5.2. | Geotechnical Characterisation of the Soil..... | 165 |
| 5.3. | Geochemical Characterisation of the Soil..... | 169 |
| 5.4. | Magnetic Permeability..... | 173 |
| 5.5. | Empirical Relationships between VWC, ARDP, BEC, Density and Temperature | 177 |
| 5.5.1. | Errors..... | 177 |
| 5.5.2. | Relationship between ARDP, BEC and VWC-Inter-Site Variation | 178 |
| 5.5.3. | Relationship between ARDP, BEC and VWC-Intra-Site Variation | 186 |
| 5.5.4. | Relationship between ARDP, BEC and Density..... | 195 |
| 5.5.5. | Relationship between ARDP, BEC and Temperature..... | 199 |
| 5.5.6. | Comparison of different models | 204 |
| 5.6. | Principal Component Analysis | 211 |
| 5.7. | Summary of Laboratory Soil Testing Results..... | 218 |
| Chapter 6: Field Monitoring: Results and Discussion | | 220 |
| 6.1. | Introduction | 220 |
| 6.2. | Weather Variation over the Monitoring Period..... | 220 |
| 6.3. | Heterogeneity and Lateral Variations | 225 |
| 6.4. | Seasonal Variations in Geophysical Properties | 238 |
| 6.5. | Seasonal Variations in Temperature..... | 269 |
| 6.6. | Diurnal Variations in Temperature and Geophysical Properties | 281 |
| 6.6.1. | Diurnal variation of temperature | 281 |
| 6.6.2. | Effects of Diurnal Variation on geophysical properties | 287 |
| 6.6.3. | Summary of Diurnal Variations | 293 |
| 6.7. | Infiltration after Rainfall Events..... | 294 |
| 6.8. | Relationships between Geophysical and Geotechnical Properties of the Soil..... | 298 |

Acknowledgements

| | | |
|--|---|-----|
| 6.8.1. | Correlation between Geophysical Parameters and Temperature..... | 298 |
| 6.8.2. | Principal Component Analysis..... | 302 |
| 6.9. | Summary of Field Monitoring Results..... | 308 |
| Chapter 7: Conclusions and Recommendations for Future Work..... | | 311 |
| 7.1. | Conclusions..... | 311 |
| 7.2. | Recommendations for Further Work..... | 318 |
| References..... | | 321 |
| Appendices..... | | 345 |
| Appendix A: MATLAB Functions and Scripts..... | | 345 |
| Appendix B: Additional Laboratory graphs..... | | 350 |
| Appendix C: Additional Field Monitoring graphs..... | | 364 |
| Appendix D: Comparison between a Commercial IMKO TRIME T3 Probe and the TDR100..... | | 368 |
| Appendix E: Further Details on Mechanisms of Permittivity and Permeability..... | | 375 |
| Appendix F: Further Details on Seasonal Variability of Geophysical Properties for each Study Site..... | | 381 |
| F.1. | Diddington Clay Field..... | 381 |
| F.2. | Diddington Pasture Field..... | 386 |
| F.3. | Cirencester Quarryfield..... | 389 |
| Appendix G: Further Details on Seasonal Variability of Temperature for each Study Site..... | | 392 |
| G.1. | Diddington Clay Field..... | 392 |
| G.2. | Diddington Pasture Field..... | 393 |
| G.3. | Cirencester Quarryfield..... | 394 |

List of Figures

| | |
|---|----|
| Figure 1.1: Some of the primary proxy methods by which archaeological features are identified using remote sensing techniques. Re-used under a creative commons share-a-like license from DART project 4 | |
| Figure 1.2: Schematic of physical, geophysical and geometric characteristics of a “typical” archaeological ditch feature. | 5 |
| Figure 2.1: An EM wave. (Conyers, 2004)..... | 13 |
| Figure 2.2: The EM spectrum and some archaeological uses. Reused under creative commons license from the DART website | 14 |
| Figure 2.3: Conceptual diagram showing the interaction of charges with an EM wave. (Cassidy 2009) ... | 16 |
| Figure 2.4: The complex permittivity as a function of frequency and the dominant polarisation and relaxation processes. (Chen and Or, 2006) | 19 |
| Figure 2.5: (a) permittivity and (b) conductivity for various types of soils with different density showing a wide variability at different volumetric water contents (Curtis et al., 2001). | 33 |
| Figure 2.6: A water molecule showing the positions of electrons in relation to the hydrogen and oxygen nuclei which give fractional charges..... | 34 |
| Figure 2.7 The relationship between water content and capillary potential for different soil textures a) Bennet Sandy Soil b) Greenville Loam c) Preston Clay (Richards, 1931). | 40 |
| Figure 2.8: SWCC for adsorption and desorption (Fredlund et al., 1994). The saturated water content for wetting cycles (θ_s') and drying cycles (θ_s) is also shown. | 41 |
| Figure 2.9: The redistribution of water over time after infiltration at t_0 for a) fine grained soils and small depths and b) coarse grained soils and high depths. (Youngs and Poulouvassilis, 1976) | 43 |
| Figure 2.10: Soil texture triangle showing the USDA (colours) and UK-ADAS (lines) soil classifications. Reused under Creative Commons from Wikipedia Commons. | 45 |
| Figure 2.11: Variable dispersion between 0 and 2GHz for different clay types at saturation (Thomas et al., 2008a)..... | 49 |
| Figure 2.12: Relationship between apparent permittivity and saturated VWC as a function of frequency for soils with different SSA (Thomas et al., 2010a) | 49 |
| Figure 2.13: a) relationship between linear shrinkage and the magnitude of dispersion between 100Mhz and 1GHz and b) relationship between linear shrinkage and dispersion when corrected by dividing both by dry density (Thomas et al., 2010a) | 50 |
| Figure 2.14: The modelled changes in relative permittivity of water between 0°C and 30°C using the Weast (1986) model | 51 |
| Figure 2.15: A schematic diagram of the TDR main components. The window on the right illustrates two waveforms, one in air and one in water (Robinson et al., 2003a). | 67 |
| Figure 2.16: Some of the different wave interpretation methods on TDR waveforms taken in water. a) Single tangent b) Duel Tangent c) Derivative method (derivative shown as dotted line)..... | 72 |

List of Figures

| | |
|--|-----|
| Figure 2.17: Comparison between TDR measured and actual BEC using a) the actual probe constant and b) a fitted probe constant using solutions..... | 76 |
| Figure 2.18: The attenuation of waveforms in distilled water and NaCl solutions. Notice the lack of a return reflection in the 0.1mol kg ⁻¹ NaCl solution. (Noborio, 2001) | 81 |
| Figure 3.1: The locations of the DART projects sites where the monitoring stations were installed | 92 |
| Figure 3.2: A geological map showing the main geology and superficial deposits at the two Harnhill sites | 93 |
| Figure 3.3: A geological map showing the main geology and superficial deposits at the two Diddington sites | 94 |
| Figure 3.4: The magnetometer survey and location of boreholes and trenches at CQF (Wilkinson, 2011). | 96 |
| Figure 3.5: The magnetometer survey and location of boreholes and trenches at CCC (Wilkinson, 2011). | 97 |
| Figure 3.6: The magnetometer survey and location of boreholes and trenches at DPF (Wilkinson, 2011). | 98 |
| Figure 3.7: The magnetometer survey and location of boreholes and trenches at DCF. | 99 |
| Figure 3.8: A schematic of the different TDR station components and their connections | 102 |
| Figure 3.9: A TDR probe used by the monitoring stations | 107 |
| Figure 3.10: The main components of the TDR during construction | 108 |
| Figure 3.11: A TDR waveform taken in deionised water | 110 |
| Figure 3.12: The $1/R_L$ values for the low conductivity solutions plotted against the conductivity for one of the probes and the linear regression ($1/K_p$) | 118 |
| Figure 3.13: Comparison of two rainfall events from weather stations c.400m apart | 121 |
| Figure 3.14: Schematic showing the layout and scale of the excavations, the locations and measurement volumes of the probes, TDR boxes and soil samples and the areas of disturbed and undisturbed soil .. | 122 |
| Figure 3.15: The feature at Cirencester Quarryfield | 124 |
| Figure 3.16: The ditch at Cirencester Cherry Copse. Photo used under Creative Commons License from Robert Fry..... | 125 |
| Figure 3.17: The ditch at Diddington Pasture field. Photo by Keith Wilkinson. | 126 |
| Figure 3.18: Different soil sampling methods. a) Monolith Tins b) Water content samples..... | 128 |
| Figure 3.19: The construction of the solar panel mounting frame and positioning of the monitoring stations | 129 |
| Figure 3.20: The insertion of the TDR probes using plastic waveguides to keep rods parallel | 130 |
| Figure 3.21: The inserted probes at DCFA in the ditch section | 132 |
| Figure 3.22: The inserted probes at DCFN in the SSM | 132 |
| Figure 3.23: The inserted probes at CCC in the ditch section..... | 133 |
| Figure 3.24: The inserted probes at CCC in the SSM. Note the rock below c. 0.2m depth | 133 |
| Figure 3.25: The location of the probes at Diddington Clay Field | 137 |

List of Figures

| | |
|--|-----|
| Figure 3.26: The location of the probes at Cirencester Quarryfield | 138 |
| Figure 3.27: The location of the probes at Diddington Pasture Field | 139 |
| Figure 3.28: The location of the probes at Cirencester Cherry Copse | 140 |
| Figure 3.29: The damaged weather station cable | 142 |
| Figure 3.30: The re-excavated probes at CCC | 143 |
| Figure 3.31: Wire mesh used to protect the probe locations from burrowing wildlife | 143 |
| Figure 3.32: A flooded monitoring station | 145 |
| Figure 3.33: The interpretation of ARDP waveforms showing a) the calculated first derivative found using the conv function in MATLAB® and a low pass filter and b) the subsequent fitted tangents. The lines formed from the localised minima are also shown. | 146 |
| Figure 4.1: The location of the chemical boreholes from the archaeological soils and SSM in relation to the trench, TDR box and geophysics grid on CCC | 153 |
| Figure 4.2: The location of the chemical boreholes from the archaeological soils and SSM in relation to the trench, TDR box and geophysics grid on CQF | 153 |
| Figure 4.3: The location of the chemical boreholes from the archaeological soils and SSM in relation to the trench, TDR box and geophysics grid on DPF | 154 |
| Figure 4.4: The location of the chemical boreholes from the archaeological soils and SSM in relation to the trench, TDR box, IMKO sensors (see Appendix D) and geophysics grid on DCF | 154 |
| Figure 4.5: Brown glass jars used for chemical sampling to avoid photochemical reactions | 155 |
| Figure 5.1: Millequivalents per 100g of Sodium, Potassium, Magnesium and Calcium for the tested soils | 171 |
| Figure 5.2: Comparison of BEC-VWC relationships between clay (DCF) and non-clay (DPF) soils | 181 |
| Figure 5.3: Comparison of ARDP-VWC relationships on fine grained (DCF) and coarse grained (DPF) soils. Topp et al. (1980) model also plotted for comparison | 182 |
| Figure 5.4: Comparison of waveform rise times between DCF SSM and DPF Ditchfill2 at 20% VWC. The effective measurement frequencies have been calculated using the method described by Robinson et al. (2003a) and are displayed in brackets on the legend | 184 |
| Figure 5.5: ϵ' and ϵ'' at 20% VWC for two samples from a) DCF SSM and b) DPF Ditchfill2. Errors are estimated as being less than 10% of the measured values. | 185 |
| Figure 5.6: The BEC-VWC relationship between the tested soils from DCF | 189 |
| Figure 5.7: The BEC-VWC relationship between the tested soils from DPF | 190 |
| Figure 5.8: The ARDP-VWC relationships between the different tested soils from DCF. Topp et al. (1980) model also plotted for comparison | 193 |
| Figure 5.9: The ARDP-VWC relationships between the different tested soils from DPF. Topp et al. (1980) model also plotted for comparison | 194 |
| Figure 5.10: The effects of density on ARDP-VWC relationships on the DCF SSM soil | 197 |
| Figure 5.11: The effects of density on ARDP-VWC relationships on the DPF Ditchfill3 soil | 197 |
| Figure 5.12: The effects of changing density on BEC determination on the DCF SSM soil | 198 |

List of Figures

| | |
|--|-----|
| Figure 5.13: The effects of changing density on BEC determination on the DPF Ditchfill3 soil | 198 |
| Figure 5.14: Temperature effects on BEC determination on different soils | 202 |
| Figure 5.15: Temperature effects on ARDP determination on different soils | 203 |
| Figure 5.16: An example of the different models fitted to data from one of the DCF soils (DCF Ditchfill1) | 204 |
| Figure 5.17: The Wensink (1993) model on the DCF soils | 207 |
| Figure 5.18: The performance of the Wang and Schmugge (1980) model on a) DCF and b) DPF | 208 |
| Figure 5.19: The Topp et al. (1980), Ledieu et al. (1986) and Curtis (2001) models in comparison to data from the tested soils..... | 209 |
| Figure 5.20: Scree Plot from the PCA analysis on geophysical, geotechnical and geochemical properties of the soil collected in the laboratory | 212 |
| Figure 5.21: Biplot of PCA analysis on geophysical, geotechnical and geochemical properties of the soil determined in the laboratory showing principal component 1 and 2 | 216 |
| Figure 5.22: Biplot of PCA analysis on geophysical, geotechnical and geochemical properties of the soil determined in the laboratory showing principal component 3 and 4 | 217 |
| Figure 6.1: The rainfall (a), evapotranspiration (b) and water balance (c) for the study period on all four monitoring locations. | 223 |
| Figure 6.2: The minimum, maximum and average air temperatures over the study period for the four monitoring locations | 224 |
| Figure 6.3: Comparison of ARDP values from DCFN (SSM) probes at different depths a) 0.1m b) 0.4m c) 0.7m and d) 1.0m | 227 |
| Figure 6.4: Comparison of BEC values from DCFN (SSM) probes at different depths a) 0.1m b) 0.4m c) 0.7m and d) 1.0m | 228 |
| Figure 6.5: Comparison of ARDP values from DCFA (Archaeology) probes at different depths a) 0.1m b) 0.3m c) 0.8m and d) 1.0m | 229 |
| Figure 6.6: Comparison of BEC values from DCFA (Archaeology) probes at different depths a) 0.1m b) 0.3m c) 0.8m and d) 1.0m | 230 |
| Figure 6.7: Comparison of geophysical values from DPF probes from 0.6m depth in the archaeological profile a) ARDP and b) BEC | 232 |
| Figure 6.8: Comparison of ARDP values from CQFA (Archaeology) probes at different depths a) 0.15m b) 0.3m c) 0.5m and d) 1.0m | 234 |
| Figure 6.9: Comparison of BEC values from CQFA (Archaeology) probes at different depths a) 0.15m b) 0.3m c) 0.5m and d) 1.0m | 235 |
| Figure 6.10: Comparison of ARDP values from CQFN (SSM) probes at different depths a) 0.15m b) 0.3m c) 0.5m and d) 1.0m..... | 236 |
| Figure 6.11: Comparison of BEC values from CQFN (SSM) probes at different depths a) 0.15m b) 0.3m c) 0.5m and d) 1.0m | 237 |

List of Figures

| | |
|--|-----|
| Figure 6.12: The ARDP variation on DCF over the study period at different depths a) 0.1m b) 0.2m c) 0.3m d) 0.4m e) 0.5m f) 0.6m g) 0.7m h) 0.8m i) 0.9m | 247 |
| Figure 6.13: The BEC variation on DCF over the study period at different depths a) 0.1m b) 0.2m c) 0.3m d) 0.4m e) 0.5m f) 0.6m g) 0.7m h) 0.8m i) 0.9m..... | 250 |
| Figure 6.14: The ARDP variation on DPF over the study period at different depths a) 0.1m b) 0.2m c) 0.4m d) 0.5 e) 0.6m f) 0.7m g) 0.8m h) 1.0m i) 1.2m | 253 |
| Figure 6.15: The BEC variation on DPF over the study period at different depths a) 0.1m b) 0.2m c) 0.4m d) 0.5 e) 0.6m f) 0.7m g) 0.8m h) 1.0m i) 1.2m..... | 256 |
| Figure 6.16: The ARDP variation on CQF over the study period at different depths between a) 0.1m b) 0.15m c) 0.3m d) 0.5m e) 0.6m f) 0.7m g) 0.8m h) 1m..... | 259 |
| Figure 6.17: The BEC variation on CQF over the study period at different depths a) 0.1m b) 0.15m c) 0.3m d) 0.5m e) 0.6m f) 0.7m g) 0.8m h) 1m | 262 |
| Figure 6.18: Average ARDP contrast as a % of the average SSM value for each month of monitoring over the three studied sites. The maximum (solid line) and minimum (dotted line) contrast values are also shown for each month | 267 |
| Figure 6.19: Average BEC contrast as a % of the average SSM value for each month of monitoring over the three studied sites. The maximum (solid line) and minimum (dotted line) contrast values are also shown for each month | 268 |
| Figure 6.20: The seasonal variation in temperature on DCF at different depths a) 0.1m b) 0.2m c) 0.3m d) 0.4m e) 0.5m f) 0.6m g) 0.7m h) 0.9m i) 1m..... | 274 |
| Figure 6.21: The seasonal variation in temperature on DPF at different depths a) 0.1m b) 0.5m c) 0.6m d) 0.8m e) 1m f) 1.2m | 276 |
| Figure 6.22: The seasonal variation in temperature on CQF at different depths a) 0.1m b) 0.15m c) 0.3m d) 0.5m e) 0.6m f) 0.7m g) 0.8m h) 1m | 279 |
| Figure 6.23: Average daily temperature contrast between archaeological soils and SSM value for the three studied sites from depths of a) 0.1m b) 0.5m and c) 1m. The errors of the temperature probes are shown as dotted lines..... | 280 |
| Figure 6.24: Diurnal temperature variation at different depths in the near surface during a period in December 2011 for a) DCF and b) DPF | 283 |
| Figure 6.25: Diurnal temperature variation at different depths in the near surface during a period in July 2012 for a) DCF and b) DPF | 284 |
| Figure 6.26: Cross correlation between air temperature and soil temperature at depths of a) 0.1m b) 0.2m c) 0.3m d) 0.4m e) 0.5m and f) 0.6m for DCF between 22 nd and 26 th July 2012. Horizontal dashed lines represent the limits above which the absolute cross correlations are significant with a confidence level of 90%. | 286 |
| Figure 6.27: Cross correlation between air temperature and soil temperature depths of a) 0.1m b) 0.2m c) 0.4m d) 0.5m e) 0.6m and f) 0.7m for DPF between 22 nd and 26 th July 2012. Horizontal dashed lines | |

List of Figures

| | |
|---|-----|
| represent the limits above which the absolute cross correlations are significant with a confidence level of 90%..... | 287 |
| Figure 6.28: Daily variation of the temperature, ARDP and BEC at depths of a) 0.1m b) 0.2m c) 0.3m and d) 0.6m for DCF over a dry period in December 2011..... | 289 |
| Figure 6.29: Daily variation of the temperature, ARDP and BEC at depths of a) 0.1m b) 0.2m c) 0.3m and d) 0.6m for DCF over a wet period in July 2011 | 290 |
| Figure 6.30: Daily variation of the temperature, ARDP and BEC at depths of a) 0.1m b) 0.2m and c) 0.5m for DPF over a dry period in December 2011 | 291 |
| Figure 6.31: Daily variation of the temperature, ARDP and BEC at depths of a) 0.1m b) 0.2m and c) 0.5m for DPF over a wet period in July 2011..... | 292 |
| Figure 6.32: Rainfall event from March 2012 on the Diddington sites (taken from DCF weather station but similar data found for DPF). | 295 |
| Figure 6.33: Cross correlation between rainfall and ARDP for DCF at depths of a) 0.1m b) 0.2m c) 0.3m d) 0.5m and e) 0.7m. Horizontal dashed lines represent the limits above which the absolute cross correlations are significant with a confidence level of 90%. | 296 |
| Figure 6.34: Cross correlation between rainfall and ARDP for DPF at depths of a) 0.1m b) 0.2m c) 0.5m d) 0.6m and e) 0.8m. Horizontal dashed lines represent the limits above which the absolute cross correlations are significant with a confidence level of 90% | 297 |
| Figure 6.35: Relationship between ARDP, BEC and Temperature for DCF during 2012 for a) the Archaeological soil profile and b) the SSM profile | 299 |
| Figure 6.36: Relationship between ARDP, BEC and Temperature for DPF during 2012 for a) the Archaeological soil profile and b) the SSM profile | 300 |
| Figure 6.37: Relationship between ARDP, BEC and Temperature for CQF during 2012 for a) the Archaeological soil profile and b) the SSM profile | 301 |
| Figure 6.38: Spearman’s rank correlation between different pairs of variables at different depths for a) DCF b) DPF and c) CQF..... | 302 |
| Figure 6.39: Scree plot from PCA using geotechnical and averaged ARDP, BEC and temperature data from DCF, DPF and CQF | 303 |
| Figure 6.40: Biplot of PCA analysis on average geophysical, geotechnical and geochemical properties of the soil from the field monitoring data showing principal component 1 and 2..... | 306 |
| Figure 6.41: Biplot of PCA analysis on average geophysical, geotechnical and geochemical properties of the soil from the field monitoring data showing principal component 3 and 4..... | 307 |
| Figure B.1: Temperature effects on BEC determination on different soils | 350 |
| Figure B.2: Temperature effects on ARDP determination on different soils..... | 350 |
| Figure B.3: Different models fitted to DCF Topsoil..... | 351 |
| Figure B.4: Different models fitted to DCF Subsoil..... | 351 |
| Figure B.5: Different models fitted to DCF Ditchfill1 | 352 |
| Figure B.6: Different models fitted DCF SSM..... | 352 |

List of Figures

| | |
|--|-----|
| Figure B.7: Different models fitted to DPF Topsoil | 353 |
| Figure B.8: Different models fitted to DPF Subsoil | 353 |
| Figure B.9: Different models fitted to DPF Ditchfill1 | 354 |
| Figure B.10: Different models fitted to DPF Ditchfill2 | 354 |
| Figure B.11: Different models fitted to DPF Ditchfill3 | 355 |
| Figure B.12: Different models fitted to DPF SSM | 355 |
| Figure B.13: Scree plot for PCA carried out on DCF only using the same variables as in Section 5.6. | 356 |
| Figure B.14: Scree plot for PCA carried out on DPF only using the same variables as in Section 5.6. | 356 |
| Figure B.15: Principal components 1 and 2 for PCA analysis carried out on the DCF soils only using the same variables as in Section 5.6. | 357 |
| Figure B.16: Principal components 3 and 4 for PCA analysis carried out on the DCF soils only using the same variables as in Section 5.6. | 358 |
| Figure B.17: Principal components 1 and 2 for PCA analysis carried out on the DPF soils only using the same variables as in Section 5.6. | 359 |
| Figure B.18: Principal components 1 and 2 for PCA analysis carried out on the DPF soils only using the same variables as in Section 5.6. | 360 |
| Figure B.19: Principal components 1 and 2 for PCA analysis carried out on the laboratory tested soils using all available variables. Note that soils have been omitted where data was unavailable for one or more variables by the PCA process | 361 |
| Figure B.20: Principal components 3 and 4 for PCA analysis carried out on the laboratory tested soils using all available variables. Note that soils have been omitted where data was unavailable for one or more variables by the PCA process | 362 |
| Figure B.21: Scree plot for PCA carried out on the laboratory tested soils using all available variables . | 363 |
| Figure C.1: Rainfall data from the Diddington sites compared to nearby weather data from weather underground for October 2011 | 364 |
| Figure C.2: Rainfall data from the Cirencester sites compared to nearby weather data from weather underground for October 2011 | 365 |
| Figure C.3: Air temperature data from the Diddington sites compared to nearby weather data from weather underground for October 2011..... | 365 |
| Figure C.4: Air temperature data from the Cirencester sites compared to nearby weather data from weather underground for October 2011..... | 365 |
| Figure C.5: Example waveforms from CQFA showing the multiplexer failure during monitoring in the left hand array (a) compared to the right hand array (b). Data taken from 25/03/2012 at 15:00. | 366 |
| Figure C.6: Example ARDP data a) before filtering and b) after filtering using removal of extreme values and median filter (DCFN probe 4) | 367 |
| Figure C.7: Example BEC data a) before filtering and b) after filtering using removal of extreme values and median filter (DCFN probe 4) | 367 |

List of Figures

| | |
|---|-----|
| Figure D.1: Schematic of the IMKO soil moisture probe arrays provided by Van Walt Ltd. Re-used under a creative commons share-a-like license from DART Project..... | 368 |
| Figure D.2: ARDP derived from both the IMKO and TDR100 probes for a period in June 2012 at depth ranges a) 10-21cm b) 50-51cm and c) 70-81cm..... | 371 |
| Figure D.3: ARDP derived from both the IMKO and TDR100 probes for a period in August and September 2012 at depth ranges a) 10-21cm b) 50-51cm and c) 70-81cm..... | 372 |
| Figure D.4: BEC derived from both the IMKO and TDR100 probes for a period in June 2012 at depth ranges a) 10-21cm b) 50-51cm and c) 70-81cm. Note the logarithmic scale used to display BEC..... | 373 |
| Figure D.5: BEC derived from both the IMKO and TDR100 probes for a period in June 2012 at depth ranges a) 10-21cm b) 50-51cm and c) 70-81cm. Note the logarithmic scale used to display BEC..... | 373 |
| Figure E.1: Electronic polarisation in the presence of a) no applied field and b) a local electrical field (E_{loc}). | 375 |
| Figure E.2: Ionic polarisation in non polar molecules due to the presence of a) no applied field and b) a local electric field (E_{loc}). After Elliott 1993 | 376 |
| Figure E.3: Orientational polarisation of polar molecules. (Robinson et al., 2003a)..... | 377 |
| Figure E.4: Maxwell Wagner polarisation in porous media (Cassidy, 2009). | 378 |
| Figure E.5: Different types of ferromagnetism (<i>sensu lato</i>). a) Ferromagnetism (<i>sensu stricto</i>) b) Anti-Ferromagnetism c) Imperfect Anti Ferromagnetism and d) Ferrimagnetism | 380 |
| Figure F.1: Photographs from the DCF excavation showing the difference in appearance of the subsoil layer in both (a) the SSM and (b) above the Ditchfill soils. | 386 |

List of Tables

| | |
|---|-----|
| Table 2.1: Common soil iron oxides in archaeological sediments (Aspinall et al., 2008). | 23 |
| Table 2.2: A selection of commonly found materials and their typical geophysical properties. (Adapted from Cassidy, 2009) | 31 |
| Table 2.3: The dielectric properties of different soil phases. | 32 |
| Table 2.4: A summary of some of the different dielectric models used for soil. Abbreviations are described below. | 54 |
| Table 2.5: The strengths and weaknesses of the different model types..... | 59 |
| Table 2.6: A summary of surrogate instruments for water content determination (IAEA, 2008)..... | 64 |
| Table 2.7: A summary of the optimum contrasts for locating ditches from earth resistance experiments. After Clark 1996..... | 85 |
| Table 3.1: Comparison of different features and technical specifications of different TDR devices. (Robinson et al., 2003a). Abbreviations are listed at the bottom. | 100 |
| Table 3.2: The power consumption of the monitoring station components | 103 |
| Table 3.3: The average monthly insolation for Cirencester and Diddington. All figures in KWh/m ² | 104 |
| Table 3.4: The errors in ARDP calibrations on each station | 114 |
| Table 3.5: Comparison of different methods for BEC determination | 115 |
| Table 3.6: KCl solution concentrations and approximate conductivity values..... | 116 |
| Table 3.7: The errors and standard deviations of BEC values derived from the TDR calibrations | 119 |
| Table 3.8: A summary of the samples collected from each site | 128 |
| Table 3.9: The depths and contexts of probes for the Cirencester sites..... | 135 |
| Table 3.10: The depths and contexts of probes for the Diddington sites | 136 |
| Table 4.1: A summary of the soil characterization tests carried out on each soil..... | 150 |
| Table 4.2: Conversion factors between gravimetric and volumetric water contents for the different soils tested based on their dry density values | 158 |
| Table 5.1: Summary of geotechnical testing results. × indicates measurements not obtained due to unsuitable soil types and samples. Data from Pring, Forthcoming. | 168 |
| Table 5.2: A summary of the Geochemical test results. × indicates measurements not obtained due to budget limitations | 170 |
| Table 5.3: Magnetic Susceptibility and Relative Magnetic Permeability of the soil. Where χ_{lf} and χ_{hf} are the measured volume specific magnetic susceptibility values at low and high frequencies respectively, χ_{fd} is the coefficient of frequency dependence and $\mu_r(lf)$ and $\mu_r(hf)$ are the calculated relative magnetic permeability values at low and high frequencies respectively | 176 |
| Table 5.4: Comparison of different R ² and RMSE for different models on the tested soils | 205 |
| Table D.1: The IMKO probe number and measurement depths | 369 |

Abbreviations

| | |
|------|--|
| AC | Alternating Current |
| ARDP | Apparent Relative Dielectric Permittivity |
| BEC | Bulk Electrical Conductivity |
| BGS | British Geological Survey |
| BSI | British Standards Institution |
| CCC | Cirencester Cherry Copse |
| CEC | Cation Exchange Capacity |
| CF | Compact Flash |
| CQF | Cirencester Quarryfield |
| CQFA | Cirencester Quarryfield Archaeology |
| CQFN | Cirencester Quarryfield SSM |
| DART | Detection of Archaeological Residues Using Remote Sensing Techniques |
| DC | Direct Current |
| DCF | Diddington Clay Field |
| DCFA | Diddington Clay Field Archaeology |
| DCFN | Diddington Clay Field SSM |
| dGPS | Differential Global Positioning system |
| DPF | Diddington Pasture Field |
| EM | Electromagnetic |
| ET | Evapotranspiration |
| FFT | Fast Fourier Transform |
| FTP | File Transfer Protocol |
| GPR | Ground Penetrating Radar |
| GPRS | General Packet Radio Service |
| GSM | Global System for Mobile Communications |

Abbreviations

| | |
|-------|--|
| GWC | Gravimetric Water Content |
| IAEA | International Atomic Energy Agency |
| IP | Internet Protocol |
| LIDAR | Light Detection and Ranging |
| MTU | Mapping the Underworld |
| NERC | Natural Environment Research Council |
| NGPD | National Geotechnical Properties Database |
| NHSS | National Heritage Science Strategy |
| OM | Organic Matter |
| PSD | Particle Size Distribution |
| PTFE | Polytetrafluorethylene |
| RAU | Royal Agricultural University |
| RF | Radio Frequency |
| SDM | Synchronised Device Measurement |
| SI | Système International d'unités |
| SIM | Subscriber Identity Module |
| SMS | Short Message Service |
| SPAW | Soil-Plant-Air-Water model |
| SSA | Specific Surface Area |
| SSM | Surrounding Soil Matrix |
| SWCC | Soil Water Characteristic Curve |
| TDR | Time Domain Reflectometry |
| TEM | Transverse Electromagnetic mode of propagation |
| VNA | Vector Network Analyser |
| VWC | Volumetric Water Content |
| WP | Wilting point |

Notations and Units

| Symbol | Units | Definition |
|-------------------|---|--|
| α | nepers per metre($\text{nepers}\cdot\text{m}^{-1}$) | Attenuation constant |
| β | Radians per metre($\text{rad}\cdot\text{m}^{-1}$) | Phase constant |
| γ | - | Propagation constant ($\alpha+j\beta$) |
| η | - | Porosity of the soil |
| ϵ | farads per metre ($\text{F}\cdot\text{m}^{-1}$) | Dielectric Permittivity |
| ϵ^* | farads per metre ($\text{F}\cdot\text{m}^{-1}$) | Complex Permittivity |
| ϵ_r | - | Relative Permittivity (ϵ/ϵ_0) |
| ϵ' | farads per metre ($\text{F}\cdot\text{m}^{-1}$) | Real part of the permittivity, representing energy storage mechanisms |
| ϵ'' | farads per metre ($\text{F}\cdot\text{m}^{-1}$) | Imaginary permittivity representing energy loss comprising of polarisation and conductivity losses |
| ϵ_p'' | - | Polarisation losses |
| ϵ_∞ | farads per metre ($\text{F}\cdot\text{m}^{-1}$) | High frequency permittivity (above which no polarisation can take place) |
| ϵ_{if} | farads per metre ($\text{F}\cdot\text{m}^{-1}$) | Static permittivity (at a frequency significantly below relaxation) |
| ϵ_0 | farads per metre ($\text{F}\cdot\text{m}^{-1}$) | Permittivity of Free Space (8.8541878×10^{-12}) |
| ϵ_a | - | Apparent Relative Dielectric Permittivity |
| ϵ_w | - | Relative Permittivity of Water (c. 80 at 20°C) |
| ϵ_{fw} | - | Relative Permittivity of free water |
| ϵ_{bw} | - | Relative Permittivity of bound water |
| ϵ_g | - | Relative Permittivity of soil gaseous phase (air) (c. 1) |
| ϵ_s | - | Relative Permittivity of the soil mineral fraction (c. 3-5) |
| K | - | Volume Specific Magnetic Susceptibility |

Notations and Units

| Symbol | Units | Definition |
|------------------------|---|---|
| ρ_b | grams per cubic centimetre ($\text{g}\cdot\text{cm}^{-3}$) | Bulk Density |
| ρ_d | grams per cubic centimetre ($\text{g}\cdot\text{cm}^{-3}$) | Dry Bulk Density |
| ρ_s | grams per cubic centimetre ($\text{g}\cdot\text{cm}^{-3}$) | Particle Density |
| ρ_w | grams per cubic centimetre ($\text{g}\cdot\text{cm}^{-3}$) | Density of Water |
| θ_v | % | Volumetric Water Content |
| θ_g | % | Gravimetric Water Content |
| σ | Siemens per metre ($\text{S}\cdot\text{m}^{-1}$) | Electrical Conductivity |
| σ^* | Siemens per metre ($\text{S}\cdot\text{m}^{-1}$) | Complex Electrical Conductivity |
| σ' | Siemens per metre ($\text{S}\cdot\text{m}^{-1}$) | Real Electrical Conductivity |
| σ'' | Siemens per metre ($\text{S}\cdot\text{m}^{-1}$) | Imaginary Electrical Conductivity |
| τ | seconds | Relaxation time |
| u | (in EM fields either Volts per metre ($\text{V}\cdot\text{m}^{-1}$) or Tesla (T) depending on electrical or magnetic component) | Amplitude |
| Γ | - | Reflection Coefficient |
| Γ_∞ | - | Reflection Coefficient after multiple reflections |
| Γ_{open} | - | Reflection Coefficient from an open circuit |
| Γ_{corr} | - | Corrected reflection coefficient using open circuit measurement after Lin et al. (2008) |
| μ | Henries per metre ($\text{H}\cdot\text{m}^{-1}$) | Magnetic Permeability |
| μ^* | Henries per metre ($\text{H}\cdot\text{m}^{-1}$) | Complex Magnetic Permeability |
| μ' | Henries per metre ($\text{H}\cdot\text{m}^{-1}$) | Real Magnetic Permeability |
| μ'' | Henries per metre ($\text{H}\cdot\text{m}^{-1}$) | Imaginary Magnetic Permeability |
| μ_0 | Henries per metre ($\text{H}\cdot\text{m}^{-1}$) | Magnetic Permeability of free space ($4\pi \times 10^{-7}$) |
| μ_r | - | Relative Magnetic Permeability (μ/μ_0) |

Notations and Units

| Symbol | Units | Definition |
|-------------------|--|--|
| μ_{∞} | Henries per metre ($\text{H}\cdot\text{m}^{-1}$) | High frequency permeability (above which no further magnetisation can take place) |
| μ_{lf} | Henries per metre ($\text{H}\cdot\text{m}^{-1}$) | Static permeability (at a frequency significantly below relaxation) |
| χ_e | - | Electrical Susceptibility |
| χ_m | cubic metres per kilogram (m^3kg^{-1}) | Mass Specific Magnetic Susceptibility |
| ψ_g | Kilopascal (KPa) | Gravitational Soil Potential |
| ψ_m | Kilopascal (KPa) | Matric Soil Potential |
| ψ_o | Kilopascal (KPa) | Osmotic Soil Potential |
| ψ_t | Kilopascal (KPa) | Total Soil Potential |
| ω | radians per second ($\text{Rad}\cdot\text{s}^{-1}$) | Radian frequency equal to $2\pi f$ |
| λ | metres (m) | Wavelength of electromagnetic radiation |
| A | square metres (m^2) | Cross sectional area |
| a | - | Empirical variable |
| B | Tesla (T) | Magnetic flux density |
| c | metres per second ($\text{m}\cdot\text{s}^{-1}$) | Speed of Light in a vacuum (299792458) |
| C_L | metres (m) | Cable Length |
| D | Columbs per square metre (C/m^2) | Displacement Vector |
| E_{loc} | Volts per metre ($\text{V}\cdot\text{m}^{-1}$) | Local electrical field strength |
| f | Hertz (Hz) | frequency of electromagnetic radiation |
| f_{rel} | Hertz (Hz) | Relaxation frequency |
| f_{eff} | Hertz (Hz) | Effective measurement frequency |
| F | - | Conversion factor for changing gravimetric to volumetric water content for soils of a particular dry density |

Notations and Units

| Symbol | Units | Definition |
|-------------|--|--|
| H | Ampere per metre ($A \cdot m^{-1}$) | Magnetic field strength |
| Ins | Watt-hours per square metre (Wh/m^2) | Solar insolation |
| j | - | Imaginary unit equal to square root of -1 |
| K_H | centimetres per day ($cm \cdot day^{-1}$) | Hydraulic conductivity |
| K_p | - | Probe constant |
| K_T | Watts per meter Celsius ($W \cdot m^{-1} \cdot ^\circ C^{-1}$) | Thermal Conductivity |
| L_A | metres (m) | Apparent Length |
| L_{cal} | metres (m) | Calibrated Electrical Length |
| L_{start} | metres (m) | Calibrated Electrical Length to probe head |
| L_{end} | metres (m) | Calibrated Electrical Length to end reflection |
| L_g | metres (m) | Apparent length of waveform in air |
| L_w | metres (m) | Apparent length of waveform in water |
| L_{win} | metres (m) | TDR window length |
| m | grams (g) | mass |
| m_s | grams (g) | mass of dry soil |
| m_w | grams (g) | mass of water |
| P | Watts | Power |
| \vec{P} | Columbs per square metre (C/m^2) | Polarisation Vector |
| P_e | Columbs per square metre (C/m^2) | Electrical Polarisation |
| P_i | Columbs per square metre (C/m^2) | Ionic Polarisation |
| P_o | Columbs per square metre (C/m^2) | Orientalional Polarisation |
| P_{mw} | Columbs per square metre (C/m^2) | Maxwell-Wagner Polarisation |
| P_{off} | metres (m) | Probe Offset |

Notations and Units

| Symbol | Units | Definition |
|--------------------|--|------------------------------|
| Q | cubic metres per second (m^3/s) | Water Flowrate |
| R_L | Ohms (Ω) | Load Resistance |
| R_c | Ohms (Ω) | Cable Resistance |
| R_0 | Ohms (Ω) | Series Resistance |
| T | Degrees Centigrade ($^{\circ}\text{C}$) | Temperature |
| t | seconds (s) | time |
| t_r | seconds (s) | TDR rise time |
| W_{panel} | Watts | Solar panel Wattage rating |
| W_L | % | Liquid Limit of the Soil |
| W_p | % | Plastic Limit of the Soil |
| V | metres cubed (m^3) | Volume |
| V_C | metres cubed (m^3) | Cylinder Volume |
| V_t | metres cubed (m^3) | Total Sample Volume |
| V_w | metres cubed (m^3) | Volume of water |
| v | metres per second ($\text{m}\cdot\text{s}^{-1}$) | velocity |
| v_p | metres per second ($\text{m}\cdot\text{s}^{-1}$) | propagation velocity |
| x | metres (m) | distance |
| Z | Ohms (Ω) | Impedance |
| Z_p | Ohms (Ω) | Probe Impedance |
| Z_s | Ohms (Ω) | Sample Impedance |
| Z_{out} | Ohms (Ω) | Output impedance of TDR (50) |

Chapter 1: Introduction

1.1. Background

This PhD project formed part of the 3 year DART project (Detection of Archaeological residues using Remote sensing Techniques 2010-2013), a multi-university and multi-disciplinary project with researchers and partners in computer vision, geophysics, remote sensing, knowledge engineering and geotechnical engineering. It aimed to improve the detection of archaeological features using the traditional remote sensing techniques using in heritage remote sensing including geophysical techniques, as well as aerial prospection techniques using airborne photography, hyperspectral and multispectral sensors.

The long term curation and protection of a fragile and finite archaeological resource is reliant on the ability to locate features in the ground to inform future development planning and land use management plans. Unfortunately, certain soil types are known to show a poor or limited response to traditional techniques, particularly clay soils (Conyers, 2004, Mills, 2003, Riley, 1983). The science behind the ideal conditions for employing these techniques is poorly understood, relying on largely anecdotal evidence (e.g. Detectation, 2012), with only a few success stories (Weaver, 2006). The National Heritage Science Strategy (NHSS) report that *“There are certain parts of the country where underlying geology can make interpretation of geophysical data more difficult. This has led to the abandonment of the use of geophysics for site prospection in these areas due to misconceptions”* (Williams, 2009a, b). As most of these methods rely on either the electromagnetic response of the soil (hyper and multispectral sensing, ground penetrating radar (GPR) survey) or the electrical or magnetic properties of the soil (magnetometry, electrical resistance survey), an improved knowledge of the changing soil conditions, and its interaction with the geophysical signal is desired, particularly on these unresponsive soil types. Whilst the use of both aerial remote sensing and geophysics have a long history of being used in order to prospect for new archaeological sites and features

Chapter 1: Introduction

(Bevan, 2000, Clark, 1996, Wilson, 1982), the science behind the geophysical contrasts which give rise to the interpretive anomalies is relatively poorly understood. This has led to a number of false interpretations and the sub optimal deployment of resources, through misplanned and mistimed surveys and flights, and a culture of relying on anecdotal evidence to explain the collected data.

Whilst soil is immensely complicated due to the high number of variable factors between soils, recent research from the Mapping the Underworld (MTU) project has demonstrated strong relationships between geotechnical and geophysical properties of the soil (Thomas et al., 2008) allowing the site conditions to be predicted. Whilst prior knowledge of the geophysical conditions of a site prior to a geophysical or aerial survey are unlikely to be recorded and stored, geotechnical databases are widely available from sources such as the British Geological Survey (BGS). Knowledge of these properties, along with a knowledge of the changes caused to them by archaeological features, and the recent climatic conditions of the site may be used to make an informed choice on sensor configuration and the period in which a survey is conducted, when no direct geophysical information is available.

Archaeological features are defined as any physical structure or element, such as a wall, ditch, post hole, pit, or floor, that is made or altered by humans but (unlike artefacts) are not portable and cannot be removed from a site (Darvill, 2008). The use of remote sensing and geophysical techniques allows the detection of archaeological features not by direct measurement of differences in underlying soil properties, but through the identification of proxy contrasts measureable at the surface. Some of the main proxies such as temperature, soil marks and crop marks and the effects of various archaeological features are summarised in Figure 1.1. Figure 1.1 indicates the impact of different archaeological features on the soils ability to retain water, thereby promoting or hindering the growth of crops leading to crop marks. At the same time, it highlights the time of day when the greatest thermal contrast

Chapter 1: Introduction

should be expected. It should be emphasised that this is relying on the fact that a contrast is measurable by proxy i.e. crop marks are observed rather than the underlying causes of their formation.

Although there is no such thing as a “typical” archaeological feature, ditch features are commonly occurring and representative of a number of periods. Figure 1.2 shows a schematic of the type of feature investigated in the current project, along with a summary of the geophysical, geotechnical and physical properties measured as part of the current work. The ability to identify these features using geophysical techniques such as GPR or earth resistance relies on a contrast in the geophysical properties in excess of the soils natural heterogeneity, especially in the interface between the feature fill soils and the surrounding soil matrix (SSM). Due to the complexity of soil, ranges of values for the measured properties and their heterogeneity are difficult to define and strongly soil and site specific and depend on the condition of the ground, especially its water content. However, typically values may be volumetric water content 0-50%; apparent relative dielectric permittivity (ARDP) 5-35; bulk electrical conductivity (BEC) between 0.0001 -1 S/m and temperature 5-20°C. The relationships between the soils geophysical, geotechnical and seasonal properties and their effects on the soils response to climatic conditions are discussed in greater detail in the literature review in Chapter 2.

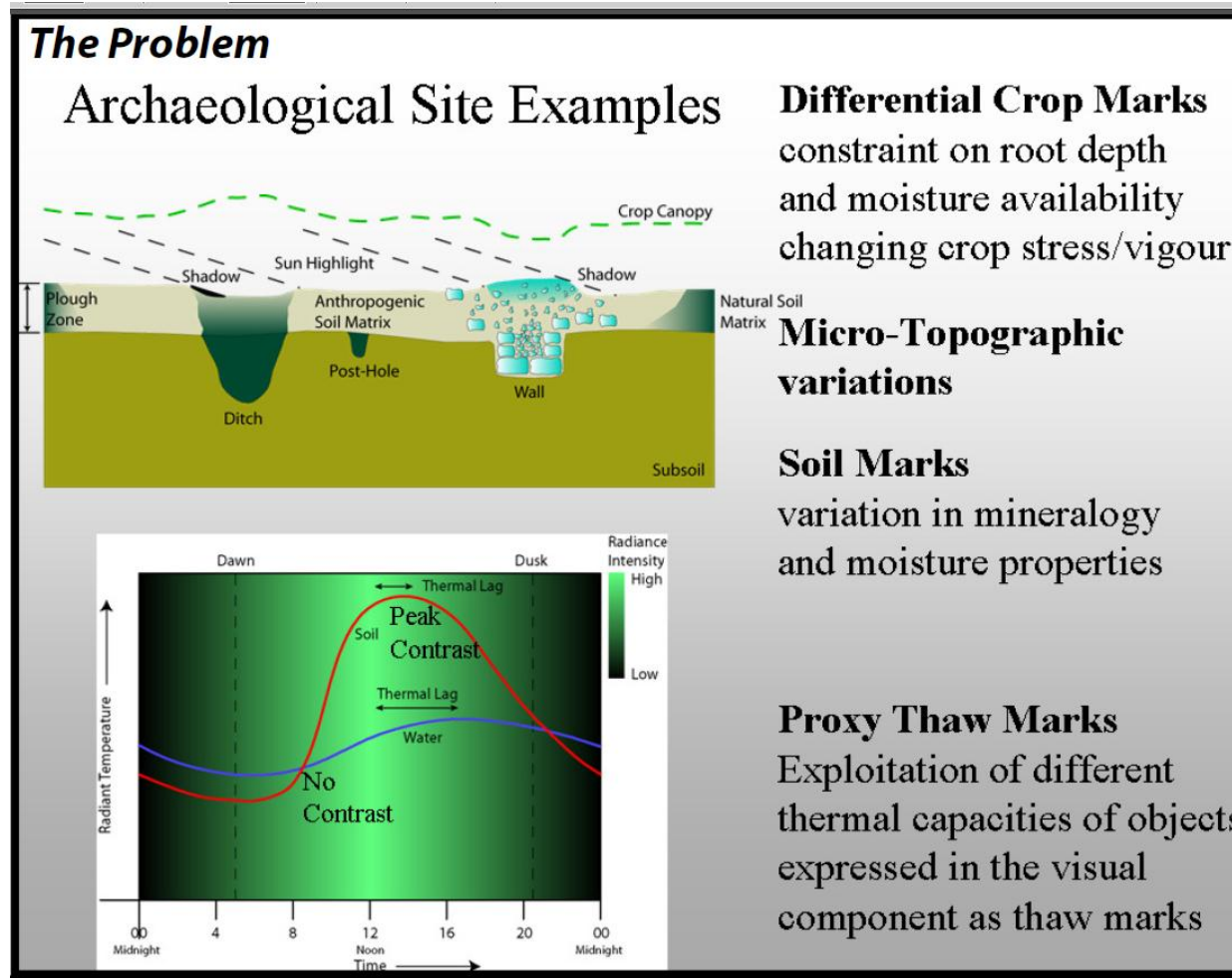


Figure 1.1: Some of the primary proxy methods by which archaeological features are identified using remote sensing techniques. Re-used under a creative commons share-a-like license from DART project

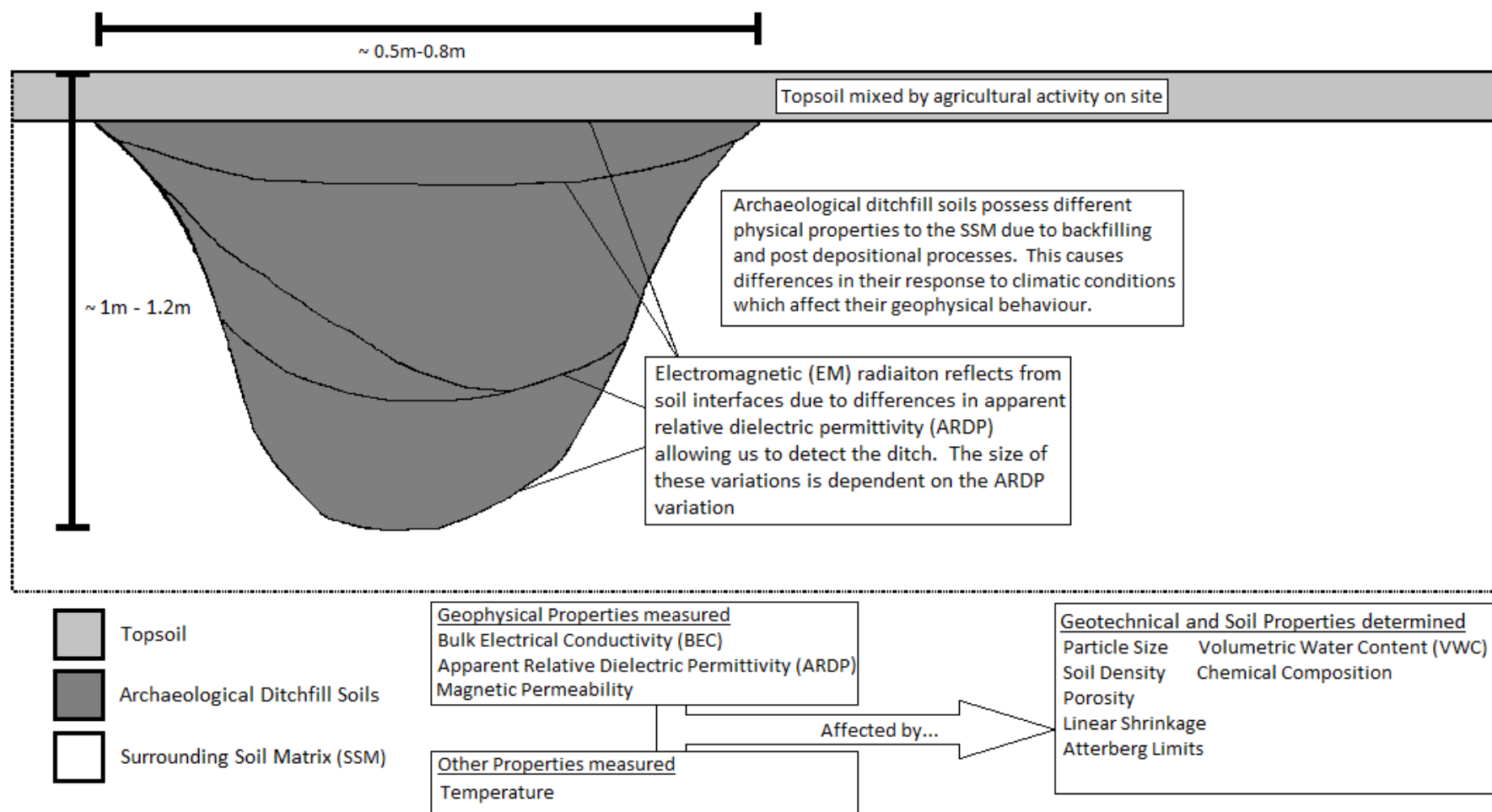


Figure 1.2: Schematic of physical, geophysical and geometric characteristics of a “typical” archaeological ditch feature.

1.2. Aims and Objectives

The aim of this project is to determine the changing electromagnetic properties as a result of seasonal changes, affecting contrast between archaeological ditchfills and the surrounding soil matrix. These will then be linked back to the known geotechnical and geochemical parameters of the soil to optimise heritage remote sensing sensor configuration and timing. This aim will be achieved by accomplishing the following objectives:

1. Conduct a critical and thorough literature study and review of the known information about time domain reflectometry (TDR), electromagnetic radiation behaviour in soils, the nature of soils and archaeological sediments, and their geophysical and geotechnical properties.
2. Develop and install autonomous remote monitoring stations to measure changing apparent relative dielectric permittivity (ARDP), bulk electrical conductivity (BEC) and temperature of the soil, both inside and outside the archaeological feature at depths of up to c.1.2m at a high spatial and temporal resolution.
3. Gather data from a number of test archaeological sites on the changing geophysical properties (ARDP, BEC), temperature and ambient weather over a 12-14 month period.
4. Link geophysical properties of the soil, measured using TDR results taken in the laboratory, to a variety of different water contents, temperatures and densities.
5. Determine the changing geophysical parameters linking these to known geotechnical properties of the soil and recent weather events on site.
6. Determine if it is possible, based on the research and data analysis, to predict the most favourable conditions to prospect for archaeological features.

1.3. Structure of the Thesis

This thesis is divided into 7 chapters. Chapter 1 is an introduction to the current research and lays out the aims and objectives of the research. Chapter 2 deals with a review of the existing state of knowledge on the geophysical properties and the techniques used which affect our ability to detect buried archaeological features. It also investigates the known links between geotechnical and geophysical properties of the soil and methods to measure these properties and concludes with the identification of knowledge gaps. Chapter 3 details the field methodology including the construction of monitoring stations and their installation, whereas Chapter 4 is concerned with the methodology of subsequent laboratory testing on soils from sites chosen, both to characterise the soils geotechnically and geochemically as well as identify their EM response under different conditions. Chapter 5 presents the findings from these laboratory studies and explores the different relationships between the geotechnical, geochemical and geophysical properties. Chapter 6 features a discussion on the data from the field monitoring stations and the results and the variability in the soil geophysical response relative to the weather and soil properties derived from the laboratory analysis. Chapter 7 presents the conclusions of the research, along with recommendations for future research.

Chapter 2: Literature Review

2.1. Scope

Archaeology literally translates as the study of ancient things (Bahn, 1999, Darvill, 2008)

although its precise definition remains a source of debate among archaeologists to this day (Drewett, 1999), with many definitions reflecting changing attitudes and opinions towards the discipline. Three different definitions are:

"A study of past societies and environments through systematic recovery of physical culture or material remains" (Darvill, 2008)

"Archaeology is not simply the finite body of artefactual evidence uncovered in excavations. Rather, archaeology is what archaeologists say about that evidence. It is the ongoing process of discussing the past which is, in itself, an ongoing process." (McEnroe, 2002)

"Archaeology... deals with a period limited to a few thousand years and its subject is not the universe, not even the human race, but modern man." (Woolley, 1961)

The majority of definitions suggest a study of material cultures, people and interactions with the landscape at some point in the past, with the main differences in the definitions centring on interpretation and the timescale over which remains are still archaeological. Whilst it has been suggested that all periods of the past should be treated with equal weight (Webster, 1974), it is clear that in practical terms, much less importance is placed on the recent past by archaeologists who are unlikely to study modern features and artefacts with the same fervour (Drewett, 1999). For the purposes of simplicity, this thesis will use the term archaeology to refer to the scientific study of the human past from all periods from the dawn of man to the present day, and the term archaeological feature to refer to the remains of structures or anthropological activities left in the landscape. Whilst it remains impossible to define a 'typical' archaeological feature, one which is perhaps most commonly occurring and representative of a number of periods is a ditch. The nature of soil in ditches depends heavily

on the provenance, function, length of usage, destruction (deliberate backfilling or infilling over time) and subsequent post depositional processes, which cause the soil to possess different geotechnical, geochemical and geophysical properties to the background soil into which the feature is cut. The contrast between these geophysical properties measured by heritage detection techniques is known to change throughout the year, but the reasons behind these changes are poorly understood. In order to optimise the detection of the fragile and finite archaeological resource, it is therefore important to gain an increased understanding on both the differences in these properties and their changes in different climatic conditions and their impact on geophysical signals. This literature review therefore focuses on electromagnetic (EM) properties, some of the key soil properties, the links between geophysical and geotechnical and geochemical properties and some of the technological methods for measuring them. Time domain Reflectometry (TDR) is particularly examined in detail as a method which is capable of long term monitoring of these properties (Curioni, 2013, Curioni et al., 2012). Previous seasonality studies on soil are also reviewed. The literature review concludes with a summary of knowledge gaps which provide the basis of the current work.

2.2. Heritage Detection Techniques

Heritage detection techniques are defined here as any non-invasive method for the investigation and mapping of archaeological features, thereby avoiding the need for an expensive excavation. Two main types of technique are used; aerial prospection techniques and ground based geophysical techniques. Although there are many differences between the two methods, the chief difference is the scale at which they operate. Aerial methods remain the preferred option for landscape prospection and geophysics the most common tool for field scale feature investigation, although landscape scale surveys are becoming increasingly common as instruments improve and larger datasets become viable (Campana and Piro, 2010, Kvamme, 2003). Both operate under similar principles, relying in a contrast in the soil

properties between the archaeological features and surrounding soil, which can be measured either directly or by proxy. A further subdivision can be made between active methods, which generate their own signals and measure the response, and passive methods, which measure responses to externally generated signals such as sunlight.

2.2.1. Aerial Prospection Methods

Aerial prospection methods are the most suitable method for prospecting for sites at a landscape scale, as they operate from either an aircraft or satellite. The vast majority of aerial techniques fall into the passive group, measuring the response to reflected sunlight, although some more recent methods such as Light Detection and Ranging (LIDAR) (Crow and Crutchley, 2010) are active. The longest standing aerial prospection method in archaeology is aerial photography with a usage dating back to 1906 in the UK (Bewley, 2003, Wilson, 1982), and rapidly gaining popularity in the interwar and post war period (Wilson, 1982). The method has become established as the dominant method for locating archaeological sites in Europe with over 50% of sites being discovered using this method (Bewley, 2003). More recently, hyper and multispectral sensors, used for geological, environmental and agricultural applications (Borengasser et al., 2007), have been employed to extend the range of reflectance detection outside of the visible spectrum, into the infrared and ultraviolet ranges (Aqduş et al., 2008). However, the use of this method in archaeology remains in its infancy, with the NHSS reporting that “Multi- and hyperspectral RS techniques have a large potential for use in archaeological prospection but are underutilized” (Williams, 2009a, b), largely due to a poor understanding of the factors which cause a detectable contrast. The aerial detection of features and the use of hyper and multispectral imaging are covered by a PhD student studying at the University of Leeds (Stott, 2014), although the present work may assist with knowledge on the formation of soil marks, and water content data may help determine the formation of crop marks.

2.2.2. Geophysical Prospection Methods

Geophysical techniques include earth resistance, magnetometry, ground penetrating radar (GPR) and low frequency electromagnetic instruments. The exact operating principles of these methods will not be covered in detail here, but can be found in any geophysical textbook (e.g. Clark, 1996, Reynolds, 1997, Scollar et al., 1990, Telford et al., 1990). An excellent review of the use of the techniques in the UK was conducted by Jordan (2009), finding a number of surveys which failed due to poor contrasts due to soil types and times of the year. Previous studies on changing contrasts are covered in greater detail in Section 2.8.1.

The principal technique for archaeological assessment is the magnetometer survey, which accounts for the vast majority of surveys in the UK (David et al., 2008). This detects archaeology through a variation in the magnetic properties of archaeological sediments and the surrounding soil. Both the mechanisms for enhancement and the detection of these by the instruments are well understood (Aspinall et al., 2008, Telford et al., 1990) and a study of these is therefore out of the remit of the DART project and this thesis.

Earth resistance survey measures the resistance of the soil and maps it either spatially or as a function of depth over a single traverse by increasing the electrode separation and calculating the apparent resistivity of the ground (Clark, 1996, Telford et al., 1990). As the method relies on variations in soil moisture and dissolved ions and the subsequent contrast between an archaeological feature and the surrounding soil, it is affected by seasonal variations in soil water content and temperature (Clark, 1996, Schmidt, 2013, Scollar et al., 1990). A full study on the impact of seasonal effects on earth resistance measurement is being carried out by a PhD student based in the University of Bradford (Fry, 2014), although supporting information can be provided by the soil monitoring stations included in the present work.

A third category, and a key growth area in UK archaeological geophysics is EM methods (Leckebusch, 2003). Both GPR and low frequency instruments such as the EM38 (Geonics

Limited, 2013) or CMD mini explorer (GF Instruments, 2014), rely heavily on both the electrical and magnetic properties of the ground, and mainly differ in their operating frequency ranges. Whilst the magnetic component remains fairly constant throughout the year, the electrical properties (conductivity and permittivity) vary seasonally with both water content and temperature, as well as with the frequency of the applied signal. A further discussion of the variation of these properties is contained in the remainder of this chapter.

2.3. EM Properties

EM radiation is all pervasive in our everyday life allowing us to see the world around us as reflected visible light, and occurring in such diverse everyday objects as TVs, microwaves and mobiles phones, as well as having specific uses in remote sensing and geophysical technologies such as GPR (Conyers, 2004). The link between electricity and magnetism was first observed by Hans Christian Ørsted in 1820, when he noticed that a current carrying wire deflected a magnetic compass needle (Aspinall et al., 2008, Cajori, 1935). However, the link between the two was not firmly cemented until the theoretical physicist James Clerk Maxwell mathematically laid out the relationships between the two (Maxwell, 1865), building on the experimental works of Ampere, Gauss and Faraday. These developed equations were later simplified by Oliver Heaviside in 1884 (Fleisch, 2008) into the four Maxwell equations which still form the basis of classical EM wave theory to this day. The theoretical nature of these equations was eventually proven in 1888 by Rudolf Hertz (Sengupta and Sarkar, 2003), who proved the transmission reflection and interference of different waves, both constructively and destructively. EM radiation is usually described in its classical representation as pairs of perpendicular time varying symbiotic electrical and magnetic fields which form orthogonal sinusoidal wave patterns with the amplitude varying as a function of time (Figure 2.1).

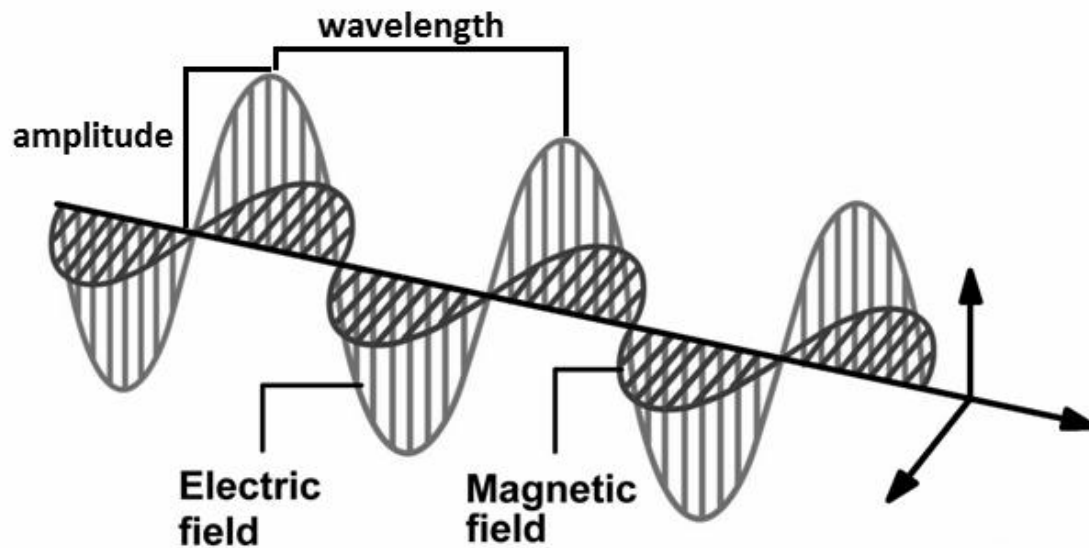


Figure 2.1: An EM wave. (Conyers, 2004)

The term, frequency (f) refers to the number of times the wave oscillates in a sinusoidal pattern as a function of time. In SI units, this is measured in Hertz (Hz), which refers to a single cycle per second or multiples of Hertz such as megahertz (MHz) or gigahertz (GHz). The wave can also be expressed as a function of wavelength (λ) in metres (m) or subdivisions of metres, where the wavelength is the distance between two peaks or troughs of the wave (Figure 2.1). As this value is clearly related to the rate of oscillation, the two parameters can be related using the speed of the wave using Equation 2.1.

$$\lambda = \frac{c}{f}$$

2.1

Where c is the speed of light in a vacuum (2.99792458×10^8 m/s)

In EM research, it is also possible to consider frequency as the change in phase angle occurring over a signal wavelength. As the signal is sinusoidal in nature, this is equal to a 360° phase change or 2π radians. This provides us with two different definitions for frequency; one based on the phase angle change, which is often referred to as angular frequency (ω) and another

based simply on the number of cycles per second (f), which is the commonly stated frequency of most signals. The two can be related using Equation 2.2 (Pollard et al., 2008).

$$\omega = 2\pi f$$

2.2

The frequency is independent of the medium in which it is travelling, although the velocity of the wave and therefore its wavelength are changed when travelling in different mediums. EM radiation can occur in many different forms from low frequency and long wavelength radio waves up to high frequency, short wavelength x-rays and gamma rays. The variety of different EM radiation types is summarised by the electromagnetic spectrum (Figure 2.2). An electrical field with a frequency of zero is one which in which current only travels in one direction and is usually referred to as direct current (DC) as opposed to those which vary and are termed alternating current (AC).

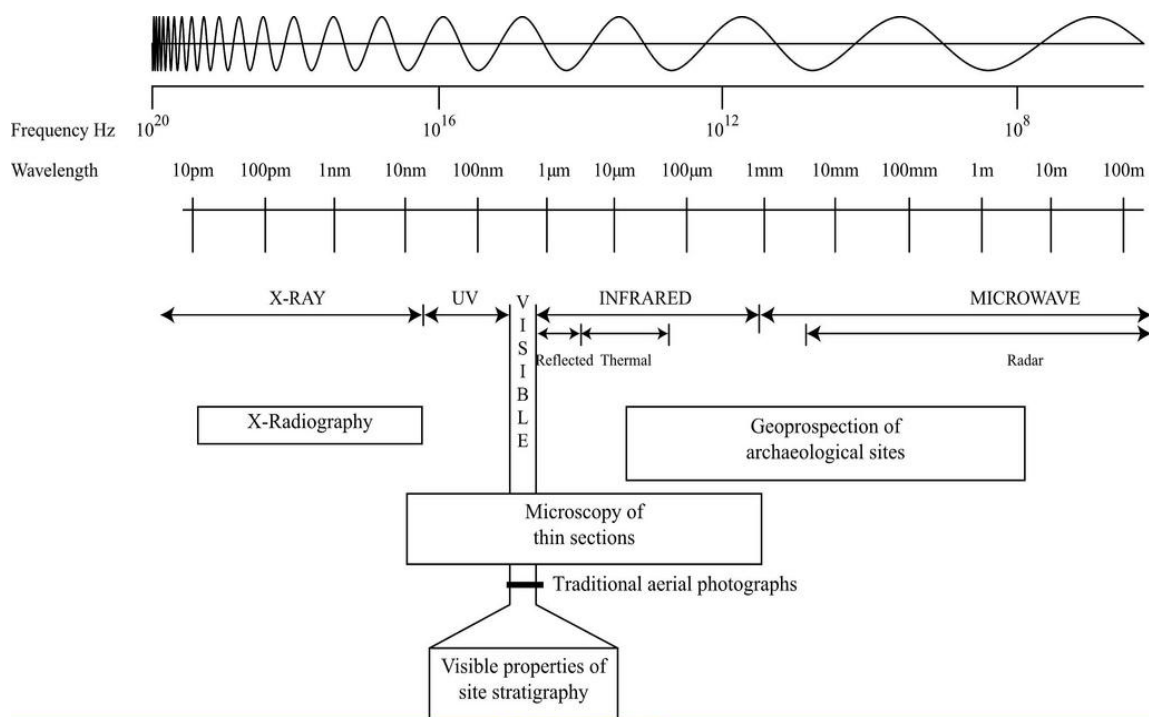


Figure 2.2: The EM spectrum and some archaeological uses. Reused under creative commons license from the DART website

It is perhaps important to note that the description of EM radiation provided above and by Maxwell's famous equations refer to a classical or wave theory of an essentially quantum system, based on particles rather than waves. Thomas Young's experiments using a double slit to show interference between different waves seemed to prove the wave nature of EM radiation and spelled the end for Newton's earlier particle theories of light (Pollard et al., 2008). However, in 1905, Einstein (Arons and Peppard, 1965) showed that light is made of discrete particles known as photons which contain a quantised amount of energy based on the frequency rather than the intensity of the light, earning the Nobel Prize for physics in 1921. The implications are clear that light, and by extension, other forms of EM radiation function as both a stream of particles and a continuous wave depending on the nature of the experiment and the type of observations made. Whilst at first this may appear to add complications to work involving EM radiation, in practice, this wave-particle duality is easy to reconcile by choosing the most appropriate theory and is now an accepted part of modern physics. In the present work, the use of classical wave theory allows us to dispense with the increased complexity of quantum particle representations, whilst still providing an accurate description of the results observed.

The propagation velocity (v) and attenuation (α) of EM signals through any medium such as the soil, is essentially governed by four main factors; the frequency of the applied signal (f), and the dielectric permittivity (ϵ), magnetic permeability (μ) and electrical conductivity (σ) of the medium. Interactions at interfaces between two media such as reflection and refraction are also defined by the differences in these properties between the two different materials. Further discussion on these properties is provided elsewhere (Cassidy, 2009, Santamarina et al., 2001), but a brief summary of each of them is provided below.

2.3.1. Electrical Permittivity (ϵ)

Electrical Permittivity is a measure of a materials ability to permit the formation of an electrical field through the polarisation of charged particles (i.e. ions, protons and electrons) contained

within it and the subsequent storage of energy. Energy stored by these separated charges is out of phase with the applied field, creating an electromotive force or displacement field (D) which opposes the applied field and causes a decrease in the velocity of the electrical field. Therefore, permittivity can be directly linked to the rate of EM wave propagation, as higher values will indicate a large storage of energy and subsequent slow speed of propagation, whereas low permittivity materials store less energy and allow faster transmission. The interaction between an EM wave and charged particles is shown in Figure 2.3.

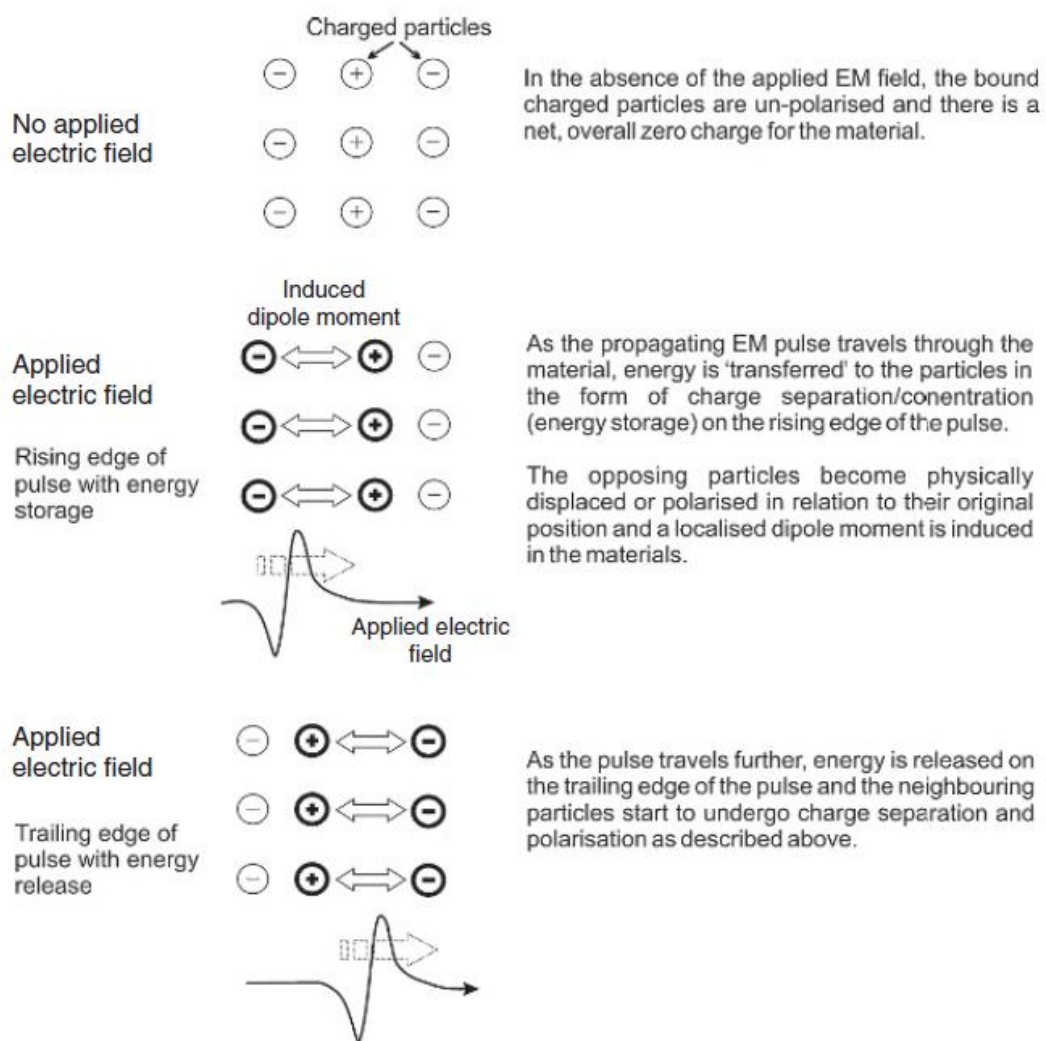


Figure 2.3: Conceptual diagram showing the interaction of charges with an EM wave. (Cassidy 2009)

The application of a local electrical field (E_{loc}) to any material causes the polarisation at both an atomic and a molecular level creating a polarisation vector (\vec{P}), which augments the displacement vector (\vec{D}) (Equation 2.3).

$$\vec{D} = \epsilon_0 \vec{E}_{loc} + \vec{P}$$

2.3

Where ϵ_0 is the permittivity of free space (8.854×10^{-12} F/m). The polarisation vector is directly proportional to the applied EM field (Chelkowski, 1980, Elliott, 1993) by a material constant known as the electrical susceptibility (χ_e)

$$\vec{P} = \epsilon_0 \chi_e \vec{E}_{loc}$$

2.4

Permittivity is usually defined as a ratio between the material permittivity and the free space value (ϵ_0). This is known as relative dielectric permittivity (RDP) usually denoted by the symbol ϵ_r . Since both ϵ and ϵ_0 are measured in the same units (Farads per metre; F/m), RDP is given as a dimensionless quantity. Furthermore, it is apparent from equation 2.4 that ϵ_r is simply one greater than the electrical susceptibility (Equation 2.5). For the purposes of convenience, unless otherwise stated as absolute permittivity, all future permittivity values will be considered relative.

$$\epsilon_r = \frac{\epsilon}{\epsilon_0} = 1 + \chi_e$$

2.5

Polarisation occurs in four main ways (Cassidy, 2009, Elliott, 1993); Electronic polarisation (P_e), Ionic polarisation (P_i), Orientational or dipolar polarisation (P_o) and Maxwell-Wagner or interfacial polarisation (P_{mw}). These are described in greater detail in Appendix E. Many materials will display more than one type of polarisation mechanism when subjected to electrical fields, and in the case of mixtures containing randomly orientated dipolar molecules,

such as soil, a combination of all of the above mechanisms are possible. The total polarisation can be given as a sum of the individual types of polarisation (Equation 2.6).

$$\vec{P} = P_e + P_i + P_o + P_{mw}$$

2.6

It should be noted that polarisation effects are not immediate and tend to lag behind the applied field often by considerable margins due to the torque and viscosity of the medium. This process, known as relaxation, causes energy to be lost as friction and heat (Kaatze, 2010) and causes imperfections in energy storage. For this reason, permittivity is often represented as a complex number (ϵ^*), consisting of real permittivity (ϵ') representing energy storage due to polarisation, and imaginary permittivity (ϵ''), representing dissipation of electrical energy due to these relaxations, conductivity (Section 2.3.3.) and resonances in the atoms and electrons of the material. It should be apparent that due to these relaxations, which peak at specific relaxation frequencies, and the different frequencies at which the different polarisation methods dominate the interaction (Figure 2.4), that both ϵ' and ϵ'' are frequency dependent quantities. The complex permittivity can be calculated using Equation 2.7

$$\epsilon^*(\omega) = \epsilon'(\omega) + j\epsilon''(\omega)$$

2.7

Where j is the complex operator ($\sqrt{-1}$). Figure 2.4 shows the real and imaginary permittivity over a wide range of different frequencies and some of the dominant polarisation and relaxation processes.

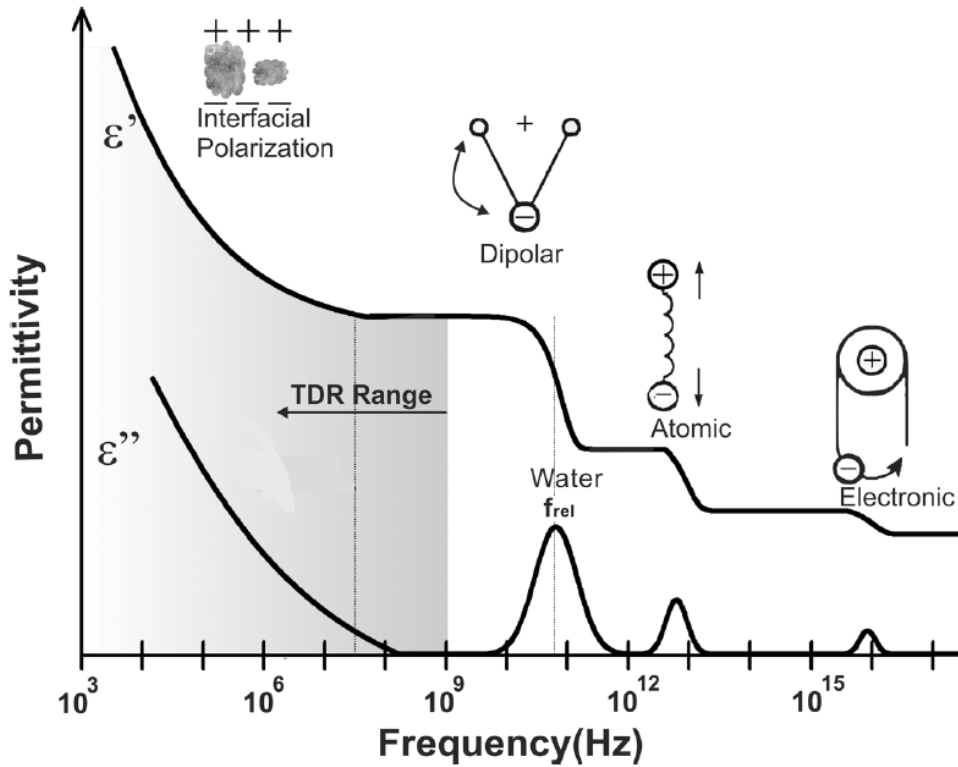


Figure 2.4: The complex permittivity as a function of frequency and the dominant polarisation and relaxation processes. (Chen and Or, 2006)

Relaxations can be defined by both a relaxation time (τ), defined as the time taken for molecules to re-randomise after removal of the electric field and a relaxation frequency (f_{rel}), which describes the frequency at which ϵ'' is at its maximum (Cassidy, 2009). The two are linked by Equation 2.8.

$$f_{rel} = \frac{1}{2\pi\tau}$$

2.8

Relaxation phenomenon in pure liquids were described by Debye (1929) and his model was later expanded to mixtures and solid materials by use of an exponent parameter (a) (Cole and Cole, 1941) to stretch relaxations over a wider frequency range and allow for multiple relaxation frequencies. This proposed Cole-Cole model (Equation 2.9) is still widely used to model polarisation and relaxation in a wide range of materials including soils (e.g. Yu et al., 2005).

$$\varepsilon^*(\omega) - \varepsilon_\infty = \frac{\varepsilon_{lf} - \varepsilon_\infty}{1 + (j\omega\tau)^{1-a}}$$

2.9

Where ε_∞ is the relative permittivity at a high frequency, above which no polarisation can take place, ε_{lf} is the static relative permittivity at a frequency significantly below relaxation, and a is the exponent between 0 and 1. Larger values stretch the relaxation whereas a value of zero is equal to Debye's original model. Since then, a number of additional models for specific circumstances based on these models with additional parameters have been developed including the Cole-Davidson (1951) and Havriliak–Negami (1967) models.

The real part of complex permittivity is often erroneously referred to as a dielectric constant, although a number of authors have noted this is incorrect due to the frequency dependence noted above, and the dependence of the value on other factors (Curioni, 2013, Evett and Parkin, 2005, Robinson et al., 2003a) which affect the ability of the material to polarise in the presence of an applied field. These include temperature, frequency of the applied EM radiation, porosity of the medium and the electrical dipole moments of the material (Sihvola, 2000).

2.3.2. Magnetic Permeability (μ)

Magnetic permeability is similar in nature to permittivity, but is a measure of a materials ability to allow the formation of a magnetic field in the presence of an external magnetising field. At an atomic level, a combination of the spin and circulation of negatively charged electrons around orbits generate EM fields in a similar fashion to a circulating current in a wire. Whilst the direction of these is normally random and displays no net force in any direction, application of an external magnetising field causes the electron orbits and spin motions to line up (Telford et al., 1990) causing the alignment of the internal magnetic dipoles, opposing the applied field and reducing its energy (Aspinall et al., 2008). This causes distorting magnetic fields, similar to the displacement fields caused by the permittivity, which affect the

propagation of the magnetic waves. It can be defined as the ratio of the magnetic flux density (B; measured in $\text{Wb/m}^2 = 1 \text{ Tesla}$) and the magnetising field (H in A/m) as shown in Equation 2.10 (Reynolds, 1997).

$$B = \mu H$$

2.10

Where μ is the magnetic permeability in Henries per metre (H/m). The relationship between the flux density (B) to the magnetising field strength (H) will depend on the ease of the material to be magnetised, a property known as the magnetic susceptibility of the material (χ_m)(Reynolds, 1997). This provides a multiplication factor for the free space permeability (μ_0), which gives the permeability of the material (Evans and Heller, 2003) using Equation 2.11.

$$\mu = \mu_0(1 + \chi_m)$$

2.11

Where $\mu_0 = 4\pi \times 10^{-7} \text{mA}^{-1}$ (Aspinall et al., 2008) or $1.26 \times 10^{-6} \text{H/m}$ (Cassidy, 2009)

Similarly to the permittivity, which is normally scaled to the free space value to give relative values, magnetic permeability is also usually expressed as relative magnetic permeability; a dimensionless ratio between the material value and the permeability of free space. Based on equations above and as with the relationship between electrical susceptibility and permittivity, it can therefore be shown that relative magnetic permeability (μ_r) is simple one greater than the materials magnetic susceptibility, χ_m (Equation 2.12).

$$\mu_r = \frac{\mu}{\mu_0} = 1 + \chi_m$$

2.12

There are several different types of magnetism occurring in materials (Aspinall et al., 2008) which are dependent on the effect of the applied field on electron motion and spin, including

diamagnetism, paramagnetism and ferromagnetism. These magnetic effects are described in greater detail in Appendix E. All materials display one or more of these magnetic behaviours, although in the vast majority of materials these effects are not very strong, and practically only material with ferromagnetic properties will have a real impact, due to weak applied fields and predominantly low susceptibility values.

Similar to the Debye (1929) relaxations in electrical polarisation, magnetic effects display time lag relaxation phenomena when measured under an EM signal as opposed to a steady magnetic field, as the dipoles realign. Therefore, much like permittivity, permeability is a frequency dependent value, and can be divided into a real component (μ') representing magnetic energy storage, and an imaginary component (μ''), representing the loss of magnetic energy. A number of researchers have used the Cole-Cole (1941) relaxation model in order to express magnetic relaxation as a function of time and frequency (Fannin et al., 2006, Meglich et al., 2008) using Equation 2.13.

$$\mu^* = \mu' - j\mu'' = \mu_\infty + \frac{\mu_{lf} - \mu_\infty}{1 + (j\omega\tau)^a}$$

2.13

Where μ_{lf} is the low frequency value of permeability, μ_∞ is the high frequency value of permeability, τ is the relaxation time and a is the Cole-Cole parameter which is based on the distribution and size of magnetic grains. In practice however, imaginary magnetic permeability is often considered to be negligible in many materials including soils and magnetic permeability is frequently considered a simple number. Furthermore, the magnetic permeability is commonly stated to be unimportant in soil (Birchak et al., 1974, Robinson et al., 1994) with the difference between air ($\mu_r=1$) and the soil stated to be negligible. However, this assumption has been found invalid in soils rich in magnetic materials where even modest amounts of magnetite (>7%) have been found to cause considerable losses and velocity retardation (Cassidy, 2007, 2009, Cassidy and Millington, 2009), although these soils are rare.

Some of the main iron oxides responsible for magnetic enhancement of soil are displayed in Table 2.1.

Table 2.1: Common soil iron oxides in archaeological sediments (Aspinall et al., 2008).

| Material | Chemical Composition | Magnetism type | Oxidation | Mass Specific Susceptibility |
|-----------|--|-----------------------------|---|------------------------------|
| Haematite | α -Fe ₂ O ₃ | Imperfect Antiferromagnetic | Fe ₃ ⁺ | 60 |
| Magnetite | Fe ₃ O ₄ | ferrimagnetic | Fe ₂ ⁺ , Fe ₃ ⁺ | 56,000 |
| Maghemite | γ -Fe ₂ O ₃ | ferrimagnetic | Fe ₃ ⁺ | 30,000 |

Anthropogenic soils have known enhancement to magnetic properties, which form the basis of magnetometer detection of archaeological features (Aspinall et al., 2008, Gaffney and Gater, 2003) both through the presence of thermoremanent magnetic materials, such as brick fragments, and through actions on the naturally occurring iron oxides. Iron oxides in the soil are affected by heating, which causes reduction of the weakly magnetic haematite (α -Fe₂O₃) into ferrimagnetic magnetite (Fe₃O₄) and subsequent re-oxidation into maghemite (γ -Fe₂O₃) forms (Aspinall et al., 2008), which can have magnetic susceptibility values many times greater. More recently, Fassbinder et al. (1990) showed that the decay of organic material enhances the magnetic response of sediments, through the actions of living bacteria which form reducing conditions. Nevertheless, the range of values occurring in the soil is not large, with 3 being an approximate highest possible value (Telford et al., 1990). Effects are limited to soils where the permeability is equal to a significant proportion of the electrical response, although in soils where the electrical permittivity is very low, this value will have a significant effect on EM signal interaction.

The magnetic permeability of soil can be assessed in the laboratory either by determining the soils attraction to a static magnet (BSI, 1999), or by use of a magnetic susceptibility meter and

conversion of the values using Equation 2.12. However, due to the previously mentioned relaxation mechanisms, these measurements should be treated with some care, as all materials display susceptibility and hence permeability variation with frequency change (Clark, 1996), so values recorded may be of limited use, particularly when looking at the interactions of higher frequency EM signals.

2.3.3. Electrical Conductivity (σ)

Electrical conductivity is a measure of a material's ability to carry an electric charge freely through it, due to the application of an applied electrical voltage or field. A material which is restrictive to these charges is termed an insulator or low loss dielectric, whereas a medium where charges are highly mobile is classed as conductive. Highly conductive materials are problematic for EM propagation, causing a loss of energy from the electrical component of the wave and therefore signal attenuation as a function of distance travelled. Reynolds (1997) states that there are three main mechanisms by which an electrical current is carried within soils and rocks, which are briefly summarised here.

Electronic or ohmic conduction is the process by which a negatively charged electron moves rapidly towards a positive charge. This is most common in metals.

Electrolytic conduction is the movement of ions with either a positive (anions) or negative (cations) charge, which are attracted towards their opposite charges. This is much slower than electronic conduction, and depends heavily on the type, concentration and mobility of the ions within the material. In soils this is the most important type of conduction, with the pore waters acting as electrolytes due to the ions dissolved within them (Santamarina et al., 2001).

Dielectric conduction occurs when an alternating current causes the electrons in an atom to be shifted slightly in relation to the nucleus. This is most common in weakly conducting materials.

Conductivity is measured in Siemens per metre (S/m), the inverse of which is resistivity (ρ), measured in ohm-metres (Ωm). It is difficult to measure σ or ρ , especially in multiphase mediums, as both values are independent of the amount of material through which the electrical current is flowing. In practice, it is therefore impossible to measure this in the real world as an amount of material must be measured and it is difficult to constrain current paths to a single phase. For this reason it is practical to measure resistance or conductance, and calculate to ignore current path lengths and assume that the material sampled is homogenous to give bulk electrical conductivity (BEC) or apparent resistivity respectively. Additionally, although conductivity is normally measured using DC, when measured with AC where current varies as a function of time, conductivity can be represented as a complex value with a real and an imaginary part (Equation 2.14).

$$\sigma^* = \sigma' - j\sigma''$$

2.14

The real part represents the effects of charge carriers moving in phase with the applied electrical field, causing energy to be lost as heat through particle collisions (Olhoeft, 2003). Where the AC frequency is too large for these charge carriers to follow the field, they lag out of phase causing charge to be stored (capacitive reactance) and the formation of a magnetic wave behind the main electrical wave (inductive reactance) (Hirst, 1966). These two effects cause charge to be stored in a similar manner to ϵ' . However, these effects are only noticeable at high frequencies, out of the range of most geophysical equipment (Cassidy, 2009), and simple values based on σ' are adequate for most applications.

2.3.4. Propagation of EM radiation

The interactions of EM radiation with a medium are strongly dependent on the three main EM parameters discussed above, with the differences in these properties governing the overall velocity (v ; measured in m/s) and attenuation (α ; measured in Np/m) of geophysical signals in each soil type (Reynolds, 1997, Telford et al., 1990). Differences in these properties between

neighbouring materials also form the basis for subsurface reflections. To simplify calculations, plane waves of a single frequency are often used, which give a reasonable approximation to real waves, although more complex calculations can be carried out by using a superimposition of a number of plane waves. The fundamental parameters discussed in Sections 2.3.1 to 2.3.3 can be broadly divided into sources of energy storage and energy losses, which can be used to calculate effective values for the real and imaginary permittivity to be used in subsequent calculations. Energy storage in soil is governed by the real (in phase) part of the dielectric permittivity (Equation 2.15).

$$\varepsilon'_{eff} = \varepsilon'$$

2.15

The factors which cause losses include the polarisation losses (see Section 2.3.1), magnetic losses (see Section 2.3.2) and DC conductivity (see Section 2.3.3). At low frequencies, the primary loss mechanism is conduction, whereas at high frequencies, the effects of molecular relaxations are dominant (Hallikainen et al., 1985). Since magnetic losses in soil are minimal, the effective imaginary permittivity, ε''_{eff} is calculated using equation 2.16.

$$\varepsilon''_{eff} = \varepsilon''_p + \frac{\sigma}{\omega}$$

2.16

Where ε''_p are the losses from polarisation lag and σ is the DC conductivity. Since the fundamental parameters are dependent on the frequency of the applied signal (see Sections 2.3.1, 2.3.2 and 2.3.3), it also follows that the effective real and imaginary parts of the permittivity calculated using Equations 2.15 and 2.16 are also frequency dependent. The propagation of EM waves in a lossy soil medium is described by the complex propagation factor (γ) which can be calculated using Equation 2.17 (Birchak et al., 1974).

$$\gamma = \alpha + j\beta$$

2.17

Where α is the attenuation constant, describing the loss of the signal (Np/m) and β is the transmission constant (radians per m) which describes the motion of the wave, which are calculated using Equations 2.18 and 2.19 (Thomas et al., 2007) respectively.

$$\alpha = \omega \sqrt{\frac{\mu\varepsilon'}{2}} \left(\sqrt{1 + \left(\frac{\varepsilon''}{\varepsilon'}\right)^2} - 1 \right)^{0.5}$$

2.18

$$\beta = \omega \sqrt{\frac{\mu\varepsilon'}{2}} \left(\sqrt{1 + \left(\frac{\varepsilon''}{\varepsilon'}\right)^2} + 1 \right)^{0.5}$$

2.19

The amplitude of EM waves decays exponentially as a function of the distance travelled (x ; in m) through the soil and the attenuation constant (Equation 2.20) (Annan, 2009).

$$u_2 = u_1 e^{-\alpha x}$$

2.20

Where u_1 and u_2 are the initial amplitude and attenuated amplitude respectively. The rate of attenuation is an important consideration in the detection of archaeological features using heritage detection techniques such as GPR because it limits the depth to which the signal can penetrate, reflect and still be detected by the sensor in question.

The phase constant, along with the angular frequency, can also be used to calculate the velocity (v ; in m/s) of the wave using Equation 2.21 (Schneider and Fratta, 2009).

$$v = \frac{\omega}{\beta} = \frac{c}{\sqrt{\frac{\mu\varepsilon'}{2}} \left[\sqrt{1 + \left(\frac{\varepsilon''}{\varepsilon'}\right)^2} + 1 \right]^{0.5}}$$

2.21

Knowledge of the wave velocity is useful for estimating the depth of buried archaeological features with EM techniques (Conyers, 2004, Conyers and Lucius, 1996). In addition, changes to the velocity also cause refraction of the signal and 'download' (reduce) the frequency and wavelength of the transmitted signal (see Equation 2.1). This affects the resolution of the survey and the size of features which can be detected, the minimum size of which is related to the wavelength, with the smallest discernible features estimated at around 25% of its value (Conyers, 2004).

Differences in dielectric properties are also responsible for reflections of EM radiation used by heritage detection techniques for the detection of archaeological feature boundaries and layers. Reflections occur at interfaces in EM impedance, according to Snell's law and Fresnel coefficients (Annan, 2009). EM impedance (Z) can be calculated using Equation 2.22 (Cassidy, 2009).

$$Z = \sqrt{\frac{j\omega|\mu'|}{\sigma' + j\omega|\epsilon'|}}$$

2.22

Where $|\mu'|$ and $|\epsilon'|$ are absolute real magnetic permeability and electrical permittivity respectively. In a non-conductive medium this is often simplified to Equation 2.23 (Annan, 2009).

$$Z = \sqrt{\frac{|\mu'|}{|\epsilon'|}}$$

2.23

In soil, where the magnetic permeability is usually assumed to be negligible (see Section 2.3.2), Equation 2.23 can be further simplified to Equation 2.24.

$$Z = \sqrt{|\varepsilon'|}$$

2.24

Reflections occur at interfaces in dielectric properties. Amplitude of the reflected energy is given by Equation 2.25.

$$v_r = \Gamma v_i$$

2.25

Where v_r is the reflected amplitude and v_i is the incident amplitude and Γ is the reflection coefficient (Schneider and Fratta, 2009), determined using the EM impedance of the two materials and Equation 2.26.

$$\Gamma = \frac{Z_1 - Z_2}{Z_1 + Z_2}$$

2.26

Where Z_1 is the source impedance and Z_2 is the load impedance (Yanuka et al., 1988). From Equations 2.22-2.26, it should become apparent that the ability to detect archaeological features using EM radiation is dependent on differences between one or more of the fundamental EM parameters (ε , μ , or σ) with respect to the archaeological feature and the surrounding soil matrix. Since the magnetic permeability of the soil does not vary greatly over time (see Section 2.3.2), of particular importance are variations in the permittivity and conductivity of the soil. It should also be apparent that since these values are frequency dependent, the velocity, attenuation and scale of reflections are also frequency dependent. Due to this, a compromise must be met between high frequency signals which have good resolution but attenuate quickly in soils with high imaginary permittivity values, and lower frequency signals which penetrate to a greater depth but are only capable of detecting larger features (Conyers, 2004).

2.4. Soil Properties

Soil has no commonly agreed definition. Gerrard (2000) states that an all embracing description of soil is “*a natural body composed of minerals, organic compounds, living organisms, air and water in interactive combinations produced by physical chemical and biological processes*”. The main phases in soil are the weathered parent mineral fraction, organic matter and water and soil gases, such as air, which fill the pore spaces between the solid particles. Weathered material overlying the bedrock is often termed the regolith, although a definition of where the two regions meet is often difficult to define (Gerrard, 2000) and the two are often considered together as a pedological organisation. Soil is, by its nature, a dynamic system and changes in physical and chemical composition occur over time due to climate, bedrock mineralogy, topography, vegetation, organic processes and human land use processes (Rowell, 1994) which makes it a highly complicated medium in which to work.

In geotechnical engineering, soil is defined as any weakly cemented or uncemented accumulation of weathered rock mineral particles containing voids filled with air or water (Knappett and Craig, 2012), the properties of which are defined by a series of classification tests. For the purposes of the current work, soil will be taken to refer to any multi-phase material comprising solid minerals, soil gases and water and which may or may not contain significant amounts of organic material. Furthermore, soils located within an archaeological feature will be termed archaeological soil. The background soils, which do not form part of the feature, will be termed the surrounding soil matrix (SSM), although it is recognised that these soils may have been anthropogenically influenced both by current land use practices and during their pedological formation. Studies have shown differences in soil properties of the two different soil types (Scollar et al., 1990, Stanjek and Fassbinder, 1995, Strunk-Lichtenberg, 1965) which are likely to have been caused by their differing depositional histories and origins, although the precise differences are likely to be a function of the nature of the soil and the processes which created the archaeological feature. Geophysical properties are a function of

the composition and physical behaviour of the soil and display a wide range of values. Typical geophysical values for a range of materials are shown in Table 2.2 indicating the broad range of different properties in subsurface features.

Table 2.2: A selection of commonly found materials and their typical geophysical properties. (Adapted from Cassidy, 2009)

| | Material | Apparent Relative Dielectric Permittivity | Bulk Electrical Conductivity mS/m |
|------------------------|-----------------------------|---|-----------------------------------|
| WATER | Freshwater | 78–88 | 0.1–10 |
| | Ice | 3 | 1–0.000001 |
| | Seawater | 81–88 | 4000 |
| ROCKS | Limestone – dry | 4–8 | 0.001–0.0000001 |
| | Limestone – wet | 6–15 | 10–100 |
| | Granite – dry | 5–8 | 0.001–0.00001 |
| | Granite – fractured and wet | 5–15 | 1–10 |
| | Sandstone – dry | 4–7 | 0.001–0.0000001 |
| | Sandstone – wet | 5–15 | 0.01–0.001 |
| | Shale – saturated | 6–9 | 10–100 |
| OTHER MATERIALS | Clay – dry | 2–20 | 1–100 |
| | Clay – wet | 15–40 | 100–1000 |
| | Concrete – dry | 4–10 | 1–10 |
| | Concrete – wet | 10–20 | 10–100 |
| | Sand – dry | 3–6 | 0.0001–1 |
| | Sand – wet | 10–30 | 0.1–10 |
| SOIL | Soil – average | 16 | 5 |
| | Soil – sandy, dry | 4–6 | 0.1–100 |
| | Soil – sandy, wet | 15–30 | 10–100 |
| | Soil – loamy, dry | 4–6 | 0.1–1 |
| | Soil – loamy, wet | 10–20 | 10–100 |
| | Soil – clayey, dry | 4–6 | 0.1–100 |
| | Soil – clayey, wet | 10–15 | 100–1000 |

2.4.1. Soil Water

It is well known that, of the different phases of which soil is composed, water is by far the most important for determining a soil's geophysical properties (Annan, 2009, Curtis, 2001, Hoekstra and Delaney, 1974, Robinson et al., 2003a, Topp et al., 1980), due to its relatively high permittivity in relation to the other phases, and ability to dissolve charge carrying ions which result in high BEC values (Table 2.3). The positive dependence of both permittivity and conductivity associated with changes in water content for a variety of different soils and densities are shown in Figure 2.5. The effect of density on geophysical properties is covered in Section 2.5.2. Whilst a simple relationship exists between permittivity and water content, the relationship between BEC and volumetric water content shows a greater spread due to other soil specific factors, such as chemical composition, pore size distribution and ion availability in the soil sample, the effects of which are discussed in Section 2.5. However, a primary dependence on water content is still apparent.

In addition to the relative importance of water content, whilst the mineral fraction and resistant organic material which form the soil skeleton change little over time (Gerrard, 2000), the relative abundance of air and water in the soil pores is in a state of constant flux due to environmental factors especially climate. Differences in the water contents of archaeological features and the SSM have also been used to predict the appearance of crop marks used in aerial detection (Evans and Jones, 1977, Jones and Evans, 1975, Stanjek and Fassbinder, 1995).

Table 2.3: The dielectric properties of different soil phases.

| Soil Phase | Relative Permittivity | Conductivity (mS/m) |
|----------------|-----------------------|---------------------|
| Soil Particles | 3-5 | 0 |
| Organic Matter | 3-5 | 0 |
| Air | 1 | 0 |
| Free Water | c.80 (20°C) | 0.1-10 |
| Bound water | 3-40 | 0.1-10 |

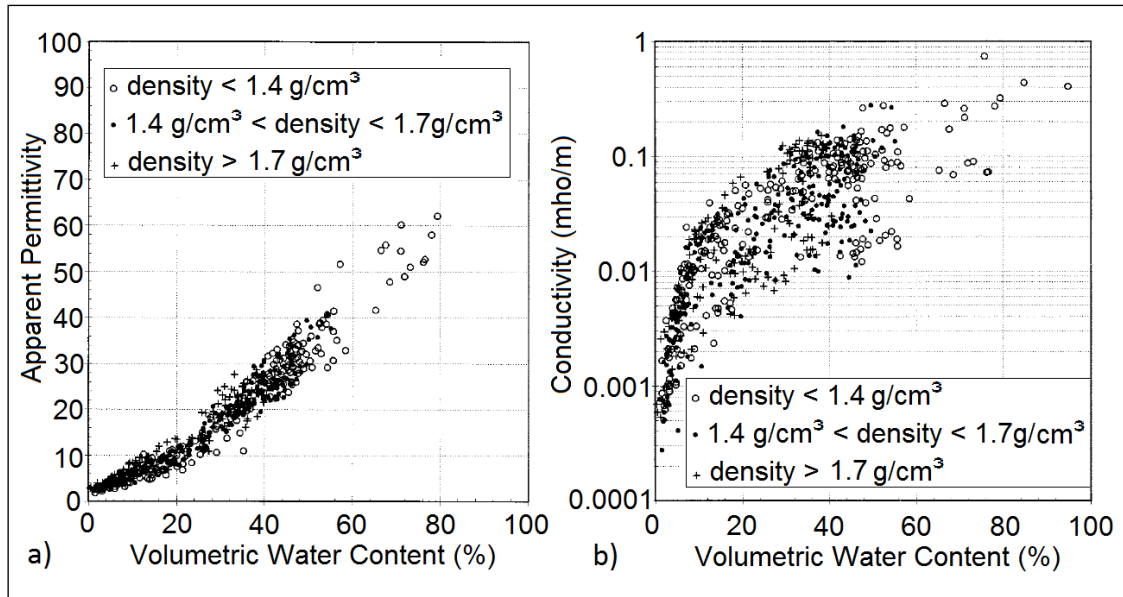


Figure 2.5: (a) permittivity and (b) conductivity for various types of soils with different density showing a wide variability at different volumetric water contents (Curtis et al., 2001).

The permittivity of water and its relaxation phenomena are well understood (Catenaccio et al., 2003, Debye, 1929, Meissner and Wentz, 2004). The high relative permittivity values of water (c.80-81) are the result of its unusual molecular structure, consisting of two hydrogen atoms which are bonded to a single oxygen atom in a tetrahedral pattern with an angle of 104.5° (Robinson et al., 2003a). The relative differences in size between the positively charged atomic nuclei causes the electron densities in the chemical bonds to be located closer to the oxygen atom resulting in a fractional charge on both atoms (Pollard et al., 2008) (positive on the hydrogen atoms and negative on the oxygen atom) and a dipolar molecule (Figure 2.6), which allows orientational as well as molecular polarisations to take place. These charges also allow water to form weak hydrogen bonds between molecules which are made and broken at a rate proportional to temperature and pressure. In addition, the dipolar charges of the water molecule attract ions which dissolve and carry charge, increasing conductivity of the solution.

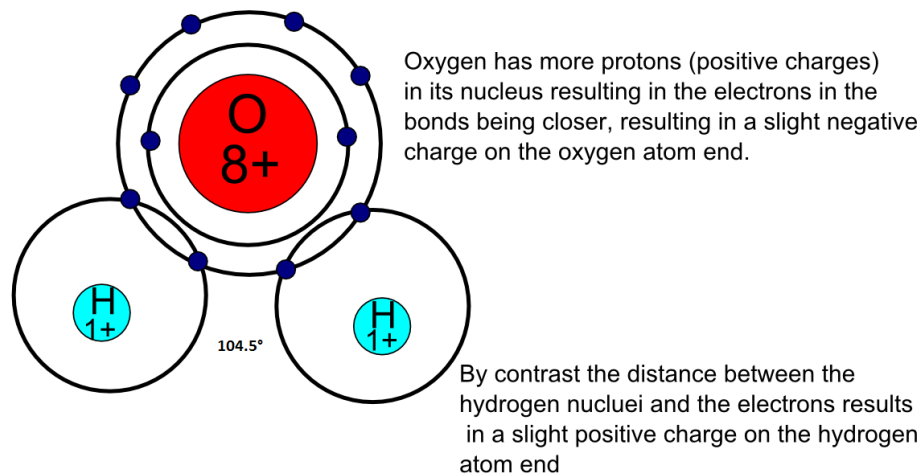


Figure 2.6: A water molecule showing the positions of electrons in relation to the hydrogen and oxygen nuclei which give fractional charges

In practice, earlier researchers into EM properties of soil discovered that the permittivity of the soil is rarely a simple relationship with amount of water, and displays EM dispersion (variable values with frequency) (Smith-Rose, 1935). This is due to the attraction between the dipolar water and the surface charges of solid particles, introducing the concept of bound water (Cownie and Palmer, 1952, Hoekstra and Delaney, 1974) with different dielectric properties. Whilst the normal relaxation frequency of water predicted by the Debye (1929) model is approximately 17GHz (Hilhorst et al., 2001), Hoekstra and Delaney (1974) were able to show that bound water relaxed at lower frequencies which were modelled using the Cole-Cole (1941) model. These effects were reported as similar for all the soils tested, although only low water contents were tested which may have failed to produce free water in clay soils.

The effects of bound water are important to consider as the reduction in relaxation frequency makes the dielectric properties of wet soil frequency dependent in the range of many heritage detection techniques, especially in soils where large amounts of bound water are present.

However, the boundary between bound and free water is not a binary divide and therefore is difficult to define as the behaviour of soil water varies with soil matric pressure (see Section 2.4.2) and distance from the soil particle (Friedman, 1998) from the tightest bound adsorption layer, which only polarises electronically and atomically, to free water capable of full rotational

polarisation. Hilhorst et al. (2001) defined the boundary between the two at 100MPa of soil matric pressure after which the soil water had a relaxation frequency of 8GHz and could be considered free in the range of most geophysical instruments whereas Wang and Schmugge (1980) suggested a value of 1.5MPa. Other authors have suggested the number of molecular layers as a guide (Borjarskii et al., 2002, Jones and Or, 2002) with numbers between 3 and 10 suggested as the divide between the two water types. Another approach has been to consider bound water as a number of different phases which depend on the strength of the attraction and the distance of the water molecules from the soil particles. Saarenketo (1998) defines these as a hydroscopic or adsorption layer which has properties indistinguishable from the soil particles; a viscous capillary layer where water is not directly bound to particles but does not flow with gravity due to surface tension effects and gravitational of free water which behaves as pure water. Each of these layers was found to have differing electrical properties and dispersive effects were mainly associated with the viscous capillary water layer, whereas the tightly adsorbed layer was insensitive to EM fields across the tested frequency range. Comparison between the above definitions of bound water are complicated by the wide range of frequencies used in determining them, and therefore for the purposes of this thesis, bound water will be defined as any which shows differing dielectric properties from pure water at the measurement frequency of the instrument in question.

Subsequent authors have most commonly correlated the bound water layer to the specific surface area (SSA) of the soil (Dobson et al., 1985, Escorihuela et al., 2007, Jones and Or, 2002, Wraith and Or, 2001), which is the ratio of particle area to mass (Santamarina et al., 2002) and primarily determined by grain size and mineral composition (Arnepalli et al., 2007). Other approaches have correlated values to either physical or chemical properties of the soil including cation exchange capacity (CEC) (Bridge et al., 1996, Saarenketo, 1998), and soil wilting point (Wang and Schmugge, 1980). As many of the above, especially SSA, are difficult to measure directly (Arnepalli et al., 2007), estimations of these properties or direct

correlations have been made using geotechnical properties (see Section 2.5). The differences in dielectric properties of bound water have also been modelled by researchers, either as a separate phase with values similar to ice (3-3.2) (Cownie and Palmer, 1952, Dirksen and Dasberg, 1993, Hoekstra and Delaney, 1974), or other static values ranging between 5 (Jones and Or, 2002) and 20-40 (Dobson et al., 1985), or by making the value of the whole water phase dependent on the degree of saturation (Borjarskii et al., 2002, Friedman, 1998) to encompass the different phases of bound water.

It has also long been known that the BEC of the soil is highly dependent on water content (Archie, 1942, Smith-Rose, 1933, 1935) with values primarily dependant of the conductivity of the pore water, as the solid phase is irrelevant in coarse grained soils (Schneider and Fratta, 2009), although some contribution from the solid phase has been noted in fine grained soils due to adsorbed water effects (Samouëlian et al., 2005). Clays with larger SSA values and CECs, which are linked to the mineralogy of the clay, create a larger surface charge density on the solid particles (Fukue et al., 1999, Samouëlian et al., 2005) and provide greater numbers of soluble ions (Friedman, 2005), thus providing higher conductivities at the same water contents than coarser grained soils. Smith-Rose (1933) noted that the relationship between the water content and conductivity of the soil is not linear with the initially steep positive relationship declining at higher water contents, and eventually ceasing to exist at water contents above 20%. A similar trend can be observed in the data of Curtis (2001). Prediction of the precise values of conductivity from the soil information requires knowledge of salt availability, the number of these salts bound to the soil particles and the methods of charge movement (Curtis, 2001).

Soil water is also important for determination of a soils thermal behaviour, both in terms of ability to store heat, determined by volumic heat capacity (i.e. heat capacity at a constant volume) and thermal conductivity (K_T measured in $Wm^{-1}C^{-1}$). The volumic heat capacity of water (4.187×10^6 SI units) is near twice that of the solid particles (2.08×10^6 SI units), and as the

gaseous phase possesses negligible properties (Davie, 2008, Scollar et al., 1990), the volumic heat of the soil determined by a sum of the volumic capacities of the other two phases. In practice, this means that wet soil has a far greater thermal capacity than dry soil with air in the pore space. Experiments have shown that thermal conductivity is primarily dependent on pore size and grain size distribution, with soil water playing only a minor role (Scollar et al., 1990, Tabbagh, 1985). Heat flux in soils (W/m^2), expressing its ability to transfer heat, is proportional to the negative temperature gradient and thermal conductivity of the soil (Equation 2.27).

$$\text{Heat Flux} = -K_T \nabla T$$

2.27

Soil water content can be measured in two main ways; gravimetrically and volumetrically.

Gravimetric water content (GWC; θ_g) is the mass of water contained within the soil as a ratio to the weight of dry soil, and can be calculated using Equation 2.28 (BSI, 1990).

$$\theta_g = \frac{m_w}{m_s}$$

2.28

Where m_w and m_s are the masses of water and dry soil respectively. Volumetric water content (VWC; θ_v) refers to the amount of water contained in the soil expressed as a volume of the total soil volume. In practice it is possible to convert between the two values if the dry density of the soil is known using Equation 2.29 (Yu and Drnevich, 2004).

$$\theta_v = \frac{V_w}{V_t} = \left(\theta_g * \left(\frac{\rho_d}{\rho_w} \right) \right)$$

2.29

Where V_w and V_t are the volume of the water and total sample, and ρ_d and ρ_w are the dry density of the soil and density of the water, which has known properties (Walker, 2011), respectively. Whilst in geotechnical engineering, GWC values are preferred (BSI, 1990), it is

conventional and appropriate to use volumetric values when dealing with EM properties (Hilhorst et al., 2001, Hoekstra and Delaney, 1974) because these relate to the number of dipole reactions taking place per a given unit volume, and relationships between permittivity and VWC have been shown to give less variable results (Hallikainen et al., 1985).

2.4.2. Soil Water Movement

The amount of water present in the soil is dependent on both infiltration during a precipitation event, and potential evaporation which removes water from the soil. In a seminal study of infiltration, Horton (1933) determined that infiltration rapidly decreases over the course of a rainfall event to a constant value known as the infiltration capacity, as pores shrink as clay particles swell, and fill with water and soil wash, reducing capillary forces. Infiltration capacity is restored to its initial value after a period of dry weather, due to the shrinkage of colloids and actions of earthworms (Beven, 2004). The main source of loss of soil water is evaporation, which depends on the amount of water and energy available as well as the air humidity, which affects its ability to carry additional moisture. Evaporation is often combined with transpiration (water movement through plants) to give evapotranspiration (ET), usually expressed as potential evapotranspiration (ET_p) which can be calculated using a number of different models (e.g. Monteith, 1965, Penman, 1948, Thornthwaite, 1948), and represents the amount of water which would be lost if soil water was unlimited (Davie, 2008). In practice, actual ET values are rarely equal to calculated potential ET unless the soil is completely saturated. The balance between potential ET and precipitation is known as the water balance, which governs the total net input of water to the soil system.

Soil water movement, in both a vertical and lateral direction, is primarily controlled by two main factors, the soil water holding capacity, which determines how much the water a soil can hold, and the hydraulic conductivity (K_H); the ability of the soil to transmit water in the presence of a hydraulic gradient. Both of these factors are a function of total porosity (ratio of void volume per soil volume), pore-size distribution and current water content of the soil and

are therefore affected by the composition of the soil, especially the particle size, density and structure. As mentioned in Section 2.4.1, water interacts with the solid soil particles and is attracted to soil particles through a combination of matric (suction) forces (ψ_m), which are due to adsorption, capillary forces and surface tension, osmotic potential (ψ_o) caused by dissolved solutes, as well as being affected by gravitational forces (ψ_g), which act against the other forces to draw water down through the profile (Foth, 1990). A combination of these forces describes the soil water potential (ψ_t) (Equation 2.30), usually expressed in units of negative pressure, which describes the amount of work needed to move soil water from its present state to a reference pool of water at zero elevation. Higher (more negative) values of soil water potential allow the soil to hold water more strongly.

$$\psi_t = \psi_m + \psi_o - \psi_g$$

2.30

In soil science, soil water potential is usually expressed in terms of a number of common reference potentials (Fredlund and Xing, 1994). In saturated soils where all the pores are full of water, the soil water potential is equal to zero, although these conditions rarely exist for long due to the effects of gravitational drainage which drain water from the largest pores, and take the soil water content to its field capacity, defined as a potential of -33KPa. The difference between the VWC and the field capacity value is known as the soil water deficit (Davie, 2008). A soil potential of -1500KPa is termed the soil wilting point, below which water can no longer be extracted from the soil by plants, and which has been shown to be roughly equivalent to the adhesion bound water in the soil (Wang and Schmugge, 1980). The water contents at which these soil water potentials occur vary by soil type and the relationship between soil water content and the potential can be described using a soil water characteristic curve (SWCC), which describes the soil water holding capacity (Fredlund and Xing, 1994). This is a function of the pore sizes and distribution as well as the soil chemistry and SSA. Lots of small pores such as in fine grained soils have a higher matric potential and those with a high

surface area and number of soluble ions have greater osmotic potential and hence display a greater holding capacity (Figure 2.7). In practice, hysteresis is displayed in SWCC (Haines, 1930) as water can enter soil pores easier than it can escape due to surface tension creating separate adsorption and desorption curves (Figure 2.8), although for convenience, often only the desorption curve is used (Fredlund and Xing, 1994). Empirical equations have been used to estimate both the soil water characteristic curve and the hydraulic conductivity, using soil textural information to calculate the porosity (Fredlund and Xing, 1994, Fredlund et al., 1994, Rawls et al., 1982, Van Genuchten, 1980) although these may not apply to all soils. A better fit can be obtained by using different equations for different parts of the SWCC based on easily obtained soil textural characteristics to obtain both parameters (Saxton and Rawls, 2006).

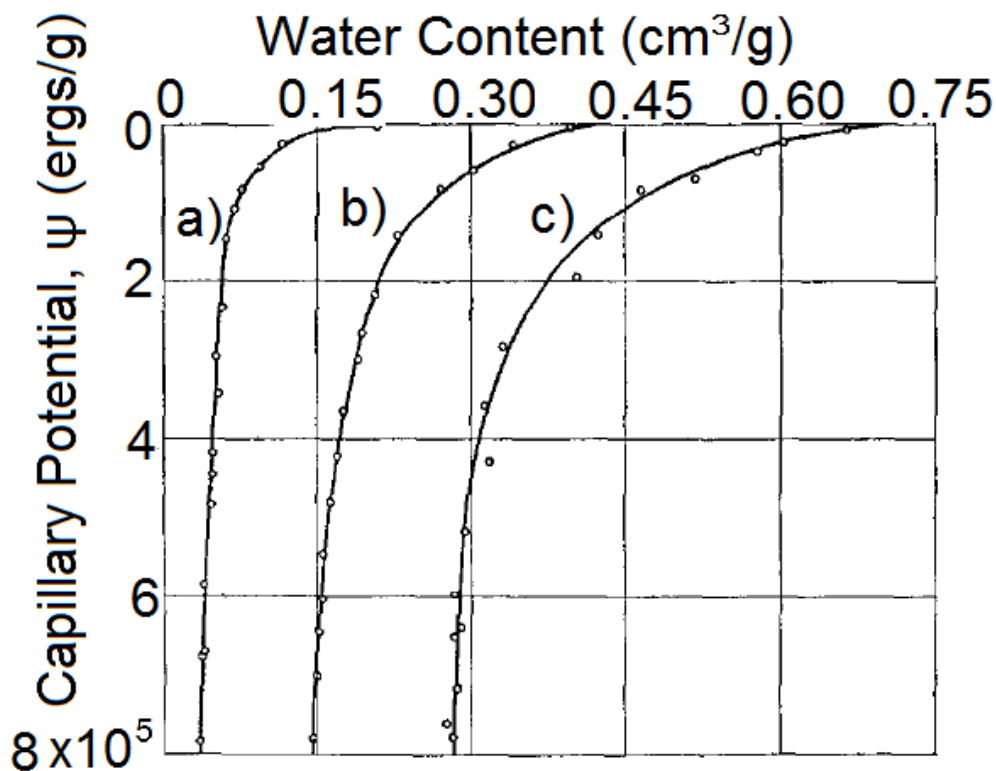


Figure 2.7 The relationship between water content and capillary potential for different soil textures a) Bennet Sandy Soil b) Greenville Loam c) Preston Clay (Richards, 1931).

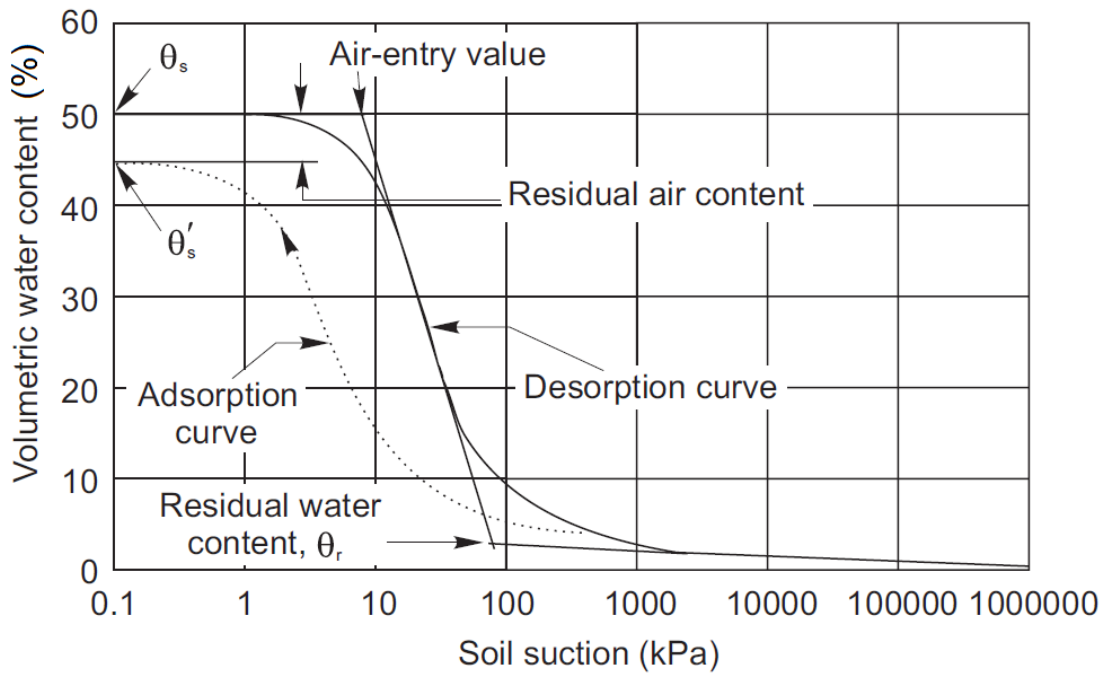


Figure 2.8: SWCC for adsorption and desorption (Fredlund et al., 1994). The saturated water content for wetting cycles (θ'_s) and drying cycles (θ_s) is also shown.

Soil water flows in interconnected pores between solid particles according to the soils hydraulic gradient (difference between soil potentials divided by distance) from areas of high potential to low potential (i.e. from wetter to drier areas) due to a combination of gravity and soil suction (Davie, 2008). The rate at which it moves is proportional to the hydraulic gradient and hydraulic conductivity (K_H) of the soil, determined by the pore size, interconnectivity and antecedent water content, until equilibrium is reached. In saturated soils, the most common equation used to describe water movement is Darcy's law (Equation 2.31).

$$Q = -K_H A \frac{\delta h}{\delta x}$$

2.31

Where Q is the flowrate, A is the cross sectional area of the pores and δh and δx are the difference in water potentials and the distance between them respectively (Davie, 2008). In unsaturated soils, Richards equation is more commonly used, which is a combination of Darcy's law with reference to number of filled pores (Youngs, 1988) affecting the hydraulic conductivity values and potential gradient. The antecedent water content of the soil has a

direct effect on the hydraulic conductivity of the soil. In coarse grained soils, maximum values of K_H exist at saturation before dropping by several orders of magnitude after an abrupt change from unsaturated to saturated soil occurs (Hillel, 1971). By contrast, finer grained soils may have higher K_H values at low water contents allowing flow to persist over a longer time period (Scollar et al., 1990), due to soil swelling closing pores as the soil gets increasingly wet. In extremely dry soils, the presence of air in the pores which creates pressure opposing the hydraulic head until it is dissolved into the water or sufficient pressure is acquired to expel the air from the pores (Davis and De Wiest, 1966). In practice, a combination of this and the size and shape of the pore make water movement not a smooth transmission as predicted by the models above, but a jerky movement as water enters pores and finds stable menisci (Youngs, 1988). Soils are rarely homogenous and a single SWCC and K_H value is rarely a sufficient description of all the different layers which have different soil potentials governing how water moves between them, as soil suction and K_H play a more significant role than gravity (Foth, 1990). The difference in properties between archaeological soils and the SSM also have the potential to affect water movement, although no studies have been found into the effects on lateral water movement due to these properties.

The differences in both soil properties and water content of the different soil layers cause water to flow both down and laterally through the profile as a sharply defined wetting front (Davie, 2008). Water moves through the soil until it meets a layer of lower hydraulic conductivity, usually caused by lower water content and lower pore connectivity where upon water movement becomes primarily lateral. As the surface soil becomes wetter, the water potential gradient between the layers increases until the wetting front continues down the profile. In practice, this means water movement slows down lower down the profile as it takes longer for water from the surface to reach and 'feed' the wetting front (Davie, 2008) which moves in a series of sharp movements. Some authors (Hewlett and Hibbert, 1967, Horton and Hawkins, 1965) have suggested water at the top of the soil profile displaces water at the

bottom, but few field studies have shown this to be true and it has been suggested that such displacement would be largely lateral rather than vertical (Davie, 2008). However, a comparison of a fine grained and a coarse grained soil (Youngs and Poulouvassilis, 1976) suggests that the displacement action is true for fine grained soils but not coarse soils where the top desaturates as the wetting front moves down the profile (Figure 2.9).

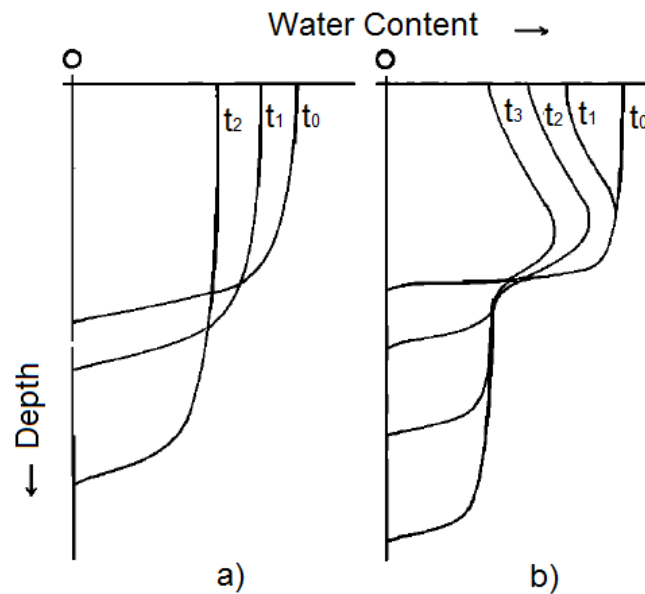


Figure 2.9: The redistribution of water over time after infiltration at t_0 for a) fine grained soils and small depths and b) coarse grained soils and high depths. (Youngs and Poulouvassilis, 1976)

A wide variety of models have been created to simulate infiltration and water movement within the soil (e.g. Green and Ampt, 1911, Horton, 1933, Phillip, 1957) based on hydrological theories and the suction, water content and infiltration rate of the soil. One more recently derived simulation model is the soil-plant-air-water (SPAW) model (Saxton, 2013, Saxton et al., 1974), which uses derived values from the empirical equations for the SWCC and K_H mentioned above to numerically simulate the major hydrological processes in order to determine the water budget in a wide range of soil and climatic conditions (e.g. Saxton and Willey, 2006, Saxton et al., 2006). More recently, the model has also been used to predict changing

geophysical parameters in the soil (Curioni, 2013) for improving utility detection using GPR (see Section 2.8).

2.5. Effects of Geotechnical Soil Properties and Temperature

Due to the importance of soil water behaviour discussed in Section 2.4, a number of other soil properties are important. Research has shown links between a number of geotechnical properties of the soil, used to characterise the soil behaviour, and the geophysical properties (Thomas et al., 2010a, b, Thomas et al., 2007, Thomas et al., 2008b, Wunderlich et al., 2010), which affect the movement and EM behaviour of the soil water. Whilst geophysical properties are rarely recorded, site investigation reports from geotechnical investigations are often more easily accessible for example the UK's National Geotechnical Properties Database (NGPD), managed by the BGS (Thomas et al., 2008b), and provide a useful predictive tool for soil geophysical properties. Heritage remote sensing techniques rely on contrasts between an archaeological feature and the surrounding soil matrix, which are likely to occur because of different soil composition due to differences in formation processes over time. Of particular importance are differences in soil SSA and porosity which affect bound water behaviour and water storage and movement (see Sections 2.4.1 and 2.4.2). Soil is a complex system, and it is rare that only a single one of the effects highlighted in this section would be in action at once, with several complementary and contradictory effects often occurring in a single soil sample.

2.5.1. Soil Texture

In geotechnical engineering, soil texture is described by the sizes of the solid soil particles (Knappett and Craig, 2012), the relative proportions of which make up the particle size distribution (PSD). Particles are categorised as either gravel (>5mm), sand (5 - 0.074mm), silt (0.074 - 0.002mm) or clay (<0.002mm) (BSI, 1990), and the relative proportions used to describe the soil as shown in Figure 2.10.

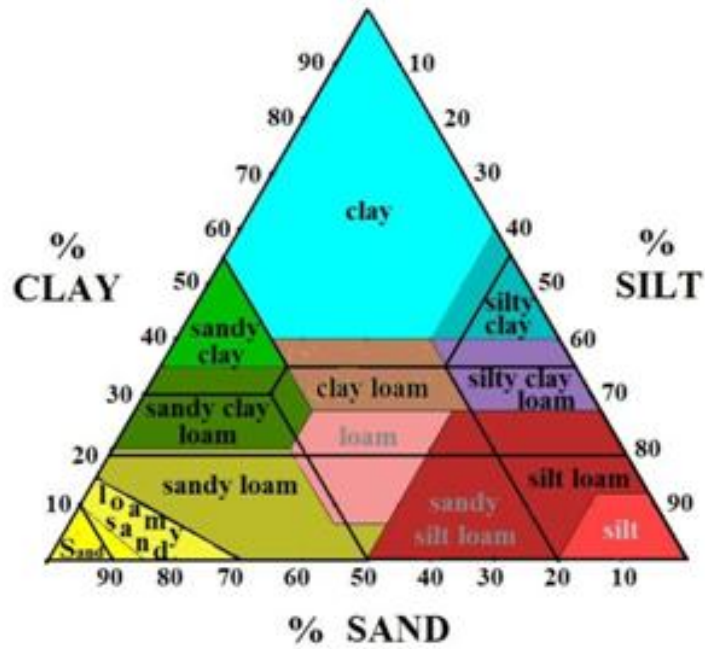


Figure 2.10: Soil texture triangle showing the USDA (colours) and UK-ADAS (lines) soil classifications. Reused under Creative Commons from Wikipedia Commons.

Whilst the differences in the relative dielectric permittivity of particles based on their size is negligible (Gong et al., 2003, Miyamoto et al., 2003) and the particles themselves are both independent of frequency and non-conducting (Heimovaara, 1994, Schneider and Fratta, 2009), fine particles have greater SSA making them important with respect to bound water (Van Dam and Schlager, 2000). A distinction may also be made between clay size particles and those of which also comprise clay minerals which possess platey, tubular or needle like forms (Knappett and Craig, 2012, Mitchell and Soga, 2005) which further increase their surface area. For this reason, the clay percentage is by far the most important textural characteristic in determining bound water, and many authors have found significant dispersion (Heimovaara, 1994) and departures from established VWC-permittivity relationships in fine textured soils (e.g. Bridge et al., 1996, Jacobsen and Schjonning, 1993). The large SSA also has a noticeable effect on measured BEC values due to the greater number of surface charges and ions available for dissolution (Section 2.4.1), meaning that many authors have expressed conductivity as a function of the soil saturation and clay content (Amente et al., 2000, Rhoades et al., 1976).

The relative amounts of different size particles, their shapes and orientations also affect the porosity of the soil affecting water storage and movement (see Section 2.4.2). Whilst if soils were made of a single grain size there would be little effect on total porosity (Foth, 1990), in reality soils are made of a distribution of different grain sizes which affect the overall total porosity and pore size distribution. In general, total porosity increases as smaller grain sizes dominate as larger grains reduce the area in which water can be held within the soil (Rawls et al., 1982), with the addition of large gravel noted to have a significant effect on total porosity (Saxton and Rawls, 2006). However, the sizes of particles also affect the pore size distribution within the soil. Coarse grained soils form fewer but larger pores than fine grained soils (Foth, 1990), giving them a higher hydraulic conductivity but lower total pore space and making their drainage easier whilst lowering their ability to hold water. In addition to the total amount of each particle size, the range of particle sizes is also important. Soils with a broad range of particle sizes have lower porosities than those predominantly made up of single size particles as the smaller particles fill in the spaces between the larger ones (Friedman, 2005, Knoll et al., 1995). Some authors have found that due to the effects of PSD on pore size, that the hydraulic conductivity and water permeability are more dependent on grain size than total porosity (Davis and De Wiest, 1966, Saxton and Rawls, 2006), proving that the size of the pores is the most important factor controlling water movement.

Although often overlooked in favour of grain size, another key component of soil is organic matter (OM), which affects the structure of the soil significantly, even in small amounts and is often found in elevated amounts in archaeological features (Scollar et al., 1990). The large cation exchange capacity of OM gives it the ability to hold water (Gerrard, 2000, Scollar et al., 1990), increasing the holding capacity of the soil and binding water in a manner similar to soil particles, especially at high water contents. Van Dam et al. (2002) found a positive correlation between permittivity measured in the field and OM that was stronger than that with grain size, although the study was limited to soils with low (<1%) clay content. Saxton and Rawls (2006)

identified that OM, whilst important in coarse textures soils, was often masked by the effects of clay in others. OM is also responsible for aggregation of soil particles, lowering the K_H of the soil (Mitchell and Soga, 2005) and the percentage of OM is an important consideration in many predictive infiltration models (e.g. Saxton and Rawls, 2006).

2.5.2. Soil Density

Density is the ratio of a soil's mass to its volume. Two types of density are measured in soils (Knappett and Craig, 2012); bulk density (ρ_b), calculated using the total mass of all soil components (solids, water etc.) and dry density (ρ_d), calculated using the mass of the dry soil. Whilst in practical terms it is easier to measure ρ_b using an undisturbed soil sample, ρ_d is more informative as a means of assessing soil compaction as bulk density relies on the saturation level of the soil, especially in expansive soils.

The relative permittivity of solid soil particles, usually between 3 and 10 but often quoted as 5 for simplification (Heimovaara, 1994), is comparatively high in relation to air (c.1) leading to higher permittivity values in high density soils when dry (Gong et al., 2003, Jacobsen and Schjonning, 1993). However, soils with low dry densities also possess a greater porosity (Boll et al., 1996, Jacobsen and Schjonning, 1993), allowing them to hold more water, and giving higher permittivity and BEC values when saturated (Schneider and Fratta, 2009). These two competing phenomena make the effects of ρ_d on measured relative dielectric permittivity dependent on the water content. Density also has a key importance in determining the SSA of the soil, as increasing the dry density of the soil causes a higher number of particles to be present per unit volume, increasing the SSA (Saarenketo, 1998, Thomas et al., 2010a, b). This increases BEC (Yu and Drnevich, 2004), and increases dispersion due to bound water effects, although these effects can be corrected for by using GWC and dividing the permittivity by dry density (Thomas et al., 2010b) to give a linear relationship between SSA and dispersion. At extremely high or low density, pore size distribution and the degree of saturation may also be

affected, influencing the pore connectivity and subsequent conductive pathways (Archie, 1942, Friedman, 2005).

Opinions on the importance of density on VWC-permittivity relationships vary greatly. Topp et al. (1980) found no noticeable effects on measurements at dry densities between 1.14 and 1.44g/cm³ above the measurement accuracy whereas Ledieu (1986) reported a slight improvement in the accuracy of the VWC-permittivity relationship when density effects were corrected for between 1.38 and 1.78g/cm³. Other authors however have reported significant departures from known relationships, especially on low density or organic soils (Kallner and Lundin, 2001, Roth et al., 1990) and the effects are often reported as being in excess of those caused by soil texture (Dirksen and Dasberg, 1993, Jacobsen and Schjonning, 1993).

2.5.3. Atterberg Limits and Linear Shrinkage

Atterberg limits describe the water content at which the soil is plastic (plastic limit) and able to undergo deformation without cracking or crumbling, and the liquid limit, the water content above which the soil flows like a slurry (Knappett and Craig, 2012). The difference between the two limits (plasticity index) can also be used with the percentage clay content to determine the activity of the clay using Equation 2.32 (Mitchell and Soga, 2005).

$$Activity = \frac{(W_L - W_P)}{\%Clay}$$

2.32

Research has linked the soil liquid limit to the SSA of the soil (Arnepalli et al., 2007, Dolinar et al., 2007, Dolinar and Trauner, 2004, Farrar and Coleman, 1967) which is based on the mineralogy and particle shape of the clay, making it a useful predictor of bound water, and giving different types of soil variable dispersive properties with frequency (Figure 2.11). In addition, the water contents between the two describe the range of water contents found in the ground in normal field conditions (Thomas et al., 2008b).

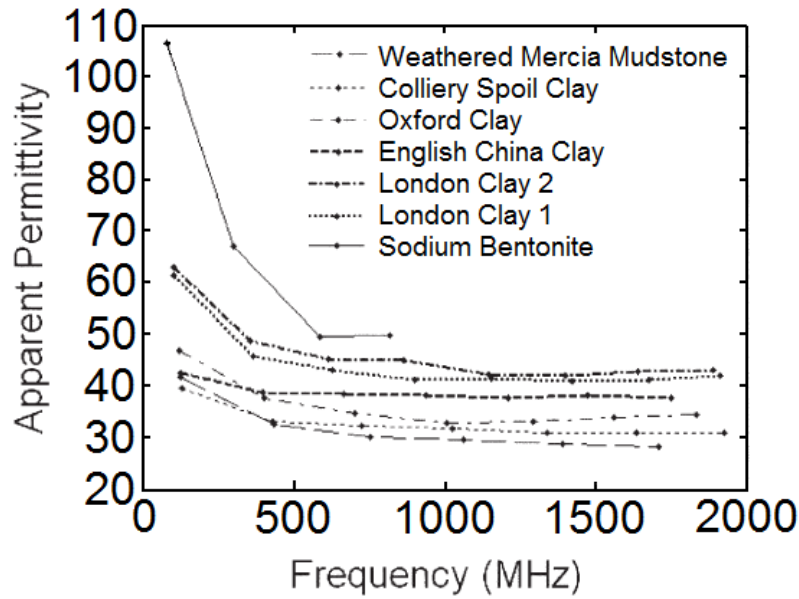


Figure 2.11: Variable dispersion between 0 and 2GHz for different clay types at saturation (Thomas et al., 2008a).

Thomas et al. (2010a) used this relationship to test the frequency dependent properties of a number of saturated fine grained soils with varying liquid limits, finding a linear relationship between the ARDP and the liquid limit at high frequencies (>500MHz) (Figure 2.12) . In addition, the dispersion, defined as the total difference between 100MHz-1GHz, was found to be greater in samples with high liquid limits.

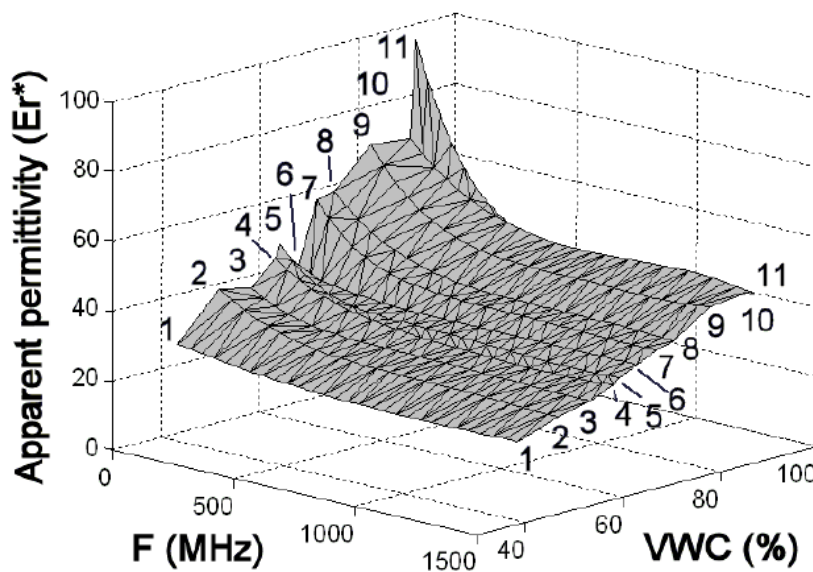


Figure 2.12: Relationship between apparent permittivity and saturated VWC as a function of frequency for soils with different SSA (Thomas et al., 2010a)

In a second paper Thomas et al. (2010b), investigated the ARDP-VWC relationships of two fine grained soils with different SSA over a range of water contents. Different relationships were identified between the three states (friable, plastic and liquid), with the ARDP rising rapidly until the plastic limit was reached whereby a linear relationship between the two was found to exist, which continued until a step change, just above the liquid limit of the soil. Correcting for density effects by dividing by ρ_d proved that dispersion was largely a function of the SSA of the soil, as well as the linear shrinkage which is discussed below.

Linear shrinkage describes the shrinkage of the soil between its liquid limit and dry states.

Whilst the liquid limit has been shown to correlate to intergrain water, linear shrinkage can be correlated to the intersheet water which is responsible for dispersion at low frequencies (Thomas et al., 2010a). A linear relationship between the two has been found, with the accuracy improved by correction for density effects (Figure 2.13).

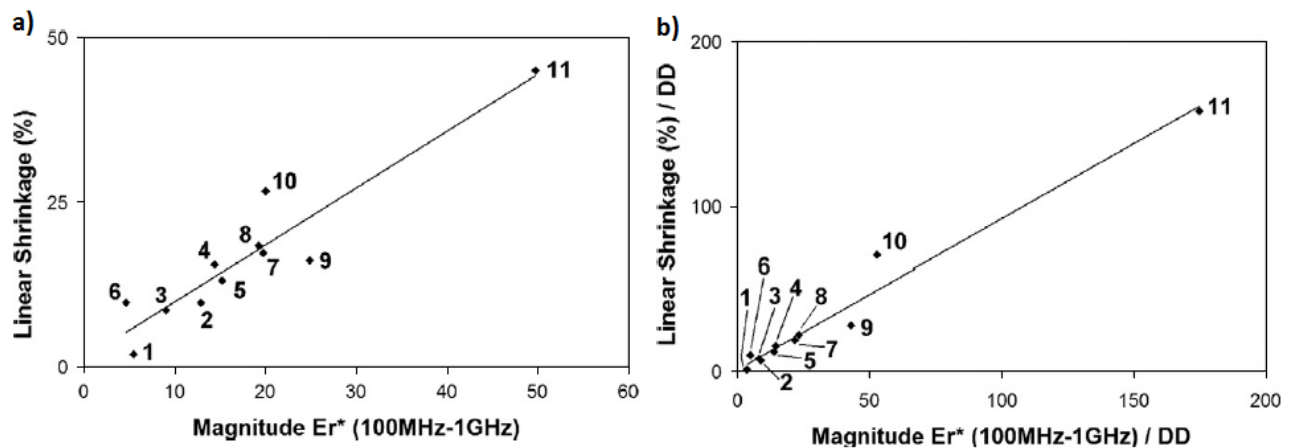


Figure 2.13: a) relationship between linear shrinkage and the magnitude of dispersion between 100Mhz and 1GHz and b) relationship between linear shrinkage and dispersion when corrected by dividing both by dry density (Thomas et al., 2010a)

2.5.4. Effects of Temperature

Temperature within the soil varies both seasonally and diurnally, as well as showing variation between archaeological and background soils, forming the basis of thermal prospection (Scollar et al., 1990). Whilst several authors have reported that in dry soil, EM properties are temperature independent (Gong et al., 2003, Seyfried and Grant, 2007, Skierucha, 2009),

temperature has a significant effect on the behaviour of water in the soil and subsequent measured geophysical properties.

The temperature dependence of the ARDP of water has long been known (Catenaccio et al., 2003, Clark, 1966, Weast, 1986) with a negative relationship between the two observed as thermal randomisation retards the water molecules ability to polarise. Weast (1986) gives the following empirical equation to normalise values to 25°C which has been used by other authors (Or and Wraith, 1999).

$$\epsilon_w(T) = 78.54[1 - 4.579 \times 10^{-3}(T - 25) + 1.19 \times 10^{-5}(T - 25)^2 - 2.8 \times 10^{-8}(T - 25)^3]$$

2.33

Where T is the temperature in °C. The modelled changes in the relative permittivity of water using this model are shown in Figure 2.14, showing a significant variation (10 units) in the temperature range likely to be encountered in soils in the UK (0°C- 30°C).

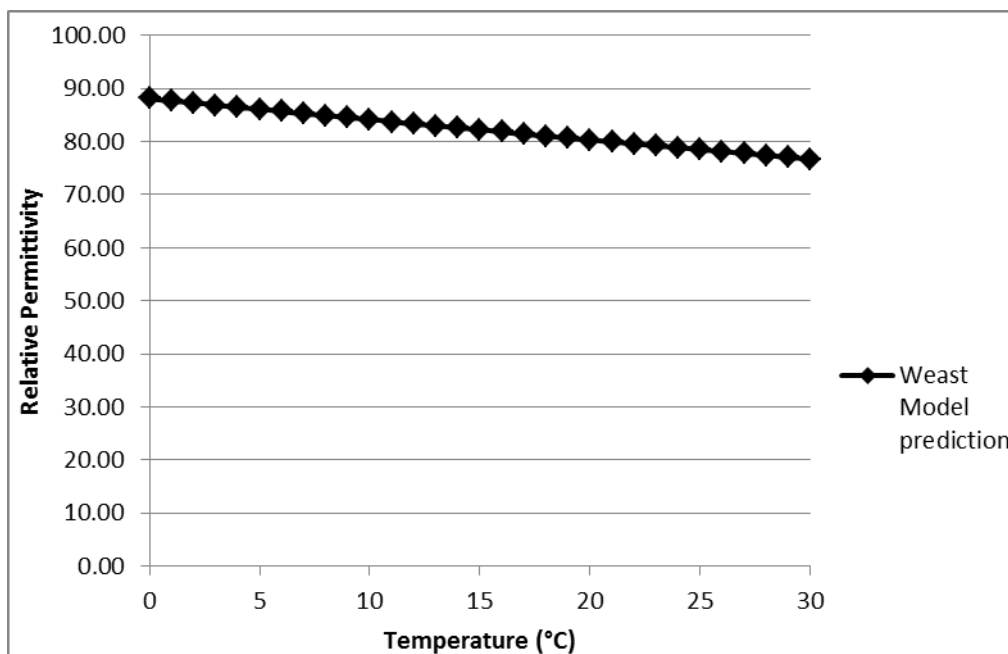


Figure 2.14: The modelled changes in relative permittivity of water between 0°C and 30°C using the Weast (1986) model

Other authors have noted that the ARDP of water drops rapidly below freezing (Hoekstra and Delaney, 1974) although large fractions of water in soil remains as liquid, even at temperatures well below the usual freezing point (Hallikainen et al., 1985). Several authors have suggested a negative temperature dependence of soil permittivity (Curioni, 2013, Gong et al., 2003, Ledieu et al., 1986, Menziani et al., 2003) on coarse grained soils, and temperature corrections based on pure water have been used (Ledieu et al., 1986). However, other authors have found positive relationships or variable responses dependent on water content (Hoekstra and Delaney, 1974, Seyfried and Grant, 2007), especially over soils with high SSA. Wraith and Or (1999) correlated these effects to the bound water fraction and suggested temperature dependence of ARDP in soil was the result of two competing phenomena; the temperature dependence of free water and the release of bound water as temperature increased, which is supported by the water content dependence of the temperature correction found by Gong et al. (2003). The point at which the dominant effect changes, known as the equilibrium water content was closely linked to SSA and attempts have been made to create models of temperature dependence accounting for both effects (Or and Wraith, 1999, Skierucha, 2009). More recently, Chen and Or (2006) suggested that rising temperatures led to the increase of the Maxwell-Wagner relaxation frequency into the MHz range providing an additional complication to the measured ARDP as a function of temperature. Additionally, measurements at 100MHz and 1.4GHz showed dissimilar effects, suggesting that positive dependence was a function of relaxation phenomena rather than a physical release of bound water (Escorihuela et al., 2007), although the large gap between the frequencies measured makes it hard to determine the relationship between temperature, frequency and ARDP.

Temperature dependence of the BEC is far simpler, with a positive correlation reported for almost all soils. The reasons for this are twofold; the lowered viscosity of the water and the increased ion mobility in the soil water (Scollar et al., 1990). The conductivity of any electrolyte with temperature is approximately linear and many authors have suggested

temperature dependent corrections to normalise conductivity values to a standard value, usually 25°C (e.g. Campbell et al., 1948, Sheets and Hendrickx, 1995). However as conductivity is also a function of the number of dissolved ions and the solid phase is generally considered to be negligible or independent of temperature, effects are larger in soils with a higher degree of saturation and higher SSA, such as wet clays.

2.6. Dielectric Mixing Models

As shown in the preceding sections, EM properties of soil are complex phenomenon, with many influencing factors. Providing an exact electromagnetic description for subsurface materials is therefore impossible (Sihvola, 2000) because of the structural complexity and lack of homogeneity in the ground, and mixing models are used to approximate the dielectric response of a soil. A huge number of these mixing models exist within the literature and have been compiled for a number of different frequencies of signal as well as the different physical properties of the soil, some of which are summarised in Table 2.4. A good review of these models was conducted by Van Dam (2005) who described four main types of model: phenomenological, volumetric, empirical and semi-empirical. The strengths and weaknesses of each model type is summarised in Table 2.5.

Table 2.4: A summary of some of the different dielectric models used for soil. Abbreviations are described below.

| | Reference | INPUTS | | | | OUTPUT | CALIBRATION | | | |
|------------------|--------------------------------|-------------------------------|-----------------------------------|------------------|----------------|------------------------|--------------------|-----------------------------------|------------------------------------|--|
| | | Volume/ Textural Inputs | Permittivity Inputs | Water content | Other Inputs | Permittivity Output | Frequency Range | No of different soils | Soil Types Calibrated for | Formula |
| Phenomenological | Debye (1929) | - | $\epsilon_{lf} \epsilon_{\infty}$ | - | τ | $\epsilon' \epsilon''$ | ∞ | - | - | $\epsilon^*(\omega) - \epsilon_{\infty} = \frac{\epsilon_{lf} - \epsilon_{\infty}}{1 + (j\omega\tau)}$ |
| | Cole-Cole (1941) | - | $\epsilon_{lf} \epsilon_{\infty}$ | - | τ, α | $\epsilon' \epsilon''$ | ∞ | - | - | $\epsilon^*(\omega) - \epsilon_{\infty} = \frac{\epsilon_{lf} - \epsilon_{\infty}}{1 + (j\omega\tau)^{1-\alpha}}$ |
| Empirical | Topp et al (1980) | - | - | θ_v | - | ϵ_a | TDR | 4 | Sandy Loam, 2 Clay Loam and 1 Clay | $\theta_v = [-5.3 \times 10^{-2} + 2.92 \times 10^{-2}\epsilon_a - 5.5 \times 10^{-4}\epsilon_a^2 + 4.3 \times 10^{-6}\epsilon_a^3]$ |
| | Ledieu et al (1986) | - | - | θ_v | (pd optional) | ϵ_a | TDR | 1 | Loam | $\theta_v = 5.69\sqrt{\epsilon_a} - 17.58$ ($\theta_v = 5.688\sqrt{\epsilon_a} - 3.38\rho_b - 15.29$) |
| | Curtis (2001) | - | - | θ_v | - | ϵ' | 0.1-1GHz | 3 | Sand to Clay | $\theta_v = 2.37 \times 10^{-4}\epsilon_a^3 - 3.421 \times 10^{-2}\epsilon_a^2 + 2.435\epsilon_a - 2.86$ |
| | Persson et al (2002) | Cl, Om (Si, Sa) | - | θ_v | pd | ϵ_a | TDR | 10 | Sand to Loam | Unknown (Artificial Neural Network) $\theta_v = [3.9 \times 10^{-2} + 3.17 \times 10^{-2}\epsilon_a - 4.5 \times 10^{-4}\epsilon_a^2 + 2.6 \times 10^{-6}\epsilon_a^3]$ |
| | Kallner and Lundin (2001) | - | - | θ_v | | ϵ_a | TDR | 3 (but at different humification) | Peat | |
| | Jacobson and Schjonning (1993) | Cl, Om | - | θ_v | pd | ϵ_a | TDR | 5 | Sandy Soil to Clay Loam | $\theta_v = -7.01 \times 10^{-2} + 3.47 \times 10^{-2}\epsilon_a - 11.6 \times 10^{-4}\epsilon_a^2 + 18.0 \times 10^{-6}\epsilon_a^3$ |
| | Roth et al. (1992) | - | - | θ_v | - | ϵ_a | TDR | 9 mineral, 4 organic, 2 magnetic | Sand to Clay | $\theta_v = -7.28 \times 10^{-2} + 4.48 \times 10^{-2}\epsilon_a - 1.95 \times 10^{-3}\epsilon_a^2 + 3.61 \times 10^{-5}\epsilon_a^3$ (mineral) $\theta_v = -2.33 \times 10^{-2} + 2.85 \times 10^{-2}\epsilon_a - 4.31 \times 10^{-4}\epsilon_a^2 + 3.04 \times 10^{-6}\epsilon_a^3$ (organic) |

| | Reference | Volume/ Textural Inputs | Permittivity Inputs | Water content | Other Inputs | Permittivity Output | Frequency Range | Number of different soils | Soil Types Calibrated for | Formula |
|------------|--------------------------------------|-------------------------------|--|----------------------------|---|------------------------|--------------------|------------------------------|--|--|
| Empirical | Herkelrath et al. (1991) | - | - | θ_v | - | ϵ_a | TDR | 1 | Organic | $\theta_v = \frac{38.2}{\left(\frac{\epsilon_a}{\epsilon_a}\right)} - 0.051$ |
| | Malicki et al. (1996) | - | - | θ_v | ρ_d | ϵ_a | TDR | 18 | Sand to Loam, Organic | $\theta_v = \frac{\sqrt{\epsilon_a - 0.819 - 0.168\rho_b - 0.159\rho_b^2}}{7.17 + 1.18\rho_b}$ |
| | Nadler et al (1991) | - | - | θ_v | - | ϵ_a | TDR | 1 | Silt Loam | $\theta_v = [-725 + 367\epsilon_a - 12.3\epsilon_a^2 + 0.15\epsilon_a^3]$ |
| Volumetric | Roth et al (1990) | V_g, V_s | ϵ_w^*, ϵ_s (estimated), ϵ_g | θ_v | T, η (estimated from ρ_d and soil information), α | ϵ_a | TDR | 13 | Mixtures of Cl, Si, Sa and Om | $\epsilon_w(T) = 78.54[1 - 4.579 \times 10^{-3}(T - 25) + 1.19 \times 10^{-5}(T - 25)^2 - 2.8 \times 10^{-8}(T - 25)^3]$ $\alpha = 0.45$ $\zeta_c = \frac{\epsilon_a}{\epsilon_w}$ $\zeta_w = \frac{\epsilon_w}{\epsilon_w(20^\circ\text{C})}$ $\zeta_s = \frac{\epsilon_s}{\epsilon_w(20^\circ\text{C})}$ $\zeta_g = \frac{\epsilon_g}{\epsilon_w(20^\circ\text{C})}$ $\theta_v = \frac{\zeta_c^\alpha - (1 - \eta) \cdot \zeta_s^\alpha - \eta \cdot \zeta_a^\alpha}{\zeta_w^\alpha - \zeta_a^\alpha}$ |
| | Dobson et al (1985) modified de Loor | V_w, V_g | $\epsilon_{fw}, \epsilon_{bw}, \epsilon_s, \epsilon_g$ | θ_{bw}, θ_{fw} | - | $\epsilon' \epsilon''$ | 1.4-18GHz | 5 | Sandy Loam, Silt Loam, Loam and Silty Clay (details in Halikainen et al (1985)) | $\epsilon_s = (1.01 + 0.44 \rho_s)^2 - 0.062$ $\epsilon'_w = \epsilon_\infty + \frac{\epsilon_{lf} - \epsilon_\infty}{1 + (\omega\tau)^2}$ $\epsilon''_w = \frac{(\epsilon_{lf} - \epsilon_\infty)}{1 + (\omega\tau)^2} + \omega\tau + \frac{\sigma_{eff}}{\omega\epsilon_0}$ $\epsilon_{\infty,w} = 4.9$ $3\epsilon_s + 2V_{fw}(\epsilon_{fw} - \epsilon_s) + 2V_{bw}(\epsilon_{bw} - \epsilon_s) +$ $2V_g(\epsilon_g - \epsilon_s)$ $\epsilon = \frac{3 + V_{fw}\left(\frac{\epsilon_s}{\epsilon_w} - 1\right) + V_{bw}\left(\frac{\epsilon_s}{\epsilon_{bw}} - 1\right) + V_g\left(\frac{\epsilon_s}{\epsilon_g} - 1\right)}{3 + V_{fw}\left(\frac{\epsilon_s}{\epsilon_w} - 1\right) + V_{bw}\left(\frac{\epsilon_s}{\epsilon_{bw}} - 1\right) + V_g\left(\frac{\epsilon_s}{\epsilon_g} - 1\right)}$ |

| | Reference | Volume/ Textural Inputs | Permittivity Inputs | Water content | Other Inputs | Permittivity Output | Frequency Range | Number of different soils | Soil Types Calibrated for | Formula |
|------------|--------------------------------|-------------------------------|---|----------------------------|--|------------------------|--------------------|------------------------------|---|---|
| Volumetric | Or and Wraith (1999) | V_g, V_s | $\epsilon_{fw}, \epsilon_{bw}, \epsilon_s, \epsilon_g$ | θ_{bw}, θ_{fw} | T, f^*, a, d, pd, α | ϵ_a | TDR | 4 | Loamy Sand, Silt Loam and clay | $\epsilon_w(T) = 78.54[1 - 4.579 \times 10^{-3}(T - 25) + 1.19 \times 10^{-5}(T - 25)^2 - 2.8 \times 10^{-8}(T - 25)^3]$ $a = 1621 \text{ \AA}K$ $d = 2.047 \times 10^3 K$ $m = \frac{k}{8\pi^2 r^3 c f^* a}$ $x_{bw}(T) = \frac{-d + T \ln(mT)}{\theta_{bw} = x A_s \rho_b}$ $\alpha = 0.5$ $\epsilon = V_s \epsilon_s^\alpha + V_g \epsilon_g^\alpha + V_{fw} \epsilon_{fw}^\alpha + V_{bw} \epsilon_{bw}^\alpha$ <p style="text-align: center;">OR</p> $\epsilon = \frac{3\epsilon_s + 2V_{fw}(\epsilon_{fw} - \epsilon_s) + 2V_{bw}(\epsilon_{bw} - \epsilon_s) + 2V_g(\epsilon_g - \epsilon_s)}{3 + V_{fw} \left(\frac{\epsilon_s}{\epsilon_w} - 1\right) + V_{bw} \left(\frac{\epsilon_s}{\epsilon_{bw}} - 1\right) + V_g \left(\frac{\epsilon_s}{\epsilon_g} - 1\right)}$ |
| | Birchak et al (1974) | V_g, V_s | $\epsilon_w, \epsilon_s, \epsilon_g$ | θ_v | α | ϵ_a | 4-6GHz | 2 | Limestone, Clay | $\alpha = 0.5$ $\epsilon = V_s \epsilon_s^\alpha + V_g \epsilon_g^\alpha + V_{fw} \epsilon_{fw}^\alpha + V_{bw} \epsilon_{bw}^\alpha$ |
| | Wang and Schmugge (1980) | Sa, Cl | $\epsilon_i, \epsilon_w, \epsilon_s, \epsilon_g$ (both real and imaginary parts. can also use refractive indices) | θ_v | Wt (estimated as WP (from Sand and Clay)), $\eta, \alpha, \sigma, \gamma$ | ϵ^* | 1.4-5GHz | 22 | Sand to Clay | $WP = 0.06774 - 0.00064 \times Sa + 0.00478 \times Cl$ $W_t = 0.49WP + 0.165$ $\gamma = -0.57WP + 0.481$ <p>if: $\theta_v \leq W_t$</p> $\epsilon_{bw} = \epsilon_i + (\epsilon_w - \epsilon_i) \cdot \left[\frac{\theta_v}{W_t}\right] \cdot \gamma$ $\epsilon' = \theta_v \cdot \epsilon_{bw} + (\eta - \theta_v) \cdot \epsilon_g + (1 - \eta) \cdot \epsilon_s$ <p>if: $\theta_v > W_t$</p> $\epsilon_{bw} = \epsilon_i + (\epsilon_w - \epsilon_i) \cdot \gamma$ $\epsilon' = W_t \cdot \epsilon_{bw} + (\theta_v - W_t) \cdot \epsilon_w + (\eta - \theta_v) \cdot \epsilon_g + (1 - \eta) \cdot \epsilon_s$ $\epsilon'' = \epsilon'' + \alpha \theta_v^2$ |

| | Reference | Volume/ Textural Inputs | Permittivity Inputs | Water content | Other Inputs | Permittivity Output | Frequency Range | Number of different soils | Soil Types Calibrated for | Formula |
|----------------|--|-------------------------------|--|------------------|---|-------------------------------|--------------------|------------------------------|---|---|
| Semi Empirical | Peplinski et al (1995b)* *Formula corrected (Peplinski et al., 1995a) | Sa, Cl | $\epsilon_{fw}, \epsilon_{bw}, \epsilon_s, \epsilon_g$ (Calculated) | θ_v | $\alpha, \beta, \omega, \tau, \rho_d, \rho_s$ | $\epsilon' \epsilon''$ | 0.3-1.3GHz | 19 | Mixtures of Cl, Si, Sa and Om | $\epsilon_s = (1.01 + 0.44 \rho_s)^2 - 0.062$ $\sigma_{eff} = 0.0467 + 0.2204\rho_b - 0.4111Sa + 0.6614Cl$ $\epsilon'_{fw} = \epsilon_\infty + \frac{\epsilon_{lf} - \epsilon_\infty}{1 + (\omega\tau)^2}$ $\epsilon''_{fw} = \frac{\omega\tau(\epsilon_{lf} - \epsilon_\infty)}{1 + (\omega\tau)^2} + \frac{\sigma_{eff}(\rho_s - \rho_b)}{\omega\epsilon_0 \rho_s \theta_v}$ $\alpha = 0.65$ $\beta' = 1.2748 - 0.519Sa - 0.152Cl$ $\beta'' = 1.33797 - 0.603Sa - 0.166Cl$ $\epsilon' = 1.15 \left(\left[1 + \frac{\rho_b}{\rho_s} (\epsilon_s^\alpha - 1) + \theta_v^{\beta'} \epsilon'_{fw}{}^\alpha - \theta_v \right]^{\frac{1}{\alpha}} \right) - 0.68$ $\epsilon'' = \left[\theta_v^{\beta''} \epsilon''_{fw}{}^\alpha \right]^{\frac{1}{\alpha}}$ |
| | Dobson et al (1985) | Sa, Cl | $\epsilon_{fw}, \epsilon_{bw}, \epsilon_s, \epsilon_g$ (Calculated) | θ_v | $\alpha, \beta, \omega, \tau, \rho_d, \rho_s$ | $\epsilon' \epsilon'' \sigma$ | 1.4-18GHz | 5 | Sandy Loam, 2 Silt Loam, Loam and Silty Clay (details in Halikainen et al (1985)) | $\sigma_{eff} = -1.645 + 1.939\rho_b - 2.25622Sa = 1.594Cl$ $\epsilon'_{fw} = \epsilon_\infty + \frac{\epsilon_{lf} - \epsilon_\infty}{1 + (\omega\tau)^2}$ $\epsilon''_{fw} = \frac{\omega\tau(\epsilon_{lf} - \epsilon_\infty)}{1 + (\omega\tau)^2} + \frac{\sigma_{eff}(\rho_s - \rho_b)}{\omega\epsilon_0 \rho_s \theta_v}$ $\alpha = 0.65$ $\beta' = 1.2748 - 0.519Sa - 0.152Cl$ $\beta'' = 1.33797 - 0.603Sa - 0.166Cl$ $\epsilon' = \left[1 + \frac{\rho_b}{\rho_s} (\epsilon_s^\alpha - 1) + \theta_v^{\beta'} \epsilon'_{fw}{}^\alpha - \theta_v \right]^{\frac{1}{\alpha}}$ $\epsilon'' = \left[\theta_v^{\beta''} \epsilon''_{fw}{}^\alpha \right]^{\frac{1}{\alpha}}$ |

| | Reference | Volume/ Textural Inputs | Permittivity Inputs | Water content | Other Inputs | Permittivity Output | Frequency Range | Number of different soils | Soil Types Calibrated for | Formula |
|----------------|--------------------------|-------------------------------|---|------------------|--|------------------------|-----------------------|------------------------------|---------------------------------|--|
| Semi Empirical | Miranov et al. (2009) | Cl | $\epsilon_{if} \epsilon_{\infty}$ (Calculated) | θ_v | Wt, ω , τ , σ_{eff} (Calculated) | $\epsilon' \epsilon''$ | 45 MHz to 26.5 GHz | 15 | Sand to Clay | $W_t = 0.02863 + 0.30673 \times 10^{-2} Cl$ $\sigma_{bw} = 0.3112 + 0.467 \times 10^{-2} Cl$ $\sigma_{fw} = 0.3631 + 1.217 \times 10^{-2} Cl$ $\epsilon_{if, fw} = 100$ $\epsilon_{if, bw} = 79.8 - 85.4 \times 10^{-2} Cl + 32.7 \times 10^{-4} Cl^2$ $\epsilon_{\infty, w} = 4.9$ $\tau_{fw} = 8.5 \times 10^{-12}$ $\tau_{bw} = 1.062 \times 10^{-11} + 3.450 \times 10^{-12} \cdot 10^{-2} Cl$ $\epsilon'_w = \epsilon_{\infty} + \frac{\epsilon_{if} - \epsilon_{\infty}}{1 + (\omega\tau)^2}$ $\epsilon''_w = \frac{(\epsilon_{if} - \epsilon_{\infty})}{1 + (\omega\tau)^2} + \omega\tau + \frac{\sigma_{eff}}{\omega\epsilon_0}$ $RI_w = \sqrt{(\epsilon')^2 + (\epsilon'')^2} + \epsilon'$ $RI_s = 1.634 - 0.539 \times 10^{-2} Cl + 0.2748 \times 10^{-4} Cl^2$ $AC_s = 0.03952 - 0.04038 \times 10^{-2} Cl$ <p>if: $\theta_v \leq W_t$</p> $\epsilon' = (RI_s + (RI_{bw} - 1)\theta_v)^2$ $\epsilon'' = (AC_s + AC_{bw}\theta_v)^2$ <p>if: $\theta_v > W_t$</p> $\epsilon' = (RI_s + (RI_{bw} - 1)W_t + (RI_{fw} - 1)(\theta_v - W_t))^2$ $\epsilon'' = (AC_s + AC_{bw}W_t + AC_{fw}(\theta_v - W_t))^2$ |

PERMITTIVITY VALUES: ϵ_a : Apparent Permittivity, ϵ^* : Complex Permittivity, ϵ' : Real Permittivity, ϵ'' : Imaginary Permittivity

PERMITTIVITY INPUTS: ϵ_s : soil fraction, ϵ_g : air, ϵ_w : water ϵ_{bw} : bound water, ϵ_{fw} : free water, ϵ_w^* : water compensated for temperature, ϵ_i : Ice, ϵ_{if} : Static permittivity, ϵ_{∞} : permittivity at infinite frequency, $\zeta_{s,w,g}$ dielectric numbers relative to water at 20°C of the soil, water, and air soil phases

VOLUMES: V_g : Volume of air, V_s : Volume of solid

WATER CONTENTS: θ_v : Volumetric water content, θ_g : gravimetric water content

SOIL PROPERTIES INPUTS: Sa: Sand, Cl: Clay, Om: Organic matter, WP: Wilting Point, η : porosity, ρ_d : Dry density, A_s : specific surface area

OTHER INPUTS: T: Temperature, ω : Angular frequency, α : Empirical factor, β : Empirical factor, TDR: TDR range of frequencies (0.01-1.5GHz) σ_{eff} : effective conductivity f^* : cutoff frequency between free and bound water, x_{bw} : Thickness of the bound water layer in Å

OTHER SYMBOLS: WP: Wilting Point W_t : transition water content, γ : Empirical factor, RI: Refractive Index, AC; Attenuation Coefficient

Table 2.5: The strengths and weaknesses of the different model types

| MIXING MODEL TYPE | STRENGTHS | WEAKNESSES |
|-------------------------|---|--|
| Effective Medium Models | Provide an accurate description of physical relationships | Geometry effects hard to determine |
| Volumetric | Relate dielectric constant to exact effects | Need very good information about soil properties Most of them require bound and free water quantities |
| Phenomenological | Provide an accurate description of physical relationships | Very complicated to implement for heterogeneous and multiphase materials |
| Empirical | Easy to implement | Have no physical basis Only valid for the soils used to calibrate them |
| Semi Empirical | Only requires very basic information | |

The main problem with all the models presented is one of comparison; many have been developed using different instruments and on a limited range of soils (Curtis, 2001), making them difficult to compare due to differences in the frequency range and soil mineralogy and properties (Wensink, 1993), and no universal calibration exists. For maximum accuracy, soil specific calibration is still the preferred option (Evet, 2003), although this method is time consuming and has little applicability for other soil studies.

2.6.1. Phenomenological Models

Phenomenological models are those which take into account the complex molecular interactions in order to understand the frequency dependent properties of the soil based on relaxation physics. Perhaps the most famous phenomenological models are the Debye (1929) model and the Cole-Cole (1941) model which relate relaxation times to the permittivity at

specific frequencies based on the relaxation times. Some models such as the Cole-Cole model also allows an empirical fitting parameter describing the spread of different relaxations which vary according to soil type (Arulanandan and Mitchell, 1968). This means that, whilst these models have the advantage of providing an exact description of the dielectric behaviour of the soil, specific calibration to determine this factor is often required, making it difficult to use these models widely over different soil types (Van Dam et al., 2005).

2.6.2. Volumetric Mixing Models

Volumetric models are those which are a weighted sum of the dielectric properties of each of the components (i.e. air, water, soil) which make up the soil based on their volumes. In its simplest form, this is calculated using Equation 2.34.

$$\varepsilon = \sum_{i=1}^n V_i \varepsilon_i$$

2.34

Where V_i and ε_i are the fractional volume and permittivity of each constituent respectively. However such an approach rarely gives satisfactory results due to the geometric distribution of the different soil constituents and interactions between them (Sihvola, 2000) and some information on the microstructure is desirable. One solution to this is to add an exponential term (α) which varies between -1 (perpendicular layers) and +1 (parallel layers) to characterize the structure and distribution of the phases (Equation 2.35).

$$\varepsilon^\alpha = \sum_{i=1}^n V_i \varepsilon_i^\alpha$$

2.35

Due to the random nature of distribution, perhaps the most popular value for α is 0.5 (Birchak et al., 1974, Heimovaara et al., 1994), turning permittivity values into refractive indices. Roth et al. (1990) suggested a value of 0.46 for a three phase model, whereas 0.65 has been

suggested for a four phase model including bound water (Dobson et al., 1985). Brovelli and Cassiani (2008) have suggested that the exponent was related to the geometry and distribution of the pores, and therefore a constant value for all soils may not be appropriate.

Another approach is to use effective medium models (e.g. De Loor, 1968, Friedman, 1998, Sihvola, 1989) are those which calculate the effective or apparent permittivity from a background permittivity and add its inclusions. Important considerations are the size of the inclusions which must be considerably smaller than the wavelength of the EM signal for the effective permittivity assumption to remain valid (Sihvola, 1989), and their shape and density which influences their dielectric behaviour and scattering effects. The complexity of calculations with irregular shaped inclusions means that geometry often has to be idealised or simplified to make them work to simple shapes such as spheres or ellipsoids (Sihvola, 2000). In practice, the lack of information about geometry have made these difficult to implement on heterogeneous or multiple phase materials, and their use in predicting soil properties is rare (Van Dam et al., 2005).

Whilst volumetric models provide a good description of physical phenomena, the chief drawbacks of these models are the need for a detailed knowledge of the fractional amounts and permittivity of the different components which are often unknowns, and the failure to provide information on the frequency dependence of the effective permittivity. For this reason, many of these are determined empirically using semi empirical mixing models (see Section 2.6.4).

2.6.3. Empirical Mixing Models

Empirical models are those which relate the permittivity to the water content on a purely mathematical basis by fitting an expression to a particular dataset, resulting in a calibration specific to the physical characteristics of the soil (Jones et al., 2002). They are normally produced by soil specific calibration, although some are widely used, especially in TDR

research, such as the Topp et al. (1980) model and Ledieu et al. (1986) model. Whilst empirical models are easy to apply, they lack an exact physical description of the processes within the soil, and fail to account for changes in the soils geotechnical properties other than the water content (Brovelli and Cassiani, 2008, Wunderlich et al., 2010), which can have significant effects on dielectric properties (see Section 2.5). For this reason, they are often found to lose accuracy when used on soils with different properties to those used to derive the relationship, especially fine grained soils, those with low density or high organic contents, and when water content falls outside the original range of measured water contents (Černý, 2009) or permittivity is measured at an alternative frequency. To counter this, special models have been created for specific soils including peat (Kallner and Lundin, 2001), by inclusion of terms such as soil texture (Hallikainen et al., 1985, Wang and Schmugge, 1980), organic matter or density (Ju et al., 2010, Malicki et al., 1996), or by usage of semi empirical models (Section 2.6.4). An alternative to using a soil specific calibration is to input the parameters into an artificial neural network (Persson et al., 2002) which has the advantage of improving accuracy, although relationships are still only valid for the range of soils used to calibrate and care must be taken to avoid “overtraining” relationships.

2.6.4. Semi Empirical Mixing Models

Semi empirical models are hybrid models, based on the volumetric and phenomenological models described above, but have additional empirical fitting parameters, calculated from other soil properties. This gives these models both the advantage of describing physical relationships, as well as the flexibility to implement these models without the need for exact measurements of each material phase, based on easily accessible data (Van Dam et al., 2005). Hilhorst et al. (2001) used soil texture to calculate matric pressure which was used with the Debye model to calculate frequency dependent permittivity. In an alternative approach, Dobson et al. (1985) used soil textural information and density to derive a 4 phase mixing model which has since been extended to lower frequency ranges using a linear adjustment

(Peplinski et al., 1995a, b). More recently, Mironov et al. (2004) developed a generalised model based on the refractive index and tested it over a larger number of soils (Mironov et al., 2009) and found a high level of accuracy using only the clay percentage as an input. In addition to being easy to implement with minimal prior information, an additional advantage is the ability of the above mentioned models to predict the real and imaginary permittivity separately, providing scope for analysis of dielectric properties of wet soil and interactions with signals used by heritage detection techniques.

2.7. Techniques for Soil Property Determination

As discussed in Section 2.4, variations in geophysical properties (ARDP, BEC) are largely caused by changes in water content of the soil, with the behaviour of the water being affected by the soil's geotechnical properties and temperature (Section 2.5). The most accurate method for determining water content remains the oven drying method (BSI, 1990) used for laboratory tests, although the technique is both destructive and labour intensive, rendering it unsuitable for a long term monitoring project in the field. Different instruments, which infer water content using known relationships with surrogate properties of the soil, have therefore been developed to overcome this, and some of the different methods are summarised in Table 2.5. However, each of these methods has its own relationships, strengths and weaknesses. The main consideration when choosing a method is the level of accuracy desired, which is affected by the relationship between the surrogate parameter and water content, which is calibrated for a particular range and set of soil conditions and may also be affected by changes in other properties, especially temperature. Another consideration is the volume of soil measured by a technique which must be above a point known as the representative elemental volume, below which variability of soil properties varies drastically with different soil types and measurement method (IAEA, 2008, Topp, 2003), and measurements may no longer be applicable at a field scale.

Table 2.6: A summary of surrogate instruments for water content determination (IAEA, 2008).

| | Method | Surrogate Measurement | Explanation |
|----------------|--|---|---|
| Nuclear | Neutron moisture meter | Count of slow neutrons around a source of fast neutrons | A radioactive source emits fast neutrons (5 MeV), which lose energy as they collide with other atoms, in particular hydrogen. The surrogate is the concentration of slow neutrons. Since the only rapidly changing source of hydrogen in the soil is water, θ_v can be calibrated vs. the count of slow neutrons. |
| Thermal | Thermal sensors | Heat conductivity or heat capacity of the soil | A pulse of heat is generated and the subsequent rise or fall in temperature of adjacent soil is measured over time. Soil is a poor conductor of heat, and water a good one, so the amount of heat or rate of heat transmission is closely related to θ_v . |
| EM | Time domain reflectometer (TDR) | Travel time of an electromagnetic pulse | A fast rise time electromagnetic pulse is injected into a waveguide inserted into or buried in the soil. The time required for the pulse to travel along the metal rods of the waveguide is determined by the bulk electrical permittivity of the soil. The θ_v is a major factor influencing the bulk permittivity. True TDR involves capture of a waveform and analysis to find the travel time of the highest frequency part of the pulse |
| | Campbell Frequency Domain Reflectometry | Repetition time for a fast rise time electromagnetic pulse | See TDR sensors; same, except reliance on reflected pulse reaching a set voltage rather than waveform analysis causes the method to be more influenced by BEC and temperature. |
| | Capacitive sensors | Frequency of an oscillating circuit | An oscillating current is induced in a circuit, part of which is a capacitor that is arranged so that the soil becomes part of the dielectric medium affected by the electromagnetic field between the capacitor's electrodes. The θ_v influences the electrical permittivity of the soil, which in turn affects the capacitance, causing the frequency of oscillation to shift. |
| | Conductivity sensors (e.g., granular matrix sensors and gypsum blocks) | Electrical conductivity of a porous medium in contact with the soil | An alternating current voltage is placed on two electrodes in a porous material in contact with the soil, and the amount of current is a measure of the conductivity and amount of water in the porous material between the electrodes. These are used for estimation of soil water tension (suction), not θ_v . |
| Other | Tensiometers | Matric and gravitational soil water potential components | Capillary forces retaining water in the soil pores are connected through the soil water to water in a porous cup connected to a tube filled with water. This generates a negative pressure within the tube, which can be measured with a vacuum gauge. These are used for estimation of soil water tension (suction), not θ_v . |

A number of reviews of the different methods have been conducted (Gardner, 1986, IAEA, 2008, Robinson et al., 2003a, Topp, 2003). Traditionally, neutron probes have been the preferred method owing to their high accuracy (Evetts and Steiner, 1995). However, the potential hazard from radiation which makes them unsuitable for unattended measurements (Topp, 2003) and use in the near surface, and the difficulty in multiplexing multiple probes with a single logger make implementation for a study with a high temporal or spatial sampling strategy problematic. Nevertheless, they remain a preferred option for a number of applications where high accuracy is desired, or for profiling the deep surface or soils with high BEC values (Robinson et al., 2003a) as well as for calibrating other surrogate methods (Gardner, 1986, Noborio, 2001).

Perhaps the area which has received the most attention in recent years are EM methods (e.g. TDR, capacitance probes, GPR etc.) which have become widespread as understanding of soil EM interactions improve (Topp, 2003). Although the operating principles vary, most of these rely on estimating one of the EM properties of the soil, usually ARDP, and correlating it to VWC using the mixing models discussed in Section 2.6. The main drawback to these methods is that they are affected by temperature, soil salinity and magnetic materials in the soil for the reasons highlighted in Section 2.3. In addition, the wide range of operating frequencies and principles make comparison between different methods difficult as variable values of EM properties are measured, especially in dispersive soils, although some attempts to compare methods have been made (Blonquist et al., 2005, Jones et al., 2005). Low frequency methods (<100MHz) such as capacitance probes have been found to give higher values of apparent relative dielectric permittivity (ARDP; ϵ_a) (Logsdon, 2008) affecting mixing models which assume $\epsilon_a = \epsilon'$ due to the effects of Maxwell-Wagner polarisation (Chen and Or, 2006, Jones and Or, 2004). In addition, these methods have been found to be more responsive to the effects of soil type, BEC (Campbell, 1990, Chandler et al., 2004) and temperature (Seyfried and Grant, 2007) than higher frequency methods. For this reason, it has been suggested that VWC

estimates are more accurate when measured at frequencies above 500MHz (Evelt and Parkin, 2005, Kelleners et al., 2005) where these effects are less apparent.

GPR has been extensively used in recent years for estimating VWC at field scale (e.g. Lambot et al., 2008, Lunt et al., 2005, Strobbia and Cassiani, 2007) due to its ability to cover large areas.

Several methods have been used for determining ARDP from the travel time of the signal including velocity estimation using reflection from reflectors at a known depth (Grote et al., 2002), multi offset methods such as common midpoint (Weiler et al., 1998) and wide angle reflection or by using borehole transillumination (Conyers and Lucius, 1996). A review of some of the different methods was conducted by Huisman et al. (2003a) which highlighted some of the difficulties with accurately interpreting the data from each other these methods. The main drawbacks of GPR for a long term study of VWC are an undefined measurement volume (Huisman et al., 2002) and its lack of automation which makes the method labour intensive.

Other techniques such as ThermoTDR, which rely on the different thermal properties of water, are still in a state of relative infancy, and unresolved problems with changing soil contact and fluctuating ambient temperature (Ren et al., 2005) make them currently problematic for field deployment. In one of the most recent reviews (IAEA, 2008), it was found that only neutron probes and TDR gave acceptable accuracy for field water balance studies, with other EM methods widely affected by the problems highlighted above.

2.7.1. TDR

TDR units consist of a high frequency pulse generator, a voltage sampling circuit with a high temporal resolution and an oscilloscope (Figure 2.15). Wide bandwidth pulses are generated using a fast rise time (c.200ps) (Cataldo et al., 2007) and transmitted through a coaxial cable. A proportion of the energy is reflected from impedance mismatches (see Section 2.3.4) which is sampled at high speed to give a graph of reflected signal over time. Knowledge of the propagation velocity in the cable allows conversion of the time to apparent length, whereas

measurement over a probe of defined length allows the velocity of the wave to be estimated and used to calculate ARDP.

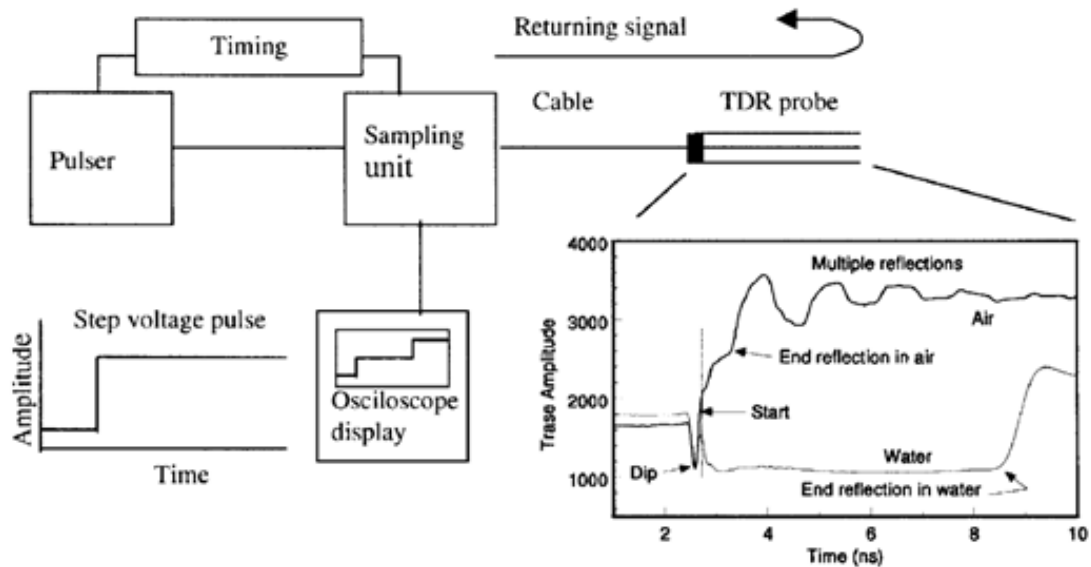


Figure 2.15: A schematic diagram of the TDR main components. The window on the right illustrates two waveforms, one in air and one in water (Robinson et al., 2003a).

TDR was originally developed as a technique for finding breaks in cables (Černý, 2009) by mapping changes in impedance as a function of apparent length, before being used to determine the dielectric properties of simple alcohols (Fellner Feldegg, 1968).

Experimentation throughout the 1970s using this technique determined the link between VWC and permittivity (e.g. Hoekstra and Delaney 1974) culminating in the seminal work by Topp et al. (1980). An empirical link was determined between the VWC and ARDP measured by the TDR (Equation 2.36) was tested over a range of mineral and organic soil with variable textures and stated as independent of temperature, soil type and density over the measured range.

$$VWC = -5.3 \times 10^{-2} + 2.92 \times 10^{-2} \epsilon_a - 5.5 \times 10^{-4} \epsilon_a^2 + 4.3 \times 10^{-6} \epsilon_a^3$$

2.36

Where ϵ_a is the ARDP measured by the TDR. Despite initial scepticism towards the universality of the relationship, especially from the remote sensing community (Topp et al., 2003), the relationship has become widely used and, along with the relatively low cost and ease of use of

the equipment, contributed to the widespread use of TDR, especially in agriculture (Jones et al., 2002). However, the widespread use of the equation has led to the discovery of deviations in the relationship on dispersive soils, such as those with very low densities, high organic contents or significant clay fractions (Bridge et al., 1996, Herkelrath et al., 1991, Jacobsen and Schjonning, 1993, Roth et al., 1990, Wang and Schmutge, 1980), and other models and empirical relationships have been created (see Section 2.6) to meet these needs. Nevertheless application of the Topp et al. (1980) model remains the standard to which other models are compared and the simplest method for determining VWC with many commercially available water content sensors using the model or a variant (e.g. IMKO GmbH, 2012).

Further work on the TDR method followed (Topp et al., 1982a, b, 2003) overcoming early scepticism and bringing the technique into a state of maturity (Topp, 2003). Other important advances included the development of multiplexers to control multiple probes (Baker and Allmaras, 1990, Evett, 1998, Heimovaara and Bouten, 1990), automated logging (Evett, 2000a) allowing rapid and unattended measurements, the determination of BEC (Dalton et al., 1984, Zegelin et al., 1989), and improvements to waveform interpretation (Evett, 2000b, Timlin and Pachepsky, 1996) and probe calibrations (Bechtold et al., 2010, Huisman et al., 2008, Robinson et al., 2003b) improving the accuracy of the technique for determination of dielectric properties. Since these experiments, the technique has been widely used for experiments in geotechnical, hydrological and geophysical studies including tracking solutes (Amente et al., 2000), infiltration studies (Bachmair et al., 2009, West and Truss, 2006), contaminated land studies (Cataldo et al., 2002), monitoring the suitability of the soil for GPR (Curioni et al., 2012), slope monitoring (Kim and Kim, 2007) and flood prediction (Menziani et al., 2003).

Modern TDR units possess good accuracy for VWC determination (<2% error) (Jones et al., 2002), and operate at frequencies similar to GPR (1MHz-1GHz) (Chen and Or, 2006, Huisman et al., 2003b, Weiler et al., 1998) making them useful for comparisons to heritage detection

techniques and making them relatively insensitive to temperature, BEC and soil type which affect low frequency techniques.

2.7.2. TDR operating principles

ARDP is determined by measuring the velocity of an EM pulse transmitted through a coaxial cable and into a probe which is inserted into the sample in question. The frequency dependent velocity of an EM pulse is determined by Equation 2.37 (Topp et al., 2000).

$$v(f) = \frac{c}{\sqrt{\frac{\epsilon' \mu}{2} \left(1 + \sqrt{1 + \left\{ \frac{[\epsilon_p'' + \frac{\sigma_{dc}}{\omega \epsilon_0}]}{\epsilon'} \right\}^2} \right)}}$$

2.37

Where $\left\{ \frac{[\epsilon_p'' + \frac{\sigma_{dc}}{\omega \epsilon_0}]}{\epsilon'} \right\}^2$ is known as the loss tangent. Since dipolar losses are usually considered to be minimal at TDR frequencies in soils (Topp et al., 1980) and magnetic permeability is usually not significantly different to unity (Robinson et al., 2003a, Topp et al., 1980), the loss tangent is usually far less than one and this equation is usually simplified to Equation 2.38 for low conductivity materials.

$$v = \frac{c}{\sqrt{\epsilon_a}}$$

2.38

Where ϵ_a is ARDP, derived from measured velocity, so termed both because it is a composite value of all of the soils constituents and, as loss mechanisms are largely ignored for the purposes of calculations, the effects of conductivity and dipolar losses are included in the response. For most practical purposes it is considered to be equal to the real part of permittivity but it is clear from combining Equations 2.37 and 2.38 it is equal to Equation 2.39 (Robinson et al., 2003a).

$$\varepsilon_a = \frac{\varepsilon' \mu}{2} \left(1 + \sqrt{1 + \left\{ \frac{\left[\varepsilon_p'' + \frac{\sigma_{dc}}{\omega \varepsilon_0} \right]^2}{\varepsilon'} \right\}} \right)$$

2.39

In cases of high imaginary permittivity values due to significant dielectric relaxations from bound water or high conductivity, travel times are therefore increased and higher ARDP values are recorded.

Reflections in a coaxial transmission line such as a TDR circuit occur at changes in impedance, according to Equation 2.40 (Yanuka et al., 1988) and a waveform is recorded from the ratio of the reflected to output signal (reflection coefficient; Γ) versus time, or more usually due to TDR's original use in cable testing, apparent distance derived from a defined propagation speed.

$$\Gamma = \frac{Z_s - Z_{out}}{Z_s + Z_{out}}$$

2.40

Where Z_s is the impedance of the sample and Z_{out} is the output impedance of the TDR unit and probe coaxial cable. Impedance changes are caused both at both the head of the probe (x_1) where the wire spacing between the central conductor and outer wires is increased and at the end of the probe (x_2) which can be identified on the waveform (Figure 2.16). Several different methods have been developed for locating these points including using the meeting points between tangents from both the end reflection and downward limb (duel tangent) or using the tangent from the end reflection and a localised minimum (single tangent). Comparison of the two methods by Timlin and Pachepsky (1996) concluded that the single tangent method provided a more accurate calibration equation for VWC determination, although Or and Wraith (1999) found the duel tangent method preferable when the BEC was high. An

alternative to fitting tangents is to use the derivative method (e.g. Cataldo, 2008), which uses peaks in the derivative of the waveform to identify the start and end reflections, and was shown to agree best with the effective measurement frequency by Robinson et al. (2005b). Some of the main methods are shown in Figure 2.16 and form the basis of automated waveform interpretation programs (e.g. Campbell Scientific, 2009, Evett, 2000b).

The velocity of the wave can be determined is determined from the travel time of the wave in the probe using Equation **Error! Reference source not found.** and a calibrated electrical length of the probe (L_{cal}) which is usually similar to the actual length but may differ due to effects of a fringing field (Robinson et al., 2003b) on the ends of the rods.

$$v(f) = \frac{2L_{cal}}{t}$$

2.41

The electrical length is usually determined using samples with known ARDP values, such as air by shorting the probe at the top and bottom of the rods (see Robinson et al., 2003b), or by taking measurements in water and fixing the probe start at the apex of the bump (Feng et al., 1999, Or et al., 1998). Robinson et al. (2003b) showed the air-water method, proposed by Heimovaara et al. (1993) whereby measurements in both air and water are used to determine travel time in the sensor, gives the most accurate results, especially in soil with layers of varying VWC. Combining Equation 2.39 and Equation **Error! Reference source not found.** shows that the ARDP can therefore be calculated using Equation **Error! Reference source not found.**

$$\varepsilon_a = \left(\frac{ct}{2L_{cal}} \right)^2$$

2.42

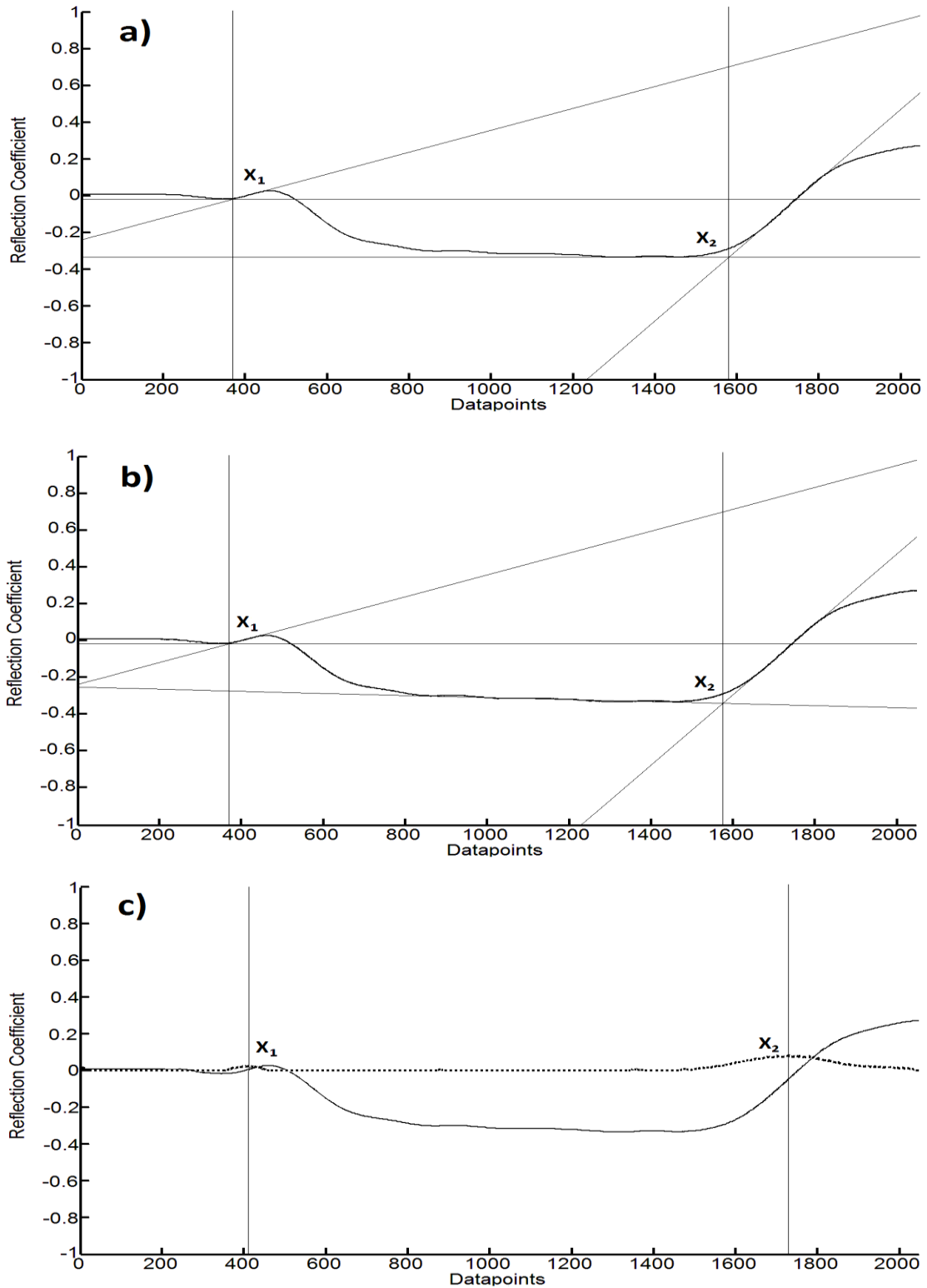


Figure 2.16: Some of the different wave interpretation methods on TDR waveforms taken in water. a) Single tangent b) Dual Tangent c) Derivative method (derivative shown as dotted line)

The difference in length between x_1 and x_2 can also be expressed as the apparent length of the measurement (L_A) as the relative propagation velocity (v_p) (ratio between the speed of light and actual velocity) is usually assumed to be one to simplify analysis. In practical terms therefore it is convenient to determine the permittivity using the L_A and L_{cal} values (Equation 2.43) (Jones et al., 2002).

$$\varepsilon_a = \left(\frac{x_2 - x_1}{v_p L} \right)^2 = \left(\frac{L_A}{L_{cal}} \right)^2$$

2.43

TDR can also be used to determine BEC using the signal reflection coefficient amplitude to measure the amount of energy lost from the pulse, a method first proposed by Dalton et al. (1984). Several methods exist including using multiple reflections to estimate the attenuation fraction from the return energy (Topp et al., 1988, Yanuka et al., 1988), and measuring the reflected to incident voltage at the probe sample interface (Dalton and van Genuchten, 1986). However, these measurements are of effective conductivity and include the effects of polarisation losses which can cause overestimation in dispersive soils. A popular method is the Giese-Tiemann (1975) method for thin sections, which has become the standard method and demonstrates the best accuracy (c.10%) when compared with a standard conductivity measurement bridge (Huisman et al., 2008, Topp et al., 1988, Zegelin et al., 1989). The technique uses a steady state reflection coefficient to calculate the load resistance (R_L) (Equation 2.44), which is measured after several multiple reflections which allow the higher frequency components of the signal to be attenuated, allowing the signal to approximate DC and making the effects of dipolar losses negligible (Castiglione and Shouse, 2003, Topp et al., 1988).

$$R_L = Z_{out} \frac{1 + \Gamma_{\infty}}{1 - \Gamma_{\infty}}$$

2.44

Where Γ_{∞} is the reflection coefficient after multiple reflections and Z_{out} is the cable and TDR impedance (usually 50Ω) (Giese and Tiemann 1975). In practice, a long but arbitrary distance is used to measure Γ_{∞} , although Lin et al. (2007) noted that the time required to reach the steady state increased with decreasing BEC, decreasing characteristic impedance, and increasing dielectric constant, and suggested that at least ten multiple reflection in the probe should take place for the DC assumption to be valid. Another consideration is the number of averages used for each reading. Bechtold et al. (2010) recommended a minimum of 16, in order to overcome the effects of electrode polarisation around the probe which causes readings to rise to a maximum value after the first few readings. Lin et al. (2008) also noted that it was necessary to correct the measured reflection coefficients to account for deviations in the TDR unit measurements from an ideal open circuit and proposed the following correction (Equation 2.45).

$$\Gamma_{corr} = \frac{2(\Gamma_{\infty} + 1)}{\Gamma_{open} + 1} - 1$$

2.45

Where Γ_{open} is the open circuit measurement taken by the TDR. This calculated load resistance is used with a probe constant based on the geometric configuration of the probe in order to find the BEC (Equation 2.46).

$$\sigma_{dc} = \frac{K_p}{R_L}$$

2.46

Where K_p is the probe constant (1/m) calculated with Equation 2.47.

$$K_p = \frac{\epsilon_0 c Z_p}{L_p}$$

2.47

Where c is the speed of light, Z_p is the impedance of the probe (Ω) and L_p is the length of the probe (m). Since ϵ_0 and c are known and L_p can be measured, the only real unknown is the impedance of the probe which relies on the number and distribution of the probe rods. The probe constant can be derived using analytical expressions (Ball, 2002) or by calibration in solutions of known conductivity (Bechtold et al., 2010, Huisman and Bouten, 1999, Huisman et al., 2008), a method which has become more popular due to variations from the idealised geometry caused by end effects (Zegelin et al., 1989) and has been shown to give more accurate results (Huisman et al., 2008).

Heimovaara et al. (1995) showed that the resistance from the probe cables (R_c) and connectors (R_0) had a significant effect on measured values and proposed a series resistor model for the TDR transmission line to improve the Giese Tiemann (1975) model and include these effects.

$$\sigma_{dc} = \frac{K_p}{R_L - (C_L R_c + R_0)}$$

2.48

Where C_L is the cable length. However, discrepancies were found between measured and fitted values of these parameters (Huisman and Bouten, 1999) leading Castiglione and Shouse (2003) to propose that the series resistor model was incorrect, and to suggest a method of scaling reflections using measurements from air and shorted probes to compensate. More recently, the series resistor model was shown to be correct as the cable resistance using the Castiglione-Shouse method was non-linear (Lin et al., 2008, Lin et al., 2007). Comparison of the three different methods showed that Castiglione-Shouse and original Giese-Tiemann models overestimated and underestimated respectively while the series resistor model was

the most accurate (Lin et al., 2007), although differences were largely irrelevant if the probe constant is determined using the solutions method and individual calibration (Figure 2.17).

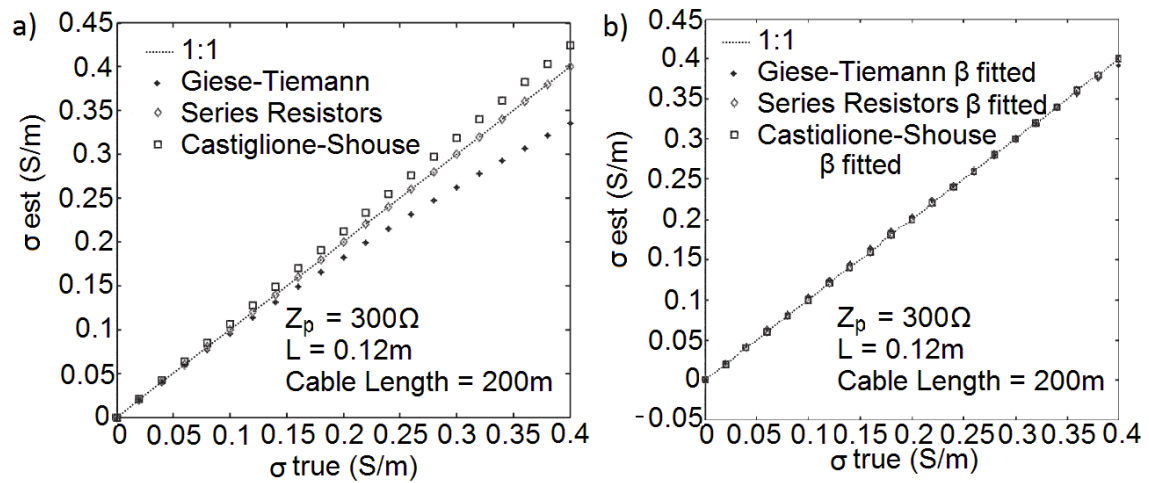


Figure 2.17: Comparison between TDR measured and actual BEC using a) the actual probe constant and b) a fitted probe constant using solutions

This approach of fitting values was confirmed by Huisman et al. (2008), who found that fitted probe constants were superior to analytical expressions such as those proposed by Ball (2002). Furthermore, they proposed a two-step calibration, first deriving K_p from solutions of low conductivity then treating R_c and R_0 as fitting parameters over the whole range of conductivity values, which was found to correct for deviations from theory and gave better accuracy than measuring the cable resistance directly. BEC is usually calculated by using Equations 2.44, 2.45 and 2.48 in order.

One important consideration is that of the signal's dominant transverse electromagnetic (TEM) mode of signal propagation (i.e. both the electrical and magnetic waves perpendicular to the direction of wave propagation) down the TDR probe rods which act as waveguides approximating a coaxial cable. However, due to the difficulty of inserting a coaxial probe into the soil, TDR probes used in field studies are rarely fully coaxial, but instead consist of a number of rods around a central conductor which are assumed to approximate a coaxial probe (Zegelin et al., 1989, Knight, 1992). The main problem with these probe configurations is that the electrical field is not spatially uniform, resulting in changes to sensitivity and measurement

volumes, with increased energy density around the electrodes causing the values of measured permittivity to differ from an arithmetic average of the different phases. This 'skin effect' is especially significant where the rod diameter is small in comparison to the electrode spacing (Knight, 1992). One solution is to use large diameter or plate electrodes but these are not practical for insertion especially in stoney soils and they also cause faster attenuation of the signal, which is detrimental in conductive soils like clay (Robinson and Friedman, 2000). In practice, three rod probes have been shown to deviate only very slightly from a coaxial cell in most conditions for determining bulk values provided that the ratio between the wire spacing and diameter is less than 10 (Knight, 1992) and the wire diameter is larger than the pore size of the soil (White et al., 1994).

2.7.3. TDR Limitations

It is important to note that TDR has a number of limitations based on the assumptions made during the process of determining EM properties of the soil which are important to consider. Perhaps the main limitation of TDR is the broadband nature of the EM pulse resulting in an undefined measurement frequency which it has been shown in Section 2.3 affects the measured permittivity values, especially in dispersive soils and makes comparisons with other methods difficult. Whilst TDR is commonly associated with high frequencies of c.1GHz where the signal is relatively insensitive to loss mechanisms (Evetts and Parkin, 2005, Topp et al., 1980), analysis of the frequency bandwidth conducted by Friel and Or (1999) using a fast fourier transform (FFT) on TDR waveforms found that most of the power is under 1GHz and biased to below 500MHz in wet soils, suggesting that the high frequencies are attenuated in lossy soils.

To address these issues, several attempts have been made to define an effective measurement frequency at which the TDR operates, usually defined as either the highest passable frequency in the EM pulse (Lin, 2003, Robinson et al., 2005b, Topp et al., 2000), the highest unfiltered frequency (Or and Rasmussen, 1999), or, more usually, the frequency in the pulse containing

the most energy (Robinson et al., 2003a). One approach is to use the rise time (t_r) of the return reflection in the TDR waveform (Robinson et al., 2005a, Topp et al., 2000). Robinson (2005a) proposed that the time between 10% and 90% amplitude should be used with Equation 2.49 to determine the maximum effective frequency (f_{eff}) in the TDR pulse.

$$f_{eff} = \frac{0.35}{t_r}$$

2.49

An alternative approach is to use modelled waveforms, with frequency dependent parameters, to determine the effective frequency (e.g. Lin, 2003) by matching the modelled permittivity, determined using Equation 2.39, to measured waveforms. Use of the technique requires accurate modelling of the whole transmission line and a careful choice of model to simulate relaxations, with both the Debye (Heimovaara et al., 1996) and volumetric models (Lin, 2003) being suggested. In practice this technique is difficult to employ on complicated systems, due to the effects of cables, connectors and multiplexors on the modelled transmission line, and has rarely been used in practical studies.

For more complex applications, the use of ARDP provides no information on the separate storage and loss of energy and therefore the dispersive nature of the soil (Thomas et al., 2008a) which may be desirable. Topp et al. (2000) used the effective frequency of the waveform, calculated from the rise time of the return reflection to separate the ARDP into real and imaginary parts. An alternative is to derive frequency domain information by using a FFT on the TDR waveforms (Friel and Or, 1999, Heimovaara, 1994, Shuai et al., 2009) or to use a vector network analyser (VNA), which measures the reflected (S_{11} scatter function) or transmitted signal (S_{12} scatter function) in the frequency as opposed to the time domain, to determine the complex permittivity (Thomas et al., 2008a). However the method remains more expensive (Cataldo, 2008) and requires careful calibration and specific, non-commercially available, probe designs so is less suited to long term analysis of the soil. Nevertheless, several

authors have compared measurements from the frequency domain to determine additional information from time domain waveforms (Heimovaara et al., 1996, Lin, 2003).

Another major limitation is the assumption the ϵ'' is inconsequential in comparison to ϵ' which is untrue in clays and organic soils containing significant amounts of bound water and high BEC values. Additional attenuation may also occur from the TDR components, with long cables and poor quality connectors and attachments (Logsdon, 2000, 2006) responsible for significant losses and acting as a low pass filter for high frequencies. These effects cause errors in real permittivity determination by increasing the imaginary component, and lowering the effective measurement frequency into a range where dipolar relaxations are more significant (Jones and Or, 2004). Several authors have shown significant overestimation of the ARDP and therefore VWC in soils with BEC values greater than 0.2 dS/m – 0.25 dS/m (Bittelli et al., 2008, Wyseure et al., 1997) with up to 20% errors in VWC detected in some cases. One solution to this problem is to use a soil specific empirical relationship between the measured ARDP and VWC, which takes into account these effects on measured values, but this method has little applicability on soils other than those for which it is calibrated upon and for comparison with other EM methods. Evett et al. (2005) created a generalised empirical calibration, taking into account both the ARDP and BEC to determine VWC using the effective frequency determined from waveforms (Equation 2.50) which allowed TDR to be compared to other EM techniques.

$$\theta_v = a + b \left[\frac{ct}{2L_{cal}} \right] + c \left[\frac{\sigma}{(2\pi f_{eff} \epsilon_0)} \right]^{0.5}$$

2.50

Where a, b and c are empirical fitting coefficients. A major drawback of this approach is that soil specific calibration is still needed to find the fitting parameters. A more generalized method by Wyseure et al. (1997) for soils with BEC above 0.2 dS/m suggested correcting the ARDP to real permittivity values at zero ohmic loss after measurements in NaCl solutions with

variable BEC values, although this failed to account for the effects of dipolar losses and surface conductivity effects.

$$\varepsilon' = \varepsilon_a + 1.432\sigma$$

2.51

Other authors such as Bittelli et al. (2008) and Topp et al. (2000) have separated the real and imaginary permittivity values from the measured ARDP values and subtracted ε'' from ε_a to relate VWC to ε' directly with some success. However, the method requires the estimation of the effective measurement frequency which may be difficult to define (see above). Strong attenuation caused by high BEC values, cables and connectors can cause additional problems with waveform interpretation as the shape of the waveform can be changed, causing the return limb to become rounded and difficult to define (Robinson et al., 2003a), especially using automated methods. In extremely high BEC values, the signal may be attenuated to the extent that a return reflection can no longer be determined (Jones et al., 2002, Noborio, 2001). One solution is to use coated rods (Kuhn and Zornberg, 2005, Moret-Fernández et al., 2009) which reduce signal loss, but these can make calibration difficult for BEC determination and reduce sensitivity and sampling area (Ferre et al., 1998, Jones et al., 2002). A more practical solution is to use shorter probes to allow a greater amount of the signal to be reflected, although care must be taken to avoid falling below a representative volume for determining VWC.

Another assumption is that the magnetic component of the soil is both negligible and uniform. Whilst magnetically enhanced soils are rare, some soils with significant amounts of magnetic material, especially those derived from magnetic parent material, can drastically alter the travel time of the signal (Cassidy, 2008, Schneider and Fratta, 2009) and thereby increasing the derived values of ARDP and VWC. Robinson et al. (1994) showed that 15% magnetite causes a 60% error in the recorded VWC, as well as increasing errors due to the difficulty in automatically interpreting the waveforms with standard software due to attenuation of the

return reflection, similar to that noted in soils with high BEC. Due to the TEM propagation mode of the signal, these magnetic effects are impossible to separate from the measurements of ARDP and BEC.

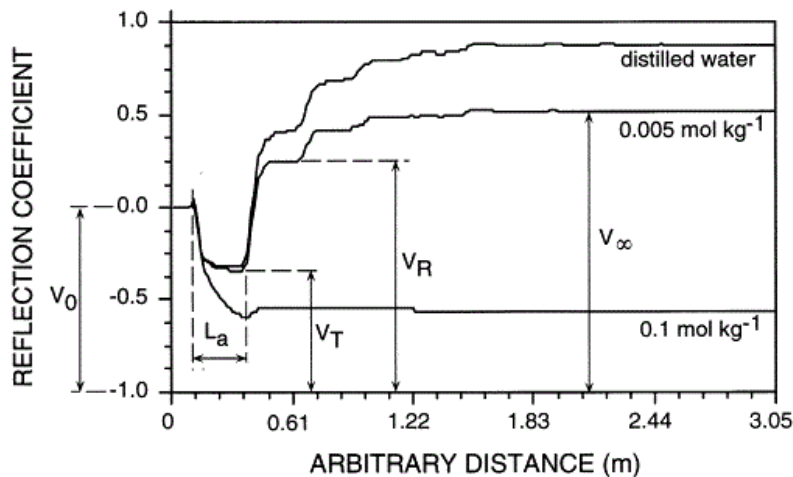


Figure 2.18: The attenuation of waveforms in distilled water and NaCl solutions. Notice the lack of a return reflection in the 0.1mol kg-1 NaCl solution. (Noborio, 2001)

The determination of ARDP also assumes that the soil sample under investigation is homogenous, but several authors have reported difficulty using TDR for VWC determination in soil where water is unevenly distributed in wet and dry layers (Dasberg and Hopmans, 1992, Nadler et al., 1991, Schaap et al., 2003), especially when a wet layer is overlying a drier layer. Errors stem from two main sources. Standard waveform interpretation techniques often fail to identify the correct end point from the probe rod end (Nadler et al., 1991) giving erroneous results by yielding incorrect permittivity values. Errors also stem from the use of bulk permittivity values, which are calculated either using an arithmetic or refractive index model depending on the wavelength to layer thickness ratio (Robinson et al., 2003a, Schaap et al., 2003). The use of the refractive index model is correct for small numbers of thick layers, whilst lots of thin layers require arithmetic averaging.

A final limitation is the physical requirement to insert the TDR probes into the soil, ensuring minimal air gaps, compaction and probe deformations which affect the measured values.

Whilst small air gaps have minimal effects, gaps making up a significant fraction of the sample

area have been shown to have significant effects on measured ARDP values (Ferre et al., 1998, Topp and Davis, 1985), and may be especially significant in soils with significant shrink-swell behaviour (Jones et al., 2002). Bending the rods on insertion, whilst having a minimal effect on measured ARDP (Graeff et al., 2010), affects the characteristic impedance of the probes, causing significant errors in BEC determination (Curioni, 2013). For these reasons, TDR probes are best deployed in soils with few gravel inclusions and using waveguides to ensure probe rods remain parallel.

2.8. Geophysical Methods and Seasonality

As discussed above, the EM properties which affect the performance of heritage detection techniques are heavily influenced by the underlying soil conditions, especially the VWC and temperature which are highly variable throughout the year. To address these issues a number of studies have been undertaken to monitor the soil properties and the performance of different instruments.

The causes of GPR anomalies have been investigated and linked to TDR readings and the soil properties, in particular the PSD and organic matter (Van Dam and Schlager, 2000, Van Dam et al., 2002). An important finding of these authors was that geophysical anomalies were caused by differences in VWC caused by the different water retention characteristics of the soil and were only visible when VWC was above 0.055. These studies proved the dependence of geophysical anomalies on the VWC and underlying soil properties, but no attempt was made to quantify how these changed over a long term period as a response to different seasonal conditions. A long term study of changing VWC in soil was conducted using regular GPR surveys over a period of 5 months to identify the optimum time to find sandy layers in the ground by Boll et al. (1996). It was found that the contrast between different sandy layers (coarse and fine) was variable with the VWC, and that layers were undetectable during extreme dry or wet conditions. TDR has also been used in combination with electrical

resistivity methods for monitoring the VWC of shale sand in France over a period of several months by Brunet et al. (2010). They were able to identify two distinct periods; a period of water content stability between September and April followed by a period of drying over the summer (June-August) which lasted until early Autumn when rain caused the soil to re-saturate to field capacity. Crucially, these surveys were able to demonstrate the seasonality of geophysical properties, and the dependence of the success of the surveys on the preceding weather conditions.

In all of the above studies, good agreement was found between TDR results and the other geophysical methods, proving its worth for predicting geophysical soil properties. However, one weakness of all of these studies is that they compared soil VWC and so rely on the models used to link the geophysical measurements to soil VWC which introduce additional errors (Huisman et al., 2001). To address this, Curioni et al. (2012) developed a TDR monitoring station capable of recording long term changes in geophysical parameters which eliminated these errors. Comparison of these results with GPR found significant seasonal variation in GPR signal penetration and ability to locate buried utilities, and a dependence on the measured properties with weather variations (Curioni, 2013).

2.8.1. Seasonality Tests over Archaeological features

Detection of archaeological features relies on contrasts in their soil geophysical properties with those of the SSM which change as a function of the prevailing environmental conditions as has been shown in Section 2.8. The differing seasonal geophysical response has usually been linked to variations in the VWC caused by the different soil properties between the two soil profiles, especially the porosity, which is said to be higher in the archaeological ditch features (Clark, 1996, Schmidt, 2013) allowing faster infiltration, and the features greater ability to hold water, due to the prevalence of fine grained particles and elevated amounts of organic matter (Scollar et al., 1990, Strunk-Lichtenberg, 1965). Based on these assumptions, the hypothetical

response of a 'typical' ditch to different weather events is predicted, a typical example of which may be as follows (Schmidt, 2013):

- During a warm period, the soil dries all but the ditch which has higher water retention characteristics. After a sustained period, the ditch also eventually dries out, making the ditch undetectable.
- After rainfall, water enters the ditch faster due to its larger pores allowing faster infiltration. After extended rainfall, the feature contrast disappears after both the SSM and ditch become saturated.
- Further drying after rainfall evaporates water from the ditch quicker due to larger pores until all soil has dried out again

Whilst discussion such as these are of some use for survey planning, their main weakness is that it is unknown how accurate these models are in real world situations, especially given the wide variety of feature dimensions and different soil types encountered, both inside the features and the SSM. These issues are partly addressed by a number of studies of seasonality of geophysical response conducted using earth resistance techniques, the earliest of which was conducted by Al Chalabi and Rees (1962) who took monthly measurements at Wall, Staffordshire. They found the ideal period was surveying during the summer months (June-September), with the best results obtained in July. Since then, a wide variety of different seasonality tests over different background SSMs and features of different sizes and shapes have been conducted (Clark, 1980, 1996, Cott, 1997, Hesse, 1966, Parkyn et al., 2011), the findings of some of which are summarised in Table 2.7. In general, the majority of these studies suggest the optimum time for heritage detection is after the dry period in Summer-Autumn, although responses vary based on the SSM soils and the nature of the archaeological ditch. Of particular importance are the dimensions of the ditch (Clark, 1996), with water deficit conditions being preferable for small-medium sized ditches and wetter conditions, near

field capacity, needed for larger and deeper ditches. Whilst ditches are usually identified as low resistance features, on deep and wide ditches anomalies have also been known to reverse as water is stored primarily in the bottom of the ditch (Clark, 1996, Gaffney and Gater, 2003).

Table 2.7: A summary of the optimum contrasts for locating ditches from earth resistance experiments. After Clark 1996

| Site | Bedrock | Dimensions of Ditch | Anomaly Type | Best Months | Peak Months |
|-----------------------------|--------------------|------------------------------------|---------------------|----------------|-------------|
| Wall, Staffordshire | Triassic Sandstone | Width: variable Depth: 3.4m max | Low Resistance | June-September | July |
| Hogs Back, Surrey | Upper Chalk | Width: 2.5m Depth: 1.1m | High Resistance | July-November | September |
| Durrington Walls, Wiltshire | Upper Chalk | Width: 17.7m Depth: 6m | Low Resistance | December-June | March-April |
| Woodhenge, Wiltshire | Upper Chalk | Width: 6.3m Depth: 2.1m | Low/High Resistance | December-June | March-April |

However several criticisms can be made of these surveys. Changes in contrast have been ascribed universally to changes in the water content of the soil and little consideration has been given to the other factors which affect BEC, such as differences in temperature, soil type, ion availability and pore connectivity between the archaeological feature and SSM, whereas it has been suggested these have a significant role at certain times of the year. For example, Scollar et al. (1990) have suggested that the year can be divided into 2 periods; a saturated period (Autumn to Spring) where temperature effects are dominant and a dry summer period where wetting and drying is the most important factor. Another weakness is the monthly measurement frequency, which is unsuitable for both assessing the response to individual climatic events and diurnal effects on geophysical measurements, due to the daily variation in temperature. A final weakness is the poor vertical resolution of the surveys which are

conducted at a single or a small number of depths of investigation which are difficult to define and may be modified by conditions at the surface due to the apparent resistivity average (Scollar et al., 1990). A consequence of these last two points is a poor understanding of infiltration phenomena in the aftermath of a precipitation event, due to a lack of suitable evidence, which can make identification of suitable survey times difficult in a year with atypical weather patterns.

Far less attention has been given to the seasonal variability in EM methods such as GPR which also vary as a function of VWC due to their dependence of both ARDP and BEC, although the soil properties and geochemistry have been used to identify the causes of anomalies. For example, Verdonck et al. (2009) used both TDR and GPR comparatively over a ditch site on a sandy soil and attempted to identify the root causes of the anomaly. They identified the presence of iron oxides which were causing water to be held within the anomaly similar to the findings of Van Dam et al. (2002), although no sharp transitions between the feature and adjacent SSM were observed. While this and similar studies (e.g. Cuenca-García et al., 2013, Wunderlich et al., 2010) have shown differences in the water content of the soil as one of the most important parameters responsible for GPR reflections, no attempts have been made to address these changes in VWC between the archaeological soils and SSM and its response to environmental variations over a long period of time.

2.9. Identified Knowledge Gaps

From the examination of the literature, several knowledge gaps have been identified. It is apparent that heritage detection techniques have variable performance throughout the year based on the EM properties of soils within archaeological features and the SSM and the contrasts between them. Previous research has demonstrated the links between geophysical properties and water content, temperature and geotechnical properties of the soil (SSA, density, PSD etc.), and a number of relationships have been identified which may potentially

be used to predict contrasts in EM properties detected by sensors. Previous seasonality testing of geophysical behaviour of archaeological ditches has been limited to measuring the apparent bulk electrical conductivity of the earth using earth resistance techniques, often at a single depth of investigation and on a coarse temporal scale (usually monthly), and correlating the results to the water content of the soil only. It is hypothesised that a greater understanding of the factors which influence the ability to detect archaeological features can be gained by a multi parametric study of the soil properties, weather and geophysical properties at a higher temporal and spatial resolution to improve the quality of future heritage detection.

In light of these findings, the identified knowledge gaps are as follows:

- There is a significant need for field measurements of the soil's geophysical properties from both the archaeological feature and the SSM over a long term period with a high temporal and vertical resolution in order to gain an improved understanding of the processes which cause the variations in contrast between EM properties which allow heritage detection which are currently poorly understood.
- Previous archaeological seasonality studies have focused on conductivity and linked purely to water content of the soil. However, few studies have considered the effects of temperature and soil properties on the BEC of the soil both inside and outside the archaeological feature. Furthermore, to the best of the author's knowledge, no studies have considered the variation in ARDP which affects the use of other geophysical techniques such as GPR and EM conductivity meters.
- Relationships between geotechnical, geochemical and geophysical properties have been identified in other works but have never been applied to compare archaeological soils and their SSM. Correlations between these properties may be of significant use for the prediction of response to heritage detection techniques. Furthermore, whilst a

number of different models for prediction VWC exist, they are far from universal in their application and some knowledge of the suitability of different models to different soil types and conditions is desirable.

- The TDR technique has been extensively used in soil science for measurement of VWC, and more recently for the long term monitoring of EM properties to improve geophysical survey. However, existing methodologies for construction of suitable monitoring stations are not robust enough for deployment in remote locations. Modification of existing designs to facilitate their use in these environments is therefore desirable.

Chapter 3: Field Monitoring Methodology

3.1. Introduction

The literature review has highlighted the dependence of current heritage detection techniques on the EM properties of the SSM relative to those of the archaeological feature to be detected, as well as the dependence of these EM properties on the soil properties, which vary temporally with changing environmental conditions and response to climatic events such as rainfall and temperature change. Methods to assess the effect of the soil properties will be discussed in Chapter 4 on laboratory based methods, but in order to assess seasonal and climatic changes of these properties and their links to weather related trends, it was necessary to develop a monitoring station capable of recording the ARDP and BEC of the soil for a long period. Time Domain Reflectometry (TDR) was chosen as the optimum method for monitoring, as it records these parameters, can be equipped for long term measurements, and can be converted to VWC, which is of value to other members of the project, for studying plant growth and the formation of crop marks for example.

3.2. Site Locations

3.2.1. Choice of Sites

In order to conduct a suitable long term monitoring experiment of changing ground conditions, suitable sites needed to be chosen to install the equipment. The main requirements for suitable sites were as follows.

1. The presence of an archaeological ditch feature. A ditch was chosen as one of the most commonly occurring archaeological targets for detection. In addition to this, it was beneficial for the feature to be of limited archaeological importance, in order to avoid an expense and complicated mitigation strategy for the excavation.
2. The presence of both a geophysically unresponsive soil (clay) and a soil which is considered to be more responsive to remote sensing and geophysical techniques. This

allowed comparison of the two different soil types to assess differences in soil response based on its physical properties as weather patterns were likely to be similar within a small area.

3. One of the sites for monitoring was to be covered by pasture which causes known difficulties for remote sensing as crop marks formation is unlikely except in periods of extreme drought.
4. In addition to these factors, the climatic conditions on the West of the country are known to be generally wetter than the east of the country (BBC, 2011), creating a difference in feature contrast and detection rates between the two sides of the country (Hanson, 2005). For this reason, it was desirable that one of the test locations should be on the East of the country with the other on the West of the country to compare the two different climatic conditions.
5. Any monitoring work needed to be subject to the approval of the landowner and any tenant farmers or land management who carried out day to day business on site.

Two monitoring locations were selected and access negotiated based on these criteria (Figure 3.1). On the west of the country, Harnhill farm, owned by the Royal Agricultural University (RAU) and located on the outskirts of Cirencester was chosen as one of the monitoring locations (Figure 3.2). One site was comprised of a limestone geology, topped with shallow soils (CCC; Cirencester Cherry Copse), providing a suitable site for a study into free draining soils, was located at OS coordinates 40800, 200695. The second site, located approximately 1.2km away at OS coordinates 40690, 200735, was located on a mudstone formation with poor drainage characteristics, allowing the soil response of traditionally unresponsive soils to be tested. On the Eastern side of the country, Lodge farm in Diddington, Cambridgeshire was chosen, as it was able to provide both a well-draining soil and clay geology, mirroring the setup on the Cirencester sites (Figure 3.3). Both sites are located atop a formation of Oxford clay but differ in their superficial deposits. One site comprised of glacially derived clay (DCF;

Chapter 3: Field Monitoring Methodology

Diddington Clay Field) providing a poorly draining site for study. The other site comprised of sand, gravel and silt of fluvial origin (DPF; Diddington Pasture field), allowing theoretically easier drainage. The site is also permanently in pasture, allowing the reasons for difficulty in detection in this condition to be assessed. Both are located in Cambridgeshire near Diddington at OS coordinates 517630, 265675 and 519175, 265268 respectively.

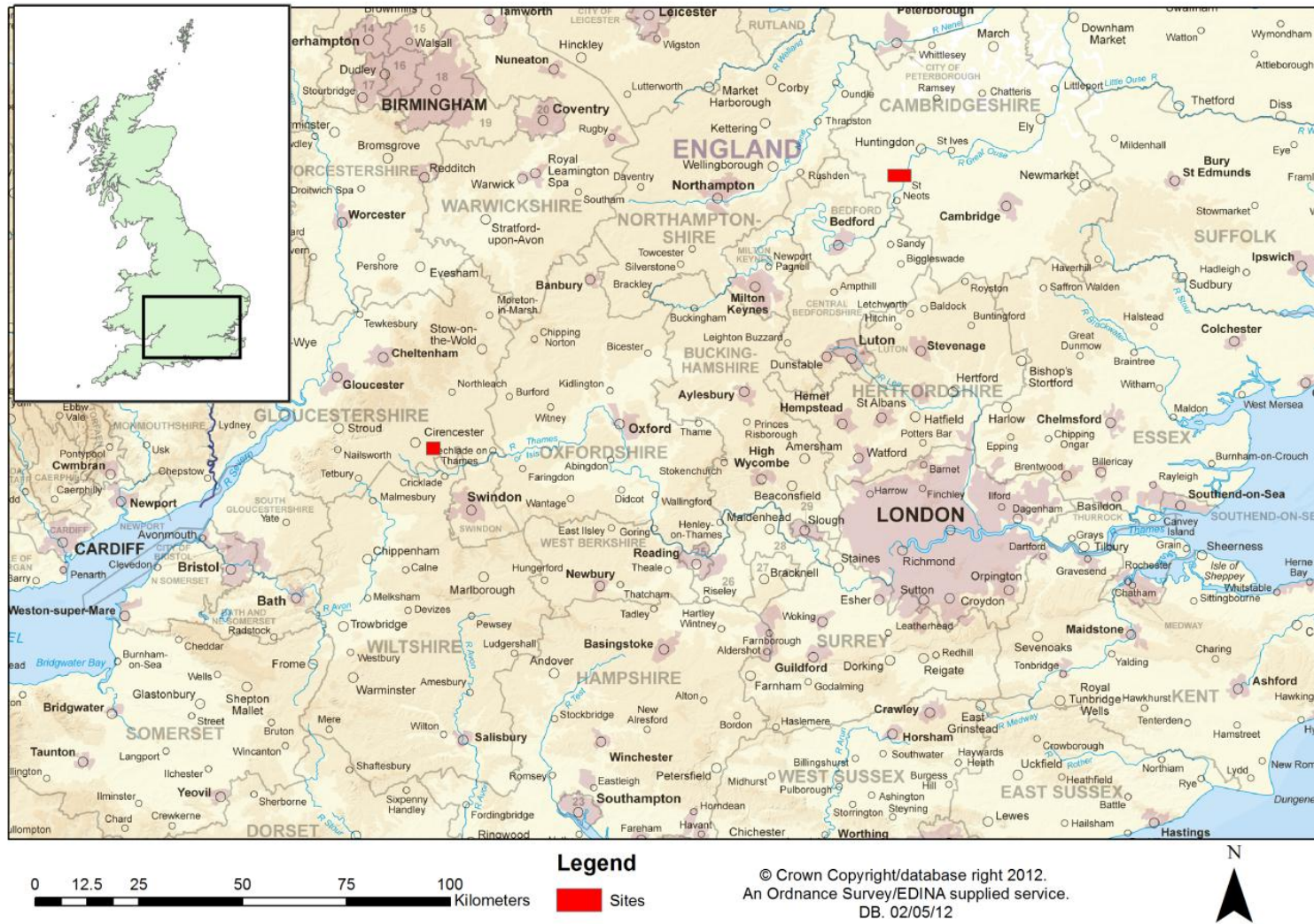


Figure 3.1: The locations of the DART projects sites where the monitoring stations were installed

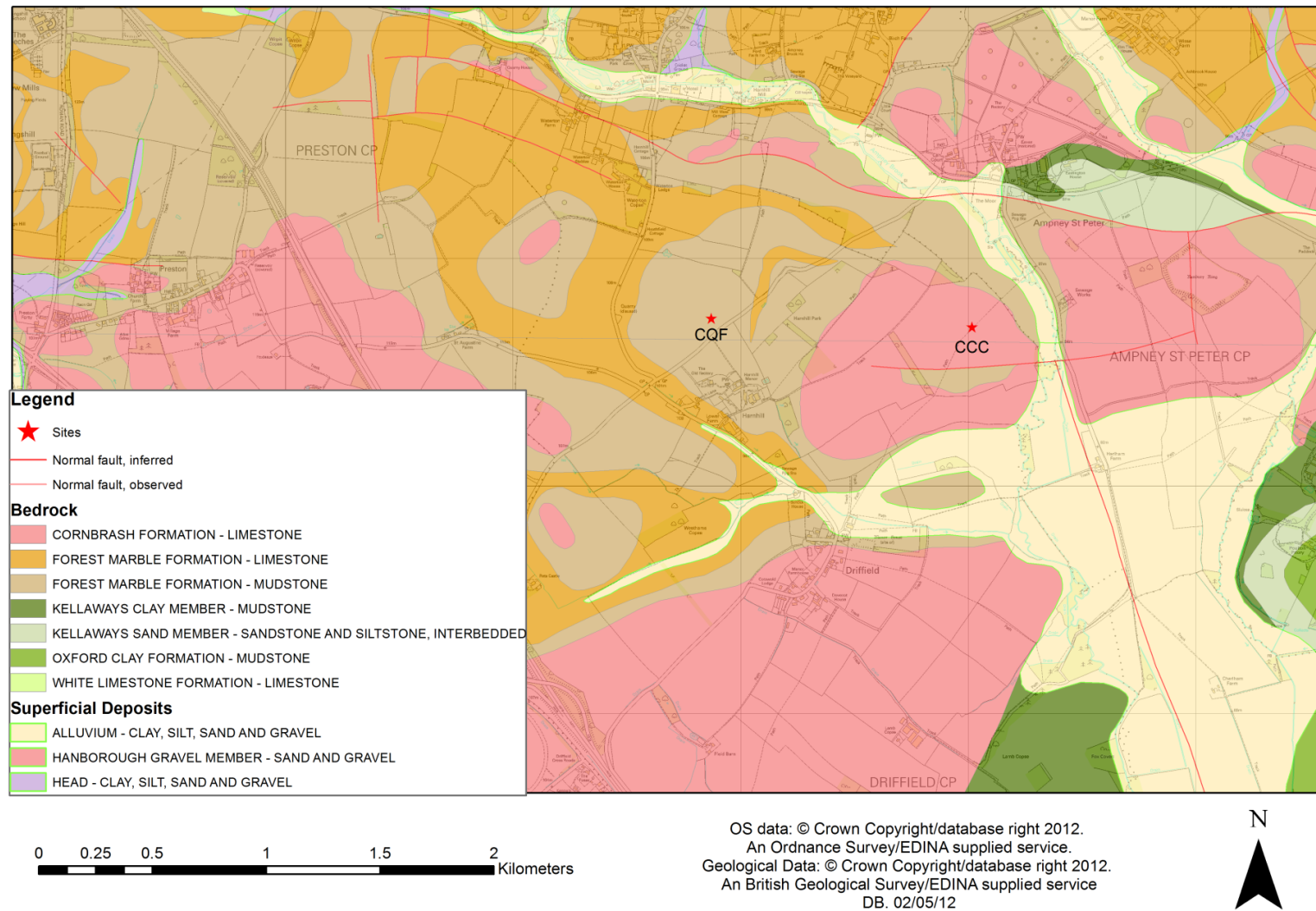


Figure 3.2: A geological map showing the main geology and superficial deposits at the two Harnhill sites

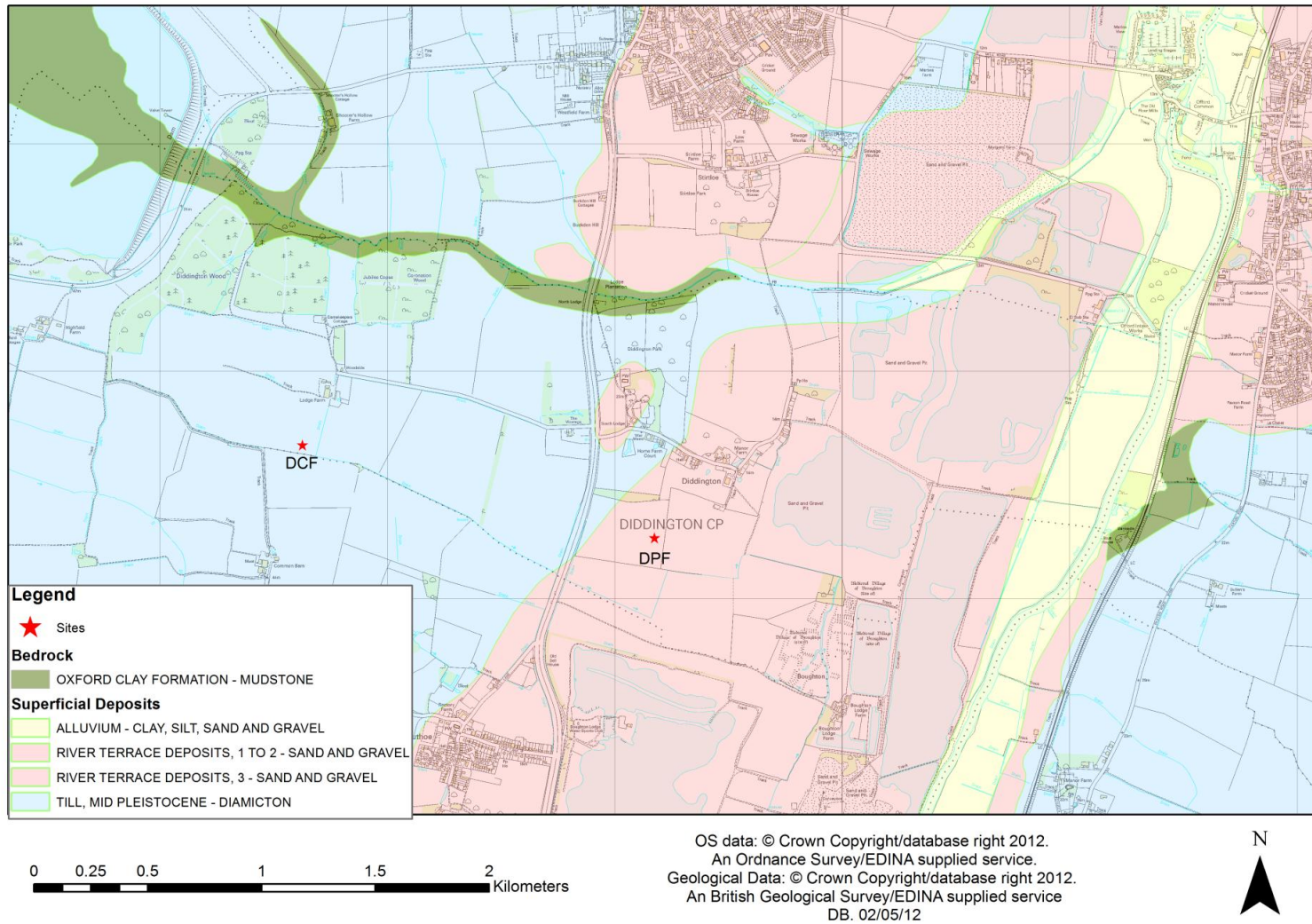


Figure 3.3: A geological map showing the main geology and superficial deposits at the two Diddington sites

3.2.2. Identification of Suitable Features

Suitable features for monitoring were located using magnetometer survey carried out using a fluxgate gradiometer at Harnhill in January 2011 (Fry, 2011b) and at Diddington in March 2011 (Fry, 2011a). Suitable features were located based on the results from these surveys, and these were cored to characterise the feature depths, fill material and confirm the geophysical anomalies were archaeological in nature. Coring was carried out at both sites in March 2011 using a Cobra TT petrol breaker vibracorer. Boreholes were logged and located using a Leica System 1200 differential global positioning system (dGPS). Cores confirmed both features at Cirencester to be suitable targets for installation as well as the selected feature at DCF. However, the feature at DPF was found to be indistinguishable from the SSM, and was noticeable as a topographic anomaly on the ground. Another feature was selected from the geophysical results and cores were collected on the 16th March 2011. The new feature was deemed suitable for installation. The proposed trench at CCC was also moved, following a decision by English Heritage to schedule the selected feature a few weeks prior to installation, as it was felt that the administrative difficulties involved with working on a scheduled monument would be a hindrance to future work on site. Further magnetometer survey using a fluxgate gradiometer was carried out on 10th April 2011 to find another suitable feature and the trench location was subsequently moved c.165 m to the North West, outside the newly scheduled area into a new feature. The trenches were planned and their locations are shown in Figures 3.4-3.6.

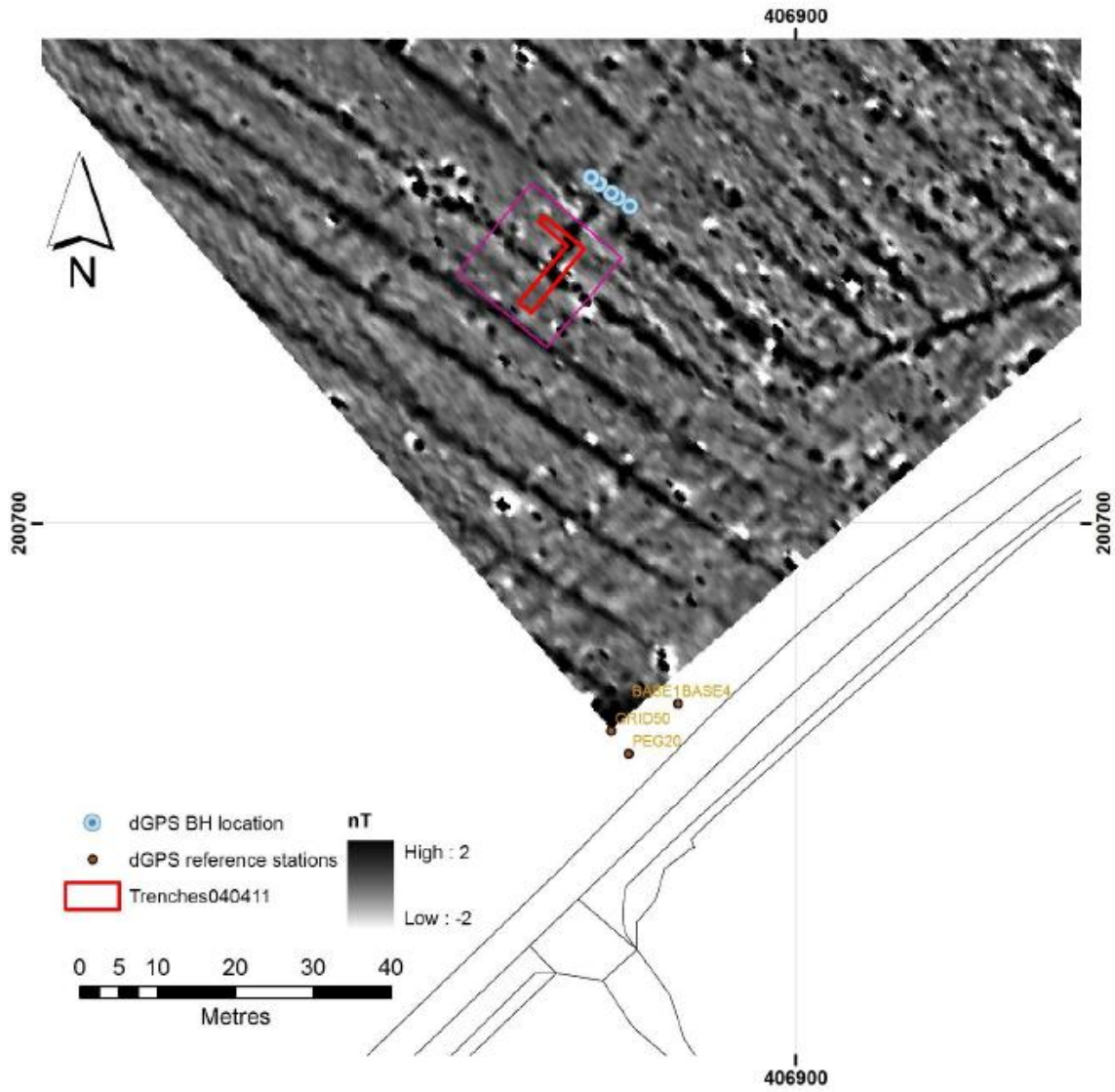


Figure 3.4: The magnetometer survey and location of boreholes and trenches at CQF (Wilkinson, 2011).

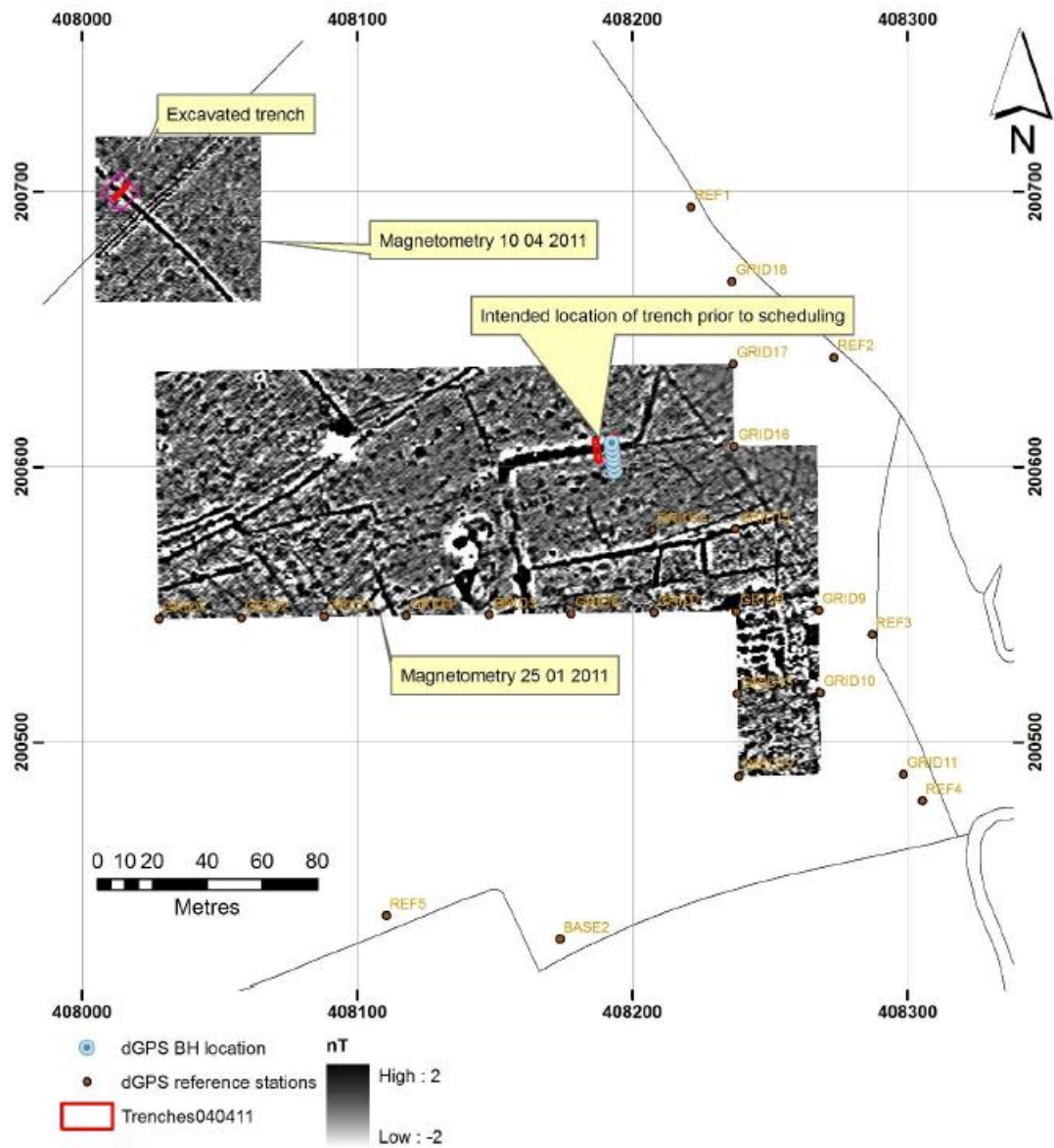


Figure 3.5: The magnetometer survey and location of boreholes and trenches at CCC (Wilkinson, 2011).

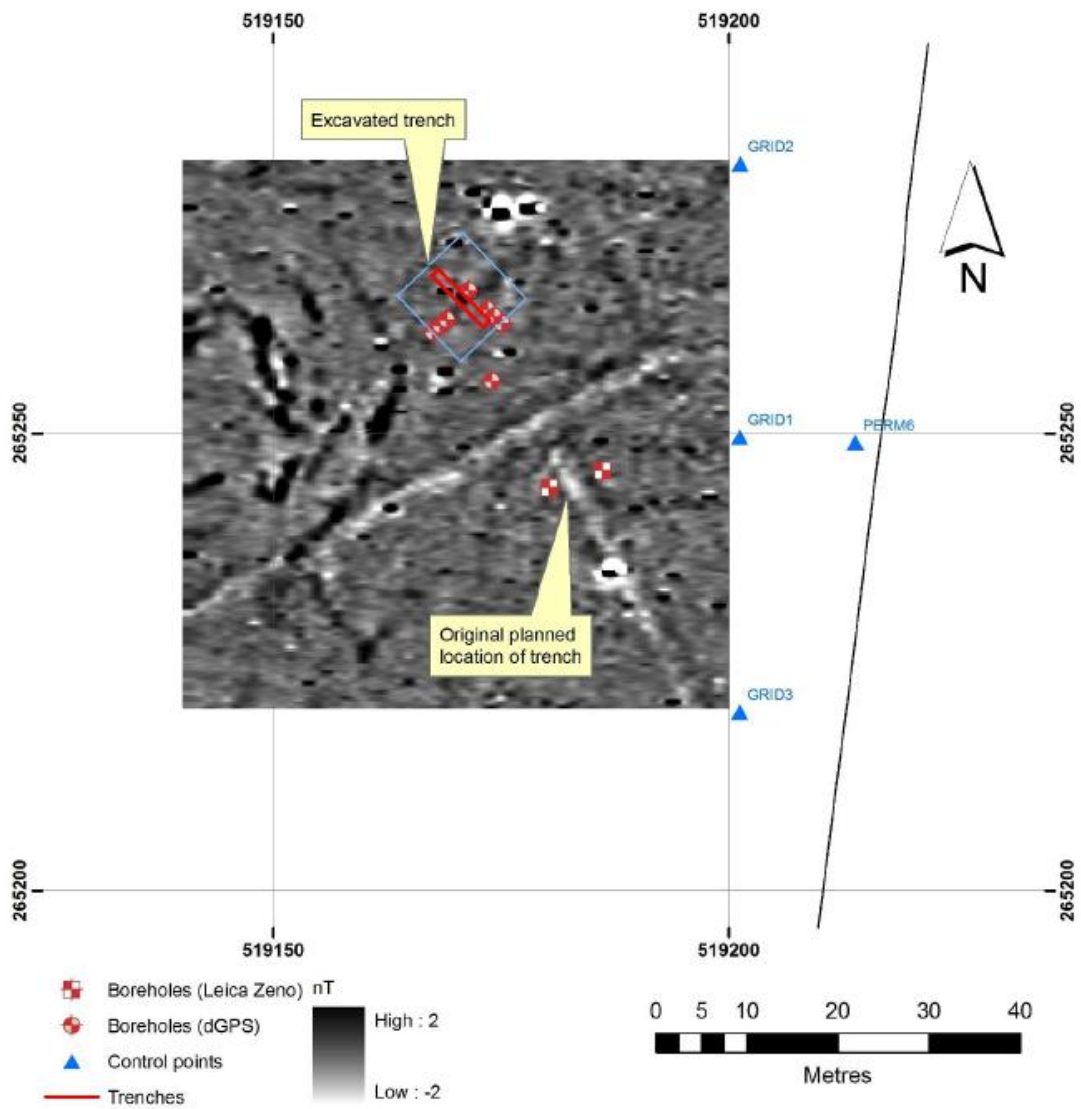


Figure 3.6: The magnetometer survey and location of boreholes and trenches at DPF (Wilkinson, 2011).

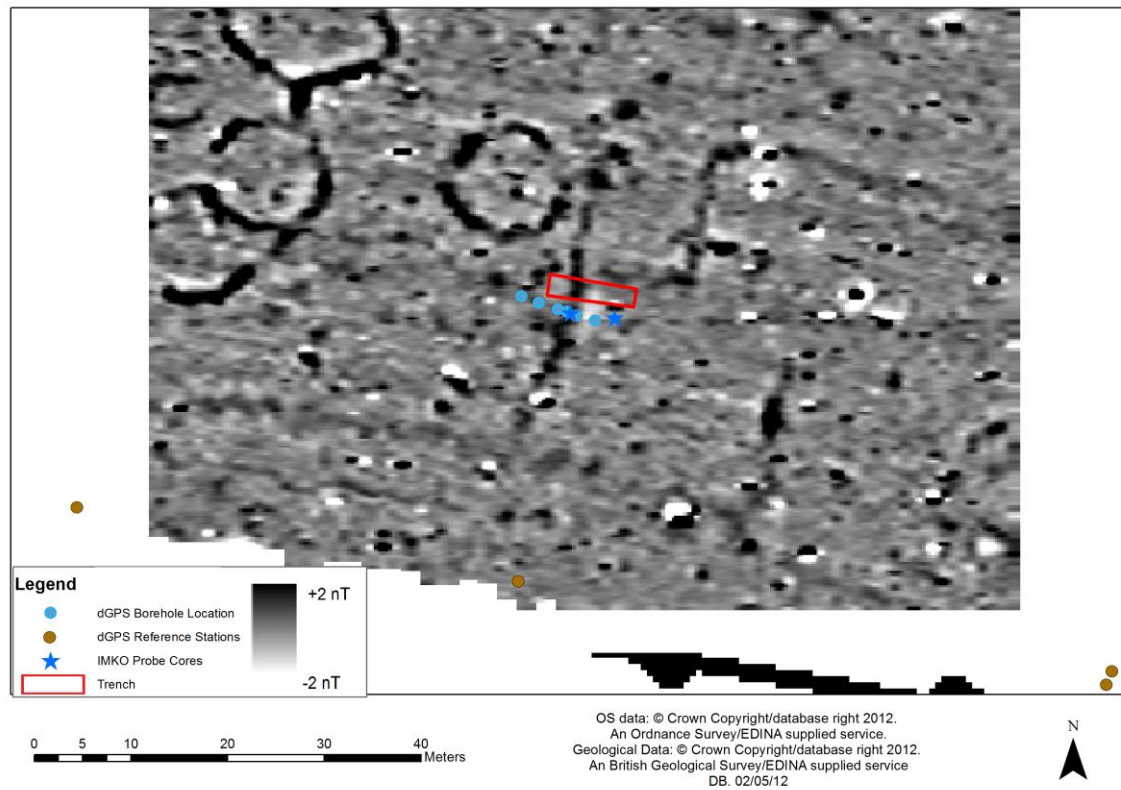


Figure 3.7: The magnetometer survey and location of boreholes and trenches at DCF.

3.3. Design of the Monitoring stations

Several different types of TDR are commercially available, with a wide range of feature and manufacturers (see Table 3.1). Key to this projects success were the ability to measure both ARDP and BEC, the need to interface with a datalogger for monitoring stability and reliability and the ability to calibrate ARDP-BEC relationships individually to study the effects of different variables. In addition, a high level of accuracy was desirable as was the ability to capture raw waveforms.

The TDR system used for the monitoring stations used in this study is the TDR100 which is manufactured by Campbell Scientific (Campbell Scientific, 2010c). This was chosen for these stations for the following reasons:

Table 3.1: Comparison of different features and technical specifications of different TDR devices. (Robinson et al., 2003a). Abbreviations are listed at the bottom.

| TDR FEATURES | TEKTRONIX 1502 (B, C) | EASY TEST FOM/mts | SOIL MOISTURE MINI TRASE | ENVIRONMENTAL SENSORS INC. MP-917 | CAMPBELL SCIENTIFIC TDR100 | SOIL MOISTURE TRASE SYSTEM I 6050X1 | MESA SYSTEMS TRIME FM2 |
|---------------------------------------|-----------------------|---------------------------|-------------------------------|-----------------------------------|--|-------------------------------------|------------------------|
| Pulse Rise time (ps) | 200 | 200 | 125-155 | >200 | 170 | 125-155 | 300 |
| Output Pulse Amplitude (V) | 0.30 | 2 | 1.6 | 0.3 | 0.25 | 1.6 | Unknown |
| Weight, (kg) | 6.5 | 3.8 | 3.4 | 5 | 0.7 | 12 | 0.9 |
| Size (cm) | 44 x 32 x 13 | 26 x 18 x 13 | 23 x 20 x 13 | 27 x 25 x 17 | 21 x 11 x 6 | 28 x 42 x 23 | 18 x 8 x 6 |
| Minimum cost to use (\$) | 11695 | 4707 | 6895 | 5350 | 3650 | 9550 | 4370 |
| Probe Compatibility | Generic | Proprietary | Generic | Proprietary or Generic | Generic | Generic | Proprietary |
| Display Options | LCD, PC | LCD, PC | PDA, PC | LCD, PC | PC, DL | LCD, PC | LCD, PC |
| ϵ_a - θ_v Calibration | None | Fixed | User Defined | Fixed | User Defined | User Defined | User Defined |
| Possible Outputs | WF | σ , θ_v , T | WF, ϵ_a , θ_v | WF, θ_v | WF, σ , ϵ_a , θ_v | WF, ϵ_a , θ_v | θ_v |
| Electrical Conductivity | Manual | ✓ | × | × | ✓ | × | × |
| Waveform size | 251 | - | 1200 | 255 | 100-2048 | 1200 | - |
| Data Storage | PC, DL | PC | PC, DL | PC, DL, IS | PC, DL | PC, DL | PC |
| Cable Connectors | BNC | BNC | BNC | BNC | BNC | BNC | Proprietary |
| Reported Accuracy | ±1% | ±2% | ±2% | ±1% | ±1% | ±2% | ±1% |
| Power Supply | AC, Battery | AC, Battery | AC, Battery | AC, Battery | Battery | Battery | Battery |

Abbreviations: WF: waveform, θ_v : VWC, ϵ_a : ARDP, σ : BEC, T: Temperature, DL: Datalogger, LCD: inbuilt display, PC: Computer, PDA: Personal Digital Assistant, IS: Internal Storage, AC: Alternating Current

Chapter 3: Field Monitoring Methodology

1. The ability to capture the data as raw waveforms as opposed to pre-calculated VWC values. This allows for a more rigorous analysis as well as providing the key geophysical parameters of the soil affecting signal transmission which are not recorded by equivalent systems. This facilitates greater analysis of the relationships between soil properties and geophysical responses which are not fully understood, particularly on fine grained and highly organic soils.
2. Calibration is manual, unlike other TDR systems which rely on factory calibrations and internal calculations and can produce inaccurate water content results in some soils, particularly those with high organic and clay contents (Bridge et al., 1996, Evett, 2003, Thomas, 2010). This allows us to develop bespoke relationships between ARDP, BEC and VWC for the soils in this project. Comparisons of the differences in VWC values derived from different models have been found to be as great as 12% (Thring, 2013). Several different mixing models can be applied to derive the VWC, and the best one determined which will help support the plant growth and development being studied by the project in the University of Leeds by providing accurate data. In addition, this allows us to develop bespoke relationships between ARDP, BEC and VWC for the soils in this project.
3. The TDR100 had already been used with good results for similar projects studying the VWC, ARDP and BEC of different soil types such as on the MTU project (Curioni et al., 2012). This meant that many elements of the monitoring station design had already been developed and tested for long term monitoring.
4. The equipment was relatively cheap in comparison to the other brands of TDR available. The need to survey several sites and financial limitations of the project grant made this an additional factor in choosing TDR equipment.

The design of the monitoring stations was based heavily on the work of Curioni et al. (2012) working on the MTU project, who demonstrated a methodology for constructing a TDR based

Chapter 3: Field Monitoring Methodology

monitoring station, capable of long term data collection. However, owing to the remote locations of the monitoring stations, several changes had to be made to the designs to make them require less direct intervention and allow site visits to be approximately monthly. The two main challenges were to firstly reduce the power consumption and improve the power supply so that the battery supply was able to last longer than the eight day period stated by Curioni (2012), and secondly, to create a system which allowed knowledge of station failure at the earliest opportunity. In addition to this, changes in the soils thermal properties were considered to be important in the heritage detection industry, particularly in remote sensing where thermal and infrared sensors are often deployed (Gumerman and Lyons, 1971, Parcak, 2009), as well as for their role in determining geophysical properties, which have a known temperature dependence as highlighted in Chapter 2. For these reasons, an increased number of thermal probes in comparison to the three used by the monitoring station previously used by the MTU project were also considered desirable. A schematic showing the finished monitoring station design is shown in Figure 3.8.

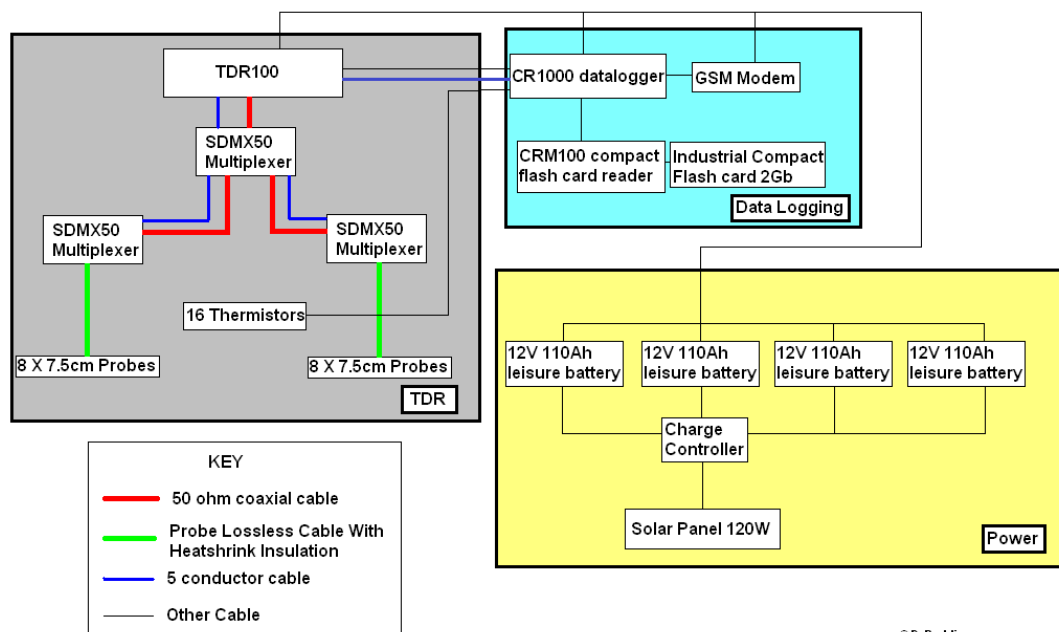


Figure 3.8: A schematic of the different TDR station components and their connections

Chapter 3: Field Monitoring Methodology

Two changes to the setup developed by Curioni et al. (2012) were made to allow the stations to run without the need to change the batteries: reducing the power they required to operate and installing a solar panel in order to charge the batteries during daylight hours of the sensors deployment. The use of CR1000 datalogger, manufactured by Campbell scientific significantly reduced the power consumption of the monitoring station, having a typical power consumption of only 192mW (16mA at 12V) during a reading (Campbell Scientific, 2010a) compared to the 12000mW (G. Curioni, pers comm.) consumed by the computer controlled station used by Curioni (2012). To expand the loggers 4MB memory, a CM100 compact flash© (CF) card reader and writer was also purchased for each unit to expand the total memory to 2GB and leave the internal logger memory free for processing tasks. The use of industrial grade CF cards, rated for many thousand read/write cycles and designed to work in a wide range of temperature and dust conditions provided a more robust memory system than a netbook, which could easily be damaged by dust or moisture ingress.

The second method of decreasing the regularity of battery changes was to design the station to incorporate a means of charging the batteries during the monitoring process. Power consumption was worked out by summing up the maximum power requirements, taken from the Campbell Scientific manuals, of all of the components of the system which require power and assuming this was the permanent drain on the batteries. These values are given in Table 3.2.

Table 3.2: The power consumption of the monitoring station components

| Component | Quantity | Maximum Power Consumption |
|-------------------|------------------------|------------------------------------|
| TDR100 | 1 | 270mA (Campbell Scientific, 2010c) |
| CR1000 Datalogger | 1 | 16mA (Campbell Scientific, 2010a) |
| SDMX Multiplexer | 3 (only 2 ever active) | 90mA (Campbell Scientific, 2010c) |
| CFM100 | 1 | 30mA (Campbell Scientific, 2008a) |
| GSM Modem | 1 | 500mA (Campbell Scientific, 2010b) |

Whilst this method may have overestimated the power drain, finding a more accurate figure for power consumption would have required extensive knowledge of the length of time each component would be operating in a full power consumption mode, which was not possible at the time of design without extensive testing which was not regarded as appropriate for this research. A total power consumption of 996mA, drawn at 12V (11.95W) per station was found, with all components operating at maximum power. Several methods to generate this power were researched based on cost, reliability and practicality, and solar panels were determined to be the best method for recharging the batteries. Maximum power from solar panels is determined by the output of the panel and the amount of solar irradiance and was estimated using an online calculator in KWh/m² assuming a south facing panel and using the nearest city available (Greenstream Publishing, 2010) and results are presented in Table 3.3.

Table 3.3: The average monthly insolation for Cirencester and Diddington. All figures in KWh/m²

| Month | Jan | Feb | Mar | Apr | May | Jun | Jul | Aug | Sep | Oct | Nov | Dec |
|-------------|------|------|------|------|------|------|------|------|------|------|------|------|
| Cirencester | 0.75 | 1.33 | 2.21 | 3.52 | 4.57 | 4.75 | 4.71 | 3.97 | 2.71 | 1.55 | 0.89 | 0.59 |
| Diddington | 0.71 | 1.36 | 2.28 | 3.47 | 4.51 | 4.68 | 4.69 | 4.04 | 2.70 | 1.65 | 0.90 | 0.57 |

The power output of a variety of different available and affordable solar panels on the market, with power outputs of between 80 and 200W, were calculated assuming a 75% efficiency using Equation 3.1 (Boxwell, 2010).

$$P = (W_{panel} * 75\%) * Ins$$

3.1

Where P is the power drain in Watt hours per day, W_{panel} is the Watt rating of the panel and Ins is the average monthly insolation. It was calculated that a 120W solar panel was able to provide enough power to recharge the batteries for the approximately 10 months of the year on average without the need to change the batteries, with December and January being the

Chapter 3: Field Monitoring Methodology

only months where a deficit of power was recorded. In practice, the solar panels proved to be even more effective than the calculation suggested, possibly due to a greater efficiency than the 75% which was used and an overestimation of the power consumption of the monitoring stations. As a result, the batteries were never changed over the full monitoring period, with the exception of a faulty battery in one of the stations.

The use of the CR1000 datalogger also allowed a greater number of temperature sensors to be installed, allowing a more detailed study of the soils thermal properties, and their effects on measured geophysical parameters to be conducted. The USB controlled thermal probes used by Curioni (2012) were replaced using 107 thermal probes (manufactured by Campbell Scientific). These operate by measuring resistive changes and converting values to temperature using the Steinhart-Hart equation (Campbell Scientific, 2003). Space on the CR1000 was provided to wire up to 16 of these probes; the same as the number of TDR probes on the monitoring station, and the maximum number were chosen to allow all TDR measurements to be accompanied by temperature data from a nearby probe.

Telemetry was needed to ensure the boxes were working without the ability to check them on a regular basis. The locations of the sites (Section 3.2) with no buildings within a local area within which to mount a radio frequency (RF) modem or similar short haul device meant that the decision was made to base communications around the use of the Global System for Mobile Communications (GSM) network, which is commonly used by mobile phones and has a wide coverage in the UK. Communication from the TDR monitoring stations was achieved by use of a Fastrack GSM modem module, supplied by Campbell Scientific for use with their dataloggers. Initial telemetry was setup using the GSM modems to send SMS (Short Message Service) messages to a mobile handset using the CS I/O port of the datalogger and the Hayes command set interface (Campbell Scientific, 2010b) of the modems to initiate a call to the SMS service centre (Campbell Scientific, 2005). Initial problems were caused by a faulty SC-WMI adaptor which was scrambling the outbound messages from the datalogger port. The problem

Chapter 3: Field Monitoring Methodology

took a while to diagnose, but was eventually diagnosed by using hyperterminal (Microsoft Corporation, 2001) to listen to the two way communication on the dataloggers CS I/O port, which showed that the outbound transmissions were clear but the modem echo of commands was scrambled. The datalogger was programmed to transmit a regular SMS message (every 12 hours), detailing the battery voltage and number of readings taken, hence indicating if there was the need for intervention to prevent major data dropouts. However, in practice, this method was found to only record the number of measurements taken by the TDR, providing no safeguard against data loss due to card storage issues (Section 3.6.5) and due to the technical limitations of the datalogger, it was impossible to enable the system to report on additions to the card data tables.

As the above method was unsatisfactory, time was later spent, after installation on developing a telemetry system in order to upload the data in pseudo real time to a file transfer protocol (FTP) server, thus allowing data skips or equipment malfunctions to be picked up and rectified in a more timely fashion. A duplicate set of equipment (TDR100, CR1000 datalogger, CFM100 card reader and GSM modem) was assembled in the laboratory and wired together in the same way as the monitoring stations. Using Campbell Scientific's device configuration utility, the port settings for the datalogger's CS I/O port were changed to include the GPRS (General Packet Radio Service) settings for the mobile phone SIM card, which were obtained online (mPhone Ltd., 2010). These were:

- Access point number
- Username and password
- Gateway IP
- FTP address, username, password and port number

Once these settings were inputted into the logger and a connection to the mobile network obtained, an attempt was made to run a script on the logger with the FTPclient used to send

some test data to an FTP server. Whilst the initial test was successful and data were received on the server, the system had many reliability issues thought to relate to temperamental hardware, especially the SC-WMI adaptors. Subsequent tests were found to work unreliably, occasionally skipping data transmission or sending incomplete records. Unfortunately, due to time constraints the precise causes of these issues were never investigated.

3.4. Construction of the stations

Each monitoring station was designed to support 16 three rod CS645 TDR probes (Figure 3.9) measuring 7.5cm (Campbell Scientific, 2008b).

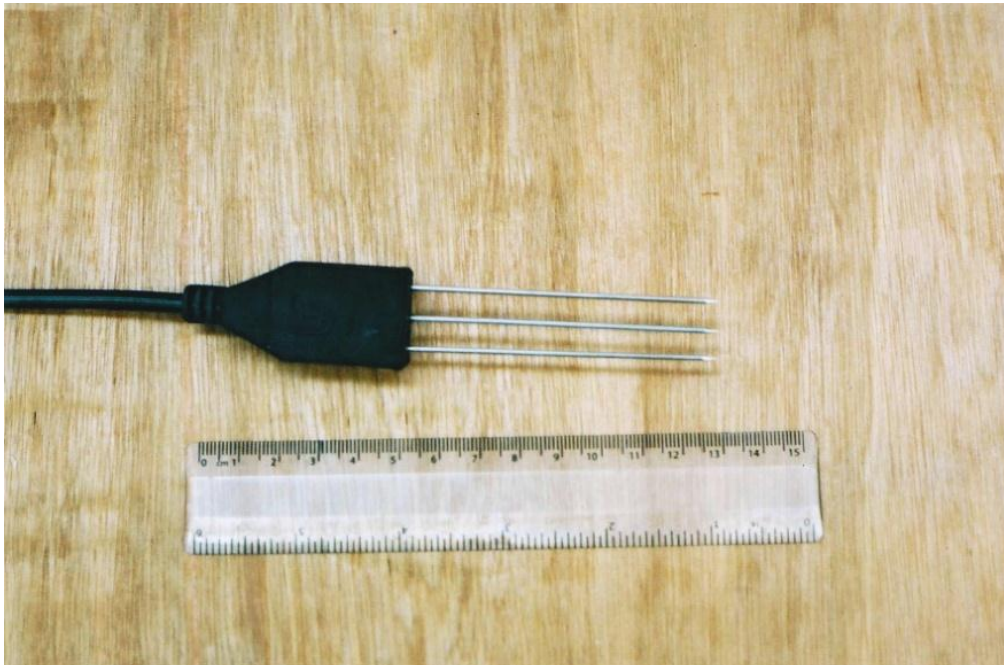


Figure 3.9: A TDR probe used by the monitoring stations

Short probes were chosen as two sites were determined to be fine grained and in cases of high conductivity the signal can attenuate in longer probes before a return reflection can be detected. The external probe cables were first measured for later calibration purposes (Section 3.5) before being covered with 4:1 heat shrinkable insulation in order to protect them against physical and chemical damage upon burial, and further insulate them against damage from burrowing animals and insects. These probes were connected to the TDR100 using three SDM50 (Campbell Scientific, 2010c) eight channel multiplexers (Figure 3.10), which were

Chapter 3: Field Monitoring Methodology

arranged in two levels, with eight probes attached to each of the second level multiplexers, and connected to each other using 50Ω impedance RG58 coaxial cables. The multiplexers, TDR and CR1000 datalogger SDM (Synchronised Device measurement) ports were all connected using 5 conductor cables to provide power and allow control from the CR1000. The CFM100 compact flash expansion was attached to the CR1000 expansion port and an industrial grade CF card inserted to store measurements. The GSM modems were connected to the datalogger CS I/O port using the supplied SC-WMI interface and SC12 cable. The temperature probes were wired to the datalogger output channels in a standard half-bridge circuit, in order to measure and log the resistive change (Campbell Scientific, 2003), which could be converted to temperature by the datalogger's internal program. All of the assembled equipment was placed in a large aluminium flight case (Manufactured by Zarges (Parsons Marketing, 2010)) with 16 holes drilled, eight on each side. Both sets of probes were then threaded out of the box through these holes through IP68 cable glands which were further sealed with silicon to stop moisture ingress. The frames to support the solar panels and weather stations were cut into pieces of the correct length, but were left unassembled for ease of transport, and assembled on site. The solar charge controller was connected to wires with crocodile clips for charging the batteries and was wired to the solar panel on site for ease of transportation.

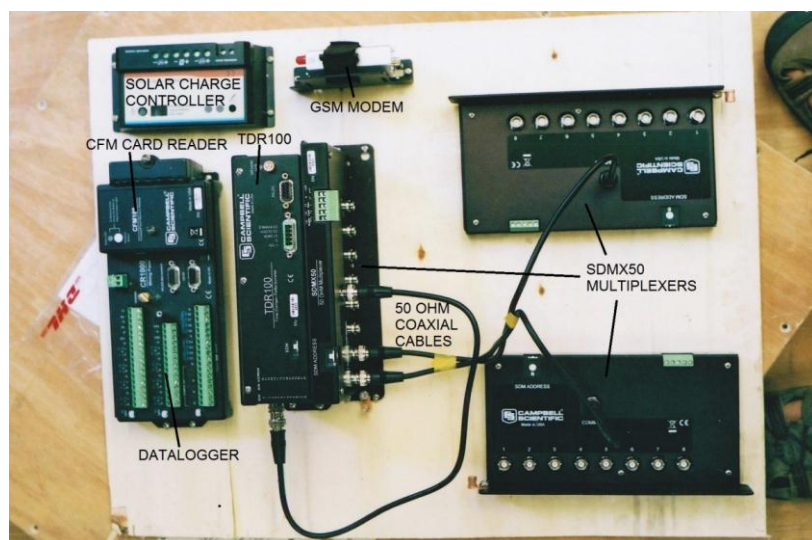


Figure 3.10: The main components of the TDR during construction

Chapter 3: Field Monitoring Methodology

To control the monitoring, a script was written for the CR1000 datalogger using the loggernet software (Stenberg, 2009). The command TDR100 was used to take readings which required a number of parameters to be set. These parameters were:

1. TDR option. This was set to one to acquire raw waveforms for detailed processing at a later date
2. MUXProbeselect. This was a number referring to the multiplexer channel to which each probe was connected and was used to refer to the probe from which the measurement was to be taken
3. WaveAve, the number of waveform to be taken and averaged per reading. This value can range between 1 and 128. More averages give smoother data improving quality but slow down measurement speed. This was set to 50 as this has been shown to provide a good compromise between the rapid acquisition of data (waveforms are collected in about 30 seconds) while still providing reasonable quality waveforms (Curioni et al., 2012).
4. Propagation velocity. The ratio between the speed of light and signal speed in the cable, was set to unity in order to simplify calibrations and use apparent lengths (L_A) as though the cable was a vacuum for measurements. This is common in many TDR applications to avoid the measurement of the cable properties (Jones et al., 2002).
5. Number of measurement points. This could be set to between 20 and 2048. The maximum was chosen, as it was felt that this allowed greater flexibility with data processing.
6. Cable length and Cable offset. These are parameters which determine the window of time from which the waveform is to be stored. For ARDP waveforms, these values needed to be determined experimentally for each probe to ensure a waveform both starting a little way before the probe head and big enough to display the maximum ARDP which was expected in the soil (Figure 3.11). These values were determined for

each probe by determining the size of the window while taking readings in deionised water, as water forms the principal component of the soils dielectric response, having the highest relative permittivity. This means that values of bulk permittivity are almost certain to be below this value, due to the mixture of dielectric materials being sampled. Whilst in practice the start of the probe head is a function of the cable length used on the probe and fixed dielectric properties within the transmission line, it has been observed that the start of the trace can move depending on the dielectric value of the soil (Heimovaara, 1993) and the temperature of the coaxial probe cables (Ren et al., 2005). For this reason, some extra length was left on both ends of the window, to allow for these shifts in waveform position under field conditions. A value of 1.2m was found to be the right length for all probes to display the maximum ARDP values, whereas the cable lengths varied between 8.8 and 9.2m. For BEC waveforms, these values were both set to one hundred to collect detailed data on the time window after all of the signal has been attenuated, from which the BEC values were derived.

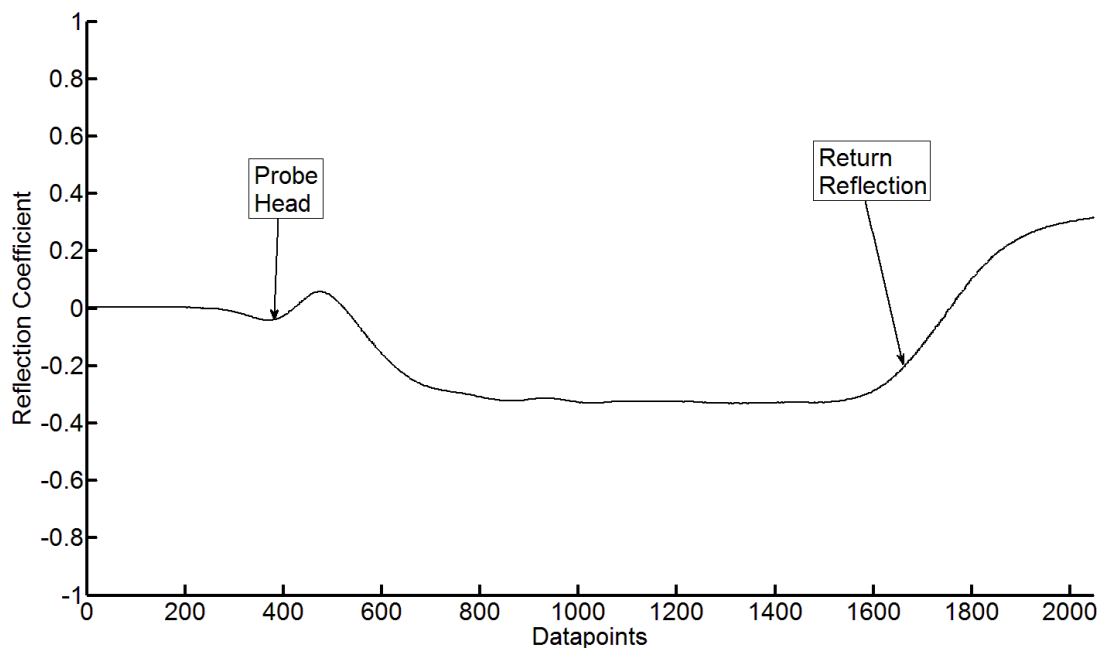


Figure 3.11: A TDR waveform taken in deionised water

In addition to these settings were the options to input a probe length and offset, but these were left at default values as they are only used when using the inbuilt permittivity determination in the CR1000. The CR1000 was scripted to take one ARDP waveform and one BEC per probe every hour as this has been shown to give a temporal resolution capable of discerning change in geophysical properties caused by environmental changes (Curioni et al., 2012). Temperature readings were placed in slow scan sequence, to avoid interference with the main readings and scripted to take place every 30 minutes using the command Therm107 with the relevant channels, using 5 repetitions per reading with the multiplier and offset being set to 1 and 0 respectively to give measurements in °C. Each data table was programmed using the cardout command to instruct the datalogger to store the data on the CF card using the CFM100 expansion.

3.5. Calibration

The station was calibrated to ensure accurate ARDP and BEC values were derived. The temperature probes were supplied factory calibrated to an accuracy of $\pm 0.3^{\circ}\text{C}$ which was assumed to be suitable for this study and hence needed no further calibration in the laboratory. The TDR100 was temporarily disconnected from the CR1000 and calibrations were carried out on the constructed monitoring stations using a laptop which was connected to the TDR100 RS232 port using a USB-serial adaptor. Waveforms were then collected manually using PCTDR. Tests on the effects of cable temperature, multiplexers and probes on measurements and calibrations using the same equipment and setup were carried out by Curioni (2013).

3.5.1. Calibration of Monitoring Stations for Apparent Relative Dielectric Permittivity (ARDP)

ARDP waveforms are commonly expressed as a function of apparent length rather than actual length with higher dielectric materials slowing down the signal more, resulting in greater apparent lengths. However, this method requires the location of the start of the waveform in

the probe head experimentally in the laboratory. The TDR probes were calibrated for permittivity readings by determining the calibrated apparent length (L_{cal}) and probe offset (P_{off} ; area of the rods covered by the epoxy resin head of the probe) for each of the probes by taking readings in air and deionised water, following the method of Robinson et al. (2003b) and Heimovaara (1993) as the exclusive use of deionised water has been shown to introduce errors, particularly at low ARDP values.

Waveforms were taken from each of the probes using the same settings that were determined for use with the datalogger script (Section 3.4). Ten waveforms in air, with the ends of the probes shorted by aluminium foil to allow an accurate determination of the ends of the rods, were recorded per probe in a temperature controlled room at 22°C ($\pm 1^\circ\text{C}$). Ten waveforms in deionised water were also recorded for each probe, with the temperature of the water being held at a constant 22°C using a water bath to allow the permittivity to be predicted (Catenaccio et al., 2003, Meissner and Wentz, 2004) for use in subsequent calibration equations.

The resulting waveforms were then analysed manually by fitting tangents to the wave using the method of Heimovaara and Bouton (1990) and Menziani et al. (1996). The apparent length of each datapoint (L_{dp}) was determined using Equation 3.2.

$$L_{dp} = \frac{L_{win}}{N_{dp}}$$

3.2

Where L_{win} is the window length in m, set as 1.2m for all probes and N_{dp} is the number of data points in the waveform (2048). This yielded the value of 0.0005859375m per data point. The probe head was located on each trace by finding the minimum caused by the impedance dip as the signal enters the probe head and finding its intersection with a tangent, fitted to the initial rising limb of the waveform. This gave a reliable, constant and easily locatable point for the

Chapter 3: Field Monitoring Methodology

waveform head (L_{start}) which is more reliable than the apex of the initial bump which can move significantly in layered systems (Robinson et al., 2003b), and which could be found even in the event of it moving due to field conditions. The end reflection (L_{end}) was found by finding the minimum values of the waveform and finding the intersection with a tangent fitted to the rising limb caused by the returning reflected signal. The apparent lengths for water (L_w) and air (L_g) were determined for each waveform using Equation 3.3 and the results averaged.

$$L_{w/g} = (L_{end} - L_{start}) * L_{dp}$$

3.3

Equation 3.4 was then used to calculate the calibrated apparent lengths of the probes.

$$L_A = \frac{(L_w - L_g)}{(\sqrt{\epsilon_w} - \sqrt{\epsilon_g})}$$

3.4

Where ϵ_w and ϵ_g are their respective known relative dielectric permittivity values. In air, this value is 1 and in water at 22°C, the value is 79.49 (Meissner and Wentz, 2004). The L_A values were then used in Equation 3.5 to calculate the probe offset (P_{off}) values for each probe using the derived apparent length of water.

$$P_{off} = L_W - (L_A \sqrt{\epsilon_W})$$

3.5

Calibration was tested using acetone, kept at 25°C using a water bath, which has a known relative dielectric permittivity value of 20.7 (Buckley and Maryott, 1958) and water at 10°C with a known value of 83.98 (Meissner and Wentz, 2004), and the maximum error on each of the probes was found to be no more than ± 0.4 . The average absolute errors for each station and the standard deviation between probes are shown in Table 3.4.

Table 3.4: The errors in ARDP calibrations on each station

| Monitoring Station | Average Absolute Error | | Standard Deviation between Probes | |
|--------------------|------------------------|--------------------|-----------------------------------|--------------------|
| | Acetone 25°C (20.7) | Water 10°C (83.98) | Acetone 25°C (20.7) | Water 10°C (83.98) |
| CQF Archaeology | 0.22 | 0.38 | 0.27 | 0.32 |
| CQF SSM | 0.27 | 0.36 | 0.20 | 0.36 |
| CCC | 0.24 | 0.39 | 0.29 | 0.38 |
| DCF Archaeology | 0.19 | 0.37 | 0.22 | 0.39 |
| DCF SSM | 0.18 | 0.36 | 0.22 | 0.37 |
| DPF | 0.22 | 0.38 | 0.26 | 0.38 |
| Mean | 0.22 | 0.37 | 0.24 | 0.37 |

3.5.2. Calibration of Monitoring Stations for Bulk Electrical Conductivity (BEC)

BEC can be derived using TDR waveforms which use a long apparent length, using the final reflection coefficient value after all of the signal has been attenuated to reach a steady state reflection coefficient (Γ_{∞}). For more accurate readings, a long window length is also used to allow all of the high frequency components to attenuate leaving a DC value (Ball, 2002) and the later values from the waveform are averaged to minimize the effects of noise on the trace. Conductivity calibrations were based on the methods of Curioni et al. (2012), Huisman et al. (2008) and Bechold et al. (2010). Initial tests were carried out to select suitable parameters for conductivity waveforms. Curioni (2012) used waveforms with apparent lengths between 0m and 200m, with the steady state reflection being derived from the final 75 datapoints. However, an apparent cable length of 100m and window length of 100m was thought to allow more datapoints in the area of interest to be averaged, reducing noise on the trace. To test this, an initial experiment was set up to compare the two methods by testing derived reflection coefficients in 2 KCl solutions, one with a high conductivity and one with a low

conductivity using two probes. Six waveforms were taken in each solution per probe, with solutions being held at a constant 25°C. The results are displayed in Table 3.5.

Table 3.5: Comparison of different methods for BEC determination

| | Solution | High (c.1.4 S/m) | | Low (c. 0.0075 S/m) | |
|---------|--------------------|------------------|--------------------|---------------------|--------------------|
| | | Mean | Standard Deviation | Mean | Standard Deviation |
| Probe 1 | Method 1 (0-200) | -0.8361 | 0.00082 | 0.8556 | 0.0042 |
| | Method 2 (100-200) | -0.8366 | 0.00045 | 0.8561 | 0.0045 |
| Probe 2 | Method 1 (0-200) | -0.8285 | 0.0074 | 0.8554 | 0.0032 |
| | Method 2 (100-200) | -0.8332 | 0.0017 | 0.8594 | 0.0045 |

Few differences can be observed at lower conductivity values between the two methods, with the 0-200 apparent length waveforms providing slightly more consistent results, albeit only slightly. At the higher conductivity values, the 100-200 apparent distance waveforms were found to give more consistent results. As several of the sites were due to be located in clay, which is associated with higher BEC values (up to 1 S/m in extreme cases; Herz and Garrison, 1998), the bespoke monitoring stations for this project therefore used an apparent cable length of 100m and a window length of 100m. The final 144 data points (1904-2048) were averaged for each waveform to reduce instrument noise and produce a reflection coefficient (Γ) from which to calculate BEC.

For each of the probes, six waveforms using the parameters set in the datalogger script were taken in air and all of these waveforms were used to find the TDRs characteristic open circuit measurement (Γ_{open}), which deviates from its theoretically correct value of 1 for a perfectly non-conducting medium (Lin et al., 2008) due to circuitry imperfections. The results of these waveforms were averaged to give a TDR100 specific open circuit reflection coefficient, which

varied between 0.95 and 0.97 and which was then used to scale all subsequent reflection coefficients between -1 and 1 using Equation 3.6.

$$\Gamma_{corr} = \frac{2(\Gamma + 1)}{\Gamma_{open} + 1} - 1$$

3.6

Table 3.6: KCl solution concentrations and approximate conductivity values

| Solution No | 1 | 2 | 3 | 4 | 5 | 6 | 7 | 8 |
|-------------------------------------|------|------|-------|------|--------|--------|-------|---------|
| Approximate Molar Concentration (M) | 0.15 | 0.1 | 0.075 | 0.03 | 0.0038 | 0.0019 | 0.001 | 0.00047 |
| Approximate Conductivity (S/m) | 1.75 | 1.21 | 0.88 | 0.35 | 0.025 | 0.012 | 0.008 | 0.0065 |

Eight solutions of different concentrations of KCl solution were used in order to calibrate, with concentrations ranging from 0.1M to 0.000001M (Table 3.6) used to provide a good range of different conductivity values which could be encountered in the soil. These were kept at a constant temperature of 22°C throughout the calibration, to avoid temperature related fluctuations in conductivity. Reference conductivities for each of the solutions were taken using a handheld conductivity meter (HI9033 manufactured by Hanna instruments) each time a new set of probes was calibrated. Each probe was used to take 3 waveforms in each solution, and the resulting load resistance (R_L) for each waveform was calculated from the corrected reflection coefficient using Equation 3.7 and the results averaged for each solution.

$$R_L = Z_{out} \frac{1 + \Gamma_{corr}}{1 - \Gamma_{corr}}$$

3.7

Where Z_{out} is the output impedance of the TDR100 (50Ω). The equation governing the relationship between the R_L values and measured conductivity is Equation 3.8.

$$\sigma = \frac{K_P}{R_L - (C_L R_c + R_0)}$$

3.8

Where K_p is the probe constant which is based on the geometry of the probe, C_L is the length of the probe cable and R_c and R_0 are the cable and series resistor parameters respectively. In order to find the unknown parameters (K_p , R_c and R_0), a two stage process was used. Since cable and series resistance effects are negligible in low conductivity solutions (Huisman et al., 2008), the other parameters R_c and R_0 could be assumed in the low range to be roughly zero. The four lowest conductivity solution values, which ranged between c.0.025S/m and c.0.0065S/m, were plotted against the TDR derived conductance (reciprocal of the load resistance) for each probe (Figure 3.12), and the gradient of a fitted linear function, found using linear regression and constrained through the origin of the graph, was calculated to find the probe constant reciprocals ($1/K_p$). The R_c and R_0 parameters were found by applying an empirical fitting method using data from all eight solutions and a Nelder-Mead simplex optimisation (Nelder and Mead, 1965), based on the `fminsearch` function in MATLAB® (MathWorks Inc., 2010)¹ to find the optimum fitting values across the whole conductivity range. Equation 3.8 was used, with the K_p fixed to those derived in the first calibration stage and the cable lengths input from those measured during the construction process.

The calibrations were tested using 3 solutions with different concentrations of KCl (conductivity values c.0.0241S/m - 0.125S/m), to those used for the calibration, with the TDR derived values compared to values derived from the conductivity meter. The average errors and standard deviations between the readings are displayed in Table 3.7. The low standard

¹ © 2013 The MathWorks, Inc. MATLAB and Simulink are registered trademarks of The MathWorks, Inc. See www.mathworks.com/trademarks for a list of additional trademarks. Other product or brand names may be trademarks or registered trademarks of their respective holders

deviations between different readings (<2%) suggest a good precision for the instruments when measuring BEC values using TDR. At low conductivity values, errors are small (<5% for all stations). In the decisiemens range, errors are more significant (up to 14.4%), although values of this magnitude are rare in soil, and the errors were deemed acceptable.

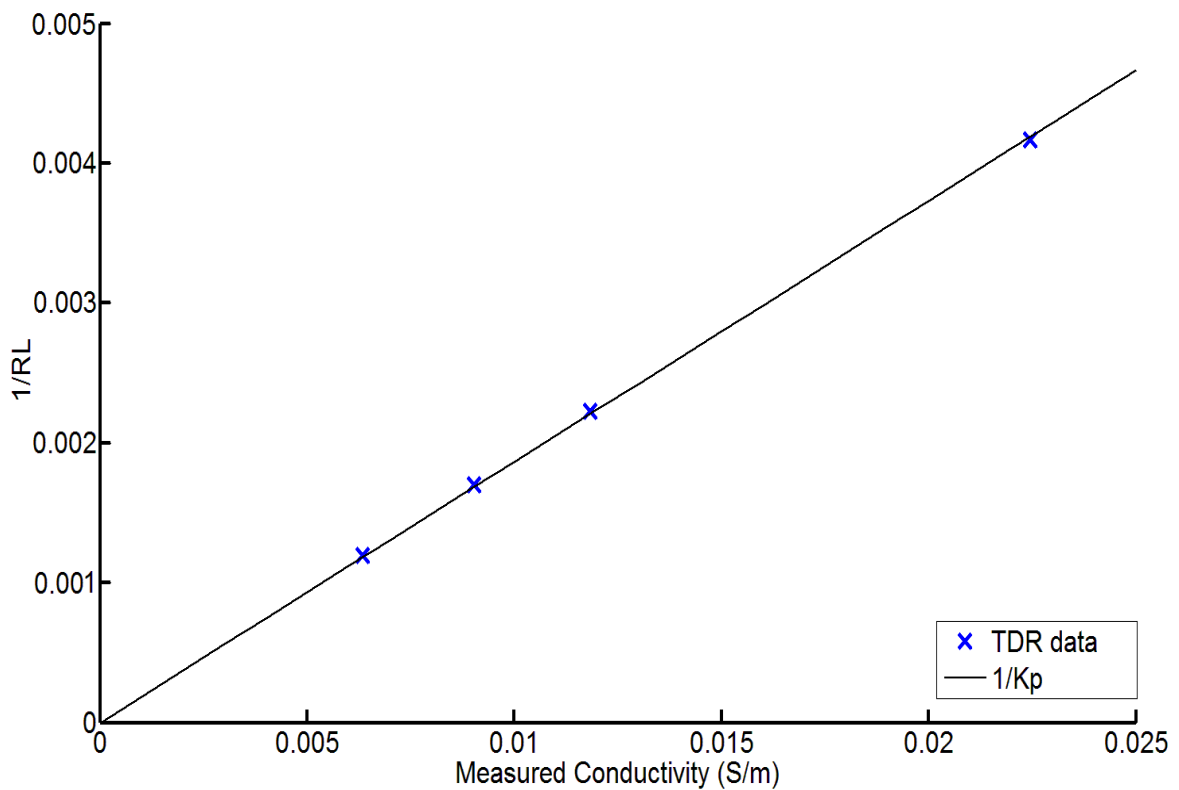


Figure 3.12: The $1/R_L$ values for the low conductivity solutions plotted against the conductivity for one of the probes and the linear regression ($1/K_p$)

Table 3.7: The errors and standard deviations of BEC values derived from the TDR calibrations

| Monitoring Station | Average Error | | | Standard Deviation | | |
|--------------------|------------------------------|------------------------------|------------------------------|------------------------------|------------------------------|------------------------------|
| | Solution 1 (c.0.0241 S/m) | Solution 2 (c.0.0430 S/m) | Solution 3 (c.0.1250 S/m) | Solution 1 (c.0.0241 S/m) | Solution 2 (c.0.0430 S/m) | Solution 3 (c.0.1250 S/m) |
| CQF Archaeology | 0.0006 (2.48%) | 0.0009 (2.09%) | 0.0022 (1.76%) | 0.0002 (0.82%) | 0.0004 (0.93%) | 0.0007 (0.56%) |
| CQF SSM | 0.0005 (2.07%) | 0.0006 (1.39%) | 0.0107 (8.56%) | 0.0002 (0.82%) | 0.0004 (0.93%) | 0.0010 (0.8%) |
| CCC | 0.0003 (1.24%) | 0.0005 (1.16%) | 0.0138 (11.04%) | 0.0003 (1.24%) | 0.0007 (1.63%) | 0.0013 (1.04%) |
| DCF Archaeology | 0.0009 (3.73%) | 0.0005 (1.16%) | 0.0171 (13.68%) | 0.0003 (1.24%) | 0.0005 (1.16%) | 0.0013 (1.04%) |
| DCF SSM | 0.0005 (2.07%) | 0.0011 (2.55%) | 0.0160 (12.8%) | 0.0003 (1.24%) | 0.0004 (0.93%) | 0.0011 (0.88%) |
| DPF | 0.0010 (4.15%) | 0.0003 (0.69%) | 0.0180 (14.4%) | 0.0004 (1.65%) | 0.0004 (0.93%) | 0.0021 (1.68%) |
| Mean | 0.0006 (2.61%) | 0.0006 (1.51%) | 0.0129 (10.32%) | 0.0002 (1.16%) | 0.0004 (1.09%) | 0.0012 (1%) |

3.6. Probe Installation Procedure

3.6.1. Introduction

Two different set-ups were used for the monitoring stations depending on the soil type present. This was based on the expected complexity of the 'difficult' soils, (i.e. fine grained soils) and financial limitations. On the geophysically unresponsive sites, two 16 probe monitoring station arrays were used (one to monitor profiles inside the archaeological ditch feature and one to monitor the SSM), whereas a single 16 probe array was used on the sites which were thought to facilitate easier detection with heritage detection techniques. Probes were installed at a variety of depths to look at vertical change in geophysical properties, and each probe was duplicated by another probe in the same context at a similar depth where

Chapter 3: Field Monitoring Methodology

technical limitations of the insertion method and the number of probes available allowed. This allowed for lateral variation and heterogeneity of the soil to be estimated, as well as providing some redundancy in case of probe failure during the monitoring period of the project.

Weather stations were also installed on all sites to record precipitation, air temperature, wind speed and direction, humidity and pressure. Two of the weather stations, located on the difficult soil at each location were also equipped with a solar radiation sensor and were therefore able to provide estimates of ET. The decision to locate a weather station at each site was made after suggestions in the literature that for single events, weather is not spatially uniform (Fiener and Auerswald, 2009). To investigate this, data from two weather stations on the University of Birmingham campus, approximately 400 m apart were plotted against each other for moderate and light rainfall events (Figure 3.13). It was found that although there were only very slight differences in the total amount of rainfall, the temporal nature of the event could vary by a number of hours. For this reason, a decision was made to locate weather stations at all sites, firstly to ensure the best data quality for looking at individual events and secondly to provide redundancy in case of equipment failure.

In addition to the bespoke TDR monitoring stations, a commercial borehole TDR sensor (TRIME T3 probe manufactured by IMKO GmbH) was installed on one of the sites (DCF) for comparative purposes. This does not form part of the present work, but a comparison between data from the two monitoring systems can be found in Appendix D.

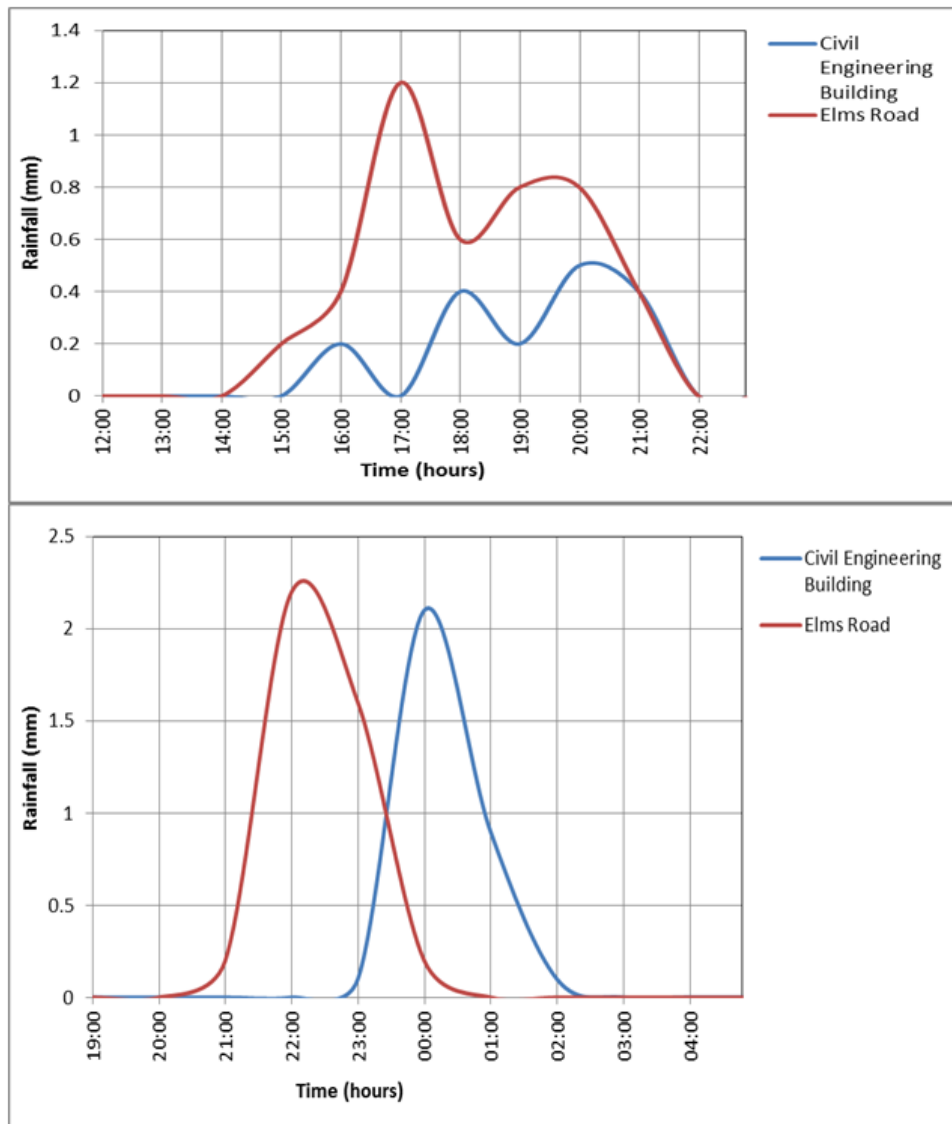


Figure 3.13: Comparison of two rainfall events from weather stations c.400m apart

A schematic showing the layout and scale of the excavations, the locations of the probes, TDR boxes, soil samples and the areas of disturbed and undisturbed soil is shown in Figure 3.14.

The volume of soil measured by each TDR probe is determined by the length of the probe and the geometry of the probe rods as it only takes measurements of the soil immediately surrounding the three electrodes in a cylinder roughly approximating a coaxial cell. The probes used in this study had a length of 75mm with rods roughly spanning 40mm giving a total soil measurement volume of about $94 \times 10^3 \text{ mm}^3$. More detailed information on the installation method and site specific details are provided in Sections 3.6.2-3.6.4.

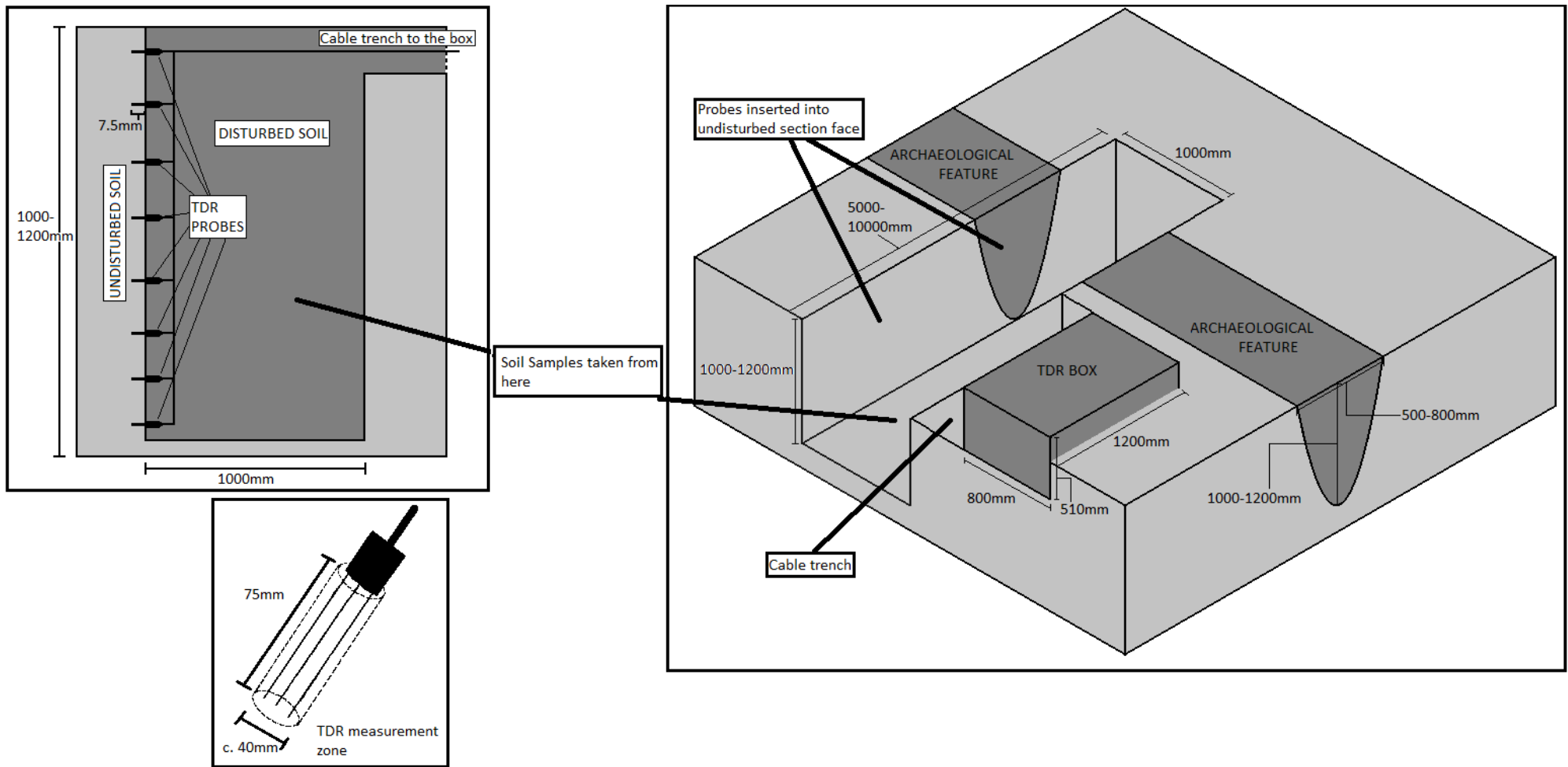


Figure 3.14: Schematic showing the layout and scale of the excavations, the locations and measurement volumes of the probes, TDR boxes and soil samples and the areas of disturbed and undisturbed soil

3.6.2. Excavations

Topsoil was stripped from the sites and initial excavations of the archaeological features were conducted by hand on a context by context basis using standard archaeological excavation tools and methods (Renfrew and Bahn, 2004). Contexts were kept separate using plastic sheets, to facilitate backfilling in a manner which preserved the conditions of the site as far as possible. Artefact finds were bagged and recorded by context, depth and location within the context layer. Following the excavation of the features, a box section was cut through the excavated section using a mechanical digger to a depth of between 1-1.2m, depending on the depth of the archaeological features. Trenches were drawn at 1:10 scale and photographed as part of the site recording process. Reference data for trench locations, including the positional nails used for section drawings were recorded using a dGPS. A full report on the excavations and installations was prepared (Wilkinson, 2011); however the key features are summarised below.

The excavations took place on 11-16th April 2011 at both sites in Harnhill, Cirencester. At CQF, excavation revealed a ditch c.1m deep which was cut through the Forest Marble formation clay. The ditch was found to contain two terracotta pipes (Figure 3.15) thought to be part of a land drainage system. Consultation with the land manager suggested that these were no longer part of the active drainage system of the field and permission was given to remove them. In another part of the trench, a concrete slab covering another drain feature containing water was found suggesting it was active. Work on this area of the trench was discontinued and attention was focused on the North East part of the trench. No additional finds were recorded, but the pipes dated the ditch to within the last 100-150 years. The site ditch was primarily filled in using reworked clay, which appeared to be darker in colour, possibly due to soil formation processes near to the surface (Wilkinson, 2011).



Figure 3.15: The feature at Cirencester Quarryfield

Excavation at the new site at CCC revealed the site to contain a rock cut ditch through the weathered Cornbrash limestone formation, with the natural depth of the soil outside the ditch only being around 0.2m-0.3m. The ditch was filled with a poorly sorted mixture of large limestone pebbles, and red brown silt and clay. Finds from the ditch, including glass and a tin can, dated the feature to within the last 100-150 years suggesting a modern field boundary feature.

Excavations at Diddington were conducted in the summer of 2011. Diddington Pasture Field was excavated on 6th-8th June. Excavation revealed that the whole site was capped below the topsoil by a dense fluvial fine grained layer with some sub-rounded flint pebbles, which ran across both the archaeological ditch and SSM soils suggesting it post-dated the formation of the feature. The ditch was cut through Pleistocene gravels and the feature fill appeared to contain finer grained material than the SSM soils. The ditch itself contained 3 different fills, each with finds including pottery, ceramics and animal bone. The bottom fill was dated to the prehistoric period using the pottery finds (Wilkinson, 2011).



Figure 3.16: The ditch at Cirencester Cherry Copse. Photo used under Creative Commons License from Robert Fry



Figure 3.17: The ditch at Diddington Pasture field. Photo by Keith Wilkinson.

Excavations at Diddington Clay Field were conducted between 22nd and 24th August 2011.

Beneath the topsoil, the soil had developed a distinct subsoil horizon which covered the whole site, which was slightly thicker over the archaeological feature and thought to have been formed due to cultivation practices on site. The ditch feature contained two fills (context 4 and 5), the upper of which consisted of reworked boulder clay with no archaeological finds suggesting a deliberate backfilling of the ditch. The lower fill was made of poorly sorted material with a high humic content, which gave it a dark appearance. Multiple uneroded pottery fragments were found, which suggested the fill dated to the Roman period. The SSM was Pleistocene compact chalky boulder clay, which appeared to be unmodified by agricultural activities on site.

3.6.3. Recovery of Soil Samples

Samples of each of the sediments encountered during the excavations were also brought back for further laboratory analysis and geotechnical characterisation which was important to link the EM behaviour of the soil to its physical properties and identify the reasons for contrasts between the archaeological features and SSM. Several different types of sample were collected for analysis. Undisturbed samples were collected using monolith tins with dimensions of 0.5m x 0.1m x 0.1m which were inserted into the side of the section using a sledgehammer and a piece of wood until the tins were fully flush against the section face (Figure 3.18). Samples were taken at depths of c.0m-0.5m and c.0.5m-1m. After the location of these was recorded on the section drawing, they were carefully removed using a spade to dig around the tin, taking care to keep the sample inside intact before being sealed in plastic to avoid moisture loss. Additional small disturbed samples were taken using a trowel from the section face for further water content testing and stored in water tight plastic containers (Figure 3.18), which were sealed using Polytetrafluoroethylene (PTFE) and electrical tape to create a good seal. Finally bulk samples were taken from the excavated material for each soil context. For samples where there was plenty of available material (e.g. SSM and topsoil), 1m³

builders bulk bags were used, whereas for soils where the amount of material was limited material was taken in 5 litre plastic sample bags.

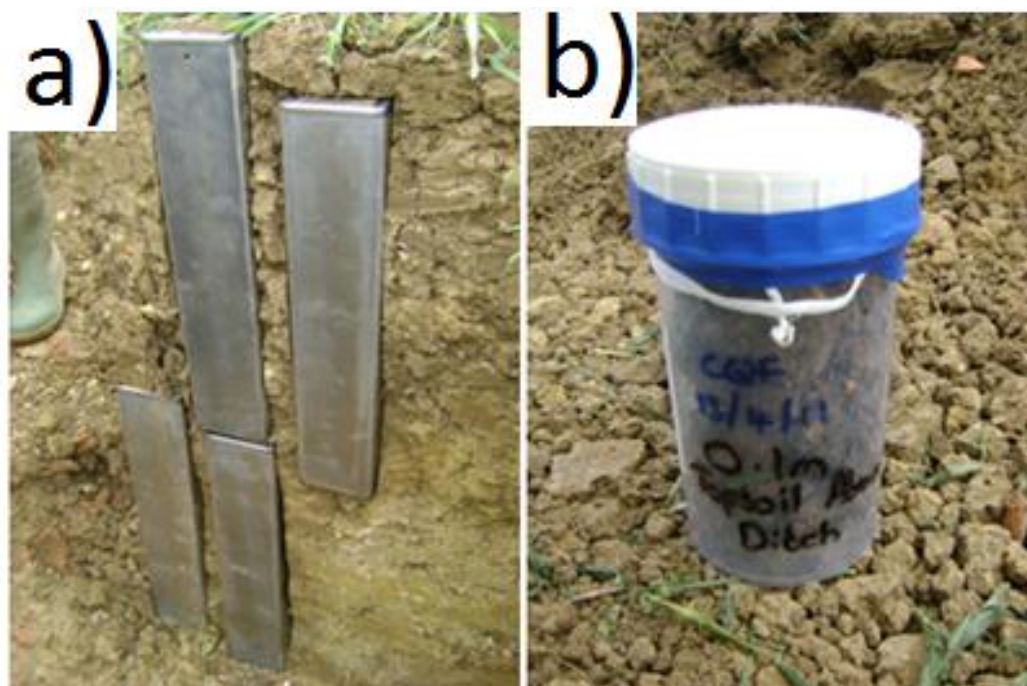


Figure 3.18: Different soil sampling methods. a) Monolith Tins b) Water content samples

Table 3.8: A summary of the samples collected from each site

| TYPE OF SAMPLE | QUANTITY TAKEN |
|-------------------------------|---|
| Monolith (undisturbed sample) | 4 per trench : 2 archaeology (c.0m-0.5m and c.0.5m-1m)and 2 SSM (c.0m-0.5m and c.0.5m - 1m) |
| Sealed moisture preserved | 2 per soil layer or archaeological sediment |
| Bulk sample | 1m ³ of archaeological sediment (separated into different amounts of sediment layers depending on availability) and 1m ³ of SSM |

A summary of the samples and the amount taken is shown in Table 3.8, with the following exceptions.

- At DPF, an undisturbed sample could not be taken below 0.5m due to the unconsolidated nature of the gravel soil.
- At DCF, Ditchfill2 was too small to sample in great detail so no bulk samples were taken.

Chapter 3: Field Monitoring Methodology

- At CCC no monolith sample was taken from the SSM profile as the depth of soil on top of the bedrock was not deep enough
- At CQF, only one monolith tin was taken from 0m-0.5m as this already reached the bottom context
- At DCF an additional monolith sample was taken from the ditch, overlapping the other two as the ditch was over 1m deep.

3.6.4. Method of Installation

A small platform was excavated for each of the monitoring stations and the solar panel mounting structures were assembled in situ. The sensor box was placed on top on the frame as per the design (Figure 3.19).



Figure 3.19: The construction of the solar panel mounting frame and positioning of the monitoring stations

TDR probes were inserted using a set of plastic waveguides in order to keep the rods parallel as shown in Figure 3.20 to minimise measurement errors caused by deviation from idealised probe geometry. The location of the probes was driven partly by necessity to avoid large

stones which have the potential to cause macrovoids and air gaps which decrease the accuracy of ARDP readings, and also bend the rods causing inaccurate determination of BEC. For this reason when a stone was encountered, the probe was taken out and reinserted nearby. The thermistor probes were inserted into holes made using a hand drill, the diameter of the probe in the section face, about 5-10cm from each inserted TDR probe, as it was felt this was close enough to provide representative temperature data from the area of the TDR probe without compromising the TDR data integrity.



Figure 3.20: The insertion of the TDR probes using plastic waveguides to keep rods parallel

Once all the probes had been inserted, their locations were recorded relative to the section drawing. At both Diddington sites, the probe locations were also recorded with a dGPS. The final locations of the probes were a compromise between a combination of the desire to study both vertical and lateral variation in soil EM properties, and the feasibility of insertion at a particular location due to stones and other insertion difficulties. Their final locations are shown in Figures 3.24-3.27 and described below in Table 3.9 (Cirencester) and Table 3.10 (Diddington).

Chapter 3: Field Monitoring Methodology

The clay sites were each equipped with two 16 probe sensors. At CQF, one 16 probe sensor (Cirencester Quarryfield SSM, hereafter abbreviated to CQFN) was placed outside of the archaeological feature with two arrays of 8 probes from 0.07m-1m, whereas the other 16 probe sensor (Cirencester Quarryfield Archaeology, hereafter abbreviated to CQFA) was placed in two vertical arrays at similar depths within the ditchfill. The locations of the probes are shown in Figure 3.26.

Similarly, two 16 probe sensors were used at DCF; one operating inside the archaeological ditch (Diddington Clay field Archaeology, abbreviated to DCFA) and one to monitor the SSM (Diddington Clay field SSM, abbreviated to DCFN). The DCFA sensors were arranged in two vertical 8 probe arrays within the ditch, at depths between c.0.07m-1m. The DCFN sensors were arranged in two vertical arrays of 7 probes each with an additional two probes (7 and 15) being used to monitor the top two contexts closer to the archaeological ditch. This allowed both the heterogeneity of these layers and the lateral dropoff in geophysical contrast to be studied in greater detail. The location of these probes is shown in Figures 3.20, 3.21 and 3.24.

On the non-clay sites, only a single 16 probe sensor was used to measure both the archaeological ditch and the SSM. At DPF, the setup was complicated by the comparatively deep excavation (1.2m) and the lack of available probes for the non-clay setup. The probes outside the archaeological feature were arranged in two arrays, one with 5 probes at depths between 0.07-1.2m and a second array of 3 probes, located closer to the ditch and concentrated on the upper regions of the soil from 0.07-0.5m. The probes inside the ditch were arranged to cover the full depth of the ditch in a single array, although one duplicate probe was installed in context 3. The layout is shown in Figure 3.27.

At CCC, installation was complicated by the shallow nature of the soil, which led to a detailed study of topsoil changes being carried out on this site. Eight of the monitoring stations sixteen probes were placed in two profiles of four probes outside the archaeology (from 0.07m-0.25m in depth) with the other eight being placed in each of the recognised archaeological contexts

inside the ditch (2 in each context). The location of these probes is shown in Figures 3.22, 3.23 and 3.27.



Figure 3.21: The inserted probes at DCFA in the ditch section



Figure 3.22: The inserted probes at DCFN in the SSM



Figure 3.23: The inserted probes at CCC in the ditch section



Figure 3.24: The inserted probes at CCC in the SSM. Note the rock below c. 0.2m depth

Chapter 3: Field Monitoring Methodology

Backfill of the trenches were conducted, taking as much care as possible to replace the soil context types in reverse order (i.e. back in the same place they were in pre-excavation) and alter the environmental dynamics of the site as little as possible. The area in the probes immediate vicinity was backfilled by hand to minimise the risk of damage to the probes, before the rest of the trench was backfilled using a mechanical digger. At several points during the process, backfilling was halted to compact the soil using the back of the digger bucket. At CQF, a petrol driven vibrating compactor was also used, although this was found to have little effect on the consolidation of the replaced material.

Table 3.9: The depths and contexts of probes for the Cirencester sites

| SITE | STATION | PROBE | APPROXIMATE DEPTH (m) | CONTEXT | SOIL TYPE |
|------|---------|-------|-----------------------|----------------|-------------|
| CQF | CQFA | 1 | 0.07 | 1 (Topsoil) | Archaeology |
| | CQFA | 2 | 0.13 | 1 (Topsoil) | Archaeology |
| | CQFA | 3 | 0.30 | 5 (Ditchfill1) | Archaeology |
| | CQFA | 4 | 0.46 | 5 (Ditchfill1) | Archaeology |
| | CQFA | 5 | 0.65 | 7 (Ditchfill2) | Archaeology |
| | CQFA | 6 | 0.70 | 7 (Ditchfill2) | Archaeology |
| | CQFA | 7 | 0.82 | 9 (Lower SSM) | SSM |
| | CQFA | 8 | 1.00 | 9 (Lower SSM) | SSM |
| | CQFA | 9 | 0.07 | 1 (Topsoil) | Archaeology |
| | CQFA | 10 | 0.15 | 1 (Topsoil) | Archaeology |
| | CQFA | 11 | 0.30 | 5 (Ditchfill1) | Archaeology |
| | CQFA | 12 | 0.45 | 5 (Ditchfill1) | Archaeology |
| | CQFA | 13 | 0.60 | 7 (Ditchfill2) | Archaeology |
| | CQFA | 14 | 0.70 | 7 (Ditchfill2) | Archaeology |
| | CQFA | 15 | 0.83 | 9 (Lower SSM) | SSM |
| | CQFA | 16 | 1.00 | 9 (Lower SSM) | SSM |
| | CQFN | 1 | 0.08 | 1 (Topsoil) | SSM |
| | CQFN | 2 | 0.15 | 1 (Topsoil) | SSM |
| | CQFN | 3 | 0.30 | 8 (Upper SSM) | SSM |
| | CQFN | 4 | 0.50 | 8 (Upper SSM) | SSM |
| | CQFN | 5 | 0.60 | 9 (Lower SSM) | SSM |
| | CQFN | 6 | 0.75 | 9 (Lower SSM) | SSM |
| | CQFN | 7 | 0.87 | 9 (Lower SSM) | SSM |
| | CQFN | 8 | 1.00 | 9 (Lower SSM) | SSM |
| | CQFN | 9 | 0.07 | 1 (Topsoil) | SSM |
| | CQFN | 10 | 0.15 | 1 (Topsoil) | SSM |
| | CQFN | 11 | 0.30 | 8 (Upper SSM) | SSM |
| | CQFN | 12 | 0.50 | 8 (Upper SSM) | SSM |
| | CQFN | 13 | 0.60 | 9 (Lower SSM) | SSM |
| | CQFN | 14 | 0.75 | 9 (Lower SSM) | SSM |
| | CQFN | 15 | 0.87 | 9 (Lower SSM) | SSM |
| | CQFN | 16 | 1.00 | 9 (Lower SSM) | SSM |
| CCC | CCC | 1 | 0.15 | 1 (Topsoil) | Archaeology |
| | CCC | 2 | 0.40 | 7 (Ditchfill1) | Archaeology |
| | CCC | 3 | 0.60 | 8 (Ditchfill2) | Archaeology |
| | CCC | 4 | 0.90 | 9 (Ditchfill3) | Archaeology |
| | CCC | 5 | 0.20 | 1 (Topsoil) | Archaeology |
| | CCC | 6 | 0.40 | 7 (Ditchfill1) | Archaeology |
| | CCC | 7 | 0.70 | 8 (Ditchfill2) | Archaeology |
| | CCC | 8 | 1.00 | 9 (Ditchfill3) | Archaeology |
| | CCC | 9 | 0.07 | 1 (Topsoil) | SSM |
| | CCC | 10 | 0.15 | 1 (Topsoil) | SSM |
| | CCC | 11 | 0.20 | 1 (Topsoil) | SSM |
| | CCC | 12 | 0.25 | 1 (Topsoil) | SSM |
| | CCC | 13 | 0.07 | 1 (Topsoil) | SSM |
| | CCC | 14 | 0.15 | 1 (Topsoil) | SSM |
| | CCC | 15 | 0.20 | 1 (Topsoil) | SSM |
| | CCC | 16 | 0.25 | 3 (Subsoil) | SSM |

Table 3.10: The depths and contexts of probes for the Diddington sites

| SITE | STATION | PROBE | APPROXIMATE DEPTH (m) | CONTEXT | SOIL TYPE |
|------|---------|-------|-----------------------|-----------------|-------------|
| DCF | DCFA | 1 | 0.10 | 1 (Topsoil) | Archaeology |
| | DCFA | 2 | 0.20 | 1 (Topsoil) | Archaeology |
| | DCFA | 3 | 0.30 | 2 (Subsoil) | Archaeology |
| | DCFA | 4 | 0.50 | 2 (Subsoil) | Archaeology |
| | DCFA | 5 | 0.70 | 4 (Ditchfill1) | Archaeology |
| | DCFA | 6 | 0.80 | 4 (Ditchfill1) | Archaeology |
| | DCFA | 7 | 0.90 | 5 (Ditchfill2) | Archaeology |
| | DCFA | 8 | 1.00 | 5 (Ditchfill2) | Archaeology |
| | DCFA | 9 | 0.10 | 1 (Topsoil) | Archaeology |
| | DCFA | 10 | 0.20 | 1 (Topsoil) | Archaeology |
| | DCFA | 11 | 0.30 | 2 (Subsoil) | Archaeology |
| | DCFA | 12 | 0.40 | 2 (Subsoil) | Archaeology |
| | DCFA | 13 | 0.60 | 4 (Ditchfill1) | Archaeology |
| | DCFA | 14 | 0.80 | 4 (Ditchfill1) | Archaeology |
| | DCFA | 15 | 0.90 | 4 (Ditchfill1) | Archaeology |
| | DCFA | 16 | 1.00 | 5 (Ditchfill2) | Archaeology |
| | DCFN | 1 | 0.10 | 1 (Topsoil) | SSM |
| | DCFN | 2 | 0.20 | 2 (Subsoil) | SSM |
| | DCFN | 3 | 0.40 | 6 (SSM) | SSM |
| | DCFN | 4 | 0.50 | 6 (SSM) | SSM |
| | DCFN | 5 | 0.70 | 6 (SSM) | SSM |
| | DCFN | 6 | 0.90 | 6 (SSM) | SSM |
| | DCFN | 7 | 0.10 | 1 (Topsoil) | SSM |
| | DCFN | 8 | 1.00 | 6 (SSM) | SSM |
| | DCFN | 9 | 0.10 | 1 (Topsoil) | SSM |
| | DCFN | 10 | 0.20 | 2 (Subsoil) | SSM |
| | DCFN | 11 | 0.40 | 6 (SSM) | SSM |
| | DCFN | 12 | 0.50 | 6 (SSM) | SSM |
| | DCFN | 13 | 0.60 | 6 (SSM) | SSM |
| | DCFN | 14 | 0.70 | 6 (SSM) | SSM |
| | DCFN | 15 | 0.30 | 2 (Subsoil) | SSM |
| | DCFN | 16 | 1.00 | 6 (SSM) | SSM |
| DPF | DPF | 1 | 0.10 | 1 (Topsoil) | SSM |
| | DPF | 2 | 0.20 | 1 (Topsoil) | SSM |
| | DPF | 3 | 0.50 | 2 (Subsoil) | SSM |
| | DPF | 4 | 0.40 | 2 (Subsoil) | SSM |
| | DPF | 5 | 0.60 | 9 (SSM/Subsoil) | SSM |
| | DPF | 6 | 0.80 | 6 (SSM) | SSM |
| | DPF | 7 | 1.00 | 6 (SSM) | SSM |
| | DPF | 8 | 1.20 | 6 (SSM) | SSM |
| | DPF | 9 | 0.10 | 1 (Topsoil) | Archaeology |
| | DPF | 10 | 0.30 | 2 (Subsoil) | Archaeology |
| | DPF | 11 | 0.60 | 3 (Ditchfill1) | Archaeology |
| | DPF | 12 | 0.50 | 2 (Subsoil) | Archaeology |
| | DPF | 13 | 0.60 | 3 (Ditchfill1) | Archaeology |
| | DPF | 14 | 0.80 | 4 (Ditchfill2) | Archaeology |
| | DPF | 15 | 1.00 | 5 (Ditchfill3) | Archaeology |
| | DPF | 16 | 1.20 | 8 (Lower SSM) | Archaeology |

Diddington Clay Field

North Facing Section
 Original Scale: 1:10
 Drawn on: 23/08/2011
 Drawn by: Rob Fry and David Stott
 Digitised on: 01/05/2012
 Digitised by: Anthony Beck

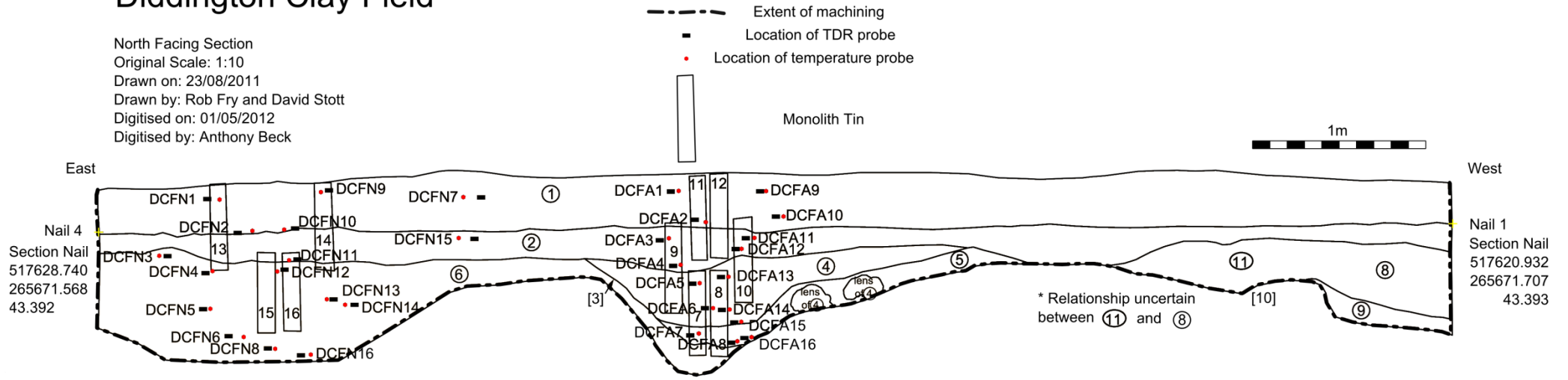


Figure 3.25: The location of the probes at Diddington Clay Field

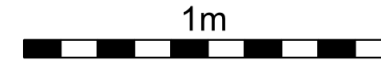
Harnhill Quarry Field

Original Scale: 1:10
 Drawn on: 23/08/2011
 Drawn by: Rob Fry and David Stott
 Digitised on: 01/05/2012
 Digitised by: Anthony Beck



Monolith Tin

- Extent of machining
- Location of TDR probe
- Location of temperature probe



West Facing Section

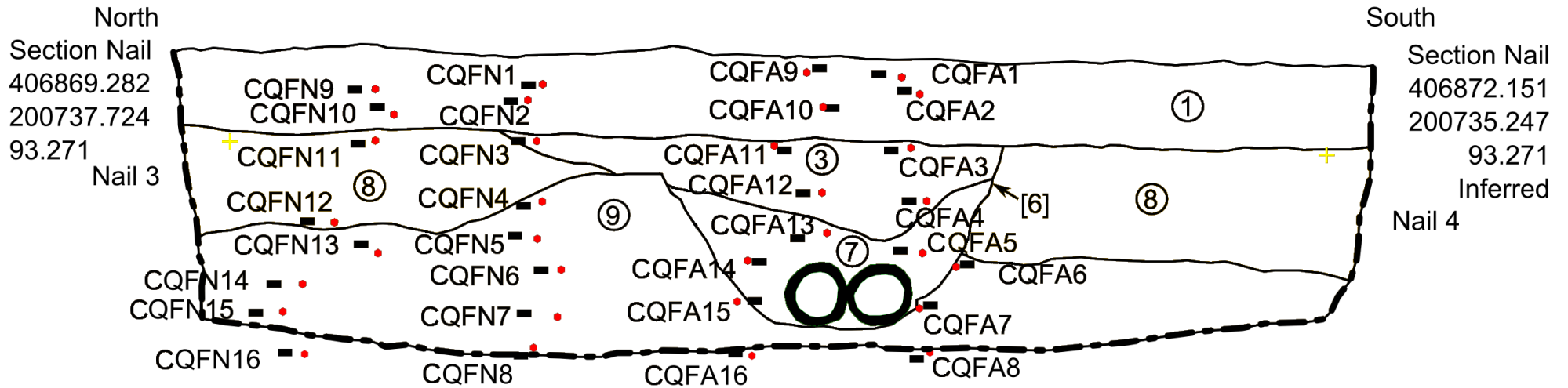


Figure 3.26: The location of the probes at Cirencester Quarryfield

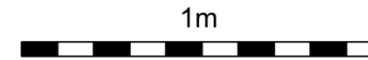
Diddington Pasture Field

Original Scale: 1:10
 Drawn on: 23/08/2011
 Drawn by: Keith Wilkinson
 Digitised on: 01/05/2012
 Digitised by: Anthony Beck



Monolith Tin

- — Extent of machining
- Location of TDR probe
- Location of temperature probe
- ◇ Bulk Sample



South Facing Section

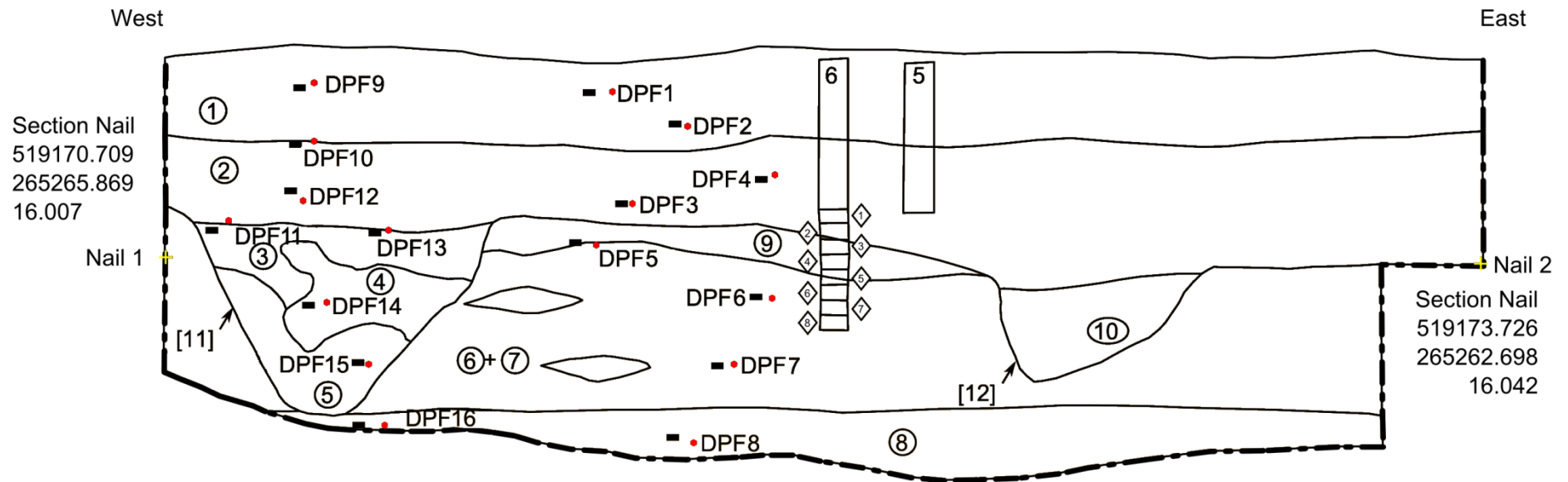


Figure 3.27: The location of the probes at Diddington Pasture Field

Harnhill Cherry Copse

South Facing Section
Original Scale: 1:10
Drawn on: 23/08/2011
Drawn by: Rob Fry and David Stott
Digitised on: 01/05/2012
Digitised by: Anthony Beck
Probe locations corrected by Armin Schmidt

- Extent of machining
- Location of TDR probe
- Location of temperature probe

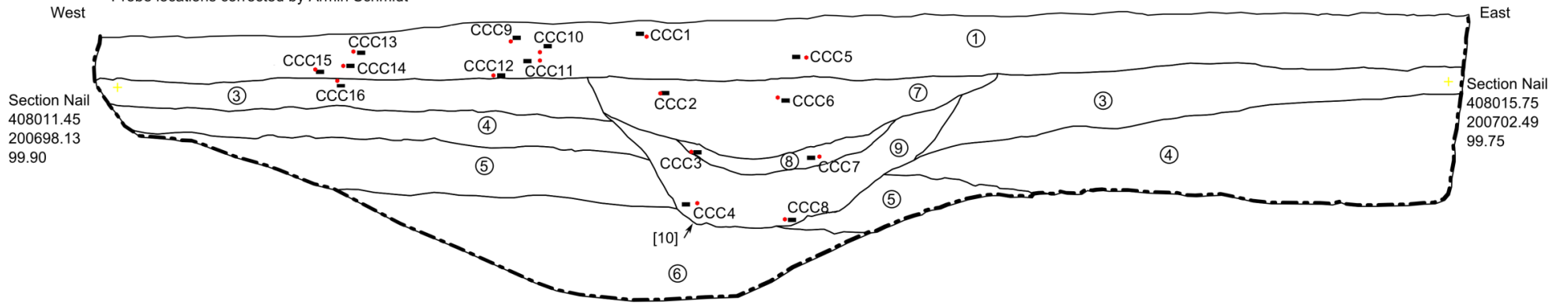
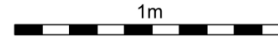


Figure 3.28: The location of the probes at Cirencester Cherry Copse

3.6.5. Post Installation Problems and Remedial action

Following the installation of the equipment on site, a number of issues affecting data collection arose at various times during the monitoring period. The problems, their causes if known and any remedial action which was taken are described below.

The initial stability of the monitoring stations was poor, with regular gaps in data where the loggers had stopped storing data to the CF cards between site visits, as well as intermittent skips of a few hours at a time, which occurred at random during the periods where data were being collected. Logger dropouts between site visits were linked to unspecified read/write failures to the CF cards, indicated by a solid yellow light on the CFM100 unit. These problems were solved by switching to a different brand of card in September 2011, which were specifically purchased from Campbell Scientific. It is thought that the problem was linked to the write speed of the CF cards used previously, although the technical specifications of both cards suggested they were identical. The intermittent skips remained, even with the new cards and seem to have been caused by the loggers scan rate being set too high, which was causing the system to skip scans and drop data in the buffer which had not already been processed and stored. To combat this, the system scan rate of the datalogger was lowered (from 2 to 10 minutes) in October 2011 to allow more processing time between groups of measurements and to avoid data in the buffer being dropped before it was transferred to the CF card. Since both these actions were taken, no further skips which could be traced directly to the datalogger processes were recorded.

Another problem was burrowing animals, which caused significant damage to the monitoring stations, both on the weather stations and some of the TDR probes. Three of the four monitoring stations had the cables between the data console and weather station sensors chewed through (Figure 3.29), causing some weather data to be lost. These cables were replaced and the cables protected by fitting animal proof insulation to the cables, including on the site where the weather station remained functional, and data collection was resumed. The

Chapter 3: Field Monitoring Methodology

site at CCC also had several of the probes dug up by a burrowing animal (Figure 3.30) in March 2012. The numbers of these probes (13 and 14) were noted so that the data quality could be monitored and the probes were reburied. Data from the right sided array of the station (probes 9-16) of the CCC monitoring station, in particular the BEC data are badly affected, suggesting that further damage may have occurred either to the probes, or to the multiplexer as a result of this damage, although permittivity and temperature data remained fairly consistent. Time and resources were not available to excavate and investigate any damage which may have occurred to the probes, although wire mesh was placed over the top of the trenches on all sites (Figure 3.31) to help deter any further damage from digging.



Figure 3.29: The damaged weather station cable



Figure 3.30: The re-excavated probes at CCC



Figure 3.31: Wire mesh used to protect the probe locations from burrowing wildlife

Data quality from the weather station at CCC was also affected by wildlife, in particular the precipitation data, as the rain gauge was frequently blocked by bird excrement, obstructing the water flow into the measurement bucket and creating a time delay between rainfall and measurement as well as restricting the maximum amount which can be recorded per archive interval. Excrement was cleared during every site visit and several methods were attempted to alleviate the problem, including spikes to prevent birds perching, and meshes over the rain gauge to stop excrement falling in, which were all ultimately unsuccessful. Due to this, data from the other site at Harnhill (CQF) had to be used in some instances. Whilst this is far from the optimum rainfall data, it is likely to have a greater accuracy than that recorded on the site itself. Another of the weather stations at DCF was found to have stopped working during a site visit in February 2012. Discussions with the manufacturer suggest that this may have been caused by a local lightning strike. The station was reset, and recorded data as normal afterwards.

During a period of extended wet weather during the end of 2012, flooding occurred at several of the monitoring stations (Figure 3.32) effectively rendering the equipment inoperable. Both stations at CQF were flooded during November 2012, the monitoring station at CCC during December 2012 and DCFA during December 2012. The station at DCFN was withdrawn from site to the laboratory during December 2012, in order to protect further damage to the equipment. The waterlogged equipment was removed from site to the laboratory at the University of Birmingham and cleaned thoroughly with deionised water and dried. However tests found that all components, with the exception of the dataloggers, were completely unresponsive, effectively ending monitoring on these sites, as time and resources were not available to replace the damaged systems and recalibration with new components on the existing probes was impossible.



Figure 3.32: A flooded monitoring station

3.7. Automation of Waveform Processing

Due to the volume of data being collected, it was deemed necessary to automate the analysis of waveforms collected by the monitoring stations. A series of functions written in a commercial software package (MATLAB; MathWorks Inc.) to deal with the large datasets were developed to analyse both ARDP and BEC type waveforms.

The analysis of the travel time for TDR permittivity waveforms, requiring the location of the beginning of the probe head and the end reflection (Menziani et al., 1996) from the probe, was conducted using the following stages. The signal waveform was separated from the header to give only the reflected signal. The tangents were found using the first derivative method (Cataldo, 2008) by using a convolution function in MATLAB® with a kernel to low pass filter the noisy data. Values of the derivative below zero were removed and the peaks were found using a one dimensional meanshift function with a bandwidth of 90.0. Error checking in the program ensured that one of the located peaks was found near the start of the waveform, and one was found later to ensure multiple peaks were not found at the start of the waveform, causing an

underestimation of the permittivity. Ten points were taken from either side of the peak location in the original signal and the gradient of the line was found using `mldivide`. The minimum of the waveform caused by the impedance change of the probe head and before the final reflection were found by finding local minima in the first 500 points and last 1500 points respectively using `min` function. The point at which the first tangent and minimum met was found to give the waveform start point (Γ_{start}) and the second tangent and minimum meeting point was used to determine the end reflection (Γ_{end}). This process is summarised in Figure 3.33.

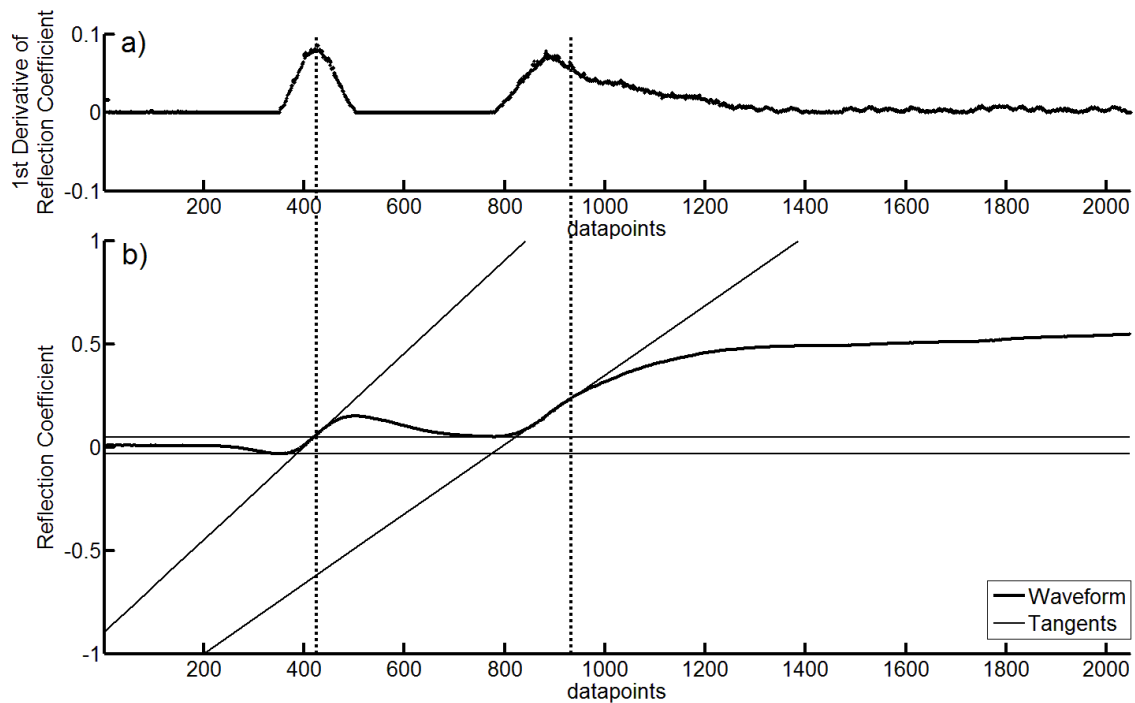


Figure 3.33: The interpretation of ARDP waveforms showing a) the calculated first derivative found using the `conv` function in MATLAB® and a low pass filter and b) the subsequent fitted tangents. The lines formed from the localised minima are also shown.

These values were used in a second function to determine the apparent relative dielectric permittivity, using the apparent length (L_A) and probe offset (P_{off}) values determined by the calibration, using Equation 3.9.

$$\varepsilon_a = \left(\frac{(\Gamma_{end} - (\Gamma_{start} + P_{off}))}{(v_p L_A)} \right)^2$$

3.9

Where v_p is the propagation speed which was set to one the as the stations used apparent length (see Section 2.7.2).

The major source of error in the automated fitting procedure comes from errors in the fitting between the tangent and the measured waveform due to noise on the trace, which in turn results in a variation in the positions of the start and end points of the measurements (and hence the apparent length). In order to assess the likely possible uncertainty in the automated tangent fitting process, a number of waveforms were tested by using only the first and last points from the extracted subsets used to determine the tangent gradients. Testing over a wide range of waveforms (approximately 1000) showed minimal uncertainty in the determination of the tangent with the final positions of the start and end points never exceeding 7 datapoints ($\approx 0.0041015625\text{m}$ of apparent length). Taking the average of the calibrated probe length of 0.075649524m and the average probe offset of 0.039469m this error is approximately equal to 0.21 permittivity units. Since this value is less than the maximum errors determined for permittivity measurements during the calibration (≈ 0.4 units), the use of an automated fitting algorithm was not thought to be noticeably detrimental to the quality of the data acquired. However, future automated fitting algorithms may include an estimation of the error using this method and output the uncertainty on every measurement in order to identify poorly interpreted waveforms. Further quality control was carried out throughout the project to examine waveforms of outlying and unusual values and identify possible problems from the interpretation method.

Separate functions were developed for processing bulk electrical conductivity data using the open circuit reflection coefficient (Γ_{open}), cable length (C_L), probe constant (K_p), cable resistance (R_c) and series resistance (R_0) values derived during the equipment calibration in the laboratory, and following a standard method of determining BEC values using TDR (Bechtold et al., 2010, Curioni et al., 2012, Huisman et al., 2008). The final 136 points were taken from the waveform and the mean was found to give a stable value for the reflection coefficient at a long time after the voltage had reached a stable state (Ball, 2002, Bechtold et al., 2010). The value was then converted to BEC using Equation 3.6 to correct the coefficient, Equation 3.7 to calculate the load resistance and finally Equation 3.8 to give BEC values in S/m, in the same way as during the calibration process.

Both scripts and functions were initially tested against manual interpretation of the data on a number of waveforms from different probes and were found to give similar results except in exceptional circumstances, such as misshapen or incorrectly logged waveforms. The scripts are provided in Appendix A.

Chapter 4: Laboratory Methodology for Soil Characterisation

4.1. Introduction

The literature review (Chapter 2) has highlighted the strong dependence of EM properties of soil on a number of the soils physical and chemical properties, including particle size distribution (particularly the amount of clay), density, magnetic susceptibility, clay mineralogy and activity and organic matter content. Furthermore, work comparing the difference in these properties between archaeological deposits and the SSM has never previously been attempted and differences in these properties seem like a logical starting place for understanding contrast in EM properties. It was therefore deemed necessary to characterise some of these variables and highlight the differences between the behaviour of archaeological and SSMs. To achieve this, a variety of different basic characterisation techniques were used on the soil samples collected from the field during the installation procedure. Tests were then carried out to demonstrate the links between seasonally changing soil characteristics (VWC and temperature) and geophysically measured responses.

Soils were taken from all 4 sites for testing, from every context described by the archaeological excavation. A summary of the different soils tested, and the tests carried out are provided in Table 4.1.

Table 4.1: A summary of the soil characterization tests carried out on each soil

| Site | Context No | Soil Name | Particle Density | Particle Size | Density | Atterberg Limits | Linear Shrinkage | Chemical Testing | Soil Description |
|------|------------|------------|------------------|---------------|---------|------------------|------------------|------------------|---|
| DPF | 1 | Topsoil | ✓ | ✓ | ✓ | ✓ | ✓ | ✓ | Plough soil |
| | 2 | Subsoil | ✓ | ✓ | ✓ | ✓ | ✓ | ✓ | Post archaeological fluvial deposit |
| | 3 | Ditchfill1 | ✓ | ✓ | ✓ | ✓ | ✓ | ✓ | Most recent archaeological fill |
| | 4 | Ditchfill2 | ✓ | ✓ | ✓ | ✓ | ✓ | × | Archaeological ditchfill |
| | 5 | Ditchfill3 | ✓ | ✓ | ✓ | ✓ | ✓ | × | Initial stabilisation archaeological fill |
| | 6 | SSM | ✓ | ✓ | × | × | × | ✓ | Gravel SSM |
| | 9 | Upper SSM | × | × | × | × | × | × | Mixture of Subsoil and SSM |
| DCF | 1 | Topsoil | ✓ | ✓ | ✓ | ✓ | ✓ | ✓ | Plough soil |
| | 2 | Subsoil | ✓ | ✓ | ✓ | ✓ | ✓ | × | Mixture of plough soil and eroded soils beneath |
| | 4 | Ditchfill1 | ✓ | ✓ | ✓ | ✓ | ✓ | ✓ | Archaeological ditchfill |
| | 5 | Ditchfill2 | ✓ | ✓ | ✓ | ✓ | ✓ | × | Initial stabilisation archaeological fill |
| | 6 | SSM | ✓ | ✓ | ✓ | ✓ | ✓ | ✓ | Chalky boulder clay |
| CCC | 1 | Topsoil | ✓ | ✓ | ✓ | ✓ | ✓ | ✓ | Plough soil |
| | 7 | Ditchfill1 | ✓ | ✓ | ✓ | ✓ | ✓ | ✓ | Most recent archaeological fill |
| | 8 | Ditchfill2 | ✓ | ✓ | × | ✓ | ✓ | × | Archaeological ditchfill |
| | 9 | Ditchfill3 | ✓ | ✓ | × | ✓ | ✓ | × | Initial stabilisation archaeological fill |
| COF | 1 | Topsoil | ✓ | ✓ | ✓ | ✓ | ✓ | ✓ | Plough soil |
| | 5 | Ditchfill1 | ✓ | ✓ | ✓ | ✓ | ✓ | ✓ | Archaeological ditchfill |
| | 7 | Ditchfill2 | ✓ | ✓ | ✓ | ✓ | ✓ | × | Initial stabilisation archaeological fill |
| | 8 | Upper SSM | ✓ | ✓ | ✓ | ✓ | ✓ | ✓ | Upper layer of clay soil |
| | 9 | Lower SSM | ✓ | ✓ | ✓ | ✓ | ✓ | × | Lower level of clay soil |

4.2. Soil Characterisation

4.2.1. Geotechnical characterisation

Geotechnical characterisation of the site was largely carried out by Laura Pring, with the assistance of the author and Laura Thring. Testing was carried out using methods described by British Standard 1377-2 (BSI, 1990) where possible although many of the tests were repeated to perform a comparison of different methods. A full discussion on repeatability and accuracy of the tests is not provided in the current work but can be found in Pring (Forthcoming).

However average results from the geotechnical characterisation of the soil are presented and discussed in Section 5.2.

4.2.2. Magnetic Susceptibility

As demonstrated in the literature review, magnetic properties have a significant effect on the propagation of EM waves, although in soil they are commonly considered insignificant. To assess this, volume specific magnetic susceptibility readings were taken by Dr. Keith Wilkinson of the University of Winchester using recovered monolith tin samples following the method of Gale and Hoare (1991) and a Bartington MS2 meter and MS2B dual frequent sensor (Bartington Instruments). Readings were taken using both the high and the low frequency setting to assess the frequency dependence of the magnetic properties. The results of the magnetic susceptibility testing are presented and discussed in Section 5.4.

4.2.3. Chemical Characterisation of the Soil

As demonstrated by the literature review (Chapter 2), electromagnetic properties of the soil are affected by chemical as well as physical properties of the soil. Of particular interest for this project are the organic matter, which affects the soils ability to hold water in a bound state (Kallner and Lundin, 2001), the iron content, which affects the magnetic permeability of the soil and soluble ions, which affect the soils conductivity, causing signal loss, and the behaviour of the bound water fraction. To assess chemical as well as physical characteristics of the soil,

chemical testing was carried out on a limited number of samples from the sites. Samples for chemical testing were acquired using a Cobra TT petrol breaker vibracorer to drill boreholes on sites at Diddington and Harnhill during February 2012. The locations of the boreholes are shown in Figure 4.1 to Figure 4.4. Owing to financial constraints, samples were taken from a limited number of soil contexts from both inside and outside the archaeological feature from each site which are summarised in Table 4.1.

Samples on site were sealed in brown glass jars (Figure 4.5) to avoid photochemical reactions from taking place and transported from site in a cool box to minimise chemical changes.

Chemical testing was carried out by Alcontrol Laboratories to determine the following things

- Sodium content
- Magnesium content
- Potassium content
- Calcium content
- Iron content
- Alkalinity, Total as CaCO₃
- Loss on Ignition
- Total Sulphates
- Soluble Nitrates
- Soluble Phosphate (Ortho as PO₄)
- Total Organic Carbon
- Total Organic matter
- pH

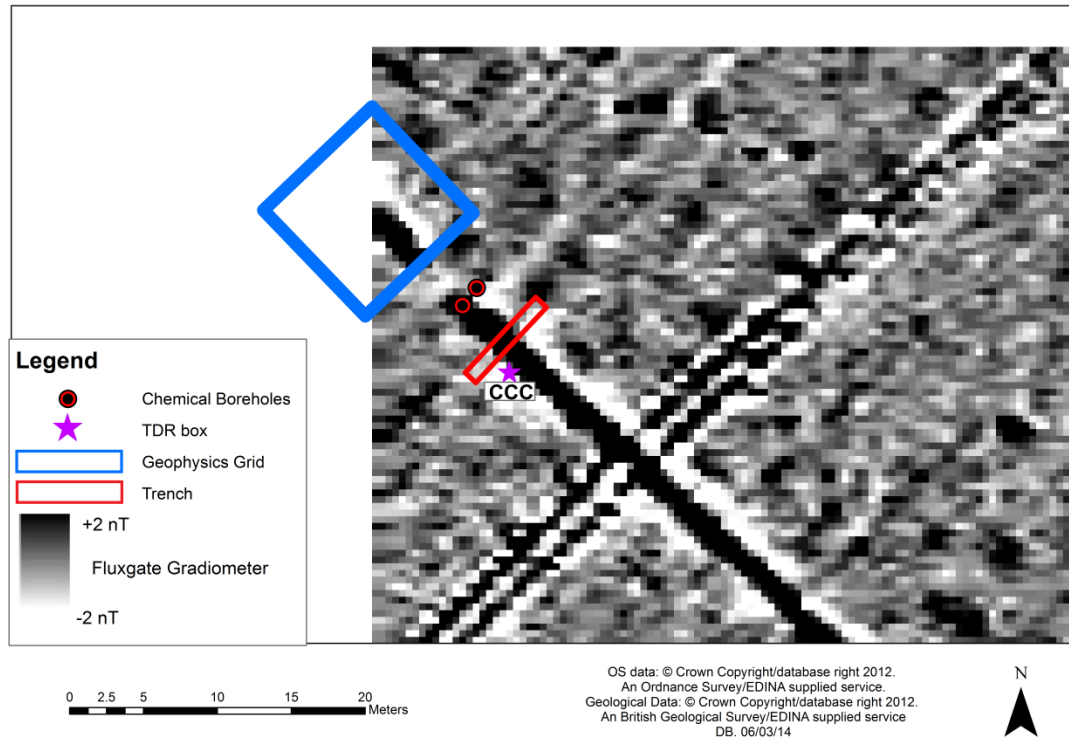


Figure 4.1: The location of the chemical boreholes from the archaeological soils and SSM in relation to the trench, TDR box and geophysics grid on CCC

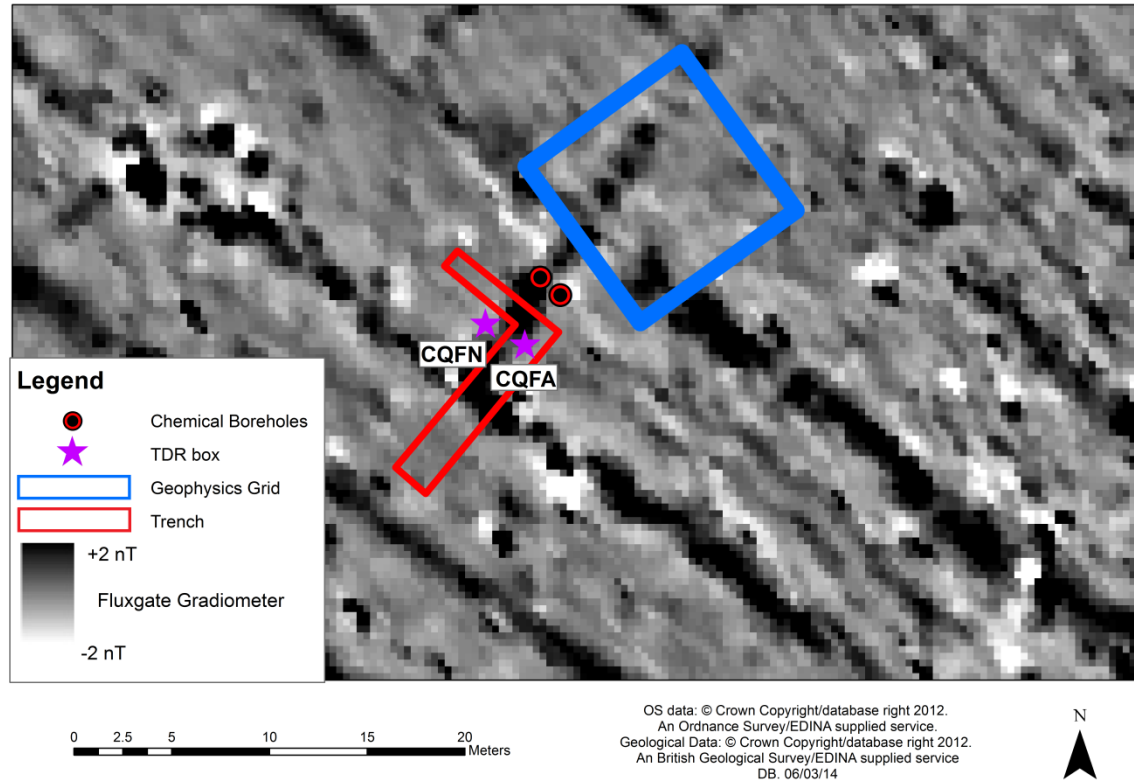


Figure 4.2: The location of the chemical boreholes from the archaeological soils and SSM in relation to the trench, TDR box and geophysics grid on CQF

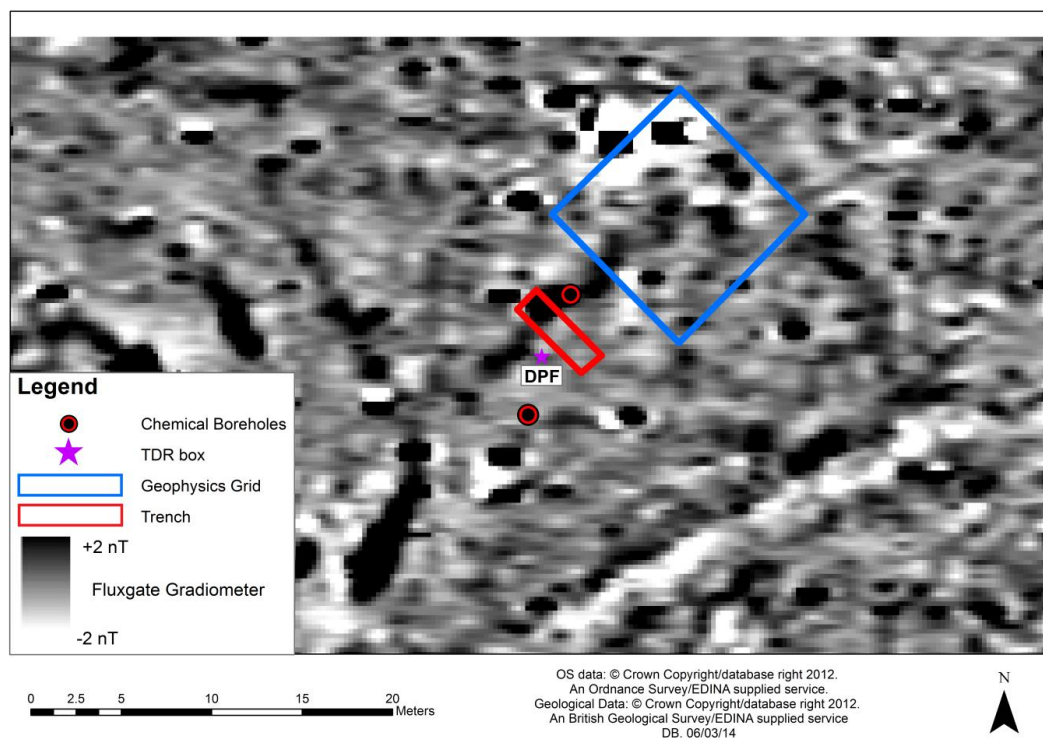


Figure 4.3: The location of the chemical boreholes from the archaeological soils and SSM in relation to the trench, TDR box and geophysics grid on DPF

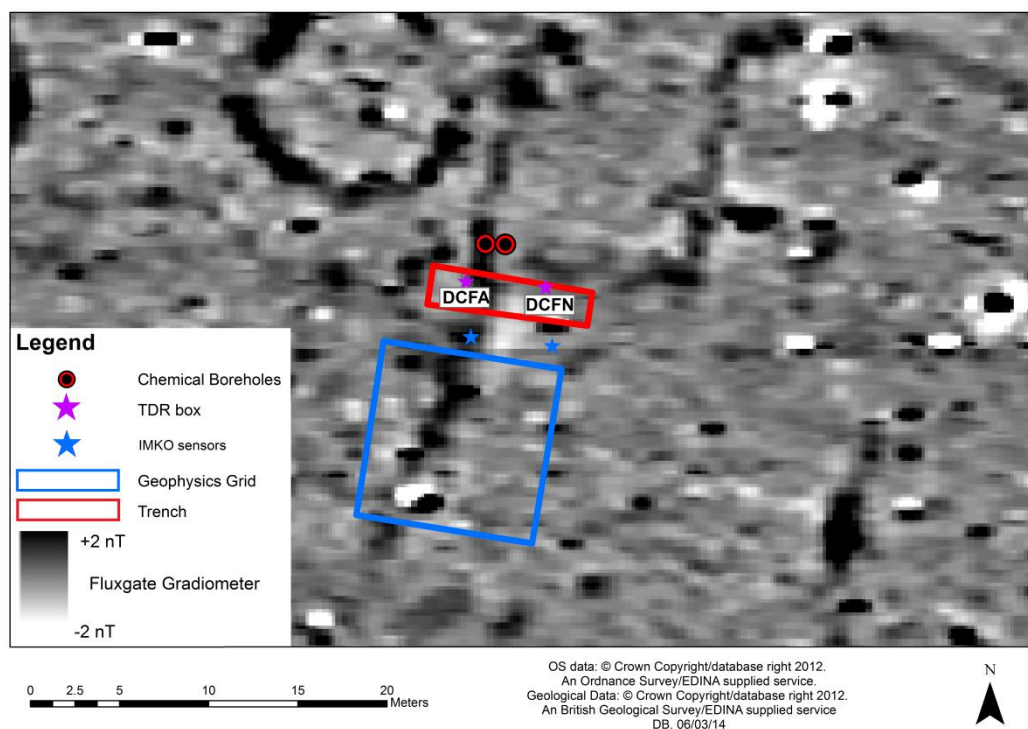


Figure 4.4: The location of the chemical boreholes from the archaeological soils and SSM in relation to the trench, TDR box, IMKO sensors (see Appendix D) and geophysics grid on DCF

The methods for each test can be found in the Alcontrol brochure (Alcontrol Laboratories, 2011). Additional measurements using the Loss on Ignition method were conducted on samples taken every 20mm down the monolith tins at the University of Winchester. These values have been averaged by context. The results of chemical testing are discussed in Section 5.2.



Figure 4.5: Brown glass jars used for chemical sampling to avoid photochemical reactions

4.3. Electromagnetic Characterisation and Water Content Relationships

4.3.1. Introduction

The properties of soil dielectric response are affected by water content (Topp et al., 1980), temperature (Or and Wraith, 1999, Wraith and Or, 1999) and density (Gong et al., 2003, Hipp, 1974), with the contrasts in these properties between archaeological features and the SSM being poorly understood. However, it is also of importance to note that each of these effects on the measured dielectric response is frequency dependent. A proposed strategy to assess the relationship between VWC and the ARDP and BEC at different temperatures, the frequency dependence of these properties, and the eventual contrast of archaeological features is presented here. Soil samples were collected from the site during the installation and were

Chapter 4: Laboratory Methodology for Soil Characterisation

used to create the samples. This allowed both ditchfill and the surrounding soil to be assessed using a method similar to that used for empirical calibrations used for soils, where samples are created in the laboratory at specific densities and water contents (Take et al., 2007) and testing using a TDR setup similar to that which was deployed in the field. The TDR measurements were used to create an empirical model to derive water content for each soil from the permittivity data being recorded in the field by fitting a curve to compare the TDR recorded values with the soil water content values and temperature of the sample. This both links the permittivity back to soil properties but also assists other members of the DART project working on plant growth and earth resistance measurements. Limited time was available for the experiment; therefore it was decided to focus on these relationships for the Diddington sites (DCF and DPF), and some soils did not yield large enough samples to make the samples necessary. Twelve different soils were tested which were

- DCF Topsoil
- DCF Subsoil
- DCF SSM
- DCF Ditchfill1
- DPF Topsoil
- DPF Subsoil
- DPF Ditchfill1
- DPF Ditchfill2
- DPF Ditchfill3
- DPF SSM

Laboratory testing was carried out in collaboration with Laura Thring, an MEng student at the University of Birmingham and forms the basis of an MEng project (Thring, 2013).

4.3.2. Sample Preparation

Soil was initially sieved to 5mm to remove any large stones which may bias the results and oven dried at 105°C for 24 hours or longer to remove all moisture. A relationship based on the known dry density of the soil was derived by calculating the GWC at a number of VWC values assuming the dry density was constant using Equation 4.1. These values were then plotted against one another and a gradient for the line was used as a conversion factor (F) between the two. The conversion factors are summarised in Table 4.2.

$$\theta_g = \frac{(\theta_v * V_c)}{(\rho_d * V_c)}$$

4.1

Where V_c is the volume of the cylinder in cm^3 . Due to the inability to obtain an undisturbed sample of DPF SSM with which to derive its dry density (see Section 3.6.3), an appropriate target dry density, representative of the field density had to be estimated. Compaction tests carried out on the soils for another project (Blick, 2012) found that the soils varied between 1.79-1.98 Mg/m^3 , in good agreement with commonly stated values for sand and gravel of 1.65-2.02 Mg/m^3 (Engineering Toolbox, 2012). An estimated dry density of 1.88 Mg/m^3 was therefore chosen for the testing. This estimation approach can be justified for a number of reasons. Since VWC values are used for the experiment, density of the soil is already accounted for in the calculation of water content (Equation 4.1). The effects of density are therefore limited to those caused by differences between the air (RDP ≈ 1) and solid fractions (RDP $\approx 3-5$) in the measurement volume, which are small and only visible in very dry soils, and bound water effects. The relatively small surface area in coarse soils in comparison to fine grained soils decreases the magnitude of bound water effects, making density a less important factor. Quinones et al. (2003) found that density was only important at extreme values and the values of all the soils and the value chosen for DPF SSM are within the commonly encountered range of values.

Table 4.2: Conversion factors between gravimetric and volumetric water contents for the different soils tested based on their dry density values

| Soil | Conversion Factor (F) |
|----------------|-----------------------|
| DCF Topsoil | 0.641 |
| DCF Subsoil | 0.6042 |
| DCF SSM | 0.5263 |
| DCF Ditchfill1 | 0.62 |
| DPF Topsoil | 0.6173 |
| DPF Subsoil | 0.6024 |
| DPF Ditchfill1 | 0.625 |
| DPF Ditchfill2 | 0.7634 |
| DPF Ditchfill3 | 0.6024 |
| DPF SSM | 0.5319 |

No one standardised method of sample preparation for TDR testing has been agreed, with several authors defining different methods. The methods used to prepare the soil were therefore developed based on ideas from the literature, experience of other researchers and based upon practicality as problems became apparent during testing. Following initial experimentation on the wide range of soils, two different methods were used to create the soil samples needed for this project as it was found that different methods were needed; one beginning with dry soil and another where saturated soil was dried to a particular VWC value.

In coarse grained soils and soils with a low VWC, samples with known water content were created by using thoroughly mixing a known volume of dried soil and deionised water, a method used successfully by other researchers (Ollerton, 2012, Quinones et al., 2003, Take et al., 2007). Many of the soils formed aggregated lumps following the initial drying from a saturated state. In these cases the soil was wetted to a low water content (c.10% VWC) using deionised water and placed in a rotary mixer for a short period, breaking the large aggregates without crushing the larger soil fraction and artificially creating more fines. Another method of using a chemical dispersant, similar to those used in PSD testing such as Sodium Hexmetaphosphate (BSI, 1990), was considered but was ultimately rejected because of a potential unknown effect on the results through change of the soils chemical properties and

the charge interaction between the solid particles and water. The soil was then dried again in the oven to form a granular soil. The mass of water to be added (m_w) was determined using Equation 4.2.

$$m_w = \left(F * \frac{\theta_v}{100} \right) * m_d$$

4.2

Where m_d is the mass of dry soil to be made into a sample in g. Deionised water was added to the sample using a plant mister spray whilst the sample was being mixed to achieve a uniform distribution of water through the soil until the desired combined weight of soil and water was reached.

Whilst the above method was the most simple, in fine grained soils, it was found that the addition of water to dry soil gave poor uniformity, because the high surface area caused the water to be adsorbed to localised areas of the soil. Owing to this, samples were instead prepared by starting with the soil in a saturated state and allowing the water to evaporate from the sample with the mass of the sample being used at different points in time to determine its water content. The mass of a tray was taken and an amount of dry soil added. The target mass was ascertained by calculating the correct amount of water using Equation 4.2 and adding it to the mass of the dry soil in the tray. Water was added to the tray until the soil was oversaturated, and the soil was mixed and left for a period of homogenisation to allow all of the soil to become saturated (usually around 24 hours). The soil was then dried to the desired mass by drying in an oven for short periods with stirring taking place between each drying cycle to stop uneven drying. For both methods, the soil was sealed using plastic and left to homogenise for 24 hours before being packed as is common practice (Take et al., 2007).

A large coaxial cell was considered for use as the packing cylinder, with the bottom being unscrewed to take TDR measurements, as the method has the potential to provide more

accurate VNA readings, as the cell will sample a greater volume of soil. However, the method has a number of disadvantages.

- The cell would have needed to be large enough to avoid any boundary effects when the TDR probe is inserted. No cell this big currently exists so a new cell would need to be constructed.
- Only one cell was likely to be available allowing only one single sample to be prepared at once as opposed to multiple samples which can be prepared in inexpensive cylinders.
- The TDR probe would be unable to remain in-situ between readings and it was feared that the subsequent removal and re-insertion of the probe may cause air voids, decreasing the accuracy of the readings.

Owing to the limited time available for the experiment and the primary focus on the TDR results and model development for comparison with the field data, a coaxial probe was used instead and the soils were packed into cylinders made from 10cm lengths of plastic pipe, 10cm in diameter. The volume of these cylinders was calculated to be 785.4cm^3 . Several authors have noted that for three rod probes, 94% of the signal energy is within twice the distance between the rods (Ledieu et al., 1986, Zegelin et al., 1989), so boundary effects are assumed to be minimal, with smaller cylinders and longer probes being used by other researchers (Cataldo et al., 2010). Preliminary testing in a tank of water using a TDR probe and a piece of plastic at various distances confirmed no noticeable effects at this distance, and even less are anticipated in more conductive mediums, which attenuate the signal faster.

To ensure the bulk density remained constant and at similar dry bulk density values to the field, the method of packing the soil in stages suggested by several authors was used (Gong et al., 2003, Miyamoto et al., 2003, Ponizovsky et al., 1999). For each soil sample, the mass of

wet soil to add (m_w), assuming water was equally distributed in the sample was then calculated using Equation 4.3.

$$m_w = (\rho_d * V_c) + \left(\left(\frac{\theta_v}{100} \right) * V_c \right)$$

4.3

Where V_c is the volume of the cylinder (785.4cm^3), θ_v is the desired VWC in % and ρ_d is the dry density of the soil in Mg/m^3 determined during laboratory testing (see Section 4.1). Each cylinder volume was divided into five equal sections, and the correct weight of soil to create the desired density was divided into five equal weights. Each portion of soil was compacted into the cylinder in stages, ensuring that the soil was uniformly packed and the final weight of the soil in the cylinder was recorded and used to calculate the bulk density (Equation 4.4).

$$\rho_b = \frac{m_w}{V_c}$$

4.4

The samples were then sealed using plastic caps and silicon sealant, and a TDR probe inserted through a hole in the lid before being sealed in place with PTFE and electrical tape to minimise evaporation losses throughout the measurement procedure. A small sample of the soil was also used for water content testing at the packing stage to assess possible evaporation over the measurement period.

In addition to creating a wide range of water contents for each soil, one fine grained and one coarse grained soil (DCF SSM and DPF Ditchfill1) were also selected to test the effects of varying the density. Additional samples at different water contents were made for these samples for dry densities of $\pm 10\%$ of the measured field values.

4.3.3. Measurements

Initially, for each of the samples from the site, samples were made in duplicate to assess consistency of results, with a variety of volumetric water contents from $0\text{cm}^3/\text{cm}^3$ - $0.5\text{cm}^3/\text{cm}^3$, (0-50%) in increments of $0.1\text{cm}^3/\text{cm}^3$ (10%) to represent a range of naturally occurring values. On some of the more coarse grained samples (from DPF), the saturation point of the soils was found to be below 50% VWC meaning the higher VWC values could not be packed and these tests were abandoned. The 10% interval in VWC values was found on some values to be too coarse and some of the intermediate values were later prepared and tested. To test the temperature dependence of each sample, the samples were heated and cooled to different temperatures before testing, to represent normal temperature changes in the soil. Temperature change was achieved by placing the sample in an incubator set to the desired temperature for a period of 24 hours before each reading was taken. From observed field data, measurements between 0-20°C was chosen as a suitable range and a full range of measurements were taken for each sample at 0, 10 and 20°C. Two types of measurements were taken for each sample:

- 3 TDR readings using an apparent window length of 1.2m and a window start point near to the probe head on the transmission line. This is the same as the ARDP measurement recorded by the field stations
- 3 TDR readings using an apparent window length and a window start point of 100m, similar to the BEC values recorded by the field stations

TDR measurements were processed using MATLAB® (MathWorks Inc., 2010) and the scripts described in Section 3.7 and the multiple readings taken were averaged. In addition to this, a limited number of samples had additional readings taken using a VNA and coaxial probe. This used narrow frequency bandwidths between 100 MHz-2GHz and measured both the real and imaginary part of the permittivity at a variety of frequencies. This allowed the dispersive

nature of the soils to be assessed. These readings were also processed in MATLAB® using a script developed by Dr. Tong Hao.

4.3.4. Deconstruction of Samples

After all the measurements had been taken, the soil samples were deconstructed in a manner which allowed the perceived VWC values to be verified. GWC (θ_g), where required was determined by drying samples of known mass in an oven set to 105°C for at least 24 hours, then reweighing the sample. Equation 4.5 was then used to determine the GWC (BSI, 1990).

$$\theta_g = \left(\frac{(m_{w+t} - m_{d+t})}{(m_{d+t} - m_t)} \right) * 100$$

4.5

Where m_{w+t} is the mass of the wet soil and drying tin, m_{d+t} is the mass of the dry soil and drying tin and m_t is the tin mass (all masses in g). Unless otherwise stated, masses were determined using a balance (Precisa XB 4200C) to a precision of 0.01g with an accuracy of ± 0.01 g. One small sample, the standard size for water content testing according to British standards (BSI, 1990) was taken from the vicinity of the probe. The rest of the soil in the cylinder was also placed on a tray, weighed and dried to assess its GWC. Comparison of the values recorded for the small and large samples showed similar values, suggesting a uniform distribution of water in the sample. Since the size of the cylinder was known, and the weight recorded at the packing stage, the bulk density was known and the GWC of the large sample was used to calculate the dry bulk density (Equation 4.7) assuming uniformity in soil packing and moisture distribution.

$$\rho_d = \frac{(100 * \rho_b)}{(100 + \theta_g)}$$

4.6

VWC of the small sample was then calculated using Equation 4.7 and the values plotted against the recorded TDR derived ARDP and BEC values and used to examine the different VNA complex permittivity plots. The results, derived empirical models for each soil type and a full discussion of them are provided in Chapter 5 of this thesis.

$$\theta_v = \left(\theta_g * \left(\frac{\rho_d}{\rho_w} \right) \right) * 100$$

4.7

Where ρ_w is the density of water in g/cm^3 (0.999841 at 0°C, 0.9997 at 10°C, 0.998203 at 20°C (Walker, 2011)).

Chapter 5: Laboratory Soil Testing: Results and Discussion

5.1. Introduction

This chapter describes the results acquired from laboratory testing on the soils to determine their geotechnical, geochemical and EM properties. Testing was carried out on a range of different soils to characterise the soil, both geotechnically (Section 5.2) and geochemically (Section 5.3) in order to determine which soil properties affect the different signal responses and thus the geophysical soil properties. The results of the testing of the EM properties and VWC relationships with the geotechnical and geochemical properties are also explored and discussed in Section 5.5. Finally, Principal Component Analysis (PCA) was used to identify the most important soil properties for determining geophysical behaviour of the soil (Section 5.6) and the chapter concludes with a summary of the findings (Section 5.7), which will be used to help understand changing EM contrasts in the field.

5.2. Geotechnical Characterisation of the Soil

This section focuses on the results of the geotechnical testing of the soil samples recovered during the excavation of the sites. The results of geotechnical testing are presented in Table 5.1. In addition to the tested values, calculated values from these properties have also been included for comparative analysis. Porosity (η) was calculated using Equation 5.1.

$$\eta = 1 - \frac{\rho_d}{\rho_s}$$

5.1

Where ρ_d and ρ_s are the dry density and particle density in Mg/m^3 respectively (Knappett and Craig, 2012). The Activity index of the clay has also been calculated using Equation 2.32.

In general, ditches possessed geotechnical properties which were somewhere between those of the topsoil and those of the SSM, which comprised the rest of the field. However the size of these differences was dependent on the type of feature, its formation factors and the

properties of the underlying SSM, and no universal differences existed between the two soils across all sites. Differentiation between the archaeological soils and SSM on CCC was impossible due to the SSM being comprised of weathered rock unsuitable for geotechnical soil testing.

The particle size distribution (PSD) data confirm that testing was conducted on a wide variety of different soils ranging from coarse grained soil such as DPF SSM to fined grained soils such as those found on CQF and DCF. The two Diddington sites show smaller particle sizes (silt and clay) dominating in the archaeological soils in comparison to the SSM at similar depths, especially in the deepest fills. These findings are consistent with findings of other authors (Scollar et al., 1990, Strunk-Lichtenberg, 1965). More complex relationships between textures of the ditchfills and SSM exist on CQF where the fines content is greater in the upper layers of both the ditchfills and SSM, with the SSM having slightly higher clay content than the surrounding ditches. At greater depths, the reverse is true, matching the results from the Diddington sites.

Density also has an important role. On DCF the archaeological soils have a tendency to be less dense than the surrounding soils. This is likely to be the result of the backfilling process which failed to compact the returning fill to the same density as the SSM. However, the upper SSM at CQF has a slightly lower bulk and dry density. One explanation for this may be the deliberate compaction of ditchfills to a higher than usual density during the backfilling of the ditch following the installation of the pipes (see Section 3.6.2). The particle density also varies across all sites with the lowest values found in the topsoil and highest in the SSM across all sites, whilst the archaeology falls somewhere between these two values. These two densities are responsible for determining the total porosity of the soil, which affects the maximum amount of water which can be held by a soil. On DCF therefore, the archaeological soils with their lower densities also display, in general, a greater total porosity, allowing them to hold a

greater amount of water before saturation is reached, whereas the reverse is true for the upper fill and SSM on CQF. However with increasing depth, the CQF soils density inverts to follow the same trends as DCF (see Ditchfill2 and lower SSM). Comparisons between density and porosity in the archaeological soils and SSM on the non-clay sites were impossible due to the lack of comparable data from the SSM, although similar trends are thought to exist based on field observations.

Atterberg limits, related to the mineralogy of the soil, show a few differences between the archaeological soils and SSMs, with the liquid limits showing similar trends to the prevalence of fine particles discussed above. More significant intra-site differences exist especially between the topsoils and subsoils in comparison to the underlying ditchfills and SSM soils. This is perhaps unsurprising as Atterberg limits have been frequently used to predict the SSA of the soil (Farrar and Coleman, 1967, Santamarina et al., 2002), which is greater in clay soils. The linear shrinkage shows similar trends to the liquid limits, being linked to intersheet water (Thomas et al., 2010a), which is also a function of the SSA of the soil, although differences are far smaller and often undetectable. More significant differences in the Atterberg limits and linear shrinkage exist between the clay and non-clay sites, with clay soils showing higher values for both the plastic and liquid limit, as well as the linear shrinkage due to their greater surface areas. Higher values for plastic and liquid limit as well as linear shrinkage can be observed on the two Cirencester sites, which could be linked to the different underlying parent geology.

Table 5.1: Summary of geotechnical testing results. * indicates measurements not obtained due to unsuitable soil types and samples. Data from Pring, Forthcoming.

| Site | Context No | Soil Name | Particle Size | | | | Particle Density g/cm ³ | Density | | Calculated Porosity - | Atterberg Limits | | | Linear Shrinkage % | Activity Index - |
|------|------------|------------|---------------|-------|-------|-------|---------------------------------------|-----------------------------------|----------------------------------|--------------------------|--------------------|-------------------|-----------------------|-----------------------|---------------------|
| | | | %Gravel | %Sand | %Silt | %Clay | | Bulk Density g/cm ³ | Dry Density g/cm ³ | | Plastic Limit - | Liquid Limit - | Plasticity Index - | | |
| | | | % | % | % | % | | | | | | | | | |
| DPF | 1 | Topsoil | 8.1 | 39.2 | 39.0 | 13.7 | 2.60 | 1.77 | 1.62 | 0.38 | 17 | 30 | 13 | 8.3 | 0.97 |
| | 2 | Subsoil | 11.3 | 33.5 | 41.1 | 14.0 | 2.65 | 1.79 | 1.66 | 0.37 | 15 | 25 | 10 | 8.4 | 0.77 |
| | 3 | Ditchfill1 | 18.1 | 33.0 | 37.3 | 11.6 | 2.62 | 1.73 | 1.60 | 0.39 | 17 | 27 | 10 | 7.2 | 0.80 |
| | 4 | Ditchfill2 | 17.4 | 32.9 | 40.9 | 8.8 | 2.65 | 1.46 | 1.31 | 0.51 | 17 | 27 | 10 | 7.5 | 1.18 |
| | 5 | Ditchfill3 | 12.5 | 34.9 | 43.0 | 9.5 | 2.64 | 1.86 | 1.66 | 0.37 | 16 | 24 | 8 | 6.5 | 0.94 |
| | 6 | SSM | 33.3 | 47.4 | 13.3 | 6.0 | 2.69 | * | * | * | 16 | 26 | 10 | 6.8 | 1.67 |
| DCF | 1 | Topsoil | 6.3 | 22.0 | 49.8 | 21.9 | 2.58 | 1.87 | 1.56 | 0.40 | 22 | 48 | 26 | 15.2 | 1.15 |
| | 2 | Subsoil | 6.9 | 20.0 | 45.6 | 27.4 | 2.62 | 1.97 | 1.66 | 0.37 | 21 | 47 | 26 | 13.7 | 0.94 |
| | 4 | Ditchfill1 | 8.6 | 16.3 | 52.6 | 22.5 | 2.67 | 1.83 | 1.61 | 0.40 | 19 | 41 | 22 | 10.8 | 1.13 |
| | 5 | Ditchfill2 | 6.6 | 15.9 | 36.5 | 41.0 | 2.63 | 1.83 | 1.58 | 0.40 | 21 | 44 | 23 | 13.3 | 0.57 |
| | 6 | SSM | 6.5 | 16.3 | 46.3 | 30.9 | 2.83 | 2.10 | 1.90 | 0.33 | 18 | 40 | 22 | 10.5 | 0.83 |
| CCC | 1 | Topsoil | 30.0 | 7.2 | 57.7 | 5.1 | 2.60 | 1.73 | 1.37 | 0.47 | 32 | 58 | 26 | 16.5 | 5.10 |
| | 7 | Ditchfill1 | 33.7 | 8.1 | 42.5 | 15.7 | 2.57 | 1.84 | 1.47 | 0.43 | 30 | 55 | 26 | 17 | 1.66 |
| | 8 | Ditchfill2 | 35.2 | 7.1 | 36.8 | 20.8 | 2.54 | * | * | * | 30 | 56 | 26 | 18 | 1.25 |
| | 9 | Ditchfill3 | 65.7 | 3.7 | 18.1 | 12.6 | 2.55 | * | * | * | 27 | 57 | 30 | 19 | 2.38 |
| CQF | 1 | Topsoil | 5.0 | 17.3 | 39.7 | 38.1 | 2.65 | 1.92 | 1.63 | 0.38 | 26 | 53 | 27 | 18.5 | 0.71 |
| | 5 | Ditchfill1 | 2.1 | 18.6 | 37.2 | 42.1 | 2.61 | 1.97 | 1.68 | 0.36 | 23 | 48 | 25 | 17 | 0.59 |
| | 7 | Ditchfill2 | 11.9 | 21.1 | 33.1 | 33.9 | 2.67 | 2.01 | 1.69 | 0.37 | 24 | 55 | 31 | 18 | 0.91 |
| | 8 | Upper SSM | 1.6 | 18.7 | 33.9 | 45.8 | 2.73 | 1.93 | 1.64 | 0.40 | 20 | 56 | 36 | 18 | 0.79 |
| | 9 | Lower SSM | 12.4 | 18.6 | 35.4 | 29.8 | 2.73 | 2.03 | 1.78 | 0.35 | 21 | 47 | 26 | 15 | 0.87 |

5.3. Geochemical Characterisation of the Soil

The results from the geochemical testing conducted by Alcontrol Laboratories and loss on ignition test results from the University of Winchester, which have been averaged by soil context, are presented in Table 5.2. In a similar way to the geotechnical properties, the ditchfill soils are generally halfway between the properties of topsoil and SSM soils, with small intra-site differences between different soils as they are formed from similar parent material, but with much larger differences between the different fields where the underlying chemistry is different. As with the geotechnical testing, no comparative data between the archaeological soils and SSM was available for CCC due to the shallow nature of the surrounding soils (see Section 3.6.2).

Perhaps the most significant differences which affect soil water behaviour and geophysical properties can be found in the organic content of the soil seen as total organic carbon (TOC), total organic matter (TOM) and loss on ignition (LOI) results. Organic matter is important for determining both water behaviour and storage capacity and influences the structure of the soil. Across all the sites, the organic content is highest in the topsoil and decreases with depth through the soil profile as would be expected in a typical soil profile. However, perhaps more significantly there is an elevated amount of organic material in the archaeological ditchfills, which is especially pronounced on CQF and still visible on the two Diddington sites. The loss on ignition result from Winchester on DPF SSM seems to be anomalous to this, but the Alcontrol results for TOC, TOM and LOI contradict it, and inspection of the soil on site would suggest that this result is erroneous. These results are in agreement with those found in other studies (Cuenca-García et al., 2013, Strunk-Lichtenberg, 1965). Organic matter is, in general, higher on fine grained soil sites, although the highest recorded values are recorded on CCC. The most likely explanation for this is land use practices, with both clay sites under arable cultivation and the CCC site used to keep pigs, which deposit organic material, and is in contrast to the permanent pasture present on DPF.

Another important property which affects the geophysical behaviour of the soil is the availability of soluble ions, as this affects the BEC behaviour of the soil. The most common cations within the soil are H^+ , Ca^{2+} , Mg^{2+} , K^+ and Na^+ , which can be estimated from the relative amounts of these elements in the soil. Millequivalents per 100g (meq/100g) have been estimated using Equation 5.2.

$$Element_{meq/100g} = \frac{Element_{mg/100g}}{Factor}$$

5.2

Where the factor is derived from the atomic weight and valence of the mineral and were $K=390$, $Mg=120$, $Ca=200$ and $Na=230$. The results are plotted in Figure 5.1.

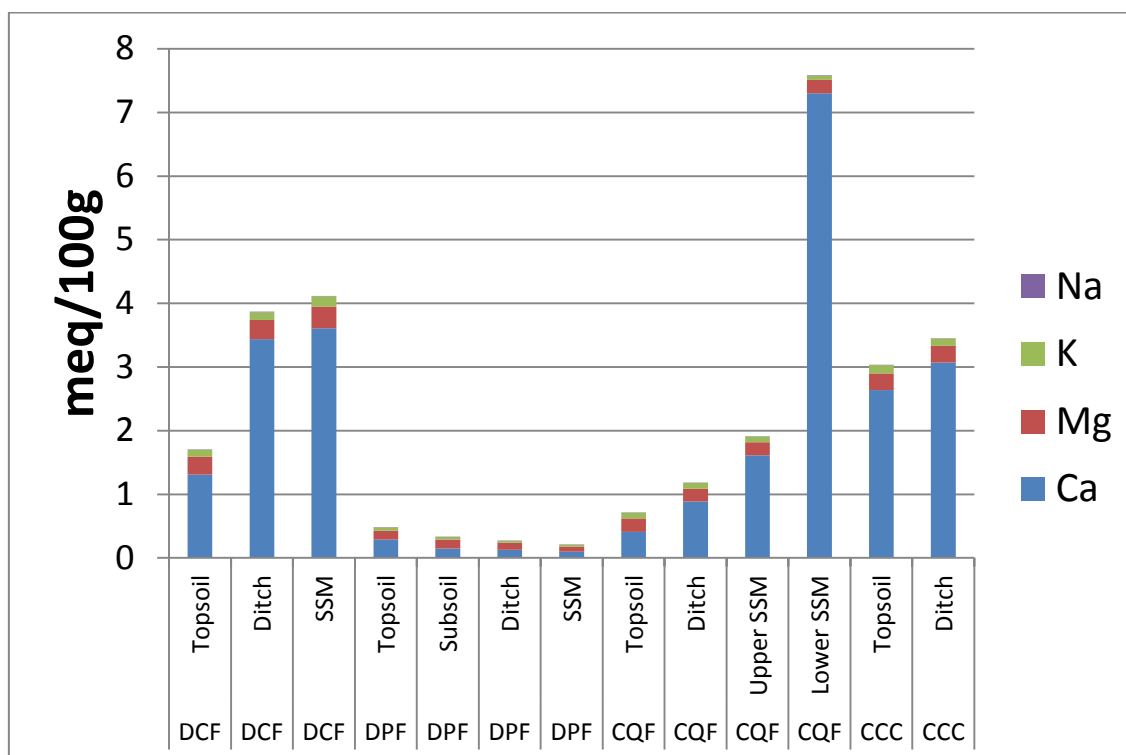


Figure 5.1: Millequivalents per 100g of Sodium, Potassium, Magnesium and Calcium for the tested soils

From Figure 5.1, it can be seen that, perhaps unsurprisingly, the highest concentrations of ions exist on the clay sites, with much smaller differences observed between the SSM and archaeological soils on each site. The majority of the variation between soils is caused by

calcium, with the other ions displaying minimal variation across a site although slight differences exist between sites. On the two clay sites values for the topsoil are lower than the underlying SSM, whereas the reverse is true on DPF. The archaeological soils measured display properties in between those of the topsoil and SSM on all of the sites where this comparison can be made.

The number of hydrogen ions can be assessed using soil pH, as the scale is a negative logarithm of hydrogen ion concentration. All of the tested soils were slightly alkaline, reflected in their pH values exceeding 7, and no discernible differences are noticeable between the coarse grained and fine grained soils. However, within each site it can be noticed that archaeological soils are more acidic than the SSM, which is reflected in lower pH and Alkalinity as CaCO_3 values on all sites between the soils. One possible reason for this is the predominance of finer grained particles (see Table 5.1) potentially providing more available ions through their increased surface area (Scollar et al., 1990, Strunk-Lichtenberg, 1965), although some differences between the fine grained and coarse grained soils would surely be apparent were this the case. Another factor may be decomposition of organic matter, which is more abundant in these soils, is also known to increase acidity (Ritchie and Dolling, 1985) as released CO_2 reacts with water to form carbonic acid. Another salt which may affect the BEC of the soil is the amount of soluble chloride within the soil. Higher quantities of soluble chloride can be observed in the topsoil and ditch section of all of the study sites suggesting these soils have the potential to be more electrically conductive when wet compared to the SSM.

Other properties have little relevance. Soluble phosphate levels remain fairly constant both between different soils on a site and between the four different study sites, with detectable values recorded in only two soils. Whilst differences in the relative abundance of nitrate can be observed within the archaeological ditchfills on the DCF and DPF sites, which may affect

plant growth and the formation of crop marks, it has little known potential to affect the soils EM properties.

5.4. Magnetic Permeability

Another important factor is the magnetic response of the soil. The results of mass specific magnetic susceptibility testing (see Section 4.2.2) have been averaged by soil context and the averages are presented in Table 5.3. The relative magnetic permeability (μ_r) has also been calculated for both the high and low frequency permittivity using Equation 5.3.

$$\mu_r = 1 + \chi_m$$

5.3

Where χ_m is the volume specific magnetic susceptibility in SI units. The coefficient of frequency dependence, expressing the dispersive nature of the magnetic component, was also determined using Equation 5.4.

$$\chi_{fd} = \left(\frac{(\chi_{lf} - \chi_{hf})}{\chi_{lf}} \right) 100$$

5.4

Where χ_{fd} is the coefficient of frequency dependence in % and χ_{lf} and χ_{hf} are the volume specific susceptibility values measured at low and high frequencies respectively (Gale and Hoare, 1991).

From this data it can be seen that most of the soils have a relative permeability of around unity, the value usually used in soil EM research. The iron content displayed in geochemical tests would suggest no significant relationship between magnetic permeability and the total amount of iron contained within the soil (Table 5.2), which is often higher in SSM. This suggests that the form of the iron oxides is the most important factor for determining magnetic permeability. It can be seen that the ditchfill soils show enhancement above the background, which allowed them to be detected using the initial magnetometer survey,

although on two of the sites (DCF and CQF) these differences are small in magnitude (c. 0.1-0.2 units). Greater differences were detected between the SSM and archaeological soils at DPF, which displayed more significant magnetic enhancement, with one of them (Ditchfill2) having a permeability of over 2 units; twice the usually assumed value. The presence of burnt material such as charcoal suggests that the iron has been converted, via the le Borgne effect, to more magnetically susceptible forms through reduction and reoxydation (Aspinall et al., 2008). All the soils at CCC showed magnetic enhancement greatly in excess of typical values. One possible explanation for this is microbially mediated enhancement by bacteria (Fassbinder et al., 1990) due to the presence of high quantities of organic material (Table 5.2) deposited by pigs kept in the field. These soils may have a significant impact on the transmission of EM radiation, affecting readings using instruments such as TDR and GPR, especially at low water contents. In addition to higher magnetic permeability values, these soils also display higher coefficients of frequency dependence, making them potentially more electromagnetically dispersive.

As mentioned in Section 2.7.3, one of the key limitations of TDR is the inability to separate electrical and magnetic effects on the propagating waveforms. An examination of the values in Table 5.3 shows that this assumption is invalid for the soils studied here, especially on DPF and CCC, where values are 1.5-3 times higher than the commonly assumed value of one, making the attribution of differences in velocity and attenuation to the electrical properties problematic. The differences between the TDR-measured real (ϵ'_{TDR}) and imaginary permittivity (ϵ''_{TDR}) can be given using Equation 5.5 or Equation 5.6 if negligible magnetic losses ($\mu'' = 0$) (Santamarina, 2001) are assumed.

$$\begin{aligned}\epsilon'_{TDR} &= \mu' \epsilon' - \mu'' \epsilon'' \\ \epsilon''_{TDR} &= \mu' \epsilon'' - \mu'' \epsilon'\end{aligned}$$

$$\varepsilon' = \frac{\varepsilon'_{TDR}}{\mu'} \quad \varepsilon'' = \frac{\varepsilon''_{TDR}}{\mu'}$$

5.6

Taking the highest measured value of approximately 3 (CCC Ditchfill1) and assuming simplified properties (i.e. no magnetic loss) we can expect the TDR to overestimate both the real and imaginary permittivity values by up to 66%, although it is worth noting that the precise effects are difficult to calculate due to the differences in operating frequencies between the magnetic susceptibility meter (kHz range) and TDR (MHz range), and the magnetic relaxation processes which are likely to make the values in the TDR frequency range significantly lower. However, it should be anticipated that the presence of this magnetic material will cause substantial increases in the measured ARDP and BEC values in line with the findings of other authors (Robinson, 1994, Cassidy, 2007 2008, 2009, Cassidy and Millington, 2009).

Table 5.3: Magnetic Susceptibility and Relative Magnetic Permeability of the soil. Where χ_{lf} and χ_{hf} are the measured volume specific magnetic susceptibility values at low and high frequencies respectively, χ_{fd} is the coefficient of frequency dependence and μ_r (lf) and μ_r (hf) are the calculated relative magnetic permeability values at low and high frequencies respectively

| Site | Context No. | Soil Name | Volume Specific Magnetic Susceptibility | | | Relative Magnetic Permeability | |
|------|-------------|------------|---|-------------|-------------|--------------------------------|--------------|
| | | | χ_{lf} | χ_{hf} | χ_{fd} | μ_r (lf) | μ_r (hf) |
| | | | SI | SI | % | - | - |
| DCF | 1 | Topsoil | 0.2148 | 0.2084 | 2.91 | 1.2148 | 1.2084 |
| | 2 | Subsoil | 0.1675 | 0.1596 | 3.76 | 1.1675 | 1.1596 |
| | 4 | Ditchfill1 | 0.1362 | 0.1268 | 6.74 | 1.1362 | 1.1268 |
| | 5 | Ditchfill2 | 0.1174 | 0.1242 | -9.53 | 1.1174 | 1.1242 |
| | 6 | SSM | 0.0615 | 0.0604 | 2.20 | 1.0615 | 1.0604 |
| DPF | 1 | Topsoil | 0.2784 | 0.2645 | 4.99 | 1.2784 | 1.2645 |
| | 2 | Subsoil | 0.1902 | 0.1748 | 8.29 | 1.1902 | 1.1748 |
| | 3 | Ditchfill1 | 0.5876 | 0.5126 | 13.39 | 1.5876 | 1.5126 |
| | 4 | Ditchfill2 | 1.0305 | 0.9045 | 13.10 | 2.0305 | 1.9045 |
| | 5 | Ditchfill3 | 0.7012 | 0.6095 | 13.08 | 1.7012 | 1.6095 |
| | 6 | SSM | 0.2208 | 0.1956 | 11.36 | 1.2208 | 1.1956 |
| CQF | 1 | Topsoil | 0.3187 | 0.2962 | 7.05 | 1.3187 | 1.2962 |
| | 5 | Ditchfill1 | 0.3210 | 0.3071 | 4.34 | 1.3210 | 1.3071 |
| | 7 | Ditchfill2 | 0.2012 | 0.1828 | 9.13 | 1.2012 | 1.1828 |
| | 8 | Upper SSM | 0.0906 | 0.0872 | 3.69 | 1.0906 | 1.0872 |
| | 9 | Lower SSM | 0.0988 | 0.0855 | 13.51 | 1.0988 | 1.0855 |
| CCC | 1 | Topsoil | 1.9699 | 1.7905 | 9.11 | 2.9699 | 2.7905 |
| | 7 | Ditchfill1 | 2.1775 | 1.9818 | 8.99 | 3.1775 | 2.9818 |
| | 8 | Ditchfill2 | 1.6523 | 1.4608 | 11.59 | 2.6523 | 2.4608 |
| | 9 | Ditchfill3 | 1.7012 | 1.4939 | 12.19 | 2.7012 | 2.4939 |

5.5. Empirical Relationships between VWC, ARDP, BEC, Density and Temperature

This section deals with the results from the laboratory testing on the soil EM properties from the Dididngton sites at a variety of different water contents, temperatures and densities described in Section 4.3. Results are discussed to examine the differences both between the two sites (Section 5.5.2) and between the different soils contained within them (Section 5.5.3). Consideration is also given to the effects of density (Section 5.5.4) and temperature (Section 5.5.5) on the measured results, and a variety of different models are fitted to find the most appropriate in different soil types (Section 5.5.6). The most important soil variables affecting the EM properties are examined through principal component analysis (PCA) in Section 5.6.

5.5.1. Errors

Errors in the experiment stem from two sources; the accuracy and repeatability of TDR measurements of ARDP and BEC and errors in the uniformity of water content distribution within the sample. To assess VWC errors, the two water content values recorded after deconstruction of the samples (small probe sample and rest of cylinder) were compared and the standard deviation and range between the two calculated. The calibration of the TDR for laboratory work displayed similar accuracy to those used in the field monitoring stations with errors no greater than ± 0.4 recorded for ARDP determination. Standard deviations taken between the three repeated readings never exceed this value, which has therefore been used to generate the error bars on subsequent plots. Errors in conductivity determined during laboratory calibration were generally between 1-5%, but could be much higher in conductive mediums. Several authors have suggested an accuracy of around 10% in comparison to DC conductivity (Huisman et al., 2008, Topp et al., 1988, Zegelin et al., 1989) and this has been used as a reasonable estimate of the error bars on subsequent data plots.

5.5.2. Relationship between ARDP, BEC and VWC-Inter-Site Variation

Data have been plotted as an average of the three different temperature readings to assess the effects of changing VWC on the different ARDP and BEC values on the two different sites. The effects of temperature are examined in Section 5.5.5. The differences in the recorded BEC values by VWC for the DCF and DPF soils are shown in Figure 5.2. The R^2 and root mean square error (RMSE) values are also presented. As expected, both soils show a positive relationship between VWC and BEC, with the DCF soils displaying both higher BEC values and greater increases per percentage increase in VWC compared with the DPF soils. This effect is likely to be caused by the higher surface area of these soils due to the finer grained texture of the clay particles, which dominate in these soils in comparison to the sands and gravels that make up the majority of the DPF samples (see Table 5.1). The greater number of ions available to be dissolved is also reflected in the geochemical data, especially in differences in the amount of calcium between soils from the two sites (see Figure 5.1). The rate of increase with increasing VWC can be seen to decrease at higher water contents, with very small increases recorded above 30-40% VWC on fine grained soils. These results are consistent with the results of similar studies relating BEC with VWC, such as Smith-Rose (1933) who found a similar maximum at around 20% VWC for the tested soils. It is suggested that this maximum value occurs at the point when all of the available ions from the soil surfaces have been dissolved and the soil water solution is at a maximum concentration of ions. The addition of further water beyond this causes no further increases in BEC and may even result in slight decreases as the soil solution becomes more diluted. This behaviour has been noted by Wensink (1993) and can be seen in the data from some of the soils in this study and is discussed in Section 5.5.3. One final observation is that the DCF soils also display a greater spread in BEC values, especially at higher water contents, reflecting differences in their maximum saturated BEC values. This difference is again reflected in the geochemical data, which show greater differences in the quantities of calcium, potassium, magnesium and sodium between the

tested soils on this site. The difference in BEC values between different soils on each of these sites and reasons for these differences are discussed in greater detail in Section 5.5.3.

The effects of changing VWC on the measured ARDP are more complicated and results for both DCF and DPF are shown in Figure 5.3. For comparative purposes, the Topp et al. (1980) model has also been included as this remains the most commonly used model for linking VWC and ARDP when using TDR. For all soils a positive relationship exists between VWC and ARDP. At low VWC values below approximately 35%, the DPF soils display lower ARDP for the same VWC in comparison to the soils taken from the DCF site. When compared to the Topp et al. (1980) model over this VWC range, it is apparent that using this model would under-predict and over-predict the water content on the DPF and DCF soils respectively. The higher ARDP values recorded for the same water contents on the DCF soils in comparison with the DPF soils and Topp et al. (1980) model is difficult to explain. The opposite effect (i.e. lower ARDP at each water content than the Topp et al. (1980) model) due to effects of bound water in fine grained soils, which reduces the real part of the permittivity (Bridge et al., 1996, Gong et al., 2003), is the most widely reported effect in clay soils. However, similar effects to those found on the DCF soils have been found when adding saline water to soils (Aqil and Schmitt, 2010). The most likely cause of this effect is the contribution of the imaginary permittivity to the recorded ARDP (Equation 2.39), which increases values when the loss tangent (ratio of imaginary to real permittivity; $\tan\delta$), commonly assumed $\ll 1$ (Robinson et al., 2003a, Topp et al., 2000), is significantly higher making the assumption of $\epsilon_a \approx \epsilon'$ invalid. The most likely cause of this is the higher conductivity values associated with these soils (see Figure 5.2) which has been known to increase the measured ARDP, and the measured values exceed the range at which this effect has been noticed (0.2dS/m-0.25dS/m) (Bittelli et al., 2008, Wyseure et al., 1997). In addition to this, the presence of significant quantities of bound water, with a rotational relaxation frequency close to the measurement frequency of the TDR (below 500 MHz according to Friel and Or, 1999), causes an increased relaxation losses in these soils, and a

smaller real permittivity as the bound water molecules cannot rotate as freely as those in free water. The effect of this is to make the loss tangent higher, similar to the effects of increased imaginary permittivity due to high conductivity discussed above, causing the TDR to record a high apparent permittivity in these fine grained soils, especially at low water contents where bound water is dominant over free water.

Under-prediction of VWC when using the Topp et al. (1980) model on the DPF soils seems to be the result of the opposite of this effect, with the soils tested here having insignificant loss mechanisms in comparison to the soils used by Topp et al. (1980) and those on DCF, and consequently smaller loss tangents. Comparison of the soil textures of the soils tested by Topp et al. (1980) show that 3 of the 4 tested soils have a higher clay content than any of the DPF soils tested, with the final Rubicon soil having a clay content higher than two of the ditchfills and the SSM. BEC values were not reported, but quoted reference values for Bainsville soil (0.1-0.3mS/cm; Schut and Wilson, 1987) are in excess of those recorded on the DPF soils.

These factors seem to suggest higher loss tangents on the Topp et al. (1980) soils than on the DPF soils indicating that some of the effects highlighted are implicit within the calibration. An alternative to this would be the contribution of the finer (silt and clay) fractions in these soils which created a significant bound water fraction due to their greater surface area. However, this seems unlikely to be a significant factor in these soils due to their predominantly coarser texture in comparison with those used to calibrate the Topp et al. (1980) model.

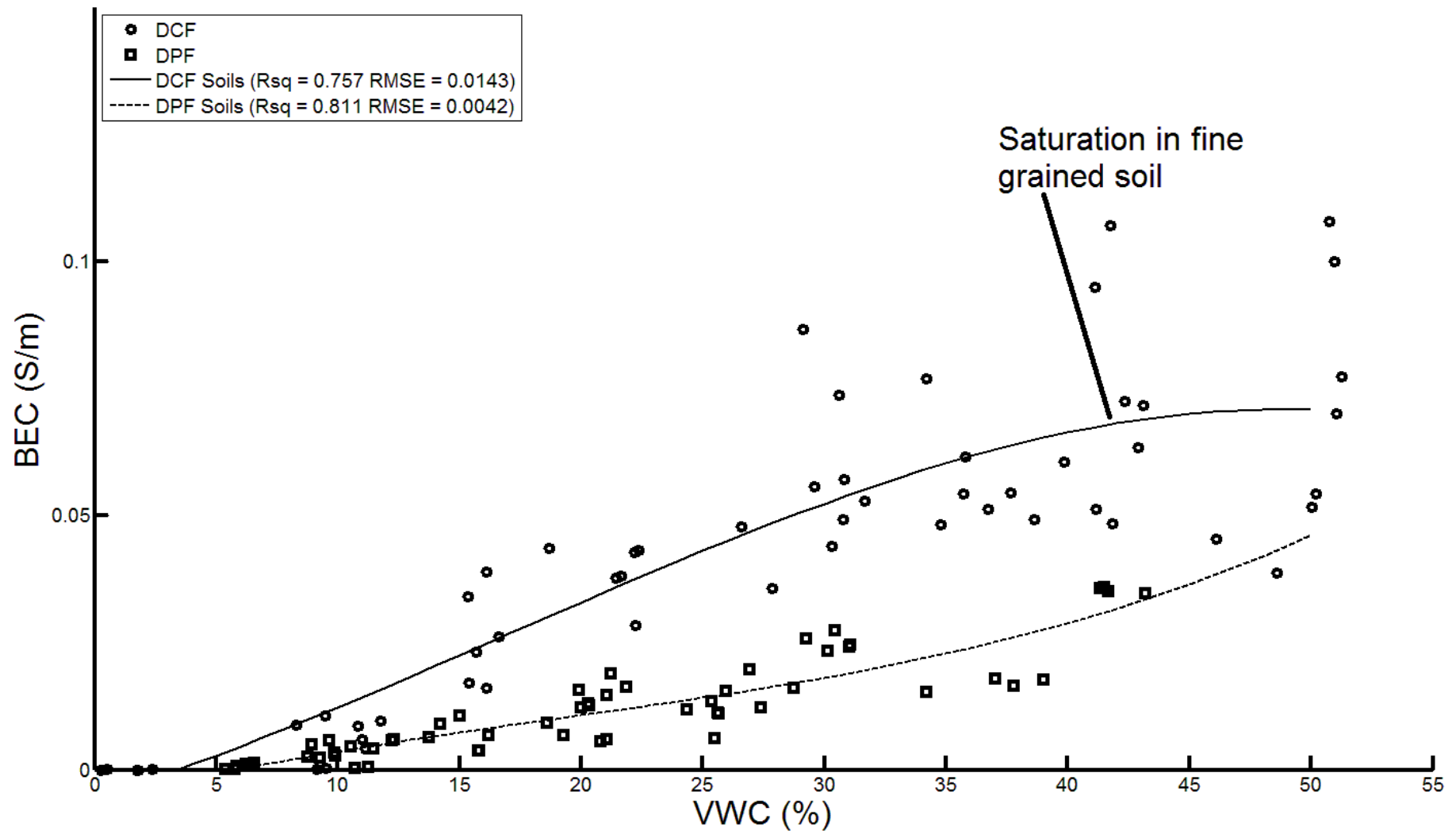


Figure 5.2: Comparison of BEC-VWC relationships between clay (DCF) and non-clay (DPF) soils

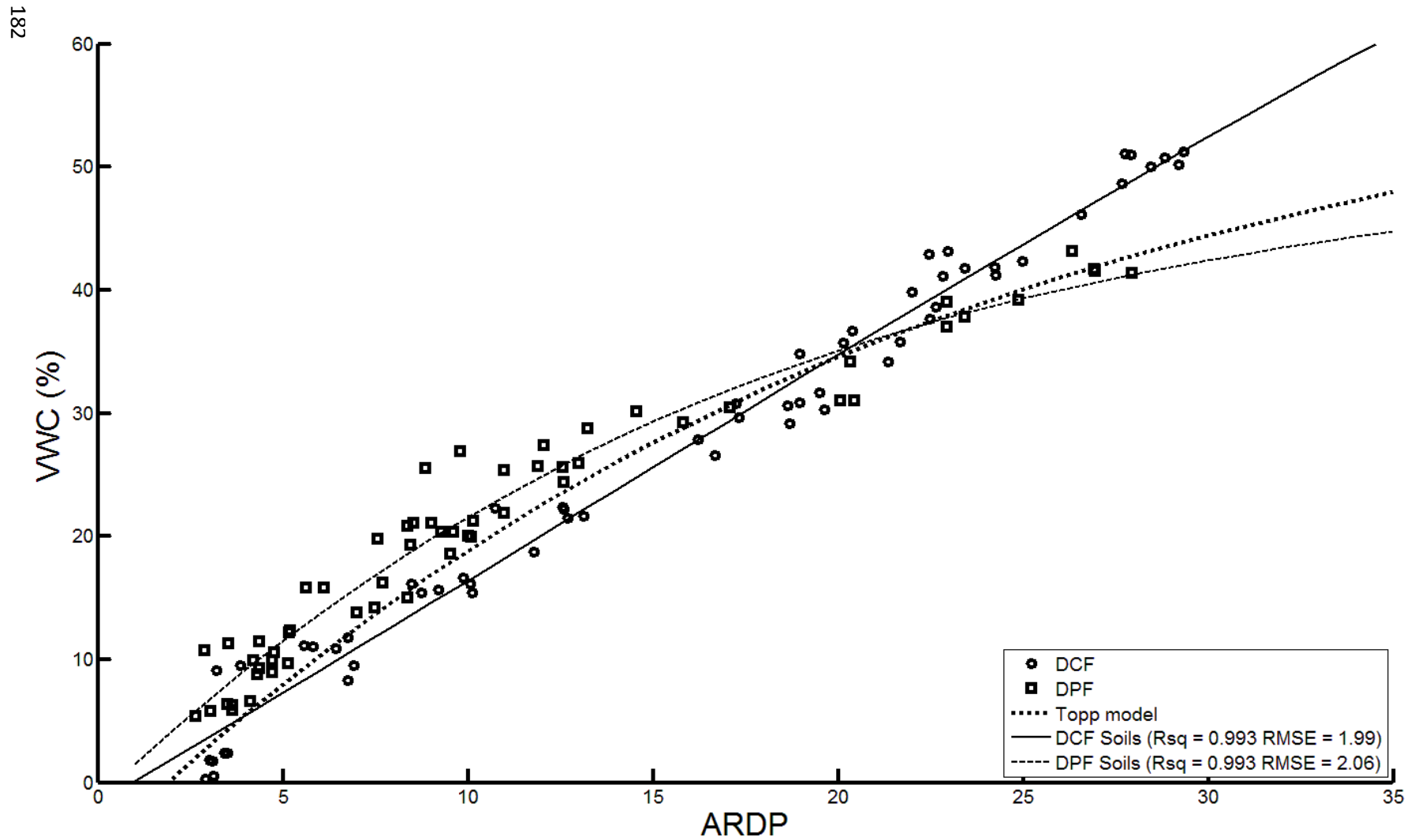


Figure 5.3: Comparison of ARDP-VWC relationships on fine grained (DCF) and coarse grained (DPF) soils. Topp et al. (1980) model also plotted for comparison

Another possible cause of higher ARDP on the DCF soils may be the contribution of interfacial polarisation to the measured values, which becomes more significant due to the lower measurement frequency in lossy soils. Chen and Or (2006) found that an increased concentration of ions raised the Maxwell-Wagner relaxation frequency for increasing solution electrical conductivity, but found the effect to be irrelevant in the TDR frequency range. However, Thomas (2008a) showed that the ARDP of clay soils did vary below 400-500MHz, particularly on soils with high liquid limits, and it can be shown that an additional effect of the losses is a lowering of the effective measurement frequency into this range. Figure 5.4 shows a comparison of two waveforms from DCF SSM and DPF Ditchfill2 soils at 20% VWC and the differences in the rise times between the two soils, defined as the time between 10% and 90% of the return reflection. From this it is clear that the DCF SSM soil takes longer for the return reflection to reach full amplitude, shown by the shallower gradient of the waveform at this point. The effective measurement frequencies (f_{eff}) have also been calculated using the method described by Robinson et al. (2003a). To illustrate the effects of this changing measurement frequency between 100MHz-1.2GHz, data taken using a VNA and a coaxial probe for the same two soil samples used for Figure 5.4 at 20% VWC are displayed in Figure 5.5. From this it is clear that ϵ'' is largely insignificant in relation to ϵ' in the DPF soil (Figure 5.5b), whereas ϵ'' forms a significant part of the reading in the DCF soil (Figure 5.5a), supporting the conclusion of a significant loss tangent in the DCF soils. However at frequencies below 400MHz, ϵ'' in the DCF SSM soil can be seen to increase dramatically while ϵ' increases more gradually, meaning the loss tangent increases as frequency decreases on this soil, leading to greater rises in ARDP values. In both soils at very low frequencies, ϵ' rises due to the effects of interfacial polarisation, although the effects are more pronounced in the DPF Ditchfill2 soil and more spread over a wider range of frequencies in the DCF SSM soil. A particular drawback of the TDR method is that the measurement frequency is undefined and further work using the

VNA and frequency analysis of TDR waveforms may be beneficial for investigating these effects, although this is not included in the present work.

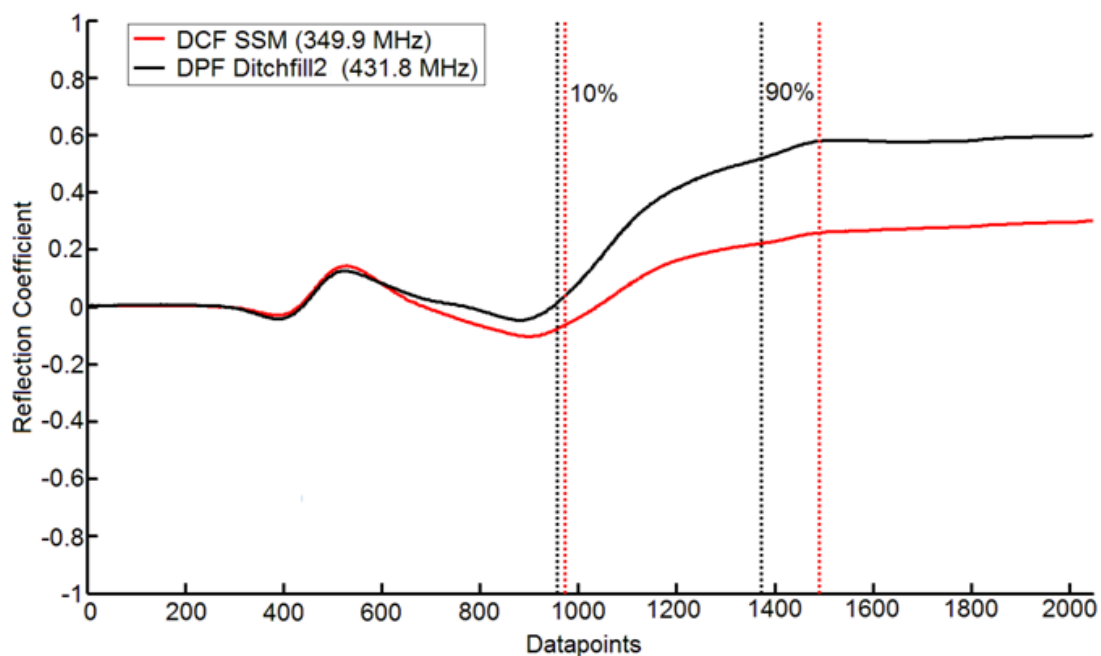


Figure 5.4: Comparison of waveform rise times between DCF SSM and DPF Ditchfill2 at 20% VWC. The effective measurement frequencies have been calculated using the method described by Robinson et al. (2003a) and are displayed in brackets on the legend

On further inspection of Figure 5.3, at higher values of VWC above approximately 30-35%, the soils from DCF have VWC values which fall above the DPF soils at each ARDP value and are under-predicted by the Topp et al. (1980) model, displaying the opposite effect to those observed in the low VWC range. The cutoff VWC value above which the relationship is reversed shows good agreement with the point when BEC reaches a stable value (Figure 5.2).

In addition, at higher water contents, the water stored in the soil is likely to have a more significant quantity of free water possessing higher permittivity values as all the soil particle surfaces are already covered from the initial water forming bound water layers. These two factors cause the imaginary part of the permittivity to become less significant in comparison to the real part which continues to increase at a steady rate due to the increased amount of

water in the measurement volume. The low ARDP values recorded at each VWC in this range near to saturation in comparison to those seen on the DPF soils seem indicative of a more significant amount of the water in the measurement volume being rotationally hindered due to bound water effects. These effects can only be observed on the DCF soils due to their higher SSAs stemming from their higher clay content and mineralogy. Above 30-35% VWC, the DPF soils agree well with values predicted by the Topp et al. (1980) model suggesting that the imaginary permittivity effects which affected the model at lower water contents are no longer significant in either soil set.

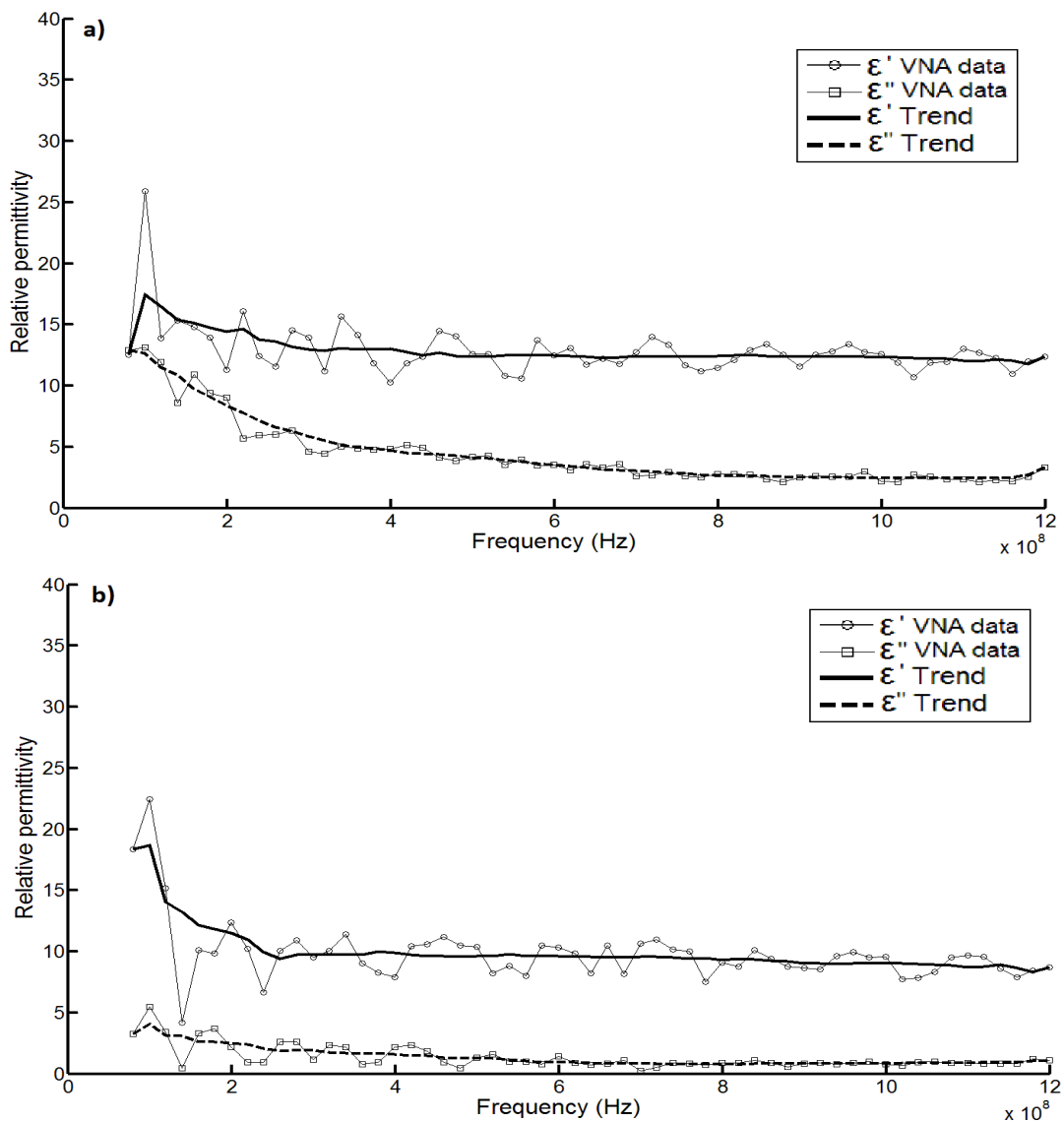


Figure 5.5: ϵ' and ϵ'' at 20% VWC for two samples from a) DCF SSM and b) DPF Ditchfill2. Errors are estimated as being less than 10% of the measured values.

It has previously been reported that fine grained soils give lower TDR measured ARDP values at the same water content in comparison to coarse grained soils (e.g. Bridge et al., 1996, Gong et al., 2003) due to bound water effects, especially at low water contents. However, it has also been reported that ARDP has an inverse relationship to frequency (Wensink, 1993) which falls in lossy soils and that measured ARDP rises as salinity (hence BEC) increases (Aqil and Schmitt, 2010). A combination of these effects has been observed here and the non-universality of the effects of the bound/free water ratio and BEC, and the influence of the loss tangent on measured values described here highlights the need for further research in order to determine within what range of soil properties each effect is dominant. Whilst some existing calibrations appear to take these effects into account on the soils for which they are calibrated, currently empirical calibrations remain the best way to ensure the best accuracy in VWC determination.

5.5.3. Relationship between ARDP, BEC and VWC-Intra-Site Variation

This section deals with differences between the soils within each site. Data have been plotted as an average of the three different temperature readings to assess the effects of changing VWC on the different ARDP and BEC values. The effects of temperature on the different soils are discussed in Section 5.5.5. Empirical models have been fitted to the data using the polyfit function in MATLAB® to fit third order polynomial curves to the data. The R^2 and RMSE are also presented. The Topp et al. (1980) model has also been included for comparative purposes, although further discussion on different models for each soil is provided in Section 5.5.6.

The relationship between BEC and VWC on the DCF soils is plotted in Figure 5.6. All of the tested soils show a positive relationship between VWC and BEC at low water contents, which tends towards a peak BEC at higher water contents. These peak BEC values are likely to occur at points where all of the available ions have dissolved and maximum ion concentration has been reached. The water content at which these peak BEC values occur varies between soils. In Ditchfill1 and the SSM, the peak BEC values are between 30-40% VWC, with substantially higher VWC recorded at the peak BEC for the topsoil and subsoil (40-50%). The VWC value at

which peak BEC values occur is likely to be linked to the ion availability and therefore chemistry and mineralogy of the soil, and can be linked to the liquid limit and clay content of the soil (Table 5.1). In two of the soils (Ditchfill1 and the SSM), a slight decrease in measured values from the peak BEC can be observed at the highest water contents. The most likely explanation for this phenomenon is that the peak ion concentration is decreased as more water is added, diluting the soil water solution. One strange result is the relatively high BEC values recorded on the DCF subsoil across the whole VWC range. Two possible explanations for this exist. Firstly, as the soil sample was collected at a later date due to insufficient sample collection during the initial excavation, it may have been affected by land use practices on site during the cultivation processes (e.g. the addition of fertiliser), which have raised its supply of available ions. Alternatively, the layer may hold nutrients due to the relative impermeability of the clay layers below. Due to budget limitations, the subsoil was not chemically sampled making determination of the precise cause difficult using the current datasets. Another interesting result is that the DCF topsoil shows a BEC value of 0 S/m at 10% VWC. One possible explanation is the distribution of water within the sample, which affects pore connectivity. As initial water is adsorbed to soil particles and may be non-uniformly distributed, the pores may not be completely connected, creating no or few conductive pathways. However no parallels for this exist to the author's knowledge within the literature and the effect may instead be explained by the error margin of the TDR in deriving conductivity. This may be especially important if the true value falls outside the range of solutions used to calibrate the probe. Several of the other trendlines also meet 0 S/m at higher water contents than 0%. However these trends are only valid for the range of VWC values over which they have been calculated.

The relationship between BEC and VWC on the DPF soils is plotted in Figure 5.7. Both the topsoil and subsoil display the highest BEC values peaking at over 0.03 S/m as well as the greatest rates of increase relative to rising VWC. This result is perhaps unsurprising given the relatively fine textures and elevated organic matter within DPF topsoil and DPF subsoil in

comparison to the other soils on the DPF site. These provide greater surface areas allowing more ions to be dissolved. This increased ion availability in these soils is also supported by the geochemical data (see Section 5.3). In contrast to the DCF soils, on DPF, the ditchfill soils, especially Ditchfill1 and Ditchfill2 display very low BEC values (never more than 0.015 S/m) and lower rate of increase in measured BEC values as VWC increases in comparison to those from the SSM . This result seems to be the opposite to that suggested by the textural and geochemical properties of these soils, which indicate a slightly higher ion availability and SSA in these soils. One explanation is that measurement samples are biased as DPF SSM contained a greater number of large stones than the other DPF samples, which were sieved out here and would be excluded from field measurements due to the need to insert probes into the sample, which results in a greater than normal prevalence of small particles with high surface areas in the DPF SSM measurement volumes than would be typically representative. Another possibility is the greater density of these samples in comparison to the ditchfill soils, the effects of which are discussed later in Section 5.5.4.

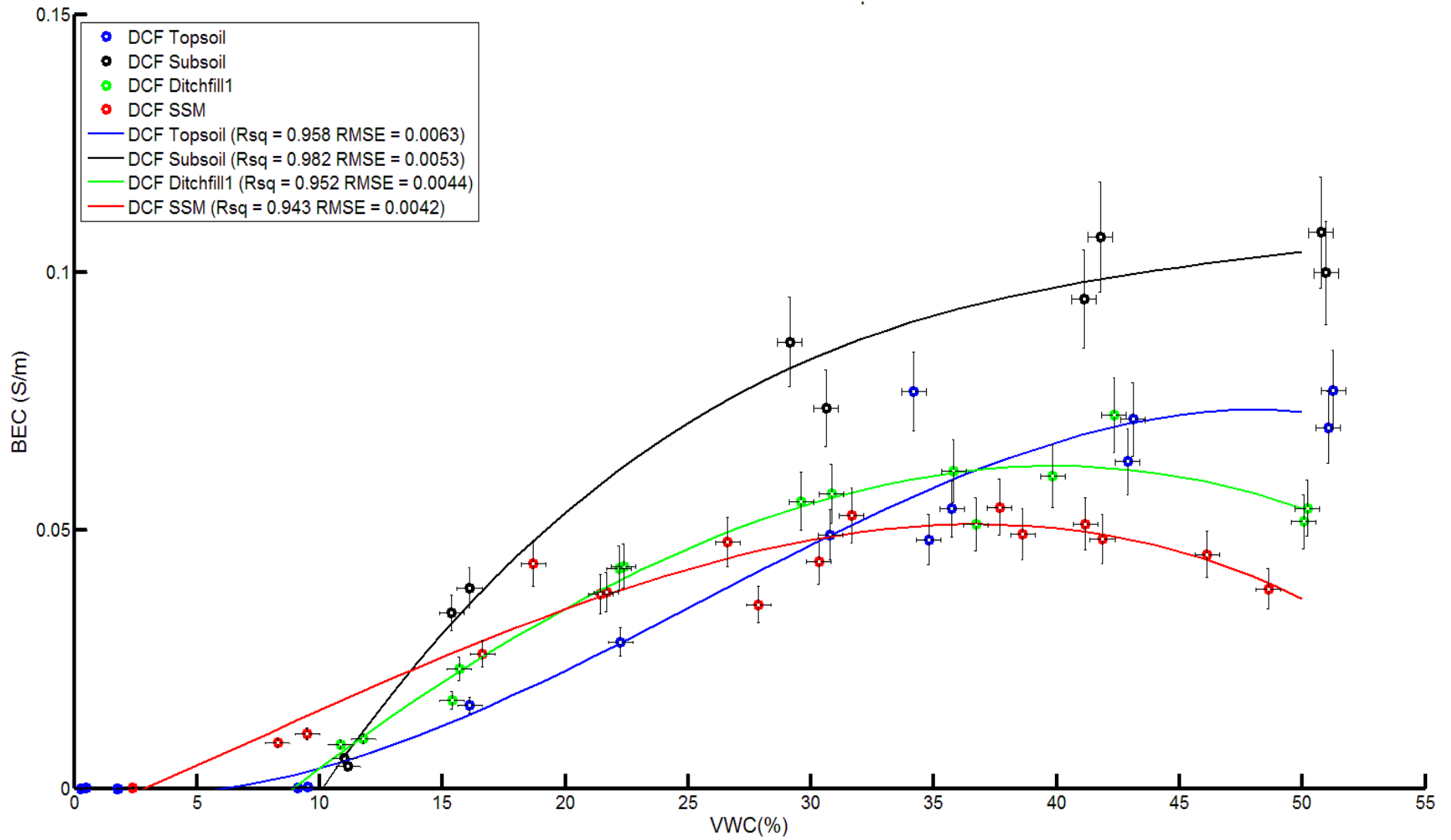


Figure 5.6: The BEC-VWC relationship between the tested soils from DCF

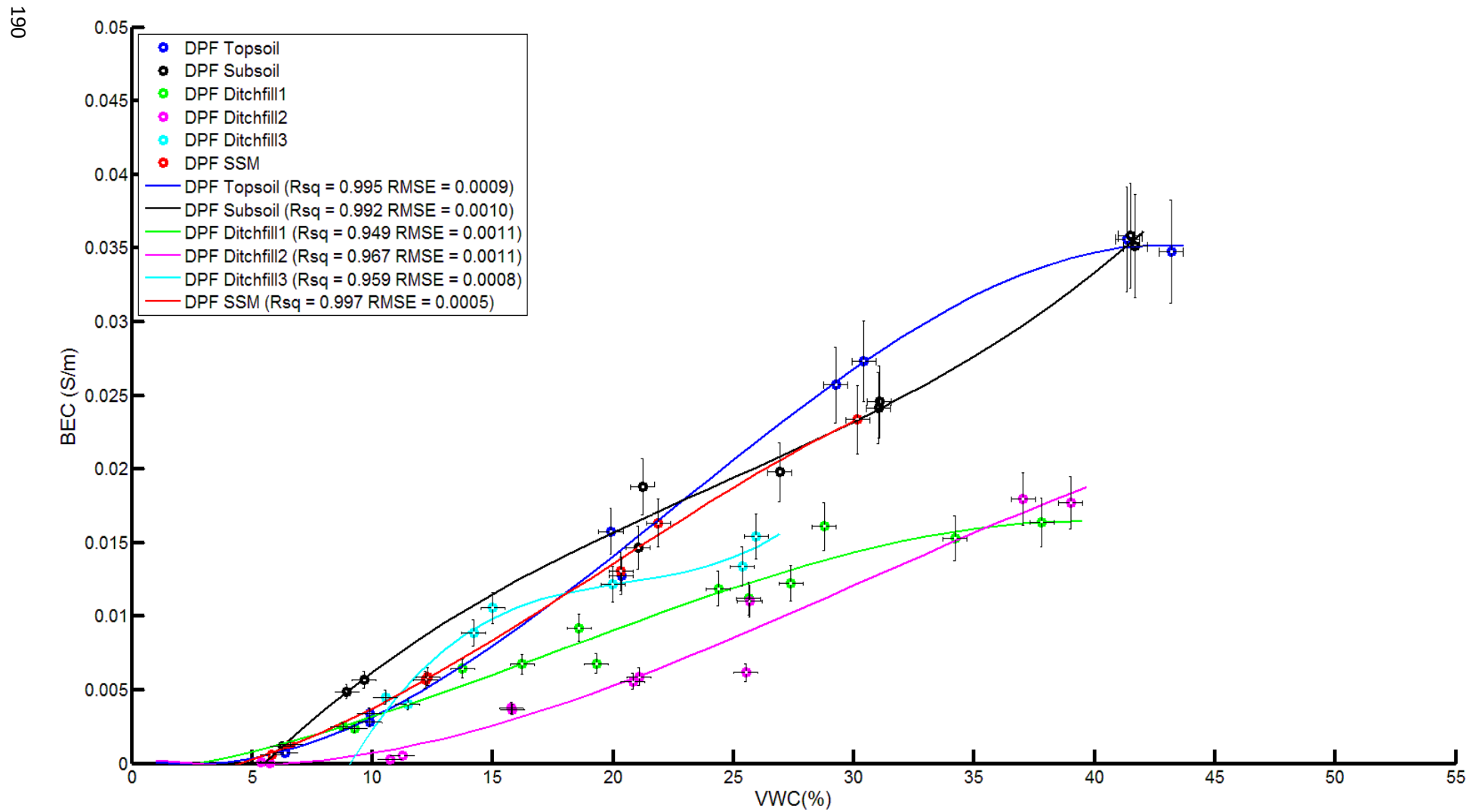


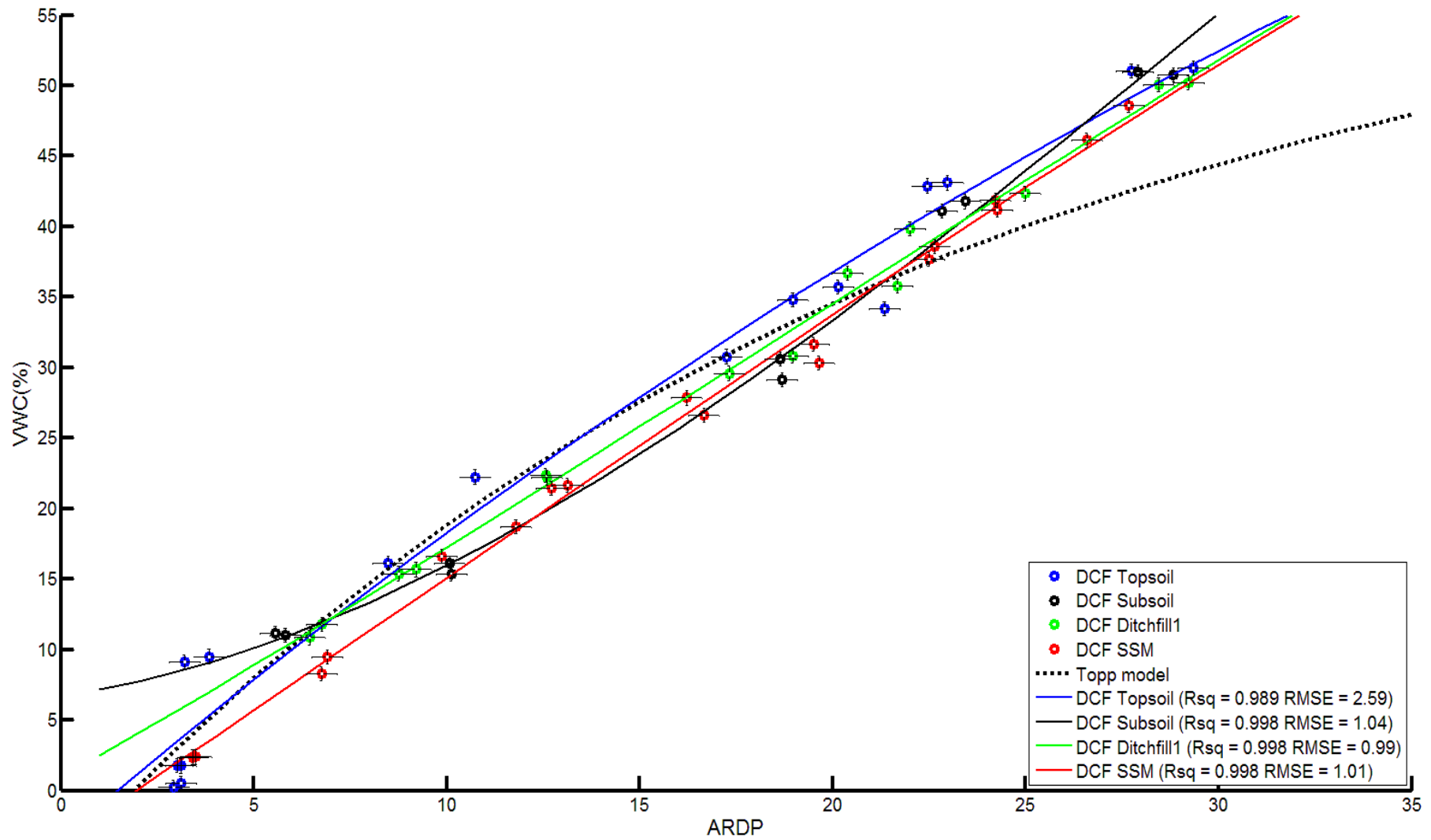
Figure 5.7: The BEC-VWC relationship between the tested soils from DPF

The relationship between ARDP and VWC on the DCF soils is plotted in Figure 5.8. At low VWCs (below 30-35%) the topsoil is most similar to Topp et al. (1980) model with the DCF subsoil the furthest from it, displaying higher permittivity values at the same water content. Taking into account the interaction between BEC and ARDP discussed in Section 5.5.2, the observed behaviour shows good agreement with the BEC values recorded in this VWC range for these soils. One anomaly to this is DCF Ditchfill1 which displays a slightly lower ARDP per unit of VWC than the SSM despite having a higher BEC (Figure 5.6). It should also be noted that DCF Ditchfill1 also has a smaller clay content than the SSM (Table 5.1) suggesting a lower SSA and less bound water in this soil, resulting in a higher real permittivity. This has the effect of making the loss tangent less significant in the ditch than the SSM. It is likely therefore that ARDP-VWC relationships in clay soils are determined by a complex interplay between the reduction in real permittivity due to bound water effects and increase in losses due to rising conductivity. At higher water contents, the amount of bound water becomes the dominant effect, with all the soils underpredicted by the Topp et al. (1980) model. The highest bound water quantities are found in the topsoil, indicated by the magnitude of their underprediction at these water contents and the small increases in measured ARDP between 0% and 10% VWC. The most likely cause of this effect is the higher quantity of organic matter in this soil. The other soils show similar trends to each other at these VWC values, indicative of their similar PSD results and suggesting negligible and stable loss tangents.

The VWC-ARDP relationships for the different soils on DPF are presented in Figure 5.9. On DPF, whilst all soils are under-predicted by the Topp et al. (1980) model (see Section 5.5.2), there are few discernible differences in the ARDP-VWC relationships of the different soils below VWC values of 30%. One exception is DPF Ditchfill2 which displays a much lower ARDP value for the same VWC in comparison to the other soils, especially at low water contents. The most likely cause of this is a lower contribution of the imaginary permittivity to the measure ARDP values than the other soils on the site, reflected in the lower recorded BEC values shown in

Figure 5.7. Another possibility is the greater pore space in this soil resulting from its low density in comparison to other soils ($1.3\text{mg}/\text{m}^3$), which leads to a greater quantity of air in the measurement volume. Density effects are discussed in greater detail in Section 5.5.4.

Towards saturation above 30% VWC, where data exist, models for all of the DPF soils fall onto the Topp et al. (1980) equation line suggesting similar behaviour to their findings, and a stable loss tangent above these water contents and a minimal quantity of bound water. Surprisingly, the comparatively large differences in the magnetic enhancement between the ditchfills and other soils (0.5-0.8 units) seem to have played little part in determination of the measured ARDP values, although other studies have suggested additional magnetic material is likely to cause overestimation of ARDP and BEC by retarding wave velocity and increasing losses in the same way as high conductivity (Cassidy, 2007, 2008, Robinson et al., 1994). One possibility is that these effects are small and being masked by other phenomena which are greater in magnitude.



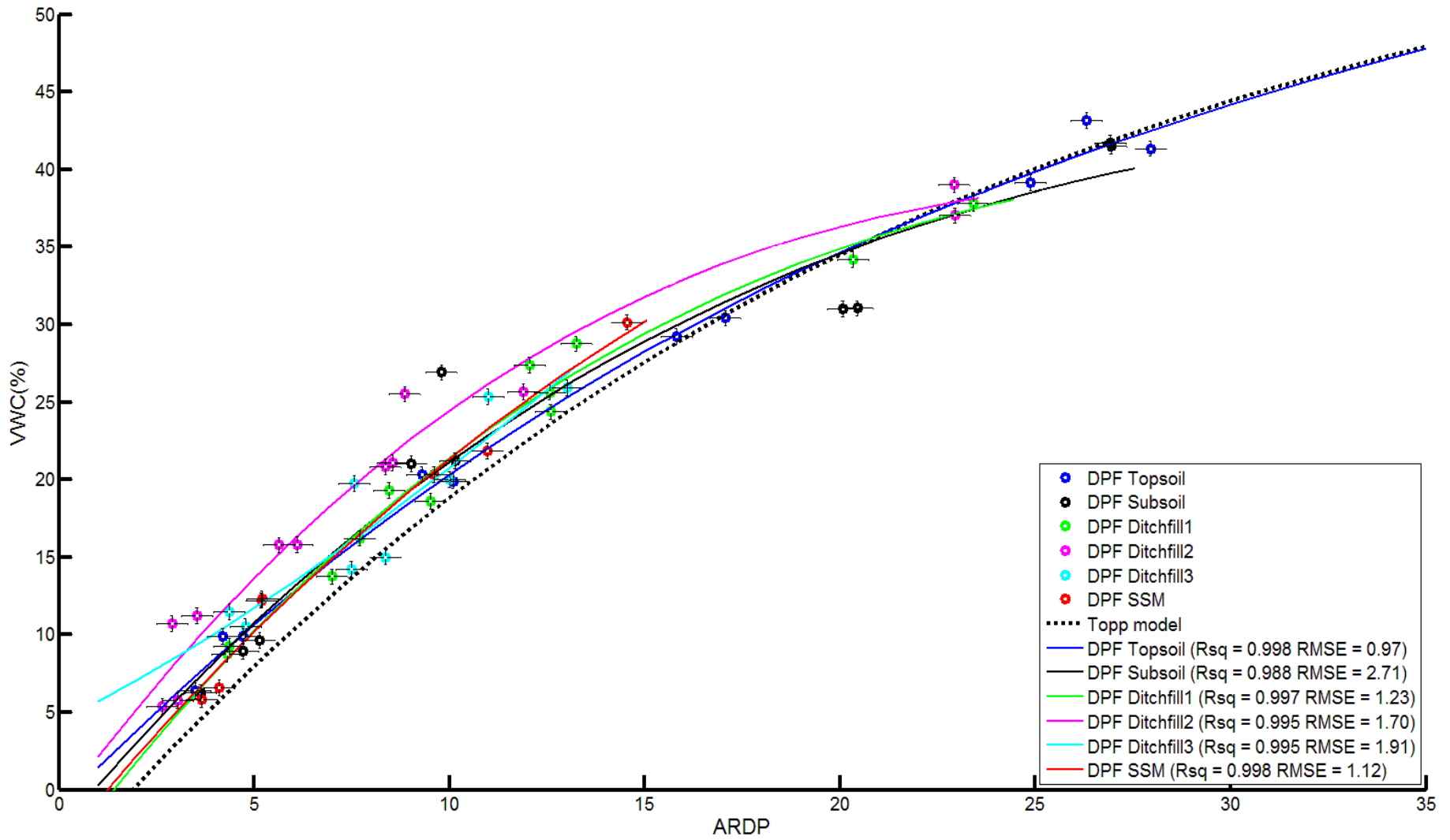


Figure 5.9: The ARDP-VWC relationships between the different tested soils from DPF. Topp et al. (1980) model also plotted for comparison

5.5.4. Relationship between ARDP, BEC and Density

Several authors have discussed the effects of density on measured ARDP-VWC relationships (e.g. Gong et al., 2003, Hipp, 1974, Malicki et al., 1996). To investigate the effects of density, two soils were chosen; one from DCF (DCF SSM) and one from DPF (DPF Ditchfill3) and additional samples were prepared which varied the density by 10% above and below the measured dry density from the field. Due to the high density of the DCF SSM soil, the samples with higher density were abandoned as it was impossible to pack to a sufficiently high density. The effects of these changes in density are displayed in Figures 5.10-5.13.

For the DCF SSM soil (Figure 5.10) there are no density related effects on the ARDP-VWC relationship at low VWC although a slight negative relationship exists between density and ARDP at higher VWC values. One explanation for this is that a decrease in density results in less solid material in the sample volume, which decreases the surface area and bound water fraction resulting in higher ARDP values due to the increased free water fraction. This difference is more pronounced at high VWC where the water forms a more significant part of the measurement value. Alternatively, the negative relationship between density and BEC discussed later in this section and shown in Figure 5.12 may further increase the contribution of the loss tangent to measured values. The results from the DPF Ditchfill3 soil (Figure 5.11) are more complex and difficult to explain. Both higher and lower density samples display lower permittivity values at the same VWC than the field density, with the lower density sample in particular being significantly outside the expected errors. One possible explanation is that multiple phenomena are taking place which dominate in the different samples. The effects in the higher density sample, which increase in magnitude with VWC, are caused in a similar fashion to those in the clay sample with increased amounts of bound water due to the greater SSA. In the lower density sample, the coarse structure of the soil may be causing the opposite effect due to the greater number of macropores which contain more air which has a lower permittivity (1 as opposed to 3-5), reducing measured ARDP values.

In addition to studying the ARDP-VWC relationship, an assessment was made on the effects of density on the determination of BEC. DCF SSM showed a small negative relationship between density and BEC at low VWC values (Figure 5.11) although differences increased with increasing water content. However, differences were rarely in excess of the maximum error for determining BEC with TDR over the measured density range. The results from the DPF Ditchfill3 soil (Figure 5.13) show the opposite trend with measured BEC increasing with measured density which slightly exceeded the predicted errors, in agreement with the findings of Yu and Drnevich (2004). These two contradictory responses between the clay and non-clay soils may suggest two conflicting phenomena. In the non-clay soil, the presence of additional solid material with increasing density means that more ions are available for dissolution. In clay soils, it is possible that this effect is counter balanced by the decrease in pore sizes between clay aggregates and pore connectivity, which decrease the cross sectional pathways for conduction. The dominant effect may be dependent on texture, and its magnitude affected by the differences in other factors, such as ion availability and VWC. Further investigation is needed to better understand the full role of density in determining geophysical properties over a wider range of soils with varying textures and chemical compositions.

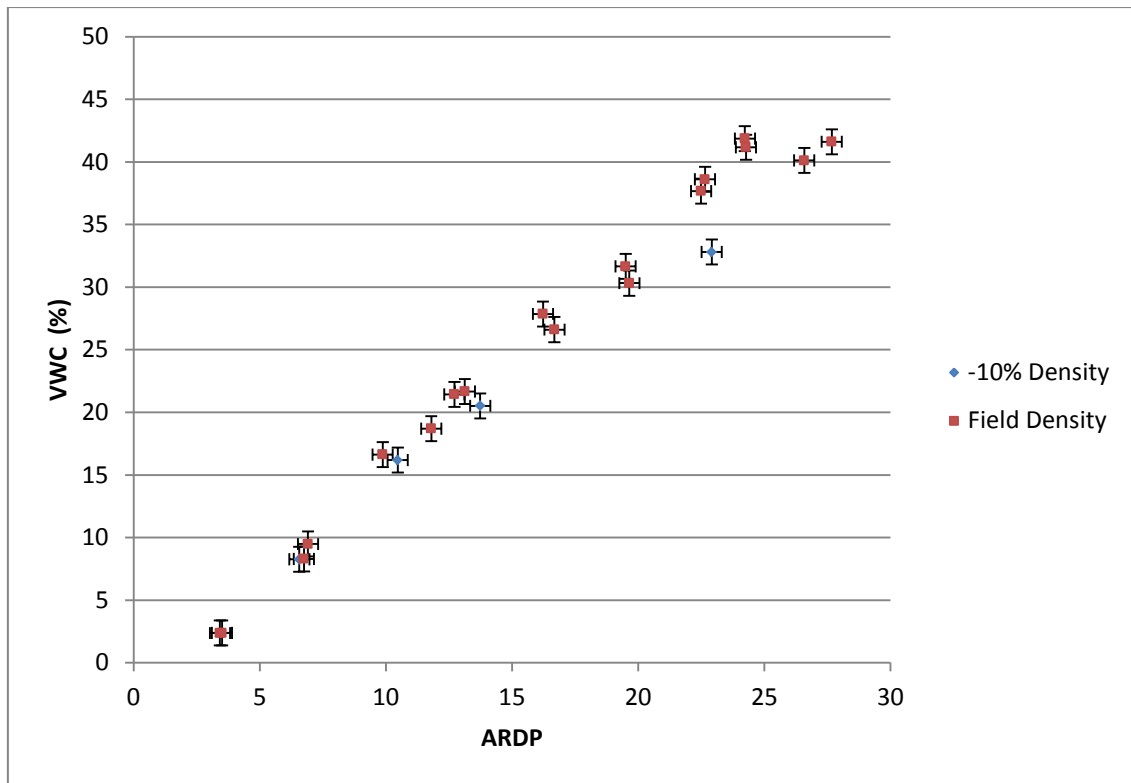


Figure 5.10: The effects of density on ARDP-VWC relationships on the DCF SSM soil

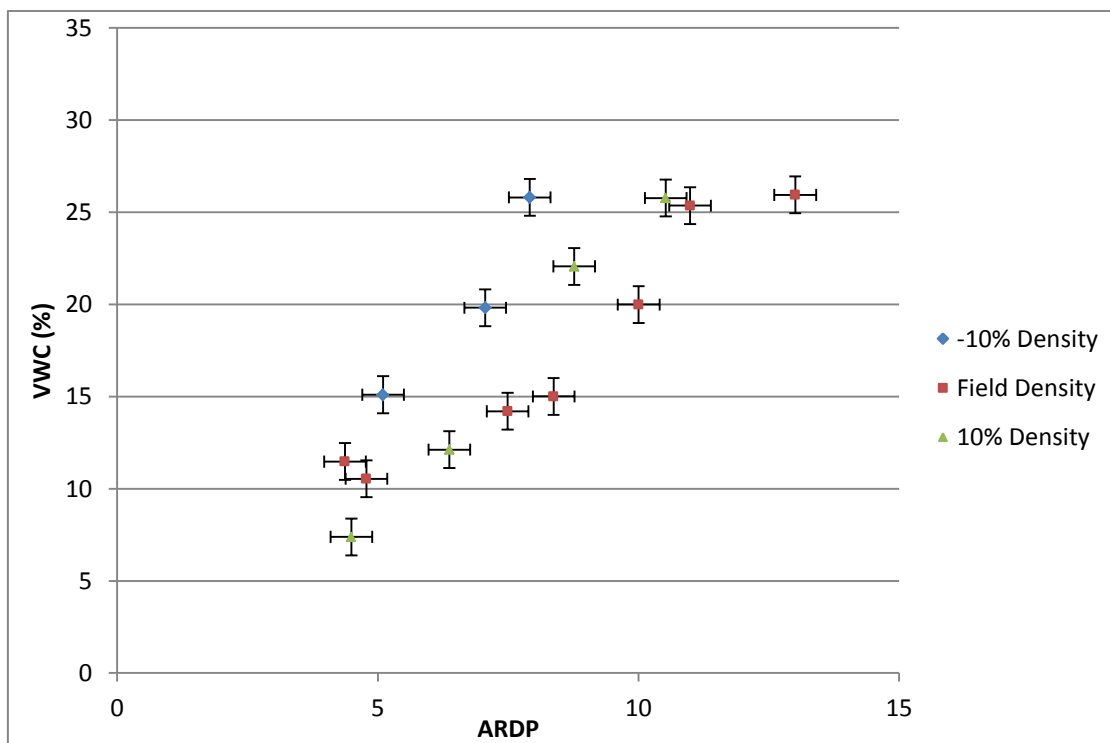


Figure 5.11: The effects of density on ARDP-VWC relationships on the DPF Ditchfill3 soil

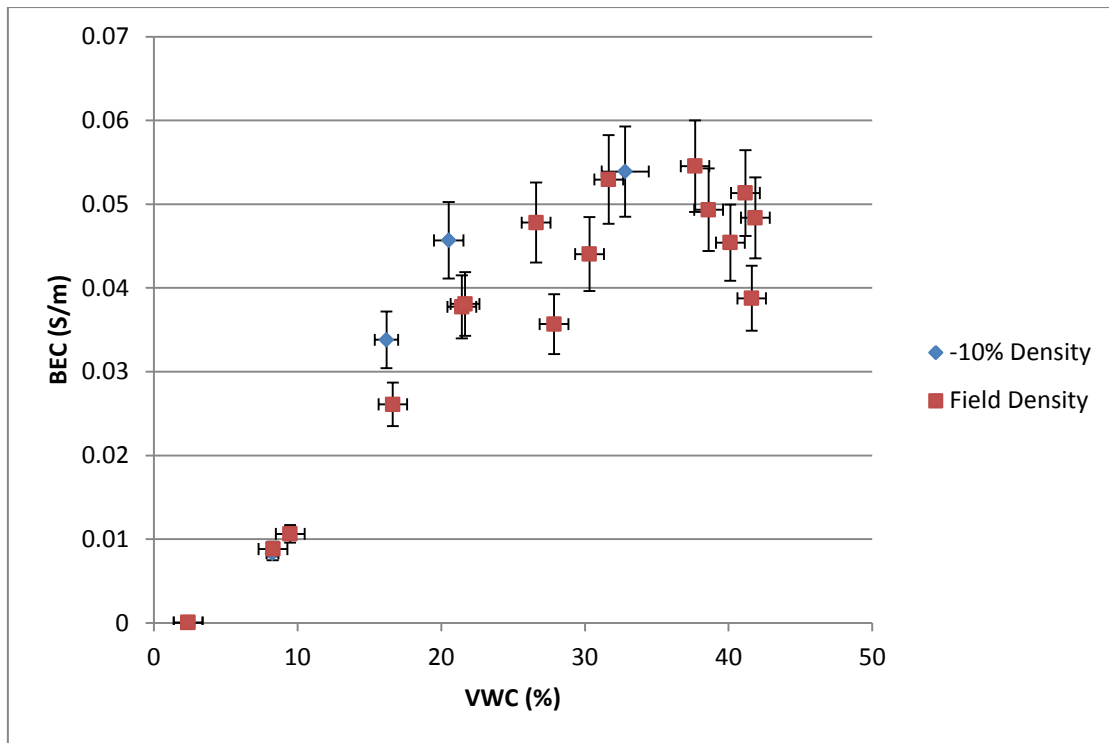


Figure 5.12: The effects of changing density on BEC determination on the DCF SSM soil

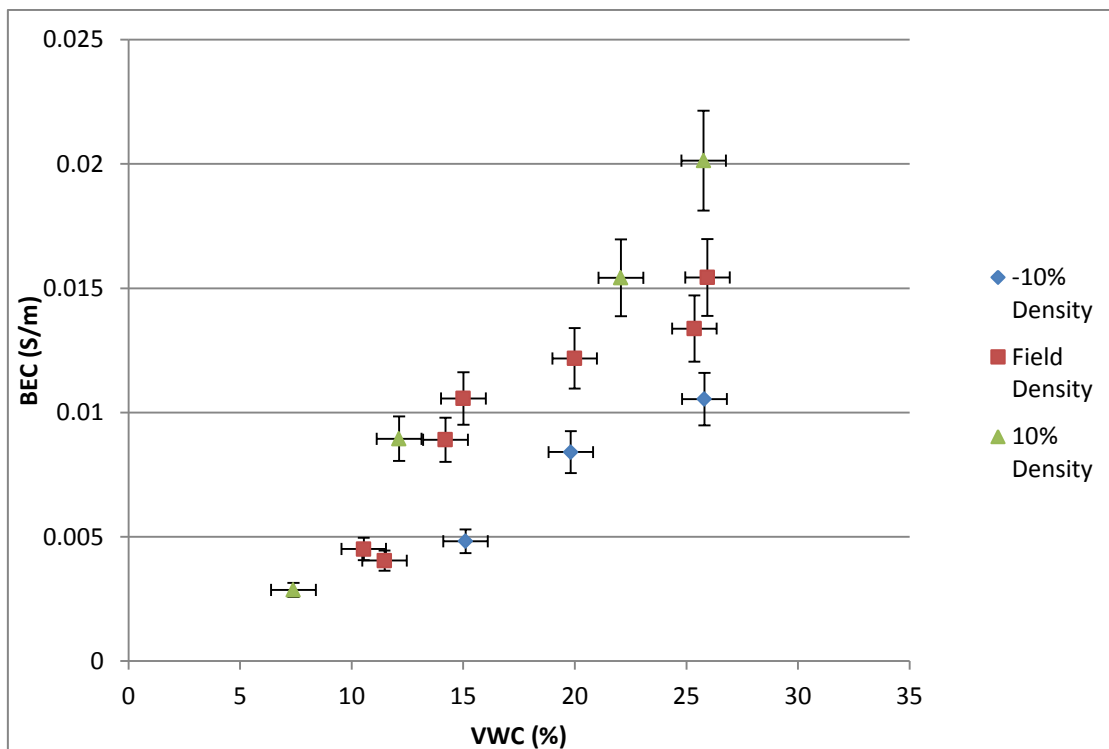


Figure 5.13: The effects of changing density on BEC determination on the DPF Ditchfill3 soil

5.5.5. Relationship between ARDP, BEC and Temperature

Several authors have commented on the effects of temperature on measurable geophysical properties (Campbell et al., 1948, Gong et al., 2003, Or and Wraith, 1999, Seyfried and Grant, 2007, Skierucha, 2009, Wraith and Or, 1999) which can affect the performance of heritage detection. In order to assess the potential changes to geophysical properties in the field as a result of seasonal temperature variations, temperature effects on BEC are plotted as the difference between the BEC recorded at 0°C and 20°C for each soil and water content in Figure 5.14. Additional plots showing the difference between 10°C and 20°C can be found in Appendix B, but were found to show similar results. The relationship between temperature and BEC can be seen to be always positive due to the increased mobility of charge carrying ions and reduced viscosity of the soil water due to the additional energy provided by heat. Temperature effects on the clay soils (red bordered bars) are greater than those on the non-clay bars (black borders) due to the higher ion concentration seen in the geochemical results (see Section 5.3) and greater surface area of these soils due to their high clay percentage. Similar results are noticeable between soils on the same site, with those soils with the highest BEC values (see Figure 5.7 above) displaying the largest effects. The magnitude of temperature effects can also be seen to increase with VWC for each individual soil, due to the additional ability of the soil to dissolve ions from the soil particle surface. However at some of the highest VWC, especially on the clay soils, these effects are seen to fall from preceding values. One explanation for this may be that, since the soil may be oversaturated at this point, the ion concentration of the soil water has dropped due to the lack of additional ions and the additional dilution effects of additional water, which is also reflected in the lower values at the highest water contents in the BEC plots above. One final observation is that the effects of temperature on BEC, especially at high water contents, appear to be more significant on the archaeological ditchfill soil on the DCF soils, and the SSM on the DPF soils. The reason for this

difference is unclear and requires further investigation, but it may have an effect on prospection at certain times of the day when temperature differences are most accentuated.

The temperature effects, measured as the difference between values recorded at 0°C and 20°C for ARDP readings are displayed in Figure 5.15. Additional plots showing the difference between 10°C and 20°C can be found in Appendix B, but were found to show similar results. The dashed lines represent the estimated errors in ARDP determination. Both positive and negative temperature dependencies are recorded. The relationship on the DCF soils is predominantly positive across the majority of the VWC range for all soils with the maximum positive relationships recorded at VWC values of 20-30% with the exception of DCF subsoil which peaks at around 40% VWC. These positive relationships are seen to decrease in magnitude until the very high water contents at which point the relationship becomes negative. This result seems to support the two conflicting phenomena of bound water release and temperature dependence of the water permittivity suggested by Wraith and Or (1999) and Skierucha (2009). The water content at which the two effects crossover has been previously linked to the SSA of the soil (Gong et al., 2003), being related to the relative quantities of bound and free water. However, as discussed in Sections 5.5.2 and 5.5.3, higher BEC values also increase the measured ARDP values especially at higher water contents, until maximum ion concentration has been exceeded. Therefore the temperature dependence of the BEC discussed above provides an additional positive effect on the measured values within these VWC ranges, offsetting the permittivity decreases expected in pure water. The high BEC values for the subsoil and this contribution of BEC to ARDP may explain the higher crossover VWC on this soil. Temperature effects on the ARDP for the DPF soils (black border) are generally much smaller than for the DCF soils and are mainly indistinguishable from errors in the TDR determination, especially at low water contents although some significant effects exist at higher VWC values. Slight positive relationships are visible in DPF Ditchfill2 and Ditchfill3 at 20-25% VWC with negative responses at higher water contents, suggesting a similar behaviour to

the DCF soils. DPF Ditchfill1 follows a similar trend, although only the negative relationship above 30% VWC shows any significant influence over the results. The largest temperature effect is recorded on the DPF SSM soil at near saturation of 30%. Whilst it should be expected that this response is negative with temperature due to the predominance of free water in the coarse grained samples (Roth et al., 1990), the measured effect is positive. One possible explanation is that large quantities of water in the soil had frozen at the 0°C reading due to the lack of dissolved ions and soil-water interaction present in the other samples with more significant fines contents. This had the effect of lowering the sample permittivity by a significant margin, and countering the normal increases in permittivity with decreasing water temperature. An alternative is the higher temperature dependence of the BEC of this soil, which increases the measured ARDP values by a significant amount in comparison to the other DPF soils.

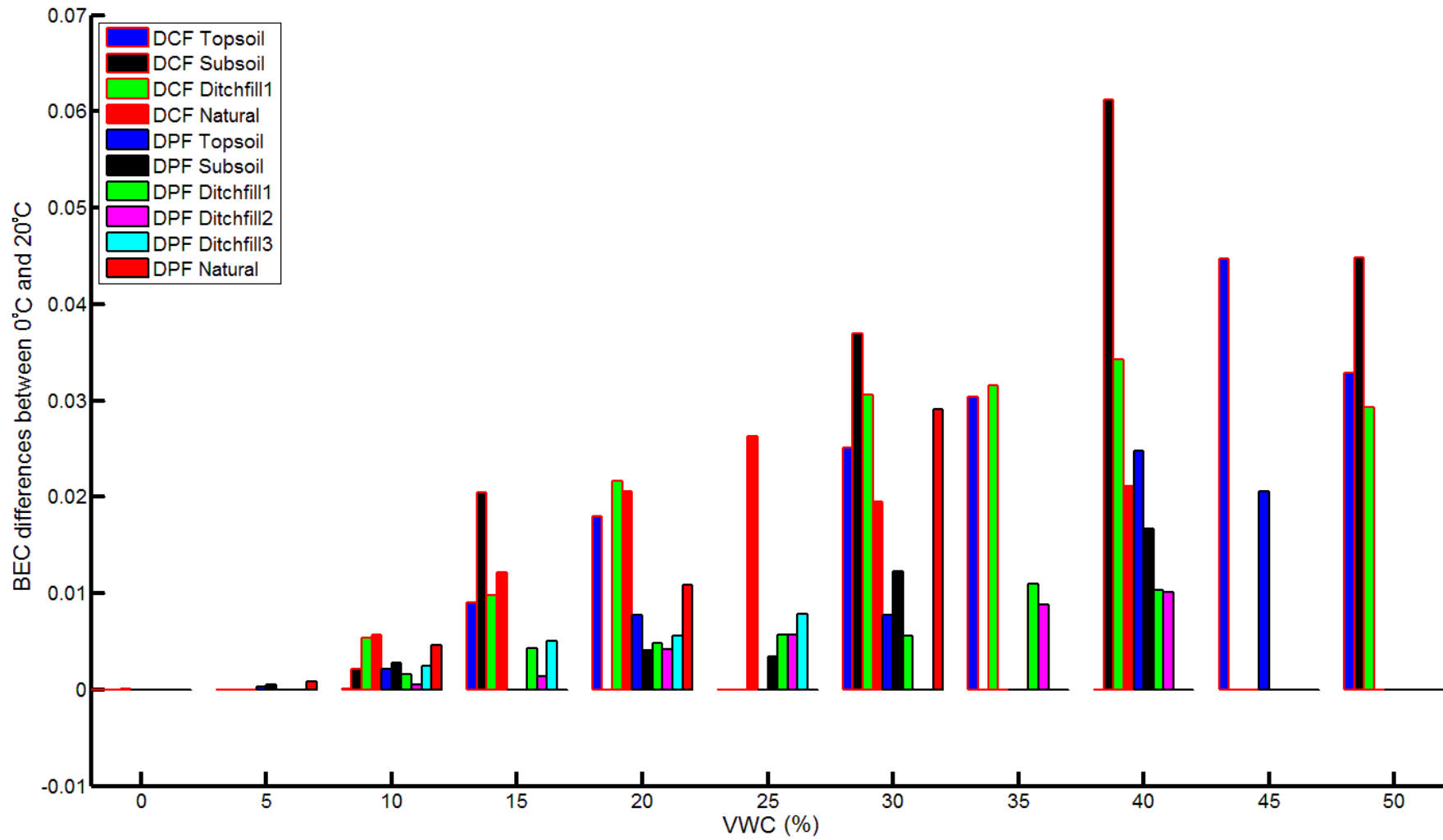


Figure 5.14: Temperature effects on BEC determination on different soils

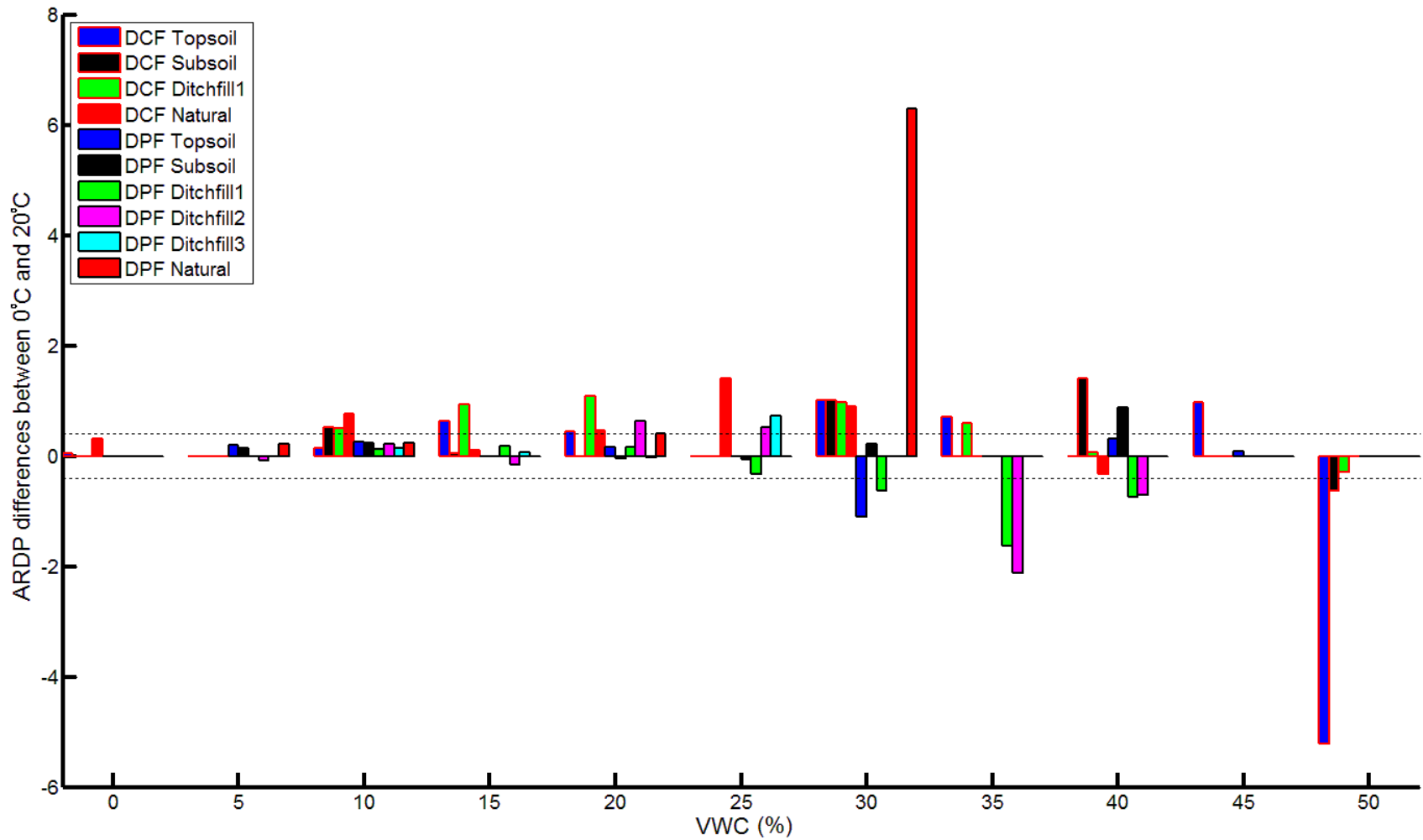


Figure 5.15: Temperature effects on ARDP determination on different soils

5.5.6. Comparison of different models

A number of different models have been suggested for linking ARDP and VWC (see Section 2.6). To identify which models are suitable for which soil type, data have been plotted against 6 different empirical equations for each of the tested soils and the R^2 and RMSE calculated for each one. The models tested were as follows:

- Topp et al. (1980)
- Ledieu et al. (1986)
- Curtis (2001)
- Wensink (1993) (1GHz model used)
- Wang and Schmutge (1980) (using clay and sand percentages and density)
- Roth et al. (1990) (using density and temperature)

An example graph is shown in Figure 5.16. Additional graphs from the other soils are shown in Appendix B. The results are displayed in Table 5.4 and the results from the soil specific empirical models fitted in Section 5.5.3 have also been included for comparative purposes.

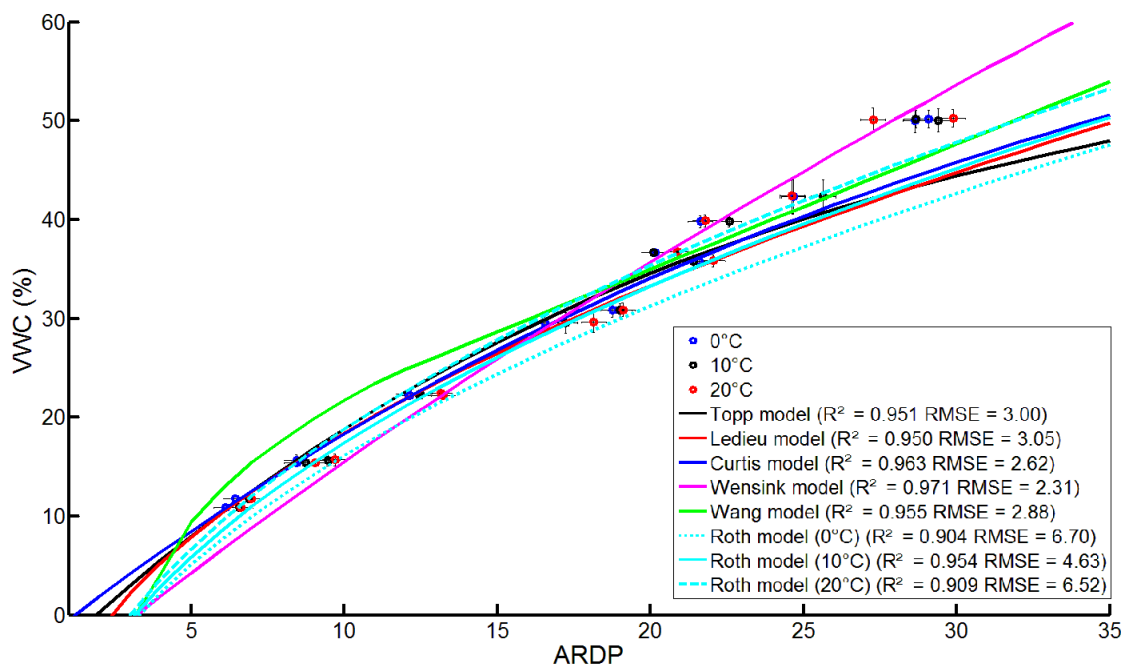


Figure 5.16: An example of the different models fitted to data from one of the DCF soils (DCF Ditchfill1)

Table 5.4: Comparison of different R² and RMSE for different models on the tested soils

| Model | Soil | DCF | | | | DPF | | | | | |
|------------------|----------------|---------|---------|------------|-------|---------|---------|------------|------------|------------|--------|
| | | Topsoil | Subsoil | Ditchfill1 | SSM | Topsoil | Subsoil | Ditchfill1 | Ditchfill2 | Ditchfill3 | SSM |
| Empirical Fitted | R ² | 0.980 | 0.991 | 0.993 | 0.995 | 0.994 | 0.974 | 0.991 | 0.983 | 0.981 | 0.990 |
| | RMSE | 2.953 | 1.927 | 1.442 | 1.234 | 1.466 | 2.929 | 1.465 | 2.188 | 2.380 | 1.897 |
| Topp | R ² | 0.948 | 0.923 | 0.951 | 0.956 | 0.976 | 0.920 | 0.926 | 0.758 | 0.711 | 0.871 |
| | RMSE | 4.142 | 4.341 | 3.005 | 3.054 | 2.114 | 3.611 | 2.585 | 5.339 | 3.466 | 3.111 |
| Ledieu | R ² | 0.941 | 0.924 | 0.950 | 0.961 | 0.969 | 0.921 | 0.903 | 0.721 | 0.673 | 0.850 |
| | RMSE | 4.417 | 4.333 | 3.045 | 2.875 | 2.367 | 3.578 | 2.946 | 5.723 | 3.690 | 3.348 |
| Curtis | R ² | 0.949 | 0.939 | 0.963 | 0.963 | 0.976 | 0.915 | 0.908 | 0.777 | 0.696 | 0.868 |
| | RMSE | 4.067 | 3.872 | 2.623 | 2.783 | 2.0967 | 3.720 | 2.872 | 5.119 | 3.555 | 3.195 |
| Wensink | R ² | 0.950 | 0.966 | 0.971 | 0.979 | 0.834 | 0.727 | 0.673 | 0.393 | 0.022 | 0.524 |
| | RMSE | 4.061 | 2.907 | 2.311 | 2.089 | 5.524 | 6.653 | 5.416 | 8.448 | 6.381 | 5.974 |
| Wang | R ² | 0.986 | 0.938 | 0.955 | 0.951 | 0.963 | 0.939 | 0.940 | 0.774 | 0.730 | 0.741 |
| | RMSE | 3.034 | 3.921 | 2.878 | 3.338 | 2.794 | 3.229 | 2.325 | 5.462 | 3.359 | 4.588 |
| Roth (0°C) | R ² | 0.918 | 0.886 | 0.904 | 0.909 | 0.914 | 0.897 | 0.901 | 0.876 | 0.886 | 0.865 |
| | RMSE | 7.173 | 8.337 | 6.696 | 6.496 | 7.312 | 7.956 | 7.070 | 8.368 | 8.899 | 10.639 |
| Roth (10°C) | R ² | 0.955 | 0.939 | 0.954 | 0.951 | 0.946 | 0.937 | 0.943 | 0.909 | 0.926 | 0.927 |
| | RMSE | 5.325 | 6.089 | 4.631 | 4.772 | 5.785 | 6.237 | 5.349 | 7.167 | 7.1605 | 7.803 |
| Roth (20°C) | R ² | 0.903 | 0.891 | 0.909 | 0.909 | 0.915 | 0.899 | 0.899 | 0.884 | 0.892 | 0.896 |
| | RMSE | 7.774 | 8.171 | 6.523 | 6.474 | 7.256 | 7.869 | 7.138 | 8.084 | 8.652 | 9.323 |

As expected, the soil specific empirically fitted models from Section 5.5.3 demonstrate the best accuracy across all the soils from both the DCF and DPF sites. However, due to the differences in underlying soil properties the other tested models all display variable fits with the different soil types, highlighting the problem with the universal application of one model, even within a single site.

For the DCF soils with the exception of the topsoil, the Wensink (1993) model displays the best fit with the highest R^2 and lowest RMSE. Thomas et al. (2010a, b) noted this was the case at higher frequencies (c.1GHz) for dispersive clay soils at water contents between the Atterberg limits. However, they also found broadband TDR readings tended towards this model only towards the liquid limit and were generally closer to the Topp et al. (1980) model due to the lower frequencies involved in the measurement. This trend is apparent on the DCF Subsoil and Ditchfill soils (Figure 5.17), especially at lower water contents, although for the SSM, the Wensink (1993) model remains an accurate fit across the whole range of measured values. One reason for the accurate fitting of the Wensink (1993) model is that it is calibrated using fine grained soils including from peat, silt and saline and non-saline clays with moderately high BEC values so takes into account the electrical and bound water effects discussed in Sections 5.5.2 and 5.5.3, whereas the other models have focused on loams where these effects are minimal. For this reason, it remains the best model for use on fine grained soils, shown by the reasonable match between the empirical model fitted to the DCF soils and the Wensink (1993) model in Figure 5.17.

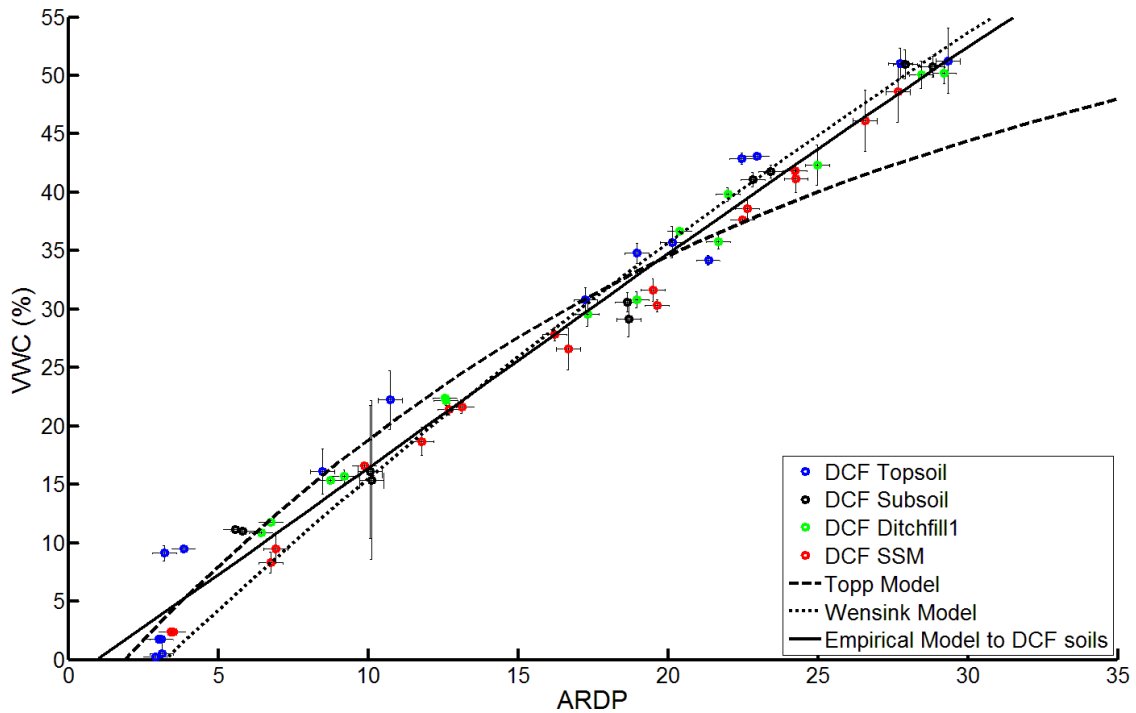


Figure 5.17: The Wensink (1993) model on the DCF soils

The Wensink (1993) model is also a good fit at higher VWC values for the DCF Topsoil (Figure 5.17), but underpredicts the VWC at lower values. This is due to the finer grain sizes of this soil in comparison to the soils used to calibrate the other tested models, which leads to a greater quantity of bound water, reflected in the accurate prediction at the higher end where these effects dominate. However, as discussed in Section 5.5.3, due to the lower BEC values on this soil in comparison to the other DCF soils, the loss tangent is not as high, reducing the electrical effects at low water contents. At these low water contents (<30% VWC) the Wang and Schmugge (1980) model provides the best results (Figure 5.18), as it accounts for a reduced rate of ARDP rise at low water contents due to bound water effects. The Wang and Schmugge (1980) model also provides a reasonable fit to other medium grained soils from DPF such as the topsoil, subsoil and Ditchfill1, but shows poor fits on soils with extremes of texture, overpredicting on fine grained soils (i.e. the other DCF soils) and underpredicting on coarse grained soils (i.e. the remaining DPF soils), especially below 30% VWC. Above this VWC, the

model predicts with reasonable accuracy for the DPF soils but underpredicts slightly for the DCF soils due to dominance of bound water effects which reduce the measured ARDP values.

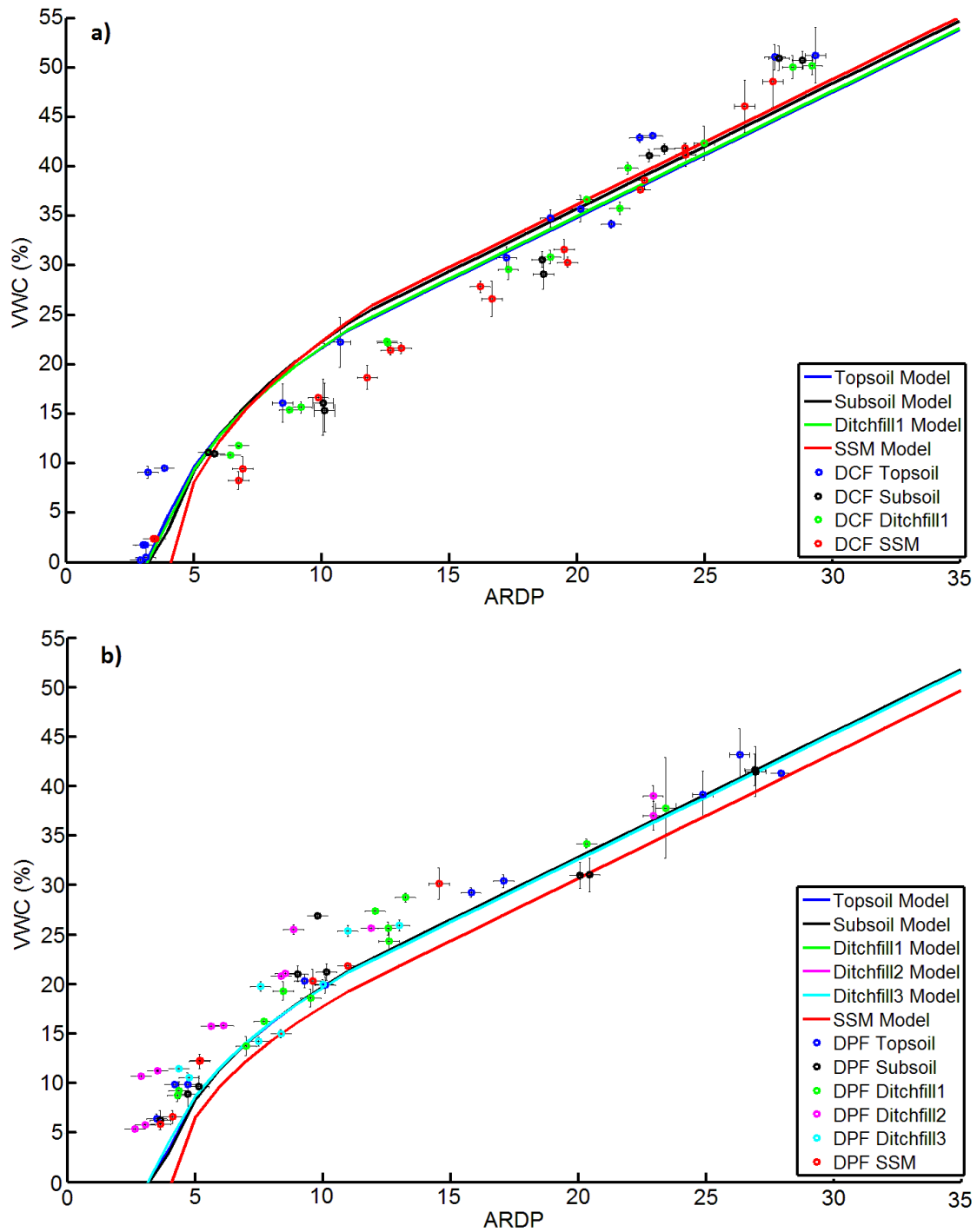


Figure 5.18: The performance of the Wang and Schmugge (1980) model on a) DCF and b) DPF

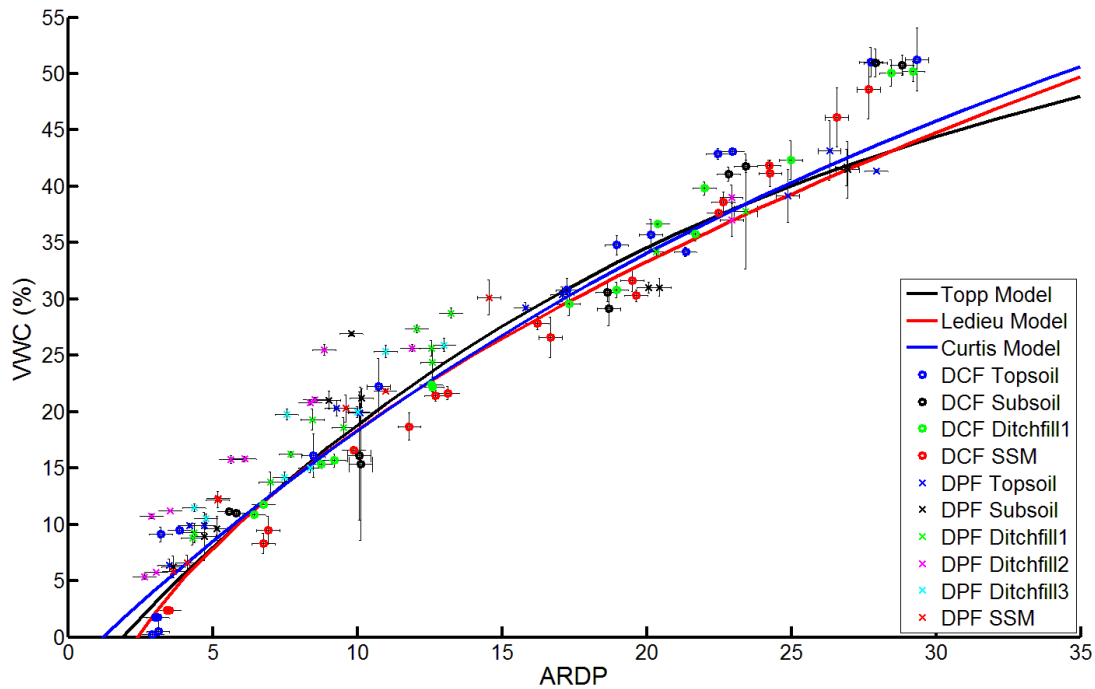


Figure 5.19: The Topp et al. (1980), Ledieu et al. (1986) and Curtis (2001) models in comparison to data from the tested soils.

The empirical models of Topp et al. (1980), Ledieu et al. (1986) and Curtis (2001) all produce similar curves which suit soils such as DPF Topsoil reasonably well (Figure 5.19). This is perhaps unsurprising as all of these models were calibrated over similar grained soils (loam-clay loam) to the soils to which the models fit well. It can also be seen that these models provide less good results on soils with very high or very low loss tangents (see Sections 5.5.2 and 5.5.3). Nevertheless the models provide an approximation which represents a good compromise between all of the tested soils, albeit with a tendency to underestimate water content at low VWC values in all soils and in the finer grained soils at high water contents.

The Roth model (1990) performs moderately poorly across all of the tested soils, albeit slightly better on the DCF soils and the DPF soils at high water contents. At low water contents, the model underpredicts and overpredicts on the DPF and DCF soils respectively for the same reasons as the other empirical models discussed above. Another particular weakness of the model is the larger errors in the 0°C and 20°C measurements as the model overestimates the temperature effects considerably. However, the model only accounts for the temperature

dependency of the ARDP in pure water and ignores bound water and BEC effects, which counter balance and often reduce these effects significantly (see Section 5.5.5). Additionally implementation of the model is problematic on soils where the density is unknown and hence using density estimates where accurate data are unavailable will further reduce the accuracy of the model.

It should be noted that none of the models provide a good fit for the DPF Ditchfills2, DPF Ditchfill3 and the DPF SSM soil with all models underpredicting the VWC, especially in the low water content range. One explanation is the soils over which all of these models are calibrated had more significant fines contents on average than these soils and therefore higher SSA. This has two implications for these soils; an increased importance of the real permittivity due to lower bound water fractions and insignificant BEC values. These two phenomena result in extremely low loss tangents for these soils, the effects of which were discussed in Sections 5.5.2 and 5.5.3. Another possibility is the effects of the low densities of the DPF soils in comparison to the soils over which the tested models were calibrated, especially in the ditchfills, which were discussed in Section 5.5.4. However from the experiments presented, it seems unlikely that these effects would be large enough to create the magnitude of errors seen here. The poor fit of the existing models to the DPF soils with the exception of the topsoil and subsoil highlights the need to empirical calibrations in the laboratory to accurately determine VWC from TDR derived ARDP readings, especially on soils where loss tangents are extremely low or high. The key factor when choosing a model is the range of soils over which the model was calibrated, which should possess similar grain sizes and ranges of BEC values to the soils in the field.

5.6. Principal Component Analysis

Principal component analysis (PCA) was conducted using the geotechnical and geochemical properties of the soil, and the measured variables for the soil samples tested in the laboratory in order to identify the most important variables for determining geophysical properties. A PCA² consists of a mathematical procedure used to reduce the complexity of datasets consisting of multiple correlated variables by rotating the data to a new co-ordinate system, determined by uncorrelated variables (known as principal components) which account for a proportion of the total data variance (Jolliffe, 2002). The PCA was carried out in MATLAB® by normalising the data to mean of zero and standard deviation of one using zscore, calculating the covariance matrix using nancov, and performing the analysis using the pcacov function. The PCA was performed with a variety of different geochemical, geotechnical and geophysical variables, although only plots using a limited range of variables are displayed in this section. The variables used were chosen according to availability of data and known effects on measured values and were as follows:

- VWC
- ARDP
- BEC
- Temperature
- Magnetic Permeability
- Gravel, Sand, Silt and Clay percentages
- Atterberg limits
- Linear shrinkage
- LOI

² Each parameter inputted into a PCA will be correlated with each other and the degree of correlation determined, which is then expressed in the Principal Components. A PCA consists of a mathematical procedure that rotates multiple times the original data organised in a matrix $n \times p$, where n are the observations (i.e. measurements) and p the parameters, in the direction of greatest variance (Jolliffe, 2002)

- Particle Density
- Bulk and Dry Density
- Porosity

Additional plots using different variable sets can be found in Appendix B.

The percentage variation accounted for by each new principal component is displayed in the scree plot (Figure 5.20). From this, it can be seen that nearly 85% of the variance is accounted for by the first four principal components, and the other principal components can be safely discarded without losing significant information.

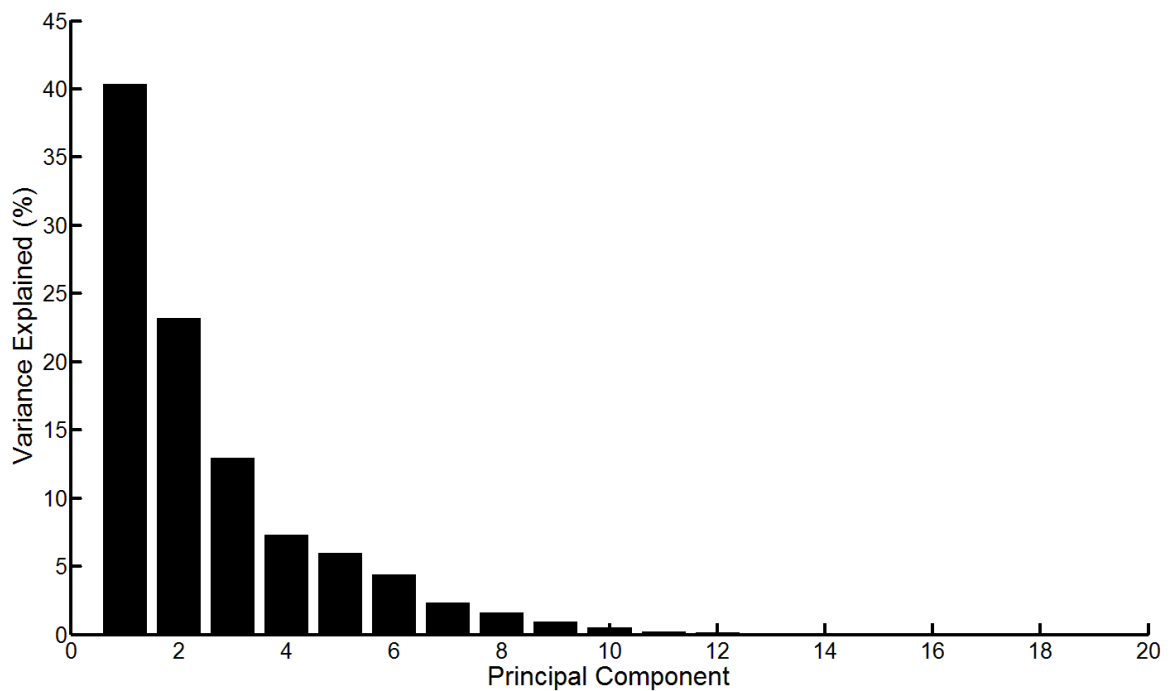


Figure 5.20: Scree Plot from the PCA analysis on geophysical, geotechnical and geochemical properties of the soil collected in the laboratory

A typical output of the PCA is the biplot which displays the samples as points and the variables as vectors in respect to a new co-ordinate system and can be used to assess the correlation between different variables. Figure 5.21 shows the biplot of the first two principal components from the laboratory testing with the DCF points shown as dots, the DPF points shown as crosses and the variables displayed as labelled vectors. Variables located near to each other in the new co-ordinate system are positively correlated, opposing variables (i.e. at

roughly 180°) are negatively correlated and those which are perpendicular (i.e. at roughly 90°) show no correlation with each other.

It can be seen that the geophysical properties (ARDP and BEC) show strong correlation with both each other and the VWC, confirming the presented results that measurements of both properties increase with water content. Clay content and the Atterberg limits (Plastic and Liquid Limit) are correlated with BEC quite strongly as expected, supporting the results of other authors who have expressed soil BEC as a function of its clay and water content (e.g. Rhoades et al., 1976). It should also be noted that the sand and gravel are negatively correlated with silt and clay showing the difference between the finer grained DCF and coarser grained DPF soils. Dry density and porosity are negatively correlated as would be expected intuitively as decreasing the solid phase of the soil increases the void space. However, these variables show poor correlation with the geophysical properties. One explanation for this is that the effects of density discussed in Section 5.5.4 varied with soil grain size and VWC and contradictory effects may have cancelled each other out obscuring a definite trend during the PCA. At first glance, temperature also seems to be relatively uncorrelated with measured geophysical values indicated by its position at a moderately wide angle in relation to BEC and ARDP in comparison to the Atterberg limits and clay content of the soil. However, it is more correlated to BEC than ARDP, shown by its relative proximity to these variables, supporting the results found in Section 5.5.5 where larger effects were found. The relatively small effect of temperature and its subsequent decorrelation in Figure 5.21 on measured geophysical values may be down to the interaction between temperature effects and other soil properties at different water contents, with temperature effects on BEC becoming more dominant as the VWC is increased and in clay soils (see Section 5.5.5). Due to the use of all data in the PCA analysis, the smaller effects at low water contents and in the DPF soils offset the contribution at higher VWC values and in the DCF soils.

In addition to looking at the variable vectors, the points representing the different soils can also be examined. It can be noticed that the individual points are clustered into different soils with the DCF points clustered on the right hand side of the plot and DPF points on the left hand side of the plot showing the strong importance of grain size on the behaviour of soil. The DCF soils are also predominantly located within a single cluster, with the exception of DCF SSM which had a higher density. The DPF soils are also located within a single cluster with the exception of DPF SSM which varied in gravel content and Ditchfill2 which had lower density than the other DPF soils (negatively correlated. Ditchfill2 also has a few points near to the other DPF soils, most likely to be those at higher water contents which show better agreement with the other DPF soils (see Section 5.5.3). DPF Ditchfill3 is excluded from the current plots due to the lack of data for certain variables (LOI and magnetic permeability). Plots using available variables showed the points clustered near to those of the topsoil, subsoil and Ditchfill1 suggesting similar behaviour to these soils. This is in agreement with the data presented in Sections 5.5.3.

Principal components 3 and 4, which are responsible for less variance than components 1 and 2, although still for a significant percentage are shown in Figure 5.22. ARDP, BEC and VWC are again strongly correlated as in the first two principal components, confirming the dominance of water content to the overall measured geophysical properties. A reasonable positive correlation between the bulk density, VWC and measured geophysical parameters can also be identified. The Atterberg limits, due to their dependence on SSA also remain correlated to the clay content as in the first two principal components, although they show a negative relationship with the measured geophysical properties. The majority of the other variables show weak or no correlations in these principal components and no clear effects can be identified.

Unlike in the first two principal components, the distribution of individual points from the different soils shows no overall patterns displaying a reasonable scatter throughout the plot, although points do seem to fall in straight horizontal lines in the direction of the VWC, ARDP and BEC parameters. This is most likely to be an artefact of the range of these values used in the experiment in comparison to the static geotechnical properties.

Based on these observations of the first four principal components, unsurprisingly, water seems to be the most dominant variable affecting geophysical measurements, shown by its correlation in all four principal components. In addition, the grain size and Atterberg limits of the soil can be considered important in determining the dielectric behaviour of the soil, as these affect the SSA of the soil, influencing bound water and BEC values.

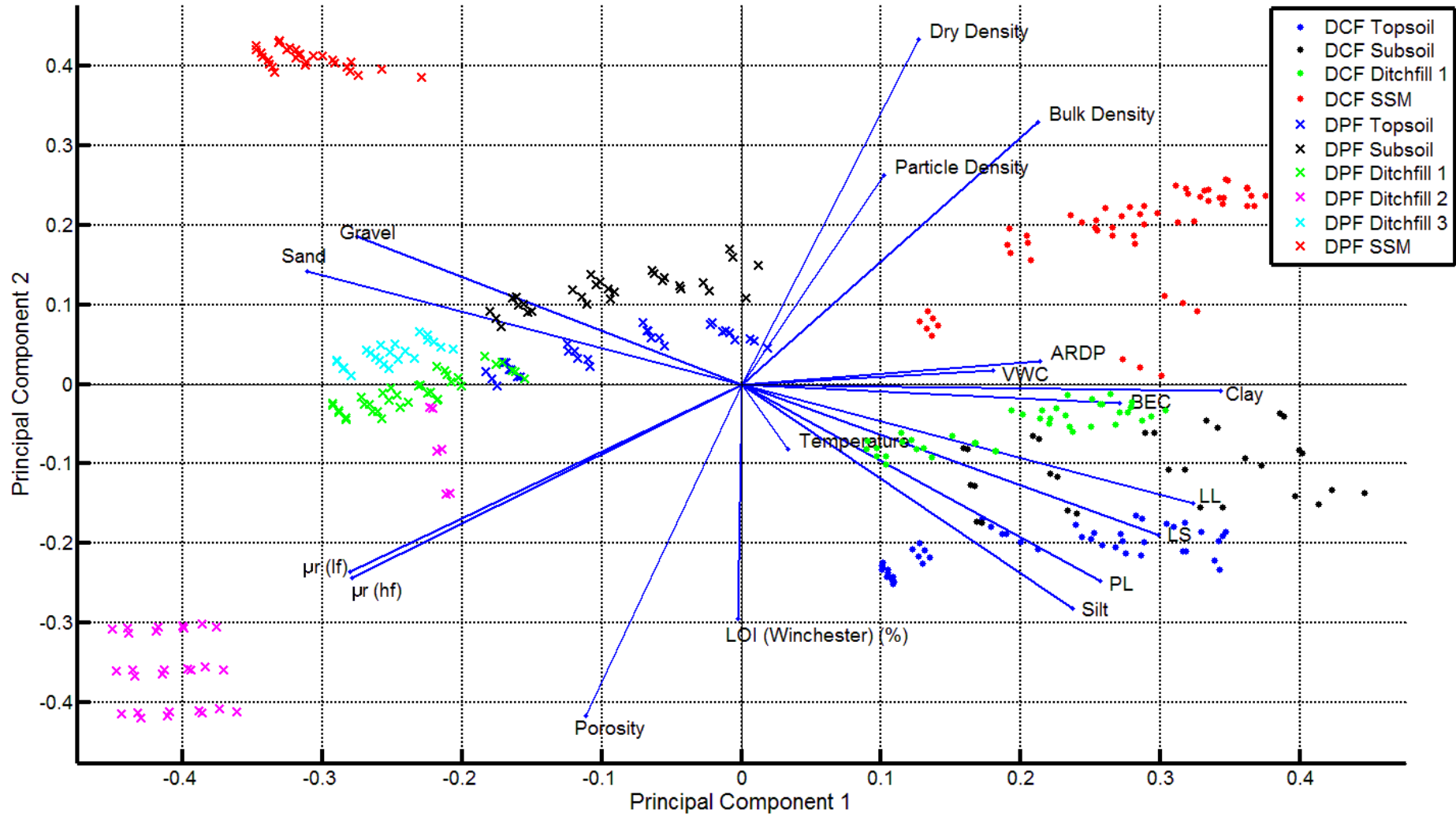


Figure 5.21: Biplot of PCA analysis on geophysical, geotechnical and geochemical properties of the soil determined in the laboratory showing principal component 1 and 2

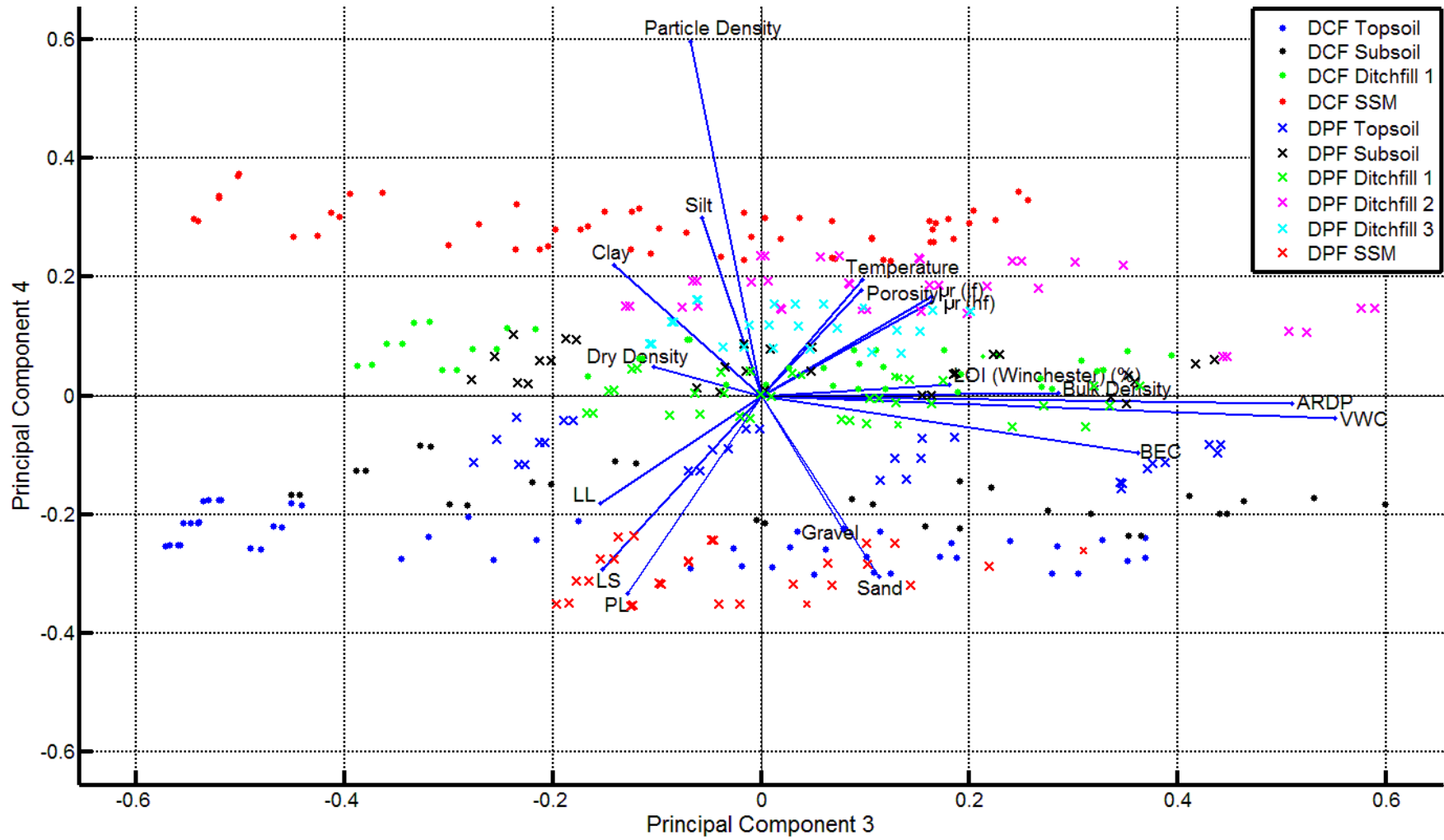


Figure 5.22: Biplot of PCA analysis on geophysical, geotechnical and geochemical properties of the soil determined in the laboratory showing principal component 3 and 4

5.7. Summary of Laboratory Soil Testing Results

The main findings of the laboratory analysis of the soils were as follows:

- The ditchfill soils predominantly display geophysical and geochemical properties which are between those of the site Topsoil and those of the SSM, although the precise nature of these properties is a result of the SSM, feature formation and subsequent land use practices. Amongst the key differences are increased levels of organic matter, smaller particle sizes, lower densities and higher magnetic permeability recorded in the archaeological soils, although these trends are not universal.
- VWC-BEC relationships increase with water content across all soils until saturation is reached and no additional ions are available at which point slight decreases were observed on some soils. The rate at which these increases occurred were greater on the fine grained DCF soils than the DPF soils due to their greater surface areas and ion availability. Smaller intra site variations were found with slightly higher BEC values recorded on the ditchfills and SSM on DCF and DPF respectively.
- ARDP-VWC relationships are complex on both tested sites. On the DCF soils the contribution of the loss tangent to ARDP, whilst frequently overlooked, cannot be ignored due to the high conductivities and significant bound water fractions which decrease the real and increase the imaginary permittivity. This makes recorded values higher on these soils at low water contents before bound water effects dominate, lowering the permittivity at higher water contents. The opposite effects were noticed on the coarse grained DPF soils due to their lower BEC and bound water fractions. Relationships can be described with reasonable accuracy using third order polynomials.
- Temperature has a large effect on the determination of BEC, with positive relationships which are proportional to the VWC and ionic content of the soil. Differences in temperature effects also exist between the archaeological ditchfills and

SSM. Temperature effects on ARDP are much smaller and often insignificant in comparison to changes in water content, due to the effects of competing phenomena of bound water release, BEC effects and temperature dependence of free water and observed patterns of positive relationships at low water contents and negatively relationships at high water contents are in agreement with other authors.

- Density of the soil creates very small effects which are often dwarfed by other variables such as VWC and temperature, and depend on the grain size and water content of the soil. On coarse grained DPF soils a positive relationship exists between density and BEC whereas a negative relationship between the two was found for the clay DCF soils. These effects were ascribed to the interplay between increased SSA and pore connectivity in the two soils. Conflicting density effects were also found for ARDP determination with positive relationships between the two found due to the release of bound water and negative effects due to the replacement of soil with air identified. Further work is needed to fully understand these effects.
- Wensink's (1993) model has been found to be a good fit for the DCF soils with the exception of the Topsoil which is closer to Wang and Schmugge's (1980) model. The Topp et al. (1980) model is an adequate fit for some of the DPF soils but some fail to show good agreement with any of the existing tested models due to the insignificance of their loss tangents. In these cases and for additional accuracy empirical calibrations are still needed.
- A PCA analysis confirmed many of the relationships noted above. In addition, VWC and soil grain size, especially clay content were identified as the most important variables when determining soil geophysical properties, with mineralogy of the soil determined through Atterberg limits also having significant effects.

Chapter 6: Field Monitoring: Results and Discussion

6.1. Introduction

This section describes the results acquired from the monitoring stations at Harnhill, Cirencester and Diddington, Cambridgeshire from both the TDR monitoring stations and the weather stations. Data from Harnhill correspond to approximately an 18 month period from April 2011-October 2012. Data from the Diddington Clay field ran from August 2011-October 2012 with a slightly longer period (June 2011-May 2013) recorded from Diddington Pasture field. Results are analysed and discussed, with reference to both the seasonal response of the soil as well as to the contrast in EM properties between the ditch and SSM soil.

The TDR data from CCC are not presented here as due to the nature of the site, it was impossible to derive geophysical readings from the SSM, although it could be assumed that the rock had a lower water holding capacity than the soil which filled the archaeological feature. Additionally, following the damage caused by animals described in Section 3.6.5, the right hand array, located in the SSM was found to give poor quality and unreliable data, especially for BEC determination. A decision was therefore made to focus on the other sites in the present work.

6.2. Weather Variation over the Monitoring Period

Long term monitoring required detailed information on the climatic variation which may affect measured geophysical values, which was collected using the weather stations. Due to system errors and cable damage (see Section 3.6.5), several periods of data were missing from both Diddington and Cirencester, which needed to be patched from nearby weather stations found from an online source (Weather Underground Inc, 2014). To test the accuracy of the patched data, comparisons were made using data from the weather stations and the online repository (see Appendix C) which demonstrated reasonable accuracy in rainfall, temperature and ET figures over a daily to monthly time frame, although more significant variation was found in

the hourly values due to microclimatic variations. For this reason, no detailed analysis has been carried out on the downloaded data (see Sections 6.6 and 6.7), which has only been used to enhance the knowledge of seasonal variations.

The weather throughout the monitoring period was atypical of a normal seasonal variation but featured both very dry and very wet periods (Fry et al., 2012). Figure 6.1 shows the monthly cumulative rainfall, ET and subsequent water balance (rainfall – ET) which allows assessment of wetting and drying cycles on each site. Summer and autumn 2011 were some of the driest recorded for nearly 100 years (Mail Online, 2012), which can be seen as high ET values exceeding the rainfall throughout the period, creating a negative water balance throughout. This was followed by an equally record-breaking warm and dry winter period especially towards the end of the period (February-March 2012) where low rainfall figures can be seen. By contrast, spring to autumn 2012 were some of the wettest ever recorded, with positive water balances recorded in April, June, October and November on all sites. Whilst atypical of 'normal' seasonal variation, these extreme weather conditions have provided a dataset indicative of both drought and saturation conditions on both fine grained and freely draining soils for both sites.

As a general observation, the Diddington site could be said to display a drier and sunnier climate, shown by the higher rates of ET and lower rainfall. This is perhaps unsurprising as the West of the country is known to be wetter (Met Office, 2014) and this was a key reason for including two study areas within the project. No great variations between the rainfall or water balance figures were recorded between different monitoring locations at the same site, with similar values recorded at both. However towards the end of the monitoring period on the CCC site rainfall is lower than on CQF. The most likely explanation for this is a reduction in the recorded rainfall due to the bird excrement blockage in the rain gauge discussed in Section 3.6.5 and it is believed that the CQF weather station collected more accurate rainfall data.

Figure 6.2 shows the variations in monthly temperatures throughout the monitoring period. All of the monitored sites displayed the same expected sinusoidal pattern, with the warmest and coldest temperatures recorded in the summer and winter periods respectively. Few significant differences could be observed between monitoring locations on either of the two sites with variations in maximum, minimum and average temperature rarely exceeding 1°C, and the largest deviations occurring at the end of the summer in 2012 (c. July-September). Differences in the average temperatures between the two different sites are also small and therefore all of the study areas show reasonable agreement throughout the study period. Slightly larger variations both between sites and study areas occurred in the maximum and minimum values, which are indicative of differing weather patterns (e.g. cloud cover, shade from nearby vegetation etc.).

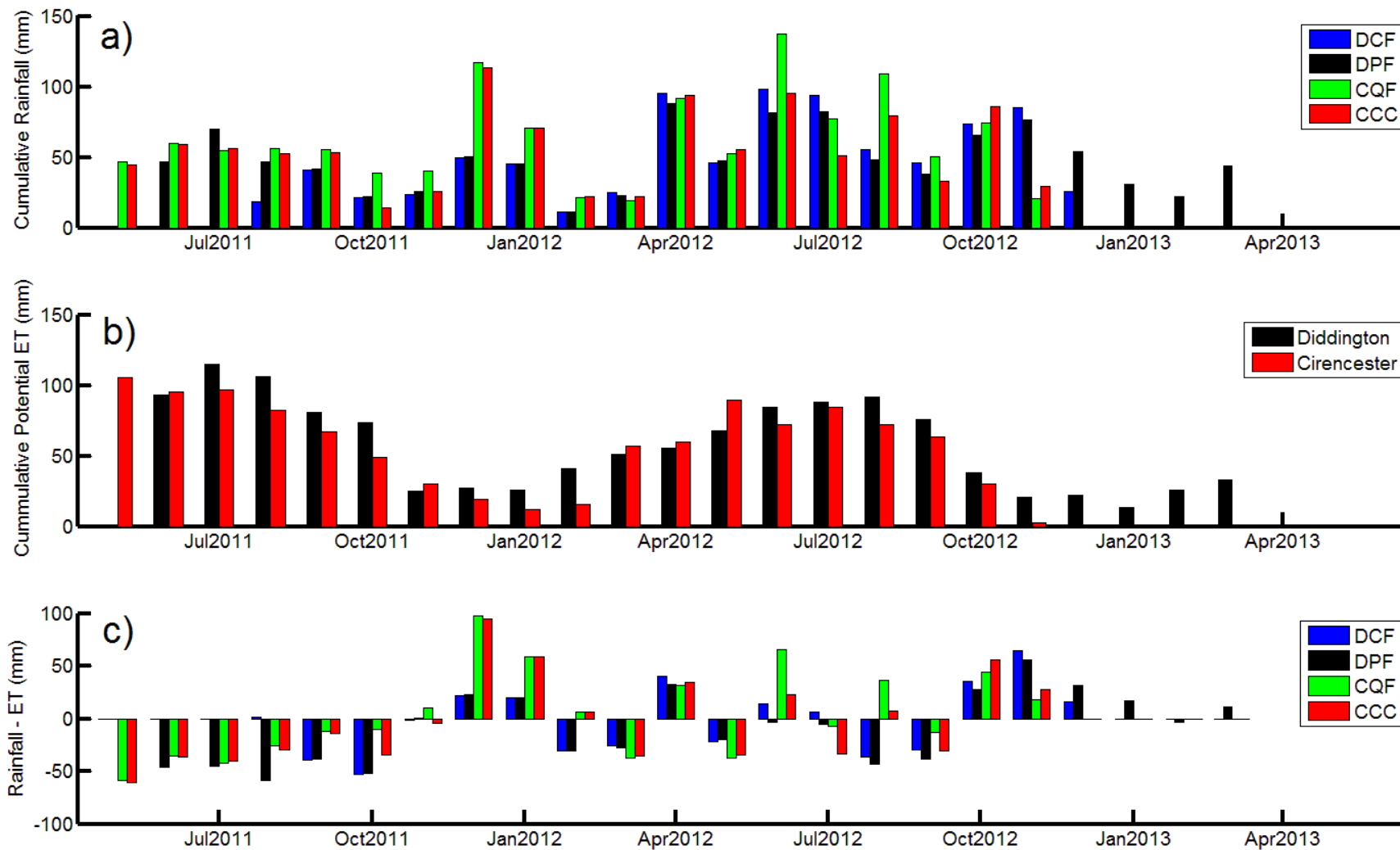


Figure 6.1: The rainfall (a), evapotranspiration (b) and water balance (c) for the study period on all four monitoring locations.

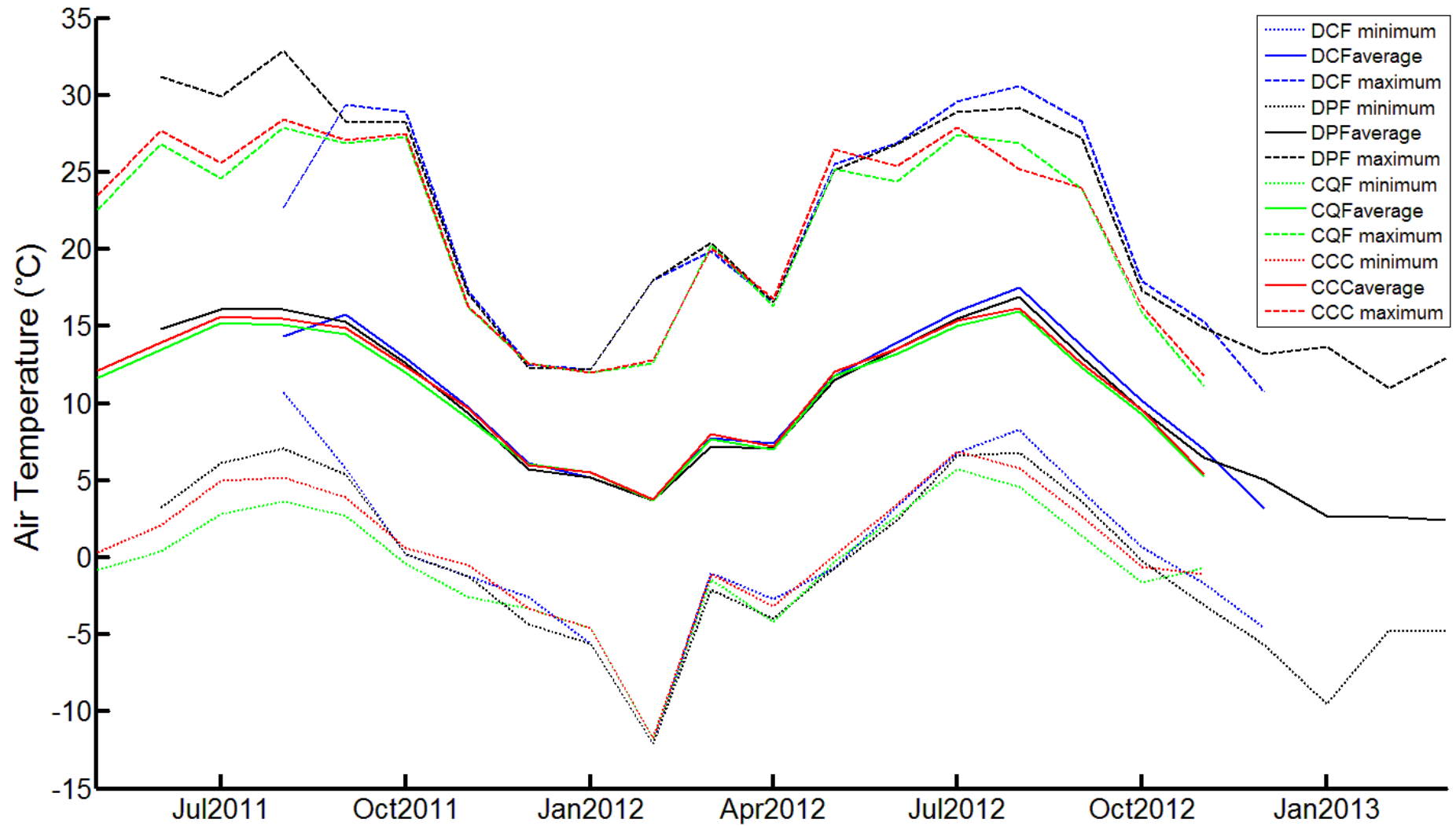


Figure 6.2: The minimum, maximum and average air temperatures over the study period for the four monitoring locations

6.3. Heterogeneity and Lateral Variations

All soils display some variation in physical and EM properties spatially. These spatial variations are important to be aware of as the magnitude of contrast between the archaeological soils and SSM must exceed this heterogeneity if features are to be distinguished from 'soil noise'.

To assess the magnitude of these variations data from two probes at the same depth and within the same soil context are compared here from several sites and depths. Several outlying datapoints were removed using a clipping procedure to remove obvious extremes and a 1D median filter in MATLAB®, although some remain. Examples of filtered and unfiltered plots are given in Appendix C.

Data from the DCF site are shown in Figures 6.3-6.6. On both the archaeological soils and SSM, the trends measured by the two arrays were consistent throughout the monitoring period, although some differences in absolute values exist, especially in the near surface probes. This finding is consistent with those of Curioni (2013). One possibility for these differences is an increased heterogeneity of these layers due to differences in the soil structure which create preferential flow paths for water infiltration (Wang et al., 2006) as well as affecting the ability of the soil to store water by affecting the pore sizes. Alternatively, these differences may be caused by the small dimension of the TDR probes, which measured small soil samples and therefore were potentially susceptible to the small scale variability in the soil properties (IAEA, 2008), especially in the presence of shrink swell patterns which can affect probe contact. At greater depths, fewer differences existed between probes at similar depths and within the same soil type (archaeological or SSM), suggesting that the soil was more homogenous and displayed less variability in soil structure. The greatest differences in geophysical properties occurred during dry periods, such as at the start of the monitoring period. Similar results were found in comparisons of water content homogeneity by Herkelrath et al. (1991) who found lower spatial variation in wet soils. It should be noted that larger variations existed in the absolute values of BEC exist in comparison to the ARDP values. Whilst these effects may partly

be the result of the lower accuracy of the TDR for BEC determination (Section 3.5.2), it is likely that the chemistry of the soil was not spatially uniform within the two measurement volumes and differences in ion availability may have influenced the measured values.

Slightly greater variability in the absolute values between probes at roughly the same depth was evident in the archaeological soils (Figures 6.5 and 6.6) compared to the SSM (Figures 6.3 and 6.4), likely due to the lower density of the ditchfill soils which created differences in soil structure and therefore distribution of pore space within which the water is stored. Due to the relatively small pore sizes of clay and the resulting suction arising from the large surface area of large numbers of small pores, even small differences in pore size may have a significant effect by reducing the soil water potential. However, the differences are still not large (maximum of approximately 1.5 relative permittivity unit and 0.004 S/m at 1m) compared to the SSM (maximum of <1 relative permittivity unit and 0.003 S/m at 1m) and are partly accounted for by the accuracy of the TDR unit (see Sections 3.5.1 and 3.5.2).

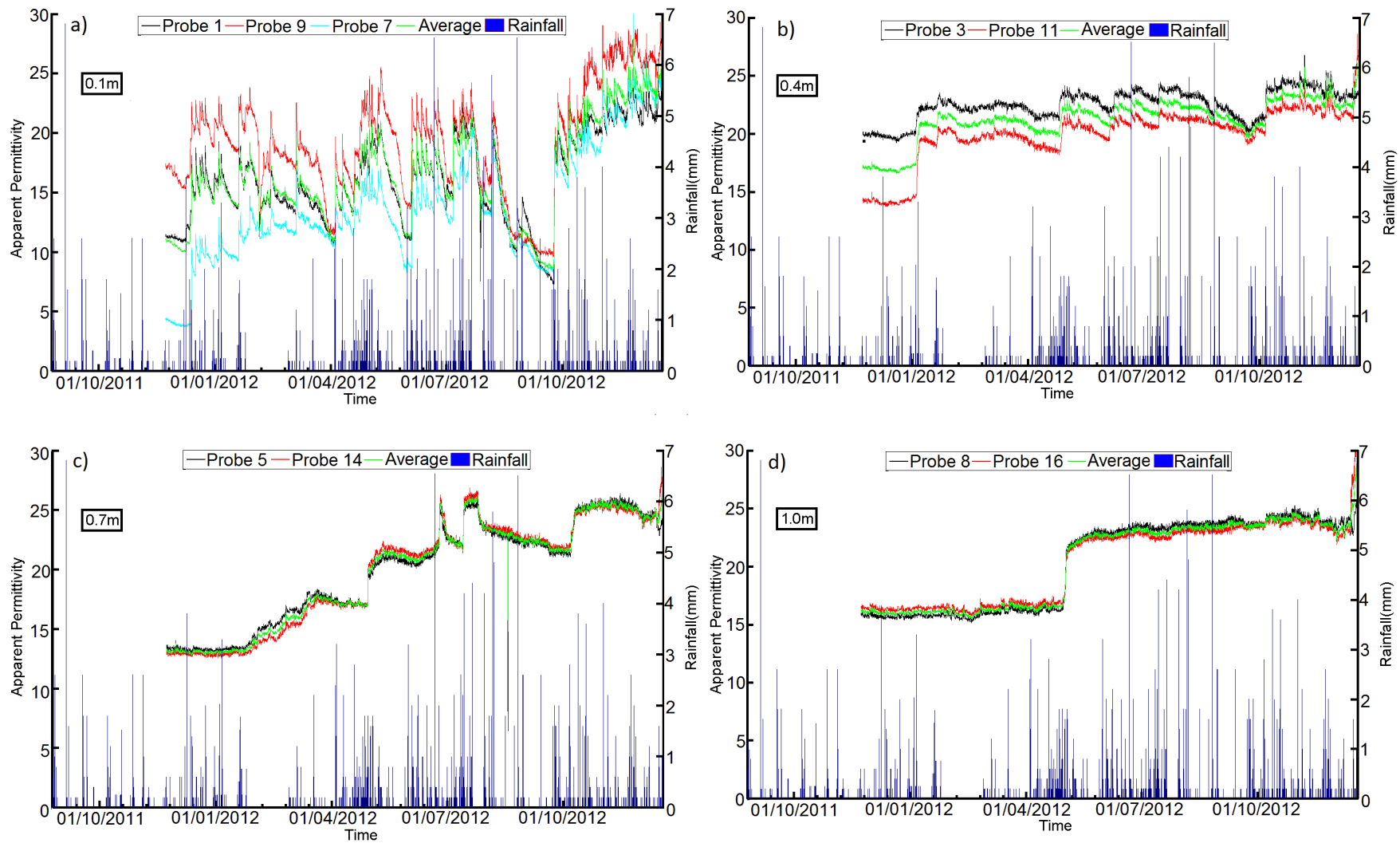


Figure 6.3: Comparison of ARDP values from DCFN (SSM) probes at different depths a) 0.1m b) 0.4m c) 0.7m and d) 1.0m

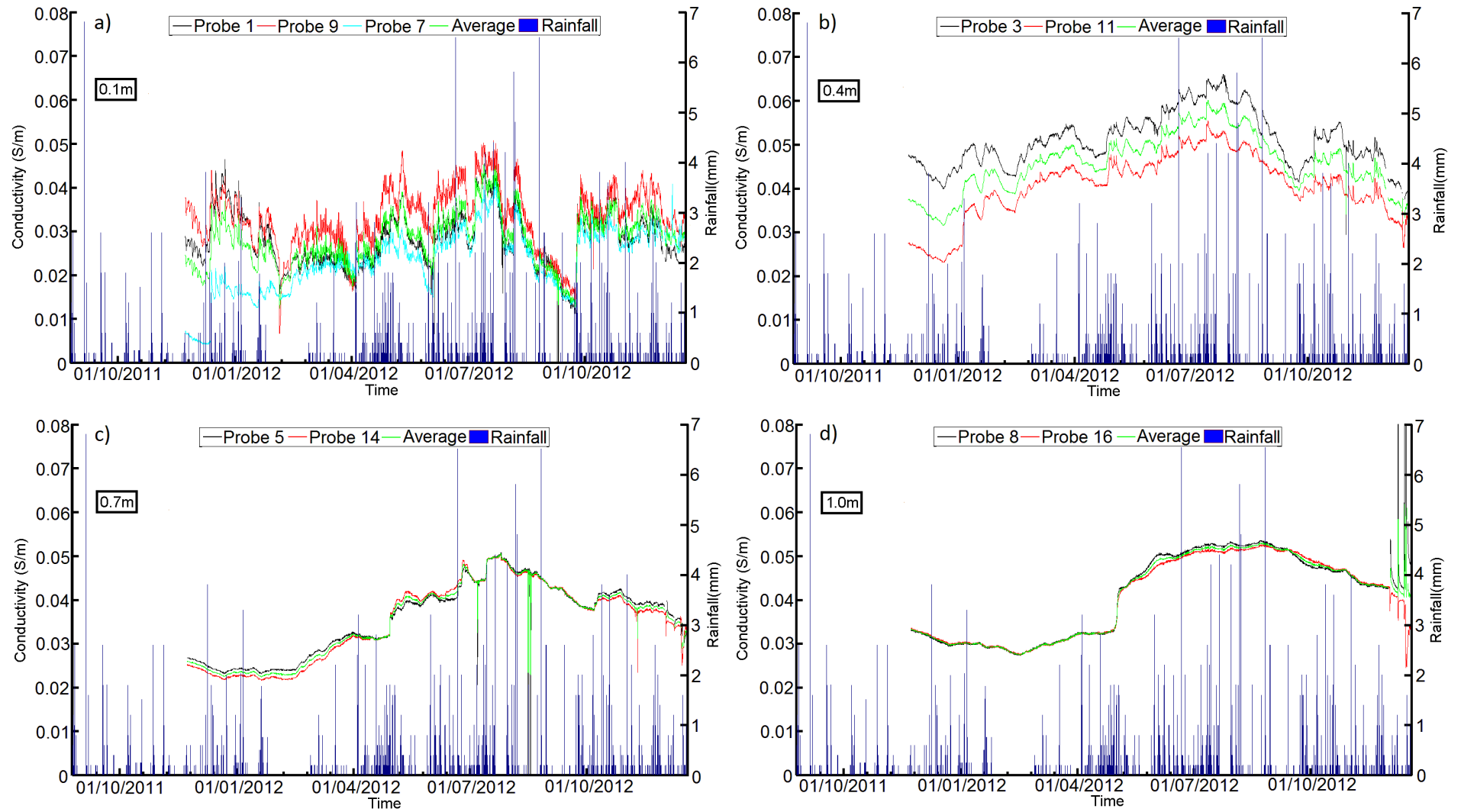


Figure 6.4: Comparison of BEC values from DCFN (SSM) probes at different depths a) 0.1m b) 0.4m c) 0.7m and d) 1.0m

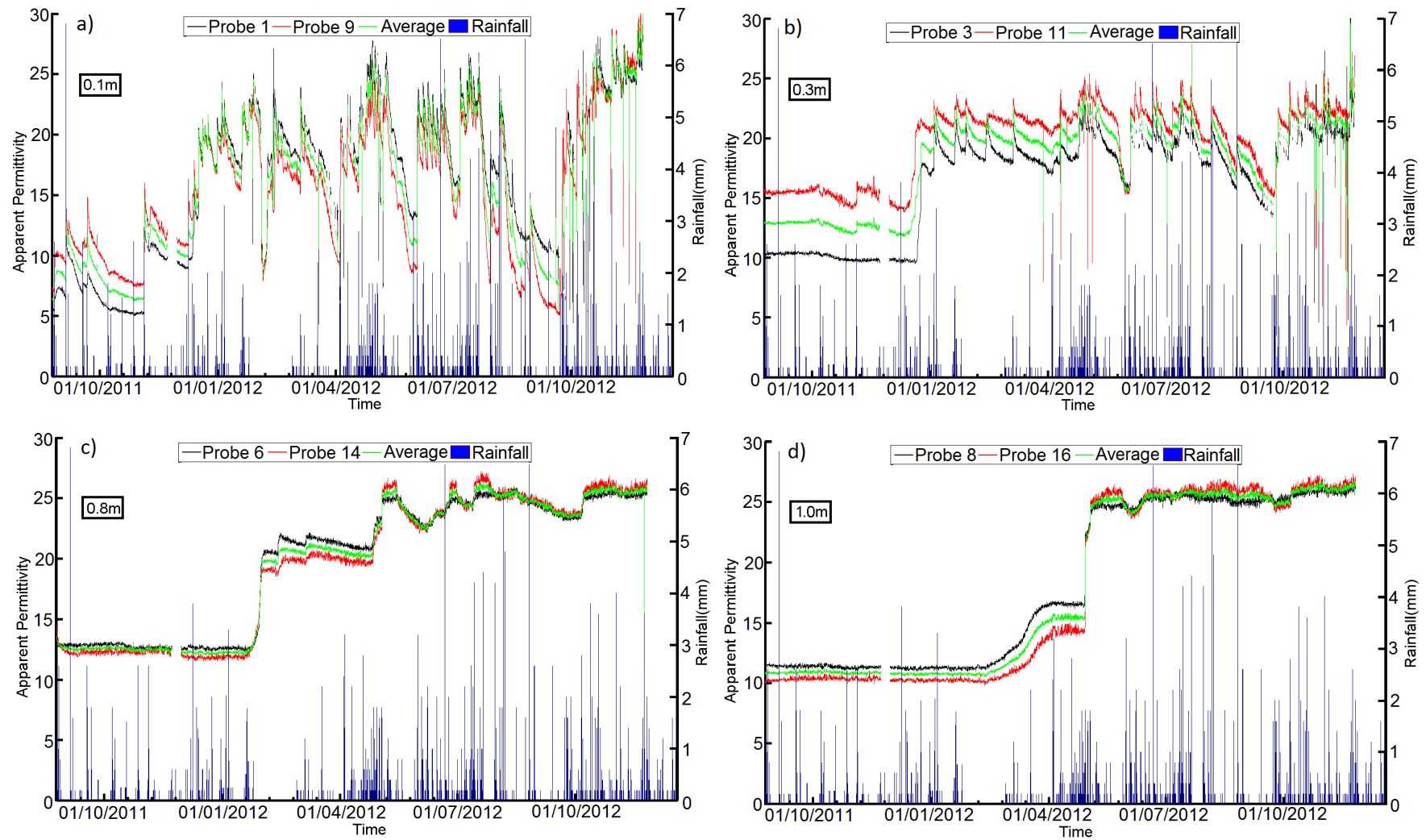


Figure 6.5: Comparison of ARDP values from DCFA (Archaeology) probes at different depths a) 0.1m b) 0.3m c) 0.8m and d) 1.0m

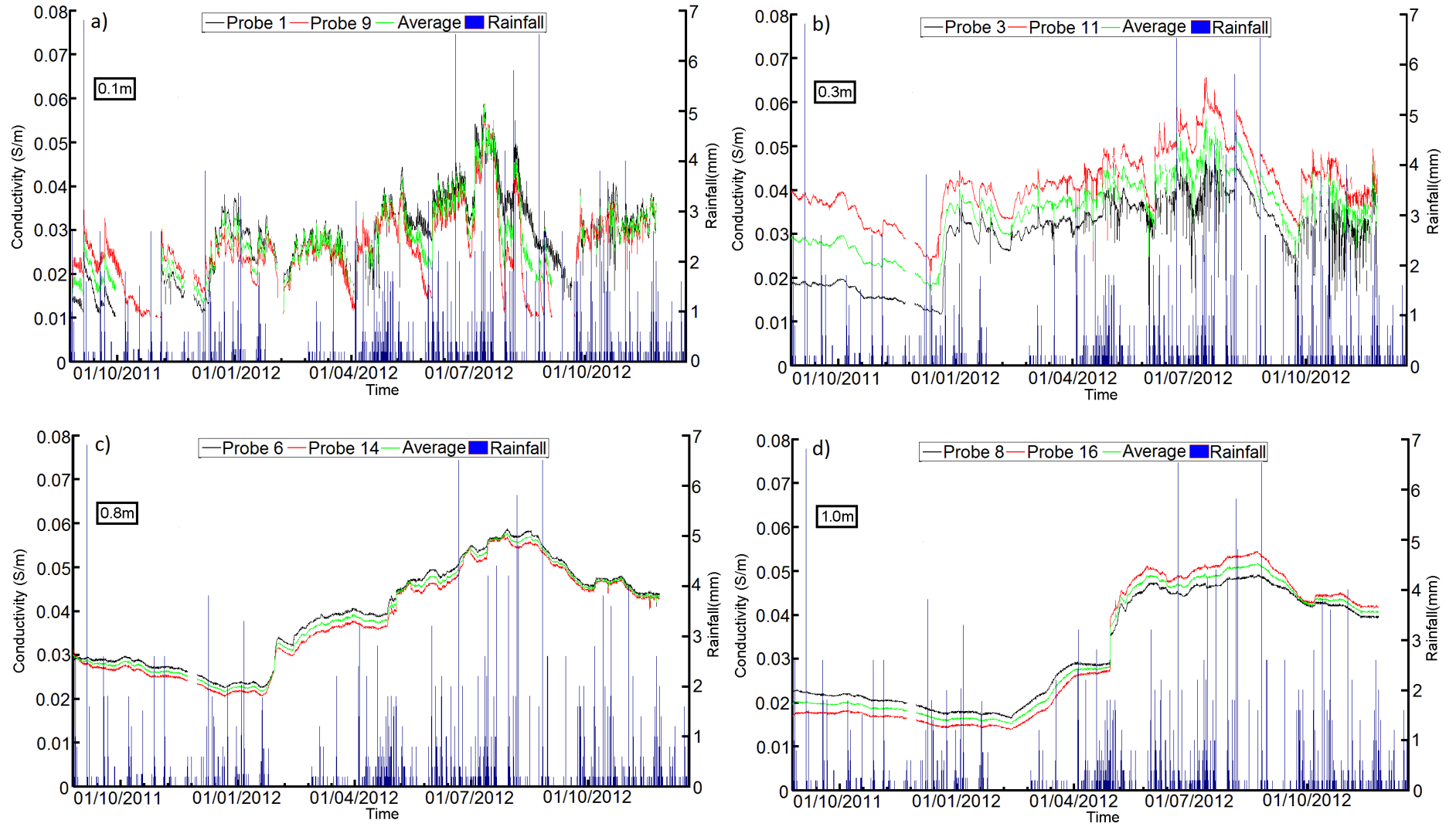


Figure 6.6: Comparison of BEC values from DCFA (Archaeology) probes at different depths a) 0.1m b) 0.3m c) 0.8m and d) 1.0m

Due to the smaller number of deployed TDR probes and their locations, DPF only had one set of probes which were suitable for comparing lateral variation (i.e. at the same depth and in the same type of soil) which were located at 0.6m depth in DPF Ditchfill1. Data for both the ARDP and BEC are displayed in Figure 6.7. Both probes showed similar trends for both ARDP (Figure 6.7a) and BEC (Figure 6.7b) and similar absolute values, with only small differences recorded between the two. The greatest differences in ARDP are recorded towards the end of the monitoring period after the upper most probes were disturbed by ploughing causing changes to the soil structure, which made the underlying soil more susceptible to differences in infiltration pathways. Slightly larger differences also exist in the measured BEC values in comparison to the ARDP values in the same way as on the DCF soils discussed above. Also it is interesting to note that unlike the DCF soils, greater differences were found in the dry soils, but the precise reasons for this are unknown.

ARDP and BEC data from the monitoring stations at CQF for both archaeological soils and the SSM from a number of depths are shown in Figures 6.8-6.11. The probes from CQFA showed large differences at all depths (Figures 6.8-6.9) apart from at 1m, although it can be noted that the probes on the left hand array of the monitoring station (probes 1-8) produced the same trends at all depths. Closer inspection of the waveforms from the different probes revealed that there was a multiplexer failure for probes 1-8 for CQFA and 9-16 CQFN towards the end of the monitoring period and those data have been discarded.

Another interesting feature is the sharp jump in ARDP and BEC occurring in early January 2012 at all of the measured depths. The immediate response at all depths makes it unlikely that this rise is the result of normal infiltration processes. One likely explanation is that the dry summer in 2011 caused the soil in the previously excavated trench to shrink away from the section face in which the probes were placed, creating a preferential pathway for water to infiltrate. These effects are important to consider for future installations on shrinkable clays and when

assessing the accuracy of readings after an extended period of dry weather. However, further research is needed into the long term consolidation effects after repeated wet-dry cycles.

Later infiltration events behave in a more typical manner, suggesting the soil swelled to fill the gap following this initial wetting event.

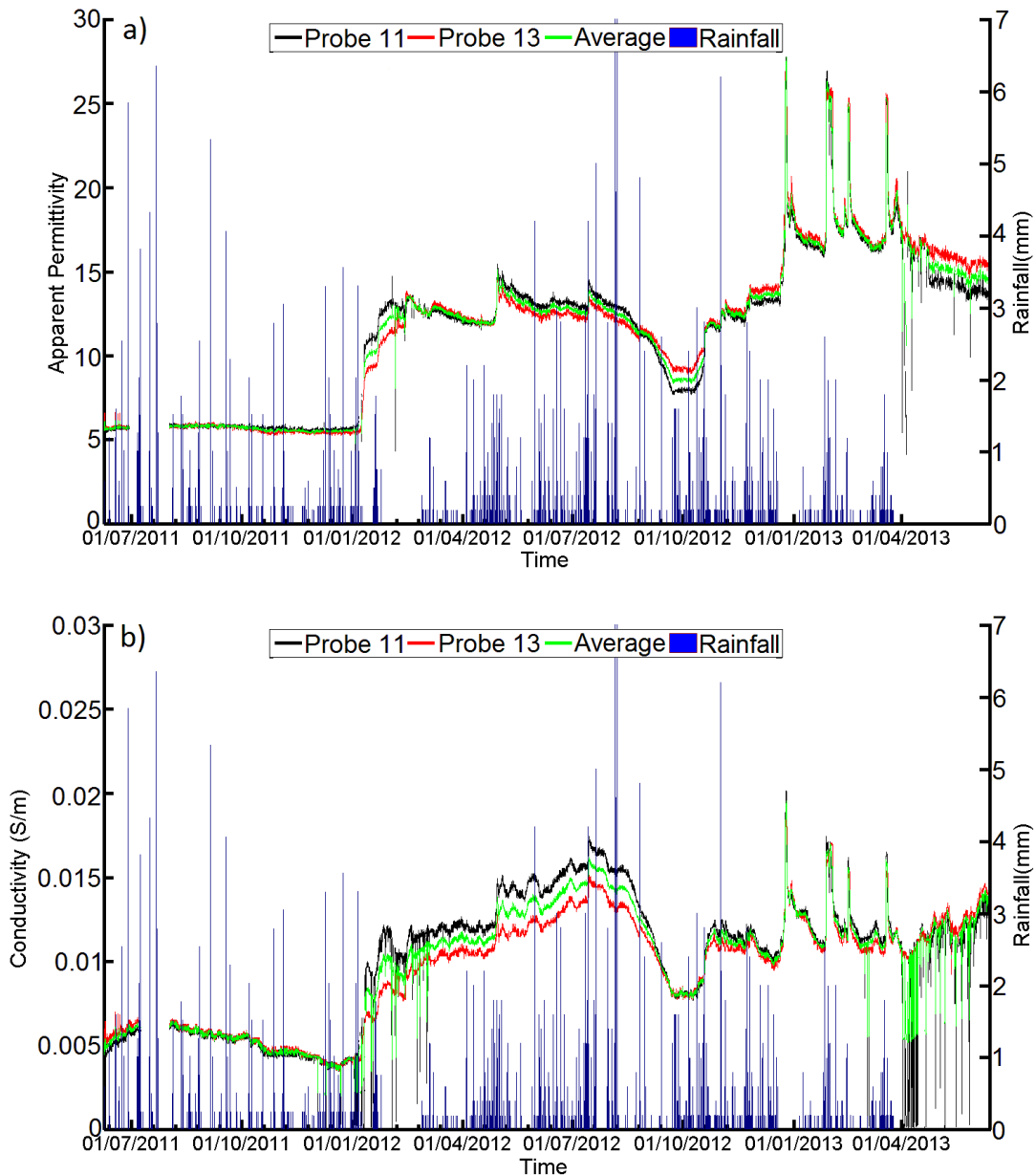


Figure 6.7: Comparison of geophysical values from DPF probes from 0.6m depth in the archaeological profile a) ARDP and b) BEC

Beyond these issues, the SSM at CQF showed very small variations in both ARDP and BEC between shallow (0.15m and 0.3m) and deep probes (1m) with the greatest variation visible in

the 0.5m probe data (Figures 6.10c and 6.11c) and several of the probes at mid ranged depths (0.6m-0.8m not displayed here). As with DCF, the greatest differences in geophysical properties occurred during dry periods, such as at the start of the monitoring period and after specific drying events when ARDP and BEC decreased. Greater heterogeneity in dry soils has also been observed by other authors (e.g. Herkelrath et al., 1991). This seems likely to be result of differential drying patterns, which appear to be more significant than infiltration patterns as infiltration events occurred simultaneously. These may be the result of very small differences in soil structure which are more significant for drying events due to the effects of hysteresis in the soil characteristic curve (Haines, 1930, Pham et al., 2005), with the drying curves possessing higher suction at the same water content in comparison with the wetting curve (i.e. making soil harder to dry than wet). Interestingly, the lateral variation appeared to be greater on this site than the other two sites, especially after drying events, although no obvious reasons exist for this.

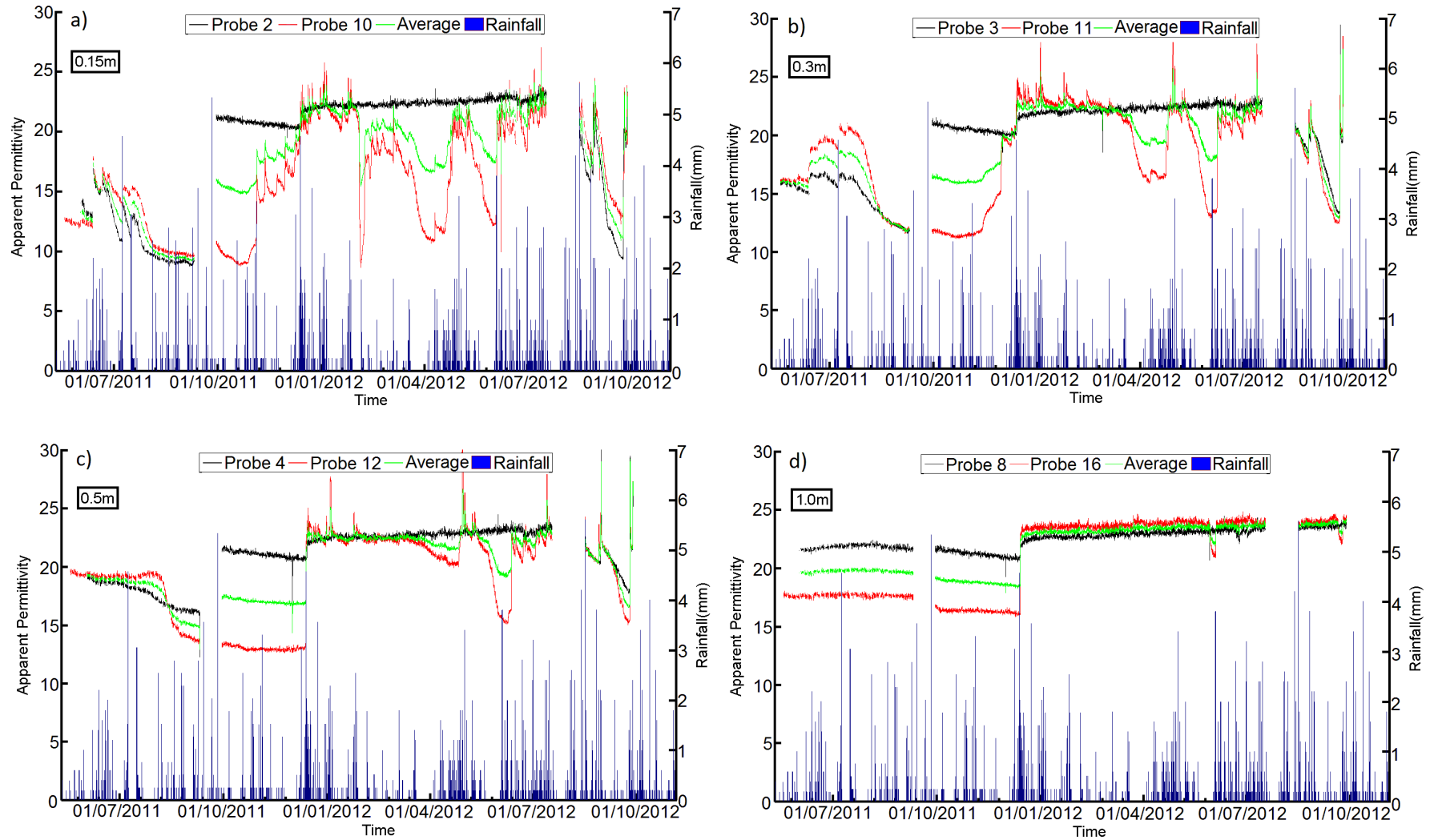


Figure 6.8: Comparison of ARDP values from CQFA (Archaeology) probes at different depths a) 0.15m b) 0.3m c) 0.5m and d) 1.0m

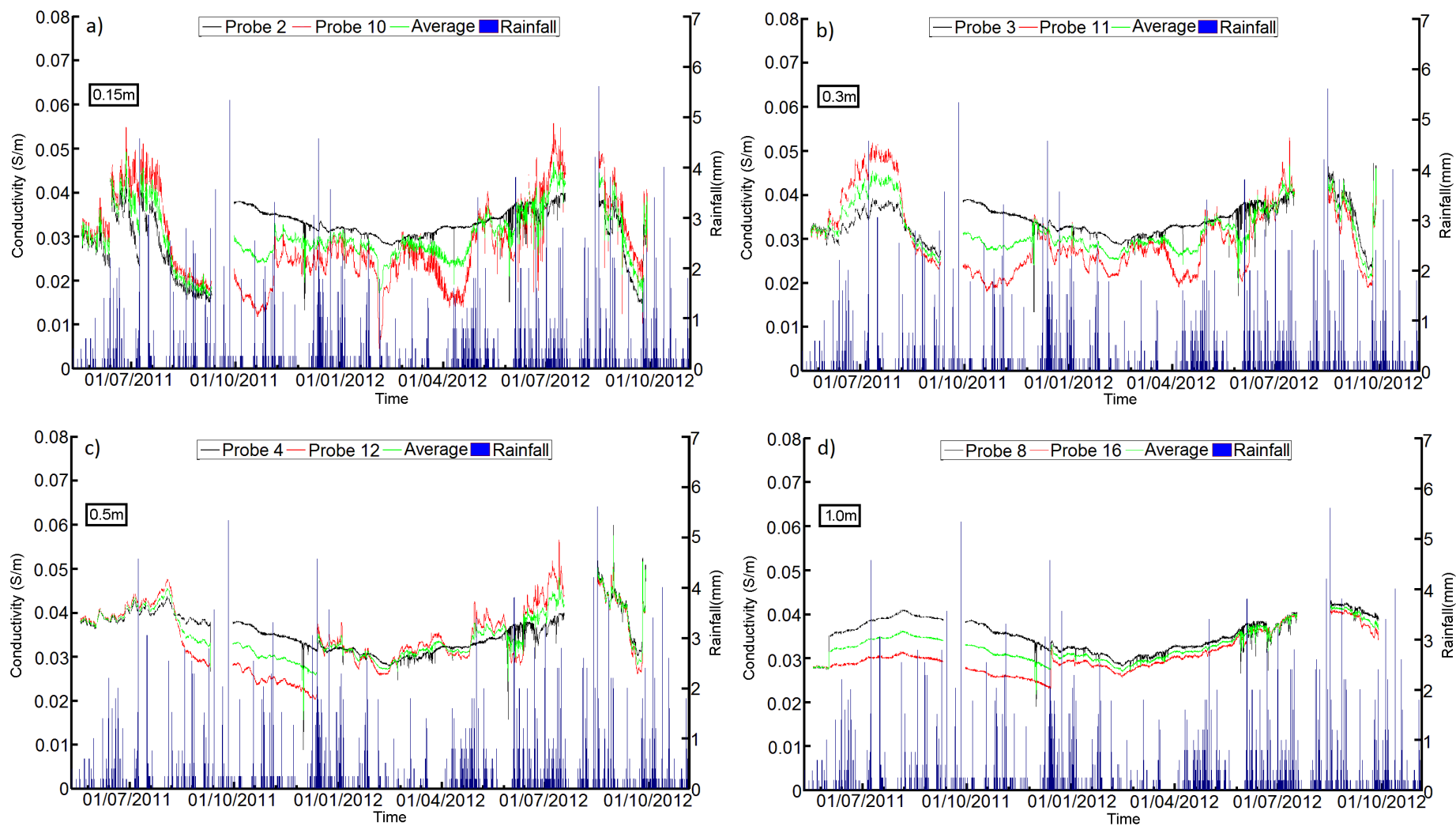


Figure 6.9: Comparison of BEC values from CQFA (Archaeology) probes at different depths a) 0.15m b) 0.3m c) 0.5m and d) 1.0m

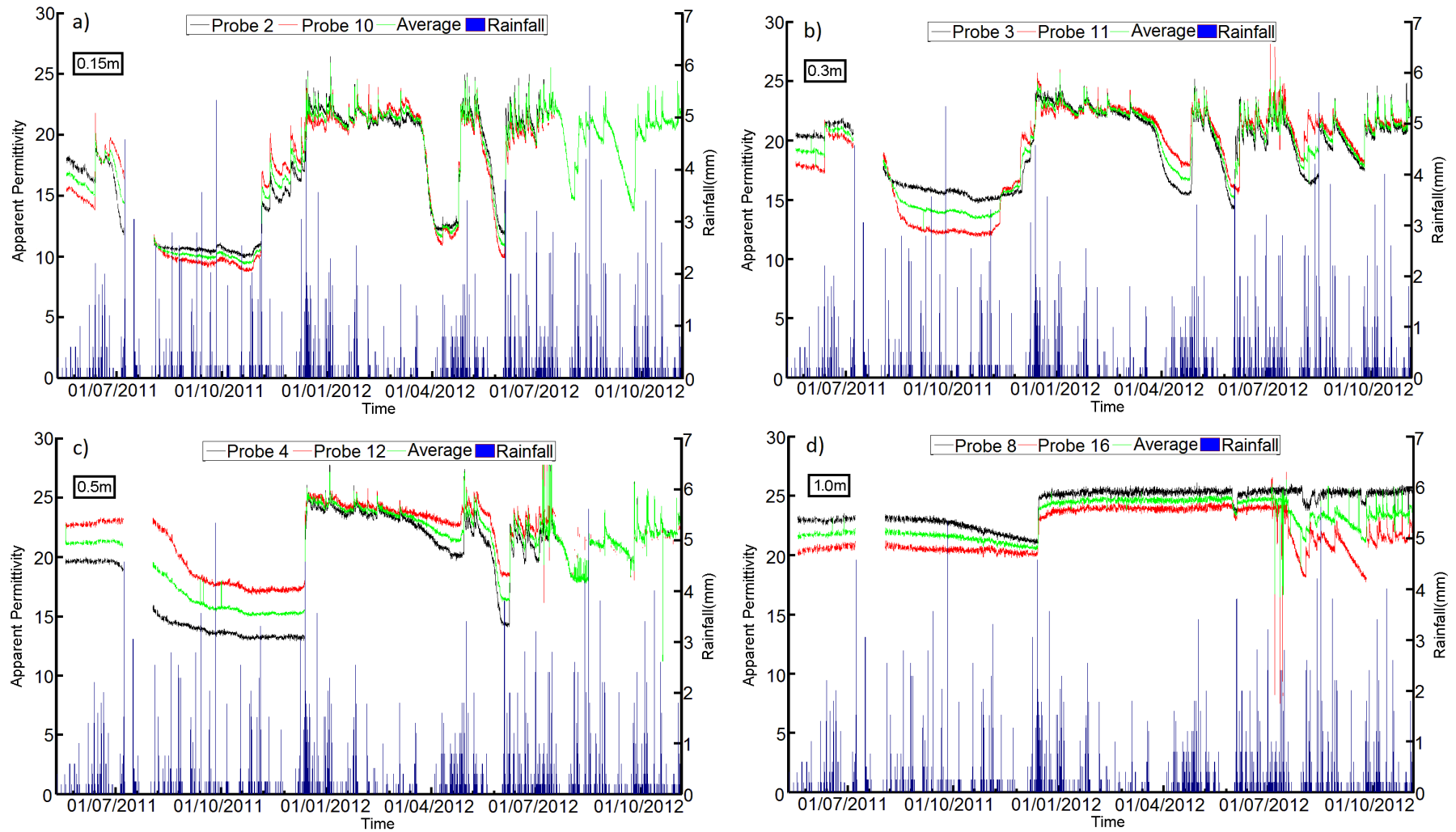


Figure 6.10: Comparison of ARDP values from CQFN (SSM) probes at different depths a) 0.15m b) 0.3m c) 0.5m and d) 1.0m

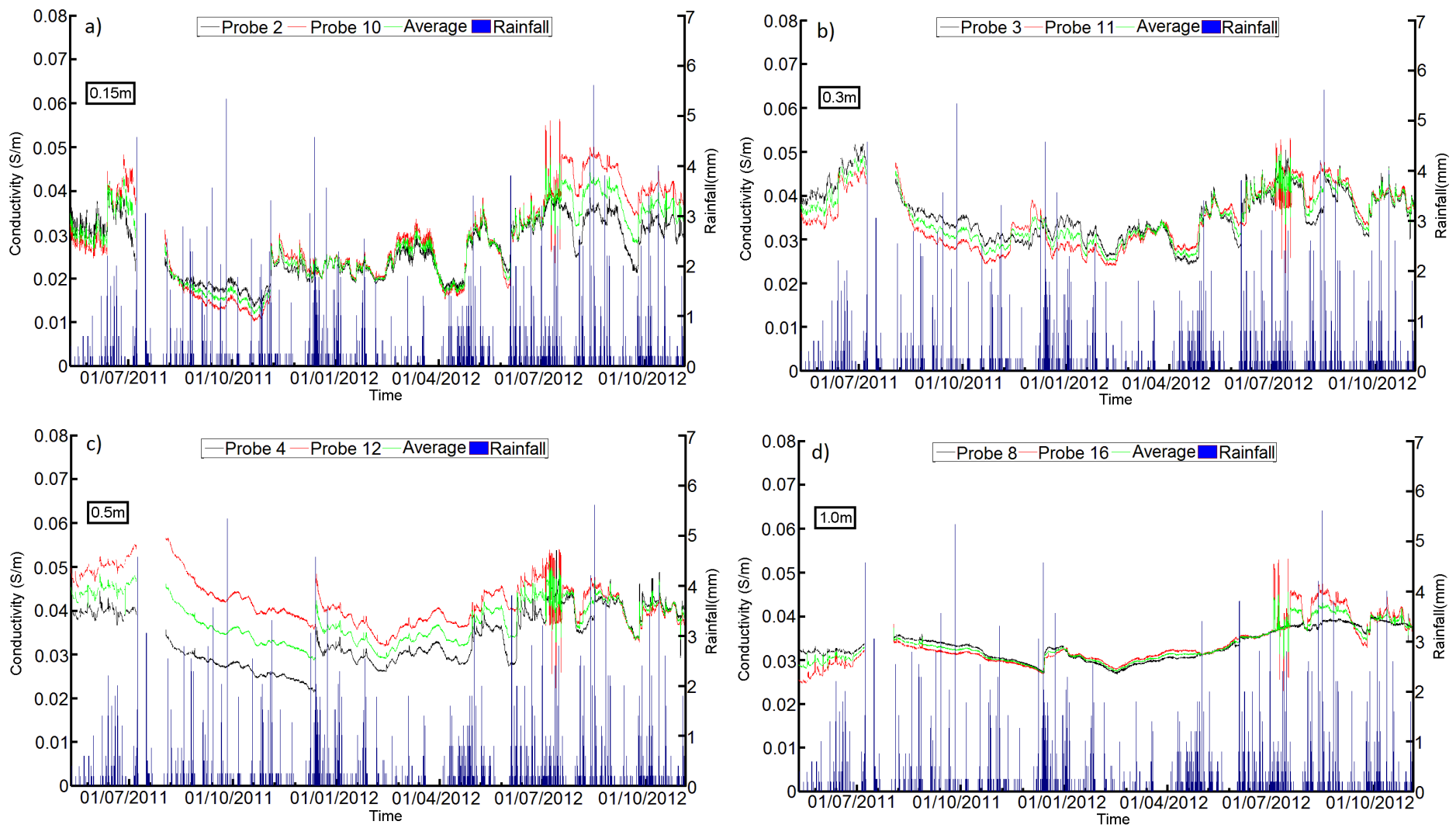


Figure 6.11: Comparison of BEC values from CQFN (SSM) probes at different depths a) 0.15m b) 0.3m c) 0.5m and d) 1.0m

A summary of the lateral variation in geophysical properties is as follows:

- For all of the soils of the same type and at the same depth, the measured trends were similar although some differences were observed in the measured values. The greatest differences in these occur during dry periods, especially at the start of the monitoring period on fine grained soils and during wet conditions on the coarse grained DPF soils.
- On DCF, greater lateral variation was observed in shallower soils due to differences in soil structure and infiltration pathways. On CQF the greatest variations were observed below the Topsoil in the upper SSM (at approximately 0.5m depth). Comparisons in the archaeological soils at CQF were impossible due to a multiplexer malfunction.
- A slightly greater lateral variation in absolute values was also observed within the archaeological soils on DCF although the differences were still small.
- A greater lateral variation was observed in BEC in comparison to ARDP which is due to the heterogeneity in soil ionic contents which caused different conductivity values even at the same water content, although the magnitude of the differences may also be affected by the lower accuracy of the TDR100 in determining BEC in comparison to ARDP.

6.4. Seasonal Variations in Geophysical Properties

This section explores the variation of ARDP and BEC over the monitoring period and compares the differences both between the archaeological and SSM soils and between the different sites. Several outlying data points were removed using clipping and a median filter as in Section 6.3 before probes from the same depths and soils were averaged. In addition, in order to produce clearer plots, data in this section have been averaged over 24 hour periods to give daily values for ARDP and BEC. Any diurnal variations have therefore been removed, although these are examined in greater detail in Section 6.6. Rainfall and ET data have also been

provided as cumulative values over 24 hour periods. Since only small differences existed in the ARDP-VWC relationships between the archaeological and SSM soil on site (see Section 5.5.3) and ARDP was not strongly affected by temperature, ARDP values provide a good analogy for water content, and differences in value can be mostly equated to differences in water movement and storage in the soil. Figures 6.12-6.17 show ARDP and BEC at a number of different depths for all three sites during the whole monitoring period. Each individual site is discussed in greater detail in Appendix F, but a summary of the observed behaviour and comparisons between the sites are provided here.

All of the measured soils showed an expected strong dependence on rainfall and ET in determining their geophysical properties, especially in the near surface. This is unsurprising given the dependence of soil EM properties to water content and the results are similar to those recorded during long term monitoring by other authors (e.g. Curioni, 2013, Menziani et al., 2003). It should also be noted that for all of the studied soils, changes with rainfall primarily affected the topsoil and subsoils down to c.0.3m with changes in the deeper soils below occurring relatively infrequently and only after very heavy rain following a period of extensive drying on the surface. This agrees with hydrological theory which suggests that surface effects are dominant on infiltration capacity and therefore drying increases infiltration as the soil shrinks and pores are reopened (Beven, 2004, Horton, 1933).

All of the studied sites were defined by two distinct periods; a very dry period with low ARDP values which responded little to rainfall events and a period of high ARDP values which remained for the rest of the monitoring period, thought to be close to the field capacity of the soil. The dry period coincided with the start of the monitoring period on both of the Diddington sites (DCF; Figure 6.12 and DPF; Figure 6.14) and may have been influenced during the installation of these sensors during the drought period which may have artificially dried the soils at greater depths than in natural soil conditions. However, the same dry period was also

observable on the CQF site (Figure 6.16) during a similar period, which occurred after an extended period of low rainfall at the end of 2011. Since monitoring commenced earlier in 2011 (May) than on the Diddington sites (DPF in June and DCF in August) allowing settling to take place, it is distinctly possible that this dry low period on all sites was the result of the extremely dry conditions in 2011. It is also interesting to note that no periods were found with intermediate value between these extremes, suggesting the soil exists in either a dry state after extensive periods of drying or a saturated state. Similar results were found also found by Curioni (2013), who found two distinct peaks when examining the frequency of occurrence of different values, and other authors (Brunet et al., 2010, Scollar et al., 1990) who highlighted a period of water content stability between Autumn and Spring followed by a period of drying over the summer (June-August) which lasted until early Autumn, when rain caused the soil to re-saturate to field capacity. Whilst the timescale of the dry and wet events does not agree here, the monitoring period was characterised by an unusually dry summer and winter period in 2011 and an extremely wet year from April 2012 onwards, which it is believed has affected typical seasonal variation. However, Scollar et al. (1990) also suggested that during the dry period, the soil was affected by wetting and drying cycles which were not visible on any of the data during the dry periods, which displayed constant or falling ARDP values, until the sharp wetting fronts which concluded the period. However, it is possible that this is due to the rarity of rainfall events which exceed measured ET values.

Measured BEC values on all of the sites showed similar trends to measured ARDP on all sites. This is unsurprising as it was shown in Chapter 5 and in the literature (Curioni, 2013, Smith-Rose, 1933) that the BEC of soil was principally determined by its VWC. However, on all sites the BEC showed variations in measured values which corresponded to rises and falls in the air temperature during similar periods. This is agreement with the findings of other authors (e.g. Campbell et al., 1948, Friedman, 2005) as well as the laboratory test results presented in Chapter 5. It also should be noted that these variations were greater during the wet period

due to the presence of additional dissolved ions which is in line with the results of the laboratory testing (Chapter 5). The effect of changing air temperature on the soil temperature at different depths in the archaeological and SSM soils is discussed in Section 6.5 and its effects on geophysical properties in Section 6.8.1.

Significant differences existed in the measured geophysical values on different soil types, with higher values of both ARDP and BEC recorded on the fine grained soils (DCF; Figures 6.12-6.13 and CQF; Figures 6.16-6.17) in comparison with the coarse grained soils on DPF (Figures 6.14-6.15) throughout the monitoring period. This confirmed the results of the laboratory experiments discussed in Chapter 5 which showed both higher BEC and ARDP values for a given water content on the fine grained soils, and the findings of other authors who have found the behaviour of both values with variation in water content to be linked to the clay content and specific surface area of the soils (Rhoades et al., 1976, Thomas et al., 2010a, b). However, water content was determined to be the most important factor for determining these properties in Chapter 5. As values on the fine grained soils were usually around double those of the DPF site for the same time periods, it is suggested that the fine grained sites also had greater water contents throughout the monitoring period as the scale of the differences in ARDP-BEC-VWC relationships between the soils developed in the laboratory were not great enough to explain a difference of this magnitude. This result is not surprising as clay soils are known to have higher soil water potentials due to their greater surface areas (Fredlund and Xing, 1994, Rawls et al., 1982, Saxton and Rawls, 2006), and it is suggested that the higher values on fine grained soils are the result of a combination of both greater water contents and differences in relationships between VWC and geophysical properties.

One key finding is that none of the studied sites appeared to show significant differences in infiltration patterns and behaviour between the archaeological soils and SSM, with major wetting fronts affecting both at roughly the same time on most sites. Exceptions to this

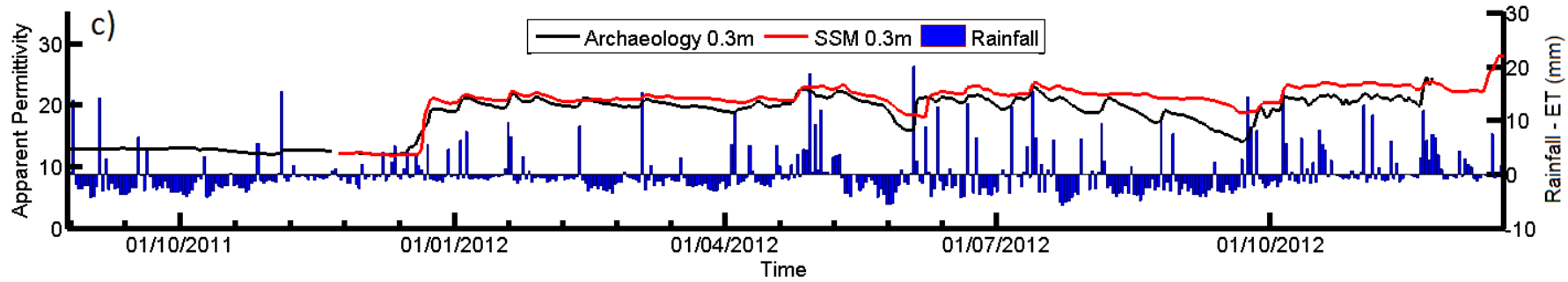
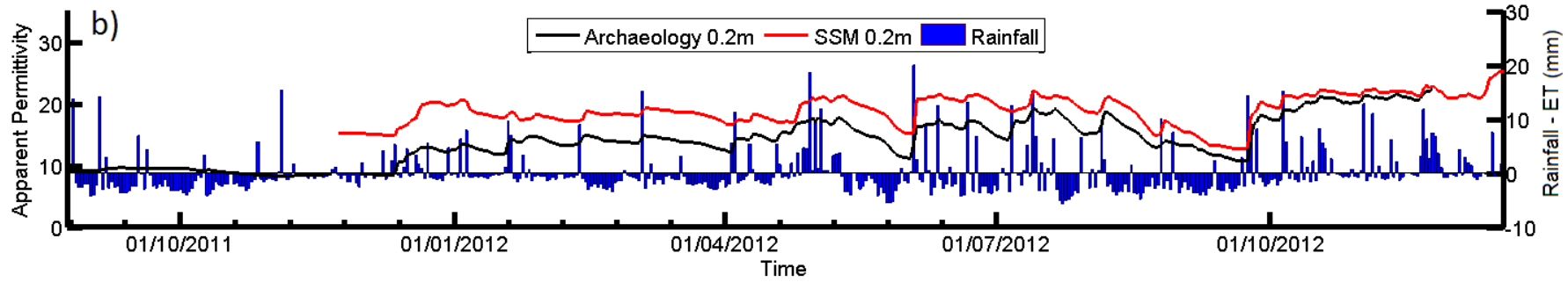
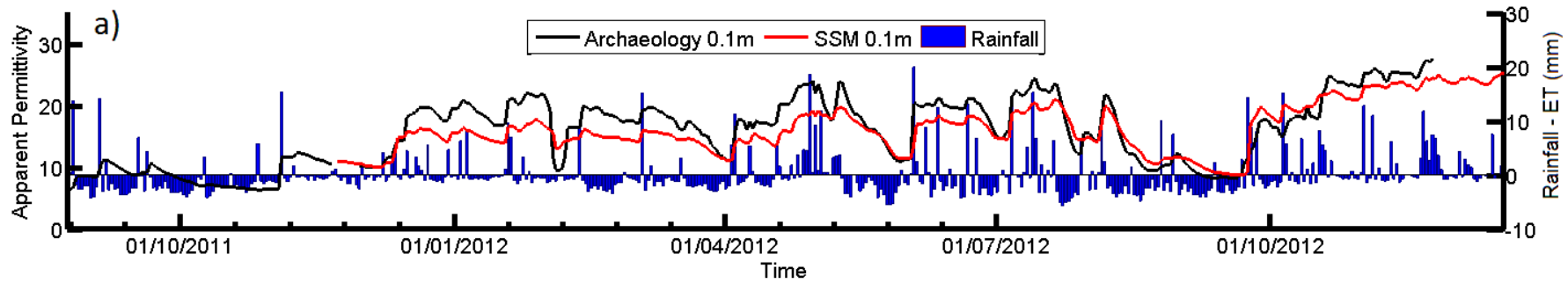
behaviour were the initial wetting front on the two Diddington sites (Figures 6.12-6.15), which moved slower in the SSM at the bottom depths. These responses can be related to the density and porosity of the soil, with faster movement in very dry soil happening in those soils with higher pore spaces within which to move water. Previous experiments on earth resistance contrast (e.g. Clark, 1980, 1996) suggested that water can infiltrate the ditch with greater ease due to lower density in comparison to the surrounding soils, although it should be noted that the temporal resolution of these surveys was limited to monthly and so processes were inferred between measurements based on rainfall data. As all subsequent rainfall events and wetting fronts behaved more uniformly between the two soil profiles once the soil was near to holding capacity, it appears that this behaviour is only true in the case of very dry soils. It is also notable that for all of the sites, the values of ARDP taken from the soil layers above did not decrease as the layers below increased and that the effect of rainfall on ARDP values at depth occurred within the same day suggesting an instant infiltration. These observations can also be seen in data from other sites (e.g. Menziani et al., 2003) and suggest that the same water was not travelling down the profile, supporting the piston-like displacement of stored water infiltration theory proposed by Horton and Hawkins (1965) and Hewlett and Hibbert (1967) as opposed to the flow through unsaturated pores. Whilst this behaviour is expected for fine grained soils (Youngs and Poulouvasilis, 1976), on the coarse grained DPF site this is an unusual result. One possibility is that the comparatively finer grained materials in the near surface soils (DPF Topsoil and DPF Subsoil) have influenced the result. A more detailed study, taken on an hourly basis, on water infiltration after a rainfall event and the differences between sites and archaeological soils and the SSM is conducted in Section 6.7.

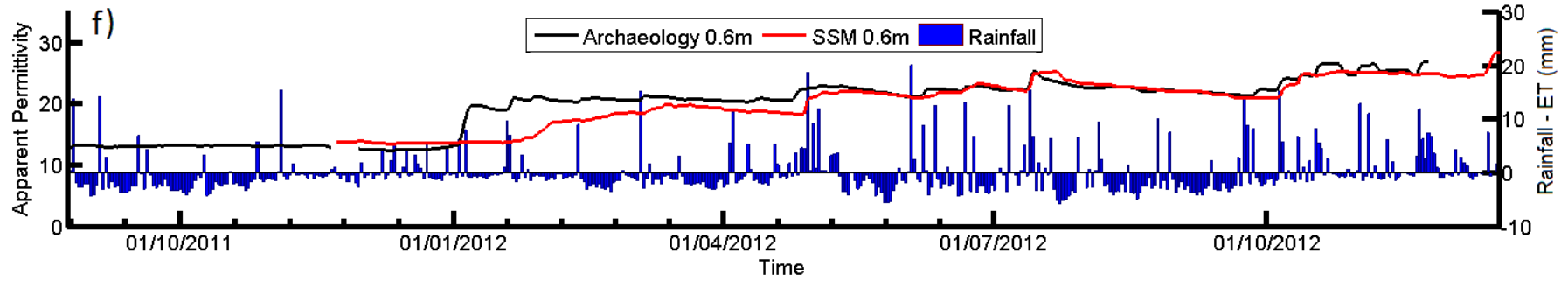
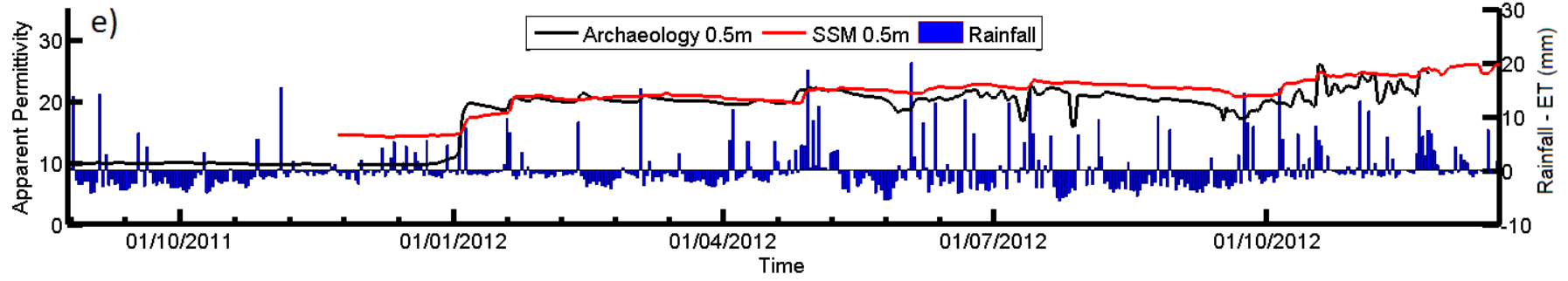
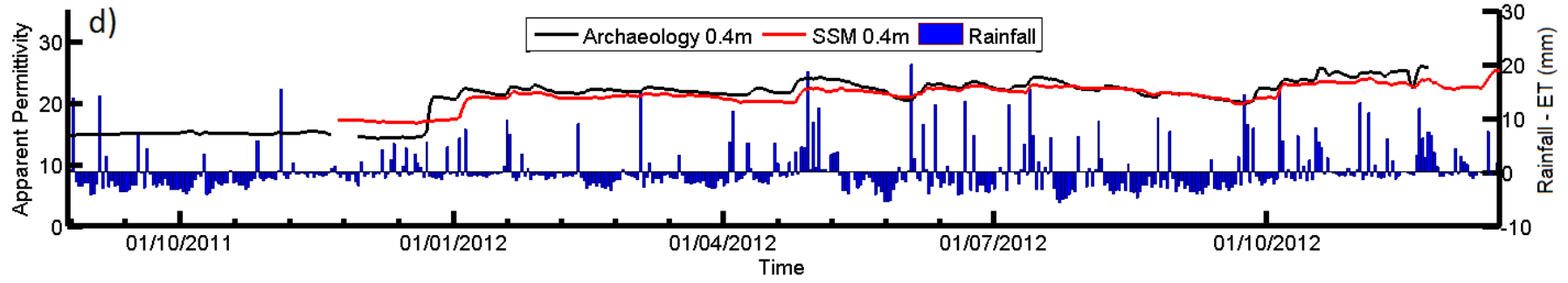
Whilst infiltration was reasonably constant between the archaeological soils and SSM, significant differences existed in drying patterns of the two soil types during a period of hot weather such as during summer 2012. For the two fine grained sites (CQF and DCF) the archaeological soils dried faster and to a greater depth, shown by the ARDP values (Figures

6.12 and 6.16) which fell at a greater rate and to a greater extent during periods in June-September 2012. By contrast, the opposite behaviour is true for DPF (Figure 6.14), as the SSM dried at a faster rate and to a greater extent in warm periods. These differences in drying, which were not present in wetting cycles, suggest different hysteresis in the soil potential between the two soil types (archaeological and SSM), and are likely to be the result of the greater porosity of the lower density soil on site which allows water to escape more freely. A period after an extended dry period may therefore provide the best time for a geophysical survey.

Due to these similarities in infiltration behaviour, for all of the studied sites, absolute contrast in ARDP throughout the year between the archaeological soils and SSM remained broadly constant during dry period at all depths and also stabilised during the wet period to a fairly constant value, especially at greater depths. This is indicative of the fact that the soil was either very dry and at residual water content or at field capacity such as during the wet period, as well as the similar behaviour in terms of infiltration behaviour which caused both soils to follow similar wetting patterns. However, on rare occasions, slightly larger differences can be observed following drying events due to the differences in drying patterns discussed earlier. It is most likely that the main differences between the archaeological and SSM soils lie in their capacity to hold water and retain it during drying events. Similar causes for GPR anomalies were identified as being caused by areas that retained more moisture than the surrounding soil (Van Dam and Schlager, 2000, Van Dam et al., 2002), due to differences in organic material, with PSD differences only visible at water contents above 0.055. However, Saxton and Rawls (2006) noted the dominance of PSD on water holding capacity in clay soils, which masked the effects of organic matter. It is likely that the differences between the holding capacities of the archaeological soils and SSM are due to differences in a combination of these factors, with the archaeological soils tending to have smaller grain sizes and higher organic content (Chapter 5). However, smaller differences could be seen on the fine grained soils both

because of their similar textures and the masking effect of the high clay contents on the organic matter identified in the literature. For example, CQF Ditchfill1 (Figure 6.16c-d) had a generally lower ARDP than the SSM at similar depths despite having a higher organic content due to it having a lower clay percentage and higher density than the upper SSM.





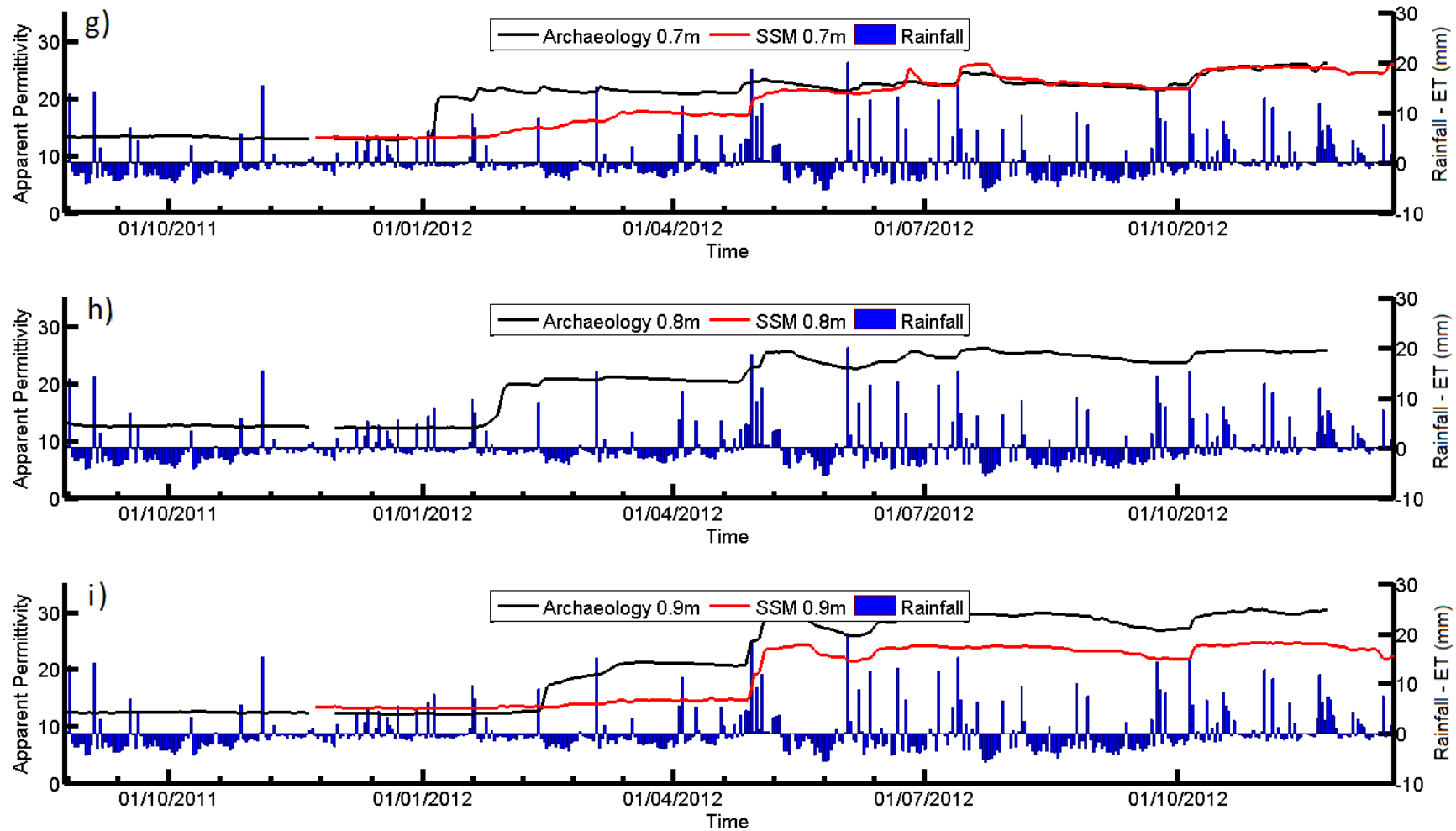
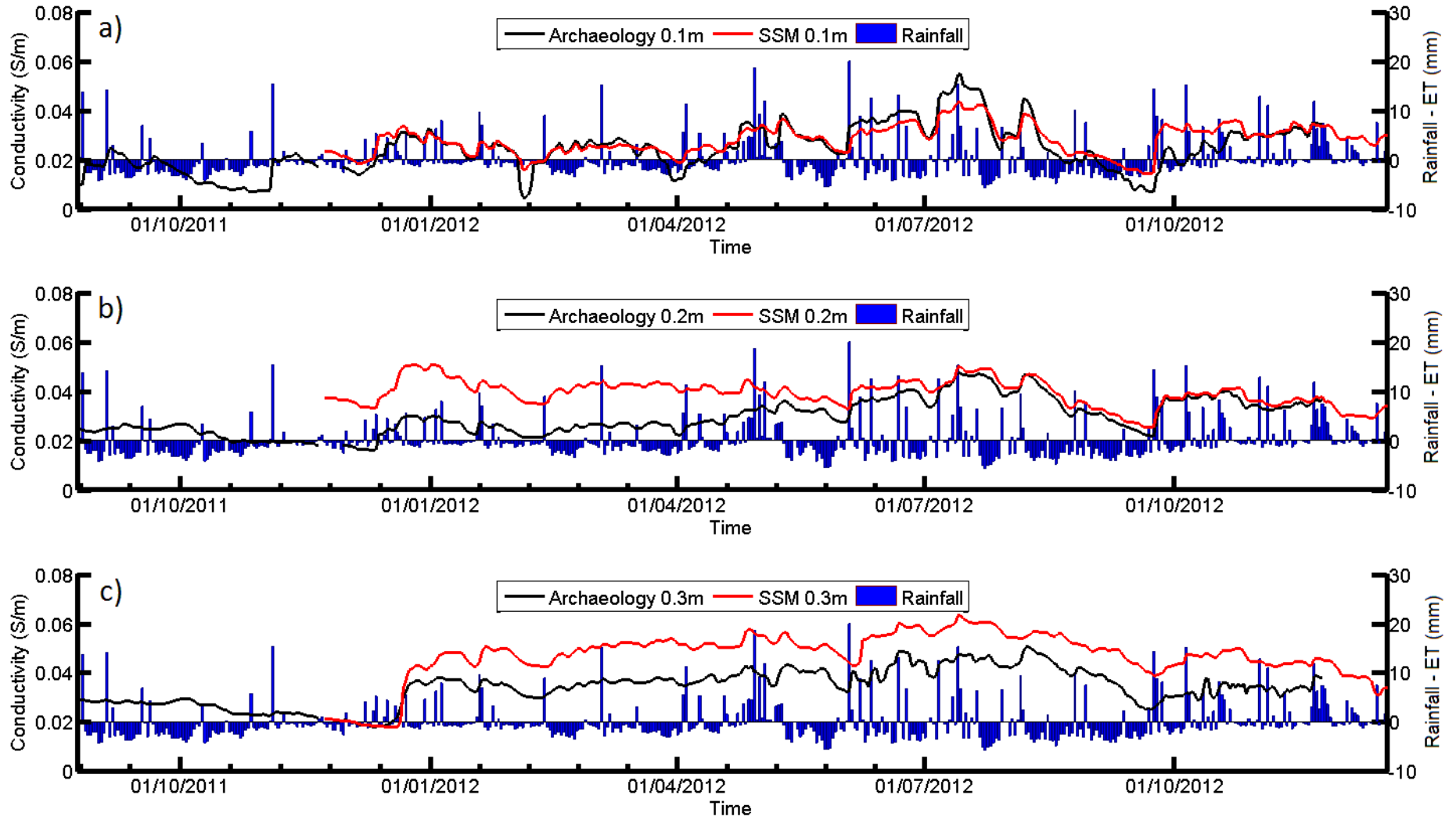
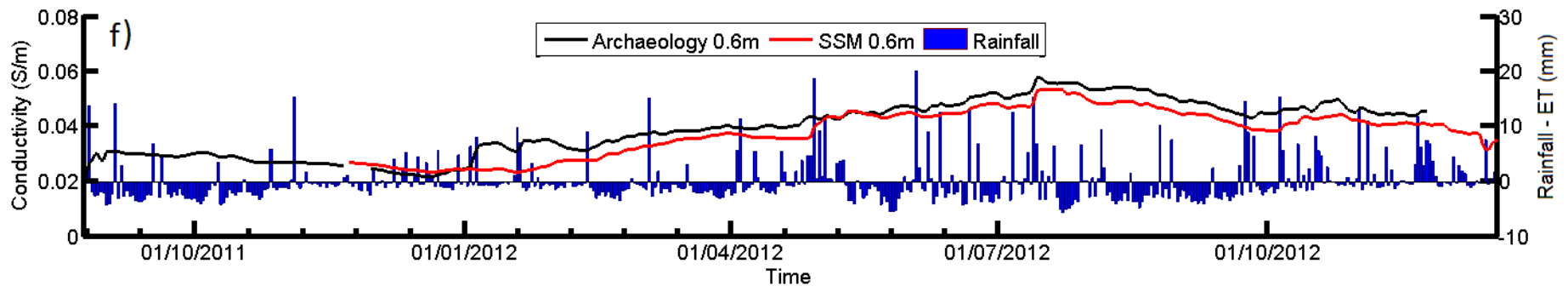
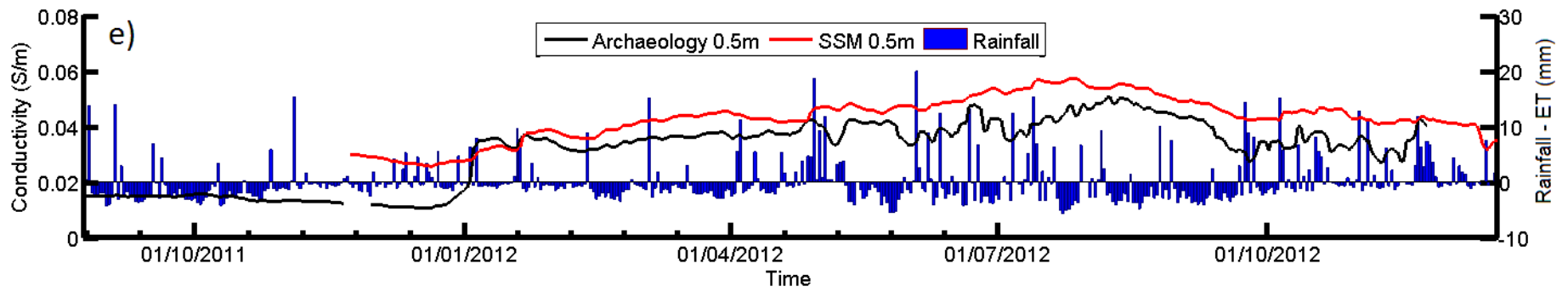
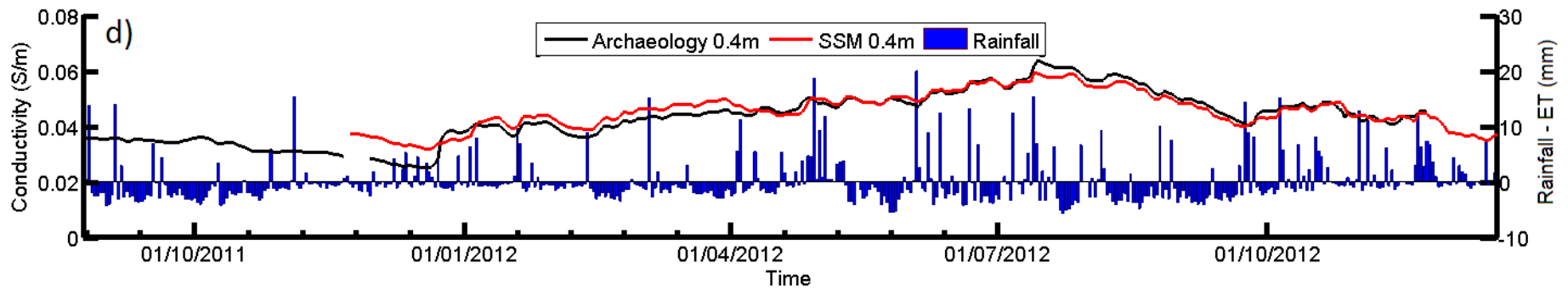


Figure 6.12: The ARDP variation on DCF over the study period at different depths a) 0.1m b) 0.2m c) 0.3m d) 0.4m e) 0.5m f) 0.6m g) 0.7m h) 0.8m i) 0.9m





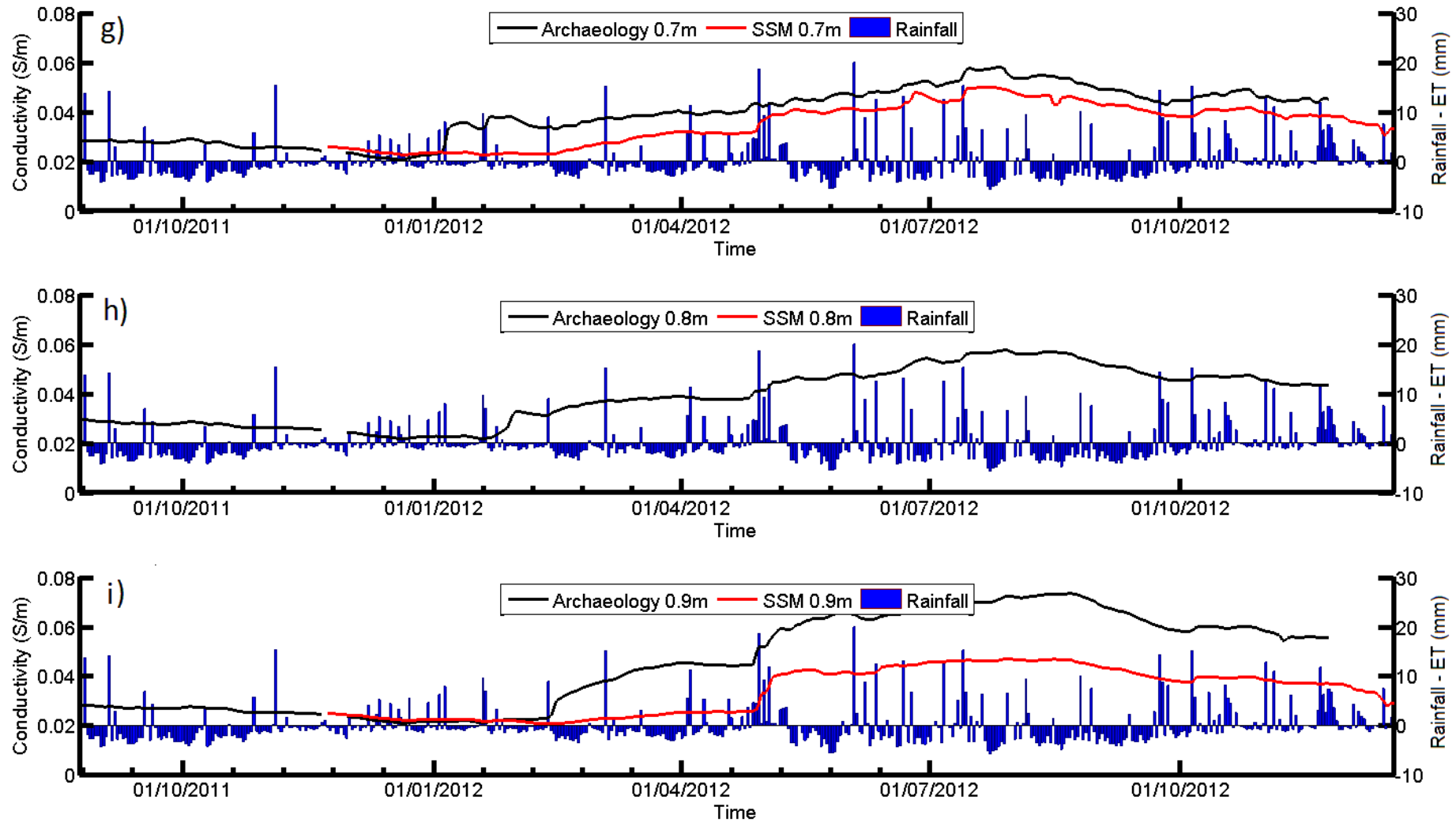
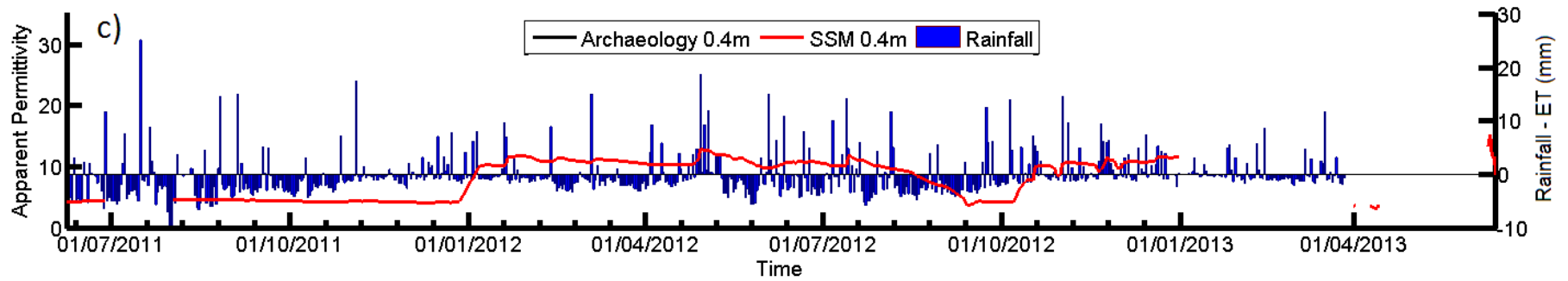
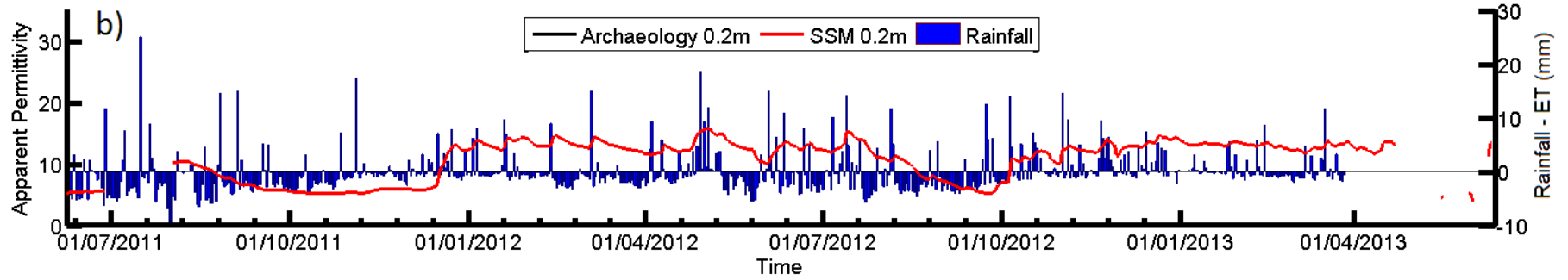
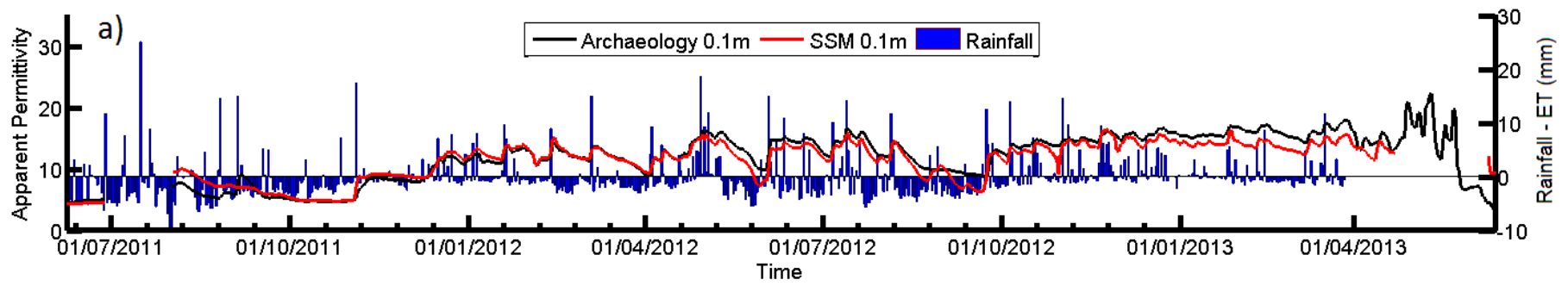
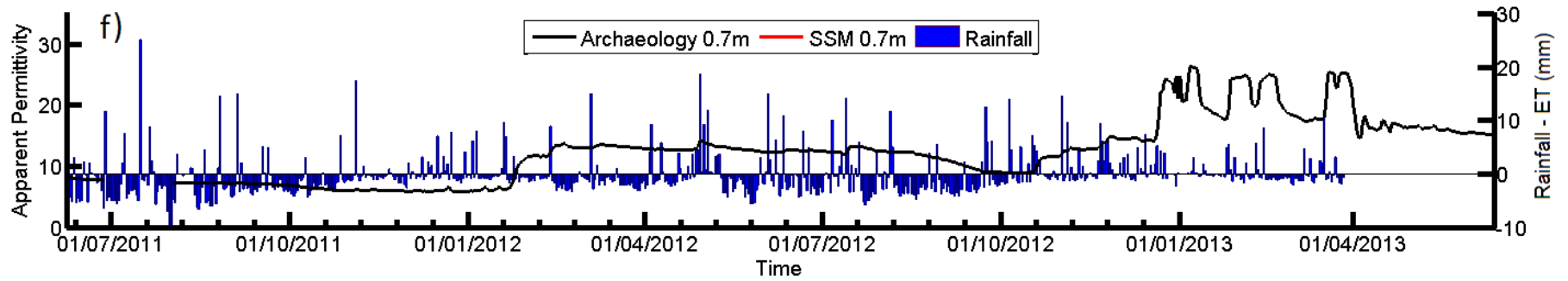
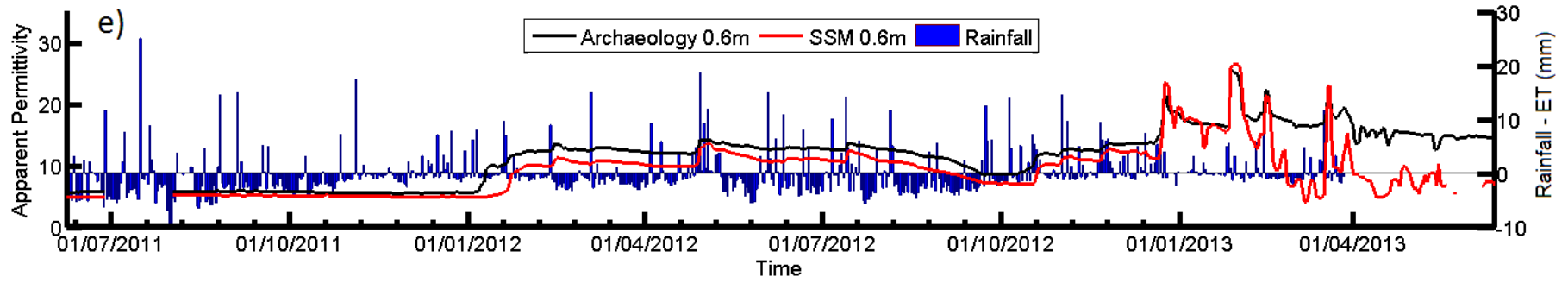
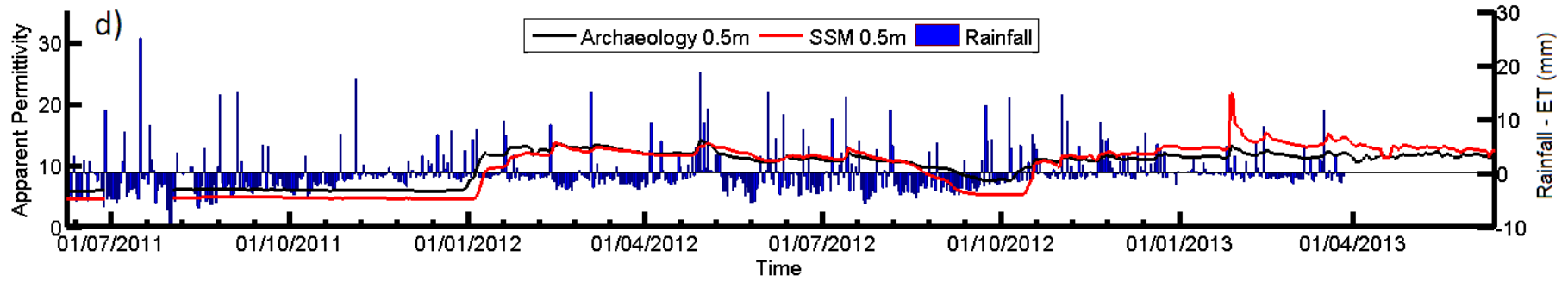


Figure 6.13: The BEC variation on DCF over the study period at different depths a) 0.1m b) 0.2m c) 0.3m d) 0.4m e) 0.5m f) 0.6m g) 0.7m h) 0.8m i) 0.9m





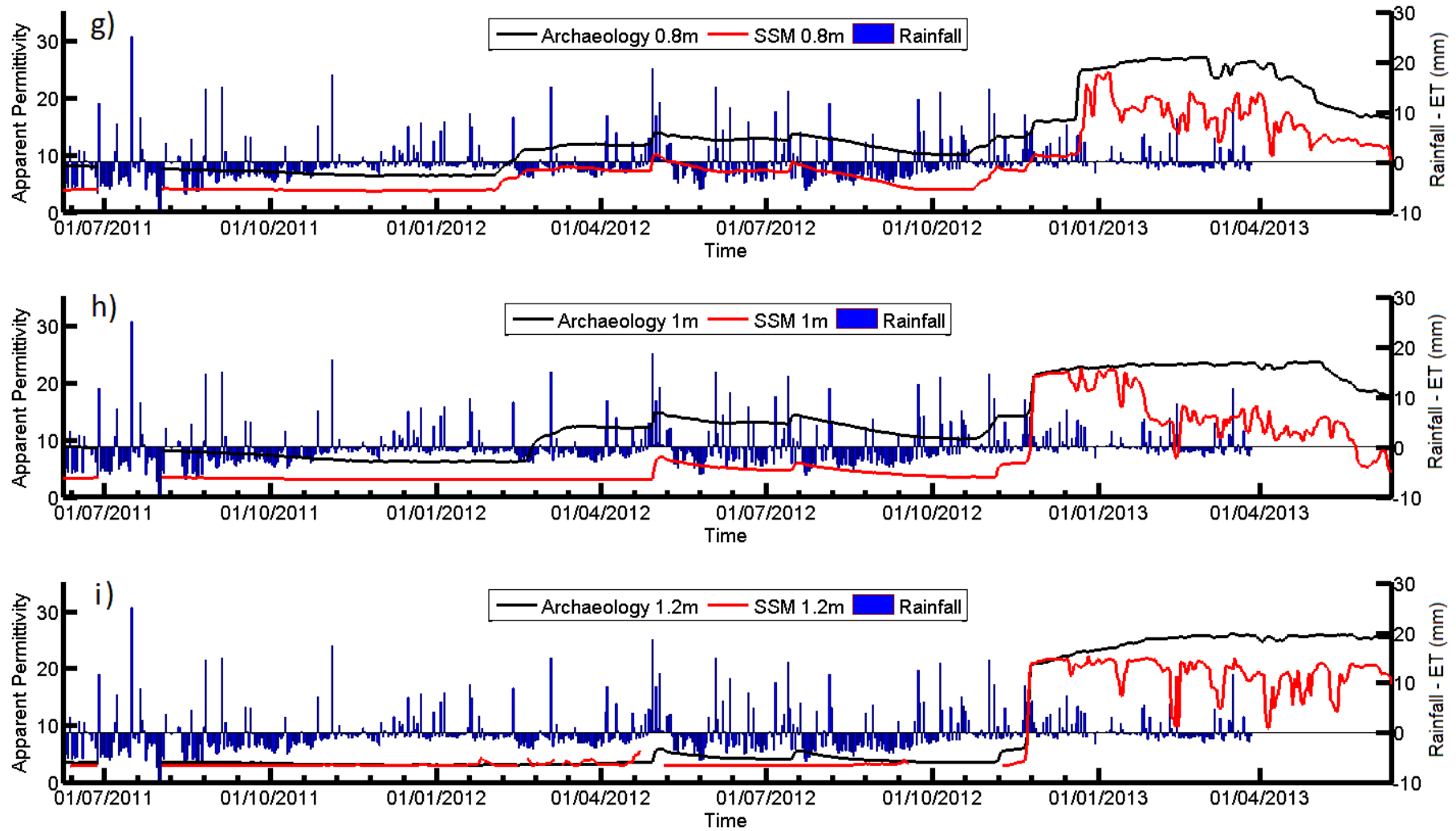
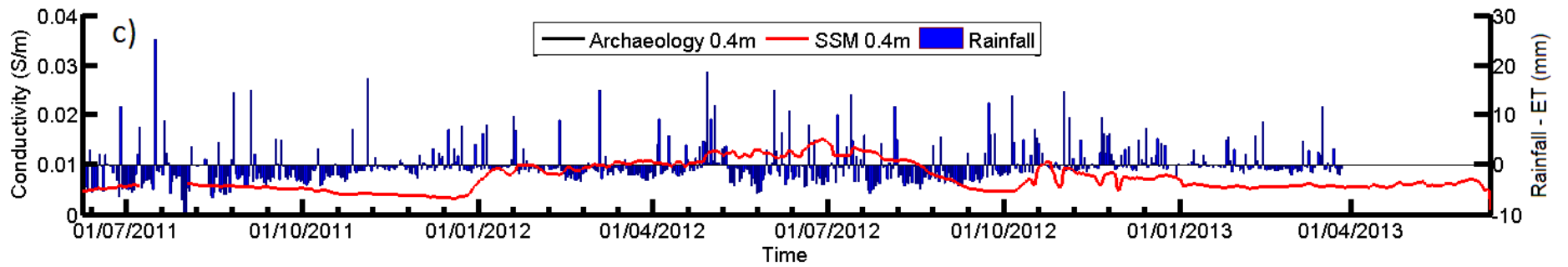
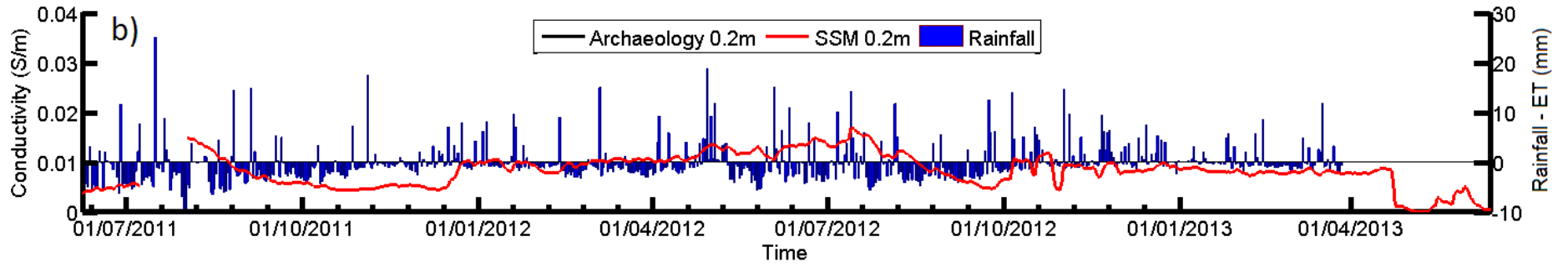
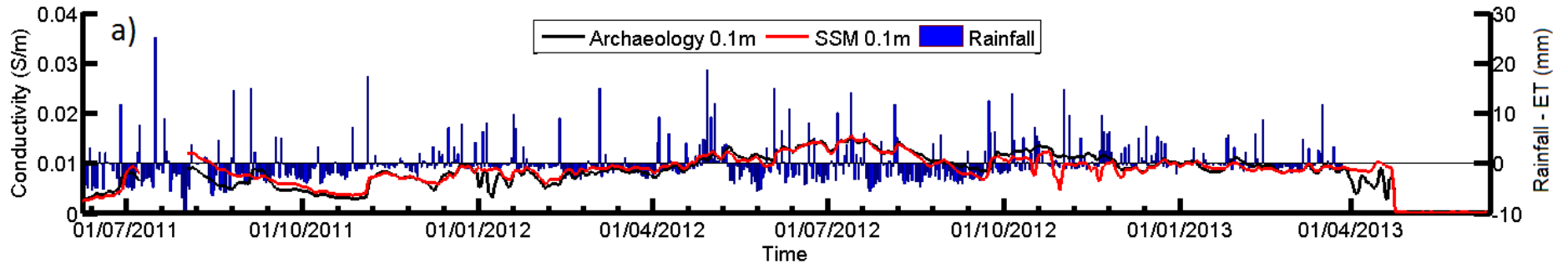
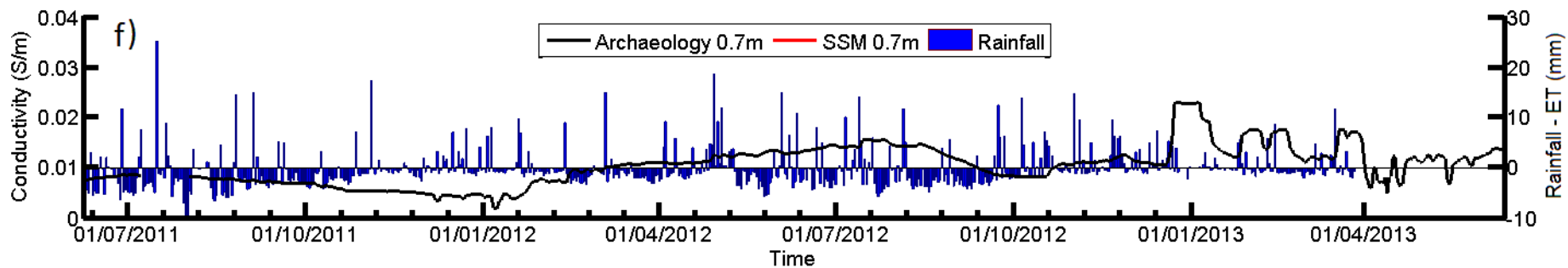
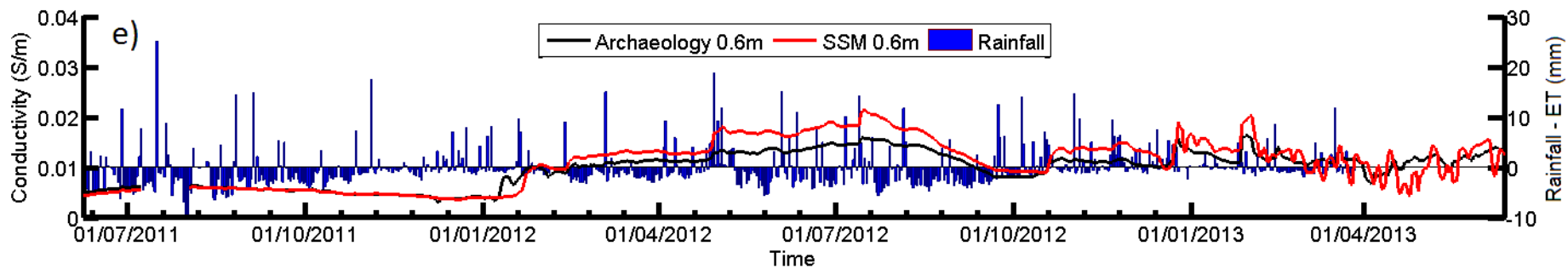
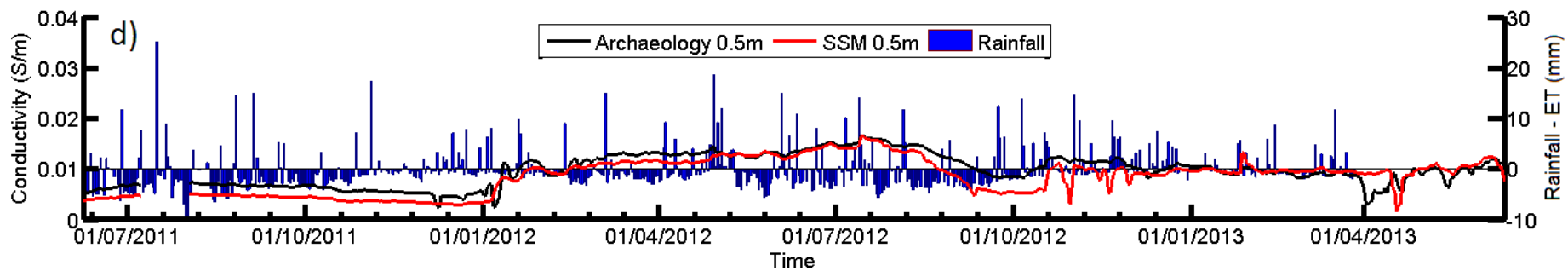


Figure 6.14: The ARDP variation on DPF over the study period at different depths a) 0.1m b) 0.2m c) 0.4m d) 0.5 e) 0.6m f) 0.7m g) 0.8m h) 1.0m i) 1.2m





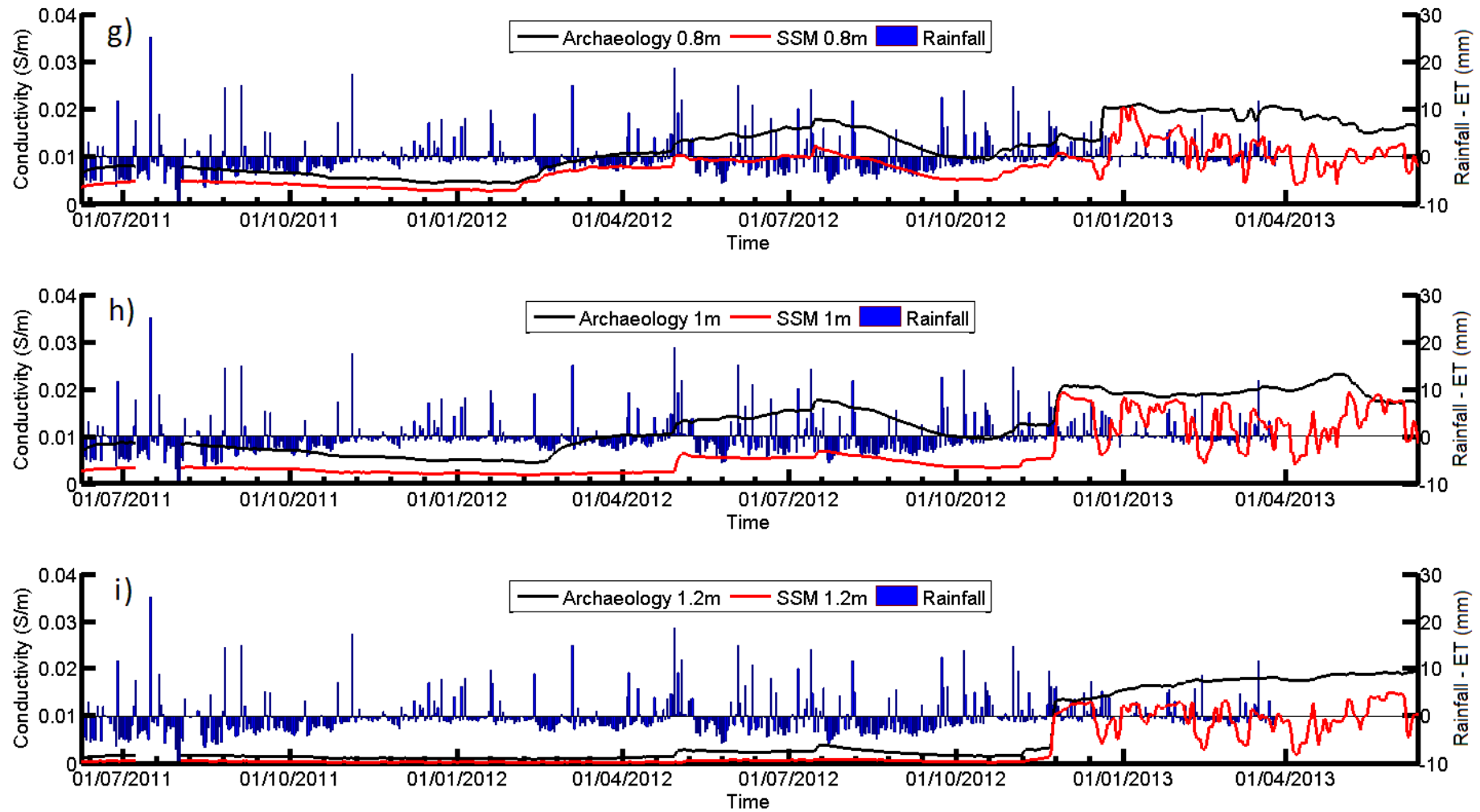
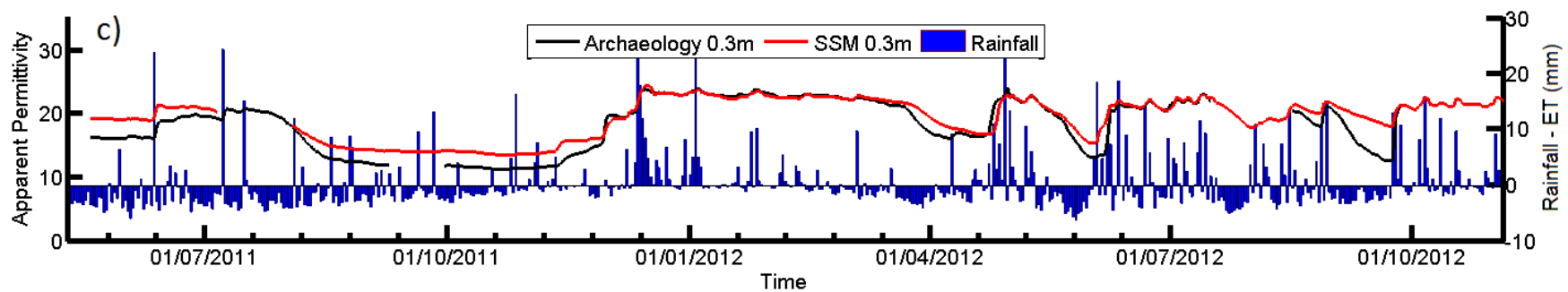
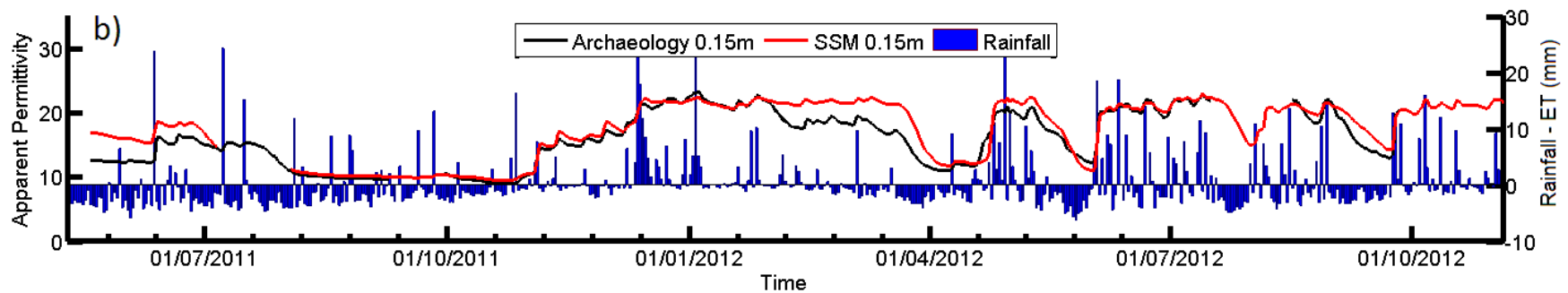
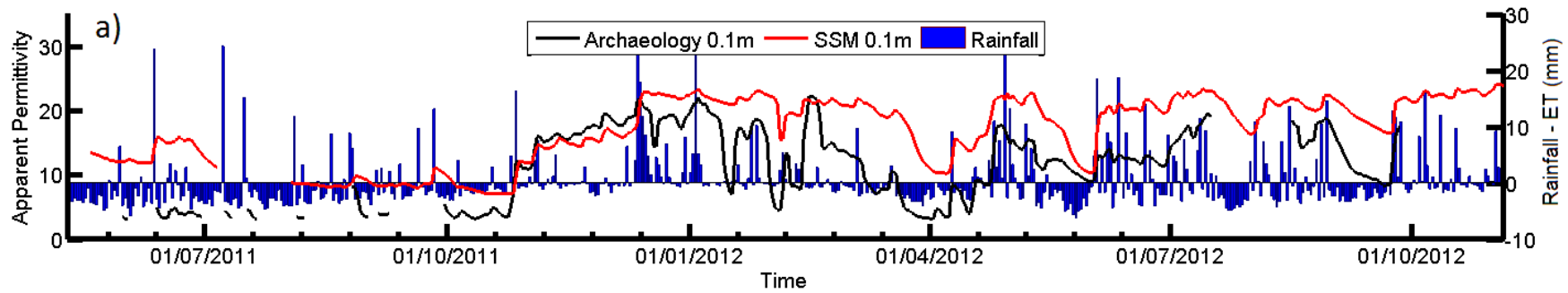
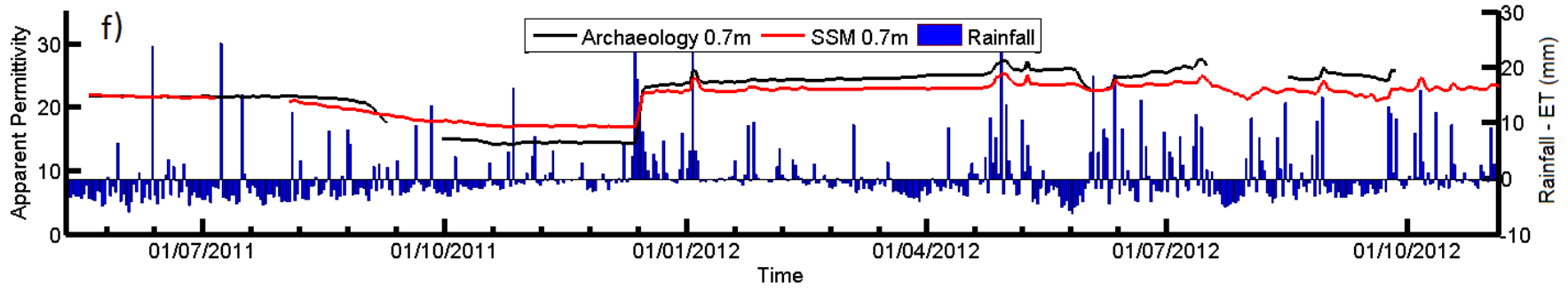
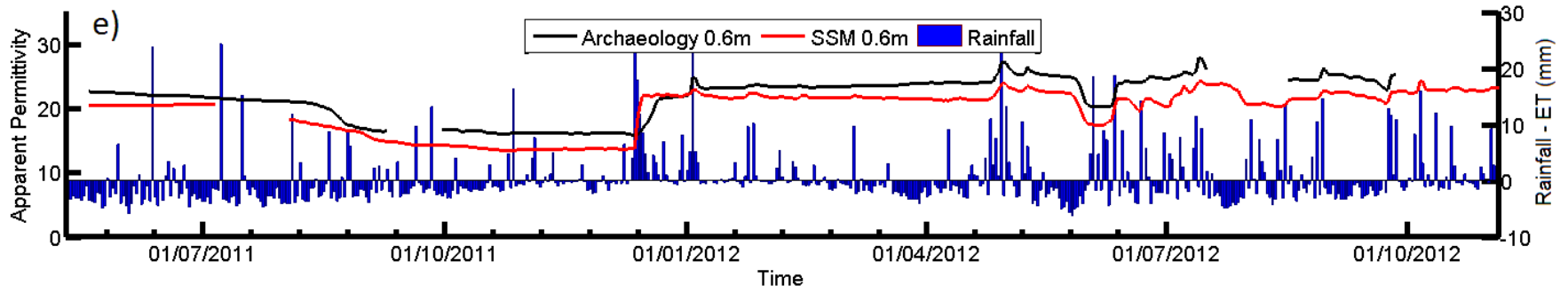
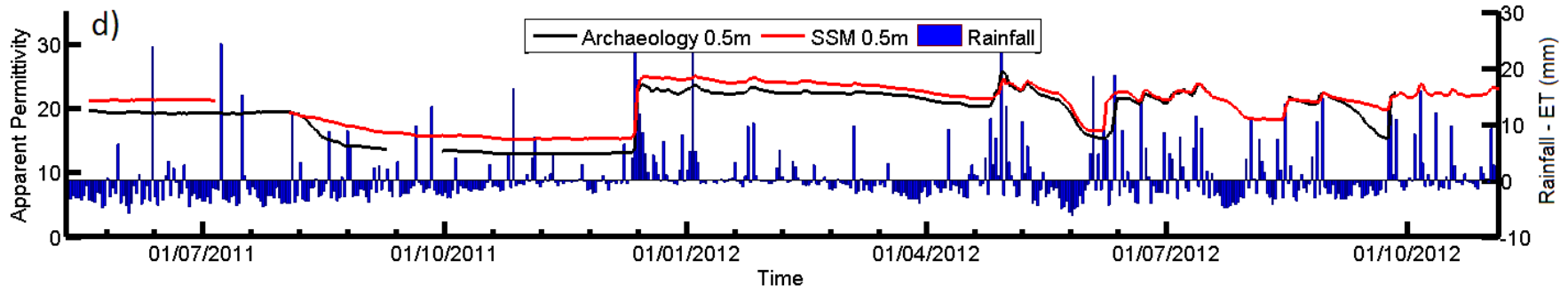


Figure 6.15: The BEC variation on DPF over the study period at different depths a) 0.1m b) 0.2m c) 0.4m d) 0.5 e) 0.6m f) 0.7m g) 0.8m h) 1.0m i) 1.2m





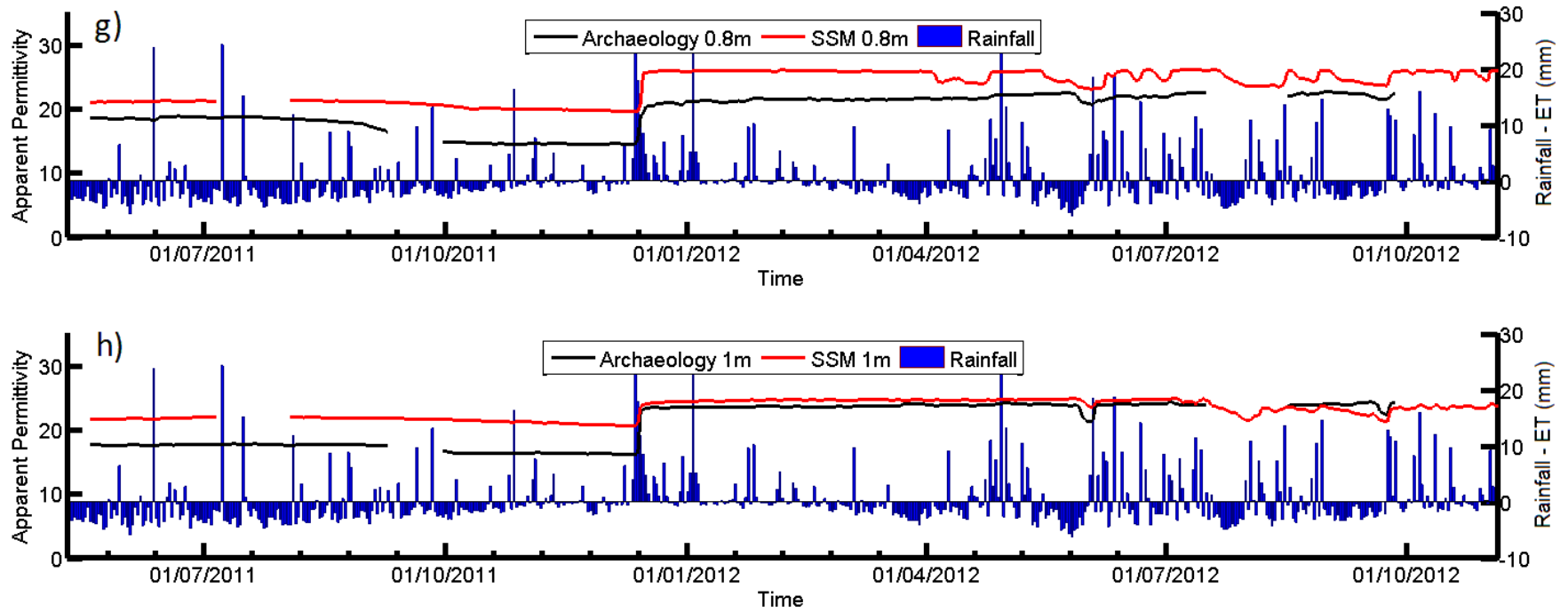
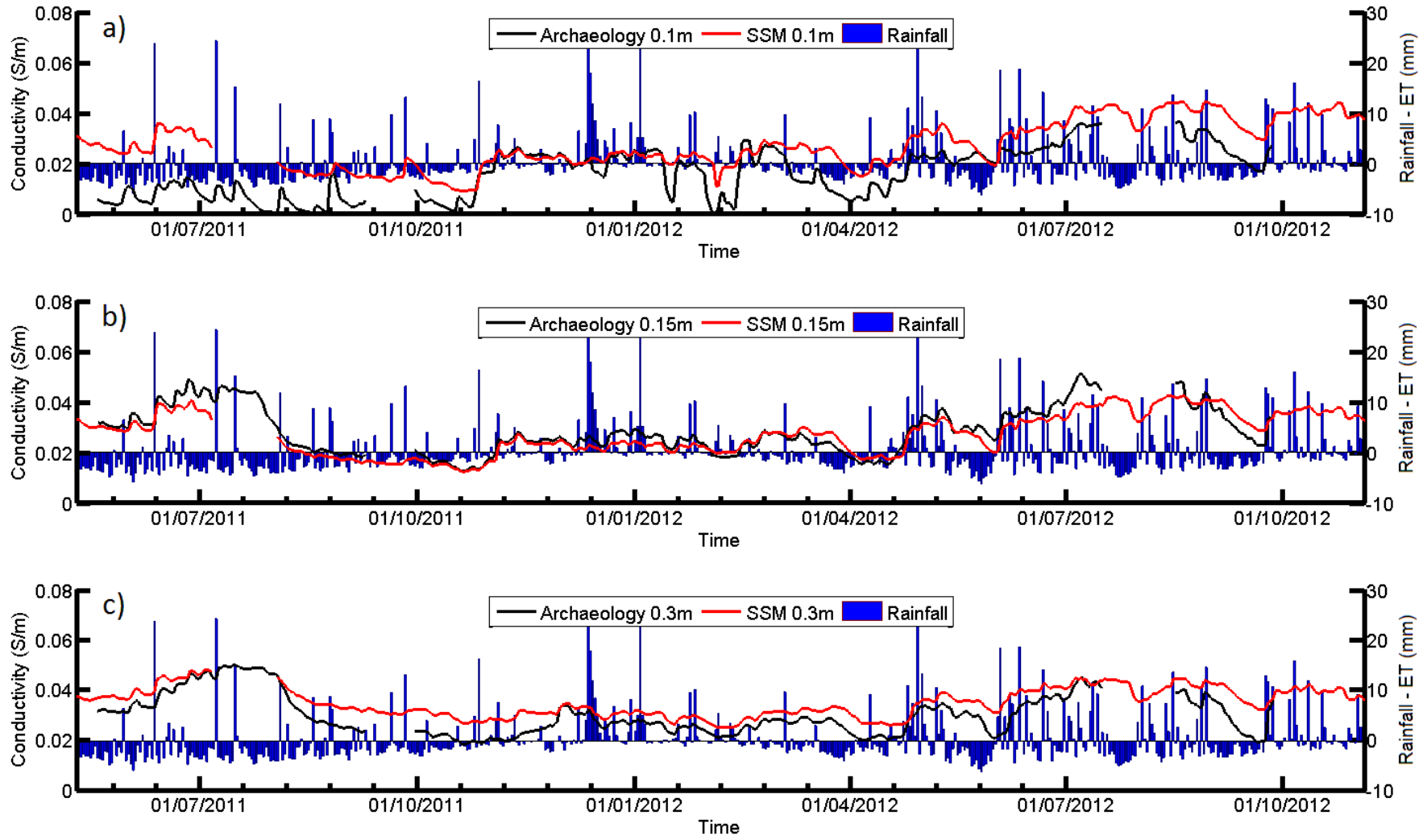
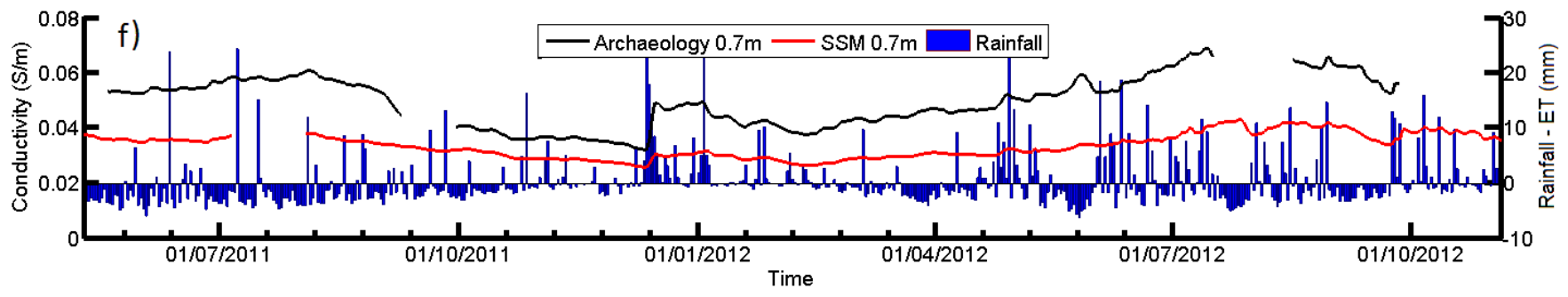
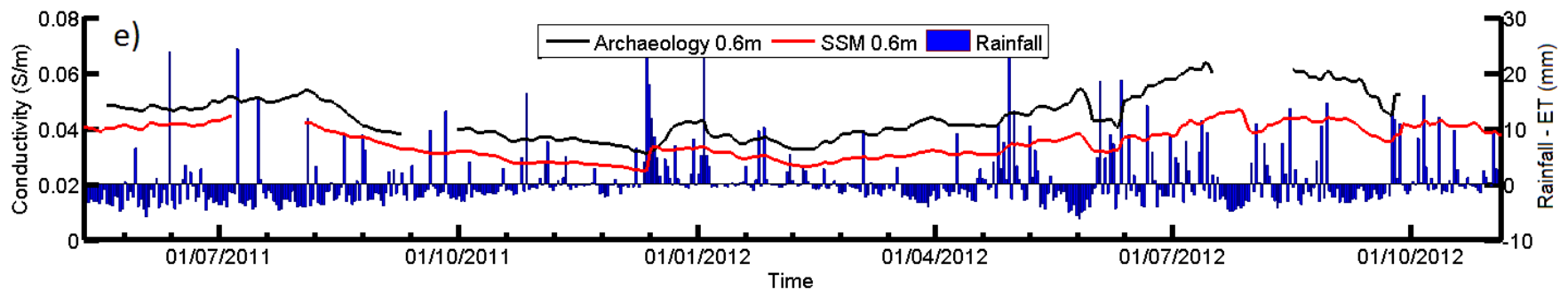
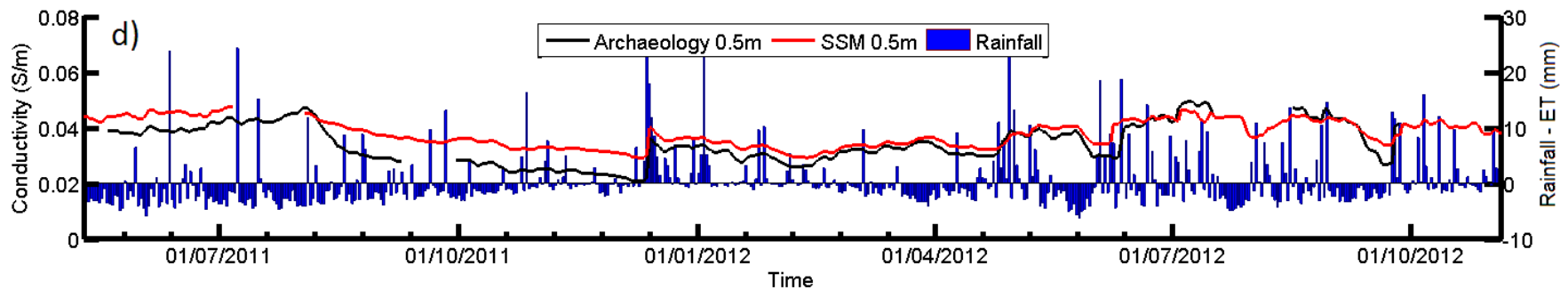


Figure 6.16: The ARDP variation on CQF over the study period at different depths between a) 0.1m b) 0.15m c) 0.3m d) 0.5m e) 0.6m f) 0.7m g) 0.8m h) 1m





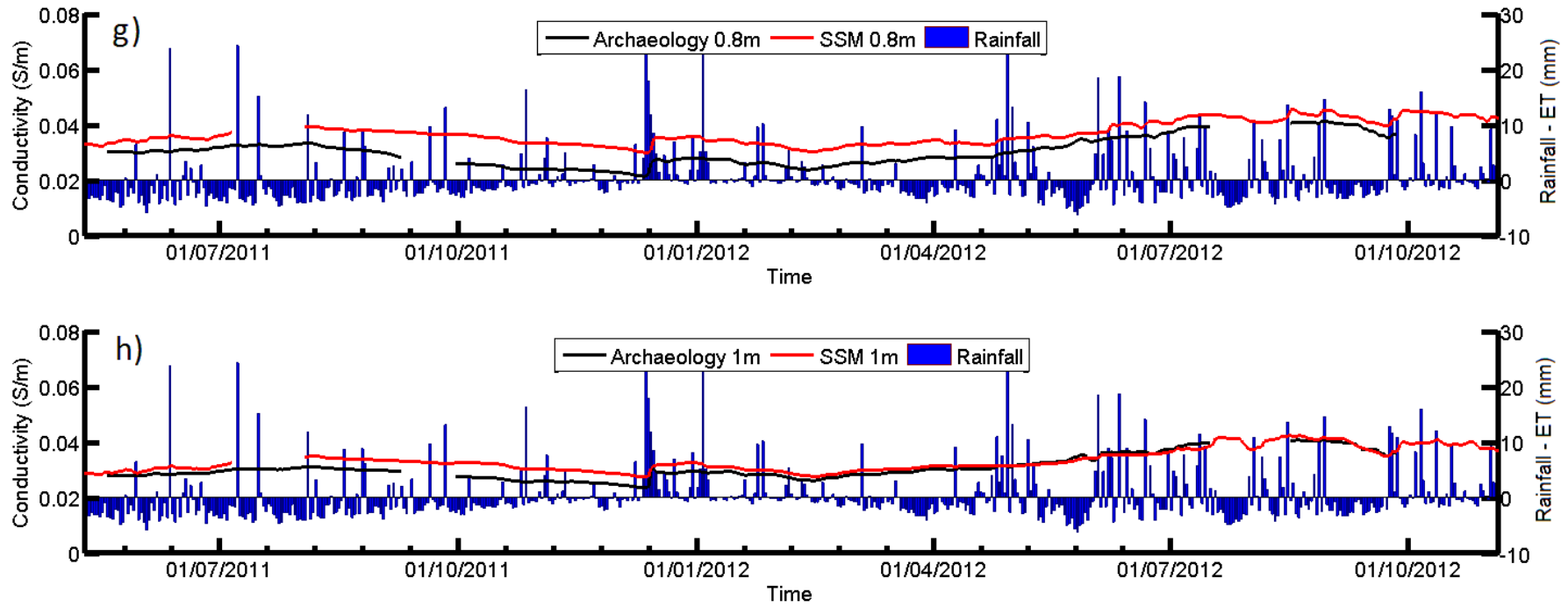


Figure 6.17: The BEC variation on CQF over the study period at different depths a) 0.1m b) 0.15m c) 0.3m d) 0.5m e) 0.6m f) 0.7m g) 0.8m h) 1m

It is important to note that in practice geophysical instruments detect anomalies relative to background values, with differences in values as a percentage of the SSM dependent on its water content at the time, causing the relative differences to change throughout the year, even if the absolute differences remain constant. It is also important to note that surface measurements are taken upon a volume of soil and although the depth of investigation can be influenced to an extent, the precise measurement volumes are unknown. For these reasons, Figures 6.18 and 6.19 show the variation in ARDP and BEC between the archaeological soils and SSM respectively, with values taken as an average of the probes at all depths and expressed as a percentage of the SSM value. Minimum, maximum and average variations are shown for each month.

Examination of the ARDP differences (Figure 6.18) show that the greatest contrasts on all of the measured sites were recorded during the dry 2011 period, where all of the soils were close to residual water content due to extensive drying and differences in the soil suction between the soil types. Interestingly, whilst the coarse grained soil shows a positive contrast during this period, suggesting the ditch is wetter, negative contrasts are recorded on the fine grained soils (DCF and CQF), suggesting the opposite trend. For DCF, this trend is reversed as the soil gets wetter although the positive contrast rarely exceeds a few percent of the SSM value, highlighting similarity of the soil properties in the two soil profiles with only a slightly higher water holding capacity in the archaeological soils. However, it seems likely that the earlier negative contrast was caused by the greater drying effect on the archaeological soils due to their faster drying from larger pores which was seen throughout the monitoring period during extended dry periods (see earlier). The comparatively large contrasts in April 2012 in comparison to the later part of the year were likely to be the result of the above mentioned differences in the movement of the initial wetting front in the dry SSM and archaeological soils. Unlike DCF, the contrast between the CQF soil profiles remained negative over the whole monitoring period due to the effect of the top ditchfill (Ditchfill1) and shallower SSM

soil which showed a greater field capacity due to their PSD and density as discussed earlier. However the size of these contrasts is smaller during the wet period in 2012, suggesting that the soils had similar saturated water contents. Over the monitoring period as a whole, the coarse grained DPF site showed a much greater difference between the archaeological soils and SSM (usually 20%-40% of the SSM values) with much smaller variations shown on the fine grained sites (< 10%), especially during the wetter 2012 period. These findings are unsurprising as coarse grained soils are known to be more responsive to geophysical techniques and the differences in soil texture and density which affect the holding capacity of the soil were greater.

The contrast in BEC (Figure 6.19) followed similar trends to the ARDP contrasts for all sites, confirming the importance of water content to BEC values, but also showed some influence of temperature. This is most notable for DCF during the summer months 2012 where ARDP differences were consistently minimal positive values between May and December but BEC responses are a much bigger during July and August due to the higher temperature, which was previously shown in Section 5.5.5 to affect the DCF Ditchfill1 soil more than the SSM.

Differences in soil temperature trends are looked at in Section 6.5, but it is important to note that higher temperatures affect the contrast even if no temperature differences exist between the archaeological and SSM soils, as variations in BEC due to water content are magnified due to the increased temperature effect in wetter soils (see Section 5.5.5). Temperature seemed to have a smaller effect on the DPF contrast, which followed the ARDP data more closely and it seems likely that this is the result of the smaller temperature dependence of coarse grained soils due to their lower ionic content discussed in Chapter 5. Unusually, virtually no differences on CQF can be observed during May to August 2012 despite negative differences in the ARDP data over the same period suggesting a difference in the absolute water content. However, as the soils in question were not included in the laboratory work in Chapter 5, no knowledge is available on VWC-ARDP-BEC relationships and it is possible that BEC is higher in the SSM at the

same VWC. This may be supported by the differences in the ionic contents of the soil which are substantially larger in the SSM (Section 5.3).

A summary of the seasonal response of the geophysical properties of the soil is as follows:

- The two fine grained sites gave higher values for both BEC and ARDP than the coarse grained DPF soil. This was due to both their higher water holding capacity and differences in their relationships between VWC and EM properties which were discussed in Chapter 5.
- All of the studied sites showed a dry period during 2011 and a wet period with no intermediate period suggesting the soil is either saturated or dry and characterised by high and low ARDP values respectively. BEC data followed similar trends to the ARDP data, being affected principally by water content, but also showed variation which followed the air temperature patterns. These temperature effects were more apparent on the fine grained sites in line with the findings of the laboratory work presented in Chapter 5.
- Rainfall events rarely affected below the surface soils on any of the sites with the greatest fluctuations in geophysical properties occurring in the top 0.3m. Infiltration to greater depths was only noted after periods of extensive drying on the surface which causes the soil to shrink and pores to open. Few notable differences were found in infiltration patterns between the archaeological soils and SSM, except for during the initial infiltration after the dry period, especially on DCF. It is likely therefore that infiltration is dependent on the antecedent water content with large differences only noticeable in very dry soils.
- For fine grained sites, archaeological soils have greater variation and dry both faster and to a greater extent after extended periods of high ET. This is thought to be the result of the lower density and greater porosity of these soils which allows the water

to escape more freely. The opposite was true for DPF, with the coarser grained SSM drying quicker due to the larger pores in these gravel soils.

- Long term differences between the archaeological and SSM soils on all sites seems to be a function of the different soil water potentials and ability to hold water between the two soils. This is heavily dependent on the SSA and therefore the clay content and mineralogy and organic matter, as well as the porosity of the soil. The differences in these properties were smaller on the fine grained sites.

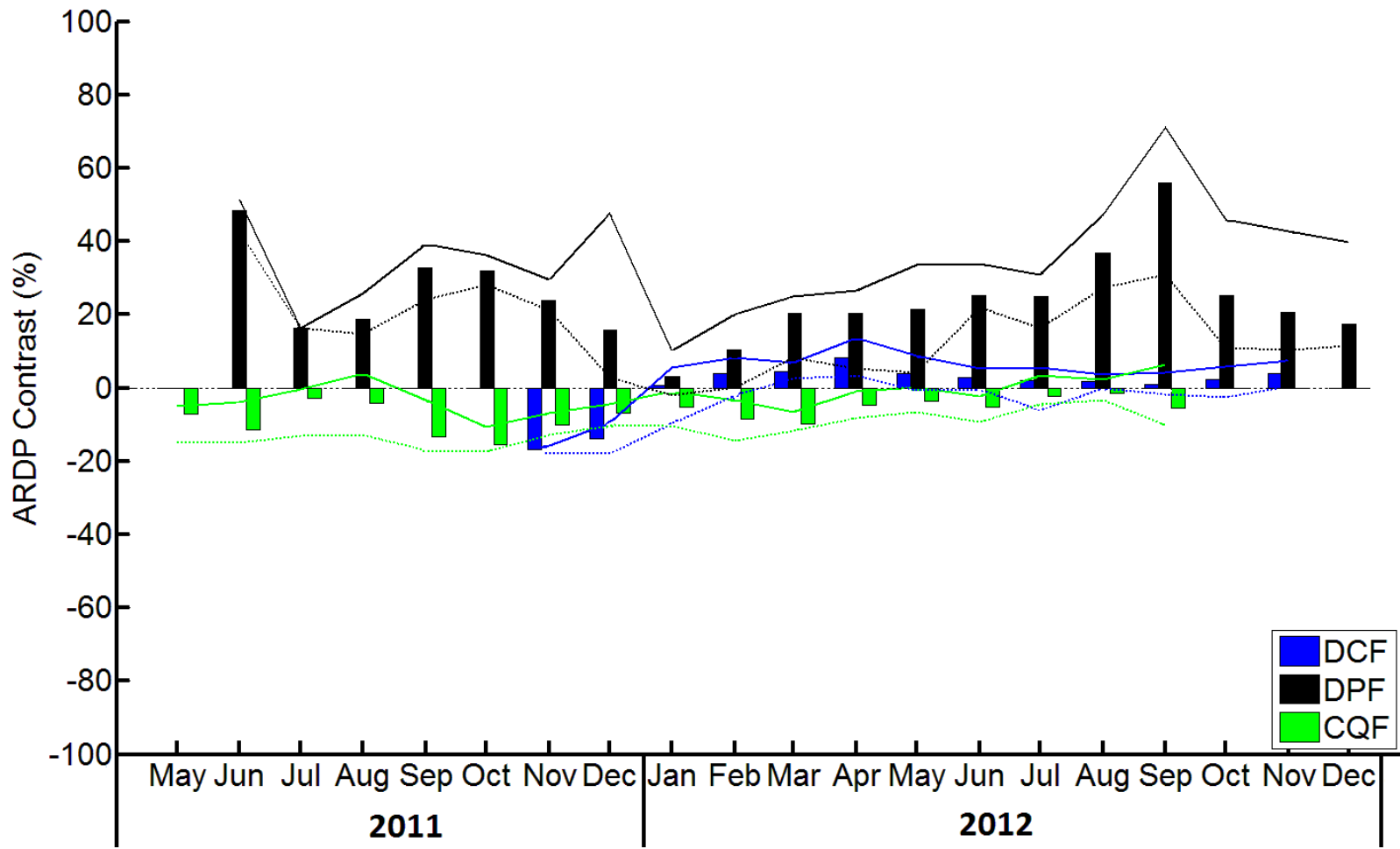


Figure 6.18: Average ARDP contrast as a % of the average SSM value for each month of monitoring over the three studied sites. The maximum (solid line) and minimum (dotted line) contrast values are also shown for each month

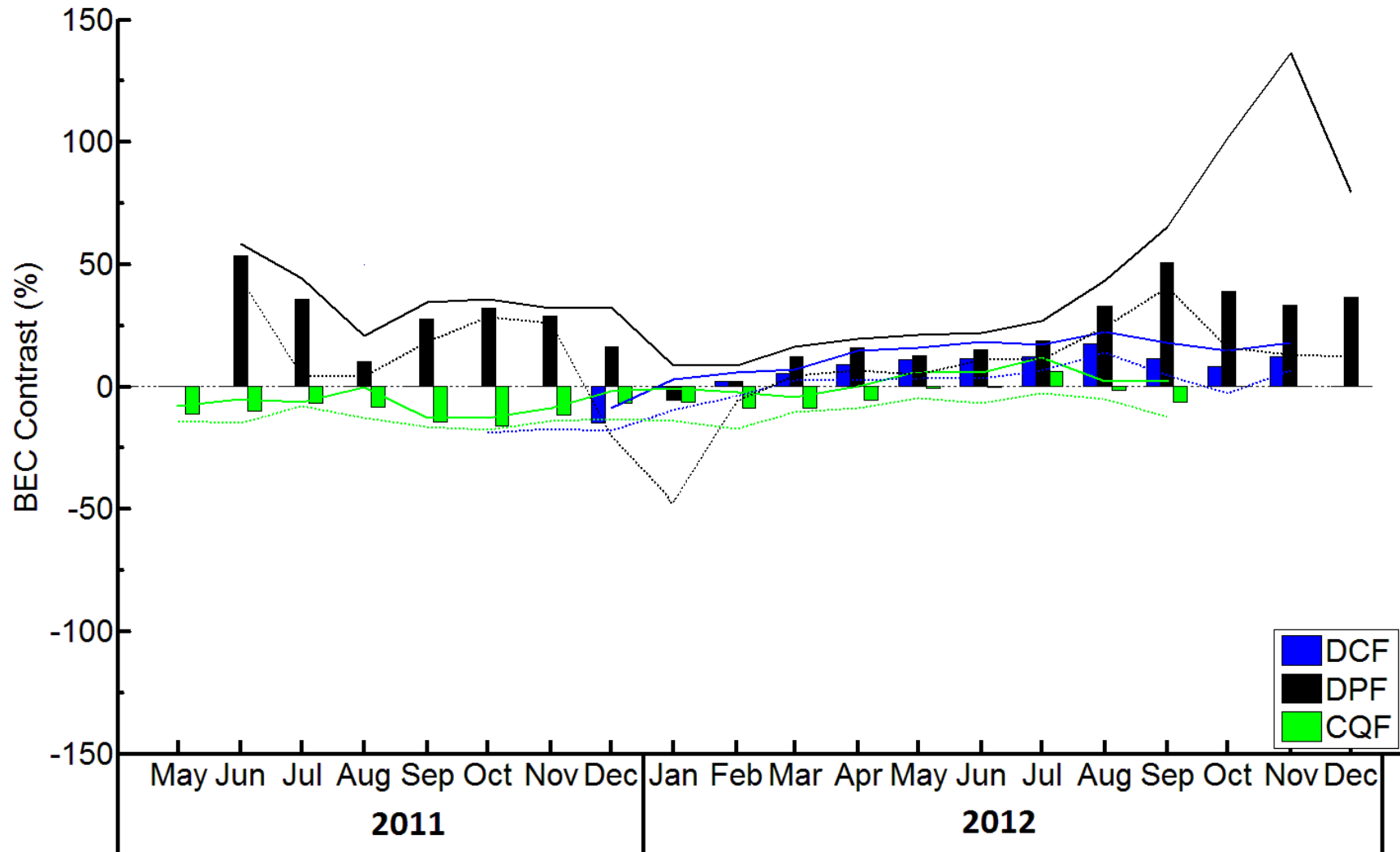


Figure 6.19: Average BEC contrast as a % of the average SSM value for each month of monitoring over the three studied sites. The maximum (solid line) and minimum (dotted line) contrast values are also shown for each month

6.5. Seasonal Variations in Temperature

This section describes the variation in soil temperature over the monitoring period for both the archaeological soils and the SSM, which is important as it affects geophysical properties, especially BEC. Probes from the same depths and soils have been averaged to give a clear view of the seasonal variation. In addition, in order to produce clearer plots, data in this section have been averaged over 24 hour periods to give daily values. Any diurnal variations have therefore been removed, although these are examined in greater detail in Section 6.6. The daily average air temperature and rainfall data has also been included for comparative purposes. Figures 6.20-6.22 show soil temperature data at a number of different depths for all three sites during the whole monitoring period. More site specific analysis and details for each site can be found in Appendix G, but some of the general behaviour and key differences between sites are discussed here.

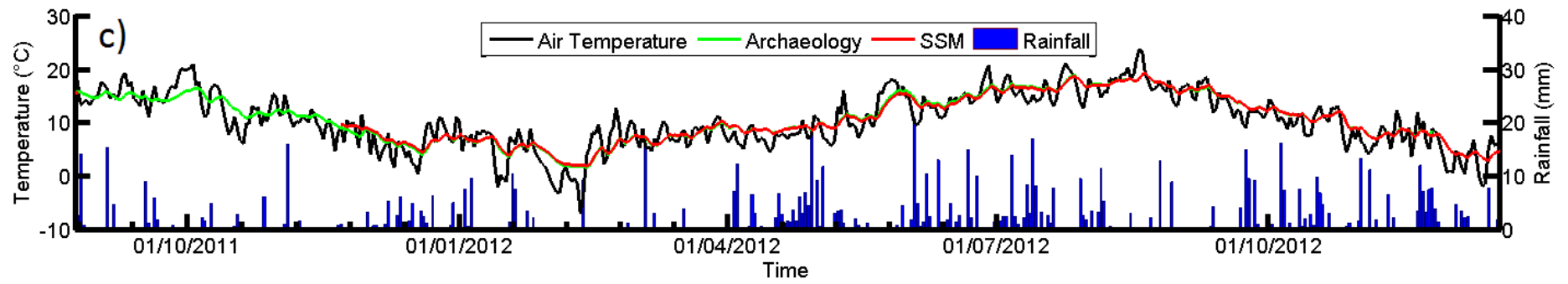
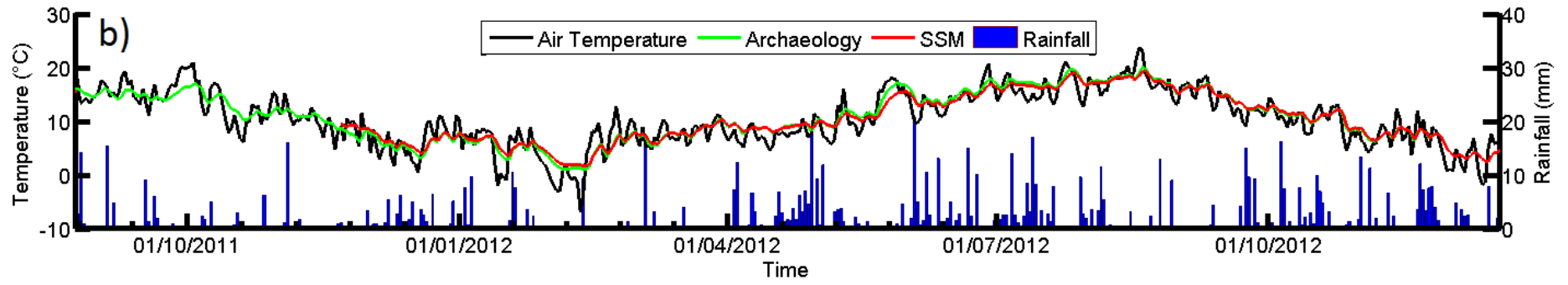
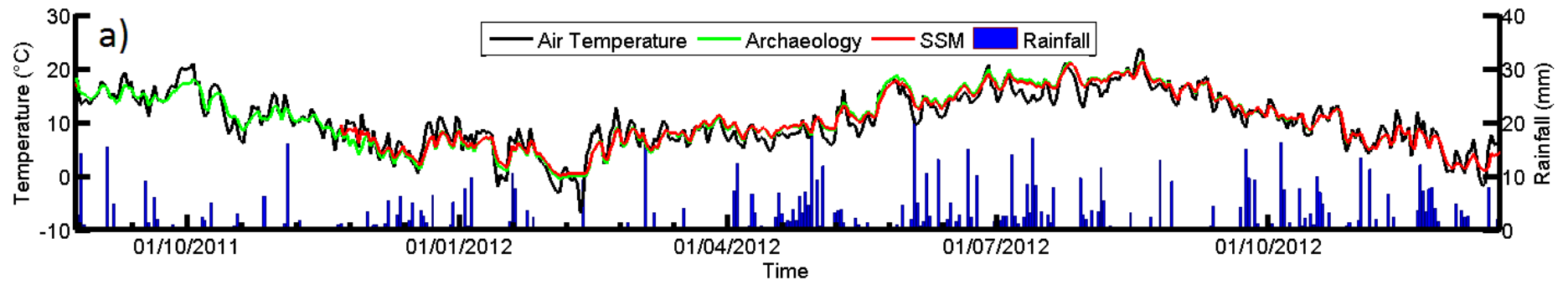
Several observed behaviours were apparent on all of the studied sites, and were applicable regardless of different soil types. On every site, both the archaeological soils and SSM showed similar overall trends in measured temperature, which closely followed the seasonal variation of measured air temperature. This meant higher and lower soil temperatures at all depths were observed in the summer and winter months respectively. However, the measured soil temperature changes were smaller than changes in the average air temperature, giving higher temperatures in the soil during the winter months in comparison to the average air temperature and lower soil temperatures during the summer months. These findings are consistent with the findings of other authors who have measured soil temperature seasonally on a wide range of different soils (Curioni, 2013, Davidson et al., 1998, Skierucha et al., 2012) and occurred due to the higher thermal inertia of the soil particles in comparison to the air (Florides and Kalogirou, 2009). It is also worth noting that in addition to these seasonal trends, smaller scale variations in air temperature took place on a day by day basis. Whilst these had a significant effect on the near surface soils, the deeper measured soils were found to show less

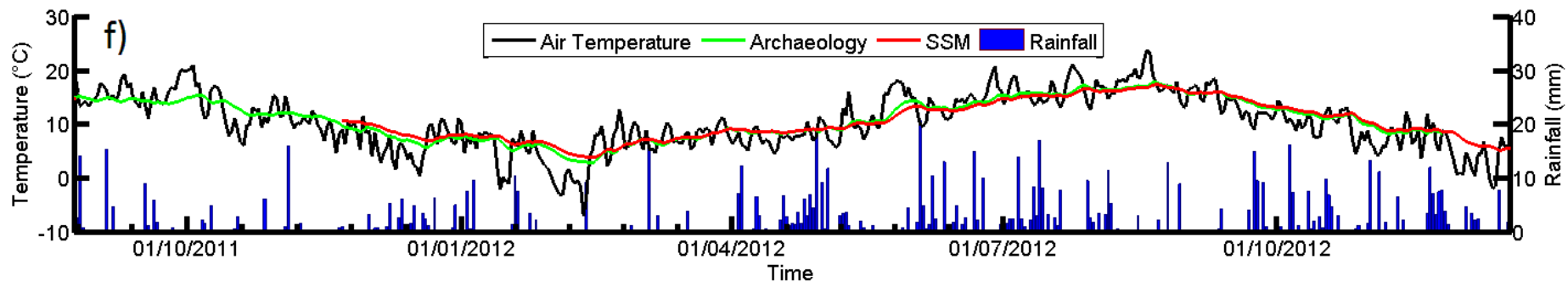
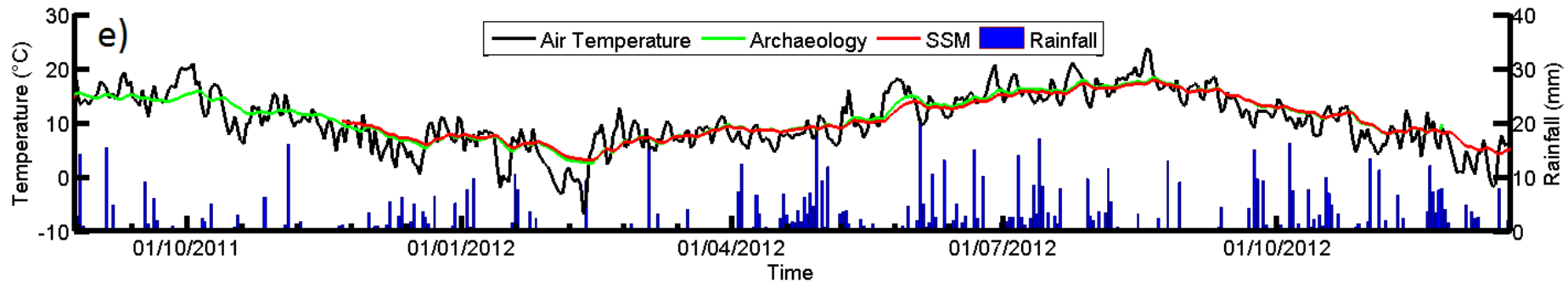
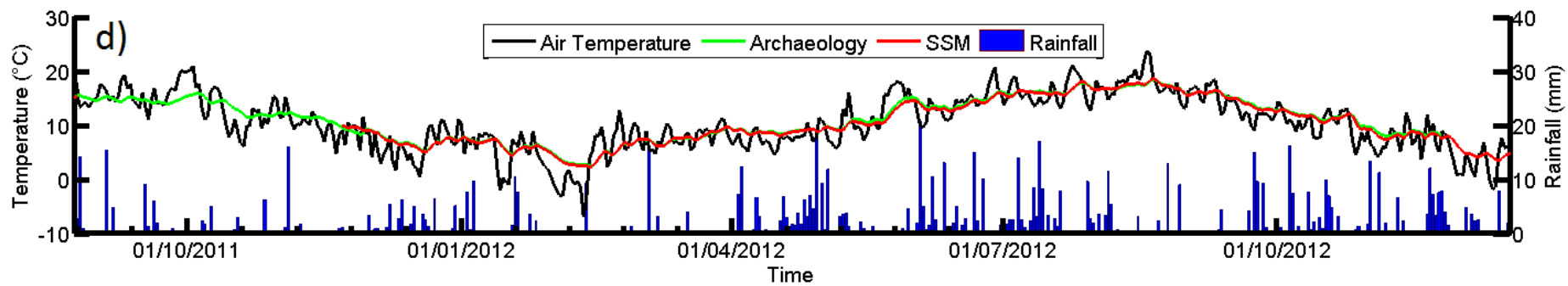
variability and in only followed the broader seasonal trends and showed smaller changes in relation to the air temperatures. This increasingly limited soil temperature variability as a function of depth is a known phenomenon (Florides and Kalogirou, 2005, Mohanty et al., 1998, van Manen and Wallin, 2012) with the upper soil commonly stated to be the most affected by small scale daily changes in the air temperature, although opinions on the depth at which these daily variations are effective varies. Interestingly, these small scale variations could be observed at greater depths on the coarse grained soils from DPF (approximately 0.5m; Figure 6.21b) than in the fine grained soils from DCF and CQF (approximately 0.3m; Figures 6.20c and 6.22c). This seems to be a function of the greater thermal diffusivity and lower thermal inertia of coarse grained and dry soils (Farouki, 1981, Scollar et al., 1990) which, for the unsaturated case, contain more air than those with fine grains. This made the soil more able to respond to temperature changes from the surface. Finally, it should be noted that the soils at greater depths showed increased lag between changes in air temperature and changes in the soil temperature. This finding was also observed by Florides and Kalogirou (2005, 2009) and van Manen and Wallin (2012) and will be examined in greater detail in Section 6.6.

Whilst both the archaeological soils and SSM on all sites showed similar behaviour in respect to these observed trends, several significant differences were noted between the two soil types on each site which gave rise to thermal contrasts at particular times of the year. On all sites, the archaeological soils were found to show both a slightly stronger response to temperature fluctuations, especially in the near surface, as well as well as a slightly shorter lag time between changes in the air temperature and soil temperature. This seems to suggest a lower thermal inertia and greater thermal conductivity in archaeological soils in comparison to the SSM. Interestingly, these differences between the archaeological profile and SSM occurred even at depths where the probes were located in the same soil (e.g. the topsoil or subsoil) suggesting that these soils were not homogenous. One possibility is that these soils were affected by differential saturation which was shown by differences in measured ARDP in

Section 6.4 which would affect the air-water ratio of these soils and therefore their thermal conductivity and inertia, although no notable differences were often visible.

The temperature contrasts between the average daily values over time for a number of depths are shown in Figure 6.23. It can be seen that for all sites, the greatest contrasts existed between the soils in the near surface (0.1m; Figure 6.23a), although these differences were also less predictable than those at greater depths due to the effects of small scale daily temperature fluctuations. The biggest negative contrasts variations occurred for all depths and sites in February and the biggest positive contrasts at the end of May to early June. Both of these periods coincided with a period of a few days where the average daily temperature was consistently high or low. Outside of these periods, temperature differences were minimal at depths of 0.5m and below (Figure 6.23b-c), suggesting that several days of stable high or low temperatures are needed to create significant contrast below the surface. It also appears that greater contrasts between the archaeological and SSM were found on sites with fine grained soils (DCF and CQF) in comparison to the observed contrasts on the coarse grained site (DPF), which rarely exceeded the margin of error on the temperature probes. However, the temperature on DPF was likely to have been affected by the grass on the surface which has reduced the measured temperature changes in subsurface soils in contrast with the bare soil on DCF and CQF.





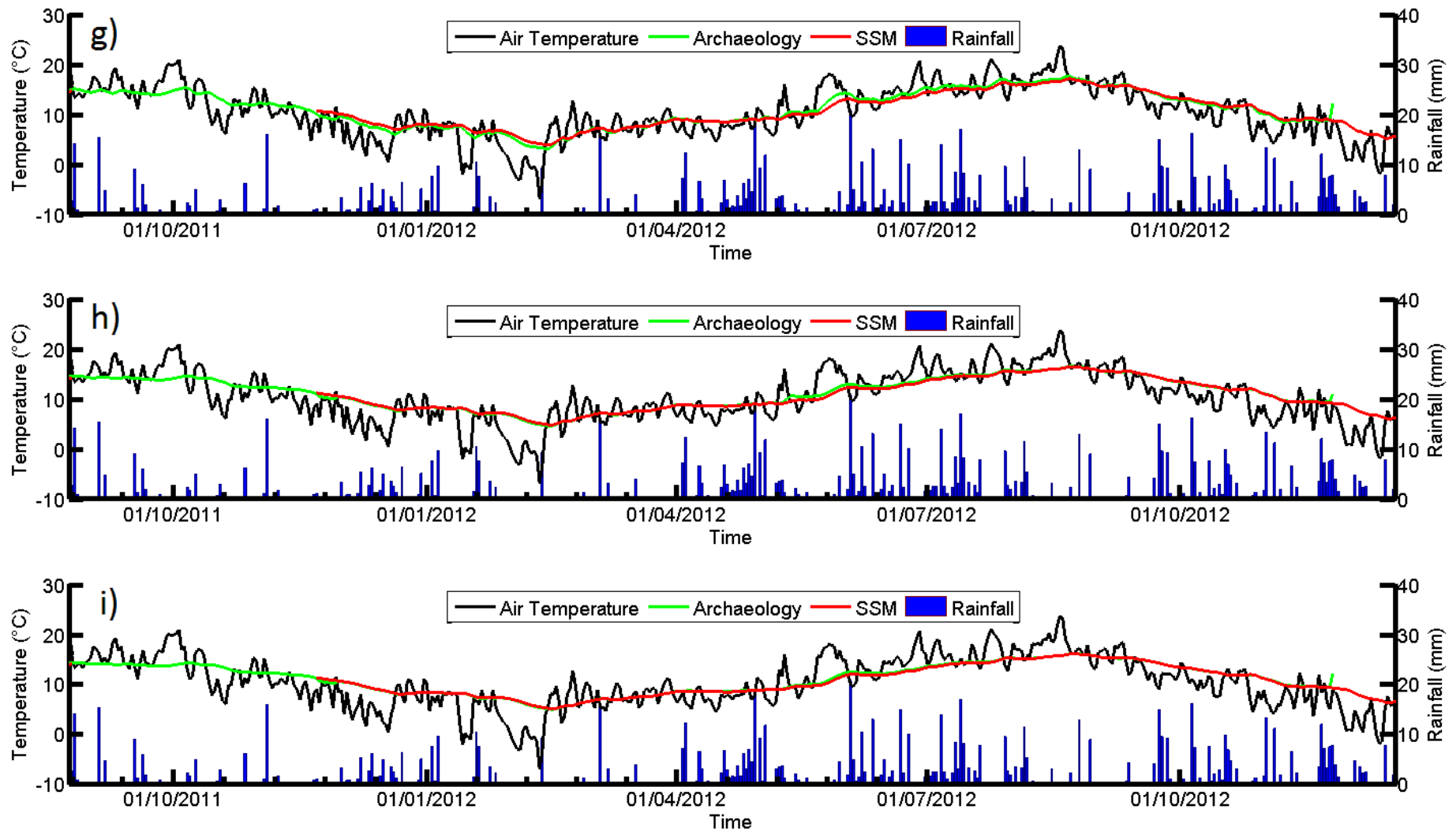
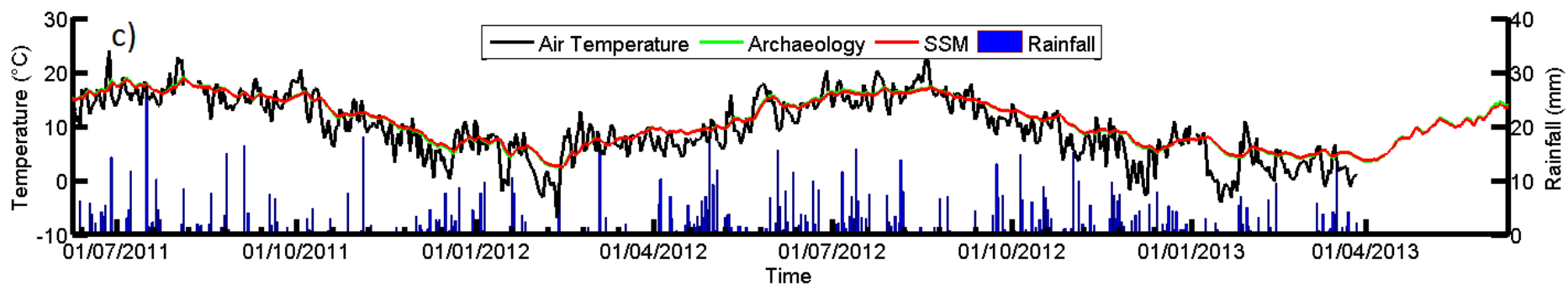
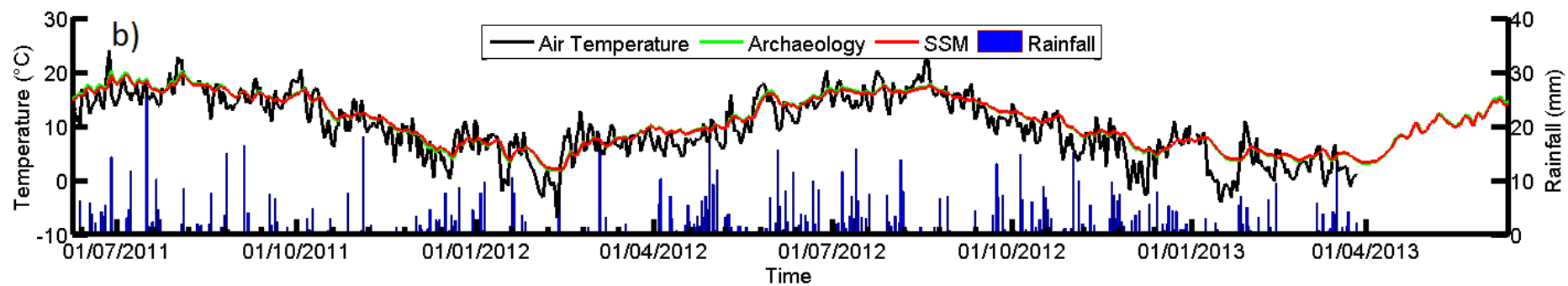
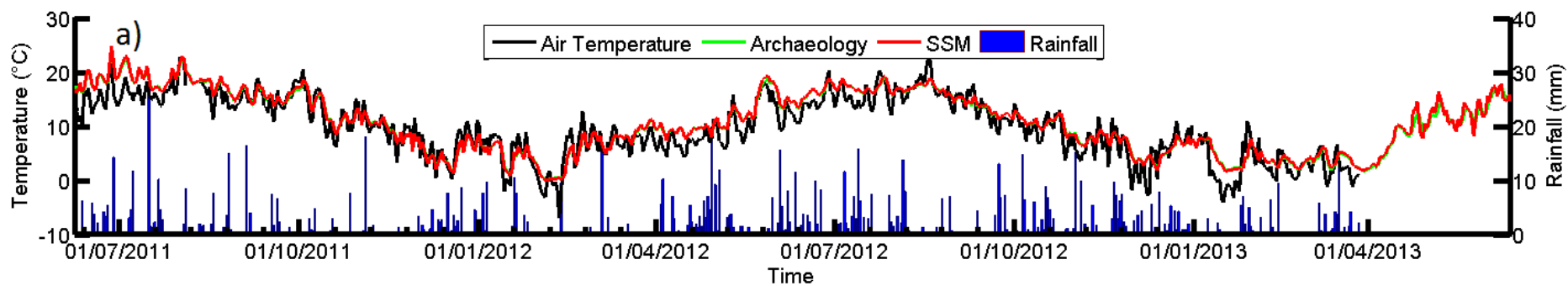


Figure 6.20: The seasonal variation in temperature on DCF at different depths a) 0.1m b) 0.2m c) 0.3m d) 0.4m e) 0.5m f) 0.6m g) 0.7m h) 0.9m i) 1m



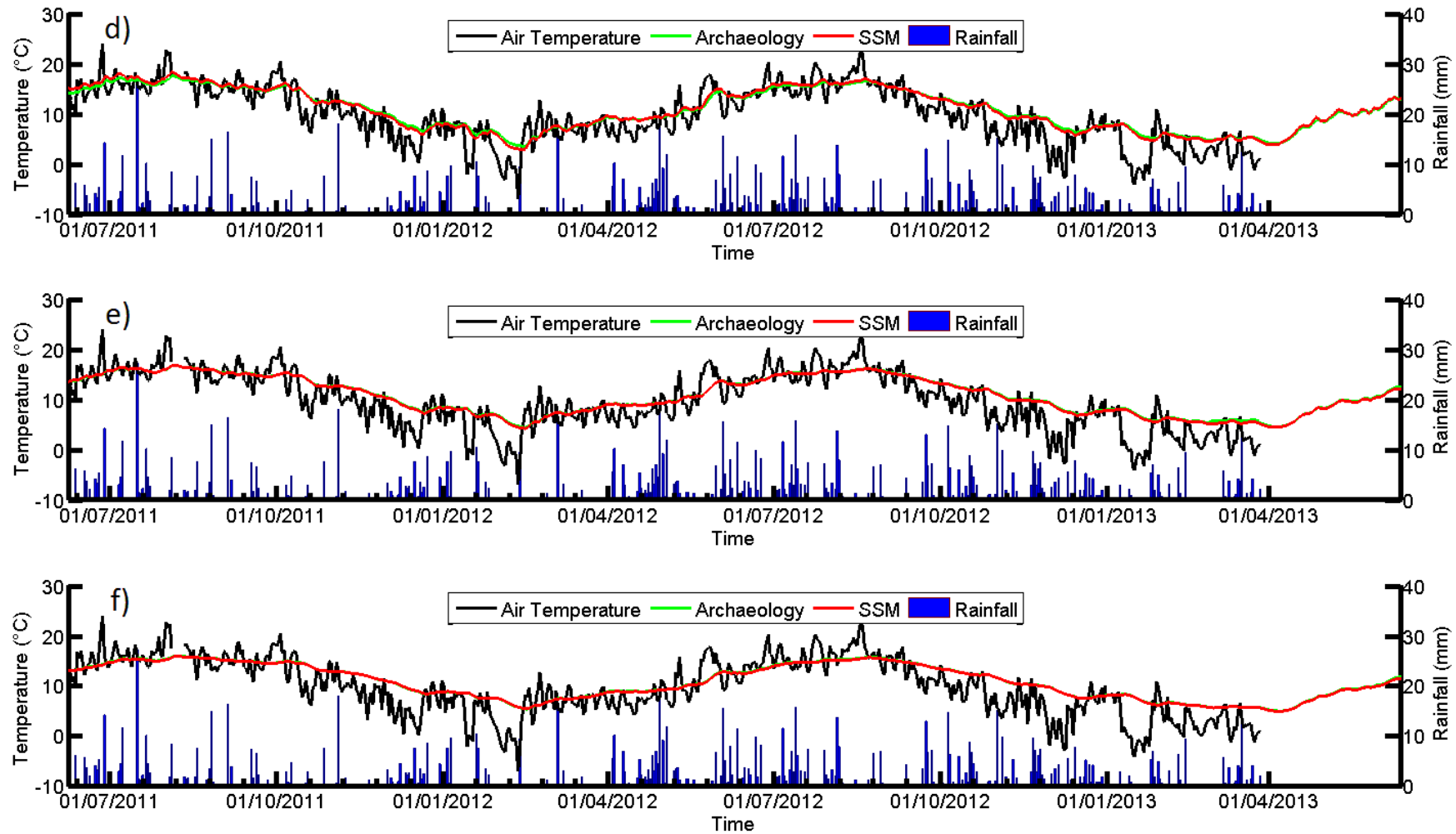
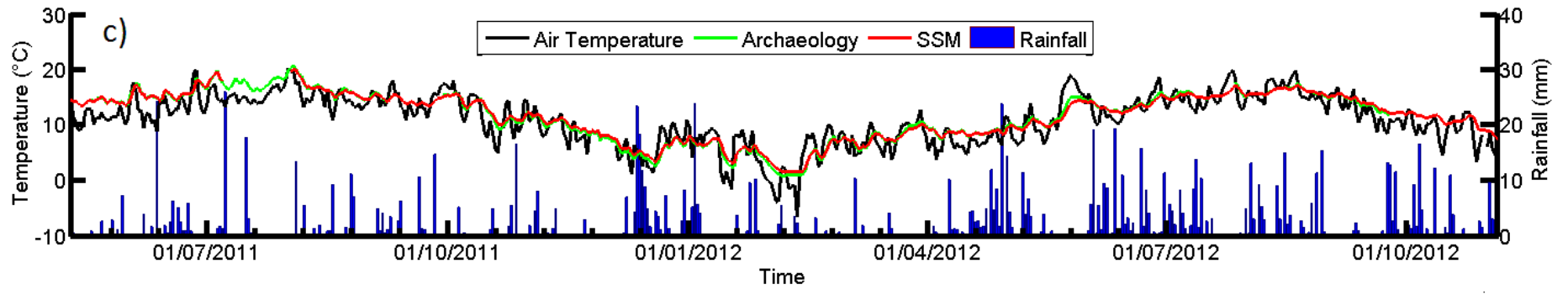
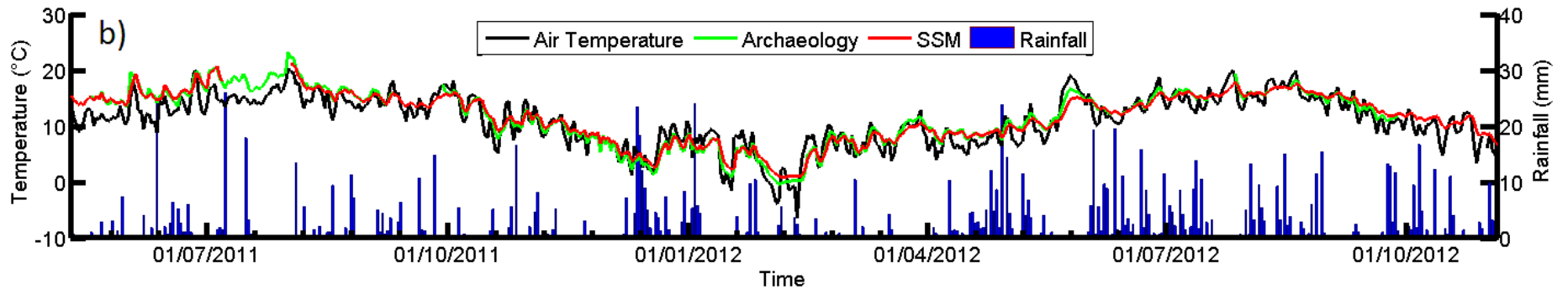
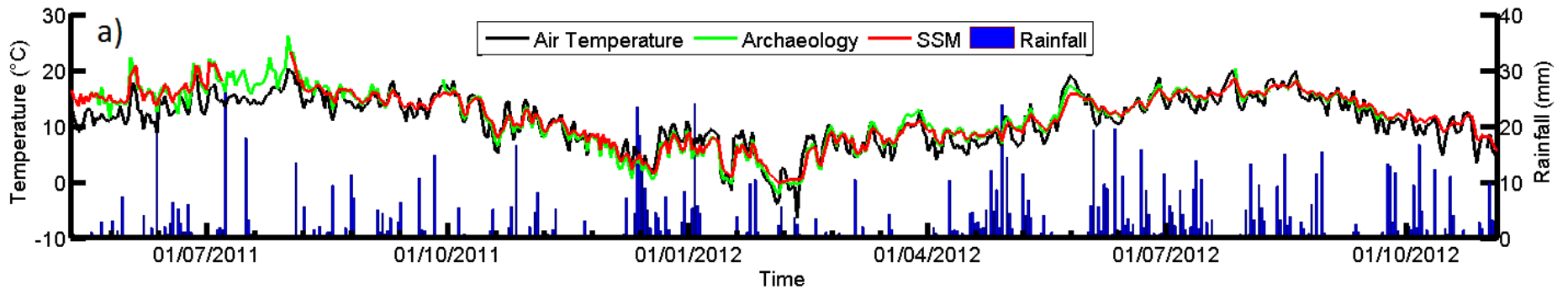
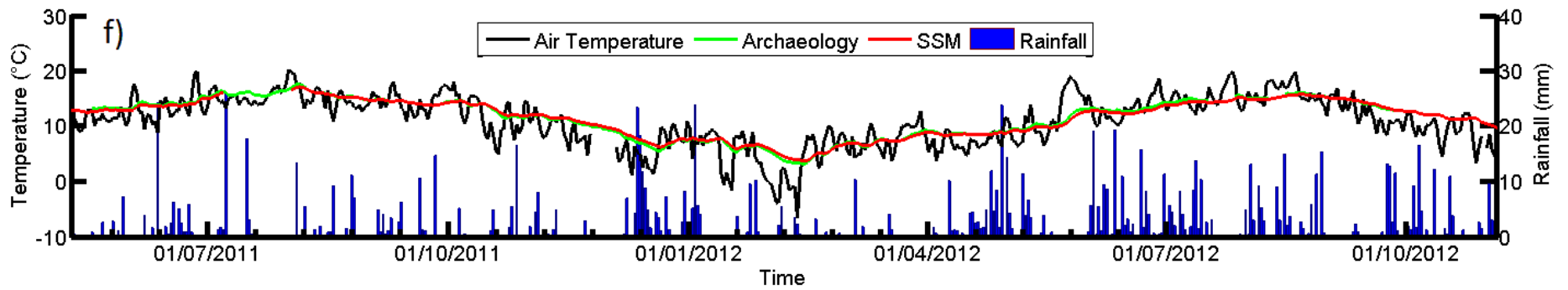
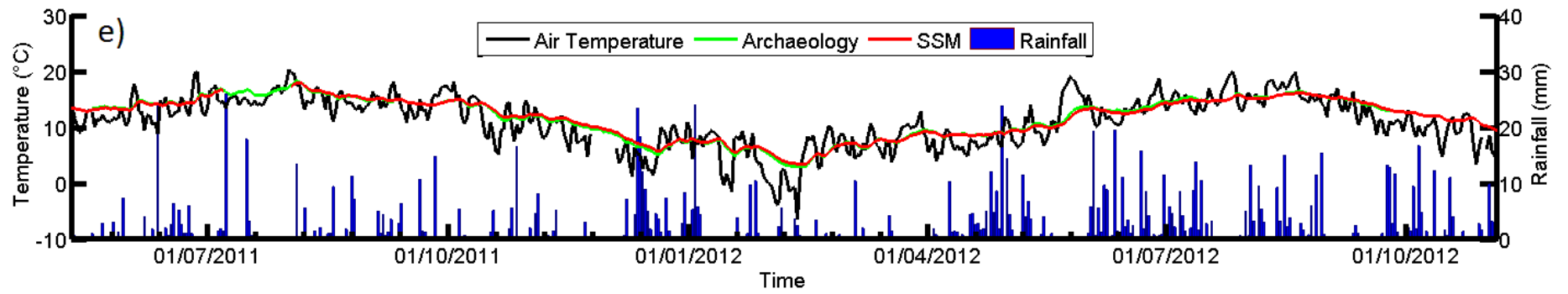
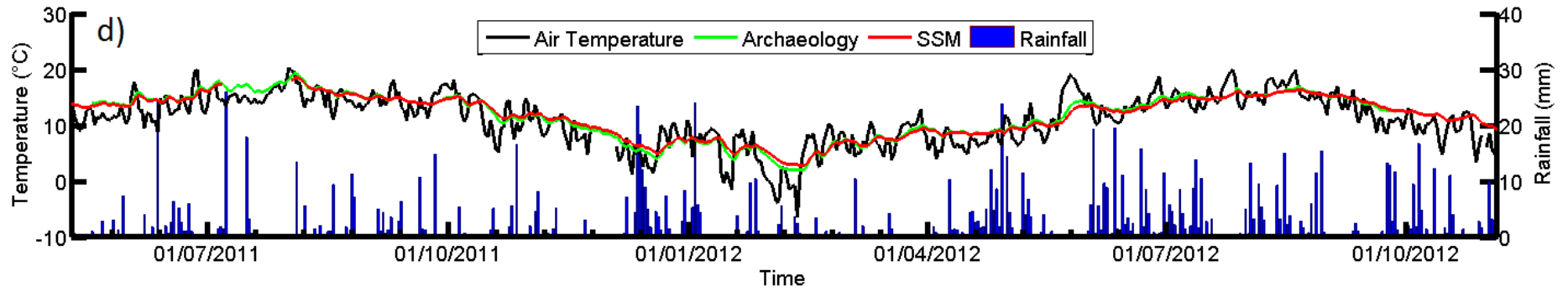


Figure 6.21: The seasonal variation in temperature on DPF at different depths a) 0.1m b) 0.5m c) 0.6m d) 0.8m e) 1m f) 1.2m





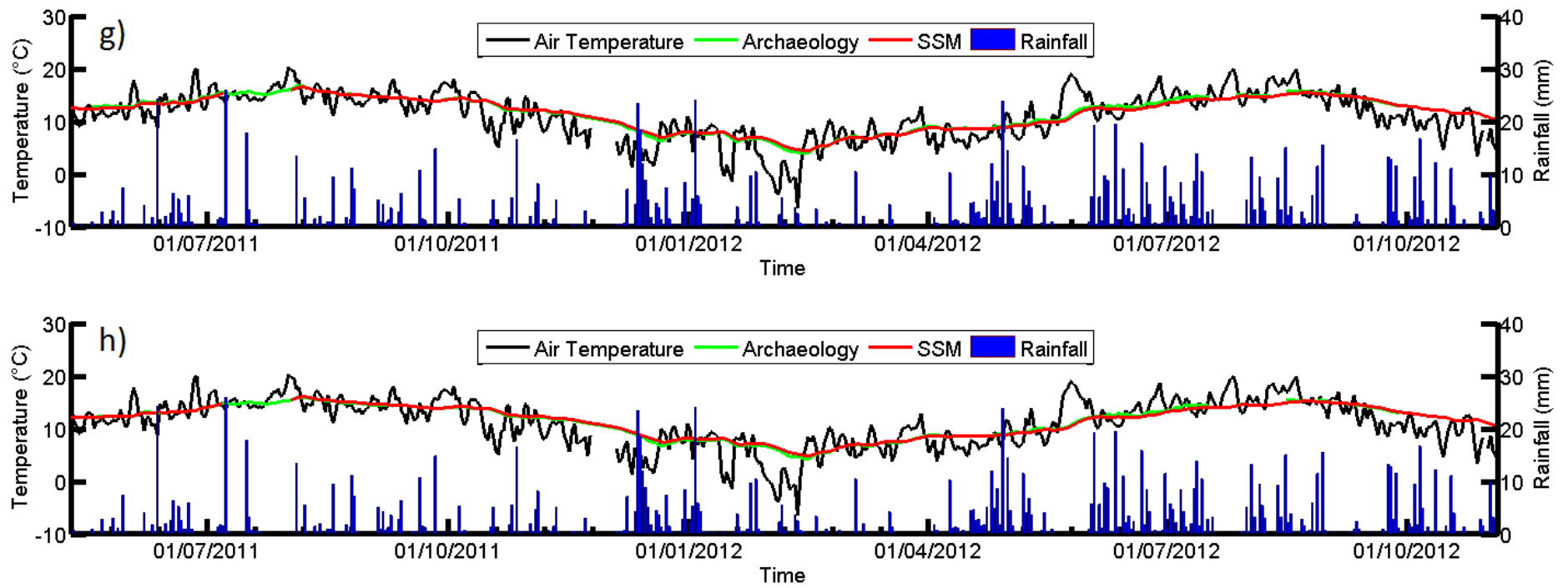


Figure 6.22: The seasonal variation in temperature on CQF at different depths a) 0.1m b) 0.15m c) 0.3m d) 0.5m e) 0.6m f) 0.7m g) 0.8m h) 1m

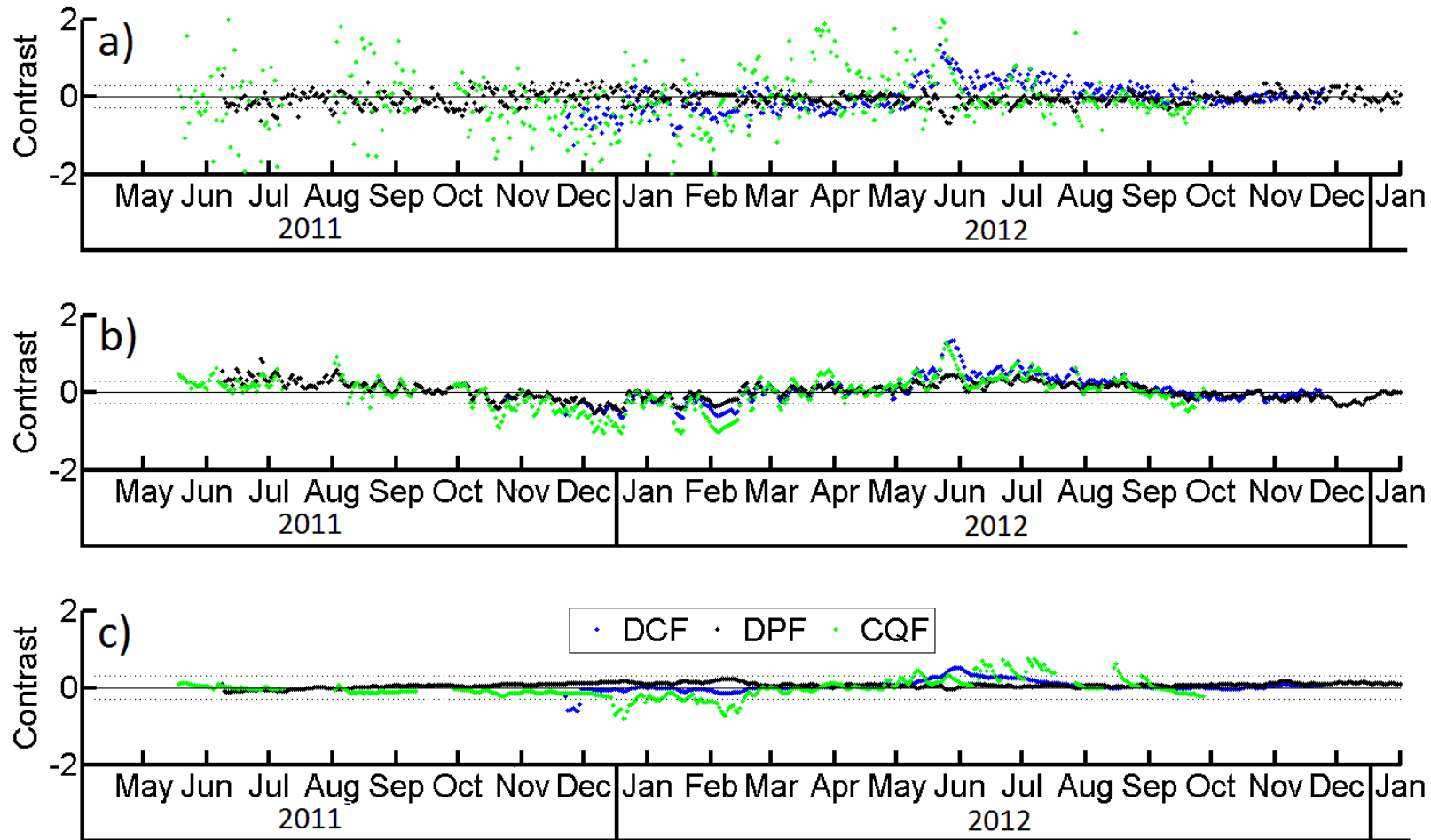


Figure 6.23: Average daily temperature contrast between archaeological soils and SSM value for the three studied sites from depths of a) 0.1m b) 0.5m and c) 1m. The errors of the temperature probes are shown as dotted lines.

A summary of the seasonal variation in soil temperature over the monitoring period is as follows:

- All of the measured sites followed the broad seasonal trends in air temperatures at depths down to 1m, with the warmest and coldest temperatures recorded in the summer and winter respectively. However, at greater depths there was less variation in the temperature in line with the findings of other studies. The near surface soils on all sites also showed some variations with daily changes in temperature, although these effects were limited to approximately the top 0.3m on the fine grained soil sites and top 0.5m on DPF.
- Both the archaeological soils and SSM followed these trends on all of the sites, although the archaeological soils were found to show a greater response to temperature changes, especially in the near surface. However, large differences only existed after an extended period of a few days of extreme high or low temperatures.
- Both absolute temperature variation and contrast between the archaeological soils and SSM were greater on the fine grained soils in comparison to the coarse grained soils, possibly due to their greater water contents and thermal conductivities.

However, this result is likely to have been affected by the vegetation cover on DPF.

6.6. Diurnal Variations in Temperature and Geophysical Properties

As demonstrated in the literature review, both ARDP and BEC have a theoretical dependence on temperature which varies according to a daily cycle. This section deals with variation of temperature on a daily basis. Two sites have been chosen (DCF and DPF), to allow comparison between fine grained and coarse grained soils.

6.6.1. Diurnal variation of temperature

The diurnal variation on DCF and DPF at a number of depths for a period in the winter of 2011, during which the soil was very dry is shown in Figure 6.24. A second period in the summer of 2012 during which the soil was wet has also been selected (Figure 6.25). Diurnal variation was

greater on both sites in the summer period due to the larger temperature changes which took place over the course of the day (approximately 15°C as opposed to approximately 5°C in December). However, during both periods, both sites showed significant diurnal variation in the top 0.1m-0.2m, with only limited daily variation observed below this depth. This shows good agreement with the literature, with the majority of diurnal variations commonly stated to be observed in the top 0.1m (Nobel and Geller, 1987), although smaller variations have been observed down to approximately 1m (Florides and Kalogirou, 2005, 2009, van Manen and Wallin, 2012). During the summer period, DCF (Figure 6.25a) also showed some diurnal temperature variations at greater depth (0.3m), which are a function of both the greater temperature differences throughout the day and the increased thermal conductivity of wet clay soil (Florides and Kalogirou, 2009, Nobel and Geller, 1987). It is also interesting to note that diurnal variation was greater in the fine grained (DCF; Figure 6.25a) soils in comparison with the coarse grained (DPF; Figure 6.25b) soils, especially during the summer period. Whilst this may have been due to differences in the soils thermal conductivity, capacity and diffusivity discussed in Section 6.5, another likely explanation is the presence of vegetation (turf) cover on the DPF site which has reduced the amount of direct sunlight on the topsoil and partially insulated the soil from changes in air temperature.

Significant differences existed in the temperature variation between the archaeological soils and SSM on DCF for both periods although larger differences can be seen during the summer months (e.g. July 2012). This is in line with the larger overall differences measured during this period, and following the findings in Section 6.5 that temperature contrasts between the two soils were greatest after extremes in temperature. The greatest differences were also primarily observed in the top 0.2m where the temperature changes were the greatest as discussed earlier. Much smaller differences between the two soil types were observed for DPF, due to the dampening effect of the vegetation on the soil temperature response discussed above, which reduced temperature extremes.

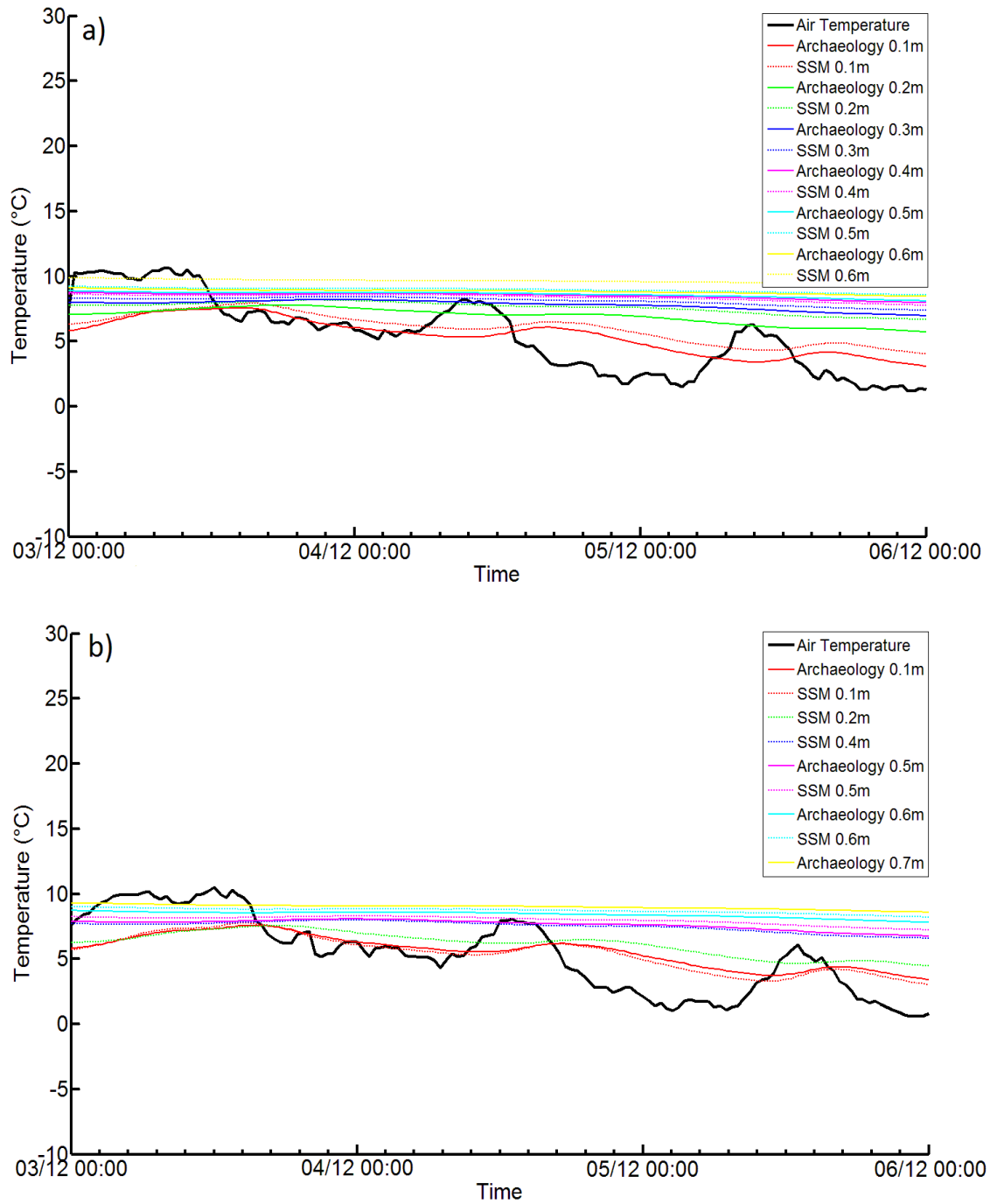


Figure 6.24: Diurnal temperature variation at different depths in the near surface during a period in December 2011 for a) DCF and b) DPF

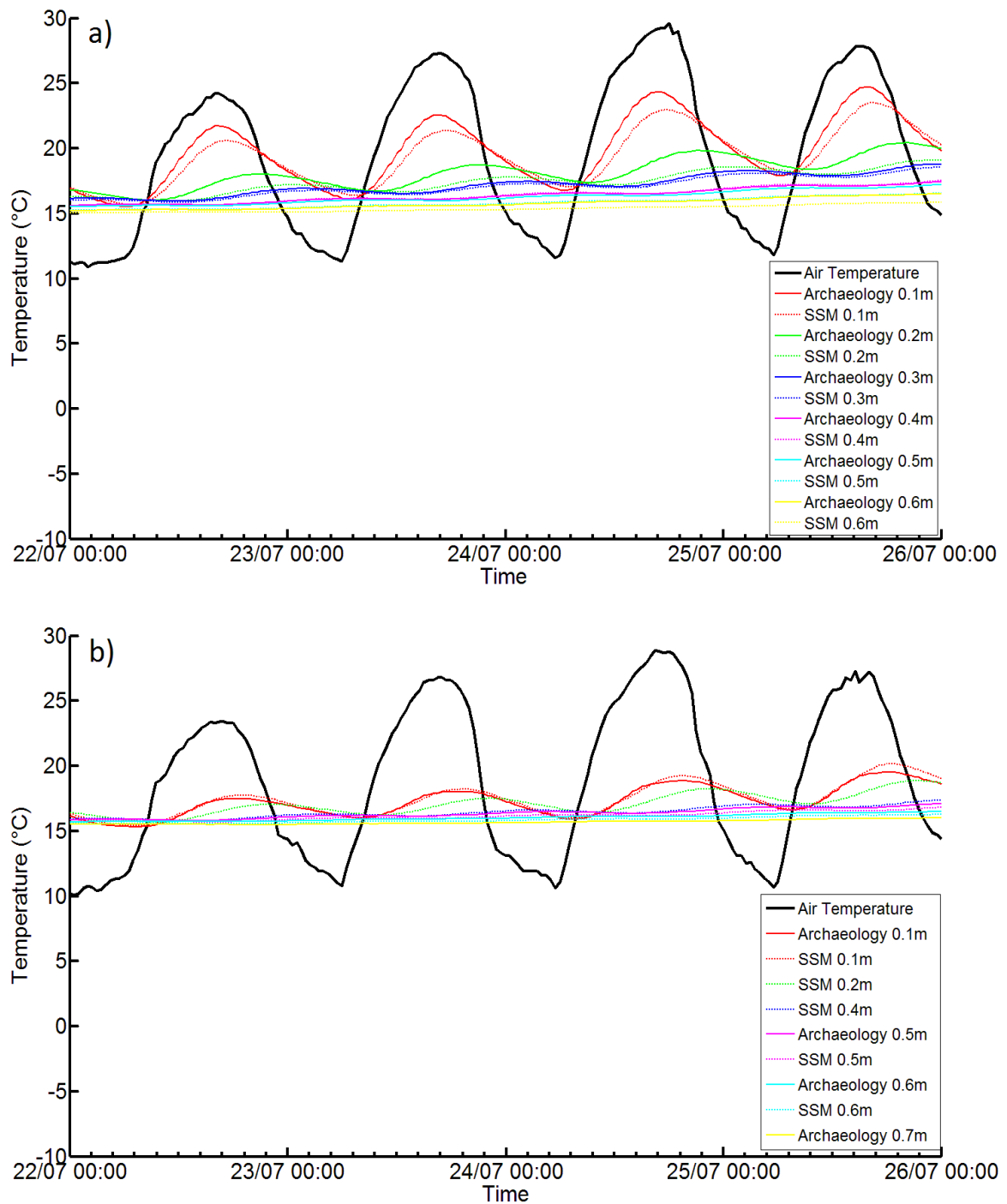


Figure 6.25: Diurnal temperature variation at different depths in the near surface during a period in July 2012 for a) DCF and b) DPF

It also can be seen that there are differences in the lagged response both between the archaeological soils and SSM, and with depth, as observed by Florides and Kalogirou (2005, 2009) and van Manen and Wallin (2012). In order to assess these differences, time domain cross correlation has also been used, which involves statistically calculating linear correlations

of two variables as a function of time by shifting one time series in relation to the other (Spiegel and Stephens, 2011). This allows the determination of the lag in temperature response from a number of different depths for each site to be calculated and displayed for both the archaeological soils and SSM. Due to the greater differences displayed, analysis has been conducted on the summer period only for the two sites. The results of the cross correlation between the air temperature and soil temperatures at different depths are displayed in Figure 6.26 (DCF) and Figure 6.27 (DPF). The two horizontal lines represent 10% significance. Both sites showed a strong correlation to air temperature, especially in the near surface probes, indicated by the high positive correlation values. However, the time of the maximum correlation varied with depth, with longer lags at greater depths confirming that the effects of diurnal variation had a greater lag as depth increases. Below 0.5m on both sites, very small correlations and long lag times were observed, confirming that only the top layers are affected significantly by diurnal variation. These findings confirm those of other authors who have measured temperatures at a wide range of depths (Curioni, 2013, van Manen and Wallin, 2012).

Whilst no significant differences were observed in the lags between the archaeological soils and SSM on DPF (Figure 6.27), largely due to the lack of temperature probes in both profiles at the near surface below 0.1m, some differences were recorded on DCF (Figure 6.26). The greatest differences were recorded at a depth of 0.2m, with the archaeological soils showing maximum correlation approximately 1-2 hours before the SSM. This is unusual as both the archaeological soil and SSM probes were in the same soil layer (DCF Topsoil). However, analysis of the ARDP data over this period in Section 6.4 (Figure 6.12b) showed the ARDP (therefore the water content) to be consistently higher at this depth in the SSM profile. Since it is widely known that water has a higher thermal capacity than soil or air (Davie, 2008, Foth, 1990), it is possible that this is causing the wetter soil to take longer to respond due to the extra energy needed to change the soil temperature. Since a similar water content difference

was recorded after significant drying events on CQF (see Section 6.4; Figure 6.16), this may potentially be important for thermal detection of archaeological features using ground based methods (e.g. Tabbagh, 1985) on fine grained soils if surveys are conducted after or during a period of warm weather when these differences are accentuated.

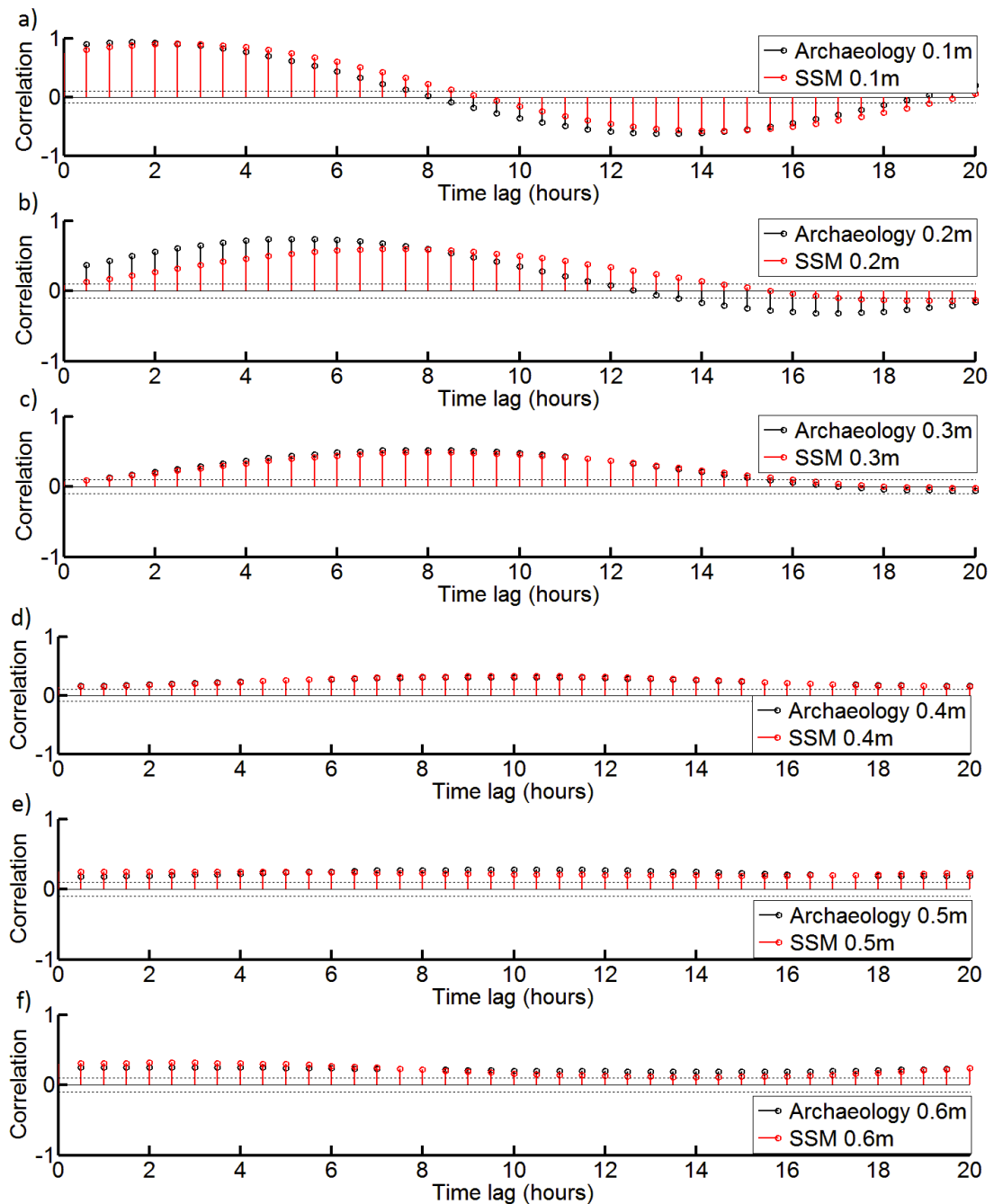


Figure 6.26: Cross correlation between air temperature and soil temperature at depths of a) 0.1m b) 0.2m c) 0.3m d) 0.4m e) 0.5m and f) 0.6m for DCF between 22nd and 26th July 2012.

Horizontal dashed lines represent the limits above which the absolute cross correlations are significant with a confidence level of 90%.

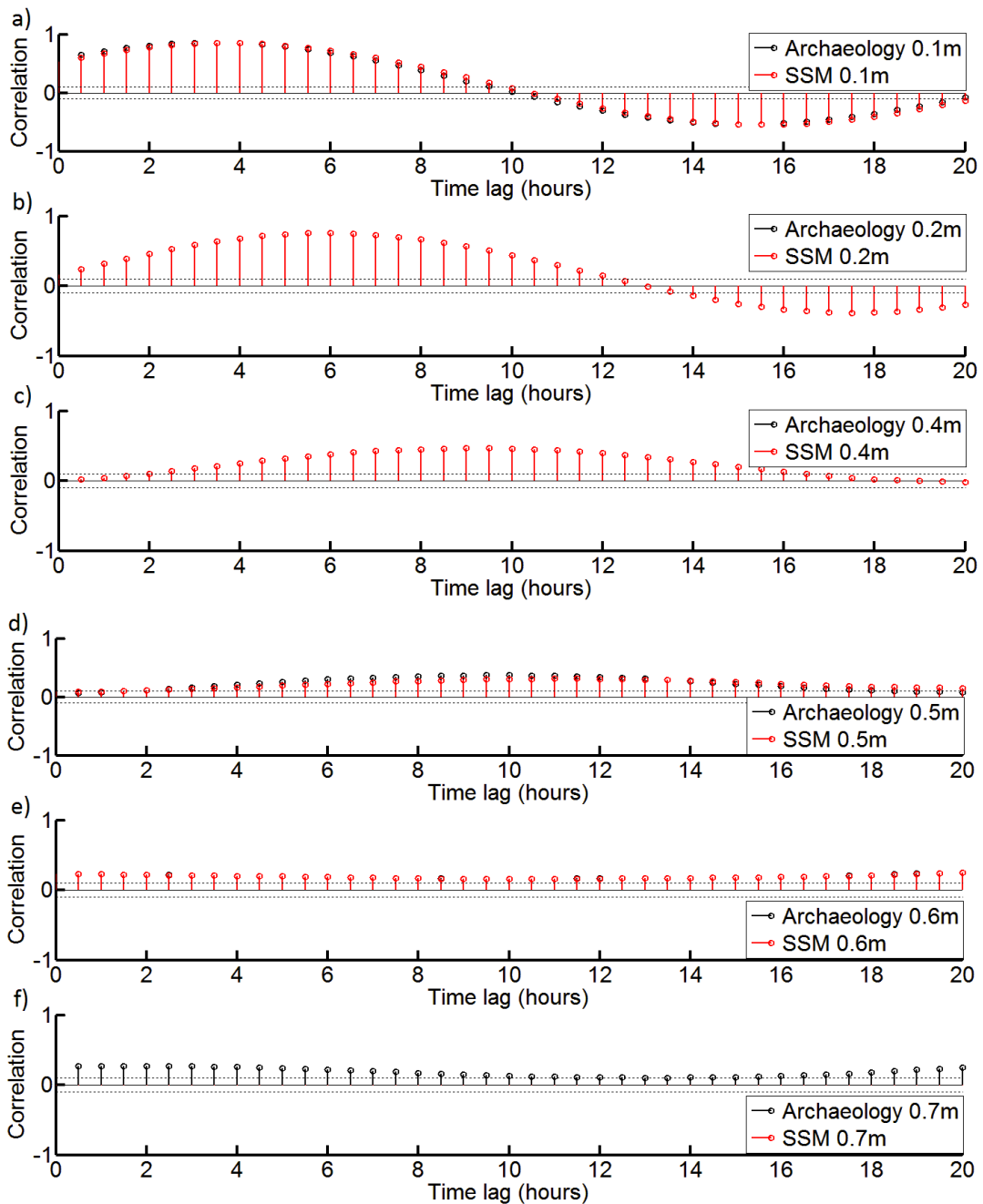


Figure 6.27: Cross correlation between air temperature and soil temperature depths of a) 0.1m b) 0.2m c) 0.4m d) 0.5m e) 0.6m and f) 0.7m for DPF between 22nd and 26th July 2012. Horizontal dashed lines represent the limits above which the absolute cross correlations are significant with a confidence level of 90%.

6.6.2. Effects of Diurnal Variation on geophysical properties

In order to assess the effect of the temperature changes described in Section 6.6.1 on measured geophysical data, temperature, ARDP and BEC data from a short period of a few

days for both a warm and a cold period has been taken for two sites (DCF and DPF) and plotted concurrently to assess daily cycles. Data have been chosen from both the dry and the wet period to allow a comparison of soil response in both conditions. Data from DCF are presented in Figures 6.28-6.29 and data from DPF are presented in Figures 6.30-6.31.

Due to the temperature behaviour of the soil discussed in Section 6.6.1, for DCF BEC was shown to have a significant diurnal variation in near surface soils. However, the diurnal effect was considerably less noticeable on the coarse grained DPF soils. Two reasons exist for this; firstly the soil temperature change was less due to the effects of the turf discussed earlier and secondly, as was shown in Section 5.5.5, the effects of changes in temperature are less significant on coarse grained soils as they both hold less water and have less dissolvable ions than their fine grained counterparts. Both sites also showed less variation in geophysical properties in the dry soil due to the reduced number of ions in solution, although it should be noted that this was partly the result of the smaller fluctuations in air temperature during the winter months from which these data were taken. As expected from the soil temperature analysis in Section 6.6.1, the effect dropped off rapidly with depth, with responses barely noticeable below the top 0.2m on either site, which was in line with results found by Curioni et al. (2012) and Skierucha et al. (2012). Slightly stronger diurnal responses were recorded in the archaeological soils from both DCF and DPF, which reflected their stronger temperature dependence shown in Section 6.6.1. The greatest contrasts occurred in the wet soil shortly after midday, although these differences were only apparent in the shallow soils. Since the diurnal effect on BEC is constrained to the top soil layers, it seems that the data presented here support the view expressed in the literature that diurnal effects have little effects on geophysical prospection (Brevik et al., 2004), with only longer term seasonal temperature changes causing significant effects on conductivity results.

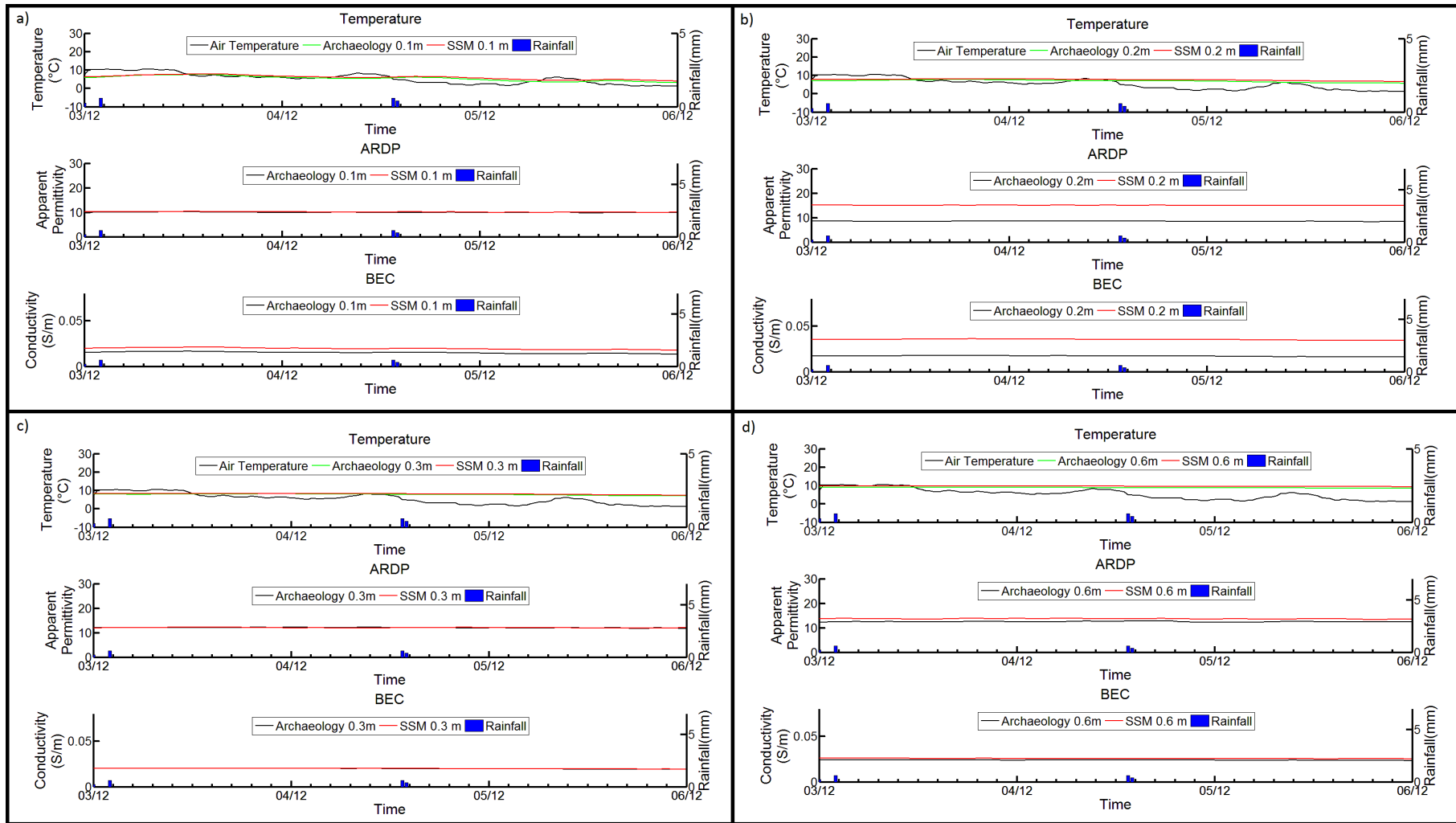


Figure 6.28: Daily variation of the temperature, ARDP and BEC at depths of a) 0.1m b) 0.2m c) 0.3m and d) 0.6m for DCF over a dry period in December 2011

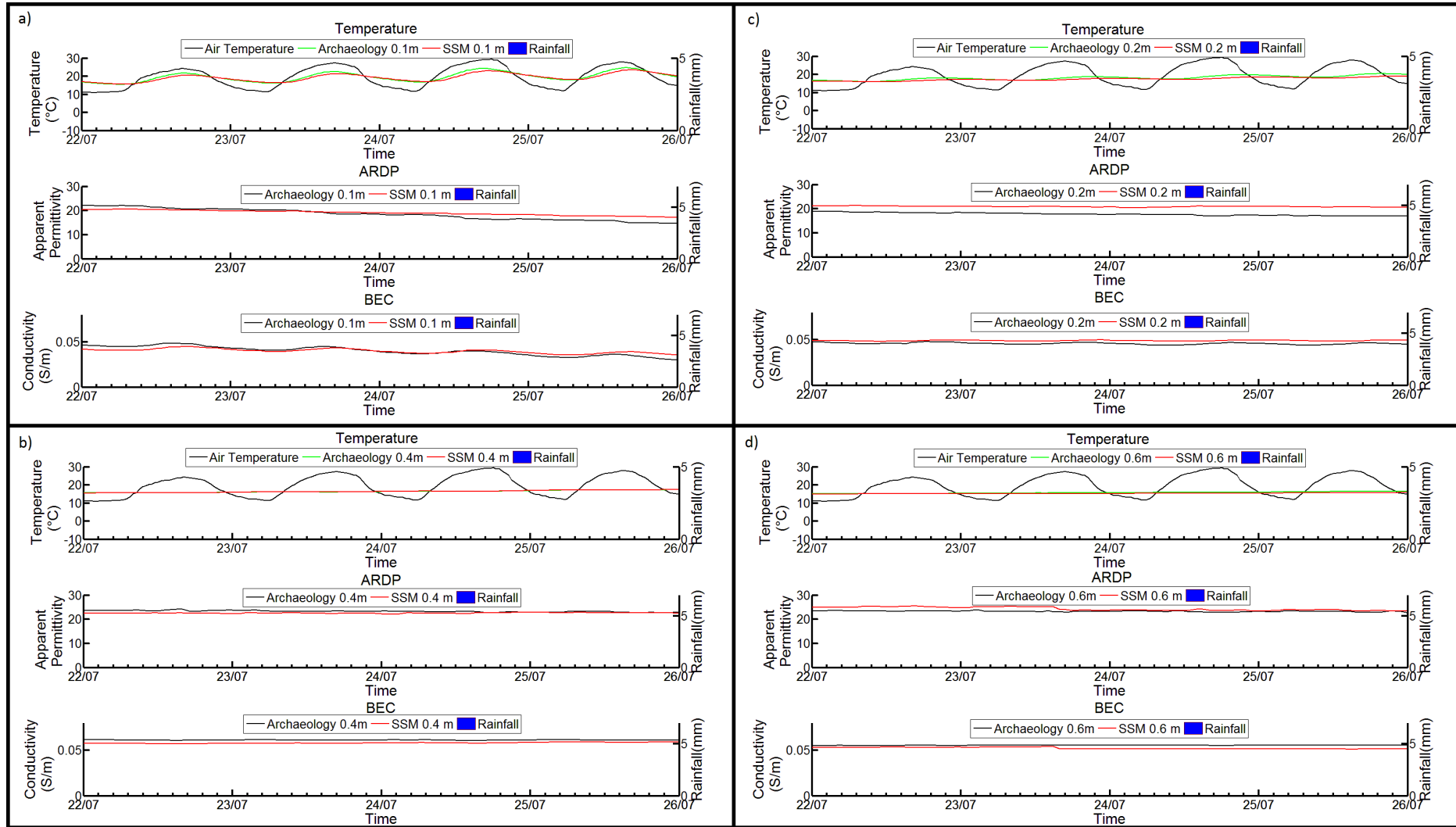


Figure 6.29: Daily variation of the temperature, ARDP and BEC at depths of a) 0.1m b) 0.2m c) 0.3m and d) 0.6m for DCF over a wet period in July 2011

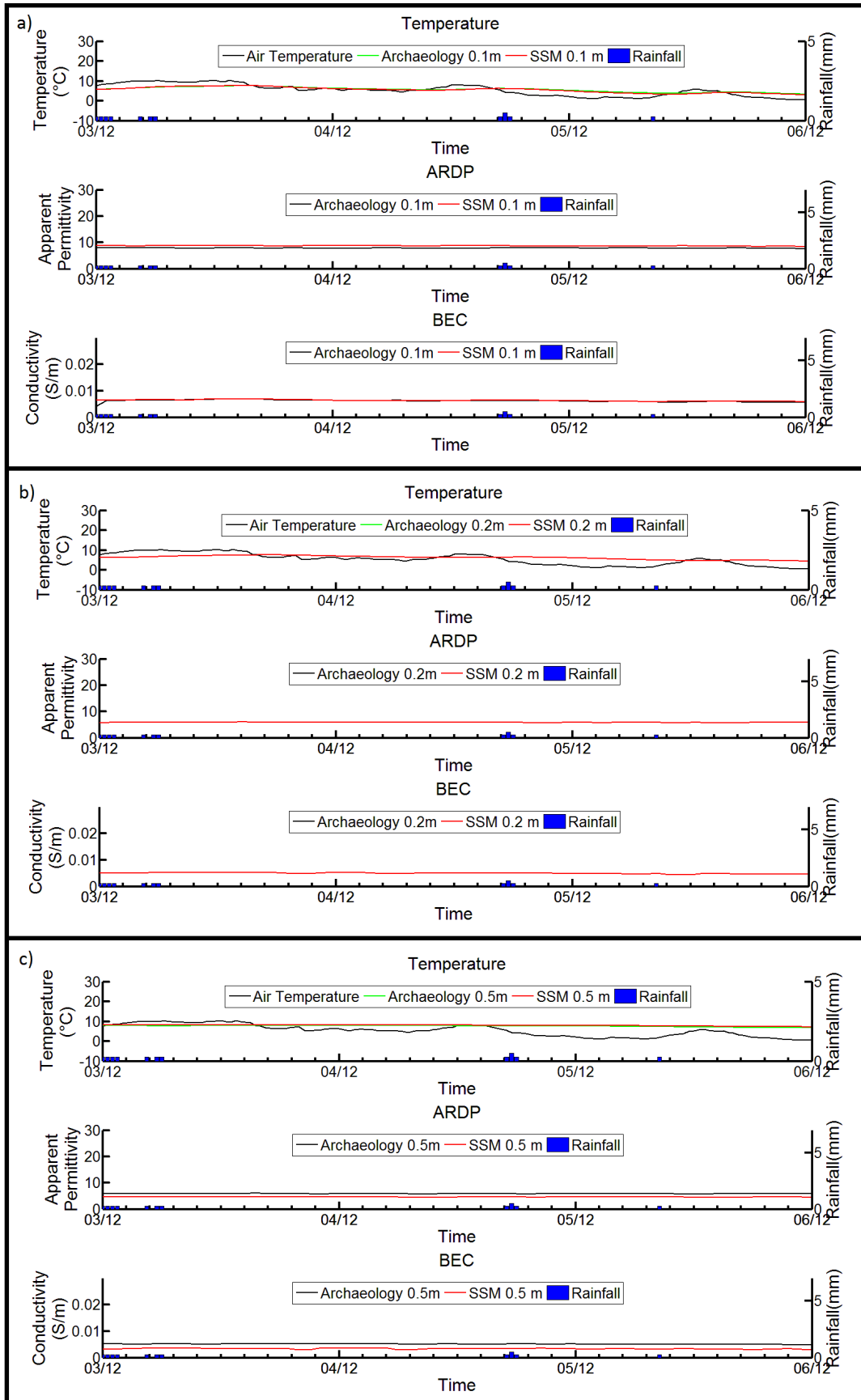


Figure 6.30: Daily variation of the temperature, ARDP and BEC at depths of a) 0.1m b) 0.2m and c) 0.5m for DPF over a dry period in December 2011

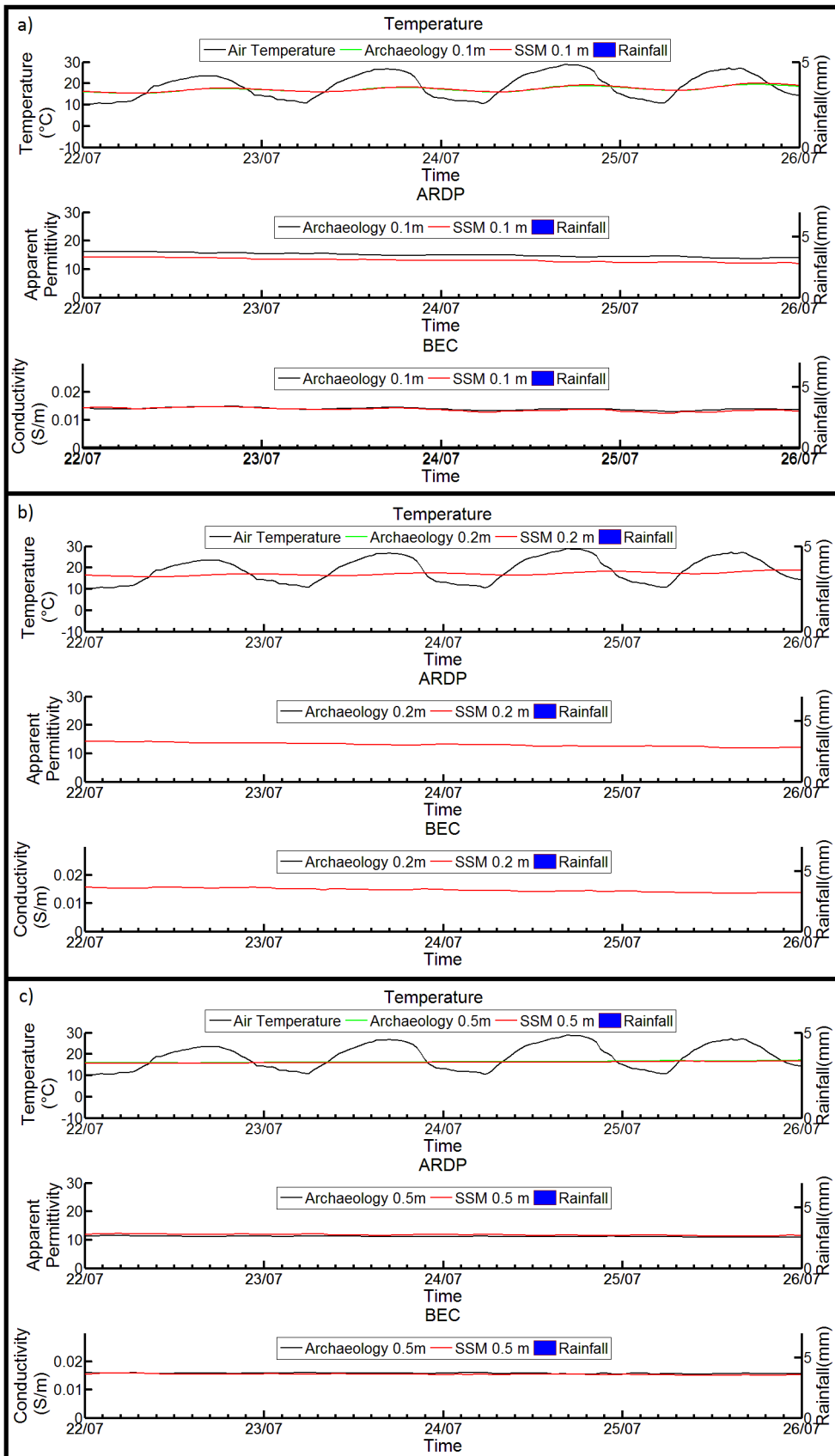


Figure 6.31: Daily variation of the temperature, ARDP and BEC at depths of a) 0.1m b) 0.2m and c) 0.5m for DPF over a wet period in July 2011

In contrast to the BEC, the ARDP was shown not to vary with diurnal variations on any of the sites even for shallow soil depths. This conflicts with the findings of Menziani et al. (2003), who found a daily cycle in TDR measured VWC due to negative temperature dependence of ARDP at depths of up to 0.4m. However, other authors have found no obvious diurnal dependence for a variety of soils (Curioni, 2013, Mohanty et al., 1998, Skierucha et al., 2012). These results also confirm the results of the laboratory analysis on the Diddington soils (Chapter 5) which showed a very weak dependence of measured ARDP with temperature due to the competing effects of the negative temperature dependency of the permittivity of water with the positive effects of rising BEC and release of bound water which cancel each other out.

6.6.3. Summary of Diurnal Variations

A summary of the results of diurnal effects on the soil is as follows:

- Both fine grained and coarse grained soils showed diurnal temperature variation in the near surface which rapidly dropped off with depth in line with the findings of other authors. However, these variations were greatest in the summer months due to the wider daily fluctuation of temperature. Smaller diurnal variation were recorded on the coarse grained soil which may be due to differences in soil thermal properties although it seems more likely to have been influenced by the vegetation cover on site.
- Significant differences existed between the archaeological profile and SSM on DCF, with the archaeological soils showing a greater temperature response, especially during the summer period where fluctuations in air temperature were greater. These effects were dampened on DPF due to vegetation cover.
- Time domain cross correlation confirmed the increased lag in response at greater depths shown by other authors. Few differences were observed in lag times between the archaeological soils and SSM, with the exception of 0.2m depth on DCF. This was

thought to be caused by the higher water content at this depth in the SSM profile which caused the soil to heat slower due to its higher heat capacity.

- In the fine grained DCF soils, BEC showed diurnal variation at the near surface, especially during warm and wet conditions. Whilst this effect was stronger in the archaeology in line with temperature changes, due to the rapid dropoff with depth these were not thought to be significant for geophysical prospection. The DPF soils showed much smaller variations as a result of both their smaller temperature changes and smaller temperature dependency highlighted in Chapter 5. Due to the concentration of these effects in the near surface, it seems unlikely that diurnal variation has a significant effect on prospection.
- ARDP showed no significant diurnal effects at any depth in agreement with the relationships between ARDP and temperature discussed in Chapter 5.

6.7. Infiltration after Rainfall Events

To assess the differences in infiltration patterns between fine and coarse grained soils and the differences between the response of the archaeological soils and SSM, an individual rainfall event from March 2012 on the two Diddington sites (DCF and DPF) has been selected for further analysis. The rainfall event is shown in Figure 6.32 and consists of a sustained period of rainfall (15.4 mm in 9.5 hours). Data, from probes averaged by depth, have been taken for the rainfall period and for a short period (c. 2-3 days) afterwards. In order to statistically determine the lag at different depths, and determine different infiltration patterns in both the archaeological soils and SSM time domain cross correlation between the hourly rainfall and measured ARDP data from the soil was conducted. These results are presented in Figure 6.33 (DCF) and Figure 6.34 (DPF). Additional rainfall events were also analysed and found to produce similar results and are not presented here.

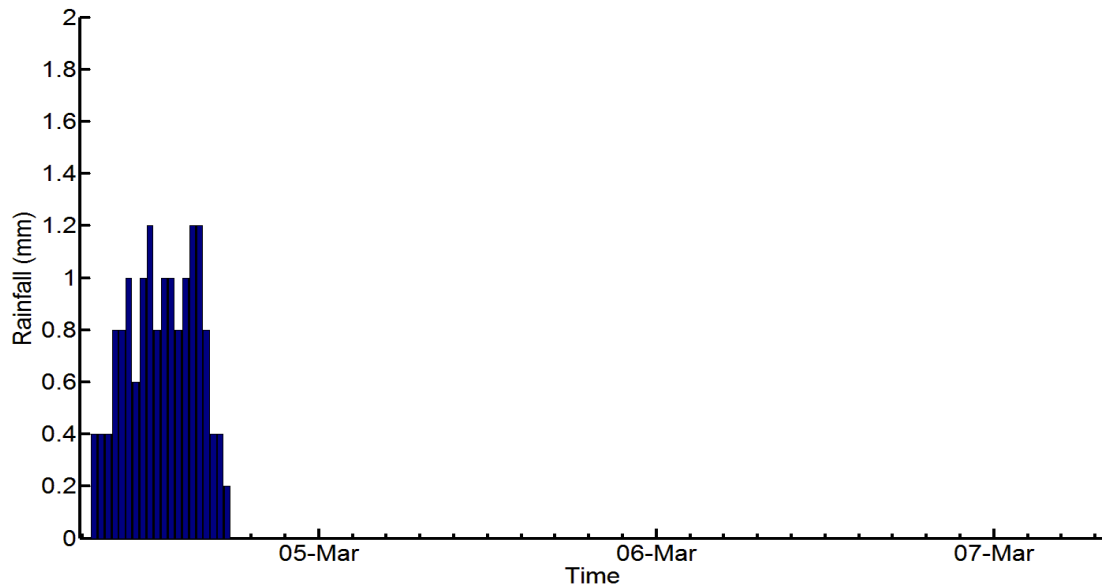


Figure 6.32: Rainfall event from March 2012 on the Diddington sites (taken from DCF weather station but similar data found for DPF).

The time domain cross correlation analysis showed a positive correlation for both sites on the near surface probes above 0.5m depth, confirming the finding in Section 6.4 that infiltration of rainfall mostly affected the near surface soil. However, whilst no significant positive correlations could be seen below this depth on DCF, water can be seen to penetrate to a greater depth on DPF, with significant correlations after 60 hours recorded at 0.6m and 0.8m depth. This seems likely to be the result of the soils free draining nature due to its coarser texture and lower soil potential which held less water in the upper layers and allowed water to drain through the soil. The negative correlation noticed for both sites during and immediately after the rainfall event on both sites, especially at greater depths was also noticed by Curioni (2013), and seems to reflect the soil’s tendency to lose water in normal circumstances due to the effects of evapotranspiration.

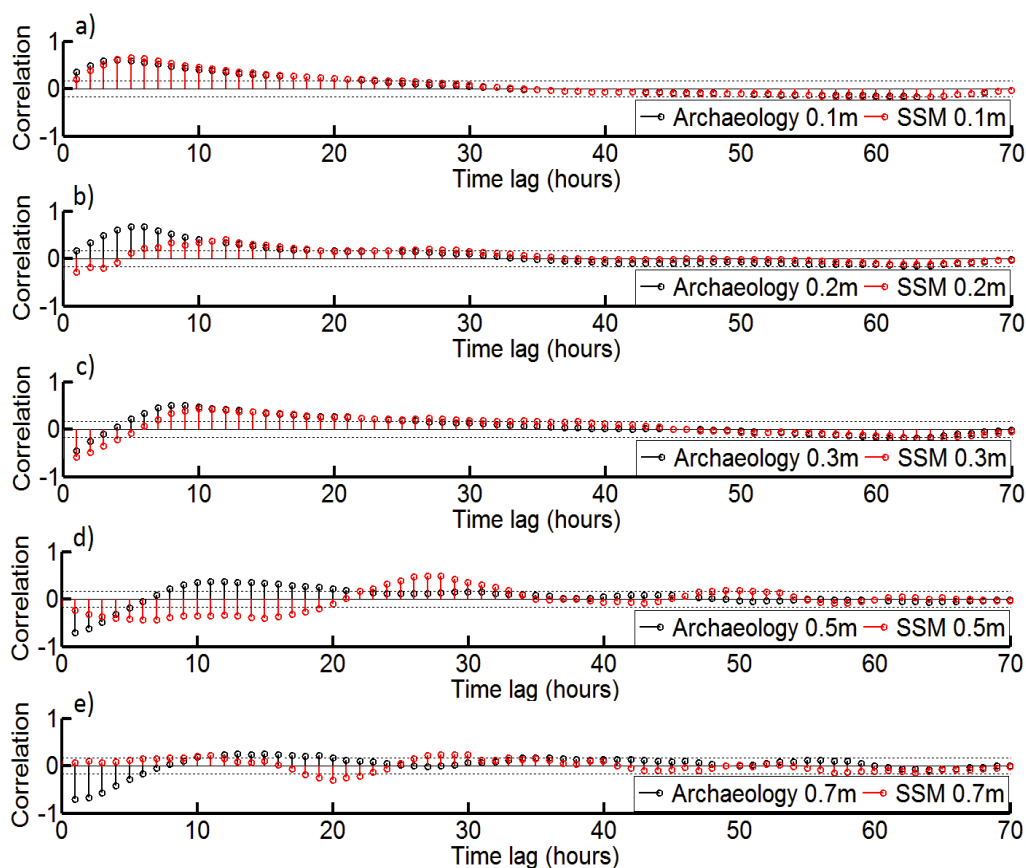


Figure 6.33: Cross correlation between rainfall and ARDP for DCF at depths of a) 0.1m b) 0.2m c) 0.3m d) 0.5m and e) 0.7m. Horizontal dashed lines represent the limits above which the absolute cross correlations are significant with a confidence level of 90%.

For DCF, infiltration was marginally faster within the archaeological feature in comparison to the SSM, especially in the near surface, although at greater depths maximum correlations were small and barely exceeded the significance line. This is due to the differences in density between the two underlying soil types which created larger pores for water to infiltrate. This effect was especially noticeable at 0.5m depth (Figure 6.33d) where a large difference existed between the two soils. In contrast, virtually no recordable differences were found in infiltration between the two soil types on DPF, with similar peaks recorded for the two soils at all of the studied depths. As both the archaeological and SSM soils are predominantly coarse grained, it is suggested that both had similar free draining properties allowing water to infiltrate at the same rate through both soils. It should be noted that differences in infiltration between the archaeological soils and SSM even on DCF are minimal, with the differences

typically being a maximum of approximately 15 hours at 0.5m. It also should be noted that correlations at greater depths are much smaller, suggesting smaller rises in geophysical values at these depths due to infiltration after rainfall events. These two factors confirm the findings in Section 6.4 that suggested that long term contrast between the archaeological soils and SSM is due to differences in their water holding capacities rather than differences in the infiltration rate. It also should be noted that infiltration is dependent on the intensity and duration of the rainfall as well as the antecedent soil water content (Saxton, 2013, Saxton and Willey, 2006, Saxton et al., 2006) and may vary accordingly.

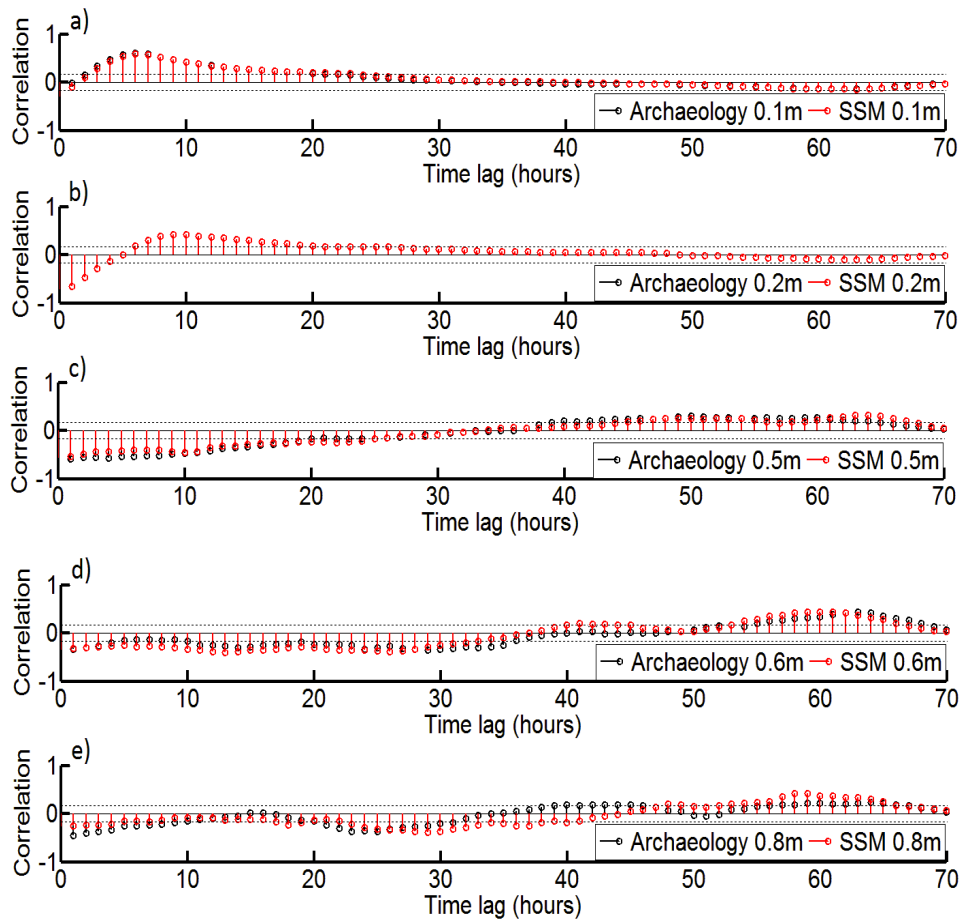


Figure 6.34: Cross correlation between rainfall and ARDP for DPF at depths of a) 0.1m b) 0.2m c) 0.5m d) 0.6m and e) 0.8m. Horizontal dashed lines represent the limits above which the absolute cross correlations are significant with a confidence level of 90%

6.8. Relationships between Geophysical and Geotechnical Properties of the Soil

6.8.1. Correlation between Geophysical Parameters and Temperature

To assess the relationships between ARDP, BEC and temperature, ARDP data have been plotted against BEC data for each of the sites and colour coded according to the temperature recorded from the nearest temperature probe. Data are presented from DCF (Figure 6.35), DPF (Figure 6.36) and CQF (Figure 6.37) for both the archaeological soil profile and the SSM.

All of the sites showed a strong positive relationship between the ARDP and BEC for both the archaeological soils and SSM. This is unsurprising given the dependence of both these properties on the VWC of the soil. However, the BEC also showed an additional positive relationship with temperature on all of the soils, shown by the warmer temperatures producing higher BEC even at the same ARDP values. This is in agreement both with the findings from the laboratory as well as those of other authors (e.g. Brevik et al., 2004, Campbell et al., 1948, Skierucha et al., 2012). However, one important point to note is that the effects of temperature on the soil BEC were not linear across the whole soil range, with greater variation to soil temperature shown at higher ARDP values (i.e. in wetter soils) on all sites. This shows good agreement with the findings of laboratory testing of the soil discussed in Chapter 5. No obvious similar relationships could be found between the temperature and ARDP in agreement with the findings of laboratory testing.

Statistical correlations between the different variables were attempted using spearman's rank coefficient³ (Spiegel and Stephens, 2011), which are presented in Figure 6.38. These predominantly showed the same correlations with strong correlations between ARDP and BEC and temperature and BEC. However, for some depths and soils, these gave inconsistent and

³ Spearman's rank coefficient ranks all of the variables before calculating the Pearson correlation coefficient between them. The method was chosen as it makes no assumptions about the underlying distribution of data which has been shown to be non-normally distributed.

contradictory results such as showing poor links between ARDP and BEC. This was likely to be due to the complexity of soil behaviour which has skewed the statistical tests.

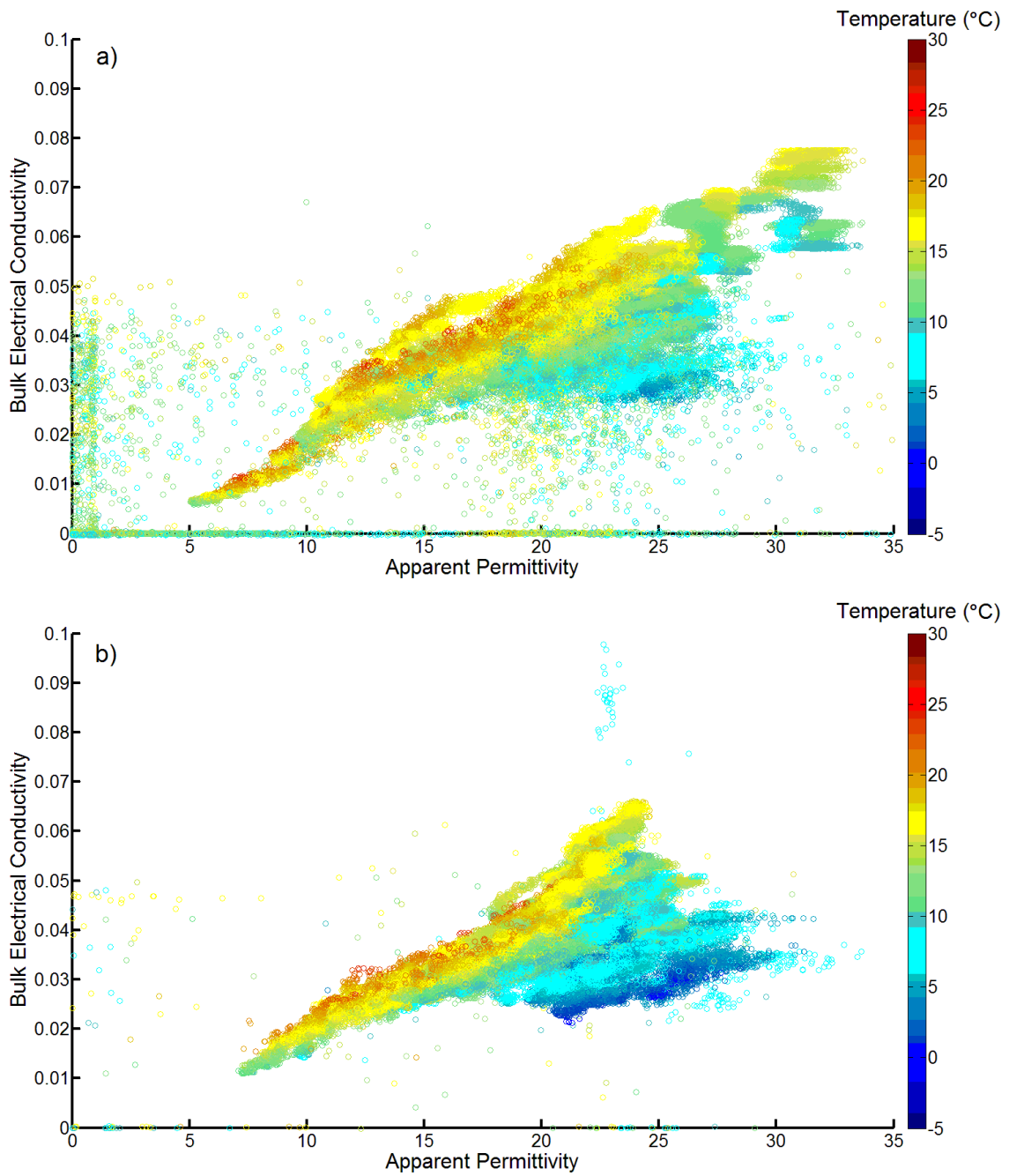


Figure 6.35: Relationship between ARDP, BEC and Temperature for DCF during 2012 for a) the Archaeological soil profile and b) the SSM profile

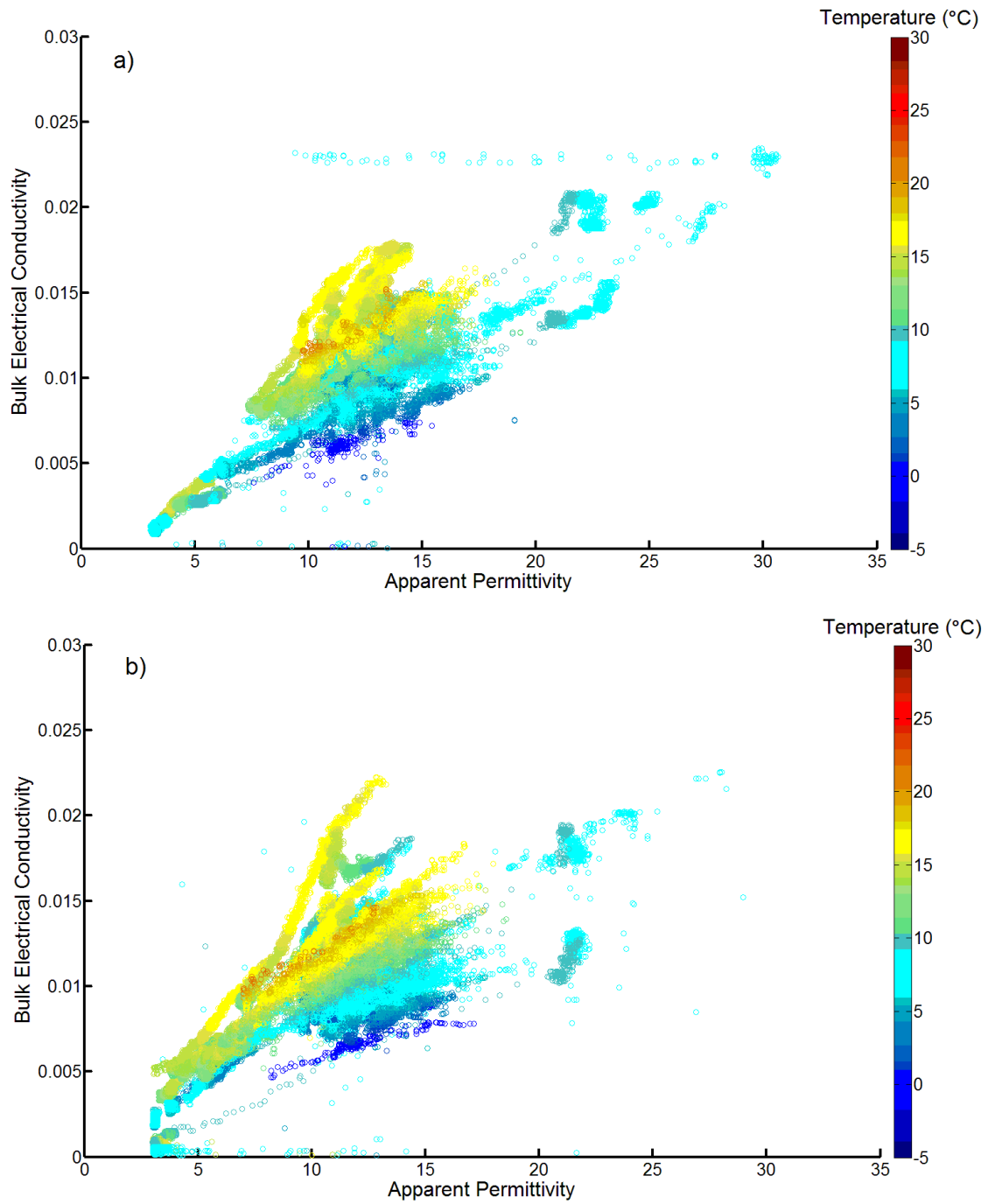


Figure 6.36: Relationship between ARDP, BEC and Temperature for DPF during 2012 for a) the Archaeological soil profile and b) the SSM profile

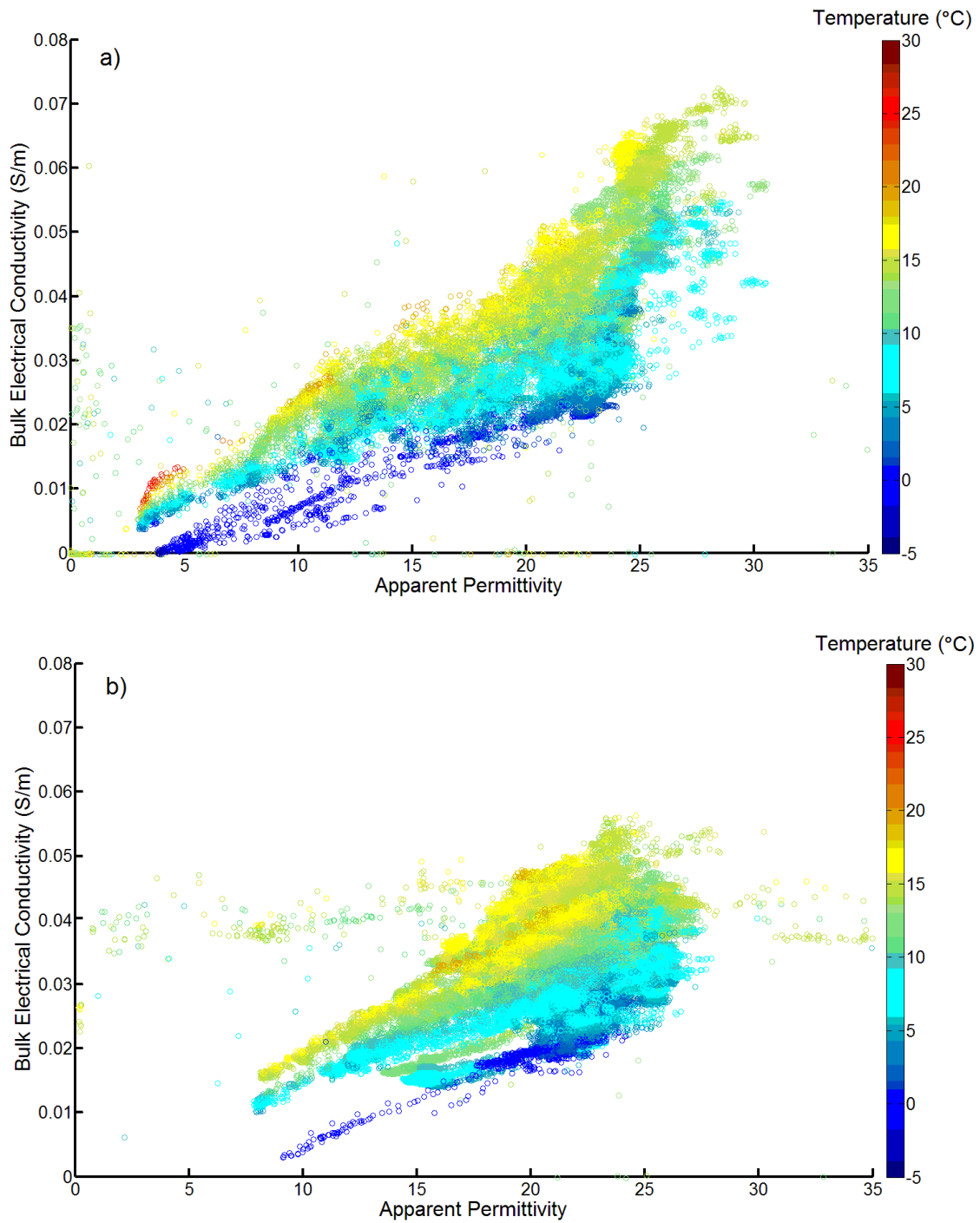


Figure 6.37: Relationship between ARDP, BEC and Temperature for CQF during 2012 for a) the Archaeological soil profile and b) the SSM profile

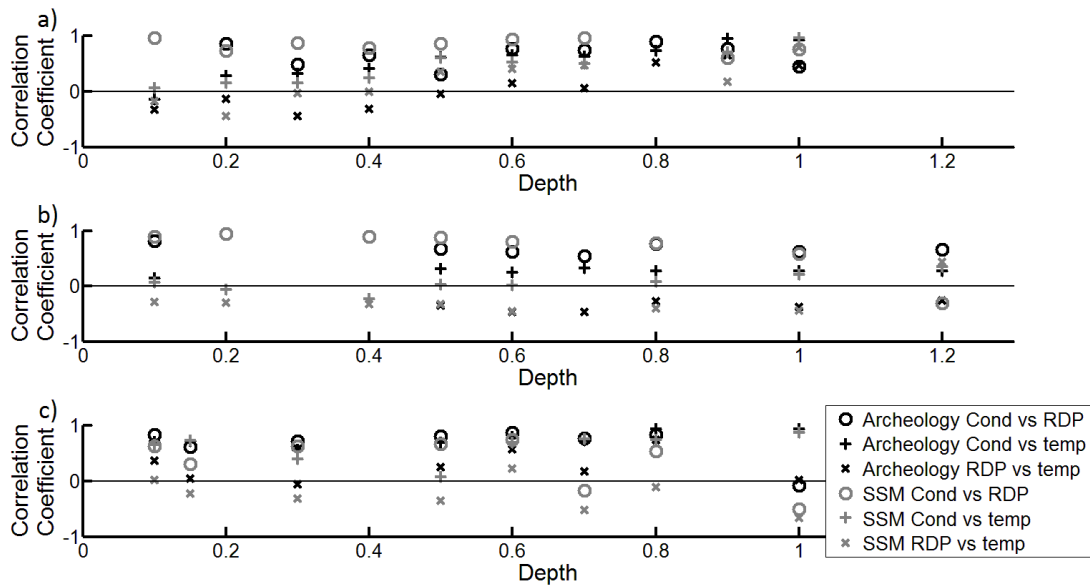


Figure 6.38: Spearman’s rank correlation between different pairs of variables at different depths for a) DCF b) DPF and c) CQF

6.8.2. Principal Component Analysis

In order to assess which variables were the most important for determining the average soil geophysical properties, a PCA was conducted using the mean values of ARDP, BEC and temperature for the monitoring period in conjunction with some of the geotechnical and geochemical properties of the soil determined during the soil characterisation tests similar to those shown in Section 5.6. Data from the three sites (DCF, DPF and CQF) over the whole monitoring period were used, and the same inputs as in Section 5.6 were used in order to produce comparable results. Analysis of the scree plot (Figure 6.39) showed that the first 4 principal components accounted for over 85% of the total variance, and the analysis focused on these as the other principal components could be safely discarded without the loss of significant information.

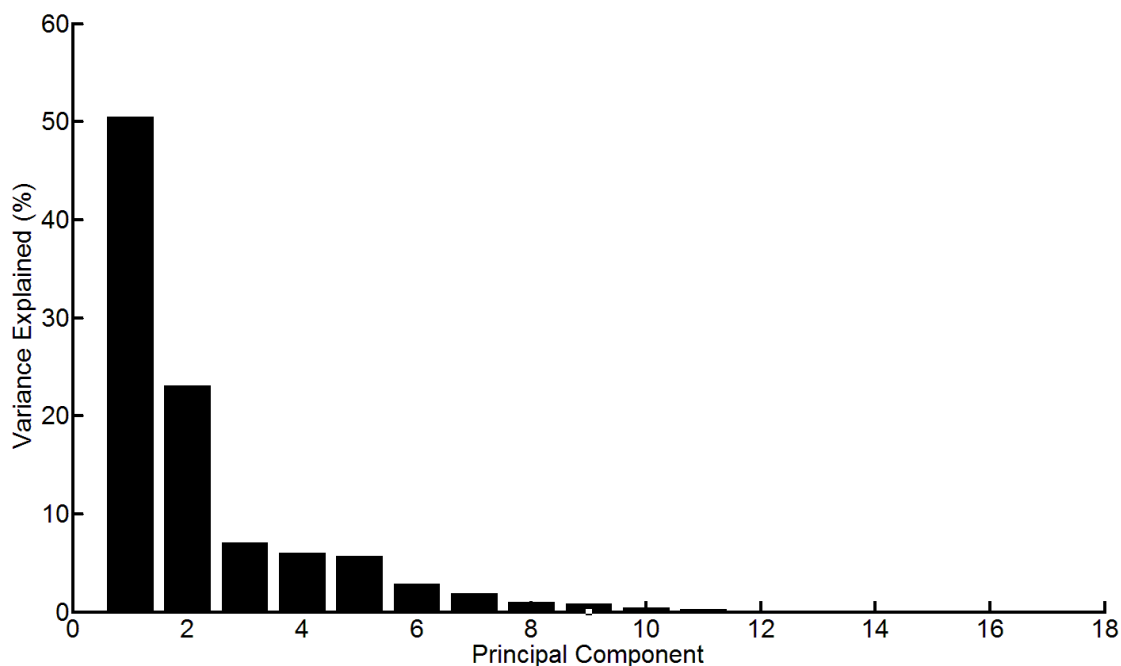


Figure 6.39: Scree plot from PCA using geotechnical and averaged ARDP, BEC and temperature data from DCF, DPF and CQF

A biplot of the first two principal components, which accounted for 70% of the variation, is shown in Figure 6.40. The plot shows good agreement with Figure 5.21 made for the soils tested in the laboratory (Section 5.6) confirming that many of the relationships found in the laboratory are also important in the field. Particle and dry density were negatively correlated with porosity as would be expected as less compact soils have a greater pore space. Similarly, gravel and sand percentages showed a negative relationship with the percentages of silt and clay indicating the differences between the fine grained soils from DCF and CQF and coarse grained DPF soils which were used in this study. This was also reflected in the distribution of the data points, with the DPF points all clustered on the left hand side of the plot near to the sand and gravel variables and the DCF and CQF points near to the clay and silt variables. The EM properties showed good correlation (positioned near to each other on the biplot) both with each other as well as with the clay percentage and the plastic and liquid limit of the soil, which reflected its mineralogy and specific surface area. This was in good agreement with the theory of ARDP and BEC determination in wet soils described in the literature review (Chapter 2), the contribution of BEC to ARDP and higher BEC values found in fine grained soils during

laboratory testing (Chapter 5) as well as the findings of other authors who have linked geophysical properties to the amount of clay (Curioni, 2013, Kachanoski et al., 1988, Kachanoski et al., 1990). However as water content was also determined to be the most important variable in Chapter 5, it also indicated that the average water content of soils was strongly determined by the clay content over the monitoring period. This supports the findings in Section 6.4 that the primary difference in geophysical behaviour is a function of the different soils ability to hold water, as these variables affect the SSA of the soil which in turn determine the soil suction potential and the SWCC. It also should be noted that data from probes located in the same soil types displayed similar behaviour shown by the clustering of these points into small groups, confirming the dependence of the geophysical properties on the geotechnical soil properties. Whilst a significant difference existed between the coarse grained (DPF) soils and the fine grained soils (DCF and CQF), shown by their groupings on either side of the plot, both fine grained sites showed similar properties and are located together on the right hand side of the plot, with the different soils (e.g. topsoil) possessing similar properties to each other. One major difference between the biplot shown here and that from the laboratory testing (Section 5.6) is that the temperature showed a far greater agreement with the measured geophysical properties than during the laboratory study in Chapter 5 and by Curioni (2013). However, as discussed in Sections 6.5 and 6.6 and in the literature review (Chapter 2), the change in soil temperature is a function of water content due to its significant effect on the thermal capacity and conductivity of the soil, and it is likely that the differences in VWC between the different soils, as well as the tendency for values of ARDP, BEC and temperature to be more static at greater depths have influenced this result.

A second biplot, showing principal components 3 and 4 is presented in Figure 6.41. This figure again confirmed the strong correlation of the measured EM properties with each other and with temperature confirming that water content is the dominant factor in determining BEC and temperature is a secondary influence, especially on BEC. The plot also confirmed the

similarity of response from probes in the same soil contexts, with the results of each soil again grouped in small clusters. Whilst the percentage variance from these two principal components is much lower, the plot appeared to confirm the secondary importance of porosity on the measured geophysical responses, shown by its proximity to the EM properties. As greater porosity increases the amount of water the soil can hold, this would again support the identification of the water holding capacity as being the key factor for determining EM properties of soil and therefore archaeological contrast.

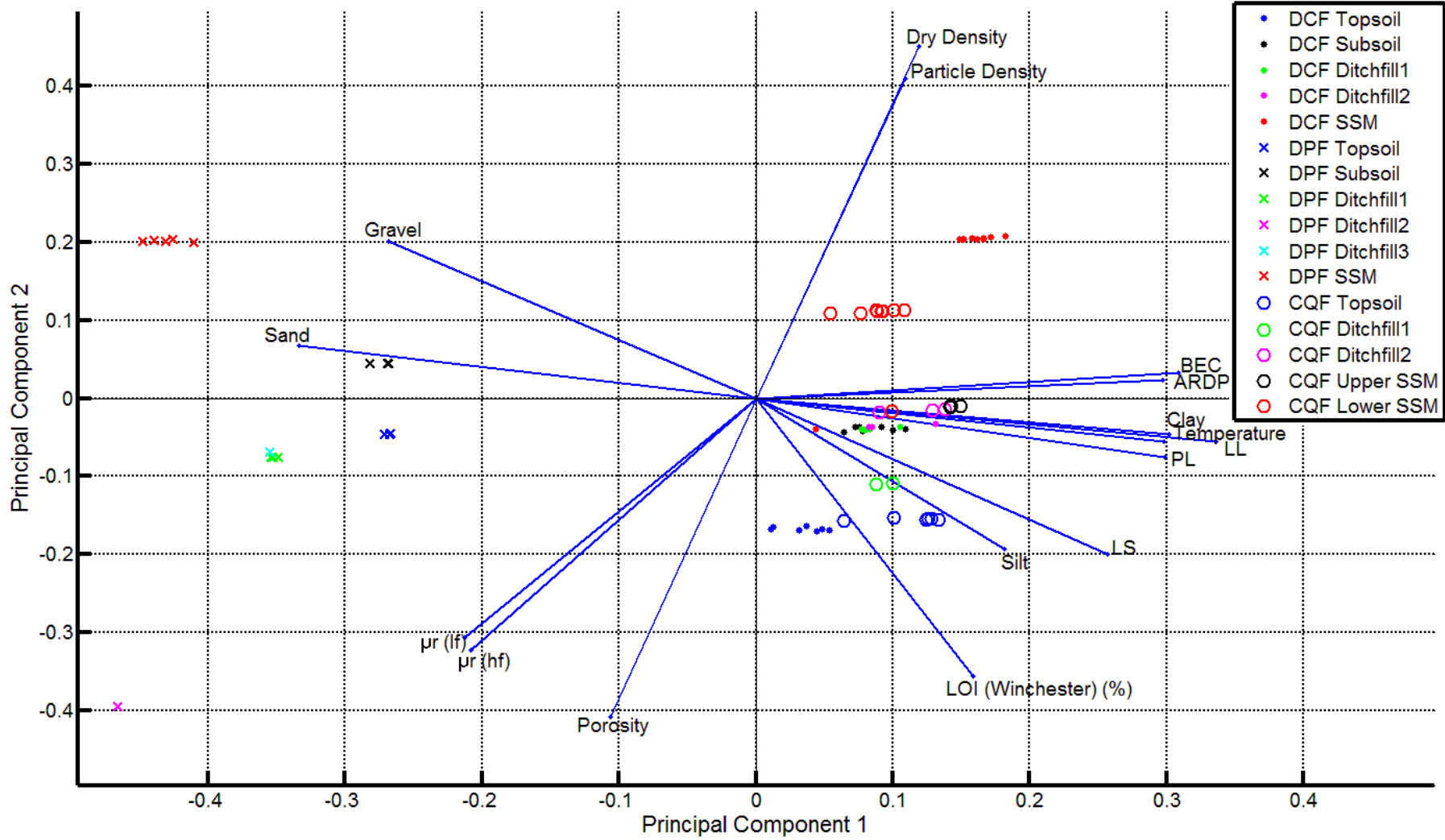


Figure 6.40: Biplot of PCA analysis on average geophysical, geotechnical and geochemical properties of the soil from the field monitoring data showing principal component 1 and 2

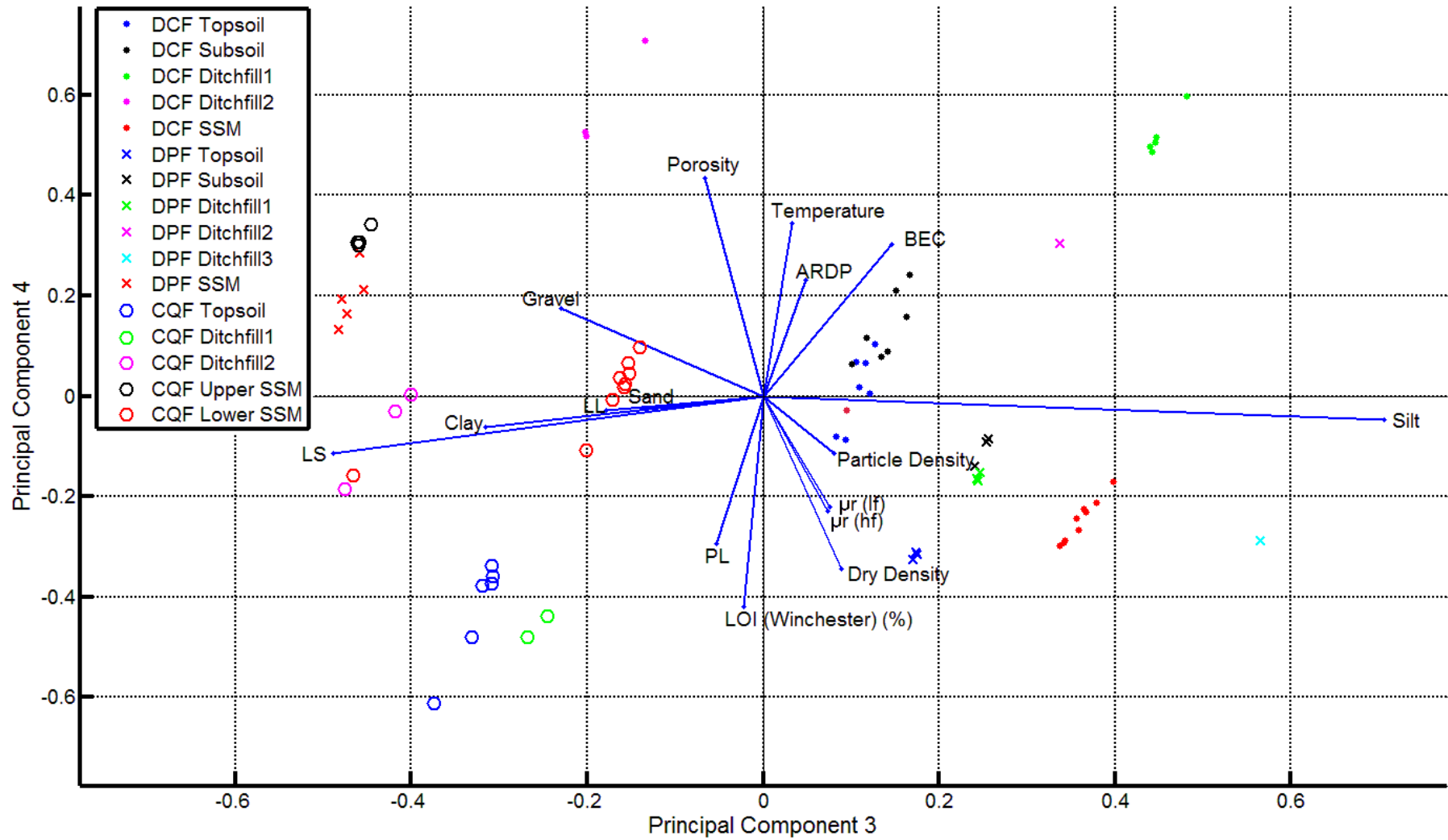


Figure 6.41: Biplot of PCA analysis on average geophysical, geotechnical and geochemical properties of the soil from the field monitoring data showing principal component 3 and 4

6.9. Summary of Field Monitoring Results

A summary of the results of field monitoring of geophysical properties and temperature for archaeological soils and the SSM on a number of different sites is as follows:

- The weather over the monitoring period showed two distinct periods; a dry period near the start of monitoring during 2011 and a wet period during 2012. ARDP and BEC data from all of the studied sites corresponded to these weather patterns with low values recorded in the dry period and high values measured after an initial wetting front. This two period model agreed with the findings of other authors although the time at which each period occurred was shifted due to the abnormal seasonal variation over the monitoring period.
- The initial wetting front was found to be slightly faster in the lower density archaeological soil due to the greater pore spaces of these soils when dry. However, few differences in infiltration were noticed for later rainfall events during the wet period, which rarely affected ARDP and BEC readings below the top few probes except after several days of drying on the surface soils. Differences were however apparent in the magnitudes and rates of drying between the archaeological soils and SSM, with the SSM drying faster for DPF and the archaeological soils on the two fine grained sites. These differences were thought to be the result of differences in the pore sizes of the soils, with larger pores allowing the water to escape more freely.
- Contrast in the geophysical properties between the archaeological and SSM soils was primarily due to differences in the water holding capacities of the soils in terms of both their residual water contents in very dry conditions and field capacities during wet periods. For this reason, the differences in the amount of fine grained particles (especially clay) and porosity between the two soils was thought to be important, and greater differences were found on DPF than on either DCF or CQF where these properties were more similar between the different soils. Higher values for both BEC

and ARDP were also found on the fine grained soils than the coarse grained DPF soils.

This was due to both their higher water holding capacity and differences in their relationships between VWC and EM properties which were discussed in Chapter 5.

- In addition to being affected by water content BEC was also affected by temperature. These temperature effects were more apparent on the fine grained sites in line with the findings of the laboratory work presented in Chapter 5.
- Temperature variations were found to follow the seasonal patterns for all sites, with daily variations also occurring in the near surface soils. However, the scale of the variation and the lag in response was found to increase with depth in line with other authors. Thermal contrasts between the archaeological soils and SSM were found to exist with the archaeological soils displaying a greater response to air temperature changes, and the greatest responses recorded after several days of extremely high or low temperatures.
- Diurnal variations were found to show no effect on ARDP and only a minimal effect on BEC due to their small magnitude and their confinement to the near surface. As such they are unlikely to have a significant effect on geophysical surveys although they may affect thermal prospection.
- Time domain cross correlation confirmed that rainfall events mainly affected the near surface soils, especially on the fine grained soils with no significant correlations below 0.5m whereas the coarse grained soils showed correlations at greater depths. An increased lag was shown to exist with depth on both sites. Whilst no differences in infiltration patterns were found for DPF, for DCF water was found to percolate through the archaeological profile slightly faster due to its lower density with a maximum difference in lags of approximately 15 hours at 0.5m depth. However, the small timescale and the small scale of the correlations suggest that these differences are unlikely to affect prospection significantly.

- ARDP and BEC were found to be positively correlated throughout the monitoring period. BEC was also shown to have a strong positive correlation with temperature which was non-linear and became greater as ARDP (and hence water content) increased. Less variation between temperature and ARDP was found. This confirmed the results of the laboratory analysis in Chapter 5, and suggests that temperature differences may drive the changing BEC contrast between archaeological features and the SSM in saturated soils.
- PCA confirmed that the geophysical properties of the soil were primarily dependent on the amount and mineralogy of the clay in the soil, with a smaller dependence on the porosity of the soil. This confirmed that the most important factor in determining geophysical contrast between the archaeological soils and SSM is their different water holding capacities.

Chapter 7: Conclusions and Recommendations for Future Work

7.1. Conclusions

This thesis described the monitoring of changing geophysical contrasts between archaeological soils and the SSM using a novel TDR monitoring strategy. The project was successful in achieving the aim of the research via the objectives laid out in section 1.2. The main finding of the thesis was that geophysical contrast between archaeological ditches and the surrounding soil was largely a function of the soils ability to hold water with few differences in infiltration speed observed, meaning the overall contrasts were determined by seasonal trends, with the optimum time for surveying thought to be in very dry conditions. Larger differences in the underlying soil properties between the archaeological ditchfills and SSM, which determine the water holding capacity (especially particle size and density) and therefore the resulting geophysical contrasts, were observed on coarse grained as opposed to fine grained soils making the timing of surveys less critical on these sites. The work was also successful in examining the relationships between geotechnical and geophysical properties and improving the understanding of geophysical behaviour across a wider range of soil types than previously studied, which is important for future work on EM radiation and soils and geophysical prediction. For both the BEC and the ARDP, which was strongly influenced by the loss tangent, the most important factors were identified as the clay content and mineralogy (identified by proxy through the Atterberg limits and linear shrinkage) and the water content of the soil.

To achieve the first objective, a thorough critical literature review was conducted. Examination of the literature showed a number of key gaps in our knowledge and understanding of the physical processes which change geophysical contrasts and allow us to detect archaeological features using heritage detection techniques. In particular, it was identified that previous seasonality studies on archaeological features were limited to monthly measurements using earth resistance techniques, which only considered changes in water content (ignoring

temperature and differences in VWC-BEC relationships) and were limited in their ability to study soil water processes due to their coarse temporal scale. Due to this, it was deemed valuable to collect data on soil water and temperature over a long term period and correlate the findings to differences in the soil properties in order to understand the geophysical behaviour of archaeological features.

In order to address these knowledge gaps and to achieve objectives 2 and 3, a new methodology was implemented for studying the geophysical properties of the soil inside and outside of an archaeological feature and the resulting contrasts with greater temporal resolution throughout the year using TDR. A modified version of the monitoring station used by the MTU project, suitable for use in remote locations, where data storage and power supply were limiting factors, was developed and arrays of TDR and temperature probes placed at depths of up to 1m-1.2m both in archaeological soils and the SSM. The modified monitoring station used solar panels which provided enough power throughout the year. Data collection was still required every month and this will need further improvement in order to achieve a fully autonomous monitoring station, although the employed design changes and methodology will be useful for further similar research. Two different sites were chosen, with each containing two study areas; one with predominantly coarse grained and one with predominantly fine grained soils. This allowed changing geophysical contrasts to be studied both in terms of different soil types and variance in climatic conditions between the East and West of the UK. The dataset possessed periods of both unusually dry weather in 2011 and extremely wet conditions in 2012, which allowed both types of soil conditions to be studied in detail, although this may have provided variation which was atypical of usual seasonal variation. In addition to the installation of monitoring stations, soils were sampled from the sites and a wide range of characterisation testing was conducted in the laboratory in order to determine the effects of different geotechnical and geochemical properties of the soil on EM properties over a wide range of water contents, both between fine a coarse grained sites and

archaeological and SSM soils, meeting the requirements of objective 4. With respect to achieving the aim of the research, the main findings are as follows:

- The project was successful in achieving the objective to develop and install autonomous monitoring stations (objective 2) and monitoring geophysical properties for a long period (objective 3). A methodology for soil monitoring projects and a design for a TDR monitoring station based on an earlier design for use in remote locations was developed, which could serve as a basis for future similar research projects. The use of dataloggers to reduce power consumption and solar panels to maintain the power supply allowed the stations to operate continuously throughout the monitoring period. However, several problems were highlighted with the methodology in this thesis especially with factors such as flooding and animal interference. Future projects involving similar soil monitoring stations should take advantage of the lessons learned in the current work to redesign the monitoring stations and installation procedure appropriately. It would be beneficial to have the telemetry system working reliably to send the data and flag up potential problems, and to redesign the station container to be more waterproof, by using marine grade cable glands for example. Subsequent installations may also consider wetting the probes in and using smaller installation trenches during installation to reduce the soil settling period. Care should also be taken when monitoring during dry periods in shrinkable clays to ensure cracks between the excavation trench wall and the soil dug during the installation process do not form and bias the results.
- Geotechnical and geochemical characterisation tests revealed a wide variety of different soil grain sizes, densities and chemical compositions between the sites. Smaller differences were also present within sites, with the archaeological soils generally possessing geotechnical and geochemical properties between those of the topsoil and SSM. Amongst the key differences between the archaeological soils and

SSM were increased levels of organic matter, smaller particle sizes, lower densities and higher magnetic permeability recorded, although these trends varied slightly for some sites and it is worth considering that no typical feature exists, with differences due to variations in feature formation, SSM soil type, environmental factors and post depositional land use.

- Laboratory testing on soils collected from two of the sites in Diddington, Cambridgeshire showed important links between the geotechnical properties of the soil and seasonally varying soil properties (i.e. the VWC and temperature), partially achieving objective 4, although further testing is needed on different soils to determine if these relationships are universally applicable. VWC-BEC relationships were found to increase until saturation was reached across all soils, although higher overall values and rates of increase were found in fine grained soils due to their greater SSA and ion availability. Smaller intra-site variations in BEC-VWC relationships were also found which were linked to differences in the clay content and geochemical differences between soils. Perhaps the most important finding was that VWC-ARDP relationships were found to be more complex and strongly dependent on the soil loss tangent rather than just the amount of bound water as previously suggested. For this reason the amount of clay, which caused lower real permittivity values due to bound water and higher losses due to the increased BEC in the frequency range of the TDR, was an important factor. It is also possible that one of the soils recorded low ARDP values due to the effects of magnetic permeability although no data were available at higher frequencies. Due to these effects fine grained soils possessed higher ARDP values than coarse grained soils at the same water content. However, much smaller differences in ARDP-VWC relationships were apparent between the SSM and archaeological soils from the same site with the exception of DPF Ditchfill2. Due to the relationship with the loss tangent, PCA analysis identified

VWC and soil grain size, especially clay content as the most important variables when determining soil geophysical properties, with mineralogy of the soil determined through Atterberg limits also having significant effects. Both ARDP and BEC relationships could be accurately described using third order polynomials, although different soils were found to fit with variable degrees of success to existing models highlighting the need for empirical calibrations for maximum accuracy.

- Temperature was found to positively correlate to BEC both in the laboratory and in the field, although larger effects were found in fine grained soils due to their greater ion availability. Minimal temperature effects were found for the determination of ARDP in data from either the laboratory or the field due to the effects of competing decreases in ARDP due to the temperature dependence of water and increases due to the release of bound water and increases in BEC. The density of the soil within the range tested in this study was also found to have minimal effects on ARDP and BEC in comparison to other factors such as VWC and temperature in the laboratory, with the exception of the low density DPF Ditchfill2 soil which displayed lower BEC and ARDP values at similar VWC values to the other soils from the same site due its unusually low density (1.3Mg/m^3). Conflicting density effects were found on fine and coarse grained soils suggesting a complex relationship with soil PSD.
- Objective 5 focussed on determining the links between geophysical, geotechnical and recent weather events and the data showed that on all sites, both the ARDP and BEC of the soil during the monitoring period were strongly correlated with the amount of rainfall and displayed two distinct periods; a dry period in 2011 where the values were constantly low and a wet period after an initial wetting front, after which the soil began to respond to further rainfall events. However, infiltration was limited on all sites with rainfall only really affecting the top 0.3m unless significant drying events had taken place at the surface, and the soil was generally affected by seasonal weather

patterns rather than individual rainfall events. BEC data were also affected by temperature variations for both periods and followed the seasonal trends of the ambient air temperature, especially on the fine grained soils and peaked during the summer months.

- Contrast between ARDP values between the archaeological soils and SSM in absolute values were relatively constant across the monitoring period. This was surprising as it was considered that the contrast between archaeological soils and SSM would provide an indication on when the most favourable conditions are to prospect for archaeological features. On closer inspection of the data, it was found to be the result of differences in the holding capacities of the different soils which were affected principally by the PSD (especially the clay content) as well as the mineralogy of the clay and, to a lesser extent, by the soil porosity. These were confirmed as the most important factors in determining the average EM properties using PCA, and the greatest differences were found between the deepest stabilisation archaeological fills and the SSM for all sites. Smaller differences in these properties and predominance of clay in both soil types on fine grained soil sites explains the poor contrast as both possess similar water contents throughout the year. On fine grained soils the best ARDP contrasts expressed as the archaeological ditch anomaly as a percentage of the SSM were found during the dry period due to differences in the residual water content, with the greatest BEC contrasts found both due to differences in the water content and during the summer where slight water content differences were exaggerated due to the effects of temperature on wet soil. The coarse grained DPF soils showed good contrast, which exceeded those found on the fine grained sites, throughout the monitoring period in both wet and dry conditions for both ARDP and BEC with the exception of during the transition between the two.

- Time domain cross correlation between the rainfall and soil after an infiltration event showed few differences between infiltration rates of the archaeological soils and SSM on coarse grained soils, although differences of a few hours were found on the fine grained soils which appeared to be the result of differences in density. One exception to this was in the initial wetting front which followed the dry 2011 period and showed infiltration was faster in the archaeological soil profile for both Diddington sites, especially DCF where the different speeds created a period of significant contrast for a several month, although for CQF similar results were found for both soils. This firstly highlights the importance of antecedent water contents on future infiltration and secondly showed a potential for surveying during the period immediately after a very dry period on fine grained soils. Significant differences were also found in drying patterns between the two soil profiles for all of the sites, especially in the near surface with the archaeological soils drying quicker for DCF and the SSM for DPF and CQF. Drying was mainly thought to be related to differences in pore size caused by density differences for DCF and CQF and by the high gravel content of the DPF SSM. Due to these variations, it may be beneficial to survey sites after a period of several days of warm sunny weather to take advantage of these differences.
- Soil temperature also displayed a seasonal response and a strong relationship with the air temperature, although both the magnitude and lag in variation were limited as a function of depth as found by other studies. For all sites, the archaeological soils were found to show both a slightly stronger response to temperature fluctuations, especially in the near surface (depths <0.3m), as well as a slightly shorter lag time (approximately 1-2 hours less) between changes in the air temperature and soil temperature. These differences were most apparent following a period of several days of consistent high or low temperatures. Greater variations and contrasts were also found on the fine grained sites which may present a good opportunity for aerial

and ground based thermal prospection techniques, although the coarse grained site was affected by turf cover. Diurnal temperature variations were shown to only affect the temperature of the top few layers for both fine grained and coarse grained sites. Cross correlation confirmed that the archaeological soils had a shorter lag in response than the SSM. However, although the temperature changes affected the near surface BEC, no correlation was found between temperature and ARDP. Due to these limitations, diurnal variations were thought to be unimportant for geophysical prospection although may be important for thermal prospection.

- One of the objectives was to determine favourable conditions for archaeological prospection (objective 6). The rich data allowed significant insight into the best timing. From the information obtained for the studied sites, it was possible to predict that the best survey results for both fine grained soils are most likely to be achieved during dry conditions such as those found in 2011 as these conditions led to the highest contrasts between the archaeological feature and the SSM. Additionally, it is recommended that due to the differences in drying patterns, surveys are conducted after several days of a warm period to accentuate water content contrasts. Surveying during the summer, especially using earth resistance techniques, is also beneficial due to the temperature effect on BEC which magnifies contrast due to water content differences. On the coarse grained DPF site, the timing of geophysical surveys was less critical with positive contrasts in BEC and ARDP found throughout the year with the exception of January and February during which time the wetting front was travelling through the profile. In contrast, thermal diurnal differences proved less significant for geophysical surveys thereby do not provide any information of the ideal time of day for prospection.

Whilst the results from this research are successful in answering the overall aim of the project, it should be noted that other soil and archaeological feature types may be more visible in different conditions and the findings are limited to similar sites, with comparable features and

soil types to those studied here. The project has also contributed with useful insight into the EM behaviour of different soil types and relationships between geophysical behaviour, geotechnical and geochemical properties, which it is hoped will feed into future studies in this area.

7.2. Recommendations for Further Work

From the research conducted and presented in this thesis, a number of recommendations and ideas for further work in this field became apparent to the author.

- Whilst the current dataset possessed both extremes of wet and dry weather, the climatic conditions were perhaps atypical of normal seasonal variation. In order to assess this, it would be beneficial to collect data over a longer period to see if the soil behaved in a similar manner with wet and dry periods as seen in the present work. In particular, it would be interesting to see if the early dry period was influenced by the installation procedure by observing if readings ever fell to values similar to those seen shortly after installation. In addition, extended monitoring would allow the soil response to be correlated to a wider range of antecedent conditions and weather histories.
- The present work focused on a number of sites but the current data are based on these specific feature types and background SSMs as perhaps there is no such thing as a “typical” archaeological feature. A natural extension of this work would be to extend the same methodology over a wider range of different size and shaped archaeological features, which have been shown to behave differently, and different SSM soil types to examine differences in their seasonal behaviours. It will also be of benefit to study a wider range of different soil types to validate the importance of different soil properties on the geophysical behaviour of soils. It is the author’s belief that prediction of the ARDP-BEC-VWC relationships without the need for specific empirical

- calibration will only become possible when these relationships are fully understood over the widest possible range of soil types with differing geotechnical and geochemical properties, which were limited due to the constraints of the current work, which only studied four different sites. Whilst studies over a wide range of soils have been carried out by other authors, these have largely only been directed at studying a single geotechnical or geochemical parameter or to develop an empirical model and a multi-parameter systematic study to take into account the interactions of different soil properties is desirable. In a similar way, further investigation into the effects of magnetic permeability on EM properties over a wide frequency range for a range of magnetic soils with varying magnetic grain sizes and chemical compositions would be of benefit as magnetic contrast exists between archaeological soils and SSM. One limitation of the TDR method (and indeed EM geophysical methods in general) is that it is impossible to separate these effects from the electrical effects of mineralogy and water content and therefore their consideration is vitally important. Whilst the magnetic properties were suggested to have significant effects, especially on BEC, measurements of these properties were only available in the low frequency range.
- Finally, a link has been drawn between the geotechnical and geochemical properties of the soils and their subsequent seasonal behaviour. By using existing databases of these properties, it may be possible to make predictions of the seasonal EM properties of the soil from geotechnical parameters through modelling such as the knowledge based system used by the MTU project or the soil-plant-air-water model (SPAW). In addition, differences were found between the properties of the archaeological soils and SSM and these models could be extended to determine the differences between features with different ditchfills to assess which features are visible in particular conditions. The current DART datasets both from this thesis and the other projects may be useful for developing these predictive models.

References

- Adeniji, A., Umara, B.G., Dibal, J.M. and Amali, A.A. (2013) Variation of Infiltration Rates with Soil Texture. A Laboratory Study. **International Journal of Engineering and Innovative Technology**, 3: 454-459.
- Al Chalabi, M.N.I. and Rees, A.I. (1962) An Experiment on the Effect of Rainfall on Electrical Resistivity Anomalies in the Near Surface. **Bonner Jahrbucher**, 162: 266-271.
- Alcontrol Laboratories (2011) "Laboratory Testing Services for Soils and Environmental Waters". Vol. 6. Flintshire, Alcontrol Laboratories.
- Amente, G., Baker, J.M. and Reece, C.F. (2000) Estimation of Soil Solution Electrical Conductivity from Bulk Soil Electrical Conductivity in Sandy Soils. **Soil Science Society of America Journal**, 64: 1931-1939.
- Annan, A.P. (2009) "Electromagnetic Principles of Ground Penetrating Radar". In Jol, H. (Ed.) **Ground Penetrating Radar: Theory and Applications**. Amsterdam, Elsevier Science pp. 4-40.
- Aqdu, S.A., Drummond, J. and Hanson, W.S. (2008) Discovering Archaeological Cropmarks: A Hyperspectral Approach. **The International Archives of the Photogrammetry, Remote Sensing and Spatial Information Sciences**, 37: 361-365.
- Aqil, S. and Schmitt, D.R. (2010) Dielectric Permittivity of Clay Adsorbed Water: Effect of Salinity. **GeoCanada 2010 – Working with the Earth.**, Calgary, AB, Canada.
- Archie, G.E. (1942) The Electrical Resistivity log as an Aid in Determining Some Reservoir Characteristics. **Transactions of the American Institute of Mining and Metallurgical Engineers**, 146: 54-61.
- Arnepalli, D.N., Shanthakumar, S., Rao, B.H. and Singh, D.N. (2007) Comparison of Methods for Determining Specific-Surface Area of Fine-Grained Soils. **Geotechnical and Geological Engineering**, 26: 121–132.
- Arons, A.B. and Peppard, M.B. (1965) Einstein's Proposal of the Photon Concept: A Translation of the Annalen der Physik Paper of 1905. **American Journal of Physics**, 33: 367-374.
- Arulanandan, K. and Mitchell, J.K. (1968) Low Frequency Dielectric Dispersion of Clay Water Electrolyte Systems. **Clays and Clay Minerals**, 16: 337-351.
- Aspinall, A., Gaffney, C.F. and Schmidt, A. (2008) **Magnetometry for Archaeologists**. Lanham; Plymouth: AltaMira Press.
- Bachmair, S., Weiler, M. and Nützmair, G. (2009) Controls of Land Use and Soil Structure on Water Movement: Lessons for Pollutant Transfer Through the Unsaturated Zone. **Journal of Hydrology**, 369: 241-252.
- Bahn, P.G. (1999) **The Cambridge Illustrated History of Archaeology**. Cambridge: Cambridge University Press.

References

- Baker, J.M. and Allmaras, R.R. (1990) System for Automating and Multiplexing Soil-Moisture Measurement by Time-Domain Reflectometry. **Soil Science Society of America Journal**, 54: 1-6.
- Ball, J.A.R. (2002) Characteristic Impedance of Unbalanced TDR Probes. **IEEE Transactions on Instrumentation and Measurement**, 51: 532-536.
- BBC (2011) **Country guides : United Kingdom** [online].
http://news.bbc.co.uk/weather/hi/country_guides/newsid_9384000/9384363.stm
[Accessed 07/05/2012]
- Bechtold, M., Huisman, J.A., Weihermueller, L. and Vereecken, H. (2010) Accurate Determination of the Bulk Electrical Conductivity with the TDR100 Cable Tester. **Soil Science Society of America Journal**, 74: 495-501.
- Bevan, B.W. (2000) An Early Geophysical Survey at Williamsburg, USA. **Archaeological Prospection**, 7: 51-58.
- Beven, K. (2004) Robert E. Horton's Perceptual Model of Infiltration Processes. **Hydrological Processes**, 18: 3447-3460.
- Bewley, R.H. (2003) Aerial Survey for Archaeology. **The Photogrammetric Record**, 18: 273-292.
- Birchak, J.R., Gardner, C.G., Hipp, J.H. and Victor, J.M. (1974) High Dielectric Constant Microwave Probes for Sensing Soil Moisture. **Proceedings of the IEEE**, 62: 93-98.
- Bittelli, M., Salvatorelli, F. and Pisa, P.R. (2008) Correction of TDR-Based Soil Water Content Measurements in Conductive Soils. **Geoderma**, 143: 133-142.
- Blick, S. (2012) **Understanding the Geotechnical Reasons for Crop Marks Caused by the Presence of Archaeology**. MEng Thesis, University of Birmingham.
- Blonquist, J.M., Jones, S.B. and Robinson, D.A. (2005) Standardizing Characterization of Electromagnetic Water Content Sensors: Part 2. Evaluation of Seven Sensing Systems. **Vadose Zone Journal**, 4: 1059-1069.
- Boll, J., van Rijn, R.P.G., Weiler, K.W., Ewen, J.A., Daliparthi, J., Herbert, S.J. and Steenhuis, T.S. (1996) Using Ground-Penetrating Radar to Detect Layers in a Sandy Field Soil. **Geoderma**, 70: 117-132.
- Borengasser, M., Hungate, W.S. and Watkins, R. (2007) **Hyperspectral Remote Sensing: Principles and Applications**. Boca Raton, FL: CRC Press.
- Borjarskii, D.A., Tikhonov, V.V. and Komarova, N.Y. (2002) Model of the Dielectric Constant of Bound Water in Soil for Applications of Microwave Remote Sensing. **Progress In Electromagnetics Research**, 35: 251-269.
- Boxwell, M. (2010) **Solar Electricity Handbook 2010: A Simple Practical Guide to Solar Energy Designing and Installing Photovoltaic Solar Electric Systems**. Ryton-on-Dunsmore: Code Green Publishing.

References

- Brady, J.E. and Holum, J.R. (1993) **Chemistry: The Study of Matter and Its Changes**. 2nd Edition. New York: John Wiley & Sons.
- Brevik, E., Fenton, T. and Horton, R. (2004) Effect of Daily Soil Temperature Fluctuations on Soil Electrical Conductivity as Measured with the Geonics® EM-38. **Precision Agriculture**, 5: 145-152.
- Bridge, B.J., Sabburg, J., Habash, K.O., Ball, J.A.R. and Hancock, N.H. (1996) The Dielectric Behaviour of Clay Soils and its Application to Time Domain Reflectometry. **Australian Journal of Soil Research**, 34: 825-835.
- Brovelli, A. and Cassiani, G. (2008) Effective Permittivity of Porous Media: A Critical Analysis of the Complex Refractive Index Model. **Geophysical Prospecting**, 56: 715-727.
- Brunet, P., Clément, R. and Bouvier, C. (2010) Monitoring Soil Water Content and Deficit Using Electrical Resistivity Tomography (ERT) – A Case Study in the Cevennes Area, France. **Journal of Hydrology**, 380: 146-153.
- BSI (1990) "Methods of Test for Soils for Civil Engineering Purposes: Part 2: Classification Tests". **BS1377-2**. London, UK., British Standards Institution.
- BSI (1999) "Magnetic Materials - Methods for the Determination of the Relative Magnetic Permeability of Feebly Magnetic Materials". **BS5884**. London, UK, British Standards Institution.
- Buckley, F. and Maryott, A.A. (1958) "Tables of Dielectric Dispersion Data for Pure Liquids and Dilute Solutions". **NBS Circular No. 589**. Washington, DC, National Bureau of Standards.
- Cajori, F. (1935) **A History of Physics in its Elementary Branches**. New York: The Macmillan Company.
- Campana, S. and Piro, S. (2010) **Seeing the Unseen. Geophysics and Landscape Archaeology**. London: Taylor & Francis.
- Campbell, J.E. (1990) Dielectric Properties and Influence of Conductivity in Soils at One to 50 Megahertz. **Soil Science Society of America Journal**, 54: 332-341.
- Campbell, R.B., Bower, C.A. and Richards, L.A. (1948) Change of Electrical Conductivity with Temperature and the Relation of Osmotic Pressure to Electrical Conductivity and Ion Concentration for Soil Extracts. **Soil Science Society Proceedings**, 66-69.
- Campbell Scientific (2003) **107 Temperature Probe User Guide**. Logan, Utah
- Campbell Scientific (2005) **Technical Note 33: Sending SMS Messages From Campbell Scientific Dataloggers using GSM Modems**. Logan, Utah
- Campbell Scientific (2008a) **CFM100 Compact Flash Module User Guide**. Logan, Utah
- Campbell Scientific (2008b) **TDR Probes CS605, CS610, CS630, CS635, CS640, CS645 User Guide**. Logan, Utah

References

- Campbell Scientific (2009) "PCTDR". 2.08 ed. Logan, Utah, Campbell Scientific Inc.
- Campbell Scientific (2010a) **CR1000 Measurement and Control System User Guide**. Logan, Utah
- Campbell Scientific (2010b) **CS-GSM Transceiver Kits (inc. Wavcom Fastrack Supreme Modules) User Guide**. Logan, Utah
- Campbell Scientific (2010c) **TDR100 Time Domain Reflectometry User's Guide**. Logan, Utah
- Cassidy, N.J. (2007) Frequency-Dependent Attenuation and Velocity Characteristics of Magnetically Lossy Materials. **IEEE Proceedings of the 4th International Workshop on Advanced Ground Penetrating Radar**, Naples, Italy: 142-146.
- Cassidy, N.J. (2008) Frequency-Dependent Attenuation and Velocity Characteristics of Nano-to Micro Scale, Lossy, Magnetite-Rich Materials. **Near Surface Geophysics**, 6: 341-355.
- Cassidy, N.J. (2009) "Electrical and Magnetic Properties of Rocks, Soils and Fluids". In Jol, H. (Ed.) **Ground-Penetrating Radar: Theory and Applications**. Amsterdam, Elsevier Science pp. 41-72.
- Cassidy, N.J. and Millington, T.M. (2009) The Application of Finite-Difference Time-Domain Modelling for the Assessment of GPR in Magnetically Lossy Materials. **Journal of Applied Geophysics**, 67: 296-308.
- Castellini, M. and Ventrella, D. (2012) Impact of Conventional and Minimum Tillage on Soil Hydraulic Conductivity in Typical Cropping System in Southern Italy. **Soil and Tillage Research**, 124: 47-56.
- Castiglione, P. and Shouse, P.J. (2003) The Effect of Ohmic, Cable Losses on Time-Domain Reflectometry Measurements of Electrical Conductivity. **Soil Science Society of America Journal**, 67: 414-424.
- Cataldo, A. (2008) Simultaneous Measurement of Dielectric Properties and Levels of Liquids Using a TDR Method. **Measurement**, 41: 307-319.
- Cataldo, A., Catarinucci, L., Tarricone, L., Attivissimo, F. and Trotta, A. (2007) A Frequency Domain Method for Extending TDR Performance in Quality Determination of Fluids. **Measurement Science and Technology**, 18: 675-688.
- Cataldo, A., Lay-Ekuakille, A. and De Carlo, C. (2002) Remote Sensing of Liquid Characteristics Using Time Domain Reflectometry. **Proceedings of the Society of Photo-Optical Instrumentation Engineers**, 4814: 465-473.
- Cataldo, A., Piuze, E., Cannazza, G. and De Benedetto, E. (2010) Improvement and Metrological Validation of TDR Methods for the Estimation of Static Electrical Conductivity. **IEEE Transactions on Instrumentation and Measurement**, 59: 1207-1215.
- Catenaccio, A., Daruich, Y. and Magallanes, C. (2003) Temperature Dependence of the Permittivity of Water. **Chemical Physics Letters**, 367: 669-671.

References

- Černý, R. (2009) Time-Domain Reflectometry Method and its Application for Measuring Moisture Content in Porous Materials: A Review. **Measurement**, 42: 329-336.
- Chandler, D.G., Seyfried, M., Murdock, M. and McNamara, J.P. (2004) Field Calibration of Water Content Reflectometers. **Soil Science Society of America Journal**, 68: 1501-1507.
- Chelkowski, A. (1980) **Dielectric Physics**. Amsterdam ; Oxford: Elsevier Scientific.
- Chen, Y. and Or, D. (2006) Effects of Maxwell-Wagner Polarization on Soil Complex Dielectric Permittivity Under Variable Temperature and Electrical Conductivity. **Water Resources Research**, 42: W06424.
- Clark, A. (1980) **Archaeological Detection by Resistivity**. PhD Thesis, University of Southampton.
- Clark, A. (1996) **Seeing Beneath the Soil : Prospecting Methods in Archaeology**. 2nd Edition. London: Routledge.
- Clark, S.P. (1966) **Handbook of Physical Constants**. Revised Edition. New York: Geological Society of America.
- Cole, K.S. and Cole, R.H. (1941) Dispersion and Absorption in Dielectrics I. Alternating Current Characteristics. **Journal of Chemical Physics**, 9: 341-351.
- Conyers, L.B. (2004) **Ground-Penetrating Radar for Archaeology**. Lanham: AltaMira Press.
- Conyers, L.B. and Lucius, J.E. (1996) Velocity Analysis in Archaeological Ground Penetrating Radar Studies. **Archaeological Prospection**, 3: 25-38.
- Cott, P.J. (1997) **The Effect of Weather on Resistivity Measurements over a Known Archaeological Feature**. M.Phil. Thesis, The University of Bradford.
- Cownie, A. and Palmer, L.S. (1952) The Effect of Moisture on the Electrical Properties of Soil. **Proceedings of Physical Society B**, 65: 295-301.
- Crow, P. and Crutchley, S. (2010) "The Light Fantastic: Using Airborne Lidar in Archaeological Survey". Swindon, English Heritage.
- Cuenca-García, C., Jones, R.J., Jones, A.J. and Poller, T. (2013) From the Air to the Atomic level of a Ditch: Integrating Geophysical and Geochemical Survey Methods at the Prehistoric Cropmark Complex of Forteviot (Perthshire, Scotland). **10th International Conference on Archaeological Prospection**, Vienna, Austria.
- Curioni, G. (2013) **Investigating the Seasonal Variability in Geophysical Soil Properties using Field Monitoring Data from Time-Domain Reflectometry Probes**. PhD Thesis, University of Birmingham.
- Curioni, G., Chapman, D.N., Metje, N., Foo, K.Y. and Cross, J.D. (2012) Construction and Calibration of a Field TDR Monitoring Station. **Near Surface Geophysics**, 10: 249-261.

References

- Curtis, J.O. (2001) Moisture Effects on the Dielectric Properties of Soils. **IEEE Transactions on Geoscience and Remote Sensing**, 39: 125-128.
- Dalton, F.N., Herkelrath, W.N., Rawlins, D.S. and Rhoades, J.D. (1984) Time Domain Reflectometry-Simultaneous Measurement of Soil-Water and Electrical Conductivity with a Single Probe. **Science**, 224: 989-990.
- Dalton, F.N. and van Genuchten, M.T. (1986) The Time-Domain Reflectometry Method for Measuring Soil Water Content and Salinity. **Geoderma**, 38: 237-250.
- Darvill, T. (2008) **Concise Oxford Dictionary of Archaeology**. Oxford: Oxford University Press.
- Dasberg, S. and Hopmans, J.W. (1992) Time Domain Reflectometry Calibration for Uniformly and Non-Uniformly Wetted Sandy and Clayey Loam Soils. **Soil Science Society of America Journal**, 56: 1341-1345.
- David, A., Linford N and P, L. (2008) "Geophysical Survey in Archaeological Field Evaluation". 2nd ed. Swindon, English Heritage.
- Davidson, D.W. and Cole, R.H. (1951) Dielectric Relaxation in Glycerol, Propylene Glycol, and N Propanol. **Journal of Chemical Physics**, 1484-1490.
- Davidson, E.A., Belk, E. and Boone, R.D. (1998) Soil Water Content and Temperature as Independent or Confounded Factors Controlling Soil Respiration in a Temperate Mixed Hardwood Forest. **Global Change Biology**, 4: 217-227.
- Davie, T. (2008) **Fundamentals of Hydrology**. London: Routledge.
- Davis, S.N. and De Wiest, R.J.M. (1966) **Hydrogeology**. New York; London; Sydney: John Wiley & Sons.
- De Loor, G.P. (1968) Dielectric Properties of Heterogenous Materials Containing Water. **Journal of Microwave Power**, 3: 67-73.
- Debye, P.J.W. (1929) **Polar Molecules**. New York: Chemical Catalog Company.
- Detectation (2012) **How far down can GPR penetrate in clay soil** [online]. <http://forum.detectation.com/viewtopic.php?t=1469&p=4258> [Accessed 20/04/2012]
- Dirksen, C. and Dasberg, S. (1993) Improved Calibration of Time-Domain Reflectometry Soil Water Content Measurements. **Soil Science Society of America Journal**, 57: 660-667.
- Dobson, M.C., Ulaby, F.T., Hallikainen, M.T. and El Rayes, M.A. (1985) Microwave Dielectric Behavior of Wet Soil-Part II: Dielectric Mixing Models. **IEEE Transactions on Geoscience and Remote Sensing**, GE-23: 35-46.
- Dolinar, B., Misić, M. and Trauner, L. (2007) Correlation Between Surface Area and Atterberg Limits of Fine-Grained Soils. **Clays and Clay Minerals**, 55: 519-523.
- Dolinar, B. and Trauner, L. (2004) Liquid Limit and Specific Surface of Clay Particles. **Geotechnical Testing Journal**, 27: 580-584.

References

- Drewett, P. (1999) **Field Archaeology: An Introduction**. London: Taylor & Francis.
- Elliott, R.S. (1993) **Electromagnetics : History, Theory, and Applications**. New York: IEEE Press.
- Engineering Toolbox (2012) **Density of Some Common Materials** [online].
http://www.engineeringtoolbox.com/density-materials-d_1652.html [Accessed 18/09/2013]
- Escorihuela, M.J., de Rosnay, P., Kerr, Y.H. and Calvet, J.C. (2007) Influence of Bound-Water Relaxation Frequency on Soil Moisture Measurements. **IEEE Transactions on Geoscience and Remote Sensing**, 45: 4067-4076.
- Evans, M.E. and Heller, F. (2003) **Environmental Magnetism: Principles and Applications of Enviromagnetics**. London: Academic Press.
- Evans, R. and Jones, R.J.A. (1977) Crop Marks and Soil Marks at Two Archaeological Sites in Britain. **Journal of Archaeological Science**, 4: 63 - 76.
- Evelt, S.R. (1998) Coaxial Multiplexer for Time Domain Reflectometry Measurement of Soil Water Content and Bulk Electrical Conductivity. **Transactions of American Society of Agricultural Engineers**, 41: 361-369.
- Evelt, S.R. (2000a) The TACQ Computer Program for Automatic Time Domain Reflectometry Measurements: I. Design and Operating Characteristics. **Transactions of American Society of Agricultural Engineers**, 43: 1939-1946.
- Evelt, S.R. (2000b) The TACQ Computer Program for Automatic Time Domain Reflectometry Measurements: II. Waveform Interpretation Methods. **Transactions of American Society of Agricultural Engineers**, 43: 1947-1956.
- Evelt, S.R. (2003) "Soil Water Measurement by Time Domain Reflectometry". In Stewart, B.A. & Howell, T.A. (Eds.) **Encyclopedia of Water Science**. New York, Marcel Dekker pp. 894-898.
- Evelt, S.R. and Parkin, G.W. (2005) Advances in Soil Water Content Sensing. **Vadose Zone Journal**, 4: 986.
- Evelt, S.R. and Steiner, J.L. (1995) Precision of Neutron Scattering and Capacitance Type Soil Water Content Gauges from Field Calibration. **Soil Science Society of America Journal**, 961-968.
- Evelt, S.R., Tolk, J.A. and Howell, T.A. (2005) Time Domain Reflectometry Laboratory Calibration in Travel Time, Bulk Electrical Conductivity, and Effective Frequency. **Vadose Zone Journal**, 4: 1020-1029.
- Fannin, P., Cohentannoudji, L., Bertrand, E., Giannitsis, A., Macoireachtaigh, C. and Bibette, J. (2006) Investigation of the Complex Susceptibility of Magnetic Beads Containing Maghemite Nanoparticles. **Journal of Magnetism and Magnetic Materials**, 303: 147-152.

References

- Farouki, O.T. (1981) **Thermal Properties of Soils**. Hanover, NH: US Army Cold Regions Research and Engineering Laboratory. Monograph 81-1.
- Farrar, D.M. and Coleman, J.D. (1967) The Correlation of Surface Area With Other Properties of Nineteen British Clay Soils. **Journal of Soil Science**, 18: 118-124.
- Fassbinder, J.W.E., Stanjek, H. and Vali, H. (1990) Occurrence of Magnetic Bacteria in Soil. **Nature**, 343: 161-163.
- Fellner Feldegg, H. (1968) The Measurement of Dielectrics in the Time Domain. **The Journal of Physical Chemistry**, 73: 616-623.
- Feng, W., Lin, C.P., Deschamps, R.J. and Drnevich, V.P. (1999) Theoretical Model of a Multisection Time Domain Reflectometry Measurement System. **Water Resources Research**, 35: 2321-2331.
- Ferre, P.A., Knight, J.H., Rudolph, D.L. and Kachanoski, R.G. (1998) The Sample Areas of Conventional and Alternative Time Domain Reflectometry Probes. **Water Resources Research**, 34: 2971-2979.
- Fiener, P. and Auerswald, K. (2009) Spatial Variability of Rainfall on a Sub-Kilometre Scale. **Earth Surface Processes and Landforms**, Landforms 848–859.
- Fleisch, D.A. (2008) **A Student's Guide to Maxwell's Equations**. Cambridge; New York: Cambridge University Press.
- Florides, G. and Kalogirou, S. (2005) Annual Ground Temperature Measurements at Various Depths. **8th REHVA World Congress Climate**, Lausanne.
- Florides, G. and Kalogirou, S. (2009) Measurements of Ground Temperature at Various Depths. **3rd International Conference on Sustainable Energy Technologies**, Nottingham, UK.
- Foth, H.D. (1990) **Fundamentals of Soil Science**. New York: John Wiley & Sons.
- Fredlund, D.G. and Xing, A.Q. (1994) Equations for the Soil-Water Characteristic Curve. **Canadian Geotechnical Journal**, 31: 521-532.
- Fredlund, D.G., Xing, A.Q. and Huang, S.Y. (1994) Predicting the Permeability Function for Unsaturated Soils using the Soil-Water Characteristic Curve. **Canadian Geotechnical Journal**, 31: 533-546.
- Friedman, S.P. (1998) A Saturation Degree-Dependent Composite Spheres Model for Describing the Effective Dielectric Constant of Unsaturated Porous Media. **Water Resources Research**, 34: 2949-2961.
- Friedman, S.P. (2005) Soil Properties Influencing Apparent Electrical Conductivity: A Review. **Computers and Electronics in Agriculture**, 46: 45-70.
- Friel, R. and Or, D. (1999) Frequency Analysis of Time-Domain Reflectometry (TDR) with Application to Dielectric Spectroscopy of Soil Constituents. **Geophysics**, 64: 707-718.

References

- Fry, R. (2011a) "Diddington, Cambridgeshire, Geophysical Report on Preliminary Fluxgate Gradiometer Survey". **DART Project Internal Report**. Bradford, UK. Available from http://dartportal.leeds.ac.uk/dataset/dart_excavation_data.
- Fry, R. (2011b) "The Royal Agricultural College, Cirencester: Geophysical Report on Preliminary Fluxgate Gradiometer Survey". **DART Project Internal Report**. Bradford, UK. Available from http://dartportal.leeds.ac.uk/dataset/dart_excavation_data.
- Fry, R. (2014) **The Study of Seasonal Variation and the Implications for Archaeological Prospection using Electrical Resistance** PhD Thesis, University of Bradford.
- Fry, R., Stott, D., Boddice, D. and Beck, A.R. (2012) What a Difference a Year Makes: Preliminary DART Datasets from Cherry Copse, Cirencester. **AARG News** 45: 42-47.
- Fukue, M., Minato, T., Horibe, H. and Taya, N. (1999) The Micro-Structures of Clay Given by Resistivity Measurements. **Engineering Geology**, 54: 43-53.
- Gaffney, C.F. and Gater, J. (2003) **Revealing the Buried Past : Geophysics for Archaeologists**. Stroud: Tempus.
- Gale, S.J. and Hoare, P.G. (1991) **Quaternary Sediments: Petrographic Methods for the Study of Unlithified Rocks**. London: Belhaven Press.
- Gardner, W.H. (1986) "Water Content". In Klute, A. (Ed.) **Methods of Soil Analysis, Part 1: Physical and Mineralogical Methods**. 2nd ed. Madison, WI, American Society of Agronomy, Soil Science Society of America pp. 493-544.
- Geonics Limited (2013) **Geonics Limited Website** [online]. <http://www.geonics.com/> [Accessed 15/05/2014]
- Gerrard, J. (2000) **Fundamentals of Soils**. London: Routledge.
- GF Instruments (2014) **GF Instruments Website** [online]. <http://www.gfinstruments.com/> [Accessed 15/05/2014]
- Giese, K. and Tiemann, R. (1975) Determination of Complex Permittivity from Thin-Sample Time Domain Reflectometry Improved Analysis of Step-Response Waveform. **Advances in Molecular Relaxation Processes**, 7: 45-59.
- Gong, Y., Cao, Q. and Sun, Z. (2003) The Effects of Soil Bulk Density, Clay Content and Temperature on Soil Water Content Measurement Using Time-Domain Reflectometry. **Hydrological Processes**, 17: 3601-3614.
- Graeff, T., Zehe, E., Schlaeger, S., Morgner, M., Bauer, A., Becker, R., Creutzfeldt, B. And Bronstert, A.(2010) A Quality Assessment of Spatial TDR Soil Moisture Measurements in Homogenous and Heterogeneous Media with Laboratory Experiments. **Hydrology and Earth System Sciences**, 14: 1007-1020.
- Green, W.H. and Ampt, G. (1911) Studies of Soil Physics, Part I - the Flow of Air and Water through Soils. **Journal of Agricultural Science**, 4: 1-24.

References

- Greenstream Publishing (2010) **Solar Irradiance Calculator** [online].
<http://www.efficientenergysaving.co.uk/solar-irradiance-calculator.html> [Accessed 10/11/2010]
- Grote, K., Hubbard, S.S. and Rubin, Y. (2002) GPR Monitoring of Volumetric Water Content in Soils Applied to Highway Construction and Maintenance. **The Leading Edge**, 21: 482-485.
- Gumerman, G.J. and Lyons, T.R. (1971) Archaeological Method and Remote Sensing. **Science**, 172:126-132.
- Haines, W.B. (1930) Studies in the Physical Properties of Soil V: The Hysteresis Effect in Capillary Properties, and the Modes of Moisture Distribution Associated Therewith. **Journal of Agricultural Science**, 20: 97-116.
- Hallikainen, M.T., Ulaby, F.T., Dobson, M.C., El Rayes, M.A. and Wu, L.-K. (1985) Microwave Dielectric Behavior of Wet Soil-Part 1: Empirical Models and Experimental Observations. **IEEE Transactions on Geoscience and Remote Sensing**, GE-23: 25-34.
- Hanson, W.S. (2005) "Sun, Sand and See: Creating Bias in the Archaeological Record". In Brophy, K. Cowley, D. (Eds.) **From the Air: Understanding Aerial Archaeology**. Stroud, Tempuspp. 73-85.
- Havriliak, S. and Negami, S. (1967) A Complex Plane Representation of Dielectric and Mechanical Relaxation Processes in Some Polymers. **Polymer**, 8: 161-210.
- Heimovaara, T.J. (1993) Design of Triple-Wire time Domain Reflectometry Probes in Practice and Theory. **Soil Science Society of America Journal**, 57: 1410-1417.
- Heimovaara, T.J. (1994) Frequency-Domain Analysis of Time-Domain Reflectometry Wave Forms. 1. Measurement of the Complex Dielectric Permittivity of Soils. **Water Resources Research**, 30: 189-199.
- Heimovaara, T.J. and Bouten, W. (1990) A Computer-Controlled 36-Channel Time Domain Reflectometry System for Monitoring Soil-Water Contents. **Water Resources Research**, 26: 2311-2316.
- Heimovaara, T.J., Bouten, W. and Verstraten, J.M. (1994) Frequency Domain Analysis of Time Domain Reflectometry Wave-Forms 2. A 4-Component Complex Dielectric Mixing Model for Soils. **Water Resources Research**, 30: 201-209.
- Heimovaara, T.J., deWinter, E.J.G., vanLoon, W.K.P. and Esveld, D.C. (1996) Frequency Dependent Dielectric Permittivity from 0 to 1 GHz: Time Domain Reflectometry Measurements Compared with Frequency Domain Network Analyzer Measurements. **Water Resources Research**, 32: 3603-3610.
- Heimovaara, T.J., Focke, A.G., Bouten, W. and Verstraten, J.M. (1995) Assessing Temporal Variations in Soil-Water Composition with Time-Domain Reflectometry. **Soil Science Society of America Journal**, 59: 689-698.

References

- Herkelrath, W.N., Hamburg, S.P. and Murphy, F. (1991) Automatic Real-Time monitoring of Soil Moisture in a Remote Field Area with Time Domain Reflectometry. **Water Resources Research**, 27: 857-864.
- Herz, N. and Garrison, E.G. (1998) **Geological Methods for Archaeology**. Oxford: Oxford University Press.
- Hesse, A. (1966) The Importance of Climatic Observations in Archaeological Prospecting. **Prospezione Archaeologica**, 1: 11-13.
- Hewlett, J.D. and Hibbert, A.R. (1967) "Factors Affecting the Response of Small Watersheds to Precipitation in Humid Areas". In Sopper, W.E. & Lull, H.W. (Eds.) **Forest Hydrology**. New York, Pergamon Press pp. 275-290.
- Hilhorst, M.A., Dirksen, C., Kämpers, F.W.H. and Feddes, R.A. (2001) Dielectric Relaxation of Bound Water Versus Soil Matric Pressure. **Soil Science Society of America Journal**, 65: 311-314.
- Hillel, D. (1971) **Soil and Water**. New York: Academic Press.
- Hipp, J.E. (1974) Soil Electromagnetic Parameters as Functions of Frequency, Soil Density, and Soil Moisture. **Proceedings of the IEEE**, 62: 98-103.
- Hirst, A.W. (1966) **Applied Electricity**. 4th Edition. London: Blackie & Son.
- Hoekstra, P. and Delaney, A. (1974) Dielectric Properties of Soils at UHF and Microwave Frequencies. **Journal of Geophysical Research**, 79: 1699-1708.
- Horton, J.H. and Hawkins, R.H. (1965) Flow Path of Rain from the Soil Surface to the Water Table. **Soil Science**, 100: 377-383.
- Horton, R.E. (1933) The Role of Infiltration in the Hydrologic Cycle. **Transactions of the American Geophysical Union**, 14: 446-460.
- Huisman, J.A. and Bouten, W. (1999) Comparison of Calibration and Direct Measurement of Cable and Probe Properties in Time Domain Reflectometry. **Soil Science Society of America Journal**, 63: 1615-1617.
- Huisman, J.A., Hubbard, S.S., Redman, J.D. and Annan, A.P. (2003a) Measuring Soil Water Content with Ground Penetrating Radar: A Review. **Vadose Zone Journal**, 2: 476-491.
- Huisman, J.A., Lin, C.P., Weihermüller, L. and Vereecken, H. (2008) Accuracy of Bulk Electrical Conductivity Measurements with Time Domain Reflectometry. **Vadose Zone Journal**, 7: 426.
- Huisman, J.A., Snepvangers, J., Bouten, W. and Heuvelink, G.B.M. (2002) Mapping Spatial Variation in Surface Soil Water Content: Comparison of Ground-Penetrating Radar and Time Domain Reflectometry. **Journal of Hydrology**, 269: 194-207.

References

- Huisman, J.A., Snepvangers, J.J.J.C., Bouten, W. and Heuvelink, G.B.M. (2003b) Monitoring Temporal Development of Spatial Soil Water Content Variation: Comparison of Ground Penetrating Radar and Time Domain Reflectometry. **Vadose Zone Journal**, 2: 519-529.
- Huisman, J.A., Sperl, C., Bouten, W. and Verstraten, J.M. (2001) Soil Water Content Measurements at Different Scales: Accuracy of Time Domain Reflectometry and Ground Penetrating Radar. **Journal of Hydrology**, 245: 48-58.
- IAEA (2008) "Field Estimation of Soil Water Content: A Practical Guide to Methods, Instrumentation and Sensor Technology". Vienna, International Atomic Energy Agency.
- IMKO GmbH (2012) **IMKO GmbH Trime System Specifications** [online]. <http://imko.de/en/abouttrime-tdr> [Accessed 08/10/2013]
- Jacobsen, O.H. and Schjonning, P. (1993) A Laboratory Calibration of Time Domain Reflectometry for Soil Water Measurement including Effects of Bulk Density and Texture. **Journal of Hydrology**, 151 147-157.
- Jolliffe, I.T. (2002) **Principal Component Analysis**. Secaucus, NJ: Springer-Verlag.
- Jones, R.J.A. and Evans, R. (1975) "Soil and Crop Marks in the Recognition of Archaeological Sites by Air Photography". In Wilson, D.R. (Ed.) **Aerial Reconnaissance for Archaeology**. London, CBA pp. 1-11.
- Jones, S.B., Blonquist, J.M., Robinson, D.A., Rasmussen, V.P. and Or, D. (2005) Standardizing Characterization of Electromagnetic Water Content sensors: Part 1. Methodology. **Vadose Zone Journal**, 4: 1048-1058.
- Jones, S.B. and Or, D. (2002) Surface Area, Geometrical and Configurational Effects on Permittivity of Porous Media. **Journal of Non-Crystalline Solids**, 305: 247-254.
- Jones, S.B. and Or, D. (2004) Frequency Domain Analysis for Extending Time Domain Reflectometry Water Content Measurement in Highly Saline Soils. **Soil Science Society of America Journal**, 68: 1568-1577.
- Jones, S.B., Wraith, J.M. and Or, D. (2002) Time Domain Reflectometry Measurement Principles and Applications. **Hydrological Processes**, 16: 141-153.
- Jordan, D. (2009) How Effective is Geophysical Survey? A Regional Review. **Archaeological Prospection**, 16: 77-90.
- Ju, Z.Q., Liu, X.N., Ren, T.S. and Hu, C.S. (2010) Measuring Soil Water Content With Time Domain Reflectometry: An Improved Calibration Considering Soil Bulk Density. **Soil Science**, 175: 469-473.
- Kaatze, U. (2010) Techniques for Measuring the Microwave Dielectric Properties of Materials. **Metrologia**, 47: S91-S113.
- Kachanoski, R.G., Gregorich, E.G. and van Wesenbeeck, I.J. (1988) Estimating Spatial Variations of Soil Water Content using Non-Contacting Electromagnetic Inductive Methods. **Canadian Journal of Soil Science**, 68: 715-722.

References

- Kachanoski, R.G., van Wesenbeeck, I.J. and de Jong, E. (1990) Field Scale Patterns of Soil Water Storage from Non-Contacting Measurements of Bulk Electrical Conductivity. **Canadian Journal of Soil Science**, 70: 537-542.
- Kallner, E. and Lundin, L.-C. (2001) Calibration of Time Domain Reflectometry for Water Content in Peat Soil. **Nordic Hydrology**, 32: 315-332.
- Kelleners, T.J., Seyfried, M.S., Blonquist, J.M., Bilskie, J. and Chandler, D.G. (2005) Improved Interpretation of Water Content Reflectometer Measurements in Soils. **Soil Science Society of America Journal**, 69: 1684.
- Kim, S. and Kim, H. (2007) Stochastic Analysis of Soil Moisture to Understand Spatial and Temporal Variations of Soil Wetness at a Steep Hillside. **Journal of Hydrology**, 341: 1-11.
- Knappett, J.A. and Craig, R.F. (2012) **Craig's Soil Mechanics**. 8th Edition. London; New York: Taylor & Francis.
- Knight, J.H. (1992) Sensitivity of time domain reflectometry measurements to lateral variations in soil water content. **Water Resources Research**, 28: 2345-2352.
- Knoll, M.D., Knight, R. and Brown, E. (1995) Can Accurate Estimates of Permeability be Obtained From Measurements of Dielectric Properties? **8th EEGS Symposium on the Application of Geophysics to Engineering and Environmental Problems** Orlando, Florida.
- Kuhn, J.A. and Zornberg, J.G. (2005) Time Domain Reflectometry Measurement and Highly Plastic Clays. **Proceedings of the Conference of the Graduate Engineering Council**, Austin, Texas.
- Kvamme, K.L. (2003) Geophysical Surveys as Landscape Archaeology. **American Antiquity**, 68: 435-457.
- Lambot, S., Slob, E., Chavarro, D., Lubczynski, M. and Vereecken, H. (2008) Measuring Soil Surface Water Content in Irrigated Areas of Southern Tunisia using Full-Waveform Inversion of Proximal GPR Data. **Near Surface Geophysics**, 6: 403-410.
- Laurent, J.-P., Ruelle, P., Delage, L., Zaïri, A., Nouna, B.B. and Adjmi, T. (2005) Monitoring Soil Water Content Profiles with a Commercial TDR System. **Vadose Zone Journal**, 4: 1030.
- Leckebusch, J.r. (2003) Ground-Penetrating Radar: a Modern Three-Dimensional Prospection Method. **Archaeological Prospection**, 10: 213-240.
- Ledieu, J., De Ridder, P., De Clerck, P. and Dautrebande, S. (1986) A Method of Measuring Soil Moisture by Time Domain Reflectometry. **Journal of Hydrology**, 88: 319-328.
- Lin, C.P. (2003) Frequency Domain Versus Travel Time Analysis of TDR Waveforms for Soil Moisture Measurements. **Soil Science Society of America Journal**, 67: 720-729.

References

- Lin, C.P., Chung, C.C., Huisman, J.A. and Tang, S.H. (2008) Clarification and Calibration of Reflection Coefficient for Electrical Conductivity Measurement by Time Domain Reflectometry. **Soil Science Society of America Journal**, 72: 1033.
- Lin, C.P., Chung, C.C. and Tang, S.H. (2007) Accurate Time Domain Reflectometry Measurement of Electrical Conductivity Accounting for Cable Resistance and Recording Time. **Soil Science Society of America Journal**, 71: 1278.
- Lindsley, D.H., Andreasen, G.E. and Balsley, J.R. (1966) "Magnetic Properties of Rocks and Minerals". In Clark, S.P. (Ed.) **Handbook of Physical Constants** New York, Geological Society of America pp. 543-552.
- Logsdon, S.D. (2000) Effect of Cable Length on Time Domain Reflectometry Calibration for High Surface Area Soils. **Soil Science Society of America Journal**, 64: 54-61.
- Logsdon, S.D. (2006) Experimental Limitations of Time Domain Reflectometry Hardware for Dispersive Soils. **Soil Science Society of America Journal**, 70: 537.
- Logsdon, S.D. (2008) Electrical Spectra of Undisturbed Soil from a Crop Rotation Study. **Soil Science Society of America Journal**, 72: 11.
- Lunt, I.A., Hubbard, S.S. and Rubin, Y. (2005) Soil Moisture Content Estimation using Ground Penetrating Radar Reflection Data. **Journal of Hydrology**, 307: 254-269.
- Mail Online (2012) **What a Difference a year makes: Map shows how England has gone from Driest in 90 years to Wettest on Record** [online].
<http://www.dailymail.co.uk/news/article-2254844/What-difference-year-makes-Map-shows-England-gone-driest-90-years-wettest-record.html> [Accessed 14/01/2014]
- Malicki, M.A., Plagge, R. and Roth, C.H. (1996) Improving the Calibration of Dielectric TDR Soil Moisture Determination taking into Account the Solid Soil. **European Journal of Soil Science**, 47: 357-366.
- MathWorks Inc. (2010) "MATLAB and Simulink Student Version R2010a". Natick, MA, The MathWorks, Inc.
- Maxwell, J.C. (1865) A Dynamical Theory of the Electromagnetic Field. **Philosophical Transactions of the Royal Society**, 166: 459-512 (reprinted in The Scientific Papers of James Clerk Maxwell, Volume I, 1952, New York, Dover, pp. 1528-1597).
- McEnroe, J.C. (2002) "Cretan Questions: Politics and Archaeology 1898-1913". In Hamilakis, Y. (Ed.) **Labyrinth Revisited: Rethinking 'Minoan' Archaeology**. Oxford, Oxbow Books pp. 59-72.
- McNeill, J.D. (1980) "Electrical Conductivity of Soils and Rocks". **Technical Note TN-5**. Ontario, CA, Geonics Ltd.
- Meglich, T., Li, Y., Van Dam, R.L. and Billings, S. (2008) Characterization of Frequency Dependent Magnetic Susceptibility in UXO Electromagnetic Geophysics. **SEG 2008 Annual Meeting**, Las Vegas.

References

- Meissner, T. and Wentz, F.J. (2004) The Complex Dielectric Constant of Pure and Sea Water from Microwave Satellite Observations. **IEEE Transactions on Geoscience and Remote Sensing**, 42: 1836-1849.
- Menziani, M., Pugnaghi, S., Vincenzi, S. and Santangelo, R. (2003) Soil Moisture Monitoring in the Toce Valley (Italy). **Hydrology and Earth System Sciences**, 7: 890-902.
- Menziani, M., Rivasi, M.R., Pugnaghi, S., Santangelo, R. and Vincenzi, S. (1996) Soil Volumetric Water Content Measurements using TDR Technique. **Annali di Geofisica**, 39: 91-96.
- Met Office (2014) **Met Office Regional Climate Summaries** [online].
<http://www.metoffice.gov.uk/climate/uk/regional/> [Accessed 09/04/2014]
- Microsoft Corporation (2001) "Hyperterminal". Redmond, WA, Microsoft Corporation.
- Mills, J. (2003) Aerial Archaeology on Clay Geologies. **AARG News** 27: 12-19.
- Mironov, V.L., Dobson, M.C., Kaupp, V.H., Komarov, S.A. and Kleshchenko, V.N. (2004) Generalized Refractive Mixing Dielectric Model for Moist Soils. **IEEE Transactions on Geoscience and Remote Sensing**, 42: 773-785.
- Mironov, V.L., Kosolapova, L.G. and Fomin, S.V. (2009) Physically and Mineralogically Based Spectroscopic Dielectric Model for Moist Soils. **IEEE Transactions on Geoscience and Remote Sensing**, 47: 2059-2070.
- Mitchell, J.K. and Soga, K. (2005) **Fundamentals of Soil Behavior**. Hoboken, NJ: John Wiley & Sons.
- Miyamoto, T., Annaka, T. and Chikushi, J. (2003) Soil Aggregate Structure Effects on Dielectric Permittivity of an Andisol Measured by Time Domain Reflectometry. **Vadose Zone Journal**, 2: 90-97.
- Mohanty, B.P., Shouse, P.J. and van Genuchten, M.T. (1998) Spatio-Temporal Dynamics of Water and Heat in a Field Soil. **Soil and Tillage Research**, 47: 133-143.
- Monteith, J.L. (1965) Evaporation and Environment. **Symposia of the Society for Experimental Biology**, 19: 205--234.
- Moret-Fernández, D., Lera, F., Arrúe, J.L. and López, M.V. (2009) Measurement of Soil Bulk Electrical Conductivity Using Partially Coated TDR Probes. **Vadose Zone Journal**, 8: 594-600.
- mPhone Ltd. (2010) **GSM, GPRS and WAP Settings** [online].
http://www.mphone.co.uk/mms_wap_settings_orange.html [Accessed 15/02/2012]
- Nadler, A., Dasberg, S. and Lapid, I. (1991) Time Domain Reflectometry Measurements of Water Content and Electrical Conductivity of Layered Soil Columns. **Soil Science Society of America Journal**, 55: 938-943.
- Nara, K. (2005) Study of the Magnetic Field Effect on Commercial Thermistors using a Water Triple Point. **Japanese Journal of Applied Physics**, 44: 1506-1507.

References

- Nelder, J.A. and Mead, R. (1965) A Simplex-Method for Function Minimization. **Computer Journal**, 7: 308-313.
- Nobel, P.S. and Geller, G.N. (1987) Temperature Modelling of Wet and Dry Desert Soils. **Journal of Ecology**, 75: 247-258.
- Noborio, K. (2001) Measurement of Soil Water Content and Electrical Conductivity by Time Domain Reflectometry: a Review. **Computers and Electronics in Agriculture**, 31: 213-237.
- Olhoeft, G.R. (2003) Electromagnetic Field and Material Properties in Ground Penetrating Radar. **2nd International Workshop on Advanced GPR**, Delft, The Netherlands.
- Ollerton, H.G. (2012) **A Calibration of a Soil for the Estimation of Water Content Using Time Domain Reflectometry**. MSc Thesis, University of Birmingham.
- Or, D., Hartwell, T., Fisher, B., Hubscher, R.A. and Wraith, J.M. (1998) "WinTDR99—Users guide (Windows-based Time Domain Reflectometry Program for Measurement of Soil Water Content and Electrical Conductivity)". **Utah Agricultural Experiment Station Research Report**. Logan, Utah.
- Or, D. and Rasmussen, V.P. (1999) Effective Frequency of TDR Travel Time based Measurement of Bulk Dielectric Permittivity. **Third Workshop on Electromagnetic Wave Interaction With Water and Moist Substances**, Russell Agric. Res. Cent, Athens.
- Or, D. and Wraith, J.M. (1999) Temperature Effects on Soil Bulk Dielectric Permittivity Measured by Time Domain Reflectometry: A Physical Model. **Water Resources Research**, 35: 371-383.
- Parcak, S.H. (2009) **Satellite Remote Sensing for Archaeology**. London: Routledge.
- Parkyn, A., Schmidt, A., Gaffney, C. and Walker, R. (2011) 'It Never Rains but it Pours': Earth Resistance Seasonality Testing in Bradford. **ISAP 2010**, Istanbul: 33-36.
- Parsons Marketing (2010) **Zarges Cases Website** [online]. <http://zargescases.co.uk/> [Accessed 02/11/2010]
- Penman, H.L. (1948) Natural Evaporation from Open Water, Bare Soil and Grass. **Proceedings of the Royal Society of London A**, 194: 120-145.
- Peplinski, N.R., Ulaby, F.T. and Dobson, M.C. (1995a) Corrections to "Dielectric Properties of Soils in the 0.3-1.3-GHz Range. **IEEE Transactions on Geoscience and Remote Sensing**, 33: 1340.
- Peplinski, N.R., Ulaby, F.T. and Dobson, M.C. (1995b) Dielectric Properties of Soils in the 0.3-1.3 GHz Range. **IEEE Transactions on Geoscience and Remote Sensing**, 33: 803-807.
- Persson, M., Sivakumar, B., Berndtsson, R., Jacobsen, O.H. and Schjønning, P. (2002) Predicting the Dielectric Constant–Water Content Relationship Using Artificial Neural Networks. **Soil Science Society of America Journal**, 66: 1424-1429.

References

- Pham, H.Q., Fredlund, D.G. and Barbour, S.L. (2005) A Study of Hysteresis Models for Soil Water Characteristic Curves. **Canadian Geotechnical Journal**, 42: 1548-1568.
- Phillip, J.R. (1957) The Theory of Infiltration: 4. Sorptivity and Algebraic Infiltration Equations. **Soil Science**, 84: 257-264.
- Pollard, A.M., Batt, C.M., Stern, B. and Young, S.M.M. (2008) **Analytical Chemistry in Archaeology**. Cambridge: Cambridge University Press.
- Ponizovsky, A.A., Chudinova, S.M. and Pachepsky, Y.A. (1999) Performance of TDR Calibration Models as Affected by Soil Texture. **Journal of Hydrology**, 218: 35-43.
- Pring, L. (Forthcoming) **Application of Geotechnical Methods to Archaeological Problems**. PhD Thesis, University of Birmingham.
- Quinones, H., Ruelle, P. and Nemeth, I. (2003) Comparison of Three Calibration Procedures for TDR Soil Moisture Sensors. **Irrigation and Drainage**, 52: 203–217.
- Rawls, W.J., Brackensiek, D.L. and Saxton, K.E. (1982) Estimation of Soil Water Properties. **Transactions of American Society of Agricultural Engineers**, 81-2510: 1316-1328.
- Ren, T., Ju, Z., Gong, Y. and Horton, R. (2005) Comparing Heat-Pulse and Time Domain Reflectometry Soil Water Contents from Thermo-Time Domain Reflectometry Probes. **Vadose Zone Journal**, 4: 1080.
- Renfrew, C. and Bahn, P.G. (2004) **Archaeology: Theories, Methods and Practice**. 4th Edition. London: Thames & Hudson.
- Reynolds, J.M. (1997) **An Introduction to Applied and Environmental Geophysics**. Chichester: John Wiley & Sons.
- Rhoades, J.D., Raats, P.A.C. and Prather, R.J. (1976) Effects of Liquid-phase Electrical Conductivity, Water Content, and Surface Conductivity on Bulk Soil Electrical Conductivity. **Soil Science Society of America Journal**, 40: 651-655.
- Richards, L.A. (1931) Capillary Conduction of Liquids Through Porous Mediums. **Physics**, 1.
- Riley, D.N. (1983) "The Frequency of Occurrence of Cropmarks in Relation to Soils". In Maxwell, G.S. (Ed.) **The Impact of Aerial Reconnaissance on Archaeology: Dedicated to Professor J K S St Joseph in token of his Outstanding Contribution to Aerial Archaeology**. London, CBA pp. 59-63.
- Ritchie, G. and Dolling, P. (1985) The Role of Organic Matter in Soil Acidification. **Soil Research**, 23: 569-576.
- Robinson, D.A., Bell, J.P. and Batchelor, C.H. (1994) Influence of Iron Minerals on the Determination of Soil-Water Content using Dielectric Techniques. **Journal of Hydrology**, 161: 169-180.

References

- Robinson, D.A. and Friedman, S. P. (2000) Parallel plates compared with conventional rods as TDR waveguides for sensing soil moisture. **Subsurface Sensing Technology and Applications**, 1: 497-511.
- Robinson, D.A., Jones, S.B., Wraith, J.M., Or, D. and Friedman, S.P. (2003a) A Review of Advances in Dielectric and Electrical Conductivity Measurement in Soils Using Time Domain Reflectometry. **Vadose Zone Journal**, 2: 444-475.
- Robinson, D.A., Kelleners, T.J., Cooper, J.D., Gardner, C.M.K., Wilson, P., Lebron, I. And Logsdon, S. (2005a) Evaluation of a Capacitance Probe Frequency Response Model Accounting for Bulk Electrical Conductivity: Comparison with TDR and Network Analyzer Measurements. **Vadose Zone Journal**, 4: 992-1003.
- Robinson, D.A., Schaap, M., Jones, S.B., Friedman, S.P. and Gardner, C.M.K. (2003b) Consideration's for Improving the Accuracy of Permittivity Measurement using Time Domain Reflectometry: Air-Water Calibration, Effects of Cable Length. **Soil Science Society of America Journal**, 67: 62-70.
- Robinson, D.A., Schaap, M.G., Or, D. and Jones, S.B. (2005b) On the Effective Measurement Frequency of Time Domain Reflectometry in Dispersive and Non-Conductive Dielectric Materials. **Water Resources Research**, 41: W02007.
- Roth, C.H., Malicki, M.A. and Plagge, R. (1992) Empirical Evaluation of the Relationship Between Soil Dielectric Constant and Volumetric Water Content as the Basis for Calibrating Soil Moisture Measurements by TDR. **Journal of Soil Science**, 43: 1-13.
- Roth, K., Schulin, R., Fluhler, H. and Attinger, W. (1990) Calibration of Time Domain Reflectometry for Water Content Measurement using a Composite Dielectric Approach. **Water Resources Research**, 26: 2267-2273.
- Rowell, D.L. (1994) **Soil Science: Methods and Applications**. Harlow: Longman Scientific & Technical
- Saarenketo, T. (1998) Electrical Properties of Water in Clay and Silty Soils. **Journal of Applied Geophysics**, 40: 73-88.
- Samouëlian, A., Cousin, I., Tabbagh, A., Bruand, A. and Richard, G. (2005) Electrical Resistivity Survey in Soil Science: a Review. **Soil and Tillage Research**, 83: 173-193.
- Santamarina, J.C., Klein, K.A. and Fam, M.A. (2001) **Soils and Waves: Particulate Materials Behaviour, Characterisation and Process Monitoring**. Chichester: John Wiley & Sons.
- Santamarina, J.C., Klein, K.A., Wang, Y.H. and Prencke, E. (2002) Specific Surface: Determination and Relevance. **Canadian Geotechnical Journal**, 39: 233-241.
- Saxton, K.E. (2013) "Soil-Plant-Air-Water Field and Pond Hydrology". 6.02.75 ed. Washington, USDA Agricultural Research Service.
- Saxton, K.E., Johnson, H.P. and Shaw, R.H. (1974) Modelling Evapo-Transpiration and Soil Moisture. **Transactions of American Society of Agricultural Engineers**, 17: 673-677.

References

- Saxton, K.E. and Rawls, W.J. (2006) Soil Water Characteristic Estimates by Texture and Organic Matter for Hydrologic Solutions. **Soil Science Society of America Journal**, 70: 1569-1578.
- Saxton, K.E. and Willey, P.H. (2006) "The SPAW Model for Agricultural Field and Pond Hydrologic Simulation". In Singh, V.P. & Frevert, D.K. (Eds.) **Watershed Models**. Boca Raton, FL, CRC Press pp. 401-435.
- Saxton, K.E., Willey, P.H. and Rawls, W.J. (2006) Field and Pond Hydrologic Analyses with the SPAW Model. **ASABE Annual International Meeting**, Portland, Oregon.
- Schaap, M.G., Robinson, D.A., Friedman, S.P. and Lazar, A. (2003) Measurement and Modeling of the TDR Signal Propagation through Layered Dielectric Media. **Soil Science Society of America Journal**, 67: 1113-1121.
- Schmidt, A. (2013) **Earth Resistance for Archaeologists**. Lanham; Plymouth: AltaMira Press.
- Schneider, J.M. and Fratta, D. (2009) Time-Domain Reflectometry - Parametric Study for the Evaluation of Physical Properties in Soils. **Canadian Geotechnical Journal**, 46: 753-767.
- Schut, L.W. and Wilson, E.A. (1987) "The Soils of the Regional Municipality of Ottawa-Carleton (excluding the Ottawa Urban Fringe)". **Report No. 58**. Ontario, Ontario Institute of Pedology.
- Scollar, I., Tabbagh, A., Hesse, A. and Herzog, I. (1990) **Archaeological Prospecting and Remote Sensing**. Cambridge: Cambridge University Press.
- Sengupta, D.L. and Sarkar, T.K. (2003) Maxwell, Hertz, the Maxwellians, and the Early History of Electromagnetic Waves. **IEEE Antennas and Propagation Magazine**, 45: 13-19.
- Seyfried, M.S. and Grant, L.E. (2007) Temperature Effects on Soil Dielectric Properties Measured at 50 MHz. **Vadose Zone Journal**, 6: 759-765.
- Sheets, K.R. and Hendrickx, J.M.H. (1995) Non-Invasive Soil Water Content Measurement using Electromagnetic Induction. **Water Resources Research**, 31: 2401-2409.
- Shuai, X., Wendroth, O., Lu, C. and Ray, C. (2009) Reducing the Complexity of Inverse Analysis of Time Domain Reflectometry Waveforms. **Soil Science Society of America Journal**, 73: 28.
- Sihvola, A.H. (1989) Self-Consistency Aspects of Dielectric Mixing Theories. **IEEE Transactions on Geoscience and Remote Sensing**, 27: 403-415.
- Sihvola, A.H. (2000) Mixing Rules with Complex Dielectric Coefficients. **Subsurface Sensing Technologies and Applications**, 1: 393-415.
- Skierucha, W. (2009) Temperature Dependence of Time Domain Reflectometry–Measured Soil Dielectric Permittivity. **Journal of Plant Nutrition and Soil Science**, 172: 186-193.

References

- Skierucha, W., Wilczek, A., Szyplowska, A., Sławiński, C. and Lamorski, K. (2012) A TDR-Based Soil Moisture Monitoring System with Simultaneous Measurement of Soil Temperature and Electrical Conductivity. **Sensors**, 12: 13545-13566.
- Smith-Rose, R.L. (1933) The Electrical Properties of Soils for Alternating Currents at Radio Frequencies. **Proceedings of the Royal Society of London**, 140: 359.
- Smith-Rose, R.L. (1935) The Electrical Properties of Soil at Frequencies up to 100 Megacycles per Second; with a Note on the Resistivity of Ground in the United Kingdom. **Proceedings of the Physical Society**, 47: 923-931.
- Spiegel, M.R. and Stephens, L.J. (2011) **Schaum's Outline of Theory and Problems of Statistics**. 4th Edition. London: McGraw-Hill.
- Stanjek, H. and Fassbinder, J.W.E. (1995) Soil Aspects Affecting Archaeological Details in Aerial Photographs. **Archaeological Prospection**, 2: 91-101.
- Stenberg, D. (2009) "Loggernet Software Development Kit". Logan, Utah, Campbell Scientific.
- Stott, D. (2014) **Understanding Contrast Formation in Archaeological Features in Optical RemoteSensing Data**. PhD Thesis, University of Leeds.
- Strobbia, C. and Cassiani, G. (2007) Multilayer Ground-Penetrating Radar Guided Waves in Shallow Soil Layers for Estimating Soil Water Content. **Geophysics**, 72: J17-J29.
- Strunk-Lichtenberg, G. (1965) Bodenkundliche Untersuchungen an Archäologischen Objekten, die durch Luftbild-Aufnahmen entdeckt wurden. **Archaeo-Physika**, 15: 175-202.
- Tabbagh, A. (1985) A New Apparatus for Measuring Thermal Properties of Soils and Rock In Situ. **IEEE Transactions on Geoscience and Remote Sensing**, 23.
- Take, W.A., Arnepalli, D.N., Brachman, R.W.I. and Rowe, R.K. (2007) Laboratory and Field Calibration of TDR Probes for Water Content Measurement. **OttawaGeo2007: The Diamond Jubilee: 60th Canadian Geotechnical Conference**, Ottawa, Canada.
- Telford, W.M., Geldart, L.P. and Sheriff, R.E. (1990) **Applied Geophysics**. 2nd Edition. Cambridge: Cambridge University Press.
- Thomas, A.M. (2010) **Measurement of Electromagnetic Signal Velocities in Saturated Fine Grained Soils**. PhD Thesis, University of Birmingham.
- Thomas, A.M., Chapman, D.N., Rogers, C.D.F. and Metje, N. (2010a) Electromagnetic Properties of the Ground: Part I – Fine-Grained Soils at the Liquid Limit. **Tunnelling and Underground Space Technology**, 25: 714-722.
- Thomas, A.M., Chapman, D.N., Rogers, C.D.F. and Metje, N. (2010b) Electromagnetic Properties of the Ground: Part II – The Properties of Two Selected Fine-Grained Soils. **Tunnelling and Underground Space Technology**, 25: 714-722.
- Thomas, A.M., Chapman, D.N., Rogers, C.D.F., Metje, N., Atkins, P.R. and Lim, H.M. (2008a) Broadband Apparent Permittivity Measurement in Dispersive Soils Using Quarter Wavelength Analysis. **Soil Science Society of America Journal**, 72: 1401.

References

- Thomas, A.M., Rogers, C.D.F., Metje, N. and Chapman, D.N. (2007) Soil Electromagnetic Mapping for Enhanced GPR Utility Location. **Proceedings of the 25th International Conference on Trenchless Installation of Utilities, No-Dig 2007**, Rome, Italy.
- Thomas, A.M., Yelf, R.J., Gunn, D.A., Self, S., Chapman, D.N., Rogers, C.D.F. and Metje, N. (2008b) The Role of Geotechnical Engineering for Informed Planning of GPR Surveys and Interpretation of Results in Fine-Grained Soils. **12th International Conference on Ground Penetrating Radar**, Birmingham, UK.
- Thorntwaite, C.W. (1948) An Approach toward a Rational Classification of Climate. **Geographical Review**, 38: 55-94.
- Thring, L. (2013) **Factors Affecting Soil Permittivity and Applications in Soil Mechanics**. MEng Thesis, University of Birmingham.
- Timlin, D.J. and Pachepsky, Y.A. (1996) Comparison of Three Methods to Obtain the Apparent Dielectric Constant from Time Domain Reflectometry Wave Traces. **Soil Science Society of America Journal**, 60: 970-977.
- Topp, G.C. (2003) State of the Art of Measuring Soil Water Content. **Hydrological Processes**, 17: 2993-2996.
- Topp, G.C. and Davis, J.L. (1985) Measurement of Soil Water Content Using Time-Domain Reflectometry (TDR) - A Field Evaluation. **Soil Science Society of America Journal**, 49: 1924.
- Topp, G.C., Davis, J.L. and Annan, A.P. (1980) Electromagnetic Determination of Soil-Water Content Measurements in Coaxial Transmission Lines. **Water Resources Research**, 16: 574-582.
- Topp, G.C., Davis, J.L. and Annan, A.P. (1982a) Electromagnetic Determination fo Soil-Water Content Using TDR. 1: Applications to Wetting Fronts and Steep Gradients. **Soil Science Society of America Journal**, 46: 672-678.
- Topp, G.C., Davis, J.L. and Annan, A.P. (1982b) Electromagnetic Determination fo Soil-Water Content Using TDR: 2. Evaluation of Installation and Configuration of Parallel Transmission Lines. **Soil Science Society of America Journal**, 46: 678-684.
- Topp, G.C., Davis, J.L. and Annan, A.P. (2003) The Early Development of TDR for Soil Measurements. **Vadose Zone Journal**, 2: 492-499.
- Topp, G.C., Yanuka, M., Zebchuk, W.D. and Zegelin, S. (1988) Determination of Electrical Conductivity Using Time Domain Reflectometry: Soil and Water Experiments in Coaxial Lines. **Water Resources Research**, 24: 945-952.
- Topp, G.C., Zegelin, S.J. and White, I. (2000) Impacts of the Real and Imaginary Components of Relative Permittivity on Time Domain Reflectometry Measurements in Soils. **Soil Science Society of America Journal**, 64: 1244-1252.

References

- Van Dam, R.L., Borchers, B. and Hendrickx, J.M.H. (2005) Methods for Prediction of Soil Dielectric Properties: A Review. **Proceedings of the Society of Photo-Optical Instrumentation Engineers**, 5794: 188-197.
- Van Dam, R.L. and Schlager, W. (2000) Identifying Causes of Ground-Penetrating Radar Reflections using Time-Domain Reflectometry and Sedimentological Analyses. **Sedimentology**, 47: 435-449.
- Van Dam, R.L., Van den Berg, E.H., Van Heteren, S., Kasse, C., Kenter, J.A.M. and Groen, K. (2002) Influence of Organic Matter in Soils on Radar-Wave Reflection: Sedimentological Implications. **Journal of Sedimentary Research**, 72: 341-352.
- Van Genuchten, M.T. (1980) A Closed-form Equation for Predicting the Hydraulic Conductivity of Unsaturated Soils. **Soil Science Society of America Journal**, 44: 892-898.
- Van Manen, S.M. and Wallin, E. (2012) Ground Temperature Profiles and Thermal Rock Properties at Wairakei, New Zealand. **Renewable Energy**, 43: 313-321.
- Van Walt Ltd. (2013) **Van Walt Ltd. Website** [online]. <http://www.vanwalt.com/> [Accessed 03/04/2013]
- Verdonck, L., Simpson, D., Cornelis, W.M., Plyson, A., Bourgeois, J., Docter, R. and Van Meirvenne, M. (2009) Ground-Penetrating Radar Survey over Bronze Age Circular Monuments on a Sandy Soil, Complemented with Electromagnetic Induction and Fluxgate Gradiometer Data. **Archaeological Prospection**, 16: 193-202.
- Vevai, J.E., Elliot, D.G. and Honeywell, W.I. (1972) Resistance Thermometry in Magnetic Fields 1. Thermistors and Platinum Thermometers at 77 K. **Cryogenics**, 12: 192-195.
- Walker, R. (2011) **Mass, Weight and Density of Water** [online]. http://www.simetric.co.uk/si_water.htm [Accessed 15/05/2012]
- Wang, J.R. and Schumge, T.J. (1980) An Empirical Model for the Complex Dielectric Permittivity of Soils as a Function of Water Content. **IEEE Transactions on Geoscience and Remote Sensing**, GE-18: 288-295.
- Wang, K., Zhang, R. and Yasuda, H. (2006) Characterizing Heterogeneity of Soil Water Flow by Dye Infiltration Experiments. **Journal of Hydrology**, 328: 559-571.
- Weast, R.C. (1986) **CRC Handbook of Chemistry and Physics**. 67th Edition. Boca Raton, FL: CRC Press.
- Weather Underground Inc (2014) **Weather Underground** [online]. <http://www.wunderground.com/> [Accessed 14/01/2014]
- Weaver, W. (2006) Ground-Penetrating Radar Mapping in Clay: Success from South Carolina, USA. **Archaeological Prospection**, 13: 147-150.
- Webster, G. (1974) **Practical Archaeology: An Introduction to Archaeological Field-Work and Excavation**. London: A. & C. Black.

References

- Weiler, K.W., Steenhuis, T.S., Boll, J. and Kung, K.J.S. (1998) Comparison of Ground Penetrating Radar and Time-Domain Reflectometry as Soil Water Sensors. **Soil Science Society of America Journal**, 62: 1237-1239.
- Wensink, W.A. (1993) Dielectric-Properties of Wet Soils in the Frequency-Range 1-3000 MHz. **Geophysical Prospecting**, 41: 671-696.
- West, L.J. and Truss, S.W. (2006) Borehole Time Domain Reflectometry in Layered Sandstone: Impact of Measurement Technique on Vadose Zone Process Identification. **Journal of Hydrology**, 319: 143-162.
- White, I., Knight, J.H., Zegelin, S.J. and Topp, G.C. (1994) Comments on 'Consideration on the use of time-domain reflectometry (TDR) for measuring soil water content' by W.R. Whalley. **European Journal of Soil Science** 45: 503-508
- Wilkinson, K. (2011) "DART: Excavation and Probe Installation at Harnhill, Cirencester and Diddington, St. Neots in April and June 2011". **DART Project Internal Report**. Winchester, UK. Available from http://dartportal.leeds.ac.uk/dataset/dart_excavation_data.
- Williams, J. (2009a) "The Role of Science in the Management of the UK's Heritage". **National Heritage Science Strategy Report 1**. Available from www.heritagesciencestrategy.org.uk.
- Williams, J. (2009b) "The Use of Science to Enhance our Understanding of the Past.". **National Heritage Science Strategy Report 2**. Available from www.heritagesciencestrategy.org.uk.
- Wilson, D.R. (1982) **Air Photograph Interpretation for Archaeologists**. London: Batsford.
- Woolley, C.L. (1961) **Digging up the Past**. Harmondsworth: Penguin.
- Wraith, J.M. and Or, D. (1999) Temperature Effects on Soil Bulk Dielectric Permittivity Measured by Time Domain Reflectometry: Experimental Evidence and Hypothesis Development. **Water Resources Research**, 35: 361-369.
- Wraith, J.M. and Or, D. (2001) Soil Water Characteristic Determination from Concurrent Water Content Measurements in Reference Porous Media. **Soil Science Society of America Journal**, 65: 1659-1666.
- Wunderlich, T., al Hagrey, S.A., Peterson, H. and Rabbel, W. (2010) Pedophysical Study of Electrical Properties and Water Content, Laboratory and Field Experiments. **Near Surface 2010 – 16th European Meeting of Environmental and Engineering Geophysics**, Zurich, Switzerland.
- Wyseure, G.C.L., Mojid, M.A. and Malik, M.A. (1997) Measurement of Volumetric Water Content by TDR in Saline Soils. **European Journal of Soil Science**, 48: 347-354.

References

- Yanuka, M., Topp, G.C., Zegelin, S. and Zebchuk, W.D. (1988) Multiple Reflection and Attenuation of Time Domain Reflectometry Pulses: Theoretical Considerations for Applications to Soil and Water. **Water Resources Research**, 24.
- Youngs, E.G. (1988) Soil Physics and Hydrology. **Journal of Hydrology**, 100: 411-431.
- Youngs, E.G. and Poulouvasilis, A. (1976) The Different Forms of Moisture Profile Development During the Redistribution of Soil Water After Infiltration. **Water Resources Research**, 12: 1007-1012.
- Yu, X. and Drnevich, V.P. (2004) Soil Water Content and Dry Density by Time Domain Reflectometry. **Journal of Geotechnical and Geoenvironmental Engineering**, 130: 922-934.
- Yu, X., Drnevich, V.P. and Nowack, R.L. (2005) Statistical Comparison of Models for Soil Dielectric Spectrum. **18th EEGS Symposium on the Application of Geophysics to Engineering and Environmental Problems**, Atlanta, Georgia.
- Zegelin, S.J., White, I. and Jenkins, D.R. (1989) Improved Field Probes for Soil-Water Content and Electrical Conductivity Measurement using Time Domain Reflectometry. **Water Resources Research**, 25: 2367-2376.

Appendices

Appendix A : MATLAB Functions and Scripts

Waveform interpretation script to find the start and end of the waveform

```

%function to interpret TDR waveforms and locate the start and end of the
%probe rods

% INPUTS - wave - the wave to be interpreted
%          %          probeno - the number of the probe used for labelling purposes
%          %          date - the timestamp of the reading
%          %          array - the array loaded from the variables script
%          %          probes - the probes array loaded from the
variables script

% OUTPUTS - start - the start of the probe head
%          %          finish - the reflection from the end of the probe

%%

function [start, finish] = Waveint (wave, probeno, date, array, probes)

A= reshape (wave, 1, 2048); % ensure waveform is in row format to make meanshift work
properly

%% create a kernal and run a conv function over the signal

K= [1 0 -1]; %kernel

o = conv(conv(A, ones(1,19), 'same'), K, 'same');%LPF and conv using kernel

o=o.*(o>0); % remove negative elements

%% Find the peaks using the meanshift

[cluster_centres] = meanshift1D (o, 90.0); %find the peaks

try

first = find(cluster_centres>200);%stop it finding silly peaks before the real one

second = find (cluster_centres>600); %to stop it finding multiple peaks at the start of the
waveform, find peaks larger than 600

first = first(1); %choose the first of these as the first peak

second = second(1);%choose the first of these as the second peak

p1 = cluster_centres (first);

p2 = cluster_centres (second);

catch ME

```

Appendices

```
close(fhband)

throw(ME)

end

p1 = int32(p1); % cast to integer
p2 = int32(p2); % cast to integer
y = A(p1-10:p1+10) ; % extract subset of signal
x = [p1-10:p1+10]; % numbering signal position from 1 in increments of 1
x = double(x);
y2 = A(p2-100:p2+10) ; % extract subset of signal
x2 = [p2-100:p2+10] ; % numbering signal position from 1 in increments of 1
x2 = double(x2);
B = [ones(size(x)); x]';
B2 = [ones(size(x2)) ; x2]';
b = mldivide(B,y');
b2 = mldivide(B2,y2');
k = b(2);
k2 = b2(2);
c = b(1);
c2 = b2(1);

%% find start and end minimum
min1 = min (A (1:500));
min2 = min (A (600:end));

%% find intersections by substituting y value into x = (y-c)/k
start = (min1 - c)/(k);
finish = (min2 -c2)/(k2);
```

Permittivity function to calculate the permittivity from the start and end points determined by Waveint function.

%function to calculate the permittivity using the start and end points of a

%TDR waveform calculated using the Waveint function

% INPUTS - start - the start value calculated from Waveint

% finish - the end point calculated from Waveint

% probeno - the number of the probe used to collect the waveform, required to load the right calibration values.

% note that the correct monitoring station Variable loading script must be run first

% La - Loaded from the appropriate variable loading script

% Offsets- Loaded from the appropriate variable loading script

% OUTPUTS - perm - permittivity from the waveform

%%

function [perm] =perm (start, finish, probeno, La, Offsets)

%declare some useful values

Vp = 1.0;

dptlength = 1.2/2048;

% work out the real start and end points

*start = start * dptlength; %work out the real start length*

*finish = finish *dptlength; %work out the real finish length*

*%Do the calculation (finish - (start + Offset)/(Vp*La))^2.*

*perm = ((finish-(start+Offsets(probeno)))/(Vp*La(probeno)))^2;*

Conductivity waveform interpretation function

%Function to interpret conductivity waveforms and output conductivity in

%S/m

%Dan Boddice

%INPUTS - wave - the conductivity waveform to be interpreted

% probeno - the probeno on the array

% date - the timestamp of the reading

% the following inputs can be left as the current values

% Kp - the array of probe constants loaded by the variables (can always leave as Kp if this is run first)

% CL - the Cable length array loaded by variables (can always leave as CL if this is run first)

% Rc - Cable Resistance array loaded by variables (can always leave as Rc if this is run first)

% RO - series resistance array loaded by variables (can always leave as RO if this is run first)

% Popen - Popen value loaded by variables (can always leave as Popen if this is run first)

% Zout - Zout value loaded by variables (can always leave as Zout if this is run first)

% array - array label loaded by variables (can always leave as array if this is run first)

% probes - the probes array loaded by the variables (can always leave as probes if this is run first)

% OUTPUTS - conductivity in Siemens per metre (S/m)

% a figure plot with labels

%%

function [Cond] =Condint(wave, probeno, date, Kp, CL, Rc, RO, Popen, Zout, array, probes)

%% Reshape the wave to ensure it is the right shape for analysis

wave = reshape(wave, [1, 2048]);

%% take the last few points and average

A = wave(1, [1973:2048]); % take the end of the waveform

A = mean (A); % find the average of the reflection coefficients

%% calculate the conductivity from the values

reflex = ((2 * (A+1))/(Popen + 1))-1; % correct the reflection coefficient

Appendices

$RL = Z_{out} * ((1+reflex)/(1-reflex));$ % **Calculate the load resistance on the probe**

$Cond = (Kp(probeno))/(RL-(CL(probeno)*Rc(probeno)+R0(probeno)));$ % **calculate the resulting conductivity**

Appendix B : Additional Laboratory graphs

The effects of temperature on the measured geophysical properties were discussed in Section 5.5.5 as the differences between the 0°C and 20°C readings. The graphs below show the differences between readings taken 10°C and 20°C. Similar trends and behaviour were observed, although the magnitude of observed temperature effects were smaller due to the smaller variation in temperature (10°C as opposed to 20°C). The effect of temperature on BEC is shown in Figure B.1 and the effects on ARDP are shown in Figure B.2.

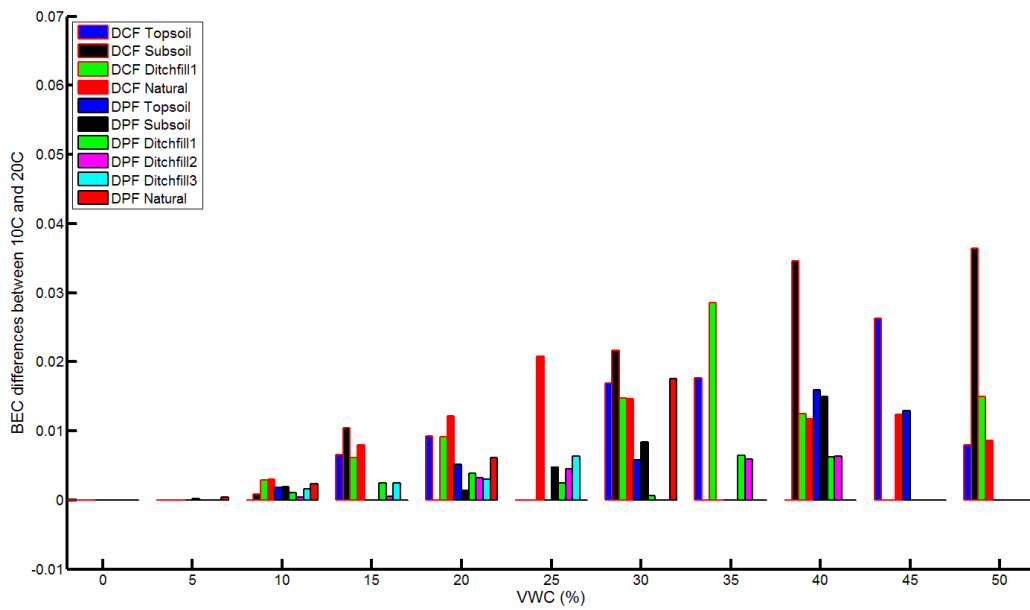


Figure B.1: Temperature effects on BEC determination on different soils

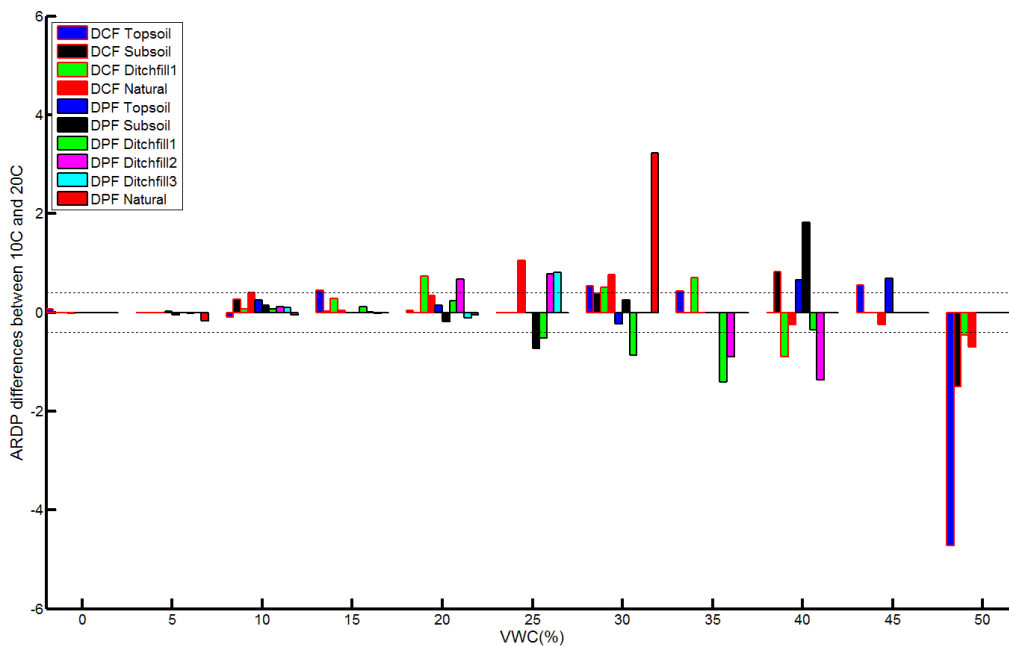


Figure B.2: Temperature effects on ARDP determination on different soils

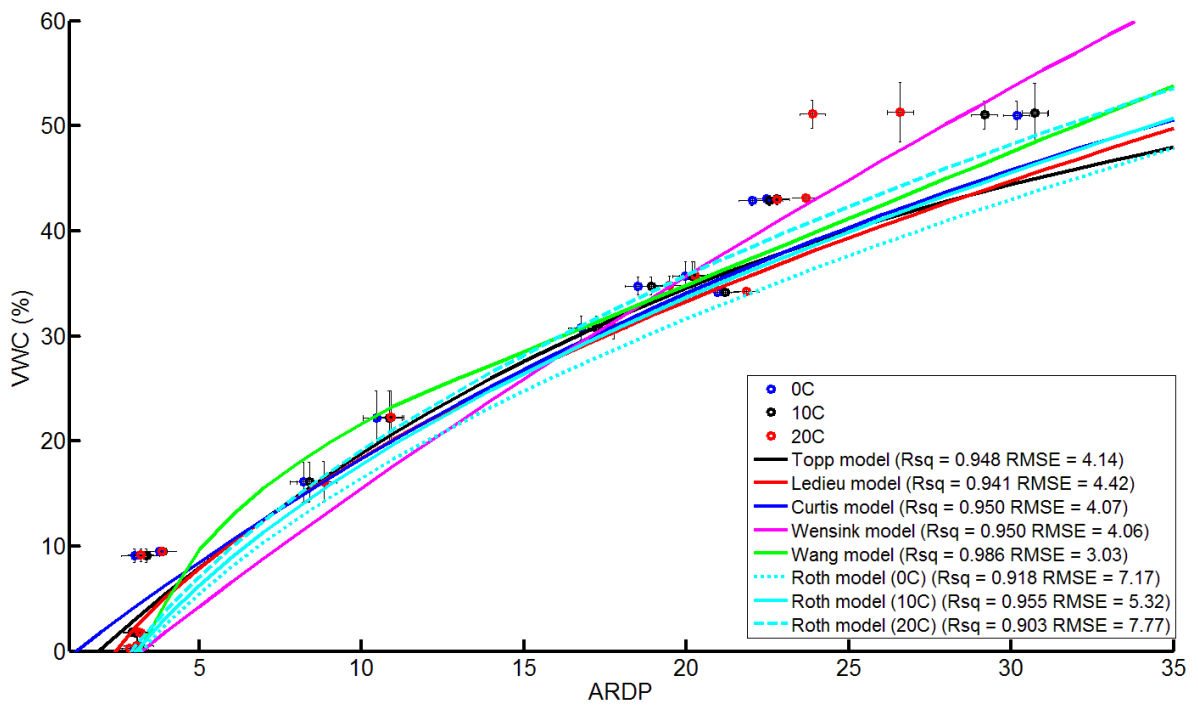


Figure B.3: Different models fitted to DCF Topsoil

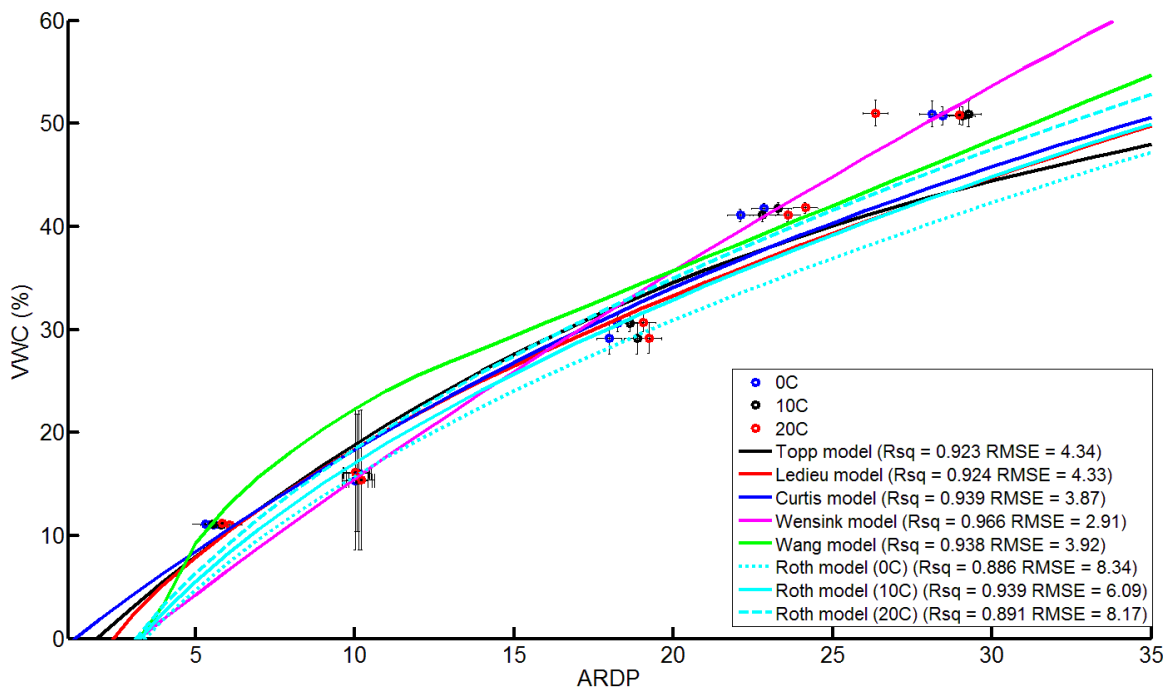


Figure B.4: Different models fitted to DCF Subsoil

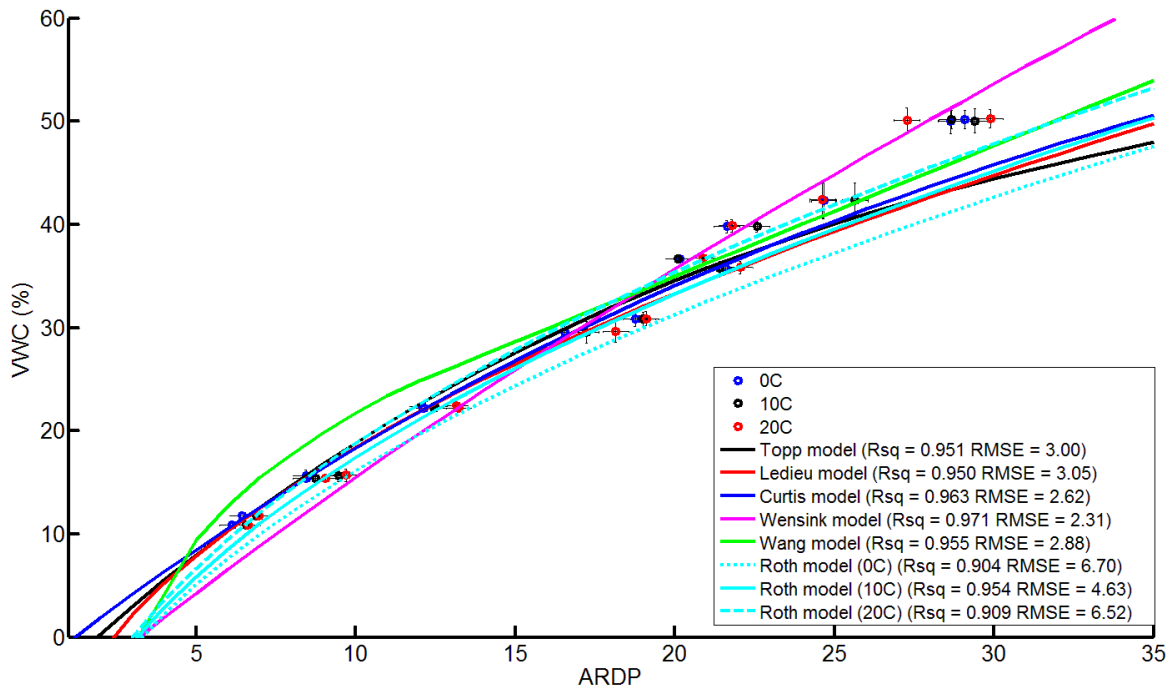


Figure B.5: Different models fitted to DCF Ditchfill1

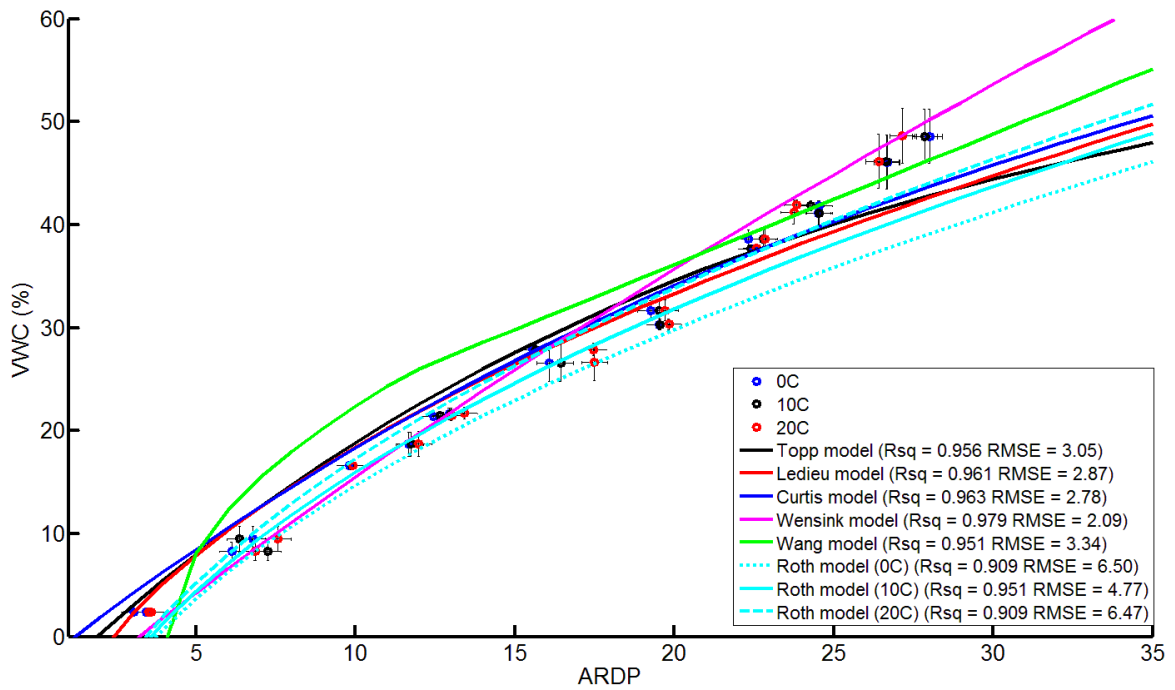


Figure B.6: Different models fitted DCF SSM

Appendices

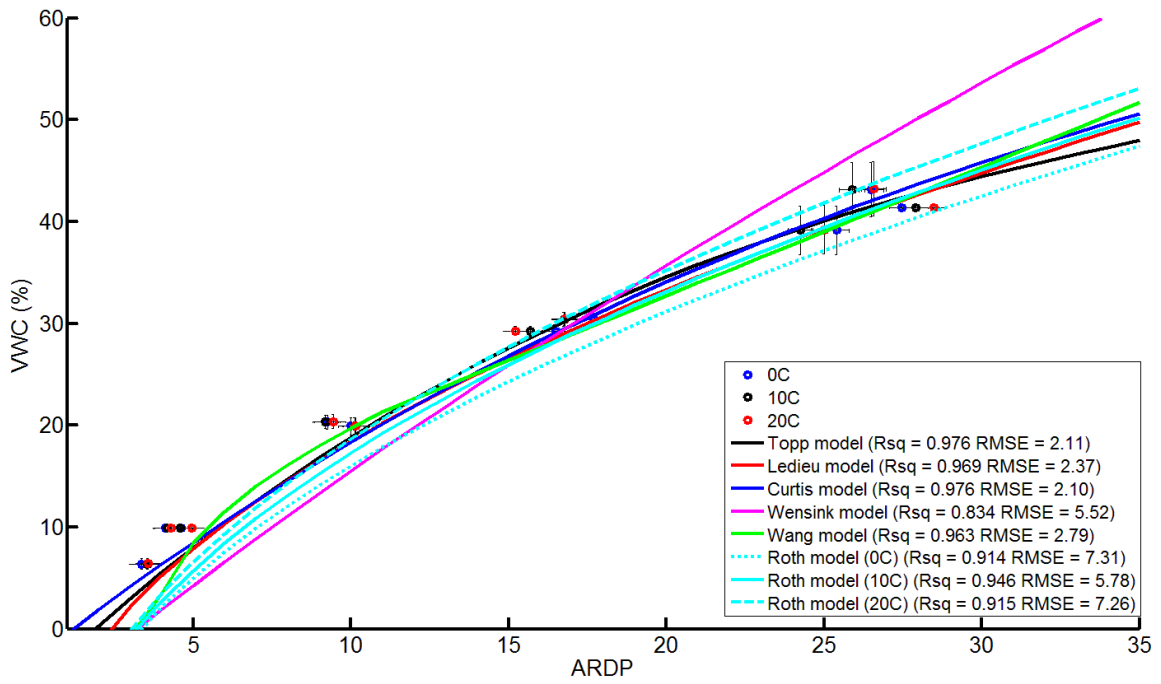


Figure B.7: Different models fitted to DPF Topsoil

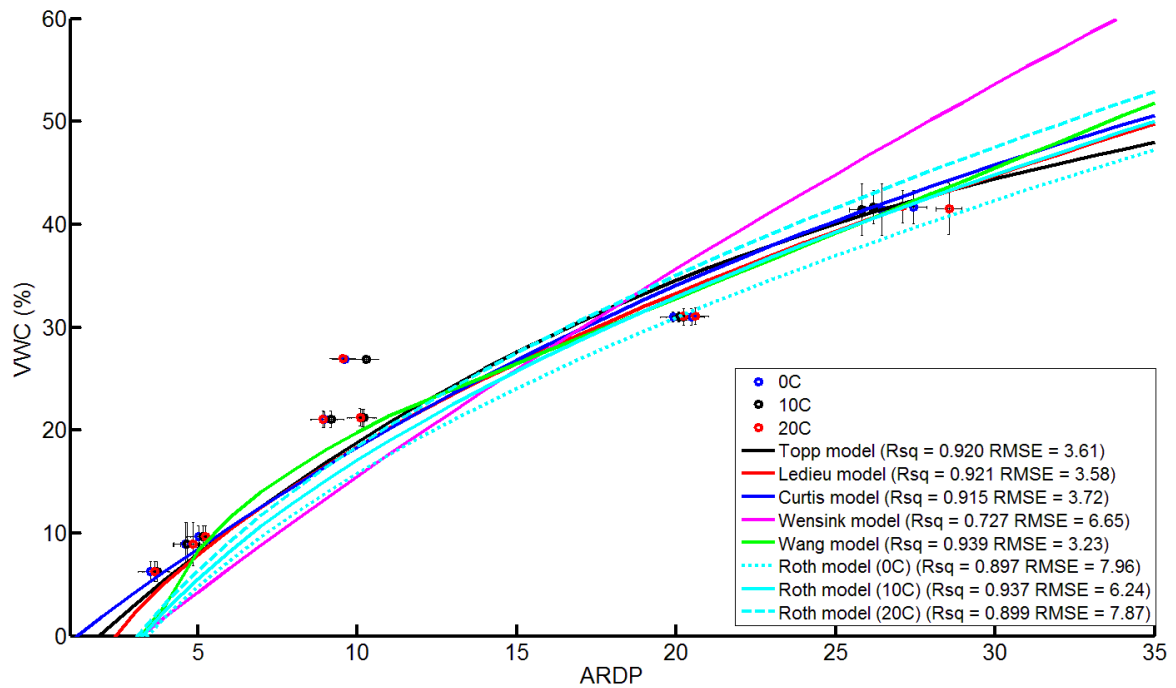


Figure B.8: Different models fitted to DPF Subsoil

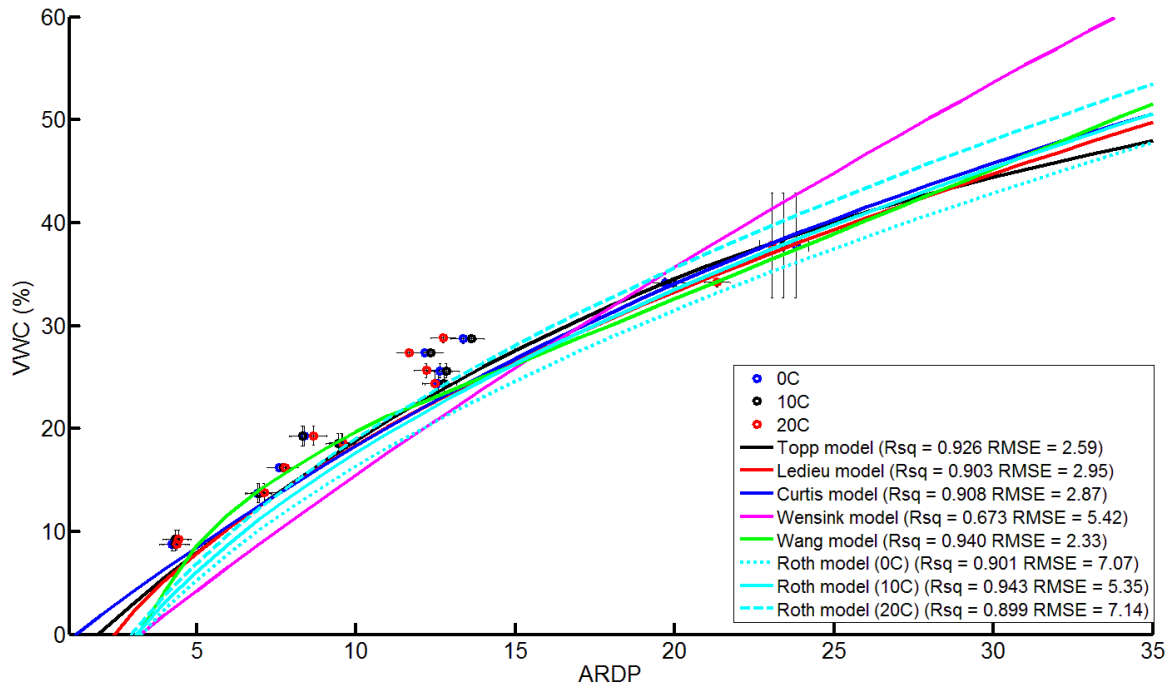


Figure B.9: Different models fitted to DPF Ditchfill1

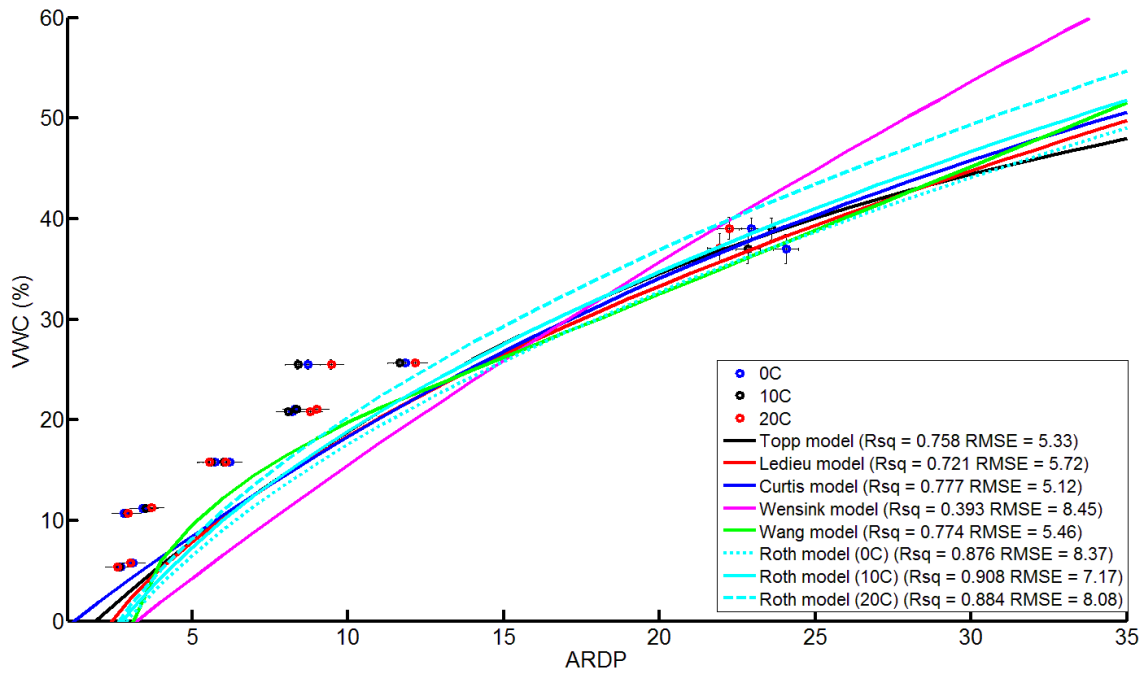


Figure B.10: Different models fitted to DPF Ditchfill2

Appendices

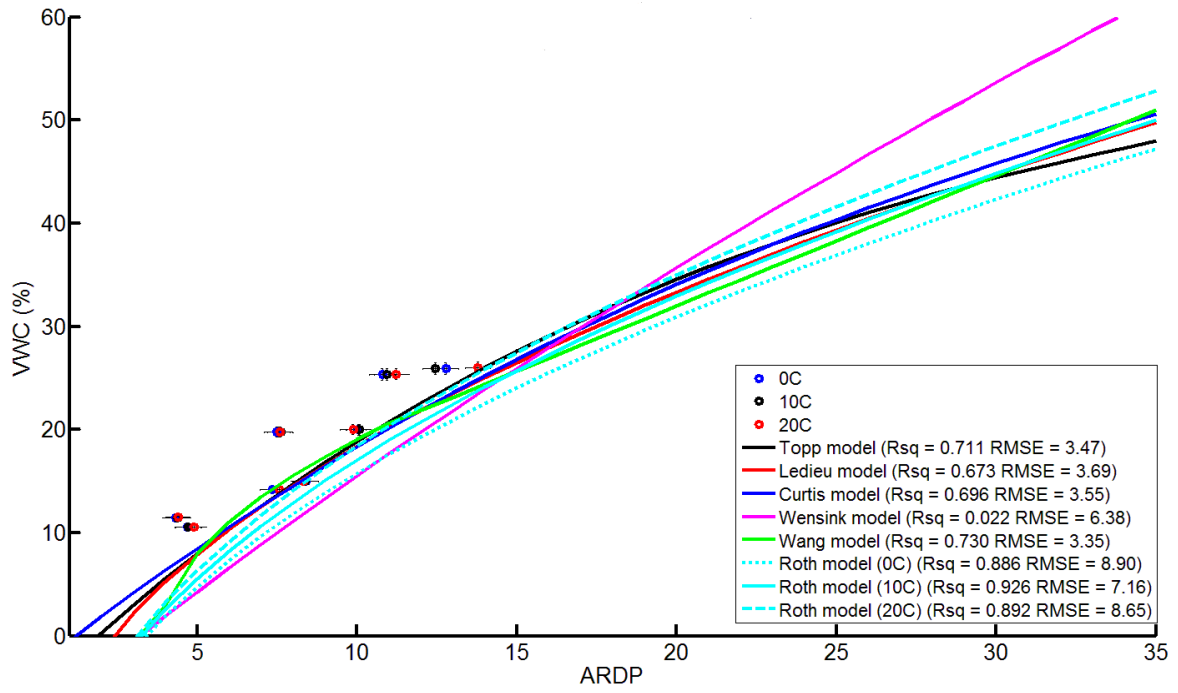


Figure B.11: Different models fitted to DPF Ditchfill3

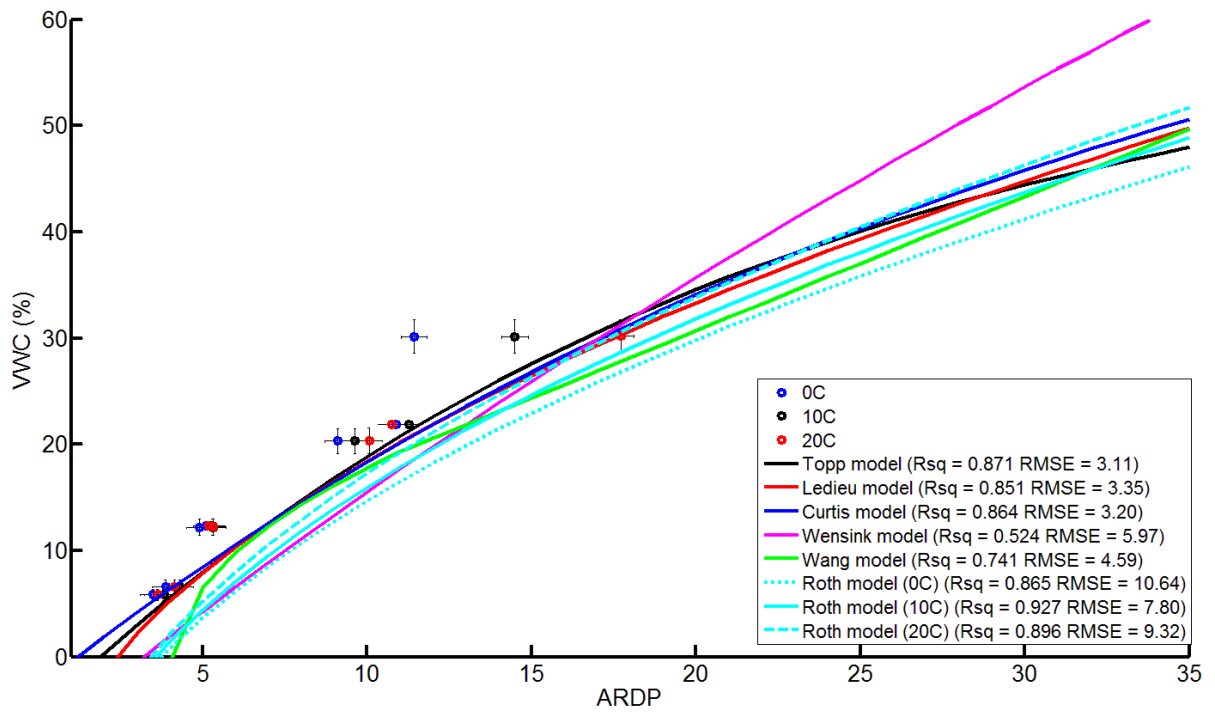


Figure B.12: Different models fitted to DPF SSM

Appendices

In addition, PCA analysis was presented in Section 5.6, which used selected variables from both Diddington sites to determine the relationships between EM and soil properties. Plots using the same variables for each site individually are shown in the following figures.

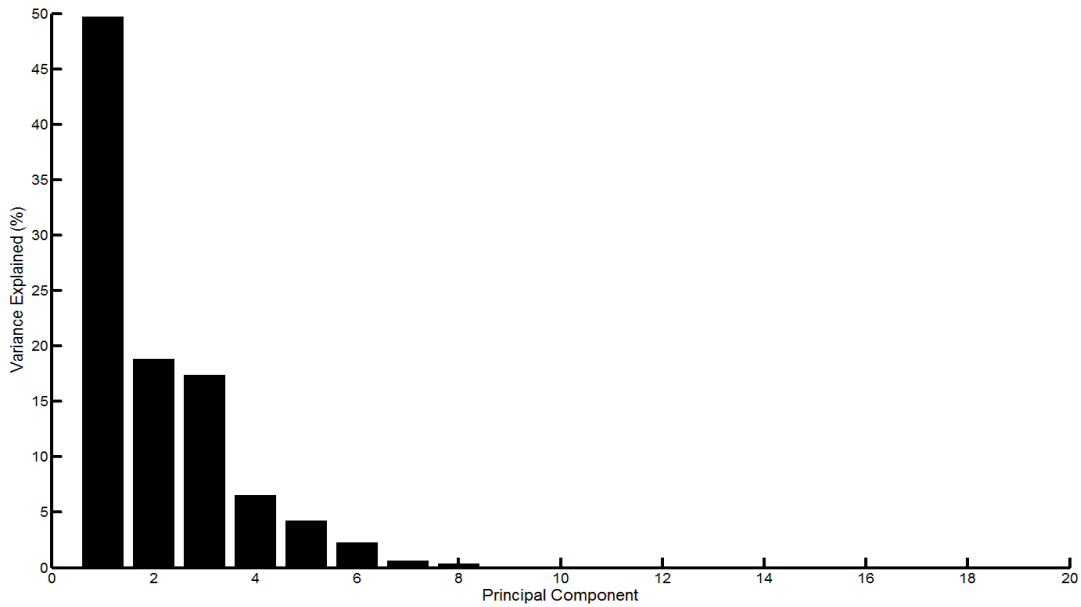


Figure B.13: Scree plot for PCA carried out on DCF only using the same variables as in Section 5.6.

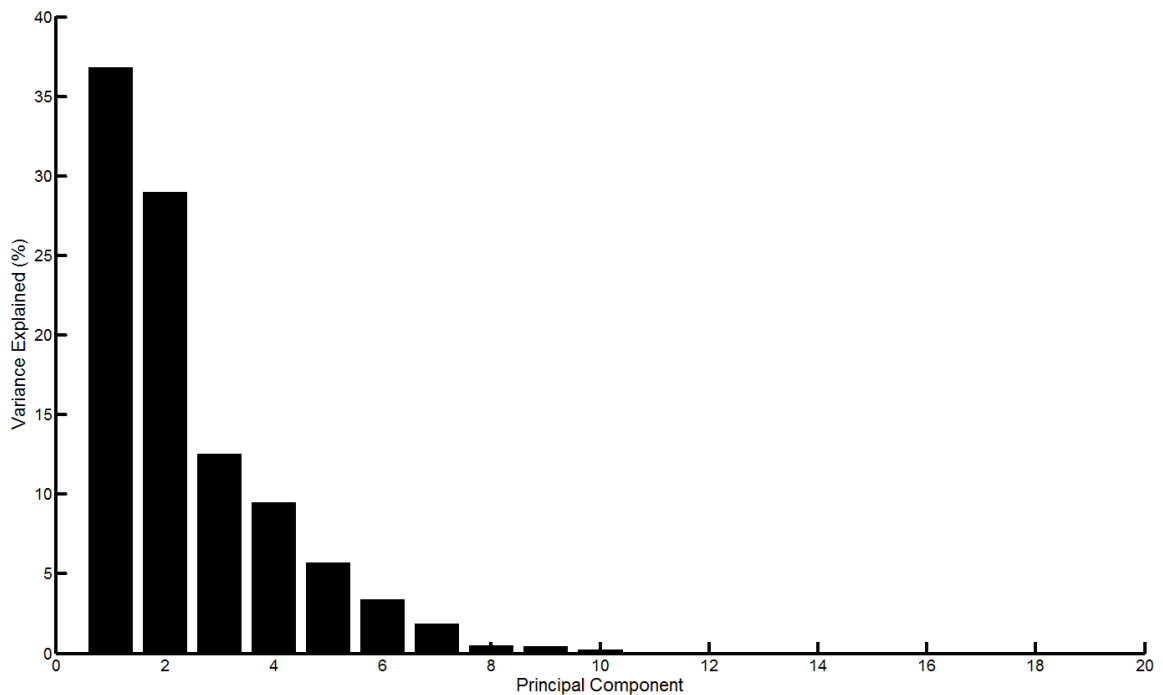


Figure B.14: Scree plot for PCA carried out on DPF only using the same variables as in Section 5.6.

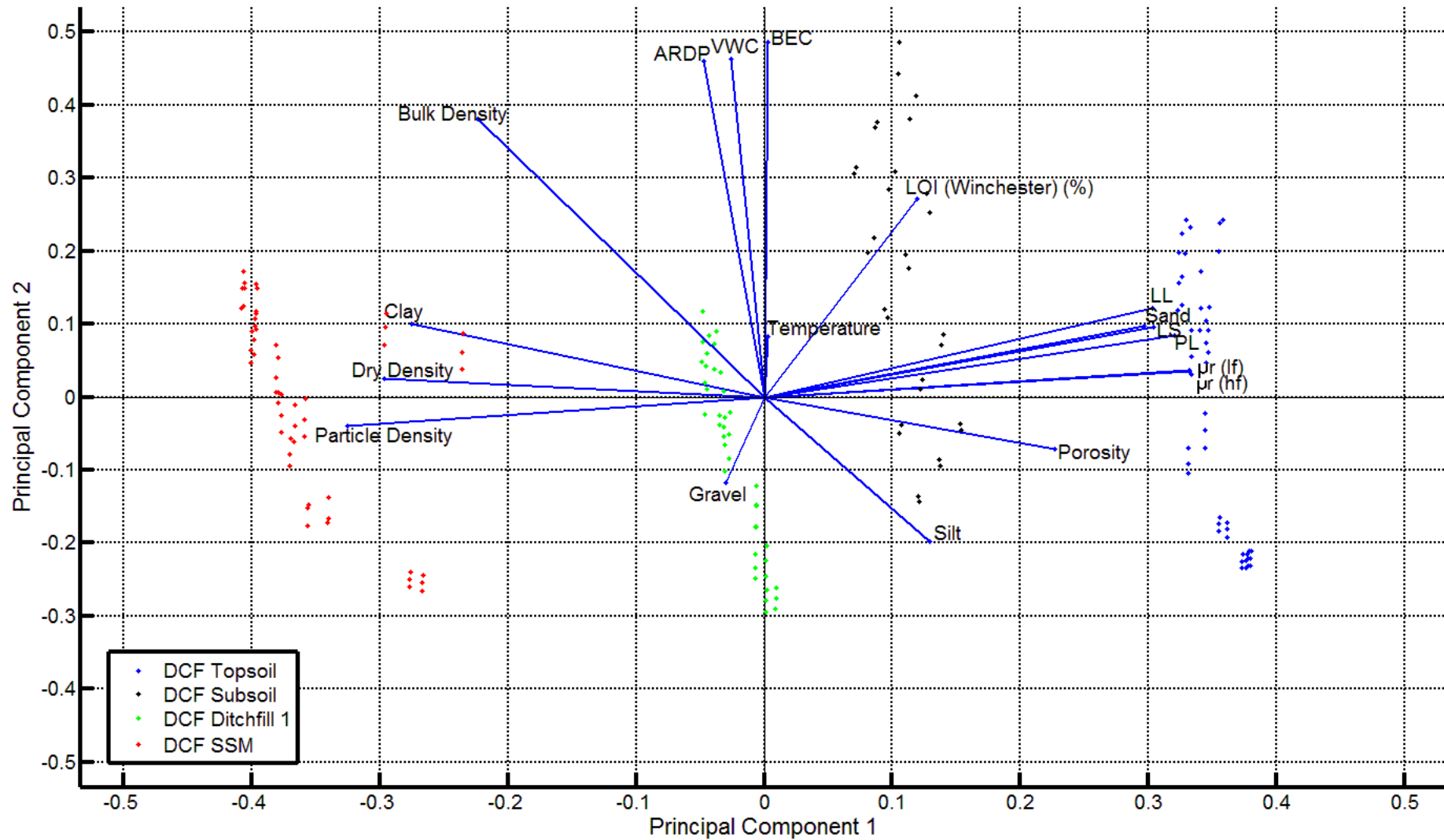


Figure B.15: Principal components 1 and 2 for PCA analysis carried out on the DCF soils only using the same variables as in Section 5.6.

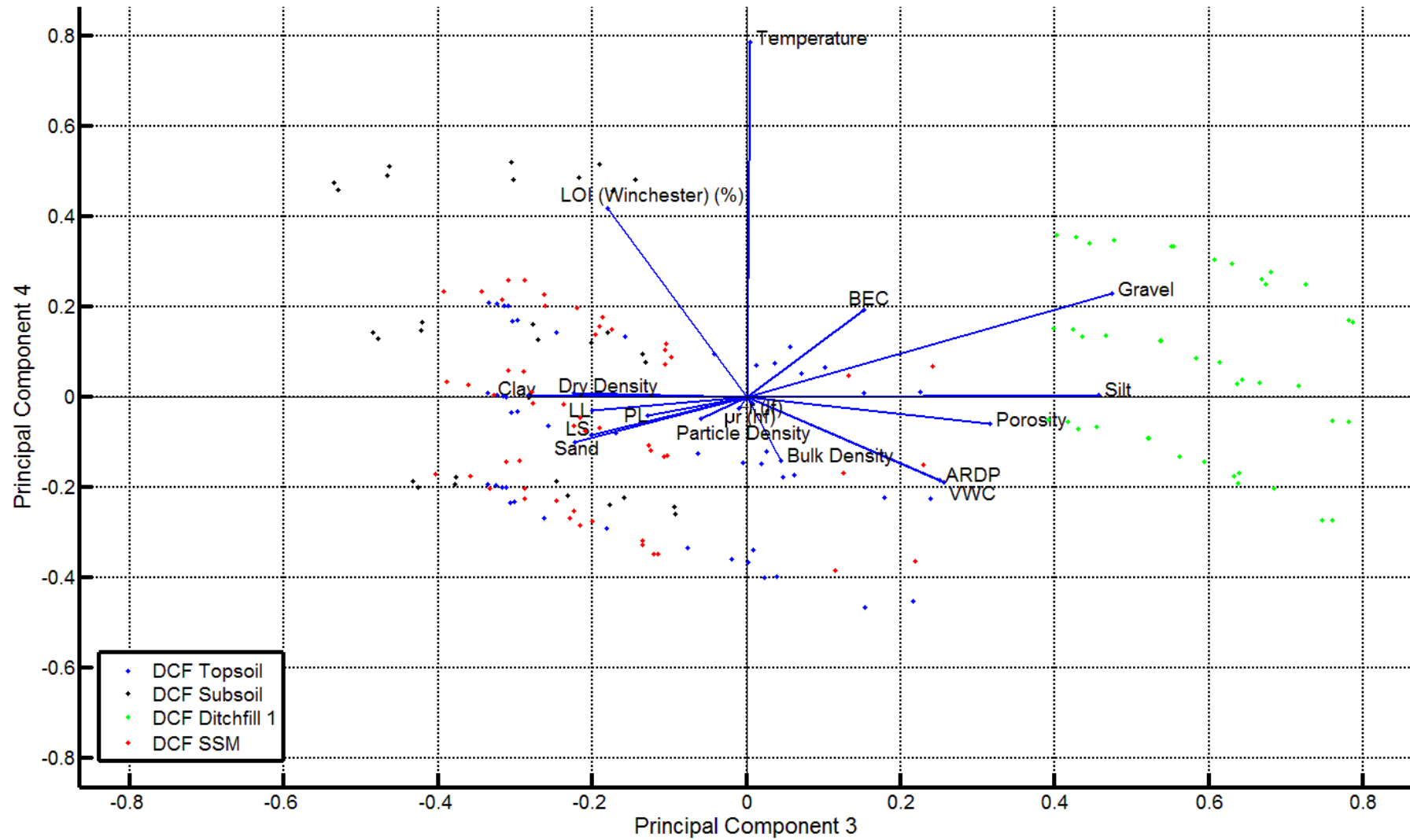


Figure B.16: Principal components 3 and 4 for PCA analysis carried out on the DCF soils only using the same variables as in Section 5.6.

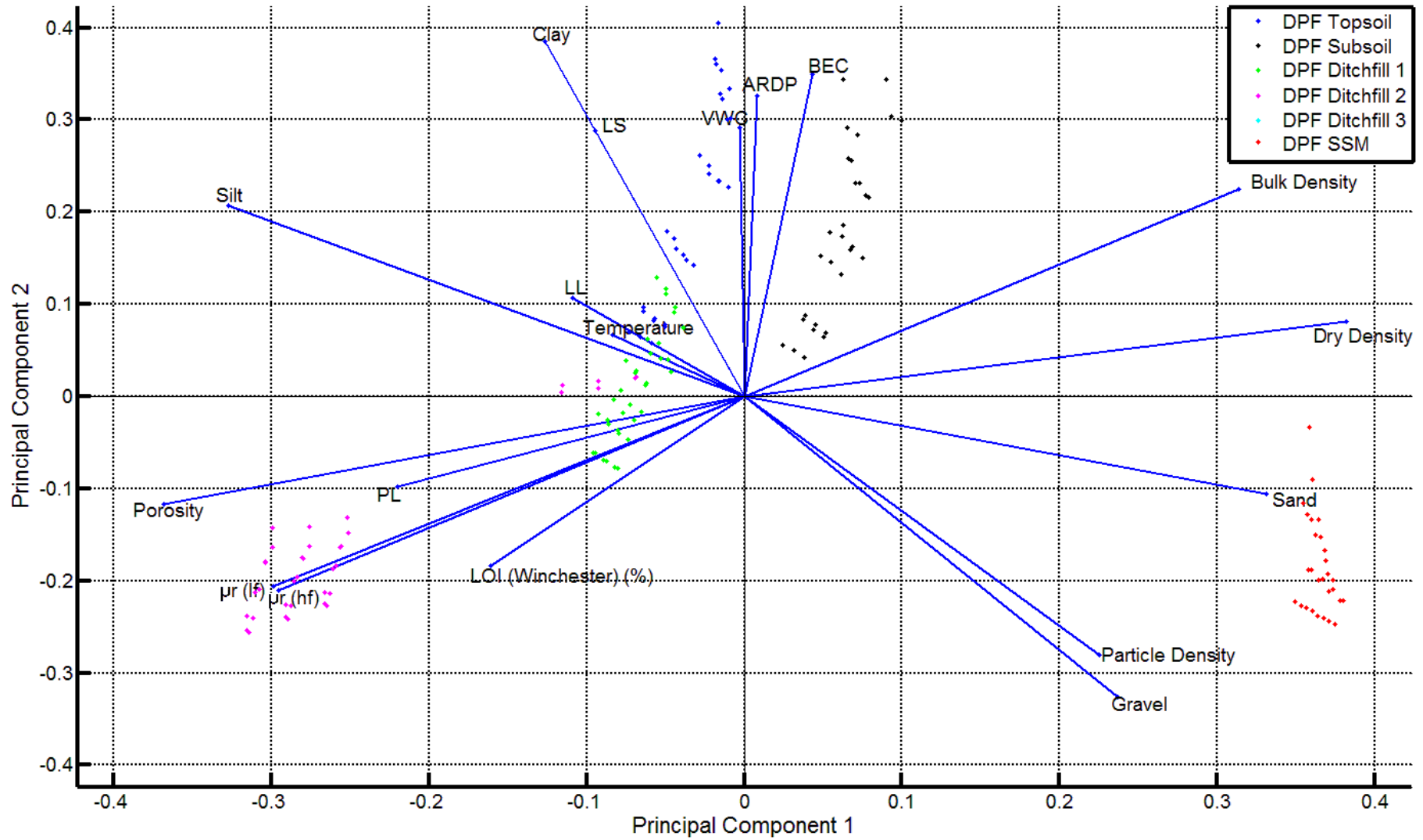


Figure B.17: Principal components 1 and 2 for PCA analysis carried out on the DPF soils only using the same variables as in Section 5.6.

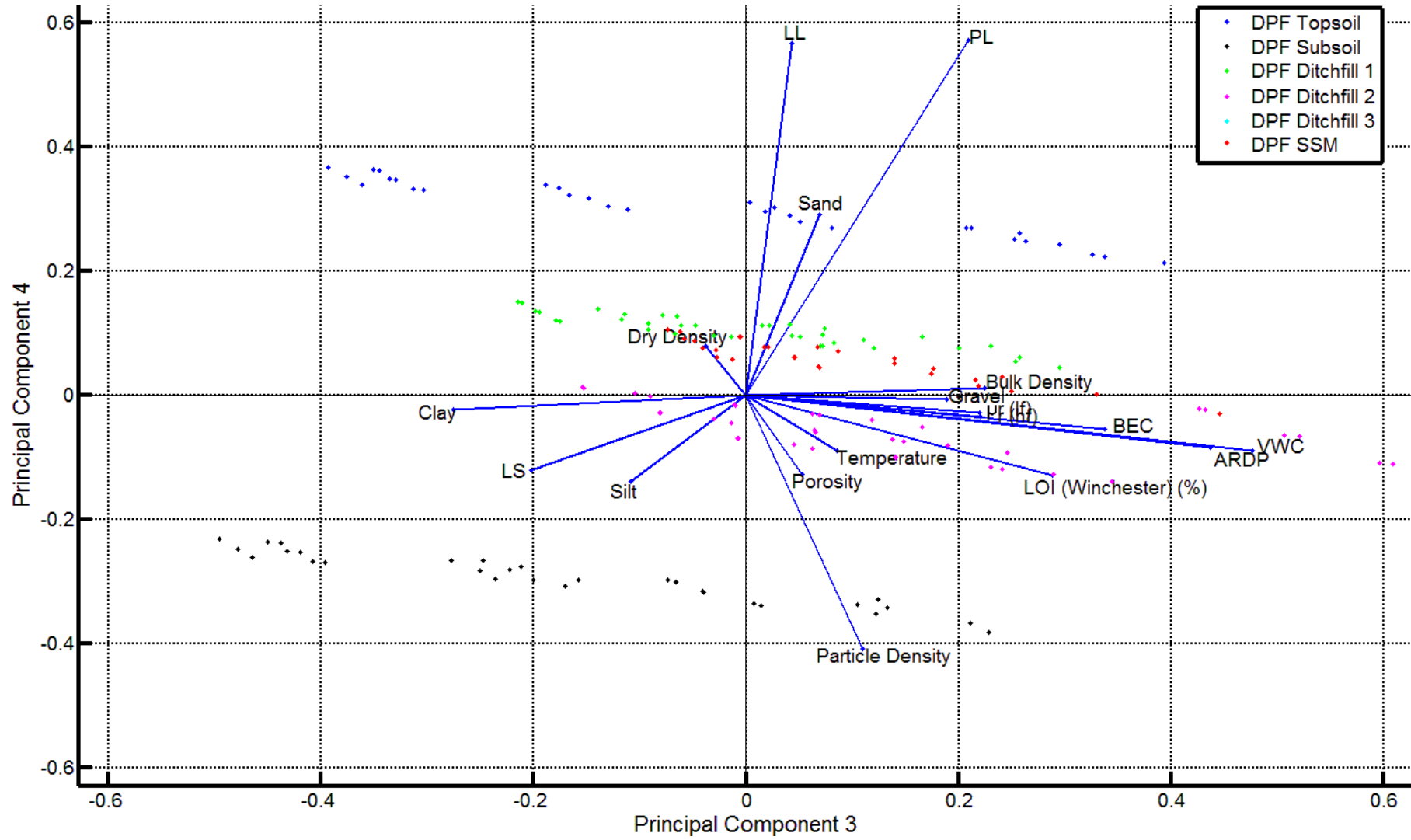


Figure B.18: Principal components 1 and 2 for PCA analysis carried out on the DPF soils only using the same variables as in Section 5.6.

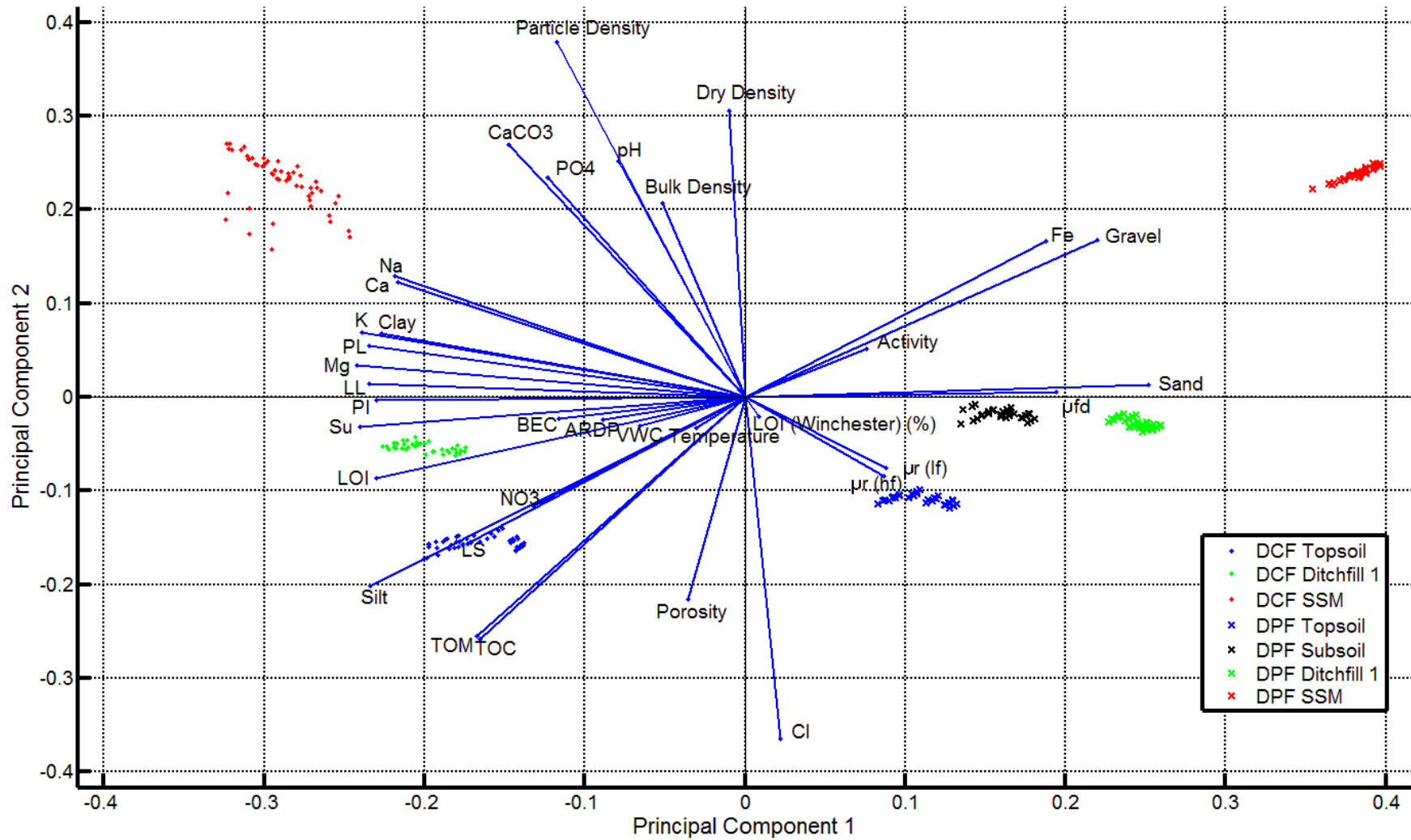


Figure B.19: Principal components 1 and 2 for PCA analysis carried out on the laboratory tested soils using all available variables. Note that soils have been omitted where data was unavailable for one or more variables by the PCA process

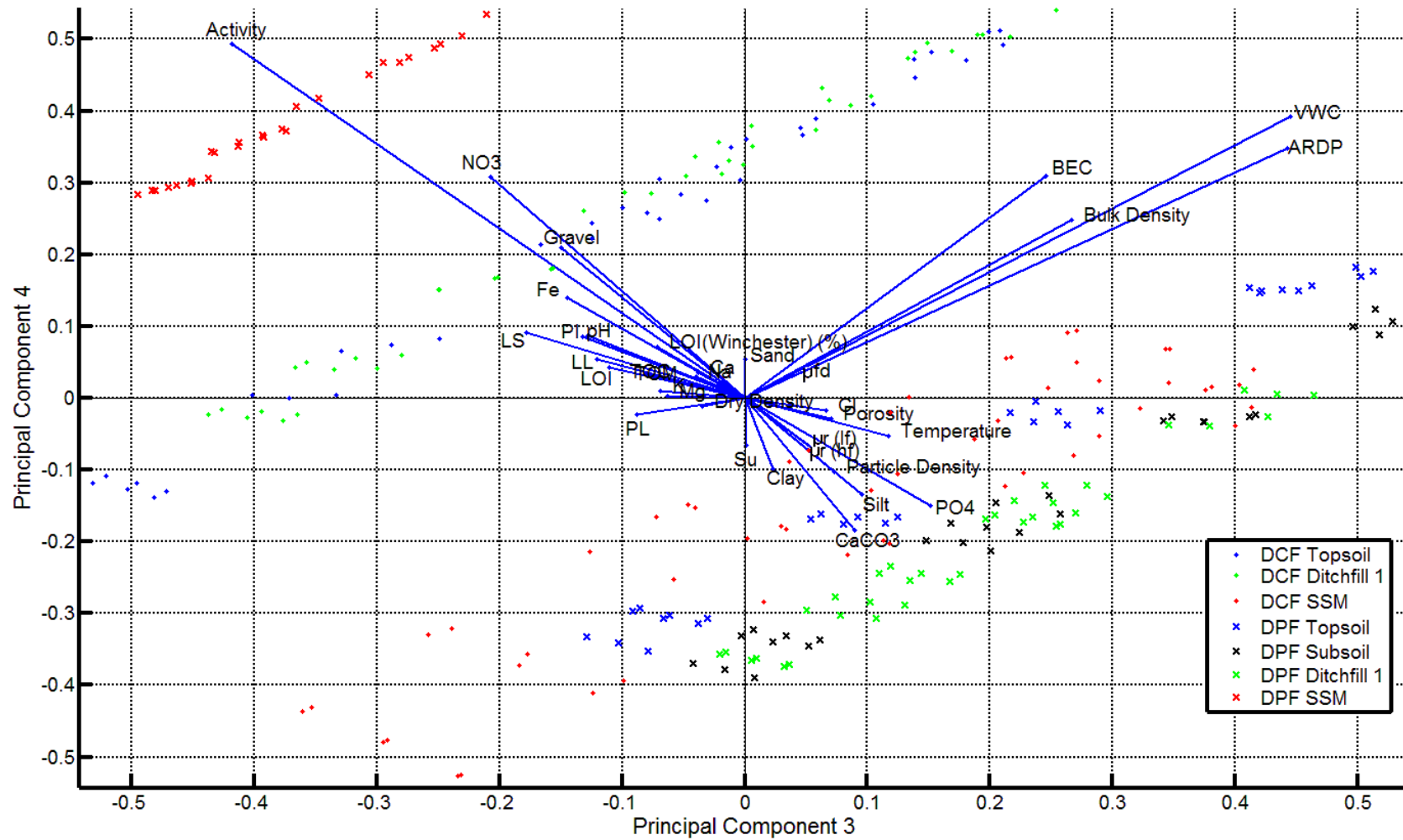


Figure B.20: Principal components 3 and 4 for PCA analysis carried out on the laboratory tested soils using all available variables. Note that soils have been omitted where data was unavailable for one or more variables by the PCA process

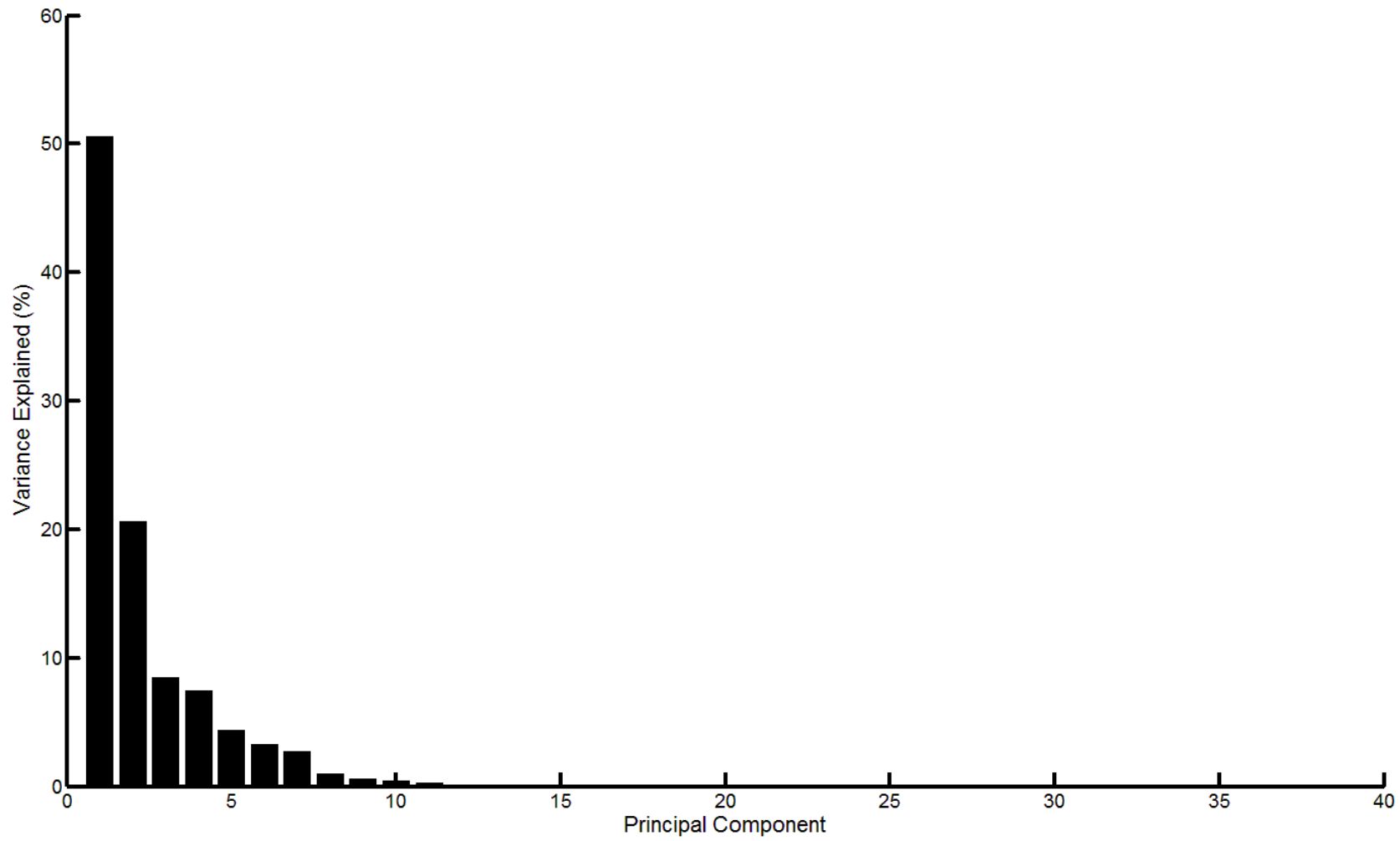


Figure B.21: Scree plot for PCA carried out on the laboratory tested soils using all available variables

Appendix C : Additional Field Monitoring graphs

Comparisons between the weather station data and data from the stations used to patch the weather data are shown for Diddington (Figure C.1) and Cirencester (Figure C.2)

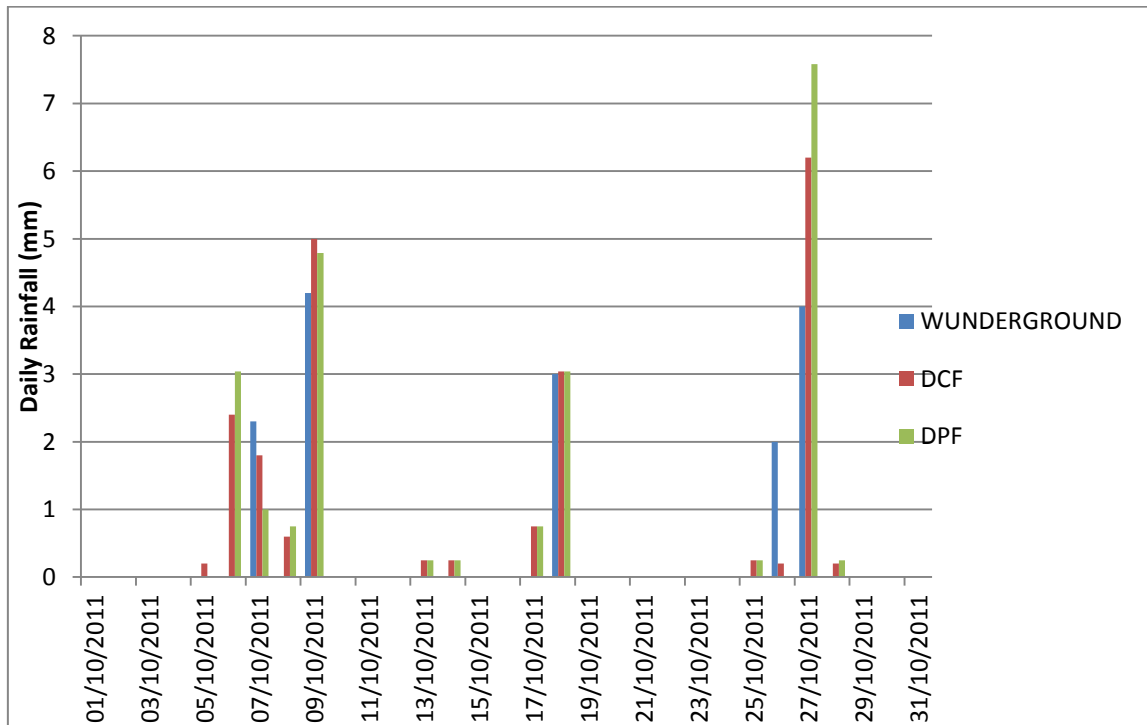


Figure C.1: Rainfall data from the Diddington sites compared to nearby weather data from weather underground for October 2011

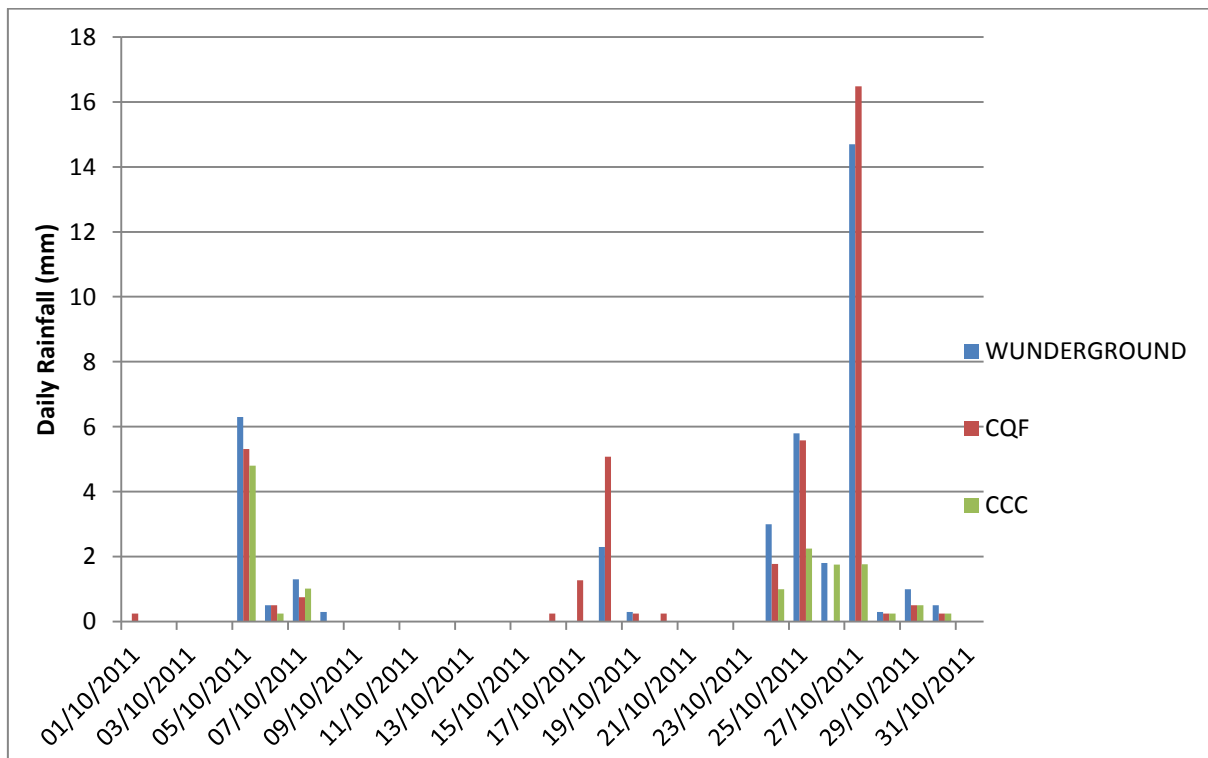


Figure C.2: Rainfall data from the Cirencester sites compared to nearby weather data from weather underground for October 2011

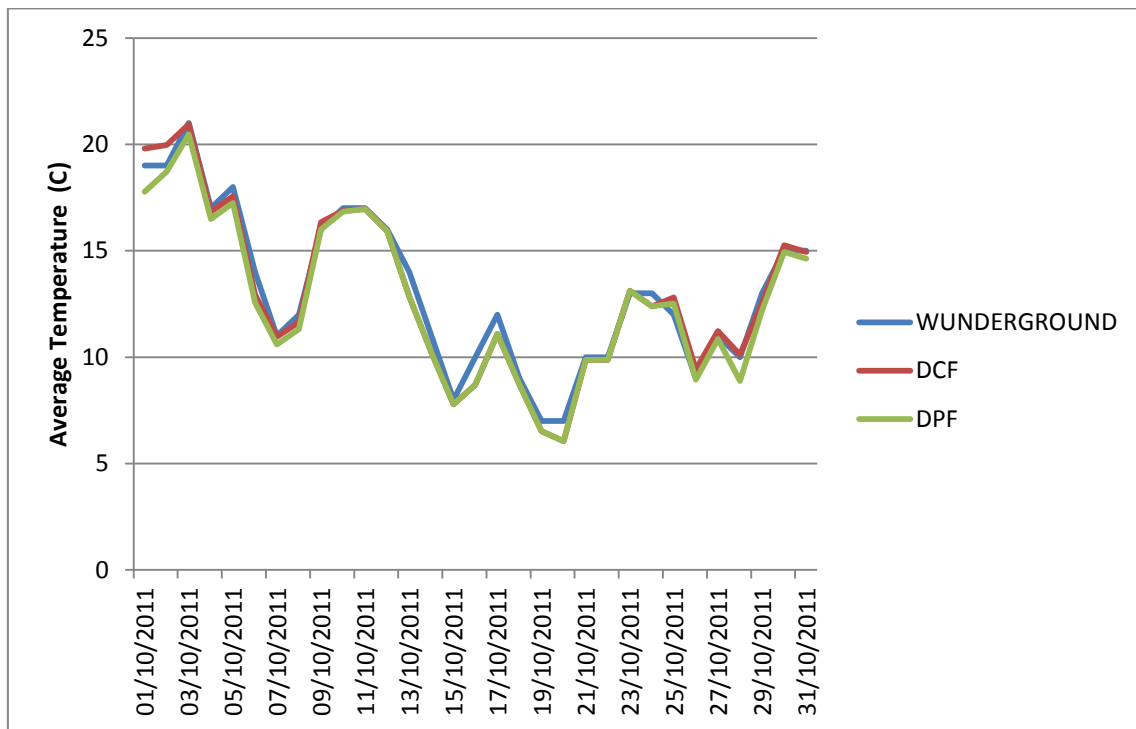


Figure C.3: Air temperature data from the Diddington sites compared to nearby weather data from weather underground for October 2011

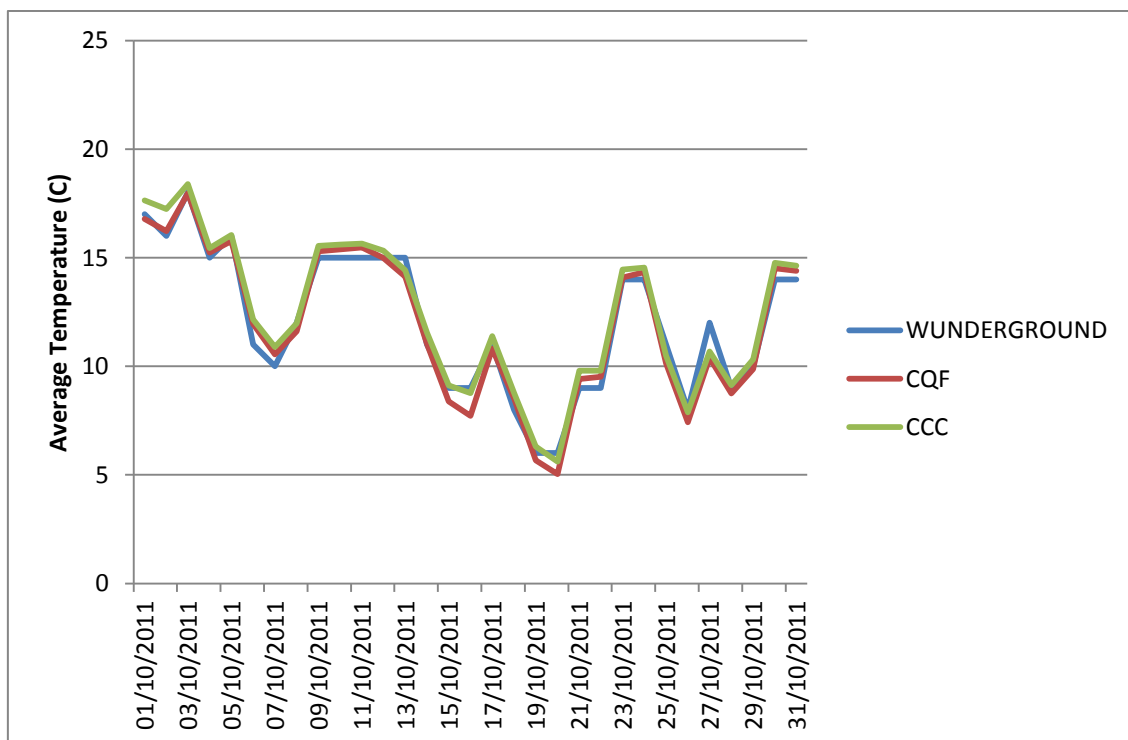


Figure C.4: Air temperature data from the Cirencester sites compared to nearby weather data from weather underground for October 2011

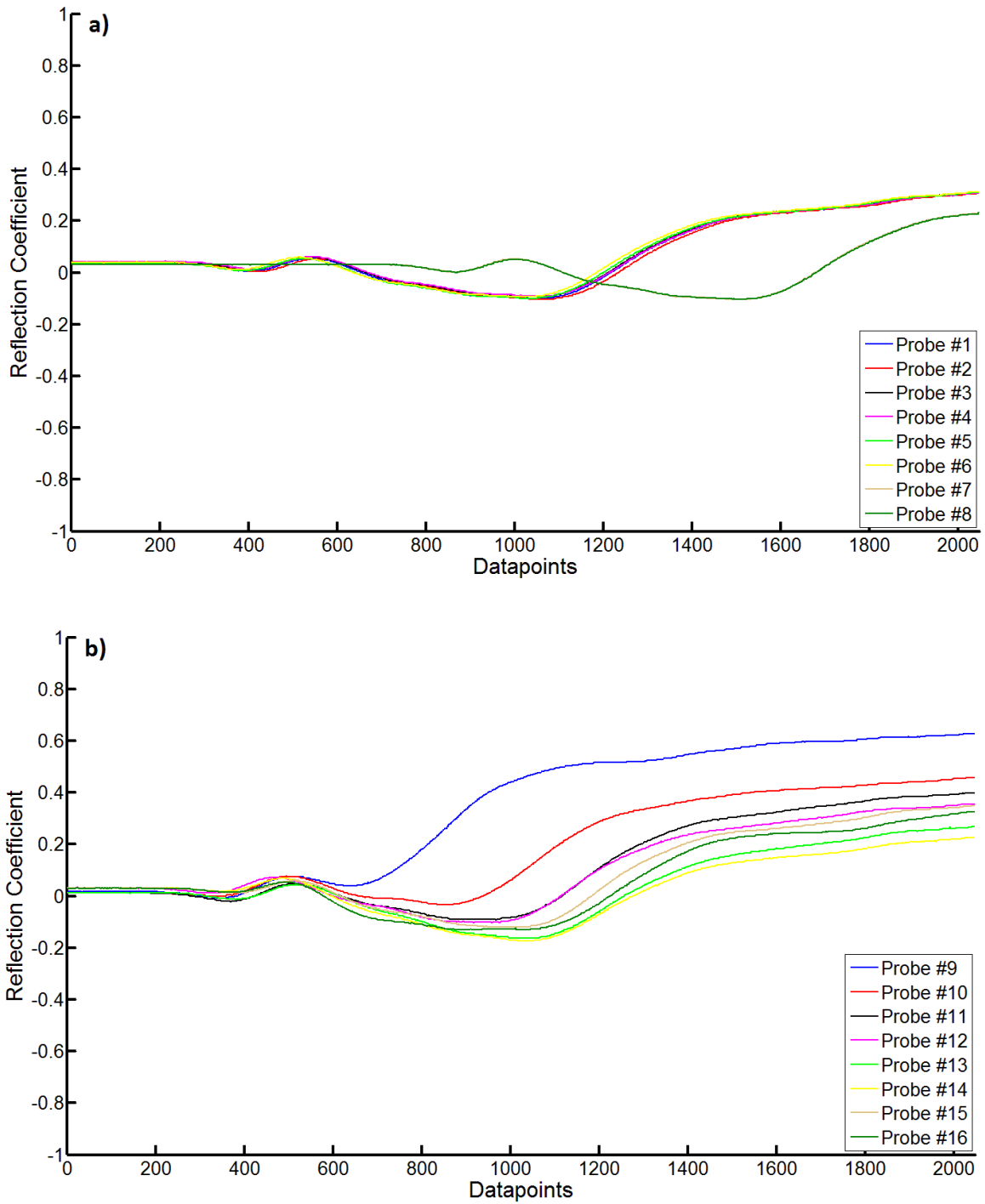


Figure C.5: Example waveforms from CQFA showing the multiplexer failure during monitoring in the left hand array (a) compared to the right hand array (b). Data taken from 25/03/2012 at 15:00.

Examples of filtered and unfiltered data are given for ARDP data (Figure C.6) and BEC data (Figure C.7)

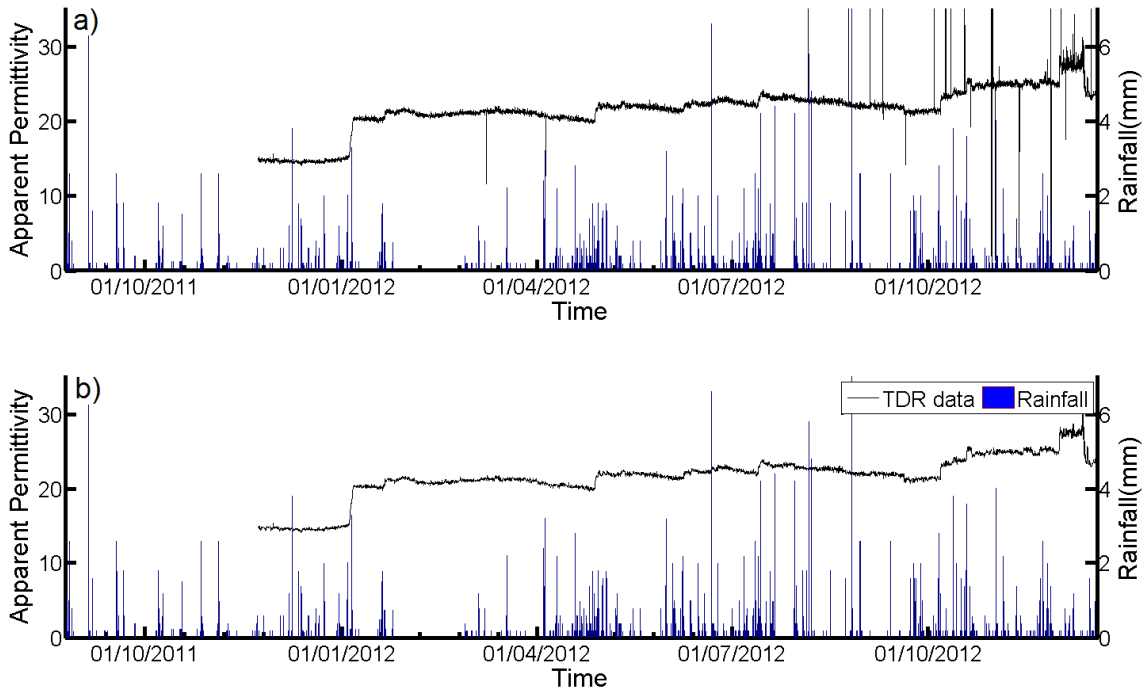


Figure C.6: Example ARDP data a) before filtering and b) after filtering using removal of extreme values and median filter (DCFN probe 4)

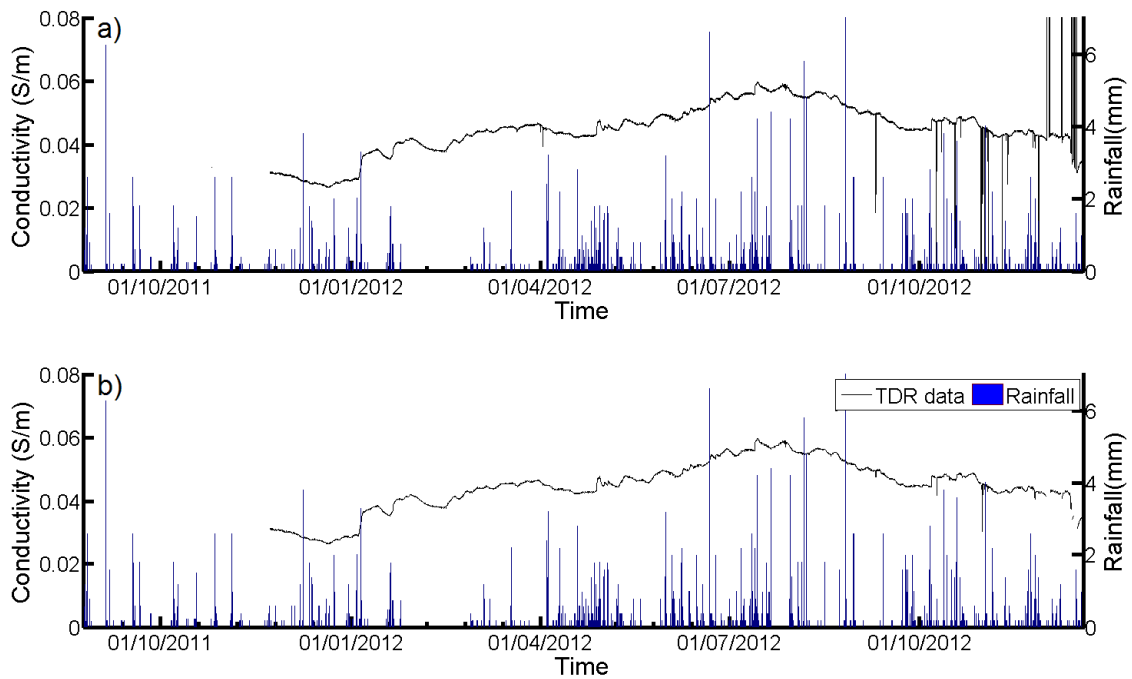


Figure C.7: Example BEC data a) before filtering and b) after filtering using removal of extreme values and median filter (DCFN probe 4)

Appendix D : Comparison between a Commercial IMKO TRIME T3 Probe and the TDR100

In order to compare the monitoring stations with a commercially used alternative, two borehole IMKO Trime T3 probe (logger and one probe generously loaned by Van Walt Ltd.) were installed at DCF on the 1st August 2011. Installation was carried out by Vincent Van Walt and Yvonne Coonan of Van Walt Ltd (Van Walt Ltd., 2013). Installation was carried out by drilling a borehole using a Cobra TT petrol breaker vibracorer to a depth of c.1m. A closed polycarbonate (TECANAT) tube, the same diameter as the hole to ensure a tight fit was inserted, and a rubber bung was used at the bottom to stop moisture ingress. The probes were then inserted into the tubes and connected to the logger, and the cables shielded from damage by pests and buried. Measurements of both VWC and BEC, derived by the loggers inbuilt calibration software were collected every 15 minutes and stored on the logger. Data from these probes was uploaded using the GSM network to a server on a daily basis and available for download. The probe numbers and their depths are shown in Figure D.1 and Table D.1.

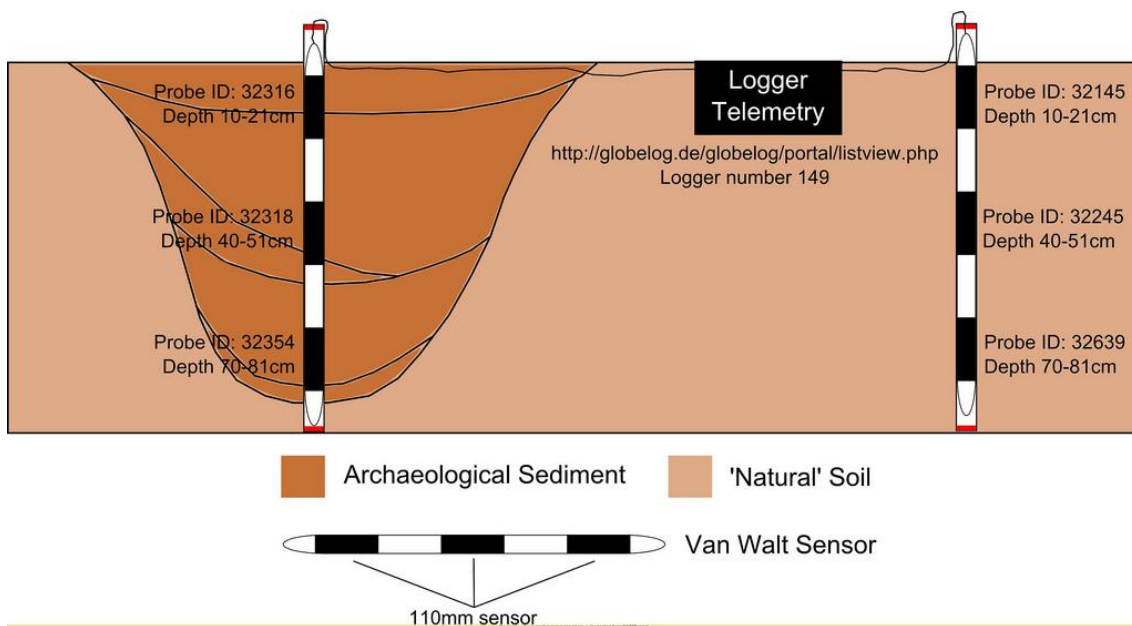


Figure D.1: Schematic of the IMKO soil moisture probe arrays provided by Van Walt Ltd. Re-used under a creative commons share-a-like license from DART Project

Table D.1: The IMKO probe number and measurement depths

| Archaeological Profile | | SSM Profile | |
|------------------------|----------------------|--------------|----------------------|
| Probe Number | Depth Measuring (cm) | Probe Number | Depth Measuring (cm) |
| 32316 | 10-21 | 32145 | 10-21 |
| 32318 | 40-51 | 32245 | 40-51 |
| 32354 | 70-81 | 32639 | 70-81 |

As with the TDR100 systems, probe failures also occurred during the monitoring period with the IMKO T3 probes. One of the probes (#32316) began giving a constant reading of 0% VWC during early 2012. The probe was removed from site and returned to the manufacturer for repair. The probe was eventually replaced with a new probe (#32317) and returned to site during April 2012. Another of the probes gave constant readings of 99% VWC and was removed from site during March 2013 and also returned for repair. Since monitoring for the project had ended on this site by this date, the probe was never replaced on site, and was returned to Van Walt Ltd. The second probe was also removed and returned to the laboratory for future use.

In order to compare the different systems, data from both the bespoke TDR monitoring stations using the Campbell Scientific TDR100 and the IMKO T3 probes were plotted for short periods and compared. In order to facilitate comparison of data in the same units and to remove the effects of assumptions inherent within the water content (such as in the loss tangent and bound water behaviour), the derived VWC data from the IMKO probes were converted to ARDP using a polynomial obtained from IMKO GmbH (Equation D.1).

$$ARDP = 5.61 \times 10^{-2} \cdot VWC + 1.68 \times 10^{-2} \cdot VWC^2 - 1.20 \times 10^{-4} \cdot VWC^3 + 2.51 \times 10^{-7} \cdot VWC^4 + 3.16$$

D.1

Appendices

Data from the TDR100 probes were averaged from the same depths as the IMKO probes.

Figures D.2 and D.3 show the ARDP from both probe types at different depths from both the archaeological soils and SSM for two different periods (18th to 25th June 2012 and 20th August to 5th September 2012). Rainfall data are also included to allow for analysis of the response of both probes to rainfall events. Similar trends can be observed for both the IMKO and TDR 100 probes with rainfall events, with both systems showing the effects of wetting fronts especially at the near surface (10-21cm). However magnitudes of rises in ARDP after the rainfall event were greater for the TDR100 than for the IMKO probe. This was due to the presence of the plastic tube which acted in a similar manner to coated rods used in lossy saline soils. This had the effect of reducing the magnitude of change in travel time with changing soil conditions (Laurent et al., 2005) therefore reducing sensitivity, especially at high ARDP values. The IMKO also seemed to record rises in ARDP at greater depths almost immediately after the rainfall event in comparison to the TDR100, shown in the archaeological profile at 71-80cm during June 2012 (Figure D.2). Since this was indicative of water reaching a greater depth, it seems likely that the inserted plastic tube created a vertical pathway for water to migrate.

The two measurement systems also showed large differences in absolute values of ARDP, especially in measurements from the bottom sensors (70-81cm; Figure D.2c and D.3c) and to a lesser extent the top sensors (10-21cm), although these may be partly due to the greater variability of geophysical properties in the topsoil (see Section 6.3). Many possibilities exist to explain these differences including variation in the effective measurement frequency of the two measurement systems, the effect of the plastic tube on the calculation of transit time and measurement volume of the two sensors and the beginnings of the equipment malfunction in the bottom sensors which occurred later on in the project and caused the bottom archaeological sensor to give erroneous readings (see Section 3.6.5 for details). Large differences also existed between the IMKO probes in the archaeological soils and SSM at 70-81cm depth which were not visible in the TDR100 data. Whilst this may have also been related

Appendices

to the aforementioned equipment malfunction, another possibility is that the access tube has created a vertical pathway for the water table to rise up to the level of the bottom SSM sensor causing abnormally high readings. Removal of the probe revealed the bottom of the access tube to contain moisture despite the seal at the bottom of the tube which may support this theory. Another possibility is that as IMKO probes are individually calibrated monitoring systems, that the calibration on one of the two probes had drifted causing them to give different absolute values to each other.

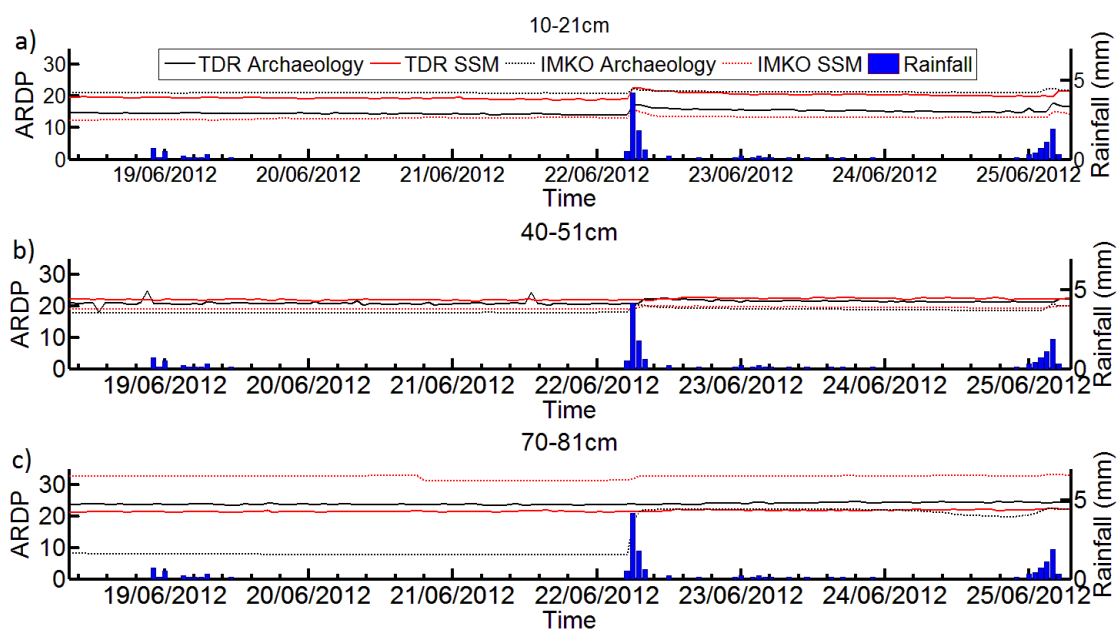


Figure D.2: ARDP derived from both the IMKO and TDR100 probes for a period in June 2012 at depth ranges a) 10-21cm b) 50-51cm and c) 70-81cm

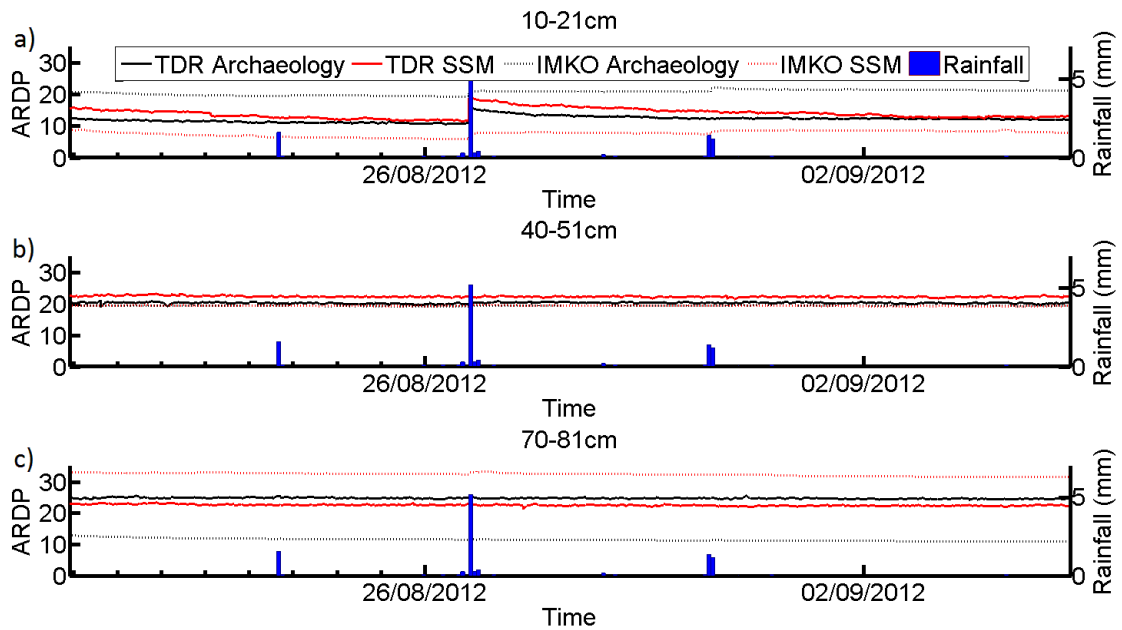


Figure D.3: ARDP derived from both the IMKO and TDR100 probes for a period in August and September 2012 at depth ranges a) 10-21cm b) 50-51cm and c) 70-81cm

Comparison of BEC values are shown for the same periods in Figures D.4 and D.5. A

logarithmic scale has been chosen in order to show the two data sets on the same plot. As with measured ARDP, both measurement systems showed similar trends in measured values and displayed the same rises after rainfall events. However, very large differences existed in the absolute values between the IMKO probes and TDR100, with the IMKO probes recording values an order of magnitude higher. Examination of these values shows them to be between 2-5mS/cm, which are in excess of typically recorded values in normal non saline clay soils of 0.1-2mS/cm (McNeill, 1980). Additional measurements taken in the laboratory on soil solutions using a DC conductivity meter confirmed the expected values to be in the range measured by the TDR100. IMKO GmbH (pers. Comm.) suggested this is the result of the coating used on the electrodes which cause large errors in BEC determination much like coated TDR probes (Moret-Fernández et al., 2009) due to the small magnitudes of measured changes, as well as the linear calibration used to convert signal loss to BEC. However, as with the ARDP measurements, the general trends were similar between the two measurement systems,

especially for the top two probes with both systems showing trends and increases after rainfall events.

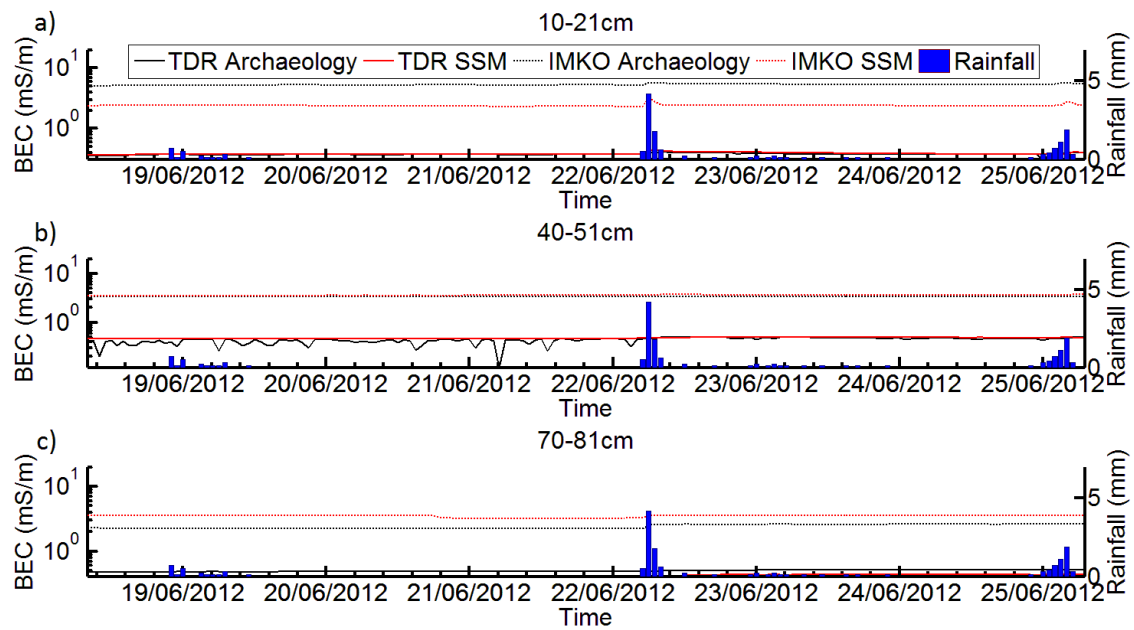


Figure D.4: BEC derived from both the IMKO and TDR100 probes for a period in June 2012 at depth ranges a) 10-21cm b) 50-51cm and c) 70-81cm. Note the logarithmic scale used to display BEC.

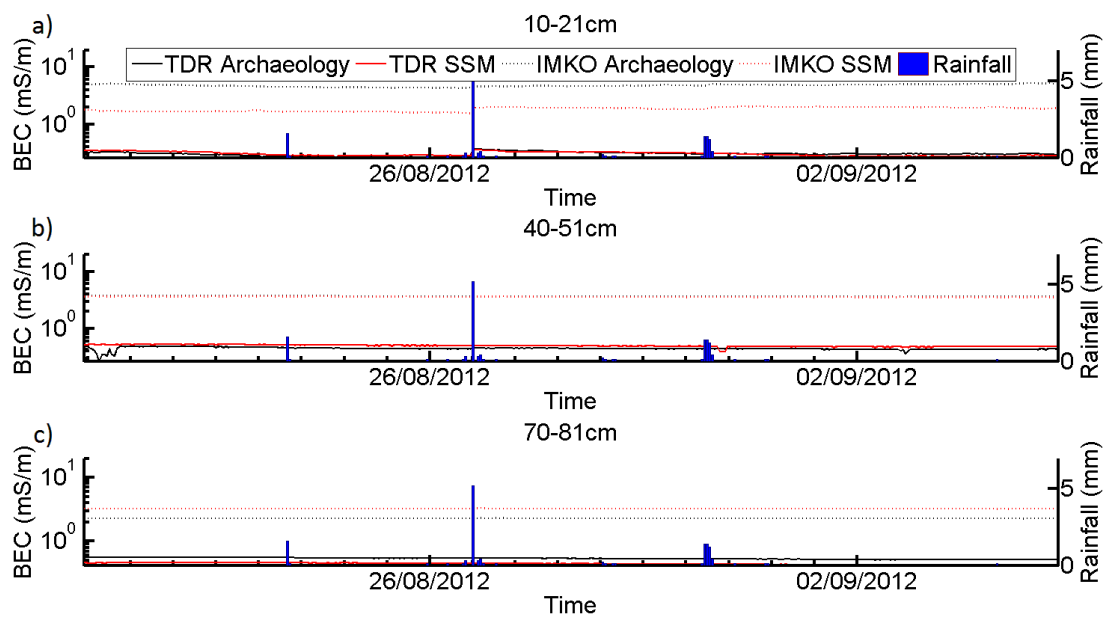


Figure D.5: BEC derived from both the IMKO and TDR100 probes for a period in June 2012 at depth ranges a) 10-21cm b) 50-51cm and c) 70-81cm. Note the logarithmic scale used to display BEC.

Appendices

The IMKO probes were found to show the similar trends in measured ARDP and BEC data to the TDR100 but had large differences in the absolute values, especially for BEC which was an order of magnitude larger. Differences were also found between the archaeological and SSM sensors which were not apparent in the TDR100 data. However, the IMKO sensor may be useful for measuring relative change in a single soil profile.

Appendix E : Further Details on Mechanisms of Permittivity and Permeability

Permittivity occurs due to four main mechanisms of polarisation; electronic polarisation, ionic polarisation, orientational polarisation and Maxwell-Wagner or interfacial polarisation

(Cassidy, 2009, Elliott, 1993)

Electronic polarisation (P_e) (Figure E.1) is the result of the separation sub-atomic charged particles. The negatively charged electrons are moved in the opposite direction to the positively charged protons in the atoms nucleus. This causes the shape of the electron density cloud to deform as a response to the applied electrical field forming an electrical dipole (Figure E.1b). Electronic polarisation is most common in electrical fields of high and optical range frequencies (Cassidy, 2009, Chen and Or, 2006).

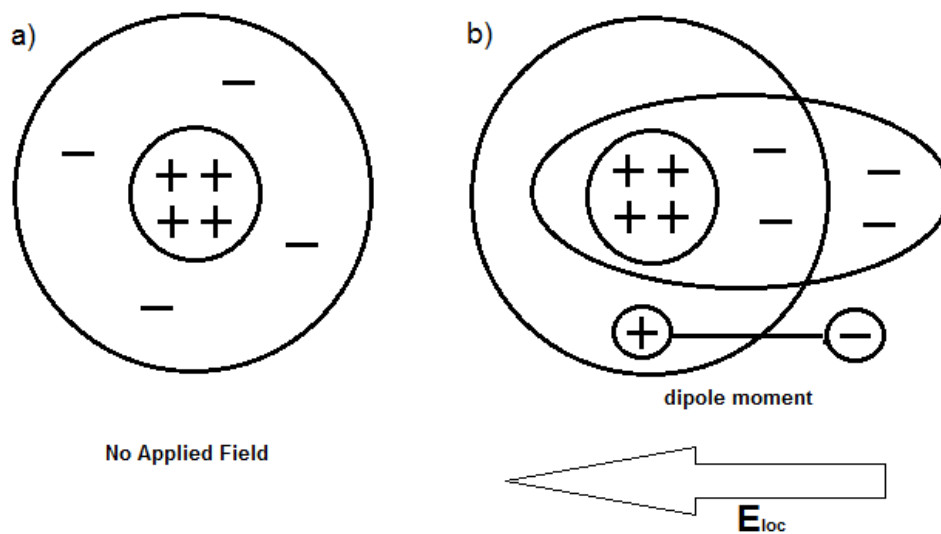


Figure E.1: Electronic polarisation in the presence of a) no applied field and b) a local electrical field (E_{loc}).

Ionic polarisation (P_i) (Figure E.2) takes place in molecules which contain an ionic chemical bond. These occur when electrons from one atom are transferred to the other, resulting in the two atoms containing opposite charges which attract each other to form a chemical bond (Brady and Holum, 1993). Application of an electrical field causes these charged atoms to drift

apart and polarise forming an electrical dipole (Elliott, 1993). Ionic polarisation is most common 10^{12} and 10^{13} Hz (Chen and Or, 2006).

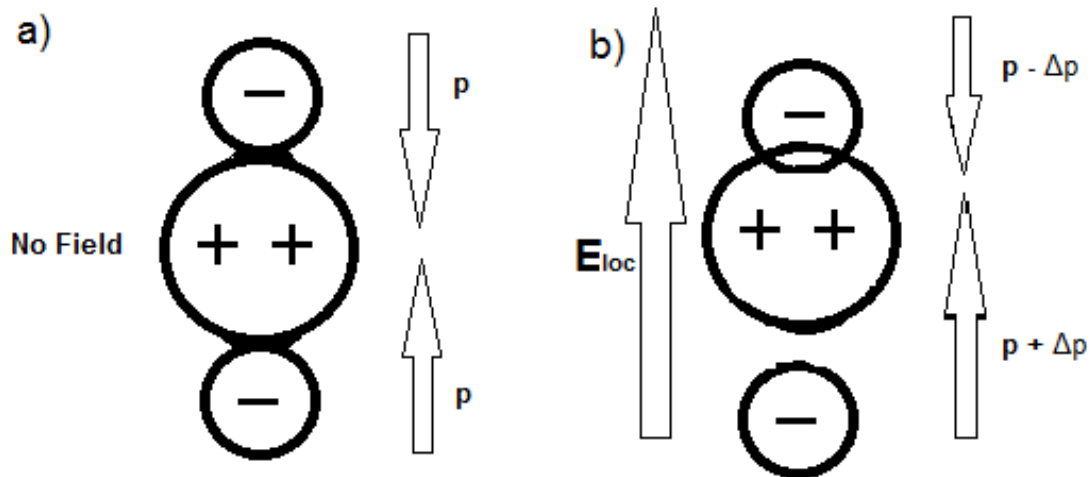


Figure E.2: Ionic polarisation in non polar molecules due to the presence of a) no applied field and b) a local electric field (E_{loc}). After Elliott 1993

Orientalional or dipolar polarisation (P_o) (Figure E.3) occurs in polar molecules which possess permanent dipole moments, due to differences in electronegativity between the atoms (Brady and Holum, 1993, Debye, 1929) such as H_2O or HCl . In the absence of an applied field, these dipoles are randomly orientated by thermal agitation, cancelling out any macroscopic effects. Application of an electrical field causes the molecules to rotate to align with it, creating a macroscopic dipole in the material, and storing energy until the field is removed and the energy released.

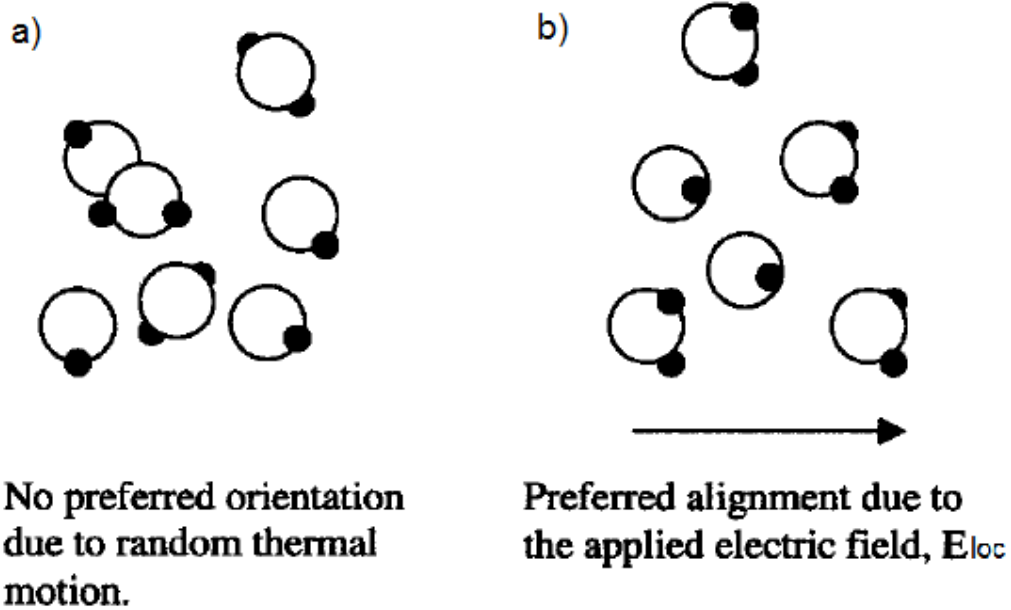
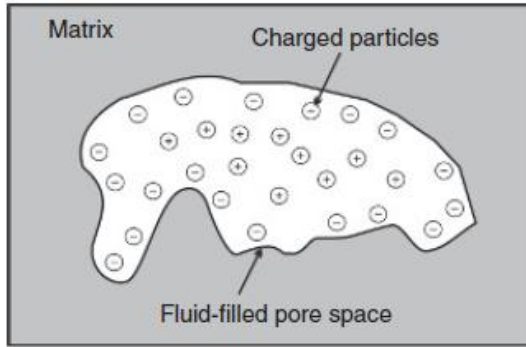


Figure E.3: Orientational polarisation of polar molecules. (Robinson et al., 2003a)

Maxwell-Wagner or interfacial polarisation (P_{mw}) (Figure E.4) occurs within mixtures of materials with different dielectric properties such as soil (Chen and Or, 2006). In absence of a field, free charges on the surfaces of particles are randomly distributed and there is no net charge. In the presence of low frequency electrical fields, free charges accumulate, forming electrical dipoles across pore spaces (Cassidy, 2009) which can cause permittivity values far greater than the sum of the individual components. These effects tend to work in the kilohertz to megahertz range (Chen and Or, 2006).

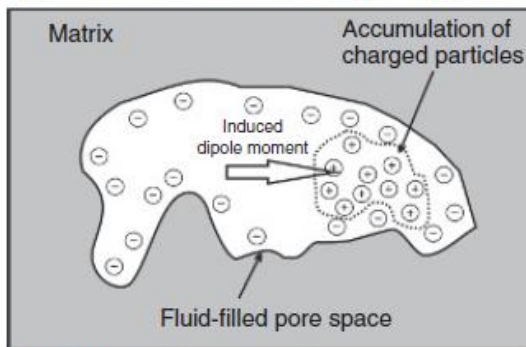
No applied electric field



In the absence of an applied electric field, the free charges (positive in this case) are distributed randomly within the pore fluid whilst the negative charges are bound to the surface of the matrix grains.

Overall, the net charge across the material is zero as the negative and positive charges effectively cancel out.

Applied electric field: Low frequency (<10 MHz)



In the presence of a low-frequency applied electrical field, the free charges separate to form an induced dipole moment across the pore space.

The relaxation response is dependent on the size of the pore space and the amount of free charge. The effect is generally restricted to frequencies below 10 MHz.

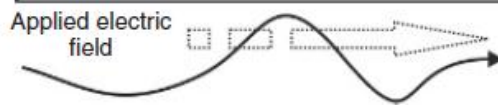


Figure E.4: Maxwell Wagner polarisation in porous media (Cassidy, 2009).

Appendices

There are 3 main types of magnetism; diamagnetism, paramagnetism and ferromagnetism (Aspinall et al., 2008).

Diamagnetism occurs in materials where all electron shells are complete and there are no unpaired electrons. The applied field causes the electrons to precess around the nucleus which gives a weak negative susceptibility. Examples of material which display this behaviour are water and quartz (Aspinall et al., 2008, Lindsley et al., 1966).

Paramagnetism occurs in materials which have one or more unpaired electrons producing unbalanced spin moments. Whilst the directions of these spins is normally thermally randomised, the presence of a magnetising field causes these moments to line up to produce a positive susceptibility, which whilst weak, is still an order of magnitude greater than diamagnetism.

Ferromagnetism (*sensu lato*) is the strongest type of magnetism, producing the highest susceptibility values which can persist to an extent, even in the absence of a magnetising field (remnant magnetisation). The orbits of unpaired electrons overlap, and the spin moments are aligned (Evans and Heller, 2003) to produce a very strong magnetic effect. The directions of the dipole moments determine the type of magnetism produced (Figure E.5). Ferromagnetism (*sensu stricto*) (a) occurs when all the dipoles are aligned in one direction, creating a magnetic moment which can persist in absence of the applied field as strong atomic interactions lock the dipoles together (Aspinall et al., 2008). If dipole coupling is anti-parallel and the numbers of dipoles in each direction are equal, then anti-ferromagnetism (b) is said to exist, which produces no magnetic moment, unless lattice defects disrupt this equality. This causes parasitic anti-ferromagnetism (c) which occurs in many iron oxides found in soil such as hematite. Finally, unequal numbers of dipoles in each direction give rise to ferrimagnetism (d), which produces a strong magnetic moment in the direction of the majority of the aligned dipoles.

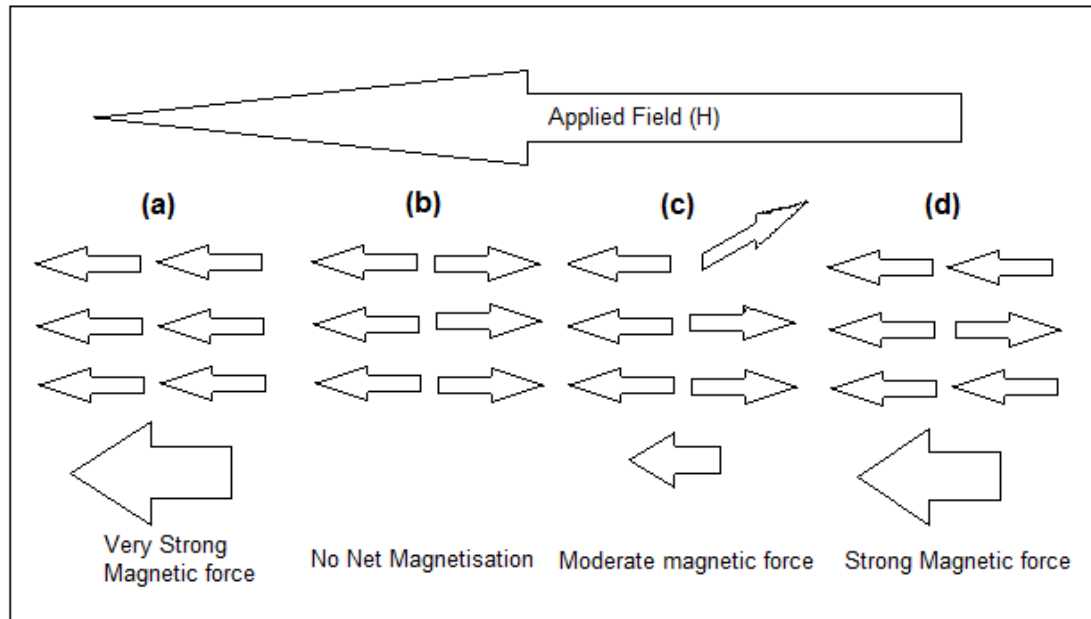


Figure E.5: Different types of ferromagnetism (*sensu lato*). a) Ferromagnetism (*sensu stricto*) b) Anti-Ferromagnetism c) Imperfect Anti Ferromagnetism and d) Ferrimagnetism

Appendix F : Further Details on Seasonal Variability of Geophysical Properties for each Study Site

F.1. Diddington Clay Field

The ARDP data presented can roughly be divided into two distinct periods; a flat period consistent at all depths where few changes are observed near to the beginning of the monitoring period and following a sharp wetting front, which moved through the profile between December 2011 and May 2012, a later period where the ARDP was seen to respond to strongly to rainfall and periods of wet and dry weather with changes in its overall value. The first c.6 months showed few changes in ARDP with consistently low values (less than 15 at all depths) recorded. Relationships developed in the laboratory (see Chapter 5) suggest that this indicates a VWC value of less than 25%. It should also be noted that values in the later monitoring periods never returned to these low values again. One possible reason for these low values is that installation took place in August 2011 during one of the driest and warmest years ever recorded in the UK, with rainfall only reaching between 65-75% of the normal average figures (Mail Online, 2012) causing an extreme drought. Since this extreme weather event was never repeated, the soil never returned to these values. Very low values were also recorded during this period on other sites (Curioni, 2013). However, given the extremely low values, it is perhaps also likely that this period was influenced by the installation method itself, which took place over a number of days with an open trench face. Although the face of the trench was cut back before installation, it is possible that the soil at depth was dried over this period due to exposure to warm air in a way which is impossible under field conditions. This would cause abnormally low permittivity as the water in the pores would evaporate and the pores would fill with air. To avoid this in future installations, it may be beneficial to artificially wet the soil before backfilling.

The end of the low period is characterised by a sharp wetting front, which travelled down the profile from December 2011 before reaching the deeper probes during May 2012 (Figure

Appendices

6.12i). However, each movement down the profile took place following a large rainstorm and the rate at which the front travelled appeared to slow down with depth. This is most likely to be due to increased resistance because of air present in the pores of very dry soils, which is harder to expel at greater depths due to the lack of a suitable pathway for it to escape (Beven, 2004, Davis and De Wiest, 1966). There is a marked difference in the movement of this wetting front below 0.5m in depth between the archaeological soils and SSM. In the archaeological soils, the initial wetting front moved quicker, arriving slightly earlier at depths between 0.4m and 0.9m (below the topsoil where the archaeological soils start; Figure 6.12d-i). It also continued as a sharp transition, whereas in the SSM, the wetting front ceased to be a steep front, but showed more gradual rises in ARDP. One likely explanation for this is the differences in pore space between the two soils, with greater porosity encountered in the less dense archaeological soils, which allowed both air to escape and the water to travel more freely.

Following this initial wetting front, the soil responded to future rainfall events with increases in ARDP values, although none of the later wetting fronts during the monitoring period produced increases in permittivity as big as this initial front. Several possibilities exist for this improvement in water conductivity following the initial wetting. Firstly, Castellini and Ventrella (2012) showed that clay is more conductive to water when wet as this improves the soil structure, although the effect was diminished as the soil got wetter due to swelling. Secondly, it is thought that the initial wetting front was responsible for expelling air from the pores (Davis and De Wiest, 1966), which provided resistance to water percolation. A combination of these two factors is likely to account for the increased responsiveness of the soil in the second part of the monitoring period. However, it is also interesting to note that the effects of rainfall events were rarely seen below 0.3m in depth. This is consistent with the findings of Curioni (2013), who also found limited infiltrations at depth, and is the result of the relatively impermeable soil layers below. Only a few notable rises occurred lower down the profile, (e.g.

Appendices

April/May 2012 and October 2012), which were all preceded by a period where ET exceeded rainfall causing drying at the surface, shown by the decreasing permittivity in the top 0.1m depth graph (Figure 6.12a), which caused shrinking on the surface and pores to open up (Horton, 1933).

Both the archaeological and SSM exhibited a similar seasonal response throughout the year and followed similar trends. Only a few slight differences in infiltration depth were visible between the archaeological soils and SSM, with slightly greater infiltration detected in the archaeological soil, which is most visible at 0.3m (Figure 6.12c) in depth. Very small differences also existed in the infiltration speeds, with ARDP rises occurring in both the archaeological and SSM soils at similar times after the initial wetting front (i.e. within 1-2 days). This similarity in infiltration behaviour is unexpected given the differences in the initial front discussed above, but may be the result of the improved soil structure in wet soil and the lack of air in the pores compared to the initial dry soil state, which reduced the effects of the earlier discussed differences in pore sizes. Perhaps the most notable differences in behaviour between the archaeological soils and SSM are the differences in drying patterns. Drying was faster in the archaeology, shown by the steeper gradient of the decreasing ARDP during periods where the ET exceeds the rainfall, such as during August and September 2012 and the end of May 2012. However, these drying effects dropped off with depth and the effect was most visible between 0.1m-0.5m depth (Figure 6.12a-e). Due to these similarities in infiltration patterns, and the lack of infiltration below the top few probes during this wet period, in both the archaeological soils and SSM below 0.4m depth (Figure 6.12e-i) relatively stable values around 20 ARDP units were recorded. On the rare occasions where rainfall or drying affected the permittivity at these depths, ARDP values tended back towards this value, and it is suggested that this is the field capacity of these soils. Since no significant differences were found in the VWC-ARDP relationships established for these soils in Chapter 5, it is suggested that both the archaeological soils and SSM had similar capacities (approximately 30-35% VWC),

Appendices

which is reflected in the similar grain sizes of these soils, although the archaeological soil's capacity was marginally higher. Contrast between the archaeological feature and the surrounding soil throughout monitoring was therefore fairly low. During the dry period at the start, the majority of depths showed either higher ARDP values in the SSM than the archaeological soils at the same depths, or few differences between the two. This showed a higher residual water content in these soils, which was likely to be a result of their higher density and lower pore space to allow water to escape, which was also reflected in the rate of drying between the two soils discussed earlier. For the rest of the monitoring period following the initial wetting front, contrast at most depths was negative (i.e. archaeological soils have lower values than SSM), rarely exceeded 1-2 ARDP units and remained reasonably constant at each depth. These small differences are unsurprising given the similarity of the properties of the two soils (see Chapter 5). The only significant contrasts were found during the initial wetting front, due to its slower movement in the SSM discussed earlier, and at a depth of 0.9m throughout the whole monitoring period which appears to be caused by differences in the holding capacity of the two soils. As the bottom DCF Ditchfill2 soil was found to have both a higher porosity and finer grains than the SSM at the same depths, and it seems likely that it had a higher soil potential and holding capacity.

The BEC data showed similar trends to the ARDP data, with the majority of the response being governed by the amount of water in the soil, as well as the temperature. This would support the findings of other authors (Curioni, 2013, Smith-Rose, 1933) as well as the experiments on soil EM behaviour carried out in Chapter 5. However, it should also be noted that there was a rise and a fall in measured values in both the archaeological soils and SSM between April and October 2012, peaking during July. Since the ARDP data showed no overall major trends due to rainfall during this period at greater depths (below 0.5m; Figure 6.13f-i), and the trend coincided with the air temperature changes noted in Section 6.2, it is thought that these trends were the result of changes in the soil temperature, which was shown to have a large

Appendices

effect on measured BEC (especially in saturated soils) in Chapter 5. A similar trend can also be noted during the initial dry period during which, in contrast to the ARDP values, measured BEC was not constant but showed a slight decrease over the period until the initial wetting front, in line with the falling air temperatures at the end of the summer 2011 period. This is an important result as, since very few changes in water content have been shown to take place at greater depths, temperature appears to have an important role in the determination of BEC in these soils. The seasonality of soil temperature is looked at in greater detail in Section 6.5 and its effects on measured geophysical properties discussed further in Sections 6.6.2 and 6.8.

As with ARDP, few large scale differences existed in the measured BEC data between the archaeological soils and SSM at the majority of depths, with the greatest overall differences shown at 0.7-0.9m due to the difference in the water storage of these soils. One particularly interesting depth is 0.3m where the SSM had a consistently higher BEC than the archaeological soil despite showing similar ARDP values. This is difficult to explain, especially as both probes were located in the same soil (DCF Subsoil) according to the section drawings, and no parallels can be found in the literature. One possibility is that the subsoil above the ditch was mixed with another soil such as the topsoil or Ditchfill1 soil during ploughing or that this layer is simply a mixing zone between the plough layer and underlying soil. Examination of the photos from site (Figure F.1) suggests that the subsoil layer was less visible as a colour difference above the ditch (Figure F.1b), which may partially support this theory although insufficient information exists to conclusively explain this phenomenon.

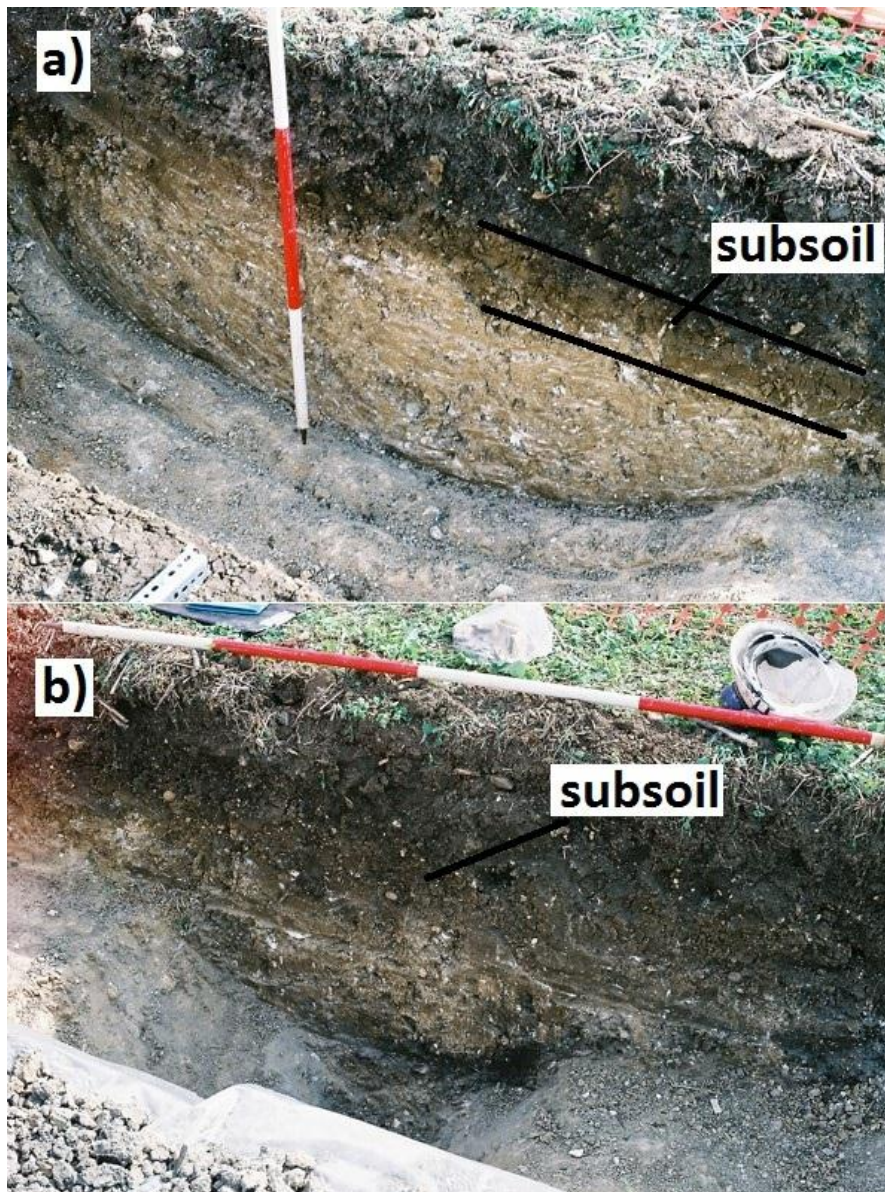


Figure F.1: Photographs from the DCF excavation showing the difference in appearance of the subsoil layer in both (a) the SSM and (b) above the Ditchfill soils.

F.2. Diddington Pasture Field

As with DCF, the monitoring period was again characterised by two main periods; a dry period of near constant values in summer 2011 followed by a period after a significant wetting front where the soil was more responsive to rainfall events. One thing to note is that the initial wetting front was less steep than on DCF suggesting a more gradual distribution of water. This is a surprising result as infiltration is generally considered to be faster in coarse grained soils

Appendices

due to their larger pores (Adeniji et al., 2013, Davis and De Wiest, 1966). One possible explanation may be that the grass was absorbing the water, reducing the ponding at the near surface and therefore the hydraulic head at greater depths, although no conclusive evidence can be found for this. It is also interesting to note that the initial wetting front was both faster and penetrated to greater depths in the archaeological soils. The reasons for this are also difficult to determine as no comparative density or porosity data exist for the SSM making comparisons problematic, although a large gravel fraction such as that found here has been noted to reduce hydraulic conductivity in dry soils (e.g. Saxton and Rawls, 2006). Towards the end of 2012 a third period was noticed, consisting of a large rise in the ARDP at greater depths (0.6m - 1.2m; Figure 6.14e-i) which seemed to unusually affect the bottom layers first, contradicting the usual models of infiltration after rainfall. One suggestion for this may be that this was caused by a rise in the water table. Excavations carried out nearby in June 2013 suggest that the water table was indeed high during this period as it was located in the bottom of the trench (c. 1.2m depth). Much of the subsequent data were very noisy and fluctuating, especially in the SSM soils. One explanation may be that the water table was fluctuating during this period due to changes in pressure, although it is more likely that this shows an equipment malfunction.

DPF also showed similar variation with depth as the DCF soils, with only the top few probes responding strongly to individual rainfall events. At the near surface (0.1m; Figure 6.14a) down to 0.5m depth (Figure 6.14d), both the archaeological soil profile and the SSM behaved in a very similar manner and had comparable responses to rainfall events, seen in the 0.1m and 0.5m graphs (Figure 6.14a and Figure 6.14d). This is perhaps unsurprising as at these depths the site was covered by the topsoil and subsoil, which were the same soils across the whole site as their deposition post-dated the archaeological feature. One slight anomaly to this finding occurred after drying during August and September 2012 which dried the SSM more than the archaeological profile, and it is suggested that some of the top of DPF Ditchfill1

Appendices

may be mixed with DPF Subsoil. Below 0.5m depth (Figure 6.14e-i), the archaeology shows consistently high ARDP values in comparison to the SSM (archaeological ditchfills start at c. 0.6m depth). Whilst this is in itself indicative of greater water contents, it was also previously found in Chapter 5 that DPF Ditchfill2 (0.8m depth; Figure 6.14g) showed very low ARDP values at the same water content in comparison to the other soils on site making these differences even greater than they appear. The consistency of these differences would suggest that the main difference between the archaeological soils and the SSM is the archaeological soils greater ability to hold water. This is unsurprising given the lower density, greater porosity and organic matter contents and smaller grain sizes of these soils discussed in Section 5.2 which gave them a greater SSA and pore space and therefore soil water potential than the SSM.

As with DCF, the measured BEC data followed similar trends to the ARDP due to its primary dependence on water content. One interesting result is that the 0.6m depth (Figure 6.15e) showed lower BEC values in the archaeological soils in comparison to the SSM despite the ARDP data (Figure 6.14e) showing the opposite result. Comparison to the section drawing showed that the archaeological probe was within the DPF Ditchfill2 soil, which was found to display lower values for both BEC and ARDP for a given water content than the other DPF soils from the laboratory work (Chapter 5).

In addition to following the broad ARDP trends such as infiltration patterns, as with DCF, the soil also showed significant temperature effects, especially during the summer 2012. However, it is important to note that the magnitude of these temperature effects was much smaller, producing a change in the order of approximately half that recorded on DCF from the coldest to the warmest period (approximately 0.01 S/m compared to approximately 0.02 S/m on DCF). This is in agreement with the findings in Chapter 5, which found reduced temperature dependence of the BEC in coarse grained soils due to the fact that the soil's lower surface area

meant fewer ions were available in solution, thereby reducing the effects of increased ion mobility caused by increasing temperature.

F.3. Cirencester Quarryfield

Data from the archaeological probes at 0.1m (Figure 6.16a) were extremely noisy. One of the two probes from this depth was already discarded as it was visible on the surface, and it is possible that a similar disturbance may have also affected the other probes, creating an air gap and lowering the measured values.

As with the other two sites, the monitoring period showed both a defined dry period during summer 2011, when the ARDP values were at a minimum, and a wet period for the remainder of the monitoring period. However, unlike the other sites, as monitoring was begun at an earlier date, the drying to the minimum value was visible during July 2011, suggesting that the values were not caused by the installation procedure but by climatic conditions. Whilst this drying could be seen at all depths following the extremely low rainfall and high ET figures, it should be noted that drying occurred at a later date at greater depths as well as being less severe which is in line with the findings of Curioni (2013). It is also interesting that the drying was more intense within the archaeological soils, especially below 0.3m depth (Figure 6.16d-h). Whilst on the other sites, this has been suggested to be the result of greater pore space allowing water to escape more easily, the opposite porosity results were found at the near surface, and the reasons for this trend are unknown.

The dry period was brought to an end by a series of rainfall events between October and December 2011 which began to wet the near surface (0.1m-0.3m; Figure 6.16a-c) during this period. However, the remainder of the profile stayed dry until heavy rain in December 2011 which caused a large wetting front which had an almost instantaneous effect on the measured ARDP. This result is similar to the behaviour of the other sites. Also, as with the other two sites, the effects of rainfall events were seen following this initial wetting front which caused

Appendices

the soil to reach field capacity. Similar patterns were also visible in infiltration patterns with rainfall during this period mainly affecting the top 0.3m for the remainder of the monitoring period and rarely affecting the deeper probes, except in cases of drying in the surface soils. The greatest differences between the archaeological soils and the SSM seemed to occur after extended periods of dry weather, which caused differential drying patterns especially in the near surface soils, which are more intense within the archaeological soils as with the initial drying phase at the start of monitoring described earlier. Over the monitoring period as a whole, at the majority of depths the SSM displayed higher average ARDP values than the archaeological soils unlike the other sites, suggesting higher water content. The exceptions to this behaviour occurred at 0.6m (Figure 6.16e) and 0.7m (Figure 6.16f) where the reverse trend is true. One possibility is that there may be differences in the VWC-ARDP relationship in these soils which were not tested in the laboratory. The chemical data suggested a greater ionic content in the SSM, and it is possible that this would give both higher BEC and ARDP values due to the effects of the loss tangent discussed in Chapter 5. However, the BEC data presented in Figure 6.17 showed the opposite trend and it seems more likely that the contrast is due to differences in water holding capacity between the soils. The probes at 0.6m and 0.7m depths within the archaeological ditch corresponded to CQF Ditchfill2 and deeper SSM (context 9) with shallower probes (0.3m-0.5m) located in CQF Ditchfill1 and the upper SSM (context 8). Comparison of the geotechnical properties of the two different ditchfills and SSM at different depths (upper and lower) showed that CQF Ditchfill1 had a lower clay content and higher density than the SSM at similar depths, whereas for CQF Ditchfill2 the opposite trend was true as with between the ditchfills and SSM on other sites. It is likely that these textural differences are chiefly responsible for the variability in the holding capacities of the soils, with differences in the clay fraction dominating in fine grained soils.

As with the ARDP data, the 0.1m probes within the archaeology (Figure 6.17a) appear to give very noisy data and very low readings and it is suggest that they were disturbed creating air

Appendices

gaps during the monitoring period. Much like the other two sites, the data showed both similar trends to those recorded in the ARDP, confirming the dominance of the water content on BEC determination, as well as showing variation influenced by changes in air temperature. Also similarly to the ARDP data, the near surface probes showed a predominantly negative contrast (i.e. the SSM has higher BEC than the archaeological soils) whilst the deeper probes located in CQF Ditchfill2 showed higher BEC in the archaeological soils. This suggests that differences in water content are responsible for determining the BEC rather than temperature differences or differences in the soil ion availability. The contrast between the archaeological soils and SSM were greatest at 0.6m and 0.7m depth, with the greatest differences during the summer months when the soil was saturated and the temperature was greatest. This is in line with the findings on other soils in Chapter 5 which determined that temperature dependence of BEC was greatest in saturated soils.

Appendix G : Further Details on Seasonal Variability of Temperature for each Study Site

G.1. Diddington Clay Field

The temperature varied following broadly seasonal trends in air temperature at all depths which displayed a sinusoidal variation with the season, being warmest in summer and coldest in winter. The lowest soil temperatures were recorded during January and February 2012 during a period where the average air temperatures were at their lowest values. The highest temperatures were recorded in July and August 2012 where the average air temperatures were at their highest values. However, another important consideration is that although the air temperature followed seasonal trends, smaller scale variations took place on a day by day basis, due to differences in solar radiation, cloud cover and other meteorological phenomena which are reflected in the fluctuations in air temperature line. The measured soil temperature was always smaller than these variations, although smaller scale daily variations were greater at the surface and the effect dropped off rapidly with depth, and can barely be seen below approximately 0.4m (Figure 6.20d-i) where only the general seasonal trend can be observed. This limited variation of temperature with depth in soils is well known and has been widely reported in the literature (Florides and Kalogirou, 2005, 2009, van Manen and Wallin, 2012).

Differences in temperature between the archaeological soils and SSM are fairly small throughout the monitoring period and only slightly over the stated resolution of the temperature probes of $\pm 0.3^{\circ}\text{C}$. However, the archaeology displayed a greater response to seasonal variation with slightly lower temperatures recorded during the winter, and slightly higher temperatures recorded during the summer period in comparison to the SSM. The greatest contrasts occurred during a period of warm weather in May-July 2012 and the temperature difference was visible at all depths over this period. The greatest variations occurred at 0.2m (Figure 6.20b) and 0.5m-0.7m (Figure 6.20e-i), with the archaeological soils responding stronger to air temperature changes. Whilst the 0.2m variations may be explained

Appendices

slight differences in depth between the archaeological and SSM probes which are magnified due to strong variability of soil temperature with depth already discussed, the deeper variations are more interesting. These depths correspond to DCF Ditchfill1 soil which has a lower density than the SSM at the same depth (1.61 Mg/m^3 to 1.91 Mg/m^3) and a greater porosity (0.4 to 0.33), but both were shown to have roughly similar water content at these depths from the ARDP data (see Section F.1.). Whilst Nobel and Geller (1987) have reported on the importance of water in determining thermal conductivity, others have suggested that thermal conductivity is primarily dependent on pore size and grain size distribution, with soil water playing only a minor role (Scollar et al., 1990, Tabbagh, 1985). One possibility is that the greater porosity in soil which was at field capacity and unsaturated may have contained more air which responds more rapidly to temperature changes due to its lower thermal inertia than water or soil particles.

G.2. Diddington Pasture Field

The temperature variations over the monitoring period at a number of different depths for both the archaeological soils and SSM for DPF are shown in Figure 6.21. Results were similar to the DCF soils discussed in Section G.1. and other studies of soil temperature which have shown similar grain sized soils varying with broad seasonal trends (e.g. Curioni, 2013, Skierucha et al., 2012). However the maximum depth at which smaller scale daily variations can be seen is greater, being around 0.6m as opposed to the 0.4m recorded on DCF. The reasons for this are unknown and a wide variety of depths has been given at which small scale changes are visible for different soil types, although 0.5m seems to be the most commonly stated value (Florides and Kalogirou, 2005, van Manen and Wallin, 2012).

Much smaller differences existed between the archaeology and SSM than on DCF for all depths. At the near surface (above 0.6m), the difference between the archaeological soils and SSM showed similar trends to those observed on DCF with positive differences recorded during

the summer months and negative differences observed during the winter. However, at 0.8m depth, the opposite trend was observed, and the magnitude of differences was greater than at any other depth. One possibility is that the thermistor was affected by the magnetic nature of DPF Ditchfill2 (Nara, 2005, Vevai et al., 1972), although this seems highly improbable given the weak strength of the field and resulting temperature difference, and no obvious link to the soil properties has been found. It seems more likely that this response was the result of another factor such as a slight variation in the relative depths of the two probes. Below 1m in depth, differences between the two soils were almost impossible to observe. Whilst at 1.2m, this was likely to be because both temperature probes were in the same soil (context 8), no explanation can be found for this at 1m as large differences existed in both the measured geophysical values (and hence water content) and geotechnical properties between the archaeological soils and SSM at this depth.

G.3. Cirencester Quarryfield

Results were similar to both the other two study sites. However, the magnitude of differences between the archaeological soils and SSM was greater than on the other sites, especially at the near surface with a contrast between probes at 0.1m and 0.15m nearly always visible throughout the monitoring period. The greatest contrast seemed to have occurred during October 2011 to January 2012, which for the majority of the time had very dry soil (see ARDP data above in Figure 6.16). However, the later period of this contrast was after the wetting front, suggesting that the change in soil water content had little effect, which would agree with the findings of other authors that grain size and porosity are more important than soil VWC (Scollar et al., 1990, Tabbagh, 1985). A similar event also occurred during summer 2012 (June to July) following an extended period of warm weather during which time the archaeological soils showed a higher temperature than the SSM. These contrasts were visible at all depths, but showed a greater lag in response at greater depths in line with the earlier observed behaviour of soil temperature with depth.